

December 2012

Part I. The First Enantiospecific, Stereospecific Total Synthesis of the Indole Alkaloid Ervincidine. Part II. The Synthesis of Alpha 5 Subtype Selective Ligands for Gaba(a) /Benzodiazepine Receptors

Sundari K. Rallapalli
University of Wisconsin-Milwaukee

Follow this and additional works at: <https://dc.uwm.edu/etd>

 Part of the [Organic Chemistry Commons](#)

Recommended Citation

Rallapalli, Sundari K., "Part I. The First Enantiospecific, Stereospecific Total Synthesis of the Indole Alkaloid Ervincidine. Part II. The Synthesis of Alpha 5 Subtype Selective Ligands for Gaba(a) /Benzodiazepine Receptors" (2012). *Theses and Dissertations*. 616.
<https://dc.uwm.edu/etd/616>

This Dissertation is brought to you for free and open access by UWM Digital Commons. It has been accepted for inclusion in Theses and Dissertations by an authorized administrator of UWM Digital Commons. For more information, please contact open-access@uwm.edu.

PART I. THE FIRST ENANTIOSPECIFIC, STEREOSPECIFIC TOTAL
SYNTHESIS OF THE INDOLE ALKALOID ERVINCIDINE

PART II. THE SYNTHESIS OF ALPHA 5 SUBTYPE SELECTIVE
LIGANDS FOR GABA(A)/BENZODIAZEPINE RECEPTORS

by

Sundari K. Rallapalli

A Dissertation Submitted in

Partial Fulfillment of the

Requirements for the Degree of

Doctor of Philosophy

in Chemistry

at

The University of Wisconsin-Milwaukee

December 2012

ABSTRACT

PART I. THE FIRST ENANTIOSPECIFIC, STEREOSPECIFIC TOTAL
SYNTHESIS OF THE INDOLE ALKALOID ERVINCIDINE

PART II. THE SYNTHESIS OF ALPHA 5 SUBTYPE SELECTIVE
LIGANDS FOR GABA (A)/BENZODIAZEPINE RECEPTORS

by

Sundari K. Rallapalli

The University of Wisconsin-Milwaukee, 2012
Under the Supervision of Professor James M. Cook

Part I. The first enantiospecific, stereospecific total synthesis of ervincidine **89** has been accomplished from commercially available D-(+)-tryptophan **37** which has served both as the chiral auxiliary and the starting material. Moreover, this is the first synthesis which unequivocally sets the stereochemistry of the hydroxyl group at C-6 in stereospecific fashion, as well as the C-16 hydroxy methyl group. The stereospecific conversion of D-(+)-tryptophan **37** into the key template (-)- N_a -H, N_b -benzyl tetracyclic ketone **49** via the asymmetric Pictet-Spengler reaction (600 gram scale) and Dieckmann cyclization on multi-hundred gram scale was reduced to only two reaction vessels. The optically active tetracyclic ketone **49** was converted into the core pentacyclic framework **56** using the intramolecular palladium-mediated enolate cross coupling reaction which was developed

here in Milwaukee to afford the core pentacyclic framework **56**. This robust reaction could be scaled up to multigram scale in this series. Important to success here were the sequence of chemical reactions which included a Wittig reaction, a regioselective hydroboration and protection/deprotection steps in order to provide regiospecific oxidation at C-6. The IBX mediated oxidation and the Luche reduction using $\text{CeCl}_3 \cdot 7\text{H}_2\text{O}$ in the presence of NaBH_4 afforded the first enantiospecific, stereospecific total synthesis of ervincidine **89**. The indole alkaloid ervincidine **89** could be prepared from D-(+)-tryptophan **37** in 13 reaction vessels in 19.2% overall yield. Another important experiment was the epimerization of the C-6 alcohol with 0.2N HCl which indicated that care must be employed in isolation of these alkaloids which contain a benzylic hydroxyl group. This research process developed here also provides a general entry to the C-6 hydroxy substituted indole alkaloids of either alpha or beta stereochemistry. Two other diastereomers were made to rule them out as potential structures. This research corrects the errors in Glasby's book and Lousnamma's review and clarifies the work of Yunusov et al. as well as providing the correct absolute configuration of the C-6 hydroxyl function in ervincidine **89**.

Part II. GABA_A/BzR chloride ion channels comprise the major inhibitory neurotransmitter system in the CNS. This central role carries with it a direct influence on many diseases of the CNS. Inverse agonists acting at $\alpha 5$ subunits containing GABA_A receptors are thought to act as cognitive enhancers while eliminating unwanted side effects associated with non-selective compounds. From the recent work of Rowlett, Cook et.al. it was demonstrated that novel $\alpha 5$ selective inverse agonist PWZ-029 was evaluated as a cognitive enhancer in rhesus monkeys in the CANTAB paradigm. This ligand had

the ability to reverse cholinergic deficits in performance induced by the antimuscarinic scopolamine under mixed trial conditions. In the ORD task, PWZ-029 showed only a modest trend for enhancement of performance, but when task difficulty was increased by testing with difficult trials only, PWZ-029 robustly increased performance. This enhancement was reversed by administration of the $\alpha 5$ GABA (A) subtype selective antagonist XLI-093 and this antagonism in turn was reversed by increasing the dose of PWZ-029. In addition, PWZ-029 enhanced performance in the DNMS task using the 10 minute delay with distracters. This ligand also exhibited anxiolytic activity in some primates and was an orally active anticonvulsant in rats. These findings are consistent with a key role for $\alpha 5$ GABA_A receptors in the treatment of age-associated memory impairment and Alzheimer's disease.

To

My Parents Sugunavathi and Satyanarayana Rallapalli

and

My Husband Srihari Vedartham

and

My Son Anirudh Vedartham and Daughter Amulya Vedartham

TABLE OF CONTENTS

PART I. The First Enantiospecific, Stereospecific Total Synthesis of the Indole Alkaloid Ervincidine

1. Introduction.....	2
1.1. Classification and biological activity of the sarpagine/macroline related indole alkaloids.....	2
1.2. Previous approaches to the tetracyclic azabicyclo [3.3.1] nonane core framework 5 of the sarpagine/macroline related indole alkaloids	34
1.2.1. A racemic synthesis by Rassat et al.....	34
1.2.2. Approach to the core tetracyclic structure via the aza-Diels Alder/intramolecular Heck cyclization by Kuethe et al.	36
1.2.3. Approach to the core structure 36 via a ring-closing olefin metathesis by Martin et al.....	37
1.2.4. Synthesis of the tetracyclic core 42 via the cis-selective Pictet-Spengler reaction by Bailey et al.	38
1.2.5. Synthesis of the tetracyclic core 48 by Magnus et al.	40
1.3 Previous syntheses of sarpagine/macroline related indole alkaloids.....	41
1.3.1. Synthesis of sarpagine/macroline related indole alkaloids in Milwaukee	41
1.3.1.1. The enantiospecific total synthesis of (+)-vellosimine by Wang	42
1.3.1.2. Total synthesis of the enantiomer of macroline, the N_a -H analog of macroline and trinervine via a regiospecific hydroboration process by Liu et al.....	44
1.3.1.3. Improved total synthesis of macroline by Liao et al.	48
1.3.2. A biomimetic total synthesis of (+)- N_a -methyl vellosimine 74 by Martin et al.	50
2. Objectives and synthetic approach.....	54
3. Results and Discussion	58

3.1. The First enantiospecific, stereospecific total synthesis of the sarpagine alkaloids related to structures of the proposed ervincidine (88 and 89) including ervindicine..	58
3.1.1. Synthesis of the (-)- <i>N</i> _a -H, <i>N</i> _b -H tetracyclic ketone 50 on large scale	58
3.1.2. Synthesis of the - <i>N</i> _a -H pentacyclic ketone 56	64
3.1.3. Completion of the regiospecific, stereospecific total synthesis of ervincidine proposed by Glasby and Lousnamaa	72
3.1.4. Completion of the regiospecific, stereospecific total synthesis of ervincidine proposed by Yunusov	74
3.1.5. Completion of the regiospecific, stereospecific total synthesis of the diastereomer (118) of Ervindicine	90
4. Conclusion	91
5. Experimental Details	92
6. References:	125

Part II. The Synthesis of Alpha 5 Subtype Selective Ligands for GABA(A) /Benzodiazepine Receptors

1. Introduction	138
2. Objective of this research	146
3. Results and Discussion	148
4. Synthesis of α 5 selective BzR bivalent ligands	166
5. Synthesis of Bivalent Ligands with Oxygen Linkers	182
6. Synthesis of α 5 subtype selective inverse agonist PWZ-029	199
7. Conclusions	219
8. General Experimental Details	221
9. Computer Modeling	243

10. Electrophysiological Experiments (with Sieghart et al.)	244
11. Experiments of GABA signaling in neuroblastoma (Weiss and Cook et al.).....	254
12. Behavioral experiments (with Savic et al.).....	258
13. Two-Way Active Avoidance (AA) Paradigm (with Savic et al.)	259
14. Measurement of Locomotor Activity (with Savic et al.)	260
15. Behavior on the Elevated Plus Maze (EPM) (with Savic et al.).....	260
16. Grip Strength Test (with Savic et al.)	261
17. <i>In vivo</i> studies on XLi-093 on mice (Rowlett and Cook et al)	262
18. CANTAB work (Rowlett and Cook et al.)	264
18.5. CANTAB Tasks in Monkeys.....	266
19. Object Retrieval with Detours (ORD) Task.....	272
20. Assessment of Motor Coordination and Behavioral Effects in Monkeys.....	273
21. References.....	276
III. Appendix I: Crystal Data for 110 and 111.....	293
IV. Appendix II: Data on QH-II-066 (Lelas et al.).....	310
V. Appendix III: Data on QH-II-066 (Weiss et al.).....	344
VI. Appendix IV: Anticonvulsant screening data on PWZ-029 (Stables).....	383
VII. Appendix V: Data on QH-II-066 (Platt et al.).....	385
VIII. Appendix VI: Crystal Data for XLi-093 (33).....	419
IX. Appendix VII: SBIR grant	427
X. Curriculum Vitae	476

LIST OF FIGURES

Part 1

Figure 1. Bisindoles	3
Figure 2. Dimeric Indole Alkaloids accedinisine and N'-demethylaccedinisine	8
Figure 3. Macroline, Sarpagine and Ajmaline	8
Figure 4. Biosynthetic Relationship Between Macroline and Sarpagine.....	9
Figure 5. Biosynthetic Relationship Between Sarpagine and Ajmaline Type Alkaloids	10
Figure 6. Sarpagine Type Indole Alkaloids	54
Figure 7. The Indole Alkaloid Ervincidine	56
Figure 8. ORTEP View of the Crystal Structure of the Monol 110	72
Figure 9. ORTEP View of the Crystal Structure of the Diol 88 which shows the Alpha Hydrogen at C-6 with C-5.....	74
Figure 10: Proton Spectrum of Natural Product Ervincidine 89	78
Figure 11. Carbon Spectrum of Natural Product Ervincidine 89	79
Figure 12. Selected NOEs of Ervincidine 89	80
Figure 13. 1D NOEs Observed after Irradiation of Protons at H-3	81
Figure 14. 1D NOEs Observed after Irradiation of Protons at H-15	81
Figure 15. 1D NOEs Observed after Irradiation of Protons at H-17	82
Figure 16. 1D NOEs Observed after Irradiation of Protons at H-6	82
Figure 17. 1D NOE data H-15 irradiated.....	84
Figure 18. 2D NOESY of Ervincidine 89	89

Part II.

Figure 1. Absolute subunit arrangement of the $\alpha 1\beta 2\gamma 2$ GABA _A receptor	140
Figure 2. The schematic diagram of subunits and ligands of the benzodiazepine-GABA receptor-chloride channel complex.....	141
Figure 3. GABA, diazepam, triazolam and midazolam.....	143
Figure 4. Mode of action of benzodiazepines	144
Figure 5. Diazepam in the Pharmacophore/Receptor Model for the BzR Site.....	145
Figure 6. Distribution of $\alpha 5$ in Hippocampus.....	147
Figure 7. Diazepam (2) aligned in the pharmacophore model.....	150
Figure 8. The ligand QH-II-66, (11 , a 7-acetylenyl-1,4-benzodiazepine, in black), was designed to offer better occupation of this region and exhibit $\alpha 5$ selectivity.....	151
Figure 9. The ligand, QH-II-66 11 , aligned in the included volume of the pharmacophore/receptor model for the $\alpha 2\beta 3\gamma 2$ subtype.....	152
Figure 10. The ligand, QH-II-66 11 , aligned in the included volume of the pharmacophore/receptor model for the $\alpha 5\beta 3\gamma 2$ subtype.....	152
Figure 11. GABA activation decreases viability and induces apoptosis in neuroblastoma cells	156
Figure 12. The Oocyte Efficacy Data on PS-1-37(18).....	159
Figure 13. Ro 15-4513 (19), RY-023 (20), RY-024 (21), RY-079 (22), RY-80 (23) and the Merck compound (24).....	161
Figure 14. Subtype efficacy of RY-24 (21),	162
Figure 15. Crystal Structure of Bivalent Ligand XLI093 (33).	169
Figure 16. XLI093 (33) Aligned in the Included Volume of the Pharmacophore/Receptor Model for the $\alpha 5\beta 3\gamma 2$ Subtype.	169
Figure 17. Effects of XLI093 (33) on GABA _A receptors were tested by two-electrode voltage clamp experiments in cRNA injected <i>Xenopus</i> oocytes	172
Figure 18. <i>In vivo</i> binding of Xli-093.	174
Figure 19. XLI-093 (3.0 mg/kg) blocked the DZ-induced suppression of performance ratio on the holeboard task.	175
Figure 20. Subtype efficacy of XLI356 (34)	178
Figure 21. Visual and audio que data for XLI356	179

Figure 22. Subtype efficacy of XLi210 (35).....	180
Figure 23. Crystal structures of XLi-093, DMH-D-053, and DM-III-96.	186
Figure 24. Aromatic region of ¹ HNMR spectra of XLi-093 (33) in CD ₂ Cl ₂ at variable temperatures.....	188
Figure 25. Aromatic region of ¹ HNMR spectra of SR-II-35 (42) in CD ₂ Cl ₂ at variable temperatures.....	189
Figure 26. Aliphatic region of ¹ HNMR spectra of SR-II-35 (42) in CD ₂ Cl ₂ at variable temperatures.....	190
Figure 27. Aromatic region of ¹ HNMR spectra of XLi-093 (33) in MeOH- <i>d</i> ₄ at different temperatures.....	193
Figure 28. Bivalent ligand XLi093 (33) aligned in the included volume of the pharmacophore/receptor model for the α5β3γ2 subtype.....	194
Figure 29. The linkers of the bivalent ligands.	195
Figure 30. The conformations for dimethoxymethane.....	196
Figure 31. Newman projection for linkers B, C and D.....	197
Figure 32. Oocyte data for PWZ-029 by Sieghart et al.	204
Figure 33. Fear conditioned contextual memory	205
Figure 34. Passive avoidance task.....	206
Figure 35. Preliminary profile of cognitive enhancing and anxiolytic like effects of PWZ-029 in monkeys.	208
Figure 36. Cognitive-enhancing effects of PWZ-029 in the rhesus monkey.....	209
Figure 37. Binding affinity data of PWZ-029 (47) and Roche compound 49	211
Figure 38. Oocyte data of SR-II-097	213
Figure 39. Oocyte data of SR-III-38	215
Figure 40. Oocyte data of SR-III-61	217
Figure 41. Movement Assessment Panel for rhesus monkeys.....	274

LIST OF TABLES

Part I.

Table 1. Antiamoebic and Antimalarial Activity of Selected <i>Alstonia</i> Alkaloids ²⁴	5
Table 2. IC ₅₀ Values of Alkaloids Tested Against <i>Plasmodia falciparum</i> (K1 and T9-96 strains).....	6
Table 3. IC ₅₀ Values of Alkaloids Tested Against <i>Plasmodia falciparum</i> (K1 strain) ⁴⁷ ..	7
Table 4. Sarpagine Indole Alkaloids	11
Table 5. Macroline Related Indole Alkaloids	21
Table 6. Bisindole Alkaloids	24
Table 7. Degradation Products of <i>Alstonia</i> Alkaloids.....	33

Part II.

Table 1. <i>In Vitro</i> Receptor Binding Data on Diazepam (2) and QH-II-066 (11). Binding Affinity at $\alpha\beta\gamma 2$ GABA _A /BzR Receptor Subtypes (Values are Reported in nM)	155
Table 2. <i>In Vitro</i> Receptor Binding Data on Diazepam (2) and PS-1-37 (18) . Binding Affinity at $\alpha\beta\gamma 2$ GABA _A /BzR Receptor Subtypes (Values are Reported in nM).....	158
Table 3. EC ₅₀ and Hill Slope for Modulation of Control GABA EC ₃ by PS-1-37 (18) in <i>Xenopus</i> Oocytes Expressing Different GABA _A Receptor Subtypes. Results Represent EC ₅₀ (95% Confidence Interval for EC ₅₀) and Hill Slope (Nh) \pm SD from at Least Four Cells from Two Batches.....	159
Table 4. Modulation of Control GABA EC ₃ by Diazepam and HZ166 (7) on <i>Xenopus</i> Oocytes Expressing Different GABA _A Receptor Subtypes. Values are Presented as Mean \pm SEM of at Least Four Oocytes from at Least Two Batches	160
Table 5. <i>In Vitro</i> Receptor Binding Data of $\alpha 5$ ligands. Binding Affinity at $\alpha\beta\gamma 2$ GABA _A /BzR Receptor Subtypes (Values are Reported in nM)	163

Table 6. <i>In Vitro</i> Binding Affinities at GABA _A /BzR Subtypes. ^a Values Reported are in nM.	170
Table 7. Percent of α 5GABAA binding sites occupied by XLi-093 and DZ at doses used in the behavioral studies.....	176
Table 8. <i>In Vitro</i> Binding Affinities of bivalent ligands at GABA _A /BzR subtypes.....	178
Table 9. EC ₅₀ and Hill Slope for Modulation of Control GABA EC ₃ by XLi 210 (35) in Xenopus Oocytes	181
Table 10. Modulation of Control GABA EC ₃ by XLi 210 (35) on Xenopus Oocytes Expressing Different GABA _A Receptor Subtypes.....	181
Table 11. <i>In Vitro</i> Binding Affinities of bivalent ligands at GABA _A /BzR subtypes. ^a Values Reported are in nM.	185
Table 12. The Molecular Composition and Stable Conformation of Various Bz BS Bivalent Ligands.	187
Table 13. <i>In Vitro</i> Binding Affinities of bivalent ligands at GABA _A /BzR subtypes....	203
Table 14. EC ₅₀ and Hill Slope for Modulation of Control GABA EC ₃ by SR-II-097 (57) in Xenopus Oocytes Expressing Different GABA _A Receptor Subtypes.	214
Table 15. Modulation of Control GABA EC ₃ by SR-II-097 (57) on Xenopus Oocytes Expressing Different GABA _A Receptor Subtypes.....	214
Table 16. EC ₅₀ and Hill Slope for Modulation of Control GABA EC ₃ by SR-III-38 (58) in Xenopus Oocytes Expressing Different GABAA Receptor Subtypes.	216
Table 17. Modulation of Control GABA EC ₃ by SR-III-38 (58) on Xenopus Oocytes Expressing Different GABA _A Receptor Subtypes.....	216

Table 18. EC50 and Hill Slope for Modulation of Control GABA EC₃ by SR-III-61 (**49**) in Xenopus Oocytes Expressing Different GABA_A Receptor Subtypes.218

Table 19. Modulation of Control GABA EC₃ by SR-III-61 (**49**) on Xenopus Oocytes Expressing Different GABA_A Receptor Subtypes.....218

Table 20. Schedule of CANTAB tests for a single dose of compound plus vehicle 271

ACKNOWLEDGMENTS

This PhD degree would not have been possible without the help and support of many people. I would like to thank my advisor Professor James M. Cook, for his enthusiastic supervision and patience during this work. I am grateful for his advice and guidance throughout my work at UW-Milwaukee. He has and will always be an inspiration and motivation to me.

I would like to thank the members of my doctoral committee, Professor's Hossain, Schwabacher, Pacheco and Dietz, for their suggestions and instructive discussions during my graduate studies at UW-Milwaukee. I am also very grateful to Dr. Föersterling for his instruction and guidance for the NMR studies. I thank Mr. Neal Korfhage for his expertise in glassblowing which enabled me to set up equipment that may have otherwise been impossible. I would also like to acknowledge Mr. Frank Laib for mass spectral analysis and CHN analysis. I greatly appreciate Dr. Jeffery R. Deschamps for his outstanding help in X-ray analysis of the key compounds during my research. Thanks to Elise Nicks, Mary Eckert and Wendy Grober for all their help during my graduate studies at UW-Milwaukee.

I would like to thank my in-laws Krishnamacharyulu and Satyavathi Vedartham who helped me in the last semester of my PhD degree. It would have been difficult to write and defend my thesis without their help. I would like to thank my brother Krishna Rallapalli and my sister in-law Chandra Rallapalli who have always been of great support. Thanks to my brother for always being around whenever I needed him. My life is indebted to my parents who have always been my pillar of strength. Without their support and guidance, this achievement would not have been accomplished. This PhD

degree is dedicated to my dad who longed to see me with a doctorate degree. I would like to thank my husband Srihari Vedartham who has always encouraged and supported me during this endeavor. All these six years he never complained about the long drive to Chicago for his work. I would like to thank him for all his help at home and also for his professional advice. Without his patience, vision and guidance it would have been impossible to continue and finish my education. Srihari has always been by my side through thick or thin. Special thanks to my son Anirudh Vedartham who went through a lot of hardship during the initial stages of my PhD program. He never showed tantrums as a toddler and without his support it would have been impossible for me to reach this milestone.

It was a pleasure to share doctoral studies with past and current members of the Cook group. I would like to thank Dr. Srirama Sarma Pullela, Dr. Ranjit Verma, Dr. Ojas Namjoshi and Dr. Michael Lorenz, and for all their help and guidance during the years of my PhD program. It was a pleasure to share and eat lunch every day with Dr. Ojas Namjoshi and Ms. Poonam Biawat. I would like to thank Ms. Poonam Biawat and Mr. Toufiqur Rahman for all the help with my thesis corrections and printing. I would also like to thank my colleagues Dr. Michael VanLinn, Dr. M. Shahjahan Kabir, Dr. Wenyuan Yin, Dr. Terry Clayton, Dr. Rahul Edwankar, Dr. Chitra Edwankar, Mr. German Fonseca, Mr. Christopher Witzigman, Mr. Michael Poe, Mr. Phanibabu Tiruveedula and Mr. Toufiqur Rahman for providing amicable atmosphere to work. I would also like to acknowledge the financial, academic and technical support of the Department of Chemistry at UW-Milwaukee, the Graduate School at UW-Milwaukee, and the NIMH.

**I. THE FIRST ENANTIOSPECIFIC, STEREOSPECIFIC TOTAL
SYNTHESIS OF THE INDOLE ALKALOID ERVINCIDINE**

1. Introduction

1.1. Classification and biological activity of the sarpagine/macroline related indole alkaloids

Alkaloids are of importance due to their biological activity. They are distributed diversely and have been isolated from plant and animal sources worldwide.¹⁻⁵ Indole alkaloids are of prominence because of the similarity with tryptophan which is an essential amino acid. The medicinal properties⁶ of these indole alkaloids remain of great interest as well as the nature of their structure and stereochemistry. From the synthetic point of view, these complex molecules remain of paramount significance. The enantiospecific and regiospecific synthesis of alkaloids or their enantiomers has always been a challenge to the synthetic chemist.⁷⁻⁹ Synthetic routes are designed and revised continually in order to provide material for testing and for commercial uses. For all of these reasons, indole alkaloids play an important role in organic chemistry. This chapter includes the various classes of ajmaline and sarpagine-related indole alkaloids and also provides the previous synthetic methods to construct these molecules.¹⁰

Biological activity of sarpagine/macroline related indole alkaloids

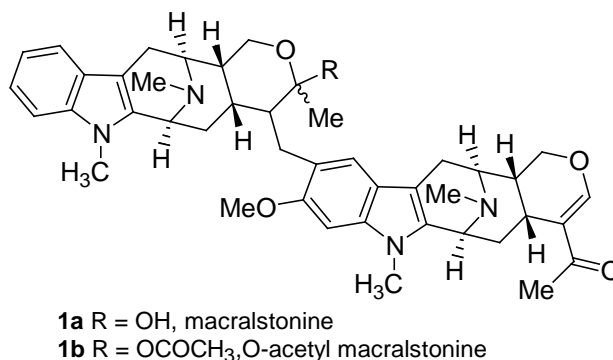
Indole alkaloids of the sarpagine/macroline/ajmaline type comprise one of the largest groups of structurally related indole natural products.¹⁰ These indole alkaloids are primarily isolated from three plant families: *Apocynaceae*, *Rubiaceae* and *Loganiaceae*.¹¹⁻¹³ Interest in the macroline/sarpagine alkaloids originated as a result of folk tales that described the medicinal properties of the plants from which these alkaloids were isolated.^{9,14} Various species of *Rauwolfia* which are broadly distributed among Asia

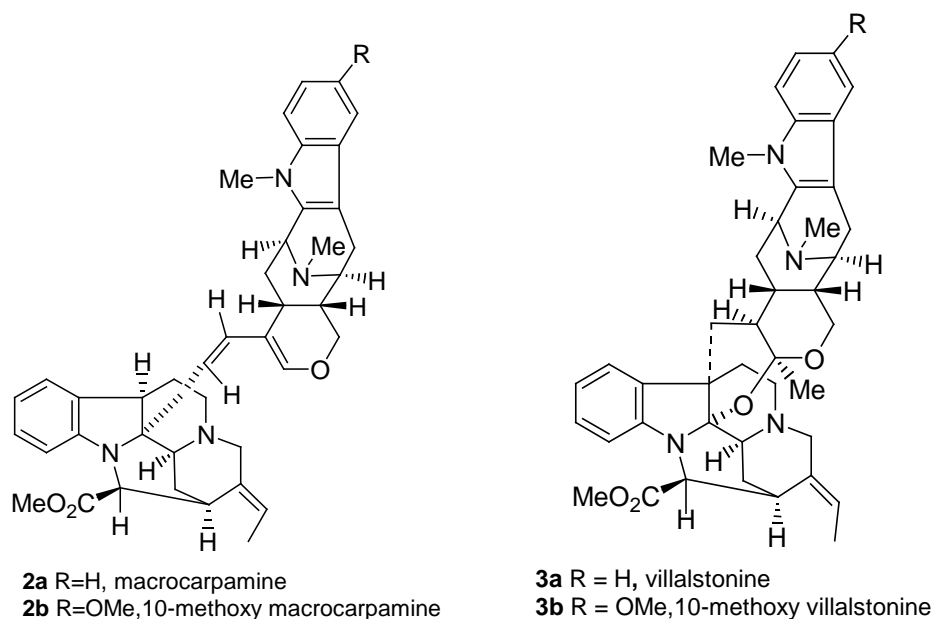
and Africa¹⁵⁻²⁰ are widely used in traditional Chinese medicine for the treatment of neuralgia, migraine²¹ and hypertension.^{18,20,22}

As early as 1958,²³ and later in 1967²⁴ the bisindole macralstonine **1a** (Figure 1), which had been isolated from *Alstonia macrophylla* Wall and *Alstonia muelleriana* Domin, was shown to exhibit potent hypotensive activity.

Nine alkaloids from *Alstonia angustifolia* were tested by Wright et al.²⁵ for antiprotozoal activity against *Entamoeba histolytica* and *Plasmodium falciparum* in vitro (Table 1). Three dimeric alkaloids, macralstonine O-acetate **1b**,²⁶ (-)-macrocarpamine **2a**,²⁷ and (+)-villalstonine **3a**^{28, 29} (Figure 1) were found to possess significant activity against both protozoa. Macrocarpamine **2a** was found to be the most active antiamebic compound with an antiamebic activity one fourth that of the standard drug emetine. Villalstonine **3a** was found to be the most potent alkaloid against *P. falciparum*, and was about fifteen

Figure 1. Bisindoles





times less active than the antimalarial drug chloroquine. The acetate of macralstonine **1b** was much more active against both protozoa when compared with the parent macralstonine **1a**. The monomeric alkaloids were found to be considerably less active than the bisindoles. These results were in agreement with the studies carried out later by Houghton et al. (Tables 2 and 3).³⁰ The results of these *in vitro* studies provide some basis for the traditional use of the plant extract from *Alstonia angustifolia* for the treatment of amoebic dysentery and malaria by the people of the Malay peninsula.^{31,32}

Table 1. Antiamoebic and Antimalarial Activity of Selected *Alstonia* Alkaloids²⁵

Alkaloids	<i>E. histolytica</i> ED ₅₀ (95% C. I.) μM	<i>P. falciparum</i> ED ₅₀ (95% C. I.) μM
alstonerine	75.3(65.0-85.6)	46.3(27.7-77.3)
alstophylline	67.7(57.2-78.2)	82.3(65.9-102)
macralstonine	inactive at 70	inactive at 178
O-acetyl macralstonine	15.51(14.78-16.24)	3.43(1.86-6.34)
villalstonine	11.8(11.7-12.0)	2.92(1.11-3.14)
pleiocarpamine	47.4(46.8-52.90)	20.5(12.6-33.17)
macrocarpamine	8.21(7.76-8.48)	9.36(7.20-12.1)
11-methoxyakuammicine	70.5(65.3-75.6)	41.3(26.5-64.3)
norfurocurarine	84.1(82.9-89.6)	129(70.2-239)
vincamajine	inactive at 70	138(79.3-238)

ED₅₀: Effective dose at 50% inhibition. See Table 2 for source of *P.falciparum*

The bisindole alkaloid accedinisine **4a** was first reported to be isolated from the root of epithelium *T. accedens* in 1976.³³ Later in 1994, accedinisine **4a** and *N*-demethylaccedinisine **4b** were isolated from *Peschiera van heurkii*. These two bisindole alkaloids exhibited potent antileishmanial and antibacterial activities.³⁴ Dimeric alkaloids are often more potent in vivo than their monomeric progenitors. Much of the early isolation and structural work on the *Alstonia* alkaloids was performed in the laboratories of Elderfield³⁵ and Schmid^{36,37} and was followed by the biomimetic interconversions of LeQuesne et al.^{26,28,29,38-40}

Table 2. IC₅₀ Values of Alkaloids Tested Against *Plasmodia falciparum* (K1 and T9-96 strains)³⁰

Alkaloids	K1 (μM, n = 3)	T9-96 (μM, n = 3)	K1/T9-96 ratio
O-acetyl macralstonine	0.53 ± 0.09	12.4 ± 1.6	0.04
villalstonine	0.27 ± 0.06	0.94 ± 0.07	0.29
alstomacrolone	1.12 ± 0.35	10.2 ± 0.4	0.11
macrocarpamine	0.36 ± 0.06	>39*	<0.009
chloroquine diphosphate	0.20 ± 0.07	0.019 ± 0.002	10.53

K1: the multi-drug resistant strain, which is highly resistant to chloroquine; T9-96: the chloroquine sensitive strain; n: number of independent experiments; *: % inhibition at 39 μM (7.5 μg/mL), the highest concentration tested was 32.6 ± 4.1 μM. The experiment was done with infected human red blood cells.

During the structure determination of *Alstonia* bisindole alkaloids by Schmid et al.^{36,37} macrolone **6** (Figure 3) was obtained as a degradation product from villalstonine **3a**. To date, macrolone **6** has not been isolated as a natural product but it is believed to be a biomimetic precursor to many *Alstonia* alkaloids.^{26,28,29,38,39}

Studies on individual sarpagine/ajmaline indole alkaloids have shown normacusine B exhibited sedative and ganglion blocking activity,⁴¹ lochnerine elicited hypoglycemic activity,⁴² pericyclivine has been shown to exhibit weak cytotoxic activity against P-388 leukemia,⁴³ while gardnutine, gardnerine, and hydroxygardnutine have been shown to elicit ganglion blocking effects as well as anticancer activity.⁴⁴⁻⁴⁶ The mixture of constituents (normacusine B, affinisine, N_a-methylpericyclivine, and voachalotine) present in *Peschiera van Heurckii* from the tropical rain forest in Bolivia is known for its alleged leishmanicidal and bactericidal activity.³⁴ Like many quaternary alkaloids, the

major quaternary sarpagine alkaloid from *Strychnos angolensis*, 11-methylmacusine A, demonstrated muscle relaxant

Table 3. IC₅₀ Values of Alkaloids Tested Against *Plasmodia falciparum* (K1 strain)⁴⁷

ALKALOID	n	IC ₅₀ (µg/mL)
talcarpine	3	40.3 ± 2.9
pleiocarpamine	2	6.44 ± 0.98
alstoumerine	2	13.1 ± 2.7
20- <i>epi</i> -antirrhine	3	7.51 ± 1.17
alstonerine	2	9.67 ± 3.57
alstophylline	2	12.7 ± 1.7
macralstonine	3	8.92 ± 2.95
O-methylmacralstonine	2	0.85 ± 0.20
O-acetylmacralstonine	3	0.53 ± 0.09
alstomacrophylline	2	1.10 ± 0.30
villalstonine	3	0.27 ± 0.06
villalstonine <i>N_b</i> -oxide	2	10.7 ± 1.9
alstomacroline	3	1.12 ± 0.35
macrocarpamine	3	0.36 ± 0.06
chloroquine diphosphate	3	0.20 ± 0.07

K1 strain: multidrug resistant strain; n: number of independent experiments. The test was done with infected human red blood cells.

activity.⁴⁸ The crude mixture of nine alkaloids present in *Ervatamia yunnanesis* is used in Chinese folk medicine for the treatment of hypertension.²² Scientists have begun to

evaluate these alkaloids for activity against cancer^{49,50} and HIV,^{51,52} however, the paucity of isolable material from these plants has retarded in depth evaluation.

Figure 2. Dimeric Indole Alkaloids accedinisine and N'-demethylaccedinisine

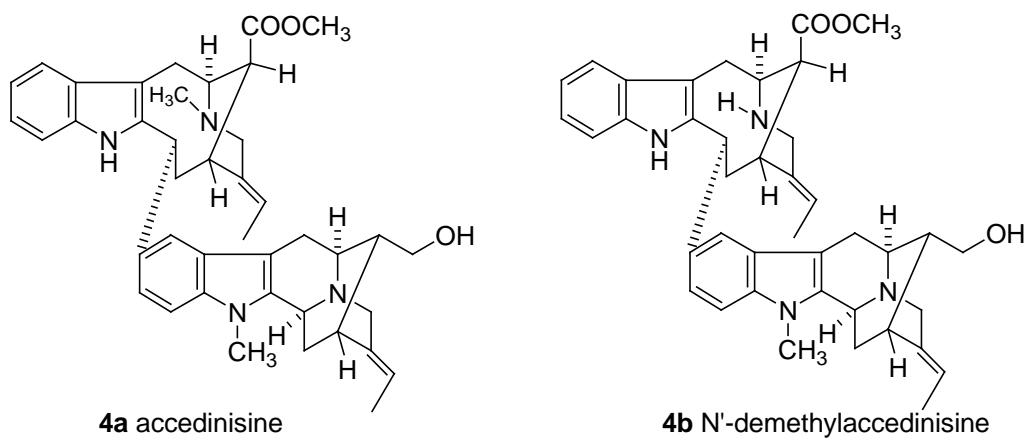
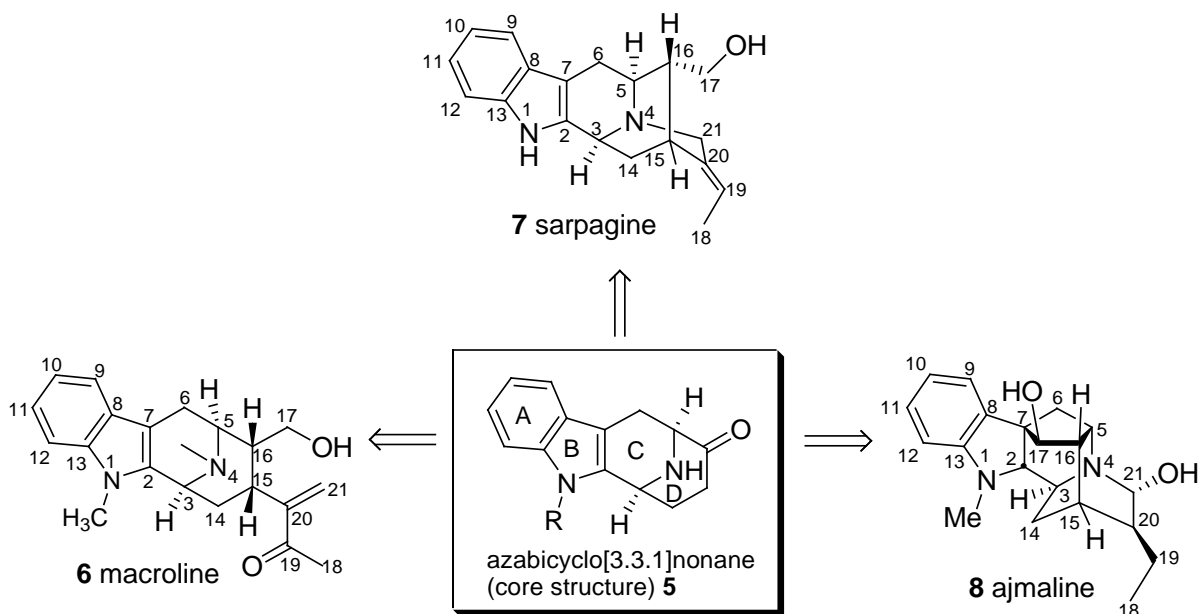


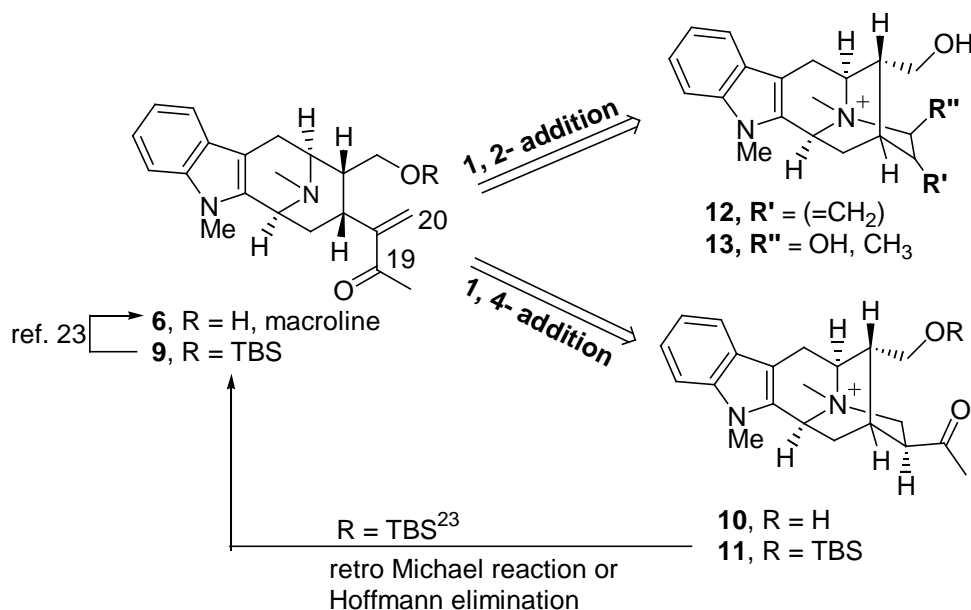
Figure 3. Macroline, Sarpagine and Ajmaline



The number of macroline-related alkaloids which have been isolated has increased rapidly. At this time, the group contains more than 150 alkaloids, of which over a 100 are monomeric indoles. The remainder belongs to the bisindole class of alkaloids.^{40,53-55} The

sarpagine group of alkaloids (represented by **7**, Figure 3) is the largest class of natural products related to the macroline bases and both series originate from common biogenetic intermediates. Illustrated in Figure 3 are the basic macroline and sarpagine skeletons. The biogenetic numbering of LeMen and Taylor⁵⁶ is used throughout this chapter. Note the four stereocenters at C-3, C-5, C-15 and C-16 in macroline. The β -hydrogen atom at C-15 of this group, as well as the chiral centers at C-3, C-5 and C-16 are the same for the sarpagine series. The two classes can be related in a synthetic sense by a Michael addition of the nitrogen atom of N-4 of macroline **6** to the α , β -unsaturated carbonyl system at C-21, or by direct 1, 2 addition of N-4 to the ketone at C-19, as illustrated in Figure 4.^{54,55} Conversely, sarpagine can be converted into macroline **6** by a retro-Michael reaction or Hoffmann elimination of the N_b -methyl intermediate, as demonstrated earlier by LeQuesne et al.³⁸ (see Figure 4).

Figure 4. Biosynthetic Relationship Between Macroline and Sarpagine



The macroline/sarpagine alkaloids bear important structural similarities to the ajmaline alkaloids, the latter of which are well known for their biological activity.⁵⁷ Ajmaline **8**, is a clinically important indole alkaloid with historical significance.^{58,59} Both these bases are structurally related by the presence of the quinuclidine ring and the C-5—C-16 bond linkage. The absolute configurations of the stereogenic centers at C-3, C-5 and C-15 of both series are identical, except at C-16 which is antipodal to the sarpagine series. The biogenetic connection between the sarpagine and ajmaline alkaloids proposed earlier⁶⁰⁻⁶² was confirmed by Stöckigt et al.⁶³⁻⁶⁶ by conversion of 16-epi-vellosimine **14** into deacetylvinorine **16** in the presence of the enzyme, acetyl-CoA dependent *vinorine synthase* (see Figure 5).

Figure 5. Biosynthetic Relationship Between Sarpagine and Ajmaline Type Alkaloids

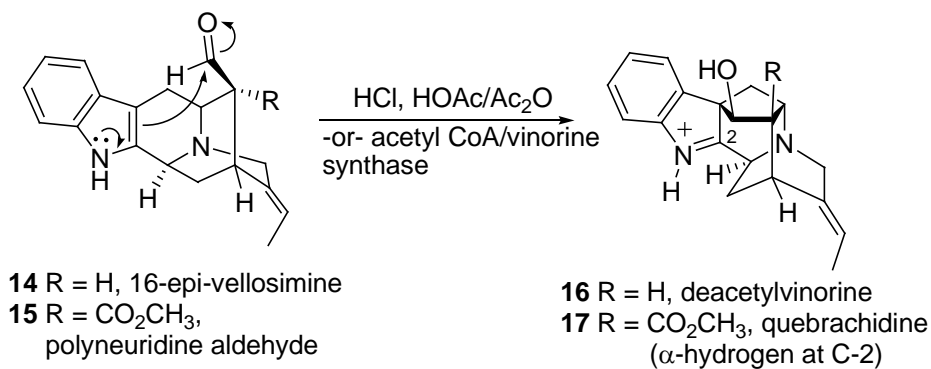


Table 4. Sarpagine Indole Alkaloids (1)⁴⁰

Structure	Alkaloid	Refs.
	R=H, R'=H, vellosimine	(40)
	R=Me, R'=H, <i>N</i> _a -methylvellosimine	(40)
	R=H, R'=OMe, 10-methoxyvellosimine	(40)
	R=Me, R'=OMe, majvinine	(40)
	R=H, R'=H, normacusine B	(40)
	R=H, R'=Ac, O-acetylnormacusine B	(40)
	R=H, R'=COPh, O-benzoyl normacusine B	(40)
	R=H, R'=Me, O-methylnormacusine B	(40)
	R=Me, R'=H, affinisine	(40)
	R=R ₁ =R ₂ =H, sarpagine	(40)
	R=H, R ₁ =Me, R ₂ =H, lochnerine	(40)
	R=R ₁ =H, R ₂ =Ac, O-acetylsarpagine	(40)
	R=Me, R ₁ =R ₂ =H, <i>N</i> _a -methylsarpagine	(40)
	R ₁ =R ₂ =H, pericyclivine	(40)
	R ₁ =CH ₃ , R ₂ =H, <i>N</i> _a -methylpericyclivine	(40)
	R ₁ =H, R ₂ =OH, 10-hydroxy pericyclivine	(40)
	R ₁ =H, R ₂ =OMe, 10-methoxy pericyclivine	(40)
	R ₁ =Me, R ₂ =OH, 10-hydroxy <i>N</i> _a -methylpericyclivine	(40)
	R ₁ =Me, R ₂ =OMe, 10-methoxy <i>N</i> _a -methylpericyclivine	(40)

Table 4. Sarpagine Indole Alkaloids (2) ⁶⁷⁻⁶⁹

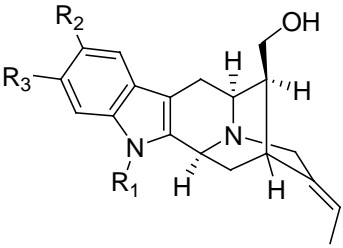
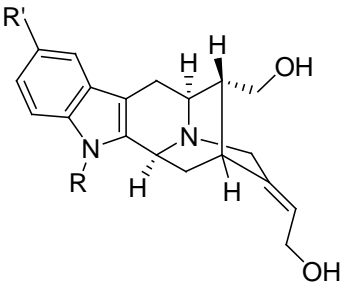
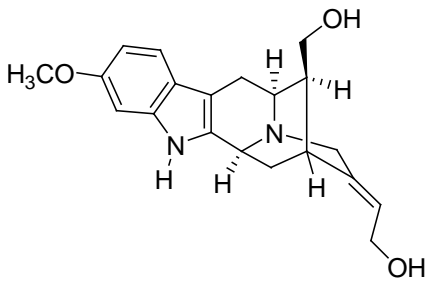
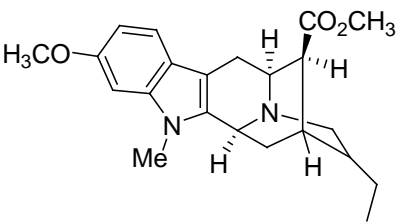
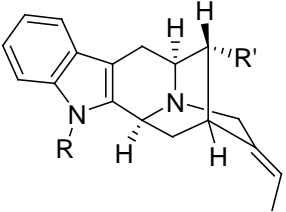
Structure	Alkaloid	Refs.
	$R_1=R_3=H, R_2=OH$, 16-episarpagine	(40)
	$R_1=R_3=H, R_2=OMe$, lochvinerine	(40)
	$R_1=R_2=H, R_3=OCH_3$, gardnerine	(40)
	$R'=OMe, R=H$, 18-hydroxy lochnerine	(40)
	$R'=H, R=Me$, 18-hydroxy affinisine	(40)
	18-hydroxygardnerine	(40)
	11-methoxy- <i>N</i> _a -methyldihydropericyclivine	(68)
	$R=H, R'=CH=CHCOCH_3$, difforine	(40, 69)
	$R=CH_3, R'=CO_2CH_3$ <i>N</i> _a -methyl-16-epipericyclivine	(40, 70)

Table 4. Sarpagine Indole Alkaloids (3)

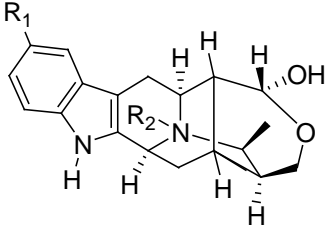
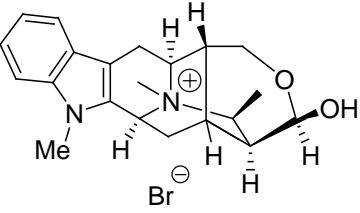
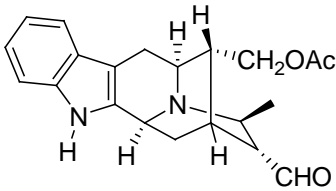
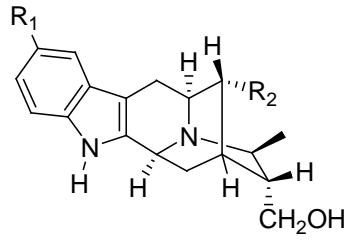
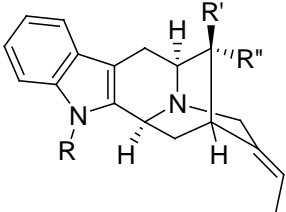
Structure	Alkaloid	Refs.
	$R_1=OH$, $R_2=CH_3$ verticillatine (Cl salt)	(40)
	$R_1=H$, peraksine (vomifoline)	(40)
	macrosalhinium bromide	(40)
	O-acetylpreperakine	(40)
	$R_1=H$, $R_2=CH_2OH$, 19(<i>S</i>),20(<i>R</i>)-dihydroperaksine	(40)
	$R_1=OH$, $R_2=CH_2OH$, 10-hydroxy-19(<i>S</i>),20(<i>R</i>)- dihydroperaksine	(40)
	$R_1=H$, $R_2=CHO$, 19(<i>S</i>),20(<i>R</i>)-dihydroperaksine-17- al	(40)
	$R=R''=H$, $R'=CH_2OH$, 16-epinormacusine B	(40)
	$R=Me$, $R'=CH_2OH$, $R''=H$, 16-epiaffinisine	(40)
	$R=Me$, $R'=CH_2OAc$, $R''=H$, O-acetyl-16-epiaffinisine	(40)

Table 4. Sarpagine Indole Alkaloids (4)

Structure	Alkaloids	Refs.
	voacoline	(40)
	trinervine	(40)
	venecurine	(40)
	R=H, R'=Me, talpinine R=OMe, R'=H, 21-hydroxy cyclolochnerine	(40) (40)
	eburnaphylline	(40)

Table 4. Sarpagine Indole Alkaloids (5)⁷⁰⁻⁷³

Structure	Alkaloid	Refs.
	neo-sarpagine	(71)
	R=H, <i>N_a</i> -demethylaccedine (amerovolfine)	(72)
	R=OH, 3-hydroxysarpagine	(73)
	ervincidine	(40, 138,139)
	R ₁ =CH ₃ , R ₂ =H, R ₃ =CH ₃ , dehydro-16-epiaffinisine	(40)
	R ₁ =H, R ₂ =OCH ₃ , R ₃ =CH ₃ , gardnutine	(40)
	R ₁ =H, R ₂ =OCH ₃ , R ₃ =CH ₂ OH, 18-hydroxygardnutine	(40, 74)
	R=H, dehydrovoachalotine	(40)
	R=OH, 17-hydroxy- dehydrovoachalotine	(40)

Table 4. Sarpagine Indole Alkaloids (6)

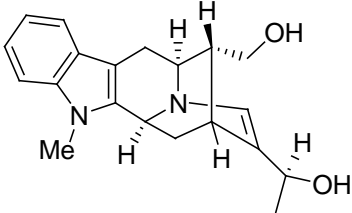
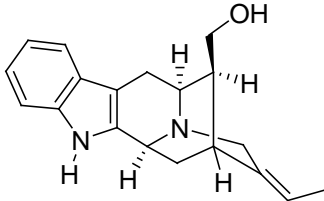
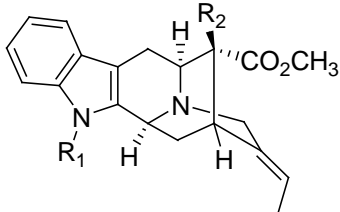
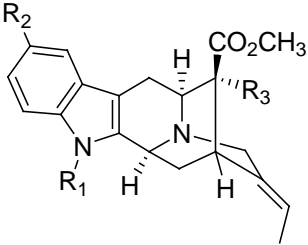
Structure	Alkaloid	Refs.
	alstoumerine	(40)
	koumidine	(40)
	$R_1=H, R_2=CHO,$ polyneuridine aldehyde (40) $R_1=H, R_2=CH_2OH,$ polyneuridine (40) $R_1=CH_3, R_2=CHO,$ voachalotinal (40) $R_1=CH_3, R_2=CH_2OH,$ voachalotine (40)	
	$R_1=R_2=H, R_3=CH_2OH,$ E-akuammidine (40) $R_1=R_2=H, R_3=CH_2OAc,$ acetylakuammidine (40) $R_1=CH_3, R_2=OCH_3, R_3=CH_2OH,$ 10-methoxy- <i>N</i> _a -methylakuammidine (40)	

Table 4. Sargine Indole Alkaloids (7)

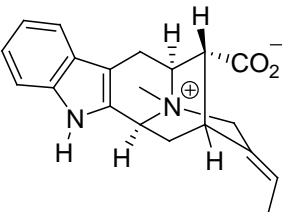
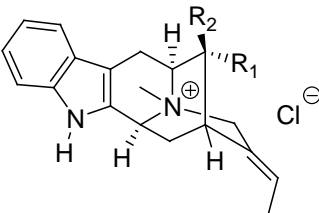
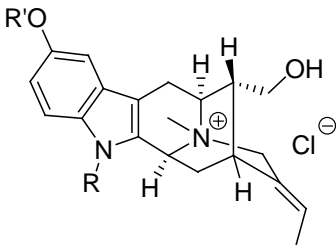
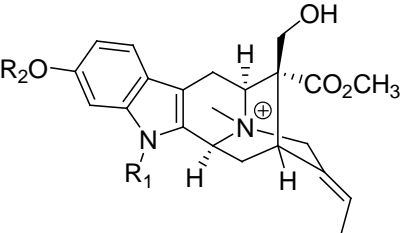
Structure	Alkaloid	Refs.
	panarine	(40)
	$R_1=CH_2OH$, $R_2=H$, macusine B	(40)
	$R_1=CH_2OCH_3$, $R_2=H$, O-methylmacusine B	(40)
	$R_1=CO_2CH_3$, $R_2=H$, alkaloid Q3	(40)
	$R_1=H$, $R_2=CH_2OCH_3$, O-methyl-16-epimacusine B	(40)
	$R_1=H$, $R_2=CO_2^-$, 16-epipanarine	(40)
	$R_1=CO_2CH_3$, $R_2=CH_2OH$ macusine A	(40)
	$R_1=CH_2OH$, $R_2=CO_2CH_3$, <i>N</i> _b -methylakuammidine	(40)
	$R=H$, $R'=H$, spegatrine	(40)
	$R=H$, $R'=Me$, lochneram	(40)
	$R=Me$, $R'=H$, <i>N</i> _a -methylsarpagine metho salt	(40)
	$R_1=CH_3$, $R_2=H$, <i>N</i> _a -methyl-11-hydroxymacusine A	(40)
	$R_1=H$, $R_2=CH_3$, 11-methoxymacusine A	(40)

Table 4. Sargine Indole Alkaloids (8)

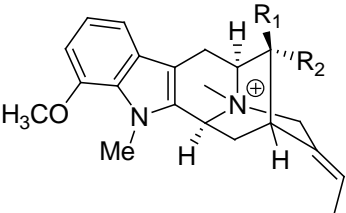
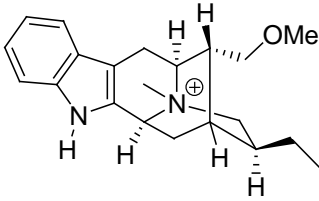
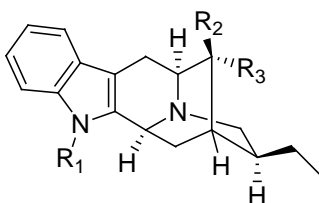
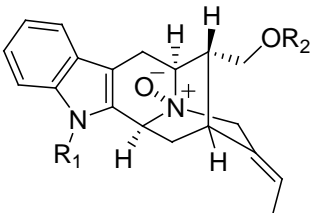
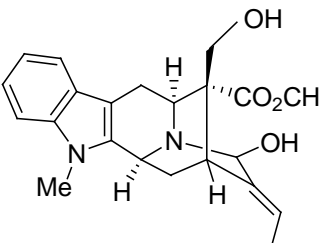
Structure	Alkaloids	Refs.
	$R_1=H$, $R_2=CO_2Et$, fuchsiaefoline (40)	(40)
	$R_1=CH_2OH$, $R_2=CO_2Me$, 12-methoxy- <i>N_b</i> -methylvoachalotine (40)	(40)
	$R_1=CH_2OH$, $R_2=CO_2Et$ 12-methoxy- <i>N_b</i> -methylvoachalotine ethyl ester (40)	(40)
	19,20-dihydro-O-methylmacusine B (40)	(40)
	$R_1=H$, $R_2=CO_2CH_3$, $R_3=CH_2OH$, 19,20-dihydroakuammidine (40)	(40)
	$R_1=H$, $R_2=CH_2OH$, $R_3=CO_2CH_3$, 19,20-dihydropolynuridine (40)	(40)
	$R_1=CH_3$, $R_2=CH_2OAc$, $R_3=CO_2CH_3$, 17-O-acetyl-19,20-dihydrovoachalotine (40)	(40)
	$R_1=CH_3$, $R_2=H$, affinisine <i>N_b</i> -oxide (40)	(40)
	$R_1=H$, $R_2=CH_3$, O-methylnormacusine B <i>N_b</i> -oxide (40)	(40)
	21-hydroxyvoachalotine (40)	(40)

Table 4. Sarpagine Indole Alkaloids (9)⁷⁴⁻⁷⁸

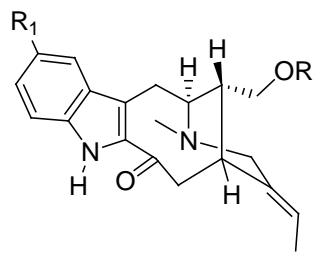
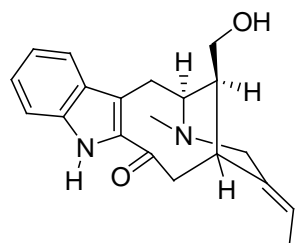
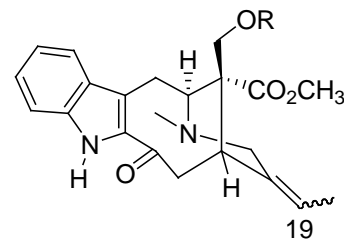
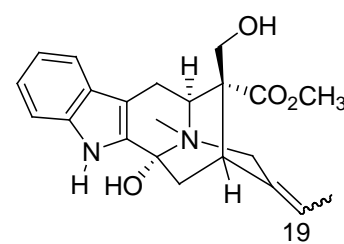
Structure	Alkaloid	Refs.
	<p>R = R₁ = H, 16-epiaffinine (75)</p> <p>R = Me, R₁ = H, hystrixnine (76)</p> <p>R = H, R₁ = OMe, pelirine (77)</p>	
	affinine	(78)
	<p>R = H, 19<i>E</i>, gelsempervine-A (79)</p> <p>R = Ac, 19<i>E</i>, gelsempervine-B (79)</p> <p>R = H, 19<i>Z</i>, gelsempervine-C (79)</p> <p>R = Ac, 19<i>Z</i>, gelsempervine-D (79)</p>	
	<p>19<i>Z</i>, 19<i>Z</i>-16-epivoacarpine (79)</p> <p>19<i>ZE</i>, 19<i>E</i>-16-epivoacarpine (79)</p>	

Table 4. Sarpagine Indole Alkaloids (10)^{71,79-82}

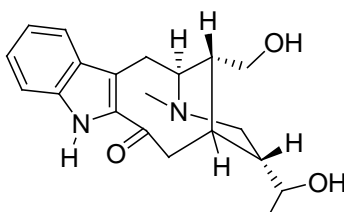
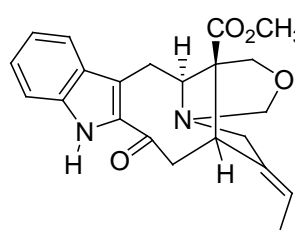
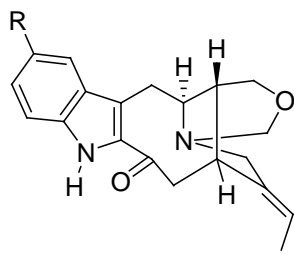
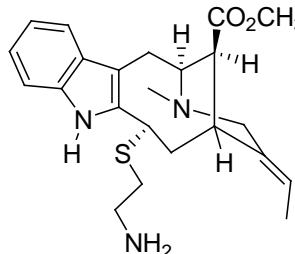
Structure	Alkaloid	Refs.
	erichsonine	(80)
	pagicerine	(81)
	R =H, amerovolficine R =OMe, 10-methoxy-16-de(methoxycarbonyl) pagicerine	(72) (82)
	pagisulfine	(83)

Table 5. Macroline Related Indole Alkaloids (1) ⁸³⁻⁸⁷

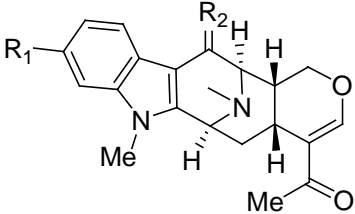
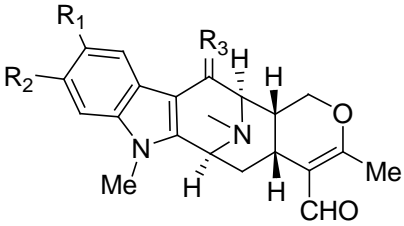
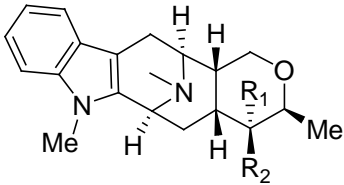
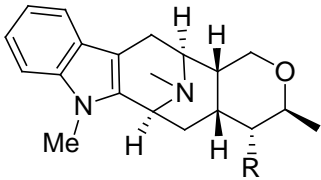
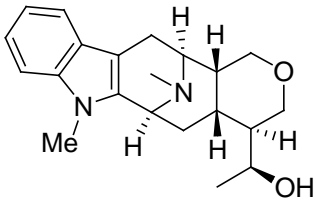
Structure	Alkaloid	Refs.
	R ₁ = R ₂ = H ₂ , alstonerine	(84)
	R ₁ = OMe, R ₂ = H ₂ , alstophylline	(85)
	R ₁ = OMe, R ₂ = O, 6-oxoalstophylline	(85)
	R ₁ = OMe, R ₂ = H, R ₃ = H ₂ , 19,20-dehydro,10-methoxytalcarpine	(27)
	R ₁ = H, R ₂ = OMe, R ₃ = H ₂ , alstophyllal	(85)
	R ₁ = H, R ₂ = OMe, R ₃ = O, 6-oxo-alstophyllal	(85)
	R ₁ = H, R ₂ = H, R ₃ = H ₂ , alstonerinal	(85, 88)
	R ₁ = H, R ₂ = CHO, talcarpine	(85, 86)
	R ₁ = H, R ₂ = CH ₂ OH, macrocarpine A	(85, 86)
	R ₁ = OH, R ₂ = CH ₂ OH, alstohentine	(85)
	R = CHO, secotalcarpine	(86)
	R = CH ₂ OH, macrocarpine B	(85, 86)
	R = CH ₂ OAc, macrocarpine C	(86)
	alstomacroine	(87)

Table 5. Macroline Related Indole Alkaloids (2)⁸⁸

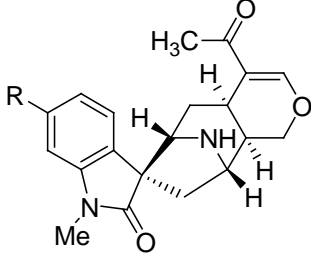
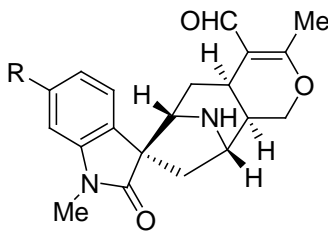
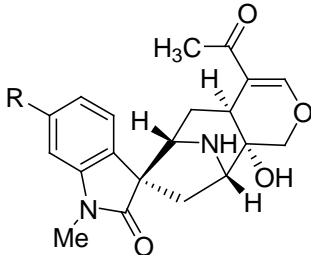
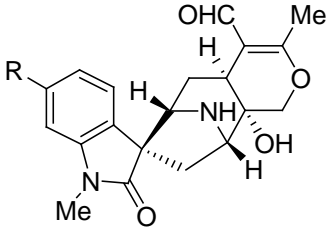
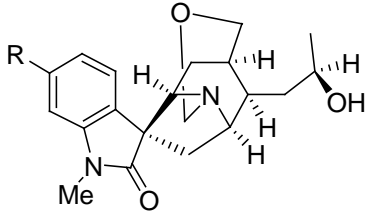
Structure	Alkaloid	Refs.
	R=H, alstonisine R=OCH ₃ , <i>N_b</i> -demethylalstophylline oxindole	(89)
	R ₁ =H, alstonal R ₁ =OCH ₃ , <i>N_b</i> -demethylalstophyllal oxindole	(89)
	R=H, 16-hydroxyalstonisine R=OCH ₃ , 16-hydroxy- <i>N_b</i> -demethyl alstophylline oxindole	(89) (89)
	R ₁ =H, 16-hydroxyalstonal R ₁ =OCH ₃ , 16-hydroxy- <i>N_b</i> -demethyl alstophyllal oxindole	(89) (89)
	macroxine	(89)

Table 5. Macroline Related Indole Alkaloids (3)⁸⁹

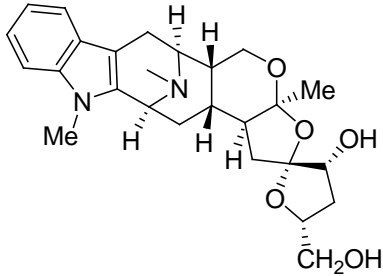
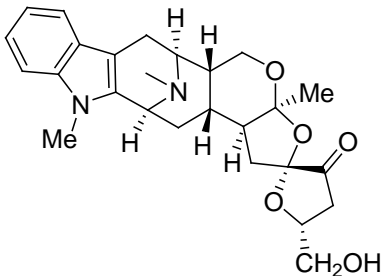
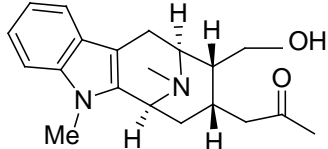
Structure	Alkaloids	Refs.
 <p>The structure of macrodasine A is a complex polycyclic alkaloid. It features an indole ring system fused to a piperidine ring, which is further fused to a hexahydroindole ring. A methyl group is attached to the nitrogen of the indole ring. The hexahydroindole ring is substituted with a methoxy group and a hydroxyl group. A side chain containing a furanose ring is attached to the hexahydroindole ring, with a hydroxyl group and a hydroxymethyl group (-CH₂OH) attached to the furanose ring.</p>	macrodasine A	(86, 90)
 <p>The structure of macrodasine B is similar to macrodasine A, but the furanose ring in the side chain is in a different conformation, and the hydroxyl group is positioned differently. It also features the indole-piperidine-hexahydroindole core and the methyl group on the indole nitrogen.</p>	macrodasine B	(86)
 <p>The structure of alstomicine is a simpler polycyclic alkaloid. It consists of an indole ring fused to a piperidine ring, which is further fused to a hexahydroindole ring. A methyl group is attached to the nitrogen of the indole ring. The hexahydroindole ring is substituted with a hydroxyl group and an acetyl group (-C(=O)CH₃).</p>	alstomicine	(85)

Table 6. Bisindole Alkaloids (1)

Structure	Alkaloid	Refs.
	<p>R =H, N'-demethylaccedinisine (40)</p> <p>R =CH₃, accedinisine (40)</p>	
	<p>R =H, desformoundulatine (40)</p> <p>R =CH₂OH, undulatine (40)</p>	
	macralstonidine	(40)

Table 6. Bisindole alkaloids (2)^{90,91}

Structure	Alkaloid	Refs.
	vobatraine	(91)
	vobasonidine	(91)
	macrospegatine	(92)

Table 6. Bisindole Alkaloids (3)⁹²⁻⁹⁴

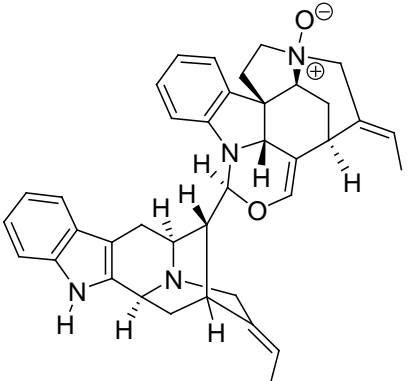
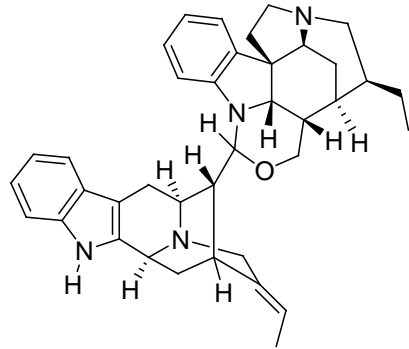
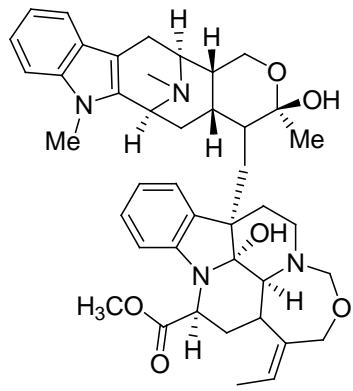
Structure	Alkaloid	Refs.
	divaricine	(93)
	geissolosimine	(40, 94)
	alstolactazine	(95)

Table 6. Bisindole Alkaloids (4)

Structure	Alkaloid	Refs.
	alstonisine	(14)
	alstomacroline	(51)
	R=H, macralstonine	(23,24)
	R=Ac, O-acetate macralstonine	(26)

Table 6. Bisindole Alkaloids (5)⁹⁵

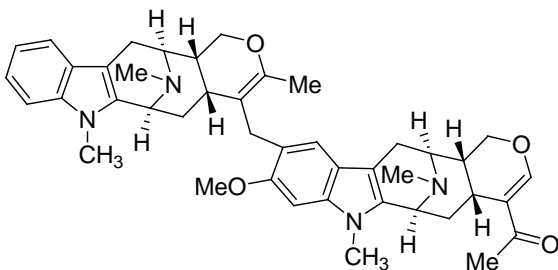
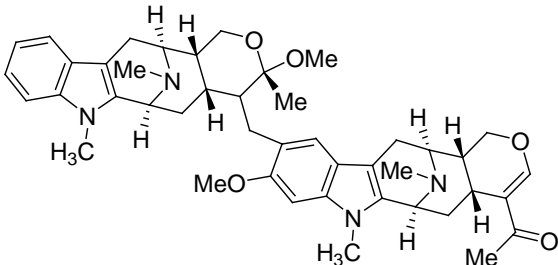
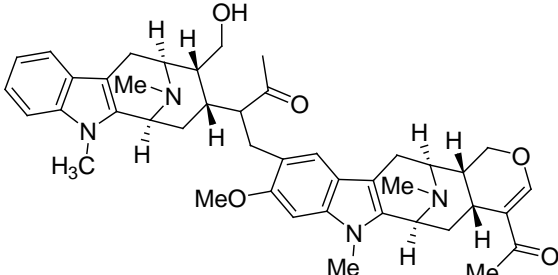
Structure	Alkaloid	Refs.
 <p data-bbox="370 743 686 772">(proposed structure by Lazar)</p>	anhydromacralstonine	(96)
	alstomacrophylline	(51)
	perhentinine	(86)

Table 6. Bisindole Alkaloids (6)

Structure	Alkaloid	Refs.
	R =H, villalstonine	(26, 27)
	R =H, <i>N</i> _b -O, villalstonine <i>N</i> _b -oxide	(28)
	R =OMe, 10-methoxy villalstonine	(26, 27)
	R =OMe, <i>N</i> _b -O, 10-methoxy villalstonine <i>N</i> _b -oxide	(26, 27)
	R =H, macrocarpamine	(25)
	R =OMe, 10-methoxy macrocarpamine	(25)
	R =OMe, <i>N</i> _b -O, 10-methoxy macrocarpamine <i>N</i> _b -oxide	(25)

Table 6. Bisindole Alkaloids (7)

Structure	Alkaloid	Refs.
	foliacraline	(27)
	alstocraline	(27)
	angusticaline	(27)

Table 6. Bisindole Alkaloids (8)^{96,97}

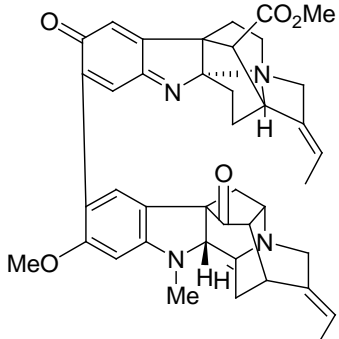
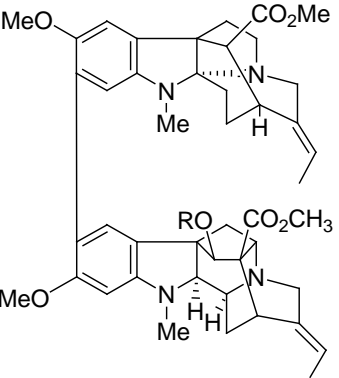
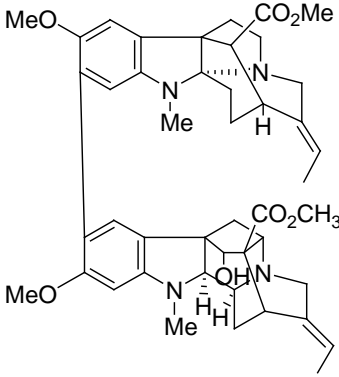
Structure	Alkaloid	Refs.
	flexicorine	(97)
	R = H, 11-methoxy-10-(11'-vincorinyl)-vincamajine R = Ac, 11-methoxy-10-(11'-vincorinyl)-vincamedine	(98)
	11-methoxy-10-(11'-vincorinyl)-17-epivincamajine	(98)

Table 6. Bisindole Alkaloids (9)^{98,99}

Structure	Alkaloid	Refs.
	11-methoxy-10-[11'(10'-methoxy-cathafoliny)]vincamajine	(99)
	pandicine	(100)
	dispegatrine	(40)

Table 7. Degradation Products of *Alstonia* Alkaloids¹⁰⁰

Structure	Alkaloid	Refs.
	R =H, villamine R =Ac, O-acetylvillamine	(36, 37) (36, 37)
	R =H, macroline R =Ac, O-acetylmacroline	(36, 37) (36, 37)
	anhydromacrosalpine-methine	(101)
	<i>N</i> _a -desmethylalstophylline	(101)

1.2. Previous approaches to the tetracyclic azabicyclo [3.3.1] nonane core framework 5 of the sarpagine/macroline related indole alkaloids

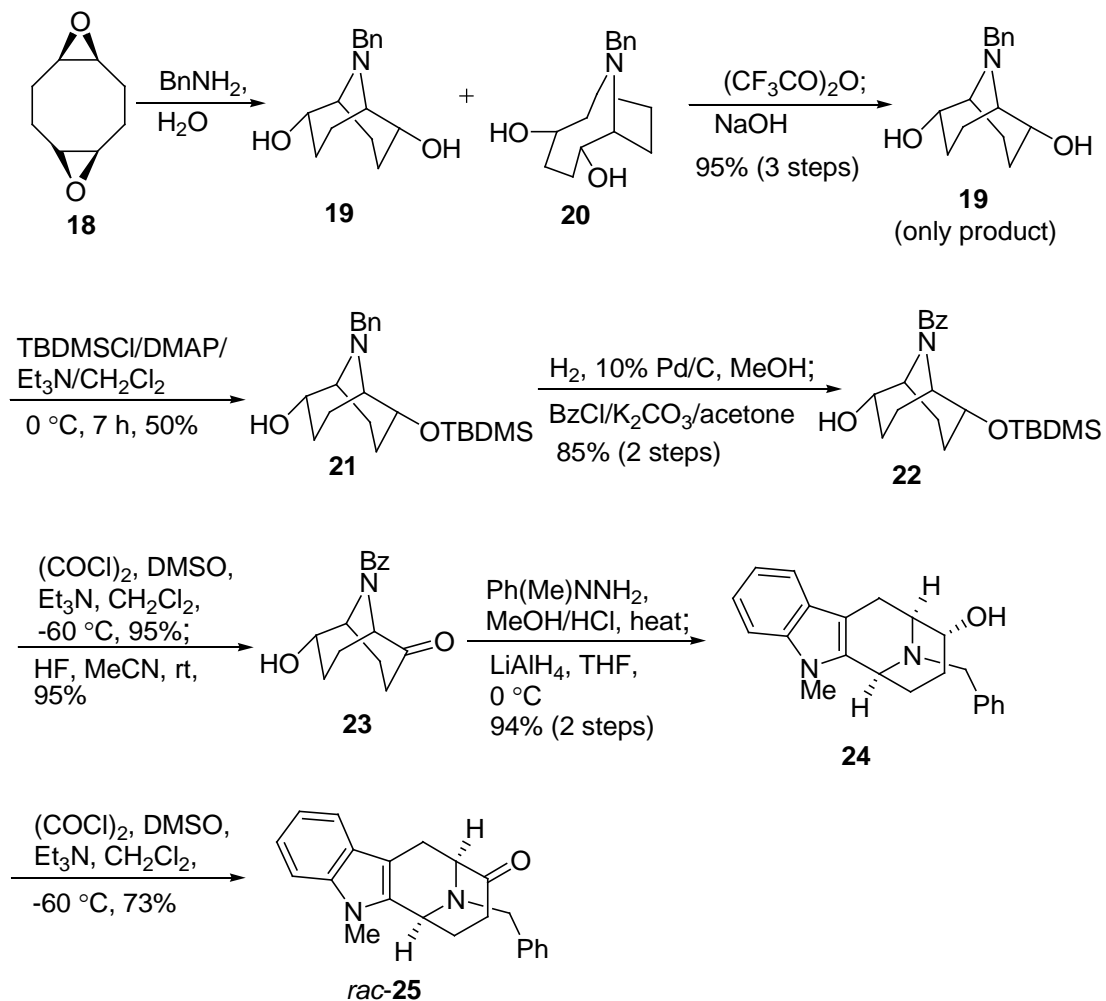
As illustrated in Figure 3, as well as Tables 4, 5, and 7, a core tetracyclic system (rings A, B, C and D) appears to be a common structural feature of the macroline related sarpagine and ajmaline alkaloids. A general approach to the synthesis of these macroline-related alkaloids should involve enantiospecific synthesis of this core structure with the correct configurations at stereocenters C-3, and C-5 and the appropriate functional groups at C-15/C-16 for further transformations. The racemic azabicyclo [3.3.1] nonane has been prepared in the late 1970's by Yoneda,¹⁰¹ Mashimo,¹⁰² Kluge¹⁰³ and Hobson,¹⁰⁴ and was later improved by Soerens¹⁰⁵ on a kilogram scale. In 1988, Zhang et al.¹⁰⁶ achieved the synthesis of the optically active tetracyclic ketone **25** in a stereospecific fashion by employing the asymmetric Pictet-Spengler reaction. Many improvements have been made to prepare both the N_a -H and the N_a -CH₃ tetracyclic ketones. Other recent routes toward the formation of the tetracyclic core, which deserve mention, include the racemic synthesis by Rassat,^{107,108} the aza Diels-Alder approach by Kuethe,¹⁰⁹ the olefin metathesis process of Martin¹¹⁰ and the *cis*-Pictet-Spengler approach by Bailey¹¹¹ and Magnus.¹¹²

1.2.1. A racemic synthesis by Rassat et al.^{59, 60}

In 2000, Rassat et al.^{107, 108} designed the synthesis of 2,6-dihydroxy-9-azabicyclo[3.3.1]-nonane **25** from the bis epoxide **18** (Scheme 1), which could be carried out on large scale. The bis epoxide **18** was easily converted into a 1:1 mixture of regioisomeric diols **19** and **20** via transannular cyclization with benzylamine in refluxing water. The undesired diol **20** was then converted into **19** by reacting it with trifluoroacetic anhydride

in refluxing dichloromethane, followed by hydrolysis with sodium hydroxide to furnish **19** in 95% yield (from **18**). This bicyclic nonane **19**, was then converted into **25**, as illustrated in Scheme 1.

Scheme 1

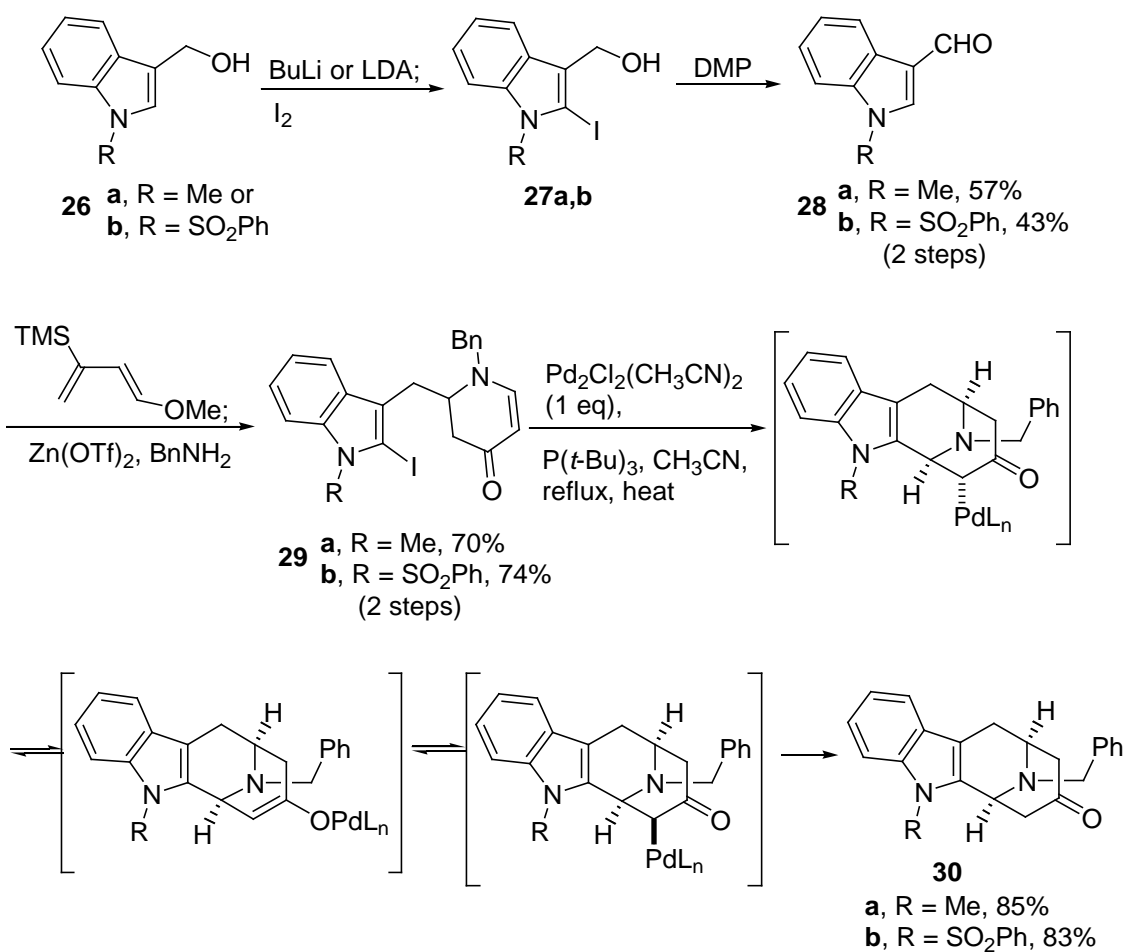


Monoprotection of the diol **19** with *tert*-butyldimethylsilyl chloride, followed by replacement of the *N*-benzyl group with the *N*-benzoyl group gave the desired monol **22**. Swern oxidation of the alcohol **22**, followed by removed of the silyl group gave **23** in 95% yield (2 steps). Fischer indole cyclization of **23** with *N*-methyl, *N*-phenylhydrazine

in refluxing methanolic HCl led to the indole, which on reduction with LiAlH_4 provided the N_b -benzyl derivative **24**. The racemic tetracyclic ketone **25** could then be obtained by Swern oxidation of **24** in 73% yield.

1.2.2. Approach to the core tetracyclic structure via the aza-Diels Alder/intramolecular Heck cyclization by Kuethe et al.⁶¹

Scheme 2

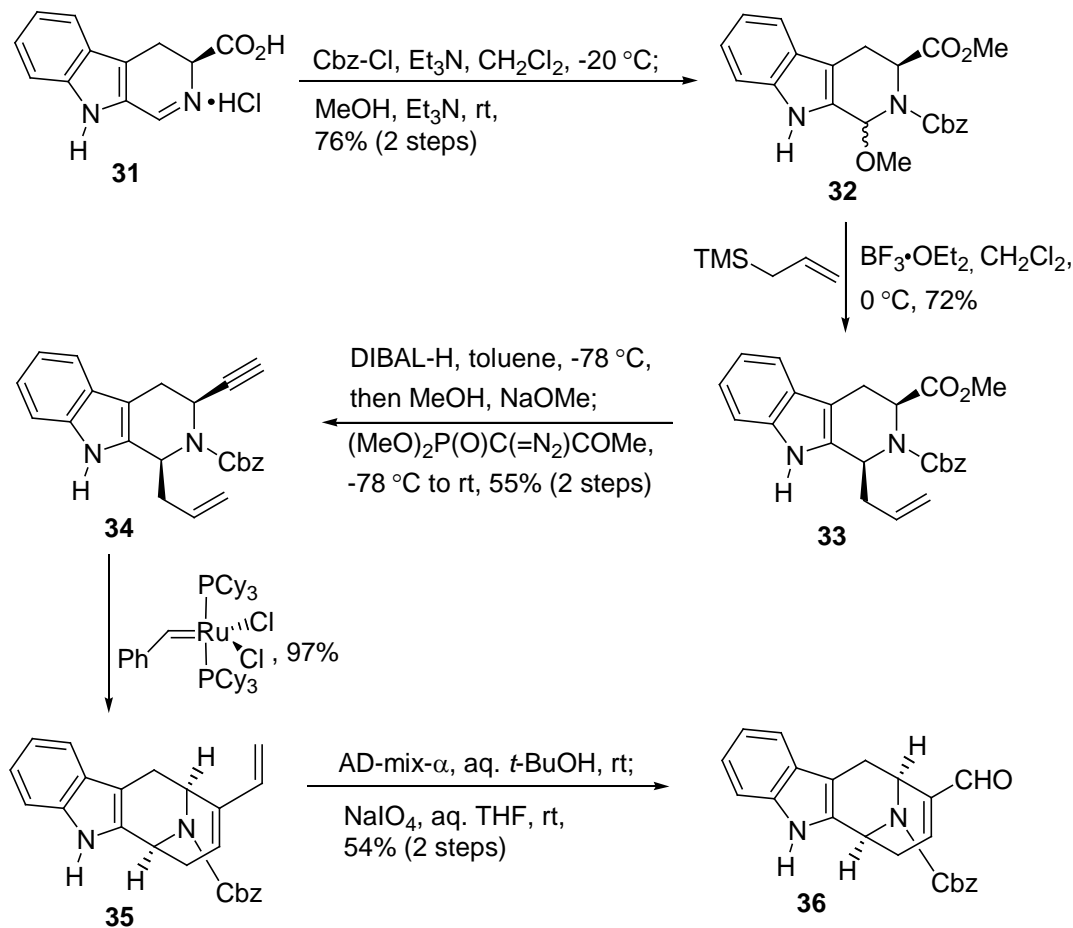


Keuthe and co-workers adopted a [4+2] annulation strategy for construction of the tetracyclic cores **30a,b**. As illustrated in Scheme 2, indoles **26a,b** on treatment with *n*-BuLi or LDA in refluxing MTBE, followed by addition of iodine furnished the iodo compounds **27a,b** individually. Dess-Martin oxidation of the primary alcohol provided the aldehydes **28a,b**. The aza-Diels Alder reaction of **28a,b** with the Danishefsky diene provided **29a,b**, which was subjected to an intramolecular Heck cyclization to furnish the desired cyclized indole scaffolds in both series **30a,b**. Although this route requires stoichiometric amounts of palladium in the Heck coupling reaction, it does provide the tetracyclic framework in five steps, albeit the carbonyl group is not in an ideal position for regiospecific transformations.

1.2.3. Approach to the core structure **36** via a ring-closing olefin metathesis by Martin et al.¹¹⁰

During their extensive study on the use of olefin metathesis reactions for the synthesis of various azabicyclo structures with the nitrogen in the one-atom bridge, Martin et al.¹¹⁰ were able to construct the tetracyclic core (ABCD rings), necessary for the synthesis of the macroline/sarpagine alkaloids. As illustrated in Scheme 3, the dihydro- β -carboline **31** (obtained from L-tryptophan) was N-protected with Cbz-Cl, followed by esterification to provide a diastereomeric mixture of amins **32**. This diastereomeric mixture of amins **32** was then treated with allyltrimethylsilane and boron-trifluoride etherate to afford the *cis*-tetrahydro- β -carboline **33** as a mixture of two compounds in a 5.5:1 diastereomeric ratio which must be separated. Selective reduction of the ester, followed by a Wittig reaction yielded the alkyne **34** in a one-pot procedure. Treatment of the alkyne **34** with

Scheme 3



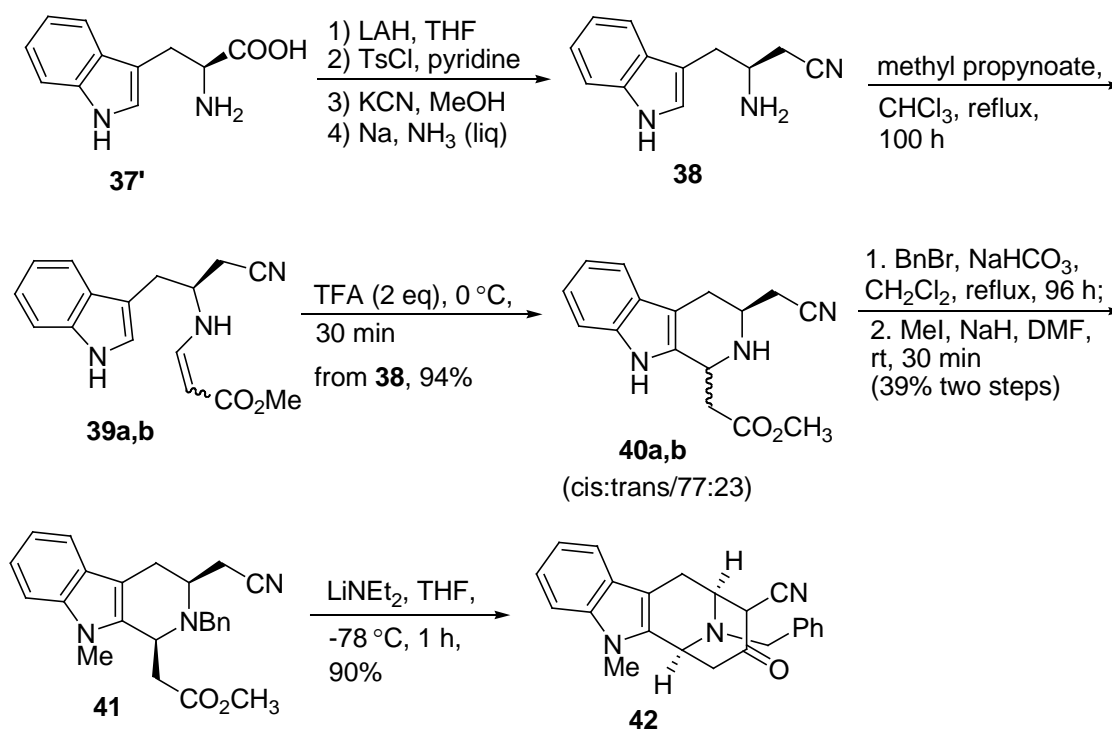
Grubb's first generation catalyst promoted the enyne metathesis to furnish the tetracyclic diene **35** in essentially quantitative yield. Selective oxidation of the exocyclic olefin provided the aldehyde **36** in 54% yield (two steps).

1.2.4. Synthesis of the tetracyclic core **42** via the *cis*-selective Pictet-Spengler reaction by Bailey et al.¹¹¹

Bailey employed the *cis*-selective Pictet-Spengler reaction to synthesize the tetracyclic intermediate **42**. As illustrated in Scheme 4, the synthesis began with L-(-)-tryptophan **37'** which was converted into the homologated nitrile **38** via the reduction/

activation/replacement sequence in 50% overall yield. The homologated nitrile **38** was then treated with methyl propynoate in refluxing chloroform for 100 hours to afford the enamines **39a** and **39b**, after which the mixture was directly added to excess trifluoroacetic acid at 0 °C to provide a mixture of *cis* and *trans* diastereomers (**40a** and **40b**) in the ratio of 77:23. The diastereomeric mixture was then converted into the *N*_b-benzyl compound, which was further methylated to provide **41** in 39% yield (2 steps). The ring closure was mediated by the action of lithium diethylamide at -78 °C on ester **41** to afford the tetracyclic core in **42** in 90% yield. Although the tetracyclic ketone **42** can be synthesized by this method, this route suffers due to the number of steps involved in comparison to other routes and also from the poor diastereoselectivity obtained in the Pictet-Spengler reaction.

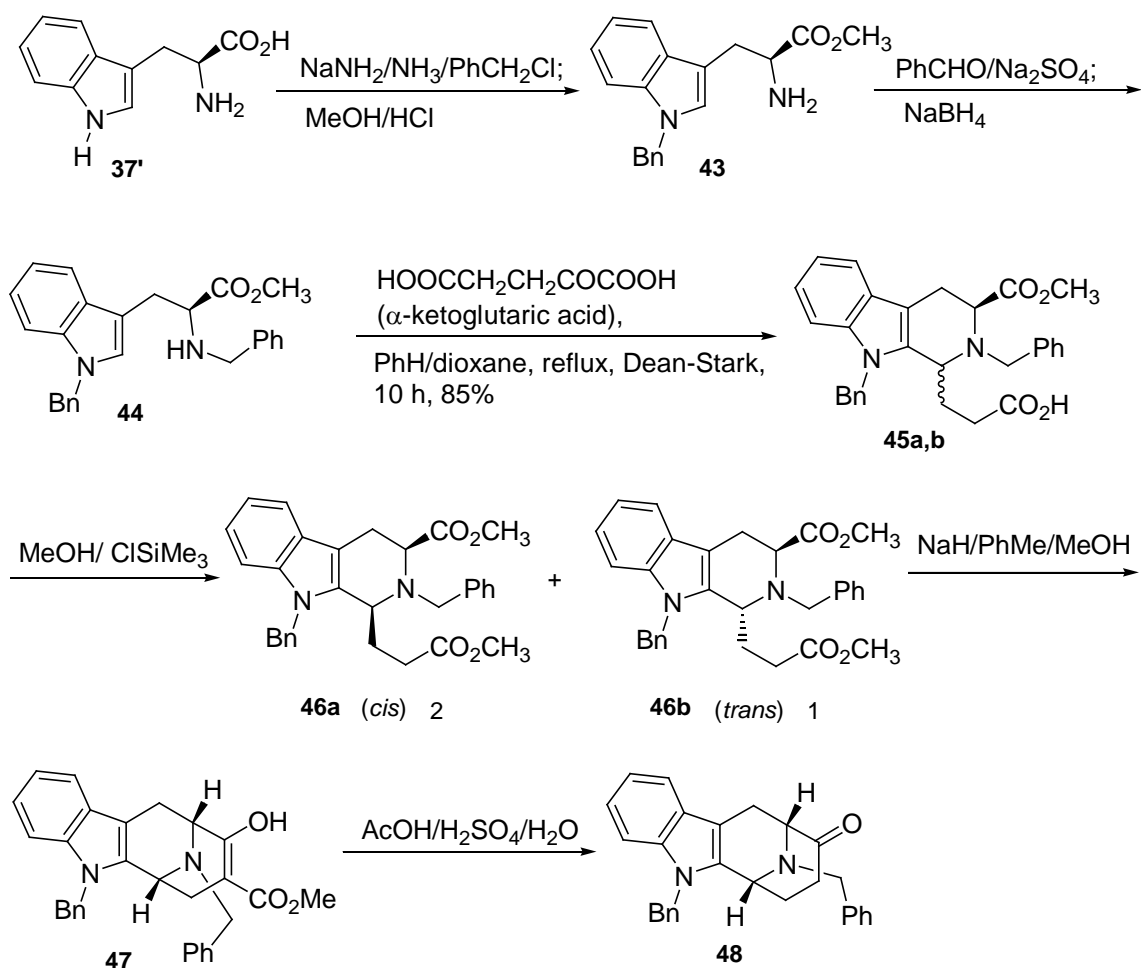
Scheme 4



1.2.5. Synthesis of the tetracyclic core **48** by Magnus et al.⁶⁴

In 1989, Magnus et al.⁶⁴ reported the synthesis of the N_a -H tetracyclic ketone **49** from L-(-)-tryptophan **37'** which he employed for the total synthesis of (+)-koumine, (+)-taberpsychine and (+)-koumidine. Illustrated in Scheme 5 is the *cis*-selective Pictet-Spengler reaction, which began with L-(-)-tryptophan **37'**.

Scheme 5



The L-(-)-tryptophan **37'** was converted into the N_a -benzyl, tryptophan methyl ester **43** by first benzylation with sodium amide/ PhCH_2Cl in 92% yield, followed by Fischer esterification of the alkylated L-(+)-tryptophan in 68% yield. This ester **43** was then

reacted with benzaldehyde at 22 °C and the imine which resulted was reduced with sodium borohydride in methanol to provide *N*_a-benzyl, *N*_b-benzyl tryptophan methyl ester **44** in 95% yield. This intermediate was then converted into a mixture of diastereomeric acids **45a/45b**, by employing the conditions of the Pictet-Spengler reaction as developed by Zhang et al.¹⁰⁶ Esterification of this mixture with MeOH/CISiMe₃ provided the esters **46a/46b** (2:1) in 80% yield. The major *cis*-diastereomer **46a** was isolated in 58% yield by crystallization from methanol and carried through to the tetracyclic ketone **48** via a Dieckmann cyclization and acid-mediated decarboxylation, as illustrated in Scheme 5 following the route developed in Milwaukee and reported in the racemic series by Yoneda et al.¹⁰¹

1.3. Previous syntheses of sarpagine/macroline related indole alkaloids

1.3.1. Synthesis of sarpagine/macroline related indole alkaloids in Milwaukee¹¹³

Vellosimine **14a** and normacusine B are the simplest representatives of the family of sarpagine indole alkaloids. Until 2000, no enantiospecific total synthesis of members of the sarpagine series was reported. The partial total synthesis of (-)-koumidine [which is similar in structure to **14a**, except it has a more stable *Z*-ethylidene double bond and the *S* configuration at C-16], was first reported by Sakai.¹¹⁴ Magnus later synthesized the enantiomer of (-)-koumidine via a Pictet-Spengler reaction. However, establishment of the double bond (*Z*:*E*=1:5.7) was not stereospecific¹¹² and the reaction was hampered by poor diastereoselectivity in the Pictet-Spengler reaction. Entry into the pentacyclic sarpagine skeleton in Milwaukee for the total synthesis of ajmaline previously, was through a macroline framework which did not have the potential for incorporation of the

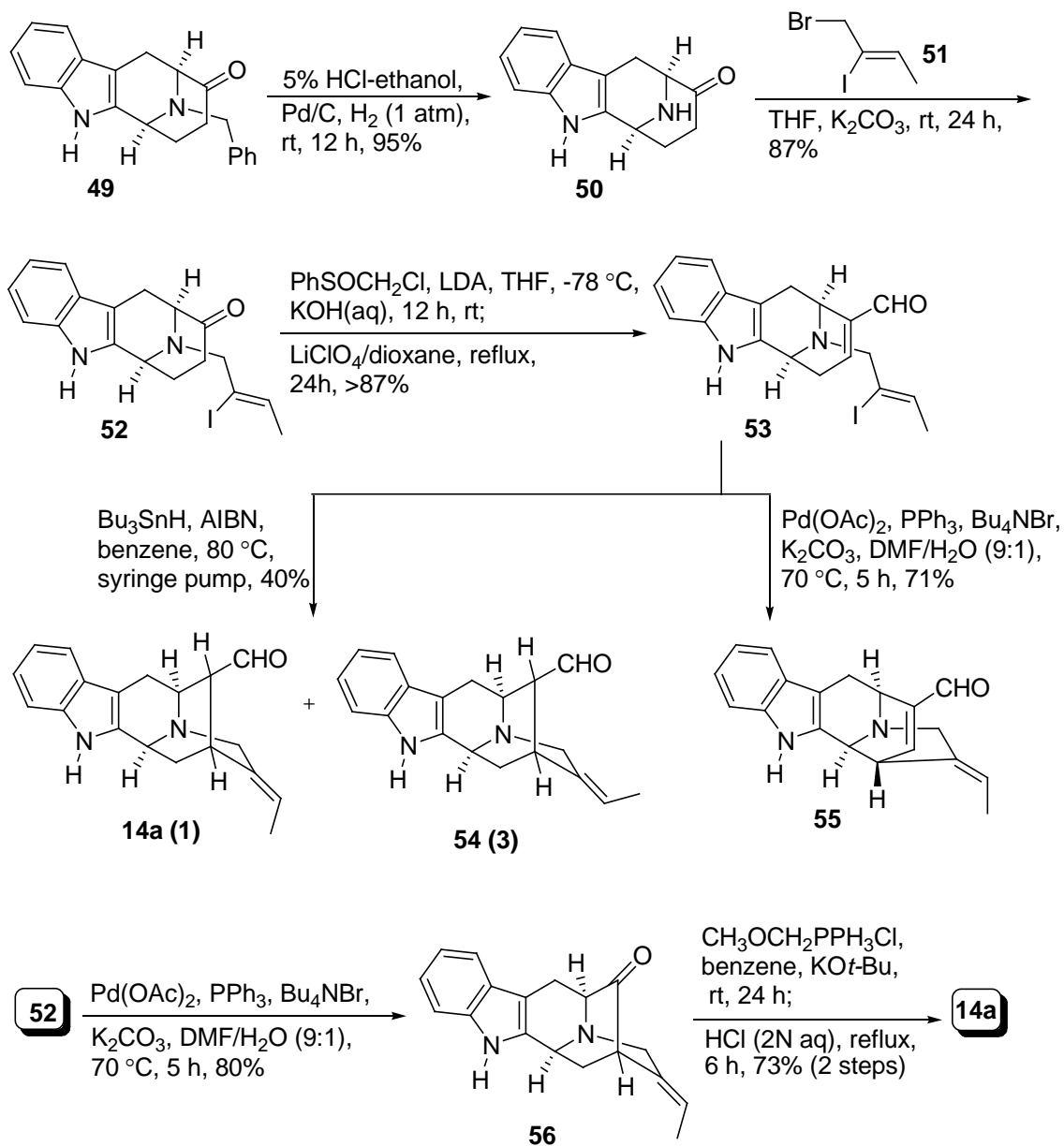
E-ethylidene double bond stereospecifically and also involved a large number of steps. Martin reported the total synthesis of geissoschizine with stereoselective establishment of the *E*-ethylidene double bond by an elimination process.¹¹⁵ Furthermore Rawal¹¹⁶ and Bosch¹¹⁷ reported the total synthesis of Strychnos alkaloids with stereocontrolled establishment of the double bond by a Heck coupling reaction.

1.3.1.1. The enantiospecific total synthesis of (+)-vellosimine by Wang^{10,118,119}

In 2000 Wang reported an efficient, enantiospecific total synthesis of (+)-vellosimine **14a** with the first stereospecific establishment of the ethylidene double bond by a key palladium (enolate-mediated) carbon-carbon bond forming process. This key reaction provided a very efficient approach and allowed a direct entry to the basic pentacyclic skeleton of the sarpagine alkaloid system, and permitted introduction of the C-19—C-20 olefinic bond with the *E* configuration, stereospecifically. The synthesis began with the tetracyclic ketone **49**, which was subjected to the conditions of catalytic hydrogenation to provide the *N*_a-H, *N*_b-H tetracyclic ketone **50** in 95% yield. Alkylation of the secondary amine in **50** with *Z*-1-bromo-2-iodo-2-butene **51**, a unit prepared by Ensley et al.¹²⁰ and employed by Rawal,¹¹⁶ Bosch¹¹⁷ and Kuehne¹²¹ provided the *N*_b-*Z*-2'-iodo-2'-butenyl tetracyclic ketone **52** in 87% yield. This *Z*-olefin **51** can now be prepared on a 500 gram scale in a regiospecific fashion in three steps from crotonaldehyde.¹²² Ketone **52** was then converted into the α , β -unsaturated aldehyde **53** in high yield (see Scheme 6).

Numerous attempts to effect the intramolecular Michael addition in α , β -unsaturated aldehyde **53** by generating a vinyl anion, followed by cyclization failed to give the desired product.^{10,119} Radical-mediated cyclization¹²¹ was then attempted on **53** by

Scheme 6



treating it with $Bu_3SnH/AIBN$ in refluxing benzene. A mixture of (+)-vellosimine **14a**, accompanied by the undesired *Z*-olefinic isomer **54** in a 1:3 (*E/Z*) ratio was obtained in 40% overall yield. The olefinic bond had isomerized under the radical conditions to provide the thermodynamically more stable olefin as the major isomer.¹⁰ Attempts to

carry out the Heck reaction under the conditions developed by Rawal,¹²³ as well as under modified conditions did not provide the desired *E*-olefin.

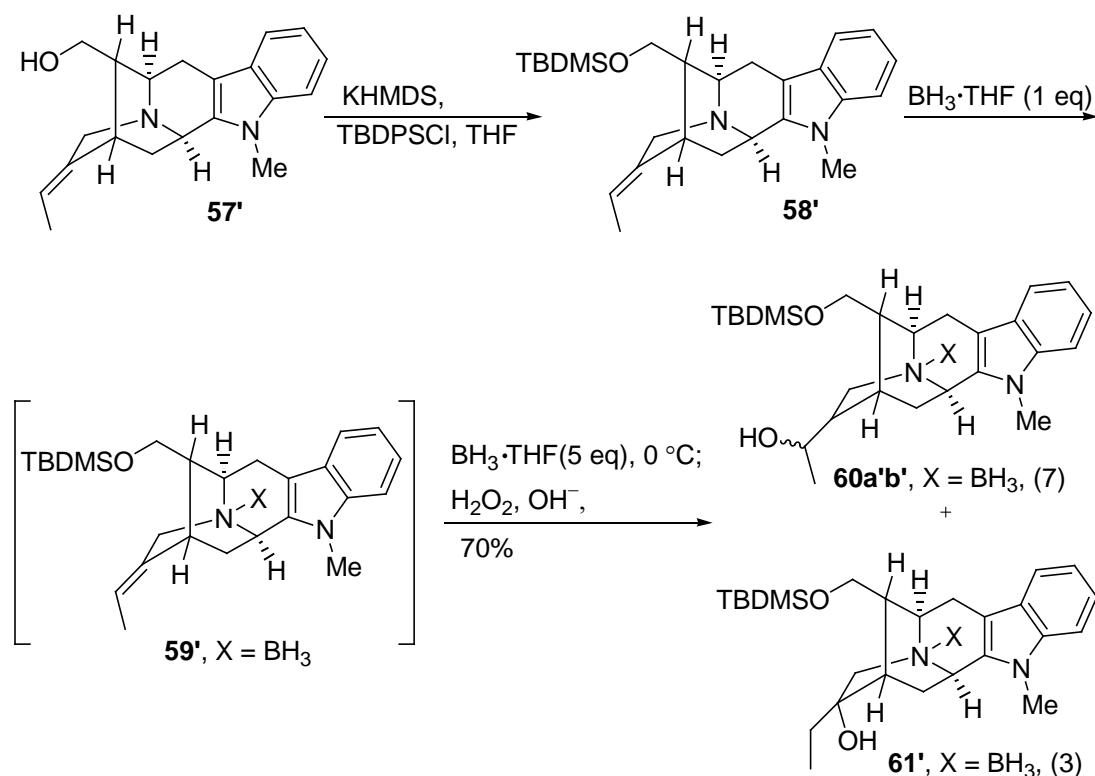
Muratake and Natsume¹²⁴ had reported a direct palladium-mediated arylation at the γ -position of a simple α , β -unsaturated aldehyde under basic conditions in high yield. When the α , β -unsaturated aldehyde **53** was stirred under similar conditions, the C-14 insertion product (aldehyde **55**) was isolated in 71% yield. With the formation of this product it was felt a similar mechanism could be envisaged to occur with iodo olefin **52**. The relative acidity inherent at the α -position of the ketone in **52** would facilitate the enolate mediated Pd(0)-cyclization into the desired sarpagine system in **14a**. When iodo olefin **52** was subjected to the optimized conditions of the intramolecular palladium-mediated cross coupling reaction (3 mol% Pd(OAc)₂, 30 mol% PPh₃),¹⁰ it furnished the cyclized product **56** stereospecifically in 80% yield. Wittig reaction of this ketone was followed by hydrolysis to provide the thermodynamically more stable α -aldehyde in **14a**. Consequently, the first total synthesis of the *N*_a-H substituted sarpagine indole alkaloid (+)-vellosimine **14a** was accomplished from commercially available D-(+)-tryptophan methyl ester **107** (Scheme 16) in seven reaction vessels in 27% overall yield. With the success achieved in stereospecific construction of the sarpagine skeleton via the enolate mediated palladium cross coupling reaction, a similar strategy was employed for the synthesis of the related sarpagine alkaloids in the *N*_a-H as well as *N*_a-methyl series.¹¹³

1.3.1.2. Total synthesis of the enantiomer of macroline, the *N*_a-H analog of macroline and trinervine via a regiospecific hydroboration process by Liu et al.¹²⁵⁻¹²⁷

From the earlier work of LeQuesne et al.,³⁸ the biogenetic origin of macroline **6** could be envisaged to arise from affinisine (enantiomer of **57'**, see Scheme 7) via a retro Michael

reaction (Figure 4). Consequently, the total synthesis of the enantiomer of macroline **6'** was designed based on this approach. Shortly after the synthesis of (+)-vellosimine **14a**, Liu¹²⁵⁻¹²⁷ followed the same strategy (from L-tryptophan **37'**) to provide the enantiomer of affinisine **57'**.

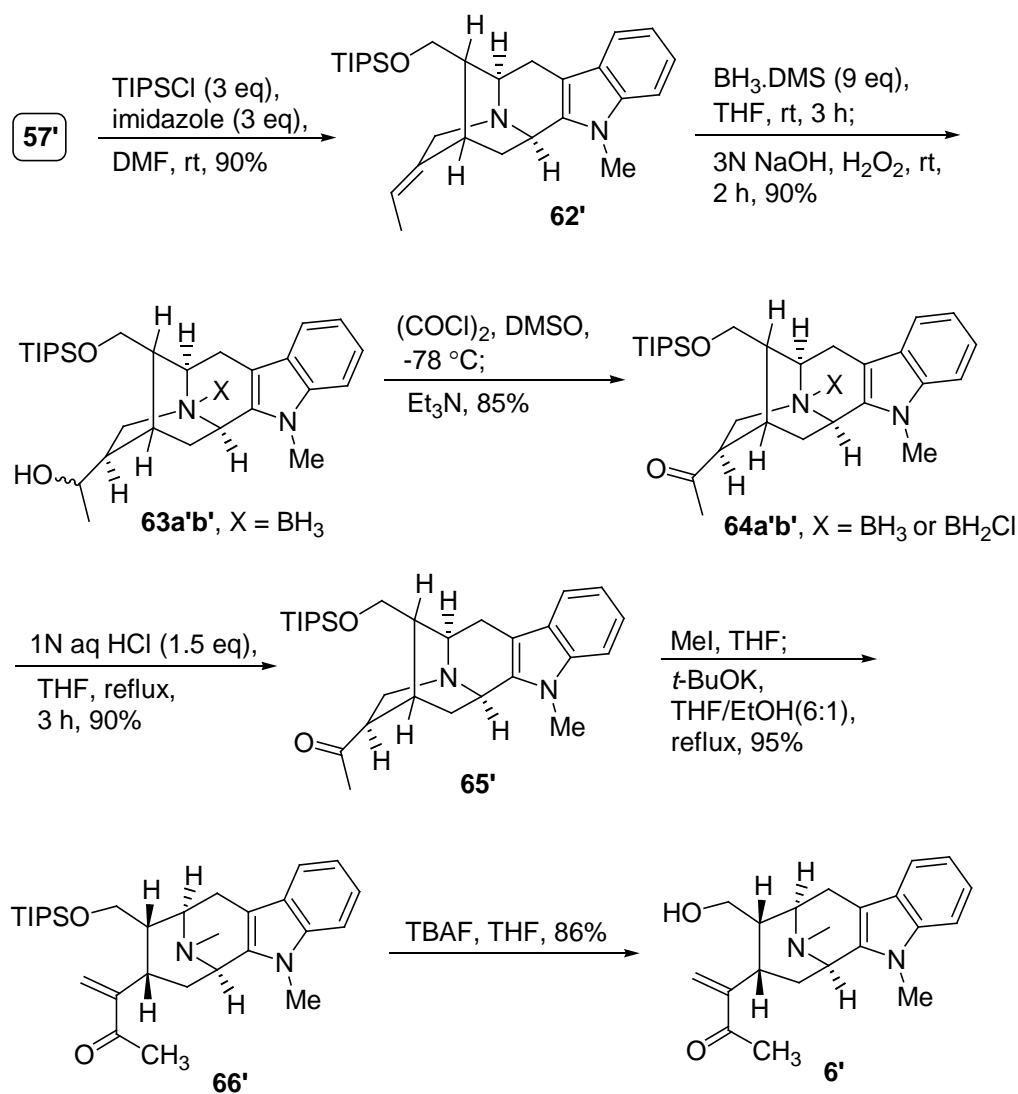
Scheme 7



The hydroxyl group of the enantiomer of affinisine **57'** was protected as the *t*-butyldimethylsilyl ether to afford olefin **58'** (Scheme 7). Hydroboration of olefin **58'** with 1 equivalent of $\text{BH}_3 \cdot \text{THF}$ at 0°C resulted in the formation of the N_b - BH_3 complex **59'**. Further addition of 5 equivalents of $\text{BH}_3 \cdot \text{THF}$ at 0°C afforded a mixture of the secondary alcohols **60a',b'** and undesired tertiary alcohol **61'** in a ratio of 7:3.¹²⁵ The poor yield (49% of the desired secondary alcohols **60a',b'**), as well as the formation of the undesired

tertiary alcohol **61'** prompted a more detailed study of this process (see Scheme 8). After executing various reaction conditions,¹²⁷ which involved the use of hindered boranes and

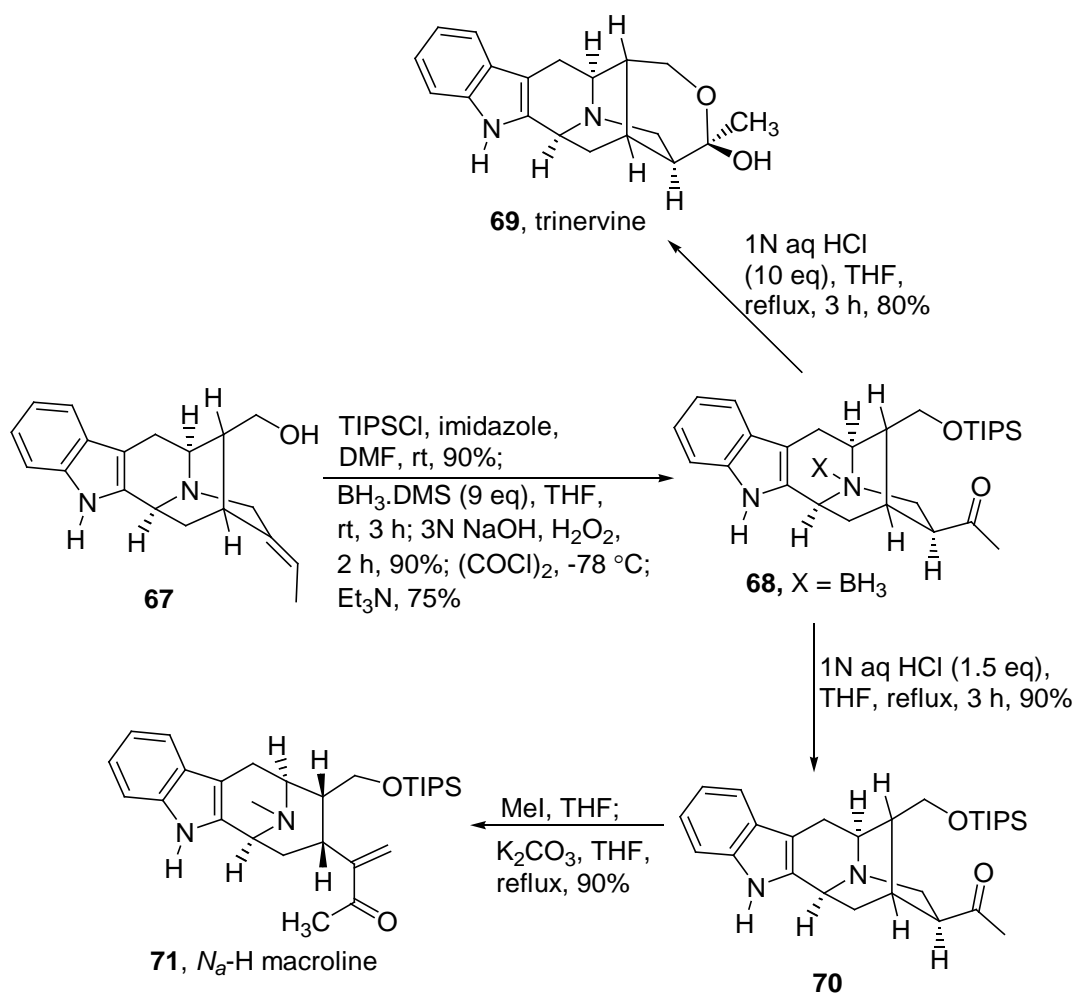
Scheme 8



a change of the reaction temperature as well as the use of a bulkier TIPS protecting group, the desired secondary alcohols could be prepared (the TIPS group was employed because it was found to be more stable and bulkier than the TBDMS). As illustrated in

Scheme 8, the TIPS group was used to protect the alcohol **57'** to provide the ether **62'** in 90% yield. Hydroboration of olefin **62'** under the modified conditions with 9 equivalents of BH_3/DMS at room temperature provided the desired secondary alcohols **63a'** and **63b'** in 80% yield after oxidative workup.^{126,127}

Scheme 9



Swern oxidation of this mixture of secondary alcohols furnished the ketones **64a,b'** in 85% yield. This mixture of ketones was heated in THF in the presence of 1.5 equivalents of HCl (1N aqueous) for 3 hours, after which ketone **65'**, which was devoid of the boron species, was obtained in 90% yield. The methylation of **65'** with methyl iodide gave the

*N*_b-methiodide salt which was subjected to the modified conditions for ring cleavage (*t*-BuOK in refluxing THF/EtOH [6:1]) to provide the enantiomer **66'** of the macroline equivalent. Deprotection of the TIPS group in **66'** with TBAF in THF afforded the enantiomer **6'** of macroline in 86% yield (see Scheme 8).

Normacusine B **67** was converted into the *N*_a-H analog of macroline **71** (Scheme 9) following the same sequence of steps as outlined for **6'** in Scheme 8. Trinervine **69**, which retained the basic sarpagine skeleton, and contained a unique hemiketal ring formed between the C-17 (OH group) and the ketone at C-19 was synthesized from intermediate **68** on stirring it with 10 equivalents of 1 N aqueous HCl in refluxing THF (80% yield). The acidic conditions at reflux released the free amine, cleaved the TIPS group, as well as catalyzed the hemiketal formation. The total synthesis of trinervine **69** was, therefore, completed in enantiospecific fashion in an overall yield of 20% (from the ketone **50**, see Scheme 6) in 10 reaction vessels (see Scheme 9).

1.3.1.3. Improved total synthesis of macroline by Liao et al.¹²⁸

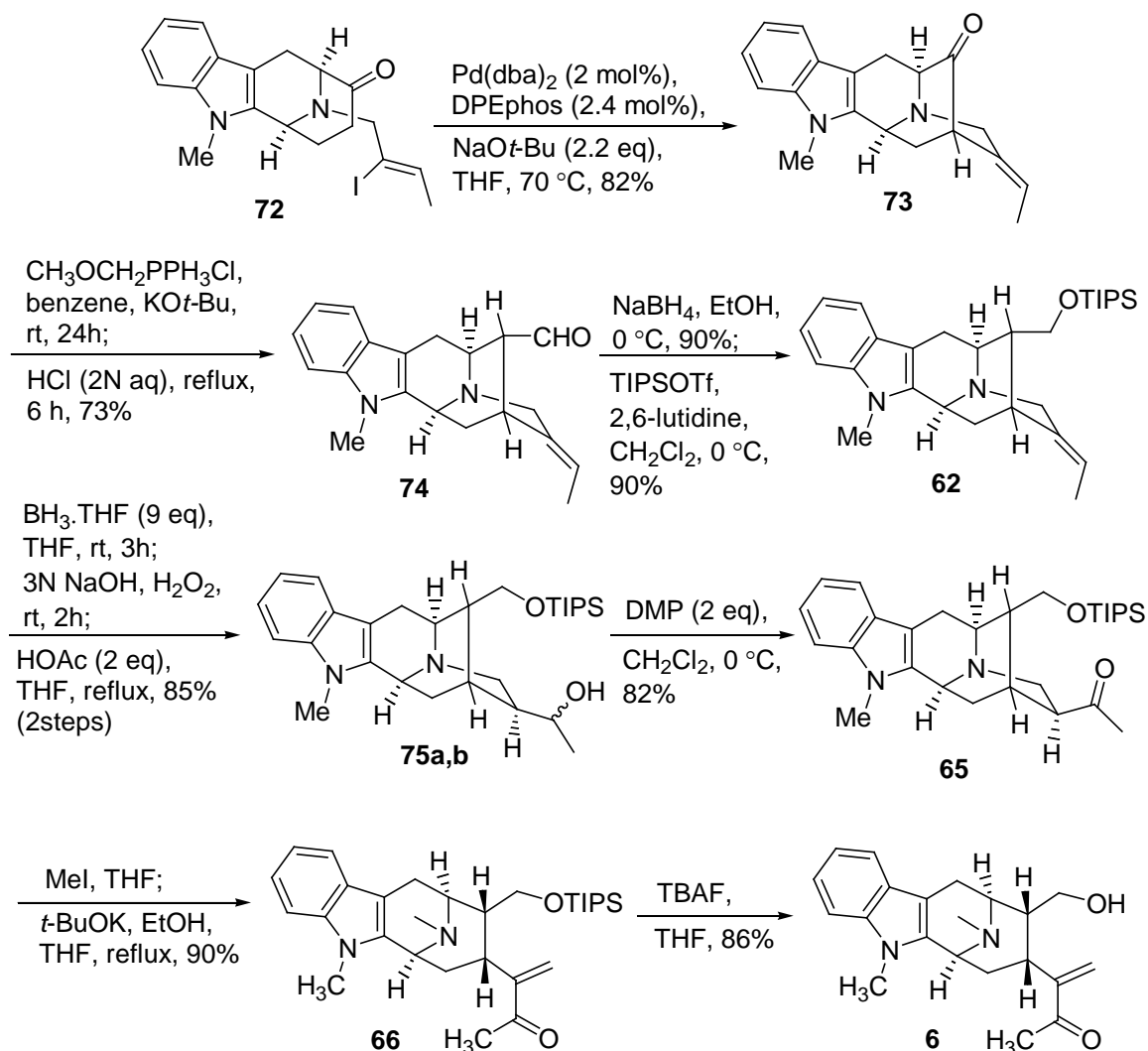
In an effort to decrease the amount of phosphine ligand employed for the cross coupling process, the Buchwald-Hartwig α -arylation¹²⁹ conditions were studied. The original Buchwald conditions¹²⁹ were modified by introducing DPEphos, a bidentate ligand with a large bite angle, a stronger base such as NaO-*t*-Bu and Pd(dba)₂ as the catalyst. The improved route toward the synthesis of macroline is illustrated in Scheme 10.

Previous to this, the same sequence of steps was carried out as depicted in Scheme 8, albeit under modified reaction conditions. The *N*_a-methylvellosimine **74** was converted into affinisine **58** (Scheme 7) by NaBH₄/EtOH reduction in 90% yield. Protection of the

OH group was carried out using TIPSOTf/2,6-lutidine in CH₂Cl₂ to provide the ether **62**.

Hydroboration followed by oxidation provided the secondary alcohols **75a** and **75b**. The

Scheme 10

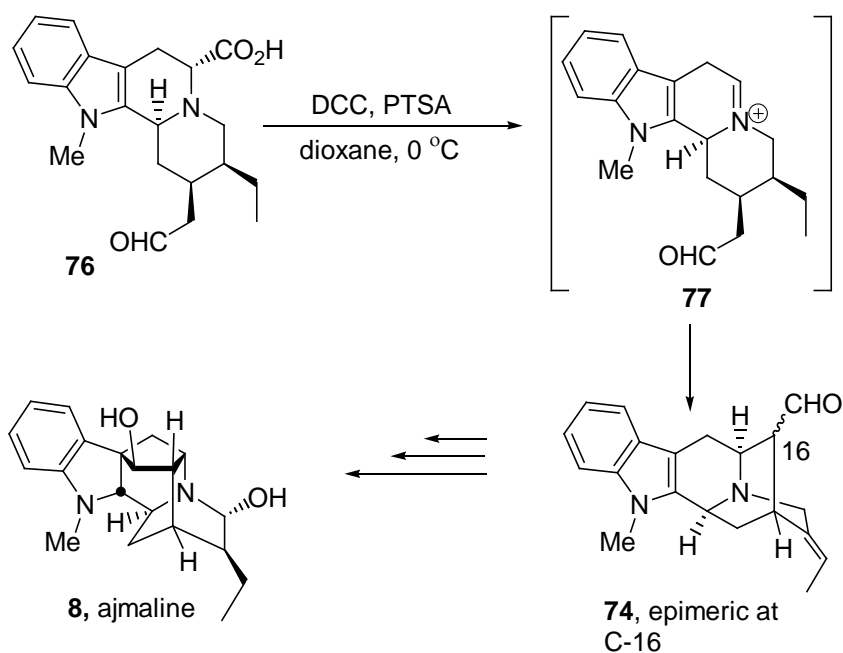


*N*_b-BH₃ complex was cleaved by refluxing with 2 equivalents of acetic acid in THF to provide the free amine **75a,b**. Because of the inconsistent results obtained in the Swern-oxidation of the secondary alcohols **75a,b**¹³⁰, Dess Martin oxidation was employed to furnish the desired ketone **65** in 82% yield. Treatment with methyl iodide in THF

provided the quaternary salt, which underwent a retro-Michael reaction to provide the macroline equivalent **66** in 20.4% overall yield from tryptophan methyl ester (not shown in Scheme). Removal of the TIPS group with TBAF monohydrate, provided **6** in 86% yield.

1.3.2. A biomimetic total synthesis of (+)-*N*_a-methyl vellosimine **74** by Martin et al.

Scheme 11



van Tamelen^{62,131} reported a biogenetic-type synthesis of ajmaline **8** in which the key step was the conversion of acid **76** into a mixture of epimeric aldehydes represented by **74** (Scheme 11). A proposition supported by a subsequent report of a biogenetic type synthesis of ajmaline was made later by van Tamelen and Olivier.^{132,133} This seminal cyclization to furnish the sarpagine skeleton proceeded via the proposed iminium ion **77**, which was generated by decarbonylation of an activated form of the carboxyl group in

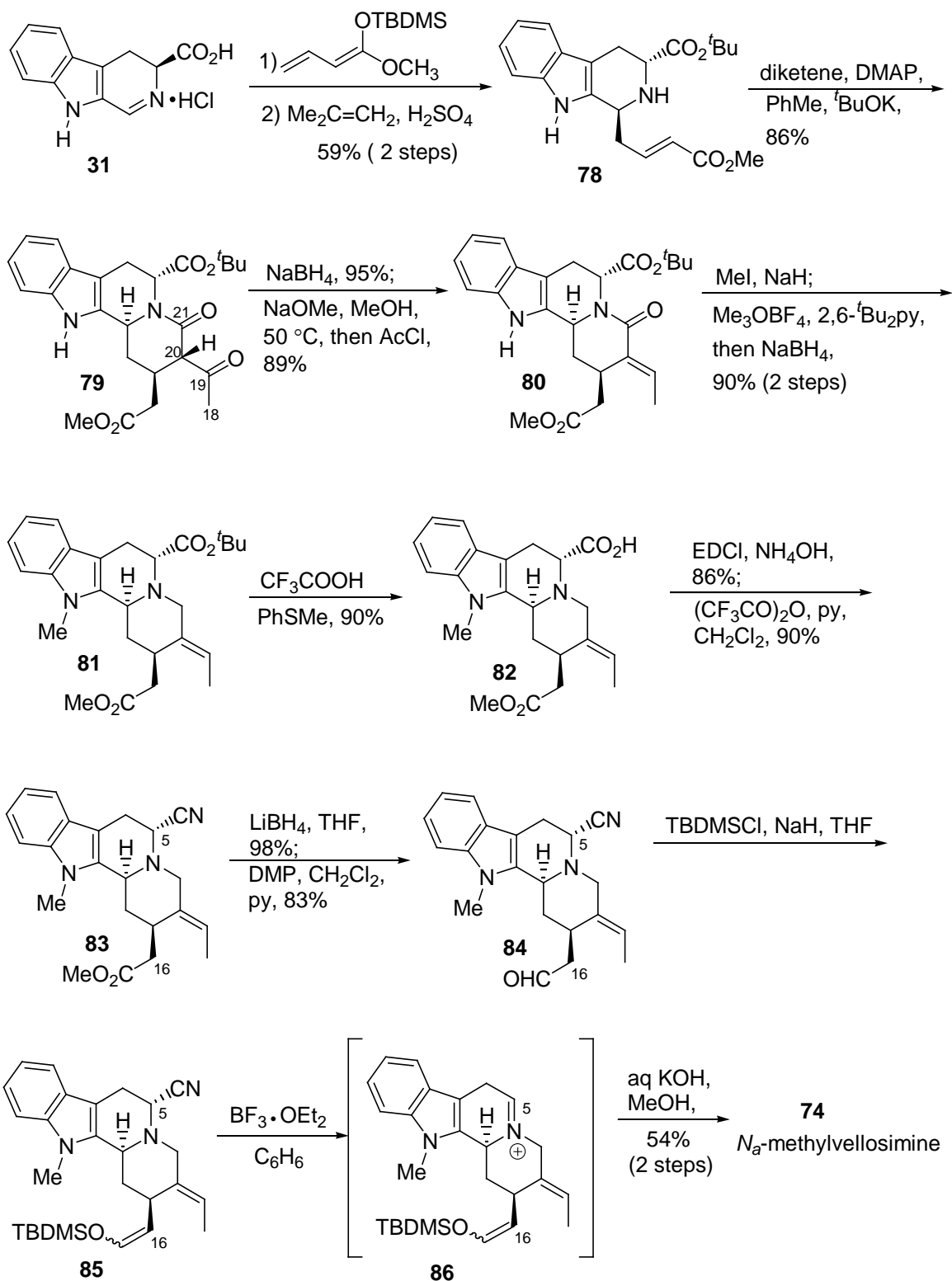
76. Aldehyde **74** was then converted into a relay compound which eventually was transformed into ajmaline **8**. Twenty-five years after van Tamelen's original work, Lounasmaa and coworkers reinvestigated this biogenetic-type cyclization.¹³⁴ They did not observe the expected "biogenetic-type" cyclization of a related iminium ion. Consequently, Lounasmaa et al.¹³⁴ reported they could not execute this type of cyclization and cast doubt on the biogenetic hypothesis of van Tamelen. It must be pointed out; however, Lounasmaa et al.¹³⁴ did not employ the exact substrate of van Tamelen. The group in Milwaukee as well as Martin and coworkers realized that Lounasmaa's work was not executed with the same substrate as van Tamelen. In order to solve this controversy, Martin et al.¹³⁵ developed a biogenetic entry into *N*_a-methyl vellosimine **74** which employed an iminium ion mediated cyclization similar to van Tamelen's original proposal.

As shown in Scheme 12, dihydrocarboline **31**, which was readily obtained from commercially available D-tryptophan **37**, was allowed to react with the vinyl ketene acetal to afford a single product and then directly converted into the *t*-butyl ester **78**. The *N*_b-acylation of amine **78** with diketene furnished an intermediate β-keto amide that underwent facile cyclization via an intramolecular Michael reaction upon addition of potassium *tert*-butoxide to give keto amide **79**.

The *E*-ethylidene side chain in amide **80** was obtained in good yield by following the reduction/activation/elimination sequence to give a single geometric isomer, as depicted in Scheme 12. The lactam **80** was then methylated at the *N*_a-indole position, after which the *N*_a-methyl amide was reduced to the amine **81** in 90% yield. This was followed by selective acid catalyzed ester hydrolysis in the presence of methyl thioanisole which

proceeded smoothly to give the acid **82**. The acid moiety in **82** was then transformed into the amide with NH_4OH in the presence of EDCl in 86% yield followed by dehydration of the amide with trifluoroacetic anhydride to provide the nitrile **83** in 90% yield. The ester group in **83** was selectively reduced in the presence of the cyano group by reaction with lithium borohydride in THF and the subsequent oxidation of the hydroxyl group with Dess-Martin periodinane gave the aldehyde **84** in 83% yield. The aldehyde **84** was then converted into the silyl enol ether **85** with TBDMSCl in the presence of NaH. The α -aminonitrile **85** was then treated with $\text{BF}_3 \cdot \text{OEt}_2$ in benzene and this was followed by exposure to aqueous potassium hydroxide in MeOH. The N_a -methylvellosimine **74** was obtained in 54% yield. This biomimetic total synthesis of N_a -methylvellosimine **74** provided experimental support for the cyclization step originally proposed by van Tamelen as one of the key steps in the biosynthesis of the sarpagine and ajmaline alkaloids. It also illustrated the Lounasmaa's criticism of the cyclization process¹³⁴ may be unfounded since he did not use the exact same substrate as van Tamelen.¹³¹

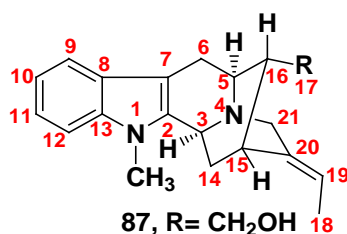
Scheme 12



2. Objectives and synthetic approach

The unique and complex architecture of the indole alkaloids coupled with their largely unexplored potential in medicine or as tools for biological studies make these compounds attractive targets for total synthesis. The sarpagine alkaloids contain the common structural element of the parent pentacyclic sarpagan ring system.⁵⁷ These indole alkaloids contain a double bond at C19-C20 and lack functionality at the C-21 position. In all known sarpagine indole alkaloids the stereochemistry at C-3 (S), C-5 (R) and C -15 (R) has been established. These three stereochemical centers have a fixed configuration because of the rigid framework of the molecule. The double bond at C19-C20 has an E-configuration. The alkaloid ervincidine belongs to the sarpagine class and has been isolated from the epigeal part of *Vinca erecta* Rgl. et Schmalh.¹³⁶ The UV spectrum is characteristic for indole bases. The IR spectrum has a broad band at 3000-3330 cm^{-1} due to the presence of OH and NH groups connected by a hydrogen bond. This alkaloid belongs to the akuammidine subgroup and is a hydroxyl derivative of tomboisine.¹³⁶

Figure 6. Sarpagine Type Indole Alkaloids



According to Glasby's book of alkaloids¹³⁷ and the review by Lounasmaa,⁵⁷ the structure of ervincidine has four stereocenters C-3 (S), C-5 (R), C-15 (R) and C-16(R). The stereochemistry of the alcohol at the C-6 position was not assigned. The paper published

by Yunusov *et al.*,¹³⁶ has reported the structure of ervincidine similar to that of the polyneuridine subclass with four stereocenters C-3(S), C-5(R), C-15(R) and C-16(S). But again the stereochemistry of the C-6 alcohol was not assigned. As illustrated in **Figure 7**, the proposed structure of ervincidine by Glasby⁵ and Lousnamaa⁵⁷ has the functional group at C-16 (R) with the alpha stereochemistry and that of Yunusov¹³⁶ has the functional group at C-16 (S) with the less stable beta stereochemistry which stimulated the interest in this indole alkaloid. The synthesis of this natural product was also challenging because the only information from the literature¹³⁶ was the optical rotation which was $+29.5^{\circ}(c\ 0.6, \text{MeOH})$.¹³⁸ No unequivocal spectral information (NMR, CHN analysis) was given. Another aspect which made the synthesis of this molecule important was the establishment of the stereochemistry of the C-6 alcohol function. Examination of both the reports from the literature^{40,136} did not assign the stereochemistry to the C-6 alcohol. The mass spectrum and the molecular ion peak of ervincidine¹³⁶ was similar to the spectra of the sarpagine and tomboisine alkaloids.¹³⁹ The difference of 16 m/e units indicated the presence of a hydroxyl group in ervincidine. The presence of an m/e ion peak at 169 in the mass spectrum suggested the presence of the hydroxyl group in the aliphatic part of the molecule possibly in ring C. On the basis of the comparison of the mass spectrum of ervincidine with that of tomboisine, akuammidine and gardenine and with the proposed biogenetic interrelationship with gardnutine and hydroxygardnutine,¹⁴⁰ the position of the hydroxyl group in ervincidine was probably at C-6.¹³⁶

Figure 7. The Indole Alkaloid Ervincidine



^a Ervincidine as proposed by Glasby¹³⁷
and Lousnamaa⁴⁰

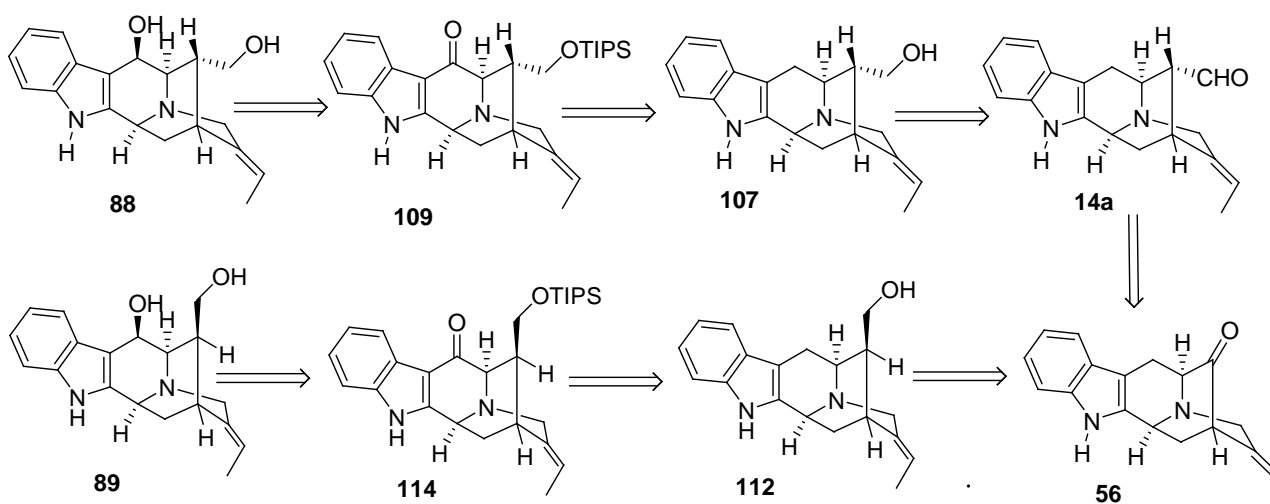
^b Ervincidine as proposed by Yunusov *etal.*¹³⁶

The objective of this research was to complete the first enantiospecific, stereospecific total synthesis of the indole alkaloid ervincidine and correct the stereochemical ambiguity reported in the literature. This ambiguity as pointed out was because the stereochemistry of the CH₂OH group at C-16 was not assigned unequivocally and neither was the hydroxyl group at C-6 position. Moreover, the design of a synthetic entry into the C-6 alcohol stereospecifically, as well as an assessment (thermodynamic stability) of the stability of the C-6 hydroxyl group was of significant importance in indole alkaloid chemistry. As shown in Scheme 13, in a retrosynthetic sense, both the diastereomers **88** and **89** might be available via a common intermediate, pentacyclic ketone **56**. The chirality of **56** was to be employed to introduce the correct stereocenters in the target alkaloids **88** or **89**.

The ketone **56** could presumably be converted into vellosomine **14a**, which could be employed as an intermediate in the total synthesis of **88**. The synthesis of the axial alcohol E-16-epinormacusine B **112** could be achieved by a hydroboration/oxidation process. This intermediate once obtained, might further provide 6-hydroxy-16 demethoxycarbonyl polyneuridine **89** via protection/deprotection of hydroxyl group,

selective oxidation by IBX at C-6 and a reduction. The chirality of **56** was to be employed to introduce the correct stereocenters in the target alkaloids **88** or **89**.

Scheme 13. Retrosynthetic Analysis of ervincidine **88** and **89**



The important initial stereogenic centers would be established from the 1, 3 *trans* transfer of chirality in the asymmetric Pictet-Spengler reaction.¹⁴¹⁻¹⁴⁶ The retrosynthetic strategy rests on the general approach which has been used to synthesize the macroline-sarpagine type alkaloids in Milwaukee. The thermodynamically stable α -aldehyde **14a** would arise via Wittig reaction on the pentacyclic ketone **56**. The N_a -H, N_b -H tetracyclic ketone **50** should be available from D-(+)-tryptophan **37** on a large scale via the asymmetric Pictet-Spengler reaction and the Dieckmann reaction as key steps.¹⁴⁷⁻¹⁴⁹ This synthetic strategy was an efficient way to provide **56** in gram quantities. The less stable β -axial alcohol could be synthesized using the pentacyclic ketone **56** via a Wittig reaction coupled with a hydroboration/oxidation following the published procedure.^{122,150,151}

3. Results and Discussion

3.1. The First enantiospecific, stereospecific total synthesis of the sarpagine alkaloids related to structures of the proposed ervincidine (**88** and **89**) including ervindicine

3.1.1. Synthesis of the (-)-*N*_a-H, *N*_b-H tetracyclic ketone **50** on large scale

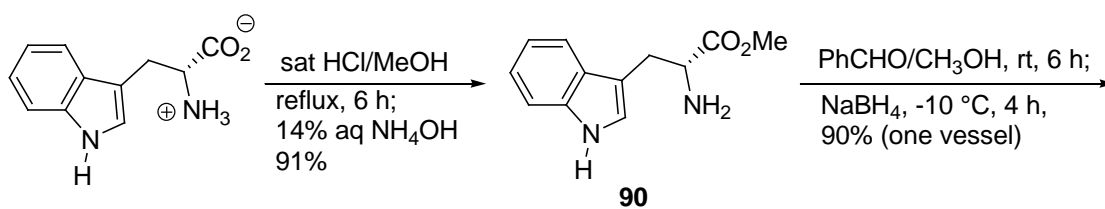
As planned, the synthesis of isomers of ervincidine **88** and **89** began with the preparation of the (-)-*N*_a-H, *N*_b-benzyl tetracyclic ketone **49** as the key building block on large scale following the procedure developed in Milwaukee. As illustrated in Scheme 14, Fischer esterification of (+)-**37** with methanolic hydrogen chloride gave the methyl ester **90** on 400 gram scale. This was then converted into *N*_b-benzyltryptophan methyl ester **91** on stirring with benzaldehyde (1.1 equivalents) at room temperature (6 hours), followed by reduction of the imine which resulted *in situ* with sodium borohydride [-10 °C to -8 °C (2-5 hours, according to the scale)]. The optical purity of the *N*_b-benzyltryptophan methyl ester **91** prepared in this manner was found to be greater than 98% ee as determined by comparison to data from authentic samples.¹⁴⁹

To introduce the desired stereocenter at C-1 the asymmetric Pictet-Spengler reaction¹⁴¹⁻¹⁴⁶ was employed with methyl 4,4-dimethoxy-butyrates **95**,¹⁴⁶ (which can be prepared on a kilogram scale) and *N*_b-benzyl tryptophan **91** to provide the *trans* diester **92b** as a single diastereomer in 92% yield. This process was scaled up to the 400 gram level and purification was achieved by recrystallization from ethanol. As shown in Scheme 15, the lone pair of electrons of the *N*_b-nitrogen atom of **91** (Scheme 15) presumably attacked the oxonium ion and this was followed by loss of the elements of methanol to form the iminium ion intermediate **96**. Attack of the iminium ion at the indole C-3 position could

form either the anti spiroindolenine **98b** or the syn spiroindolenine **98a** intermediate. The anti intermediate **98b** could rearrange directly into the desired *trans* diester **91b**; however, in the case of the disfavored syn spiroindolenine **98a**,¹⁵² it was felt the rearrangement to the *cis* diester **92a** would occur followed by the acid-catalyzed isomerization at C-1 to afford the more stable *trans* diester **92b**.¹⁴¹ Consequently, during the process of this Pictet-Spengler reaction, the *cis* diester **92a** derived from **97a** was indeed detected by TLC but was converted entirely into the *trans* diester **92b**, presumably via the carbocationic intermediate¹⁴³ **III** as planned. After work up, the *trans* diester **92b** was obtained as the only diastereomer in greater than 98% ee and high yield on 100 gram scale.

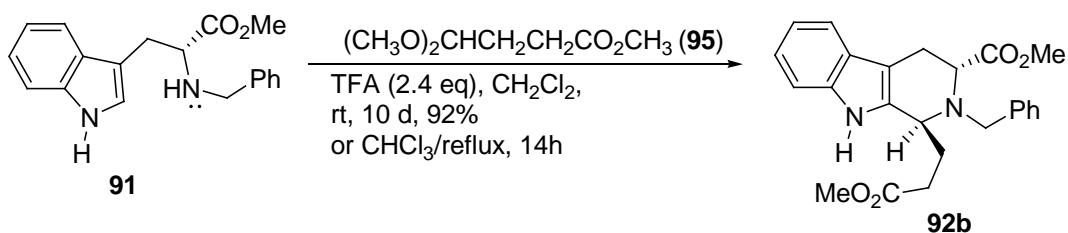
When the *trans* diester **92b** was treated with three equivalents of sodium hydride in the presence of excess methanol in refluxing toluene,¹⁰⁶ the *trans* diester **92b** was converted entirely into *trans* δ -lactam **100**. No further change was observed (Scheme 16) on prolonged heating. However, when diester **92b** was treated with nine equivalents of sodium hydride in the presence of excess methanol in refluxing toluene under these same reaction conditions for an extended period of time (72 hours), the desired Dieckmann β -ketoester **102** was obtained in 88% yield. Presumably, the δ -lactam **100** formed and then underwent ring-opening^{10,101} to provide the *trans* diester **92b** under these conditions. This diester **101a** was in equilibrium with the *cis* intermediate **101b** and the latter material was eventually converted into β -ketoester **102** via the Dieckmann process.

Scheme 14



37, D-tryptophan,

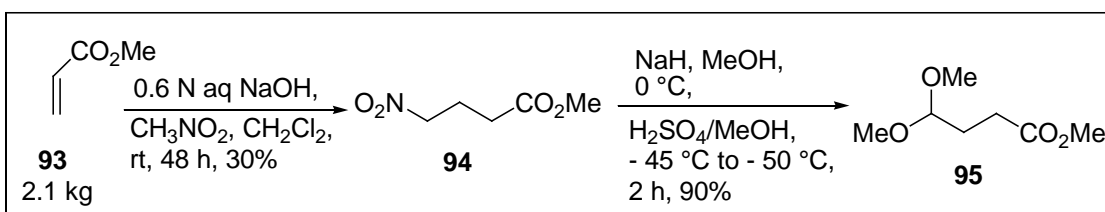
400 g scale



91

92b

trans diester only, > 98% de

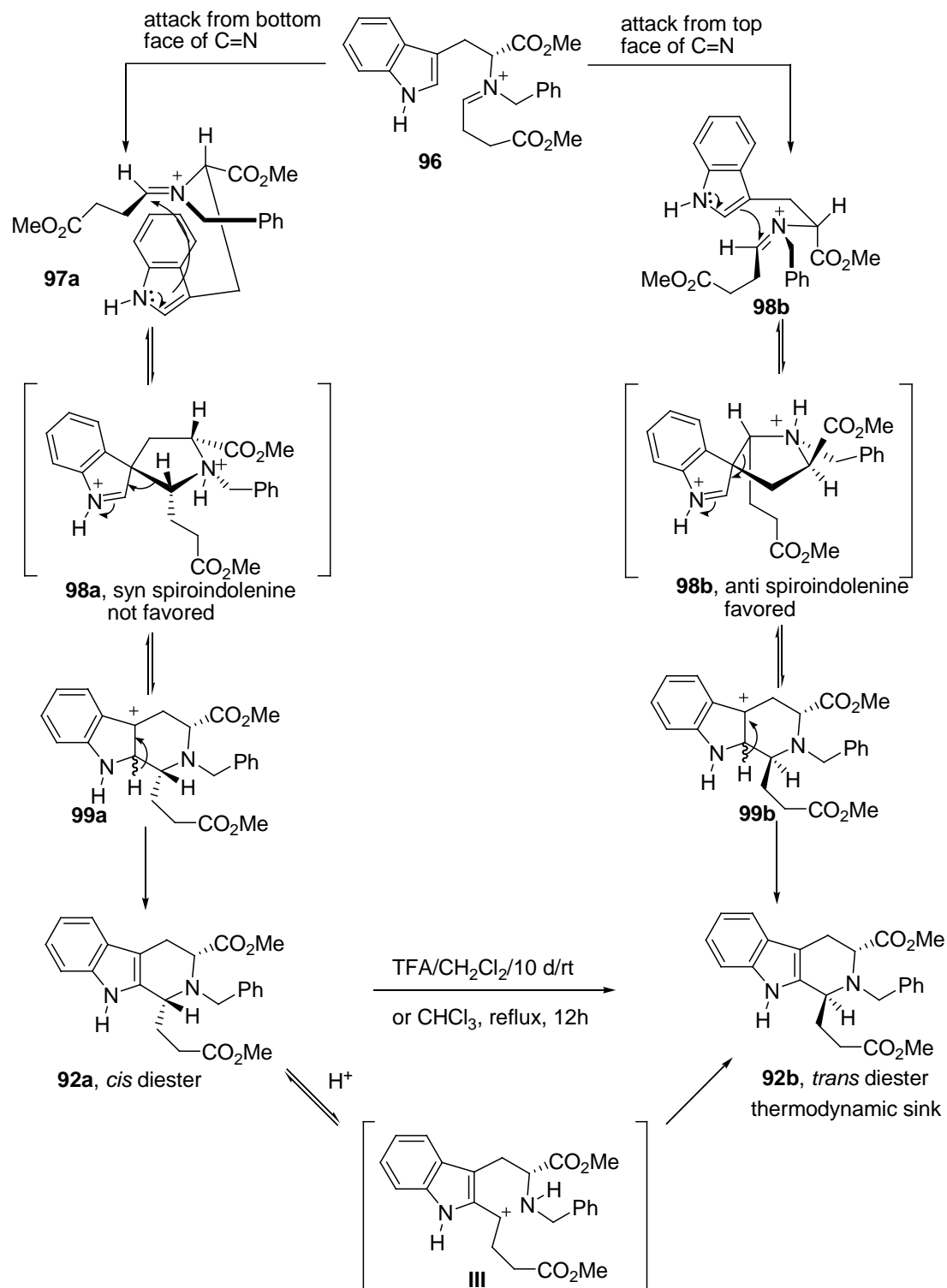


93
2.1 kg

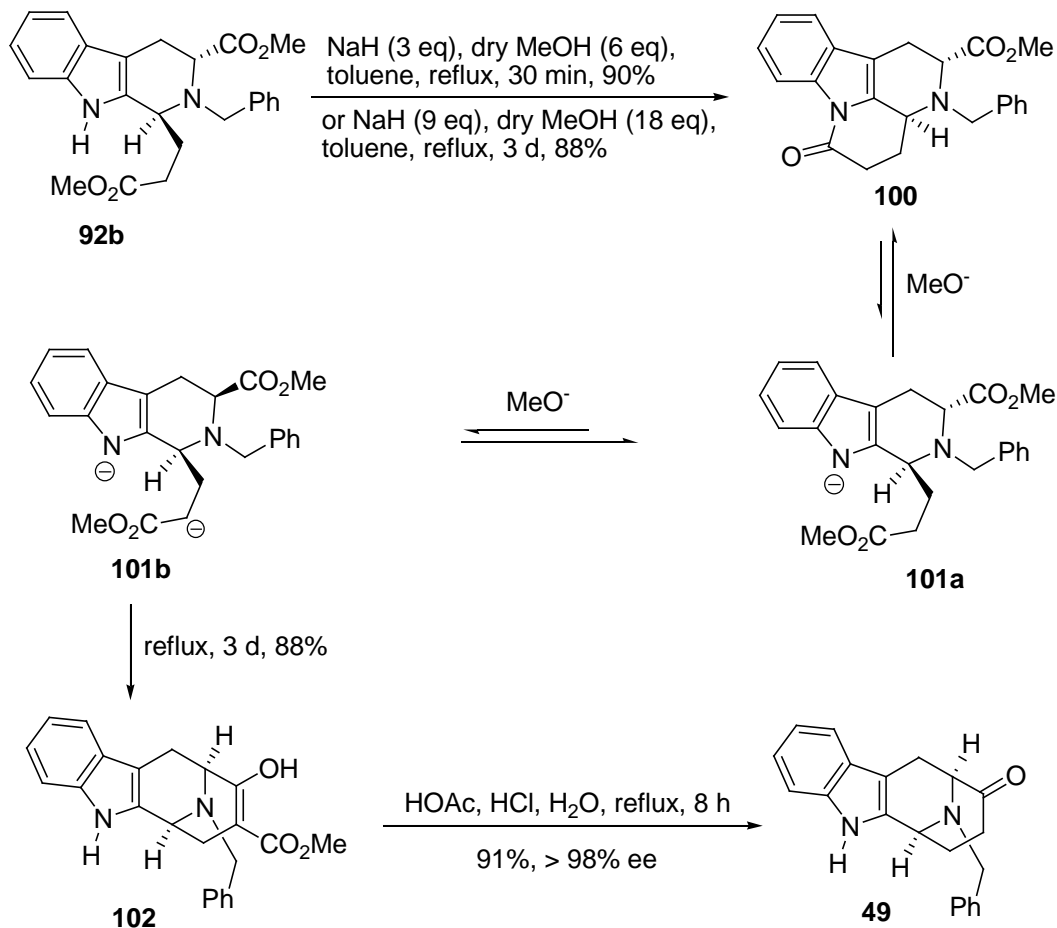
94

95

Scheme 15



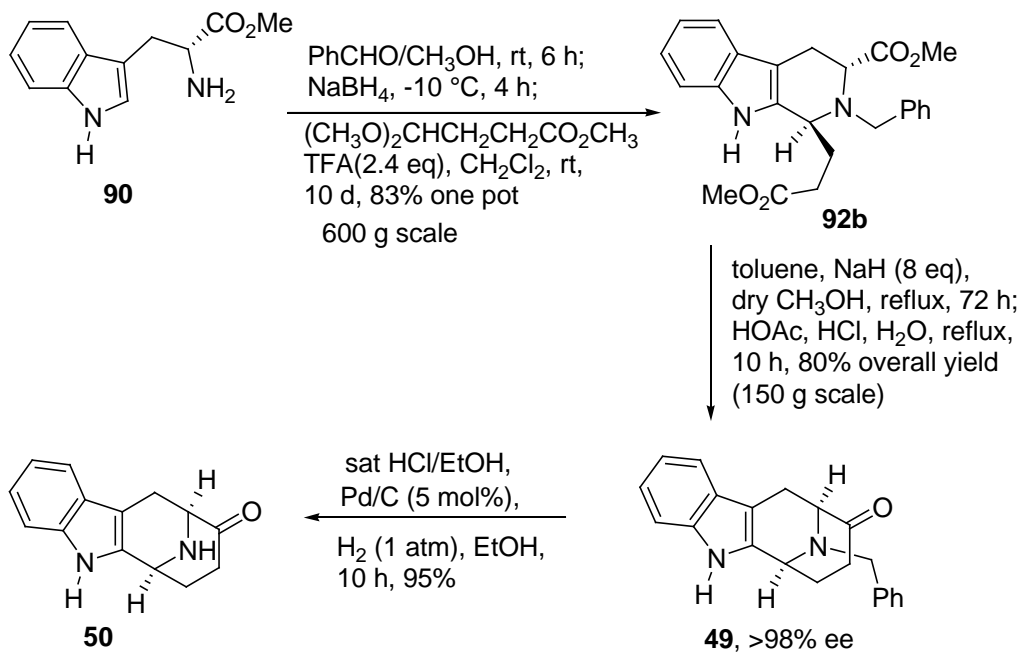
Scheme 16



It was felt the δ -lactam **100** was favored in the equilibrium over intermediates **101a** and **101b**; however, the irreversible formation of the enolate (see **102**) in the Dieckmann cyclization gradually promoted completion of the process to provide the β -ketoester **102**, exclusively (Scheme 16). Hydrolysis of the β -ketoester **102** and decarboxylation under acidic conditions was achieved in one step to provide the template (-)- N_a -H, N_b -benzyl tetracyclic ketone **49** in 90% yield. The enantiomeric purity of ketone **49** was determined to be greater than 98% ee by conversion of it into (-)- N_a -methyl, N_b -benzyl tetracyclic ketone **25** whose enantiomeric purity had been determined previously by Zhang.^{10,106,153}

D-(+)-Tryptophan methyl ester **90** can also be diastereospecifically converted (via **92b**) into azabicyclononone **49** in greater than 98% ee in a two pot process on multihundred gram scale, as depicted in Scheme 17. More specifically, after N_b -benzylation of **90** with benzaldehyde and sodium borohydride (1 eq) in methanol was completed, trifluoroacetic acid (TFA) was added to the reaction vessel at 0 °C to neutralize the alkaline mixture. After removal of the solvent under reduced pressure, CH_2Cl_2 , TFA and acetal **95** were added to the vessel at 0 °C and the modified Pictet-Spengler reaction (600 g scale) was carried out to provide the *trans* diester **92b** in 83% crystalline yield. In the second sequence (150 g scale), the Dieckmann cyclization was completed and the reaction solution was then cooled to 0 °C after which it was carefully quenched with glacial acetic acid. After removal of the solvent under reduced pressure, concentrated glacial acetic acid, aqueous hydrochloric acid and water were added to the residue in the same vessel at 0 °C. The acidic hydrolysis and decarboxylation of **102** was then executed at reflux to provide (-)-**49** in 80% crystalline yield in greater than 98% ee.¹⁰ The benzyl group in tetracyclic ketone **49** was removed by converting **49** first into its hydrochloride salt. The HCl salt of **49** was then subjected to the conditions of catalytic debenylation [Pd/C, H_2 (1 atm), bench top] to furnish the N_a -H, N_b -H tetracyclic ketone **50** in 95% yield (Scheme 17).

Scheme 17



In conclusion, the basic tetracyclic core of the *N_a*-H, *N_b*-H tetracyclic ketone **50**, which contained rings ABCD required for the synthesis of the C-19 methyl substituted sarpagine indole alkaloids was constructed enantiospecifically and stereospecifically via the asymmetric Pictet-Spengler/Dieckmann protocol on large scale.^{119,147,148}

3.1.2. Synthesis of the -*N_a*-H pentacyclic ketone **56**

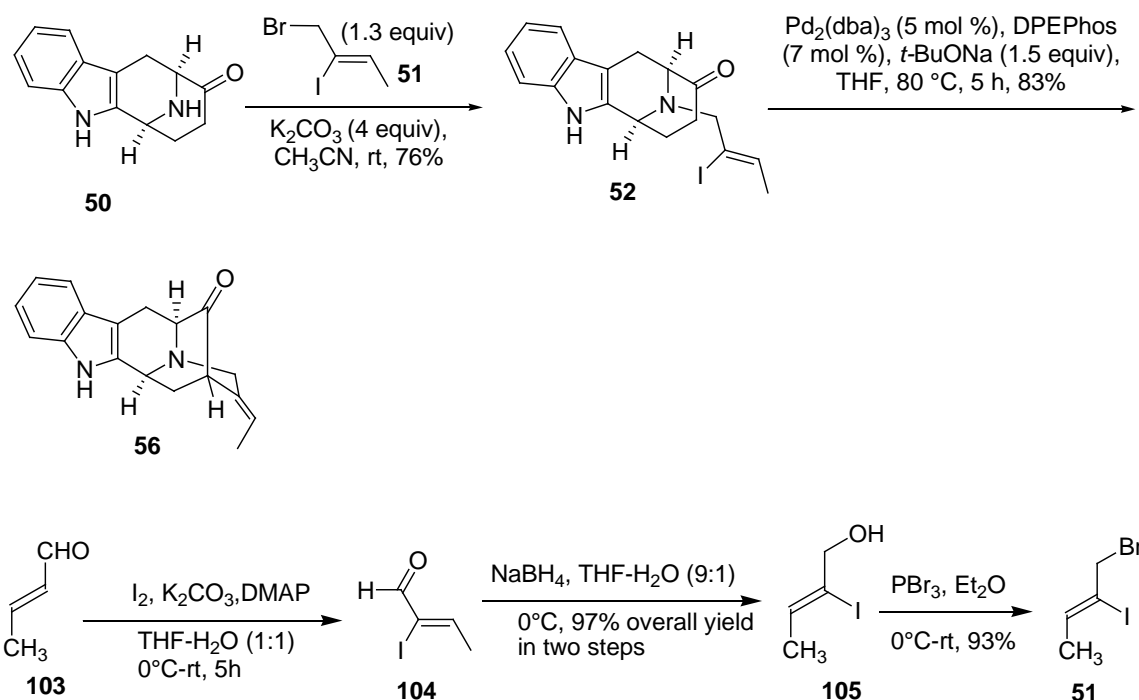
N_b-alkylation of the secondary amine **50** with (*Z*)-1-bromo-2-iodo-2-butene **51** under the conditions developed in Milwaukee (dry THF/K₂CO₃/ reflux)^{122 118,154} led to the formation of the desired product **52**, but was very sluggish, and led to considerable formation of baseline impurities. Since substitution by amines on bromides was clearly an S_N2 type process, it was then decided to increase the nucleophilicity of the amine by employing a more polar aprotic solvent. It was well known that the nucleophilic strength was dependent on the solvent employed in the S_N2 reaction. Dry acetonitrile on the other

hand proved to be the most suitable solvent for this process for the reaction went to completion at room temperature to give **52** in 76% yield. In order to increase the yield, vinyl iodide **51** was used in excess (3-4 equivalents). But this reaction condition did not improve the yield but increased the base line impurities.

Initially, the vinyl iodide **51** required for this route was synthesized according to a literature procedure.¹²⁰ However, the free-radical hydrostannation of the propargyl alcohol was difficult and the desired iodide was extremely hard to purify. Importantly, as illustrated in Scheme 18, an improved method was recently developed¹²² to prepare **51** via α -iodination of an α,β -unsaturated aldehyde **103** under the conditions of Kraft^{82,155} which exclusively formed only the *Z*-isomer **104**. This material without further purification underwent the subsequent reduction⁸³ to provide the desired alcohol **105** in 97% overall yield. This alcohol **105** was treated with PBr₃ in dry ether at 0 °C for 12 hours to provide the desired bromide **51** in 93% yield. The sequence was scaled up to the 200 g level scale starting from crotonaldehyde **103** to obtain the desired allylic bromide **51** on a large scale as well.

The ketone **52** was initially converted into the desired ketone **56** in 80% yield *via* an intramolecular palladium (enolate mediated) cross-coupling reaction analogous to the process developed by Wang *et al.*^{118,156,157} Further development for this palladium-mediated cross coupling reaction was achieved when ketone **52** was subjected in combination with 5.0 mol% Pd₂(dba)₃, 7.0 mol% DPEphos as a ligand and 1.5 equivalent of NaOtBu as a base in THF at 80 °C for 5 hours. The desired ketone **56** was obtained in 83% yield which was superior to the previously reported results (**Scheme 5**).

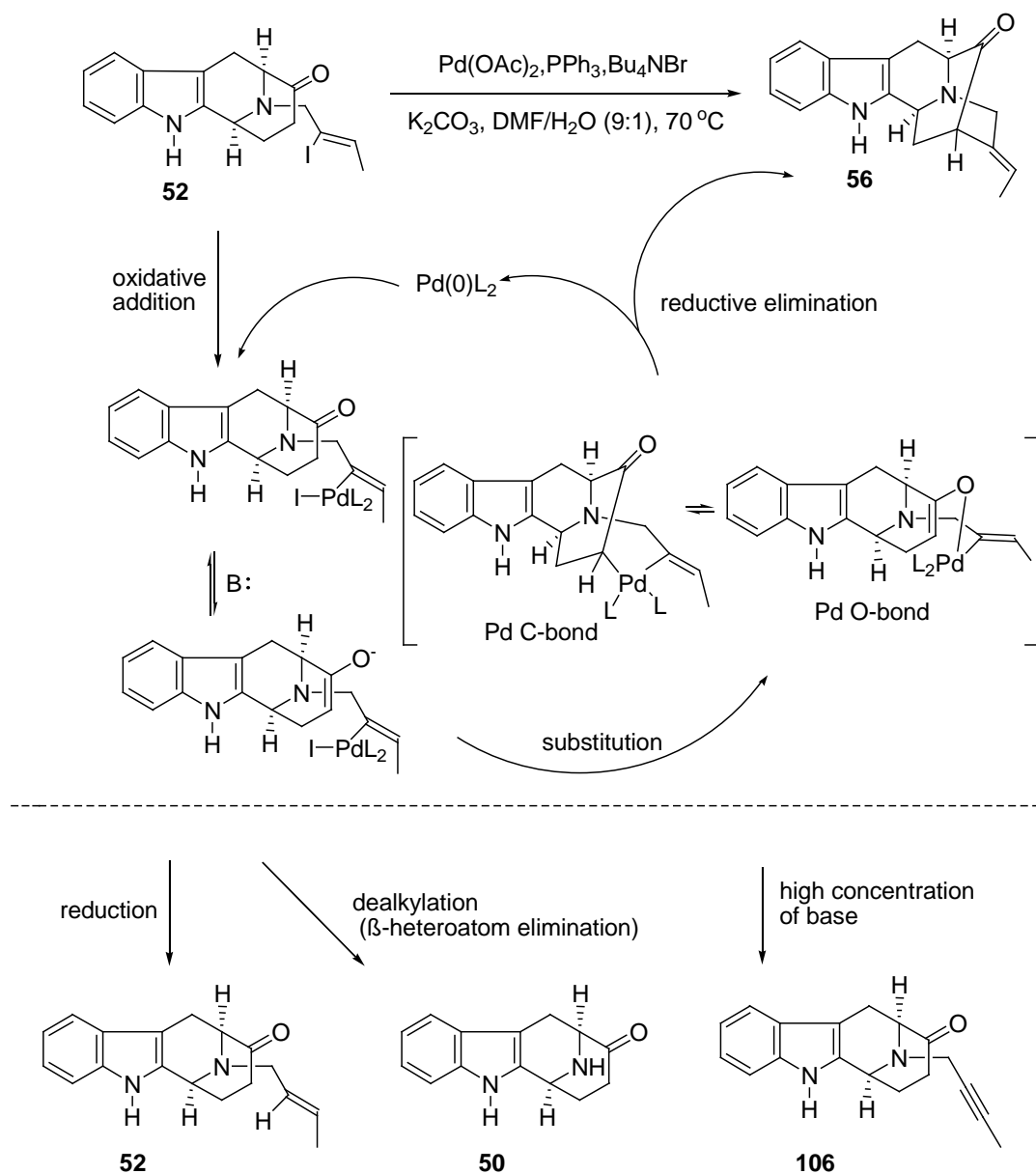
Scheme 18



A plausible Hartwig-Buchwald catalytic cycle for the enolate-driven palladium catalyzed α -vinylation reaction is illustrated in Scheme 19. It was felt the active $\text{Pd}(0)\text{L}_2$ species was generated primarily by reduction of $\text{Pd}(\text{OAc})_2$ with triphenylphosphine in this phosphine-assisted catalytic cycle.^{158,159} The active $\text{Pd}(0)\text{L}_2$ species could then undergo oxidative addition on the vinyl iodide to form a vinylpalladium(II) iodide complex. Ligation to the oxygen and rearrangement to the carbon atom at C(15) can then occur. Finally, reductive elimination of the carbon bound $\text{Pd}(\text{II})$ intermediate would furnish the desired E-olefin **56** while regenerating the active $\text{Pd}(0)\text{L}_2$ species. A key to the success of this Pd-mediated cross coupling reaction rested on the enolate concentration. This must be high enough to permit ligand substitution to occur.¹²⁵ It was well known that vinyl iodides would be quite reactive in the oxidative-addition step. If nucleophilic substitution

of the iodide by the nucleophilic enolate in the coupling process was comparably slow, the rate of byproduct formation would be significant. Eventually, a highly reproducible yield could be obtained by employing an excess of the phosphine ligand.¹⁶⁰ In the case of different substrates, sometimes it was necessary to carry out the reaction with a 10:1 ratio of PPh₃ (30 mol%) to Pd(OAc)₂ (3 mol%). The process then took three days to go to completion in comparison to that of five hours required under the original conditions, but the amount of byproducts (Scheme 19) was decreased. The yield of the sequence in this series was 81%. Furthermore, the best solvent system to date was DMF/H₂O (9/1), as compared to CH₃CN, pure DMF, or DMF/H₂O (4/1) which resulted in no reaction or low yields.¹²⁷ Because the conditions employed for the enolate driven palladium coupling process were different from the recent Buchwald-Hartwig arylation reactions,¹⁶⁰ efforts were directed toward intramolecular α -vinylation under the conditions of the arylation process.¹⁶⁰ This might permit lower catalyst loading¹⁶⁰ and be effective for both E and Z ethylenes. The homogenous reaction conditions might permit a faster rate and thereby facilitate scaleup. In fact, Liao first reported a Pd(0) catalyzed α -vinylation process in which the cheaper DPEphos was employed in the case of a Z-ethylene¹³⁰ for the synthesis of (-)-koumidine.¹⁵⁰ Moreover, utilization of this ligand for the synthesis of the E-ethylene **56** was also executed by Liao *et al.* in 80% yield.¹⁵⁰ However, a related approach has also been effective based on a palladium-catalyzed coupling of amino-tethered vinyl halides with ketones reported by Solé, Bonjoch *et al.*^{161,162} In addition, another process was also carried out with ketone **52** in the presence of 6.0 mol% Pd(PPh₃)₄ and a base PhOK (which was generated previously in the reaction vessel from 2.0 equivalent of PhOH and 1.5 equivalent of KO^tBu). The most notable aspect of the

Scheme 19



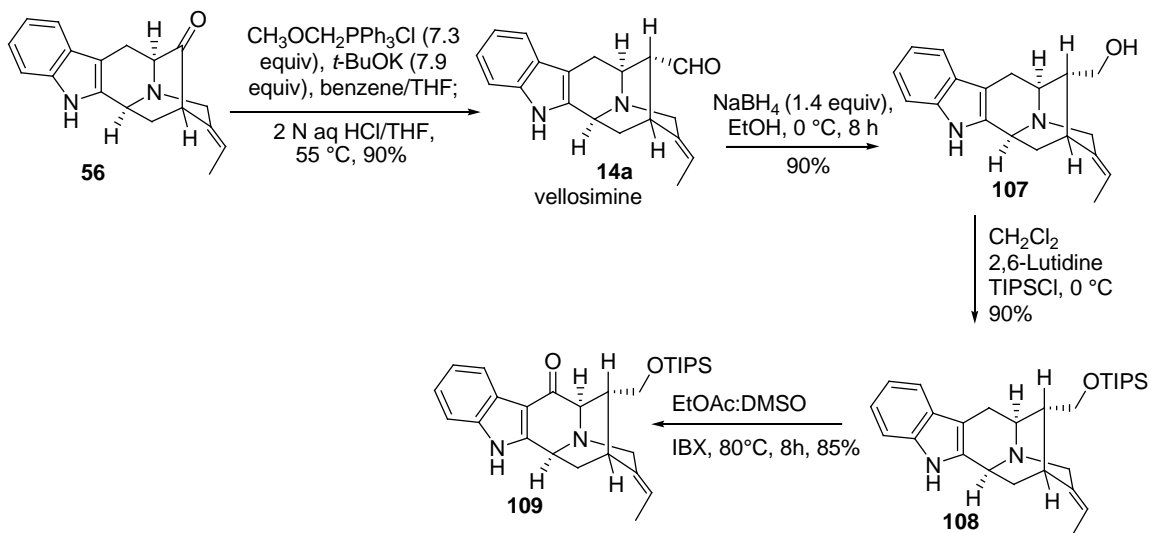
Different trace byproducts **52**, **50** or **106** are occasionally observed depending on what catalyst was employed and how much base was used.

latter attempt was that it did not require an additional ligand. The intramolecular cyclization took place to afford ketone **56** in 80% yield again in stereospecific fashion.

The use of the weaker potassium phenolate base limited the presence of any acetylene byproduct formed from loss of HI from the halide **52**.

Ketone **56** was then subjected to the Wittig reaction with methoxymethyl triphenylphosphonium chloride and anhydrous potassium *tert*-butoxide to provide a mixture of two stereoisomeric enol ethers (not shown). After a short wash column, the mixture of enol ethers was hydrolyzed under acidic conditions to provide vellosimine **14a** in 90% yield (overall yield for two steps). Since the aldehyde at C(16) was in the more stable alpha configuration because of a *syn* pentane interaction with the indole methylene bridge, the mixture was simply stirred until all of the β -epimer was converted into the more stable, natural epimer present in (+)-vellosimine **14a**. The aldehyde function of **14a** was then reduced with sodium borohydride to provide the alcohol normacusine B **106**, the spectral data of which are in complete agreement with the natural product. The C (17) functionalized alcohol was then protected as the trisopropylsilyl ether employing 2,6 lutidine as the base to provide the ether **107**. Repeated attempts to oxidize the C-6 position by DDQ on **108** were unsuccessful. The conditions employed with the first equivalent of DDQ deprotected the TIPS functional group forming alcohol **107** and the second equivalent oxidized the alcohol **107** to aldehyde **14a**. Finally, the oxidation at the C (6) position was successfully accomplished by oxidation using IBX at 80°C (radical process as shown in Scheme 21) to form the desired ketone **108**.^{130,163}

Scheme 20



The silyl analogue was then stirred in THF with tetrabutyl-ammonium fluoride monohydrate to provide the C-16 substituted monol **110**. Illustrated in Figure 8 is the ORTEP view of the crystal structure of ketone **110**.

Scheme 21

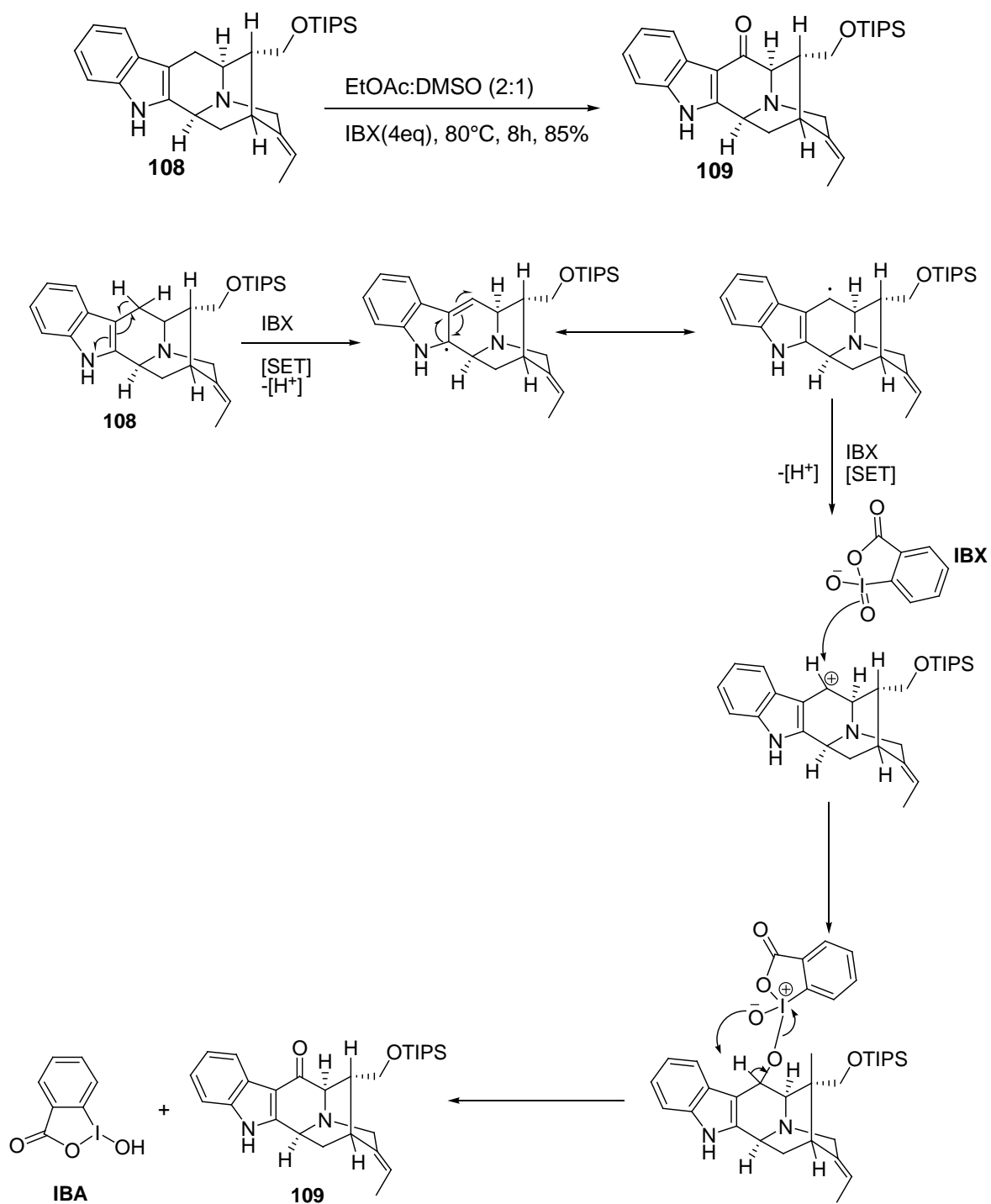
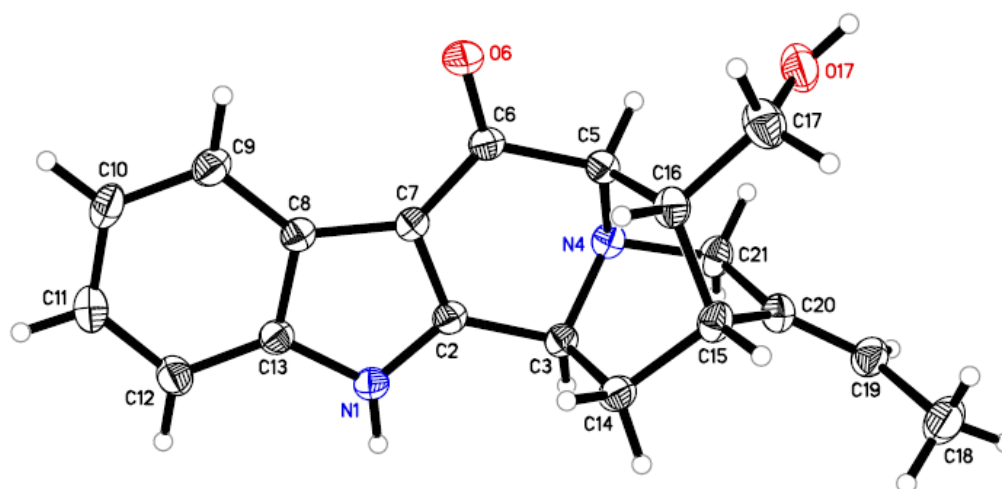


Figure 8. ORTEP View of the Crystal Structure of the monol **110**



3.1.3. Completion of the regiospecific, stereospecific total synthesis of ervincidine proposed by Glasby and Lousnamaa

The selective reduction of the ketone **110** was done by a Luche reduction¹⁶⁴ using sodium borohydride in combination with cerium chloride heptahydrate to afford the final product **88** with C-3 (S), C-5 (R), C-6 (R), C-15 (R) and C-16(R) stereochemistry as a single diastereomer. Luche reduction is a selective reduction of 1,2 enones using NaBH₄ in combination with CeCl₃. For the methanolysis of NaBH₄, CeCl₃ which is a Lewis acid catalyst is selected. The harder reducing agent (see Scheme 22) favors 1,2 reduction thus leading to the formation of a single diastereomer regiospecifically. Illustrated in **Figure 9** is the ORTEP view of the crystal structure of **88**. However, the optical rotation of this diastereomer **88** was $[\alpha]_D^{26} +79^\circ$ (c 0.6, in methanol) which is not in agreement with the value reported by Yunusov in the literature.^{40,137} The diastereomer **88** was stirred in 0.2N HCl at 0°C. Examination by TLC (silica gel; CH₂Cl₂: MeOH 9:1; R_f: 0.73) showed a new spot at lower R_f value (0.73) which indicated the complete epimerization of **111** at

the C-6 position. Unfortunately the new spot could not be isolated due to shortage of the material at this point. It is felt the C-6 alpha hydroxyl group is presumably the thermodynamically more stable isomer based on this preliminary experiment.

Scheme 22

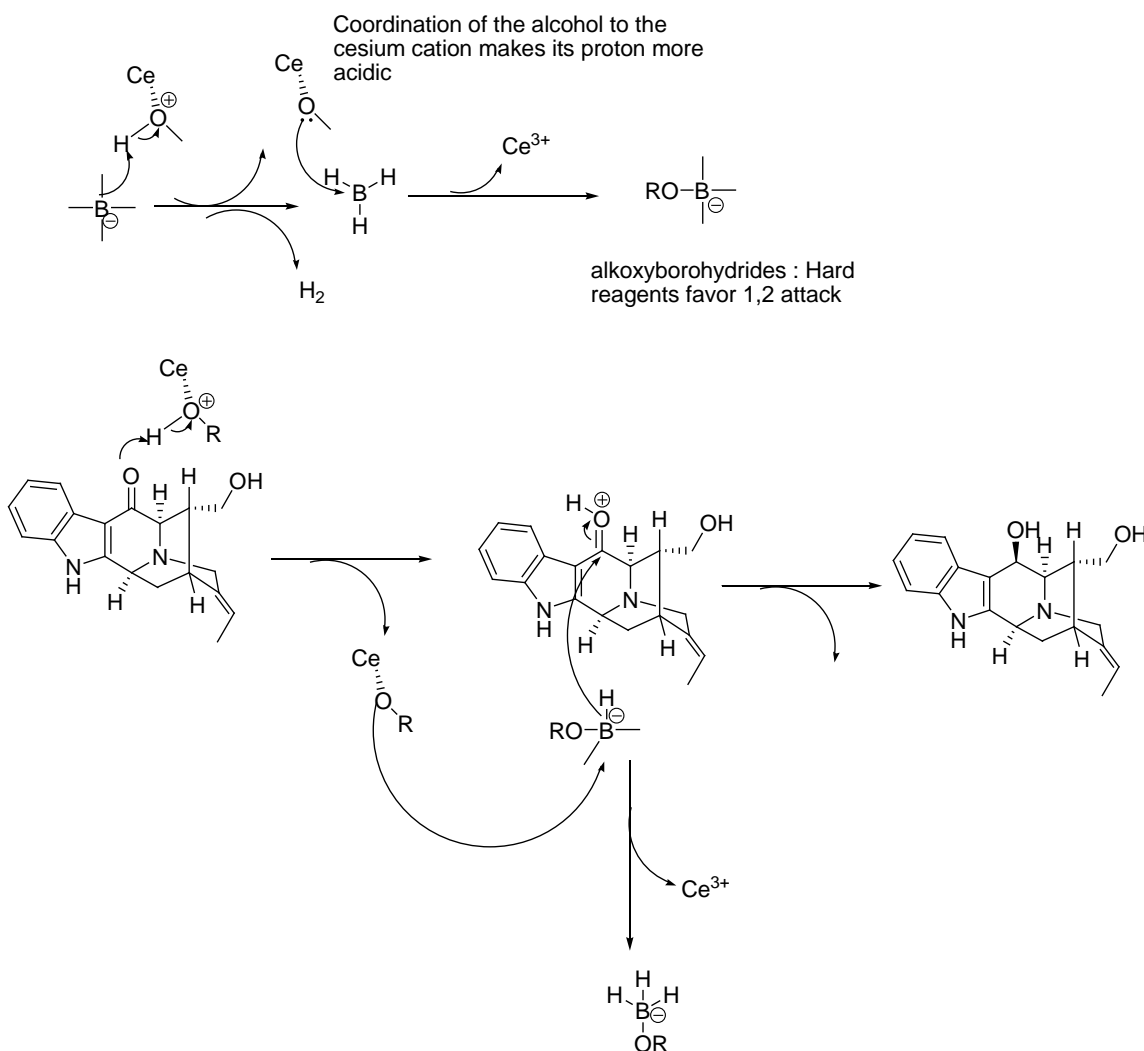
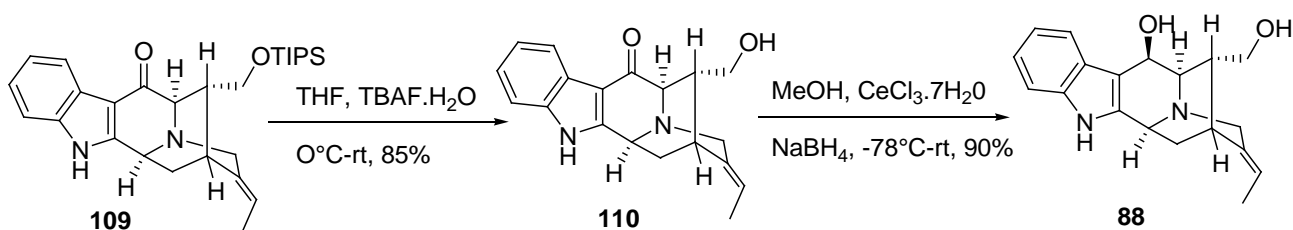
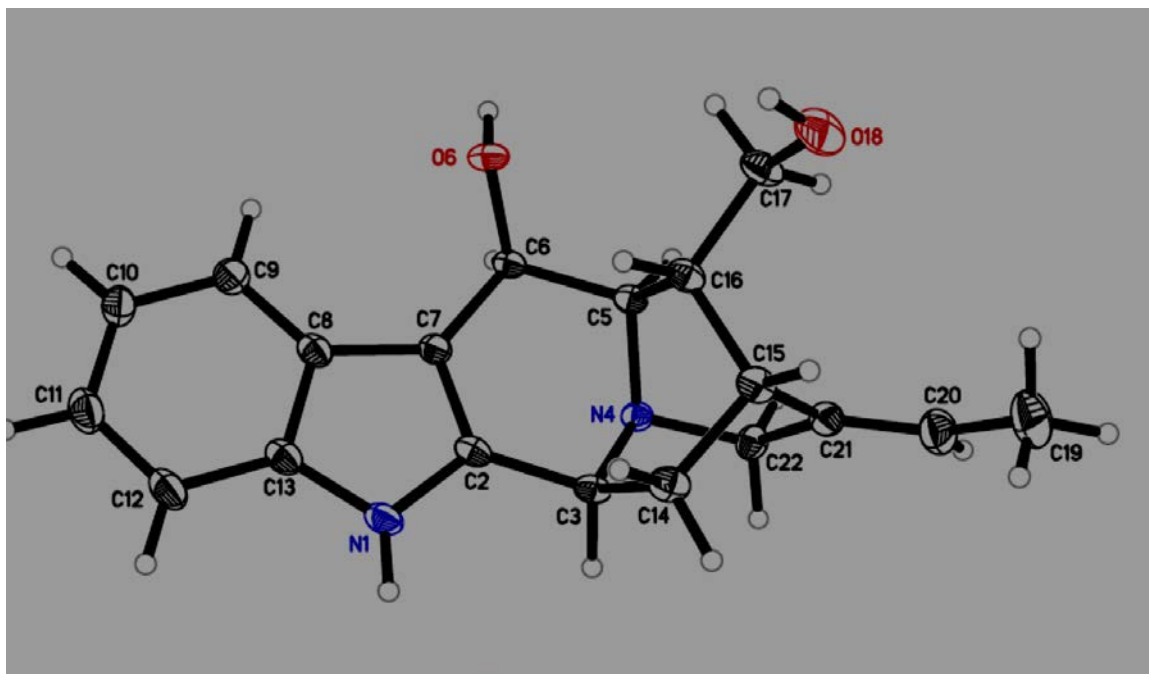


Figure 9. ORTEP View of the Crystal Structure of the Diol **88** which shows the alpha hydrogen at C-6 with C-5



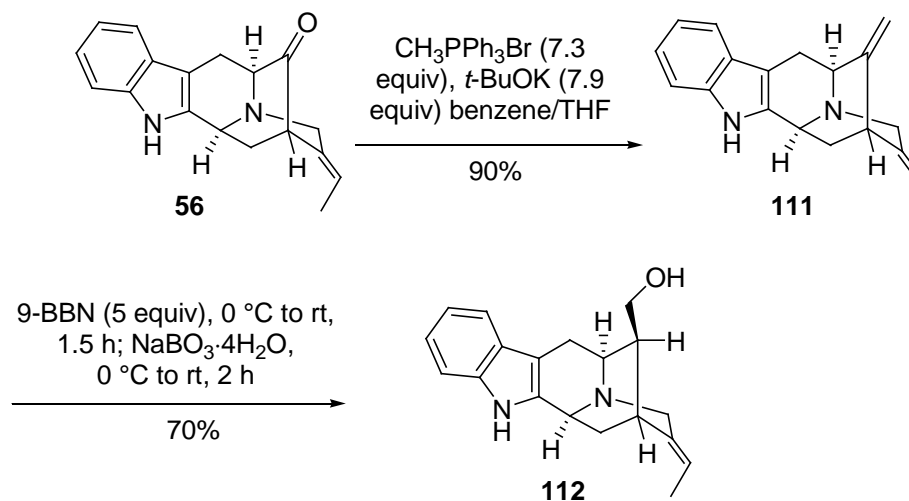
Since the optical rotation of diastereomer **88** obtained was not in agreement with the literature which was $+29.5^{40,136,137}$ the focus of this research turned towards the synthesis of the N_a -H axial alcohol at the C-16 position proposed by Yunusov¹³⁶ in order to construct the diastereomer with the polyneuridine-related stereochemistry in an enantiospecific fashion.

3.1.4. Completion of the regiospecific, stereospecific total synthesis of ervincidine proposed by Yunusov¹³⁶

The synthesis of E-16-epinormacusine B **112** began with the pentacyclic ketone **56**. The E-16-epinormacusine B **112** was obtained from **56** via a Wittig reaction which was carried out with triphenylphosphonium bromide in benzene, in the presence of potassium *t*-butoxide to afford the diene **111** in 90% yield. When the two double bonds in the diene

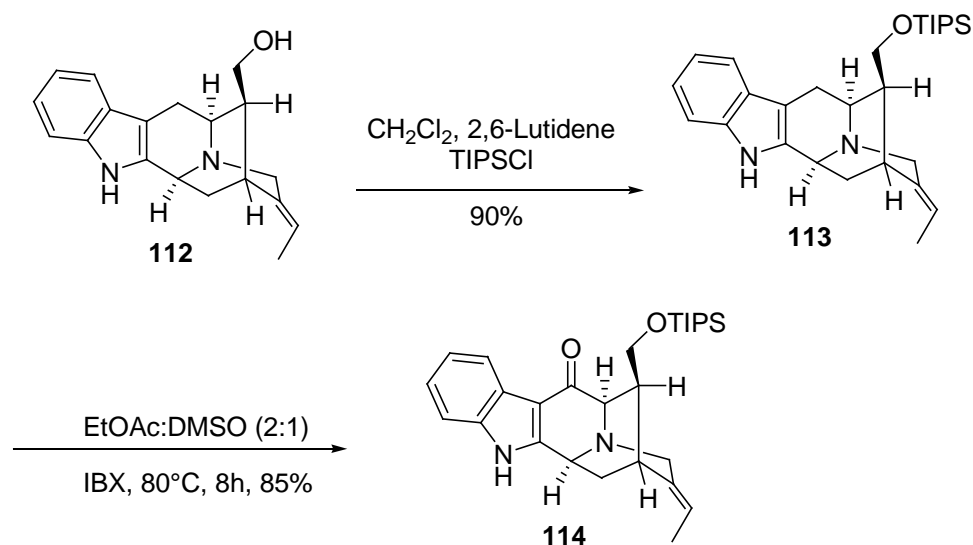
111 are compared it was felt the less hindered double bond at C(16)-C(17), relative to the ethylidene at C(19)-C(20) would be more easily oxidized with a hindered hydroborating reagent. This was in agreement with the earlier work of Magnus and Cook et al. Treatment of diene **111** with the 9-BBN reagent was chosen as the hydroborating agent to facilitate attack from the less hindered face of the C(16)-C(17) double bond relative to the C(19)-C(20) site. This also hinders the formation of the N_b-9-BBN complex which might hinder attack from the alpha face of the molecule. If it became important to obtain the alcohol with the alpha stereochemistry at C-6, simple epimerization (H⁺) should be effective based on the previous results shown here for the epimerization of **111**.

Scheme 23



The synthesis of ketone **114** from alcohol **112** was carried out analogous to the previous preparation of the TIPS derivative **108** from alcohol **107** in 90% yield. The oxidation of the C-6 position was achieved by radical oxidation using IBX^{165,166} in 85% yield.

Scheme 24



As shown in Scheme 25, the silyl group from ketone **114** was removed by treatment with wet TBAF in THF to give **115** in 90% yield. The selective reduction of the ketone **115** was done by a Luche reduction to achieve the stereospecific synthesis of the natural product ervincidine **89** as a single diastereomer in 90% yield. The optical rotation of **89** $[\alpha]_D^{26} +29.00^\circ$ (c 0.6, in methanol) was in agreement with that of the literature¹³⁶ $[\alpha]_D^{26} +29.5^\circ$ (c 0.6, in methanol) which completed the first enantiospecific, stereospecific total synthesis of the natural product ervincidine **89** (Scheme 25). The analysis of the spectral data of the alkaloid **89** follows here.

Scheme 25

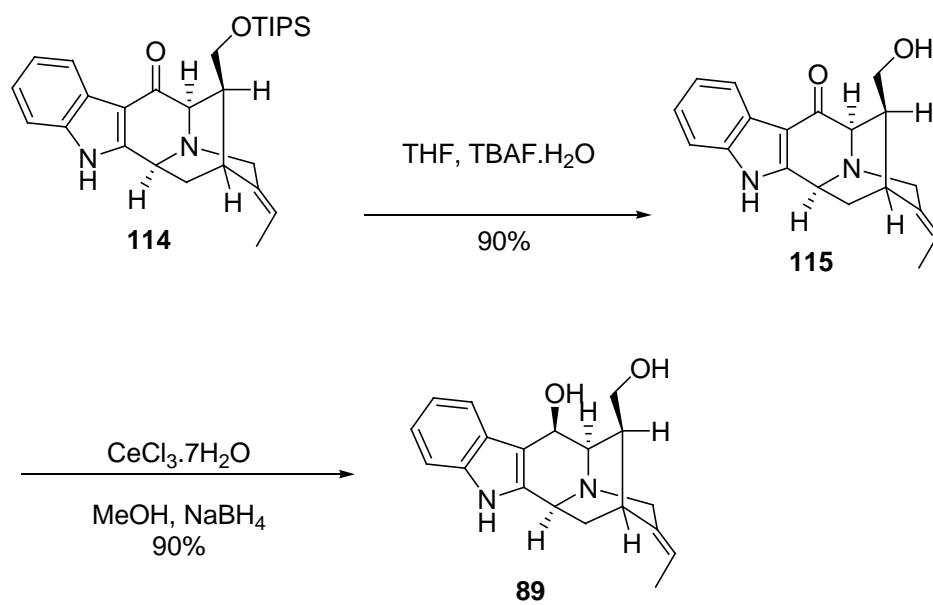


Figure 10: Proton spectrum of natural product Ervincidine 89

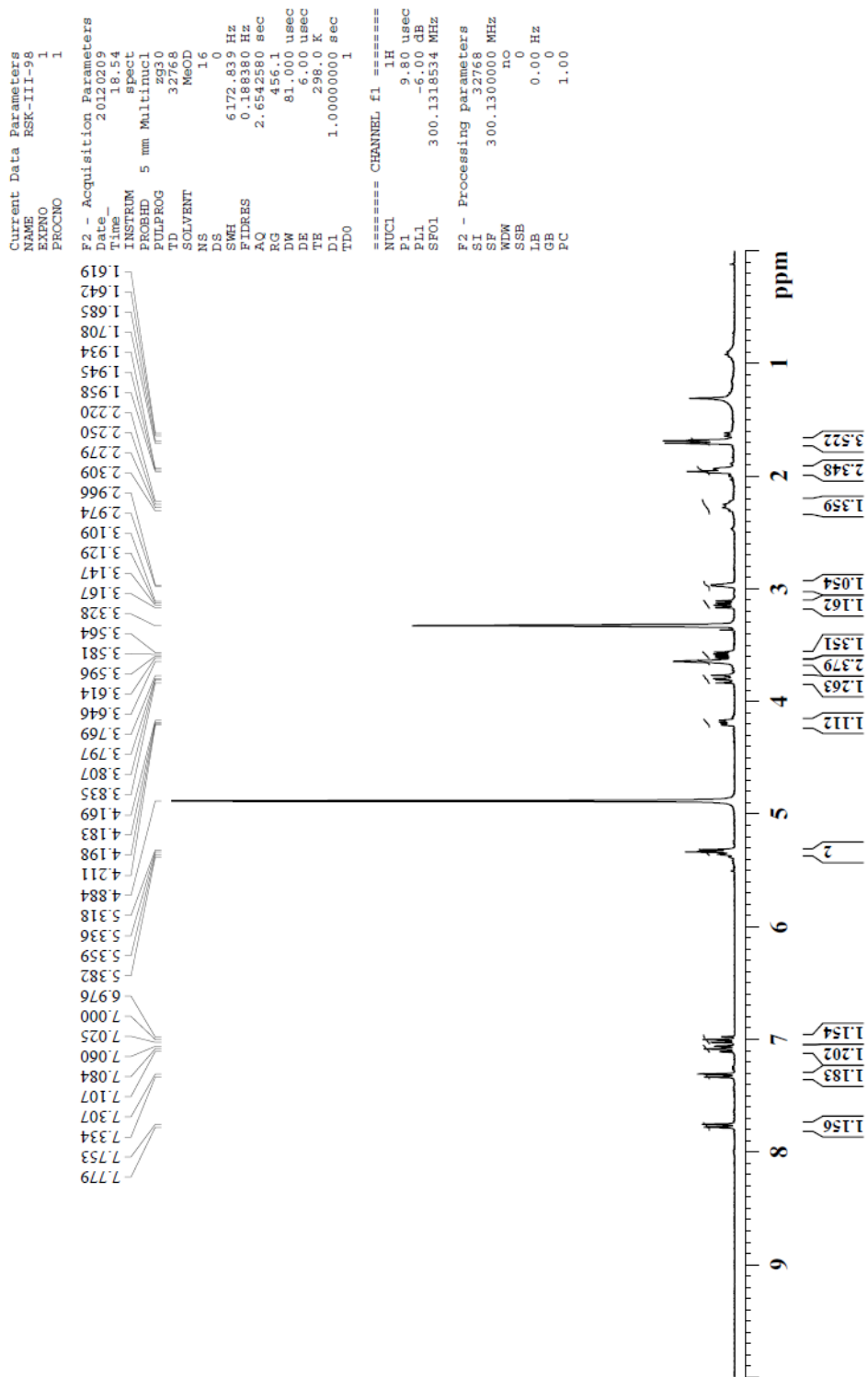
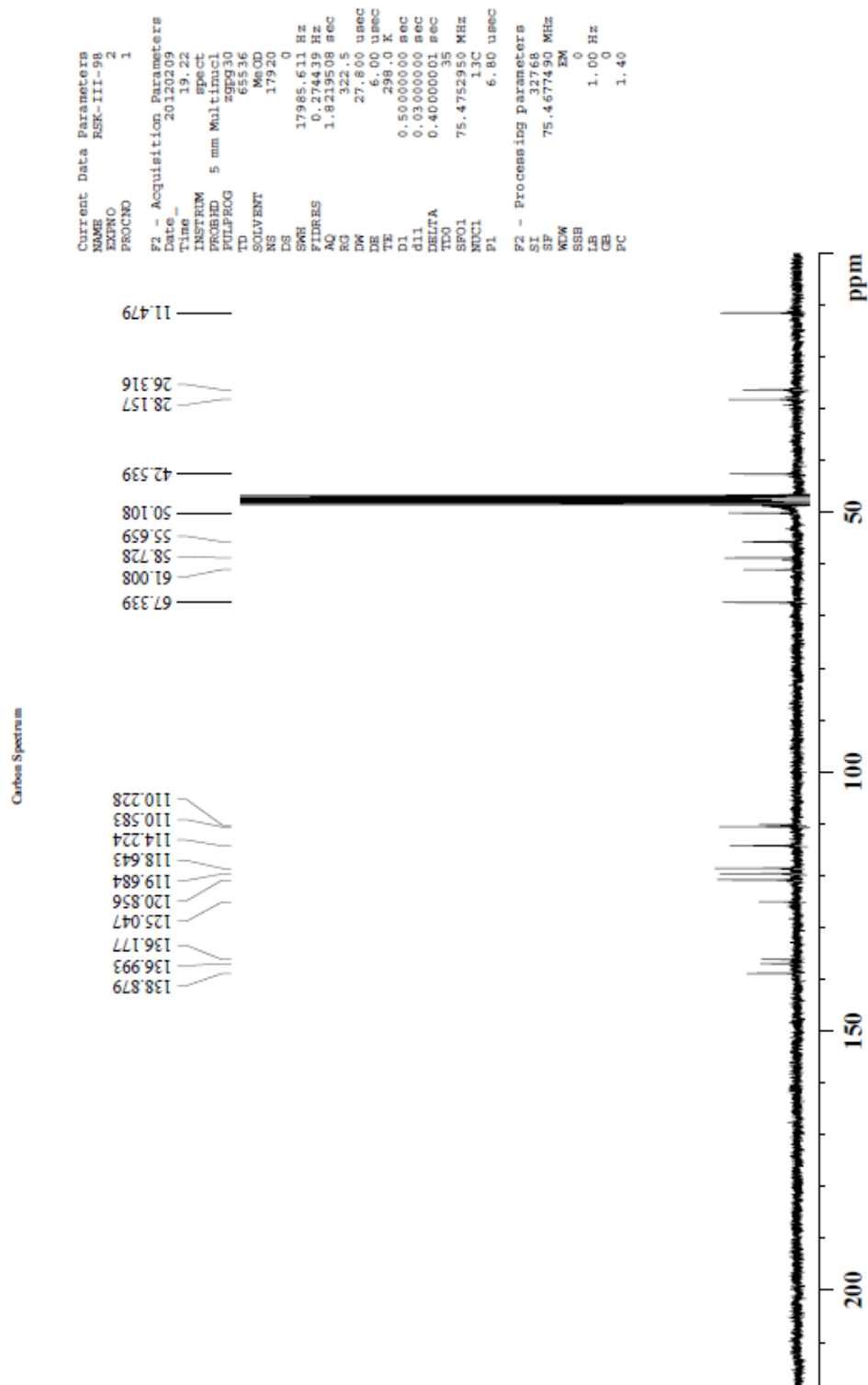


Figure 11: Carbon spectrum of natural product ervincidine **89**



To assign the stereochemistry of the C-6 alcohol a detailed study of the 1D and 2D NOESY experiments were carried out on the synthetic diol **89**. The methyl group (3H-18) detected as a three proton doublet showed strong connectivity only to H-19. The proton of the aromatic ring at H-9 and H-6, showed a weak NOE. No NOEs were found between H-15 and H-6. The protons of H-15 exhibited a strong NOE with H-17, H-16, H-14 and H-18. The proton of H-6 showed strong NOE with H-5. A weak NOE was observed between the protons labeled H-6 and H-3.

Figure 12. Selected NOEs of ervincidine **89**

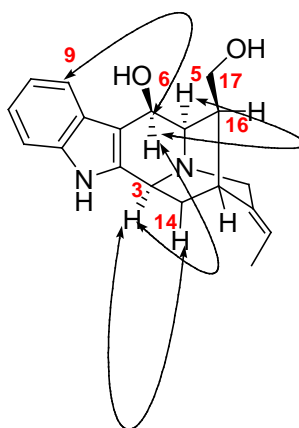
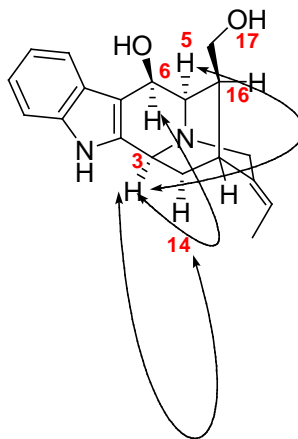
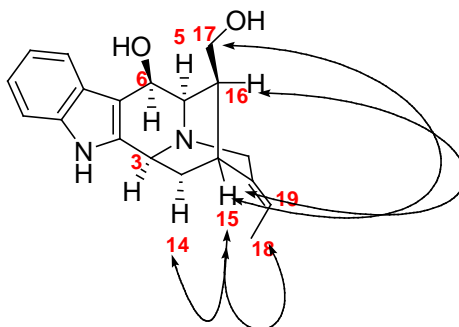


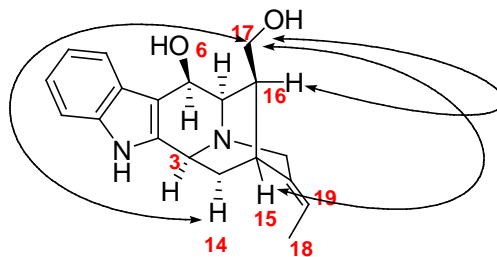
Figure 13. 1D NOEs Observed after Irradiation of Protons at H-3

Analysis of the 2D NOESY experiments (Figure 12) further confirmed, the result obtained by the 1D NOESY experiments. Good NOEs were found between H-3 and H-5 (strong) and H-14 (strong). The irradiation of the proton at C-3 resulted in the enhancement of the signals at H-5 and H-14, indicating that the protons at H-3 and H-5 (see **Figure 13**) were located in the pseudo axial position. These results were supported by examination of the 2D NOE spectrum for H-6 which exhibited cross peaks at H-5 (strong).

Figure 14. 1D NOEs Observed after Irradiation of Protons at H-15

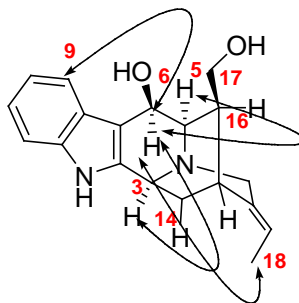
The 1D NOE signals were observed between H-15 and H-18 (strong), H-17 (strong), H-16 (strong) and H-14 (strong). The strong NOE between H-15 and with one of the H-17 protons and not an NOE with the other proton at H-17 indicated that one proton at C-17 was located in the α position while the other proton located at C-17 was found to be β . The NOE signals between H-15 and H-18 (strong), H-19 (weak) and H-5 (weak) were in agreement with the assignment.

Figure 15. 1D NOEs Observed after Irradiation of Protons at H-17

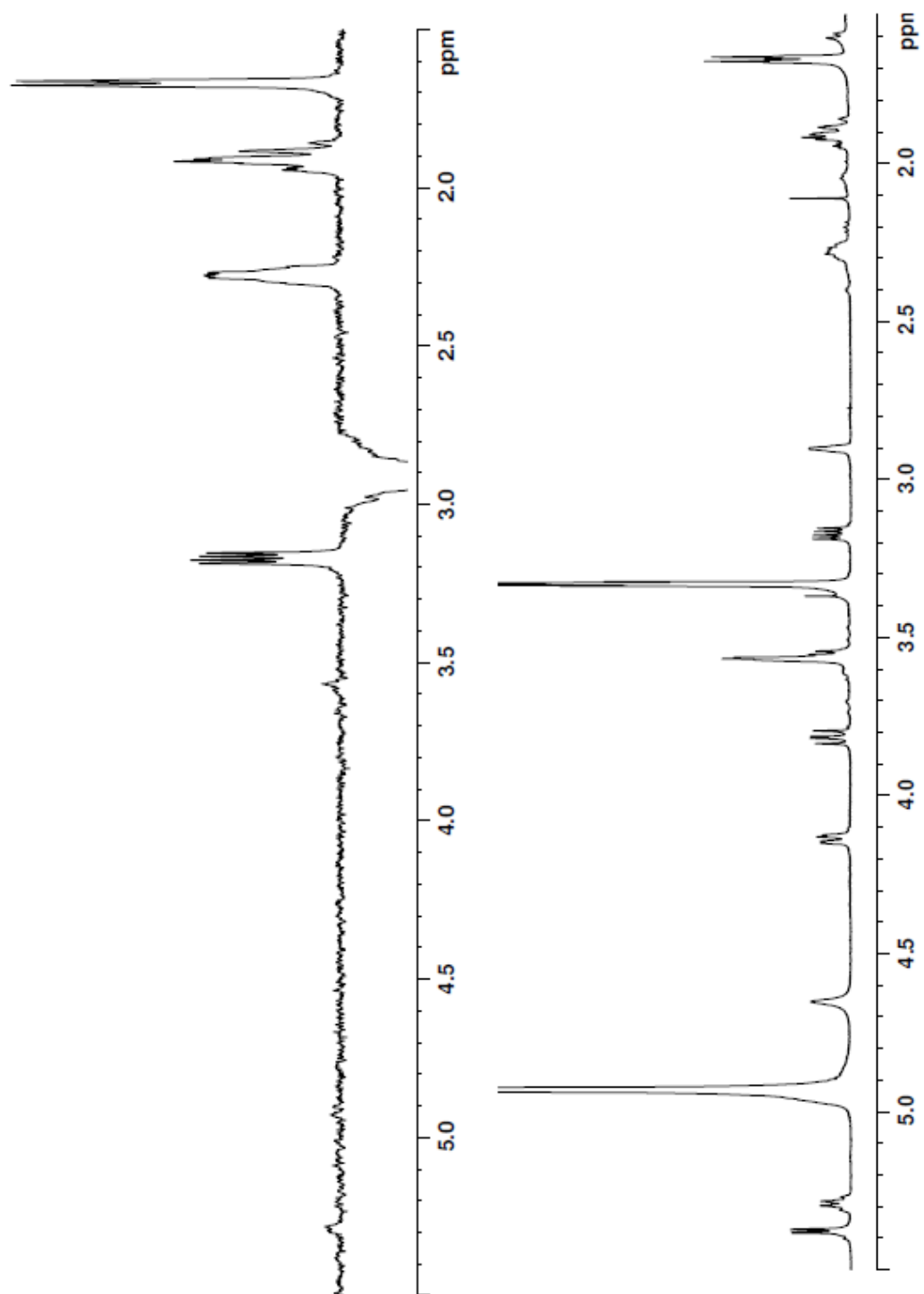


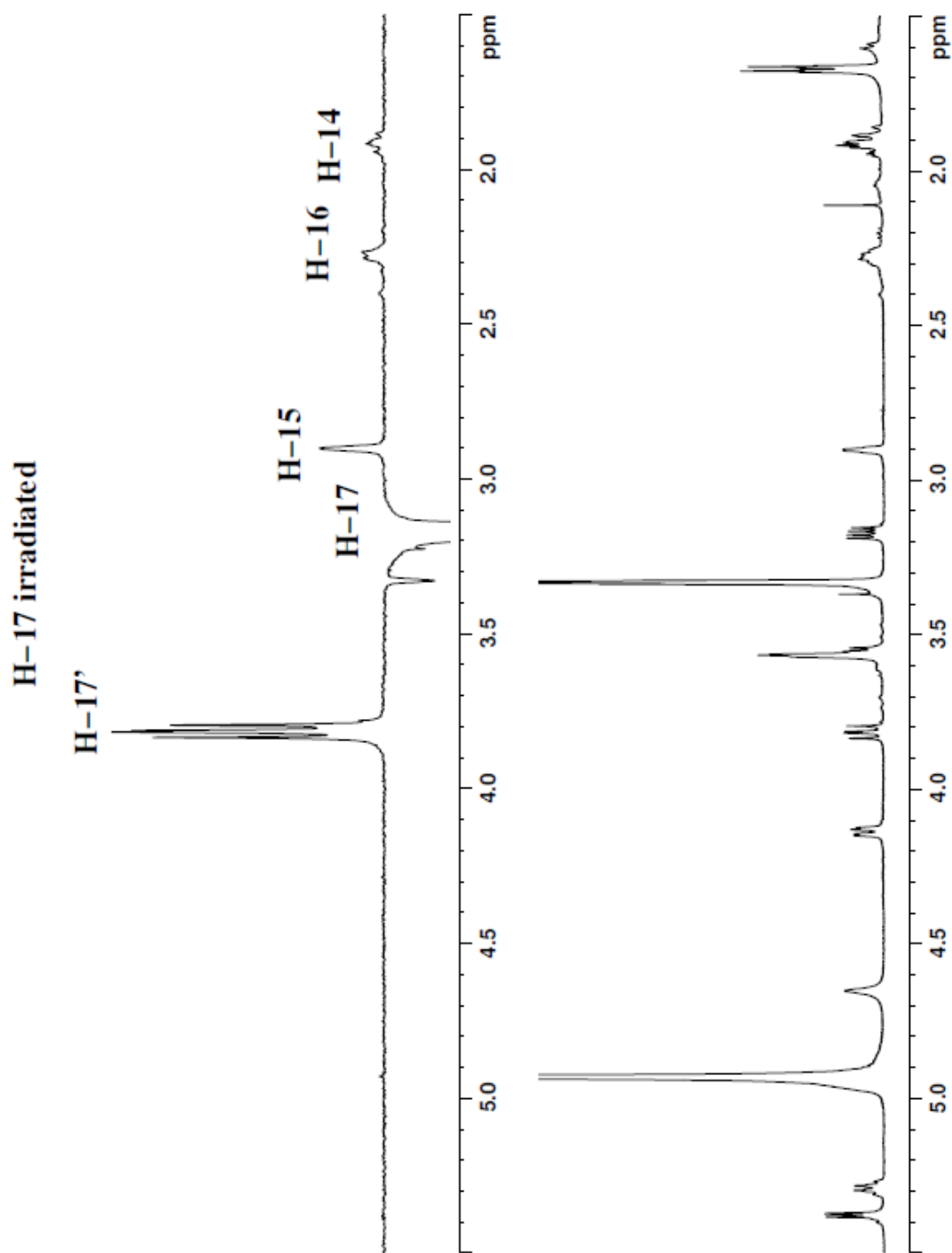
The 2D NOE signals observed between the two proton at C-17 were very strong. The signals between H-17 and H-15 (strong), H-17 and H16 (strong) and H-17 and H-14 (strong) were also strong.

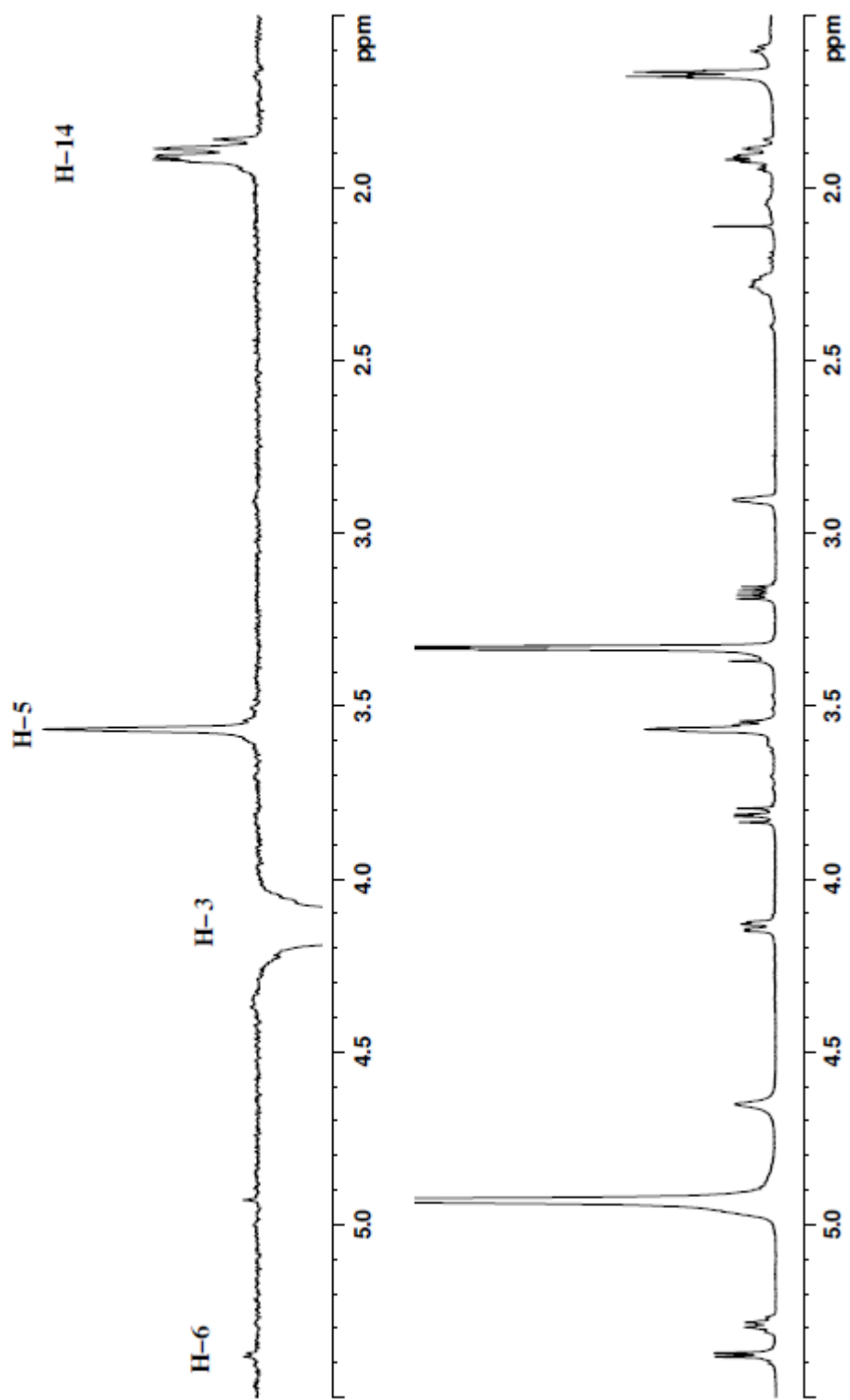
Figure 16. 1D NOEs Observed after Irradiation of Protons at H-6

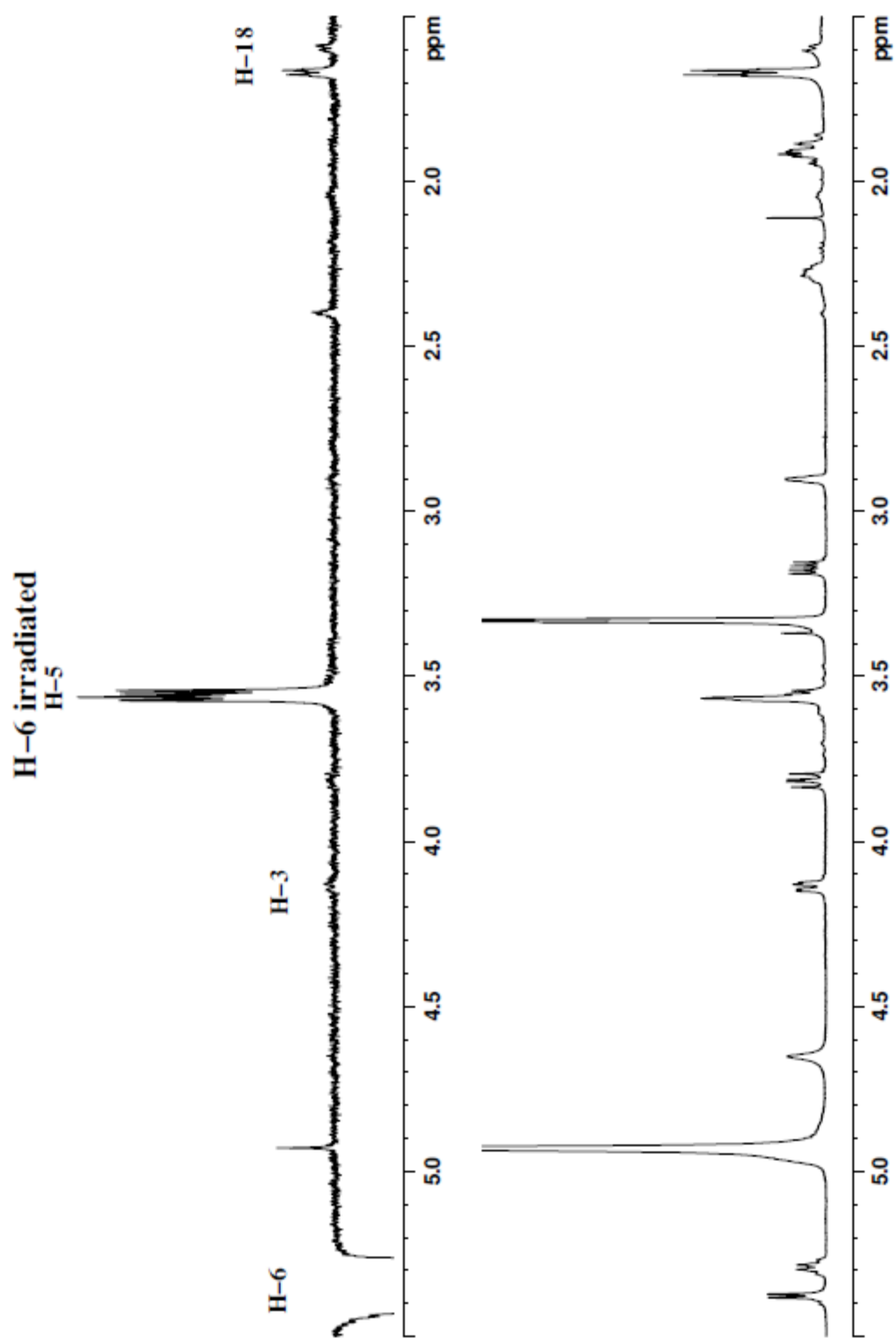


The 1D NOE signal observed between H-6 and H-5 was very strong and the NOE between H-6 and H-3 was weak. No NOE is seen between H-6 and H-15. Weak NOE signals are found between H-6 and H-9 as well as H-6 and H-18. The NOE signal between H-5 and H-16 was strong with a coupling constant of 9.8 Hz, consequently the dihedral angle between the protons at H-5 and H-16 was close to 0° (eclipsed conformation). A weak NOE was observed between H-3 and H-6. The coupling constant between H-5 and H-6 was 5.1 Hz which indicated that both the protons were cis to each other. The angle between both the H-5 and H-6 protons was about 60° (staggered conformation) from models. Both the alcohol at C (17) and the proton at the C-6 position are trans to each other. If the OH were axial and the proton at H-6 were equatorial, a strong NOE would have been observed with H-15 which in this case was not seen. In summary, the 2D COSY, NOESY and 1D NOE experiments support the structure of ervincidine **89**, as indicated in Scheme 25.

Figure 17. 1D NOE data H-15 irradiated



H-3 irradiated



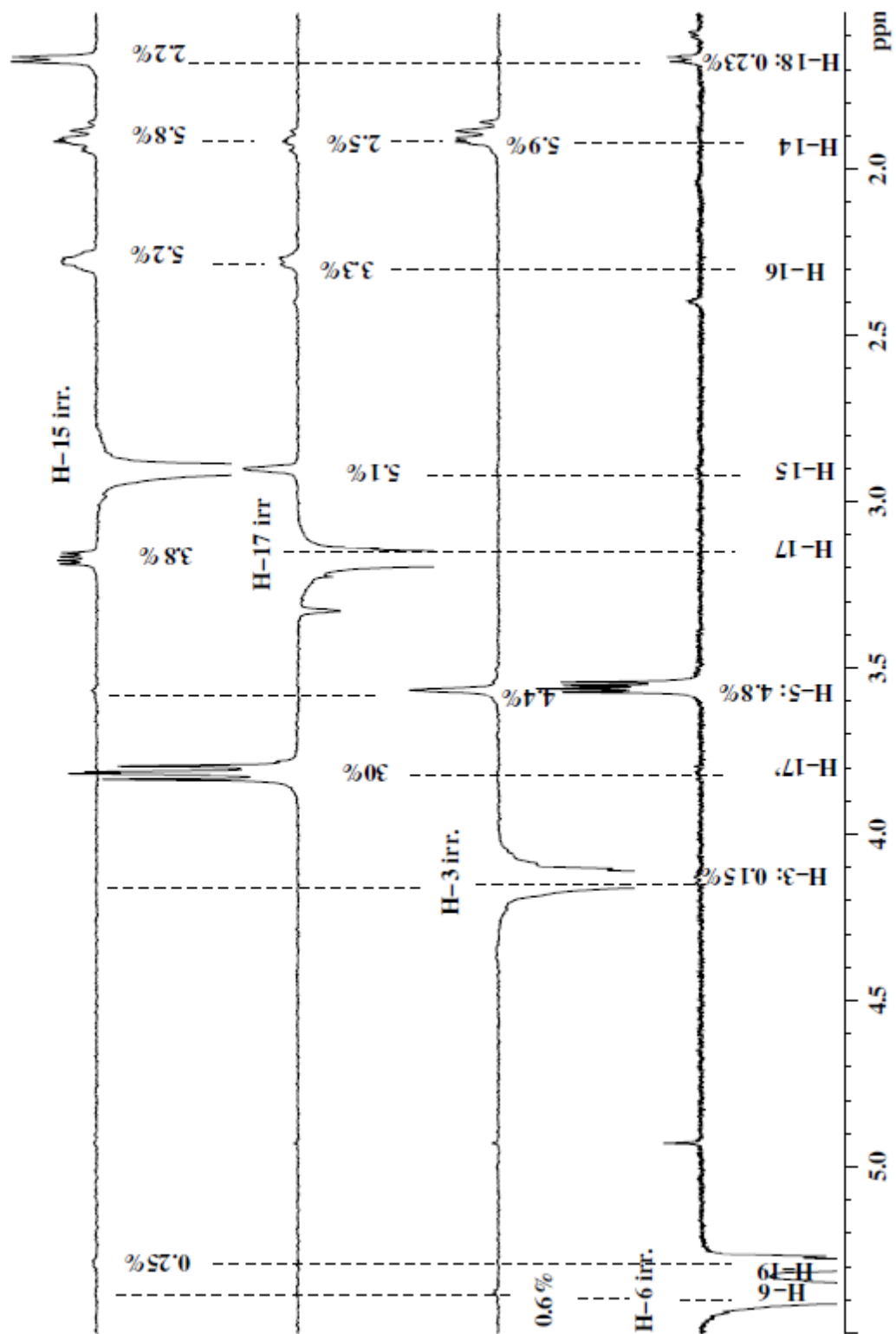
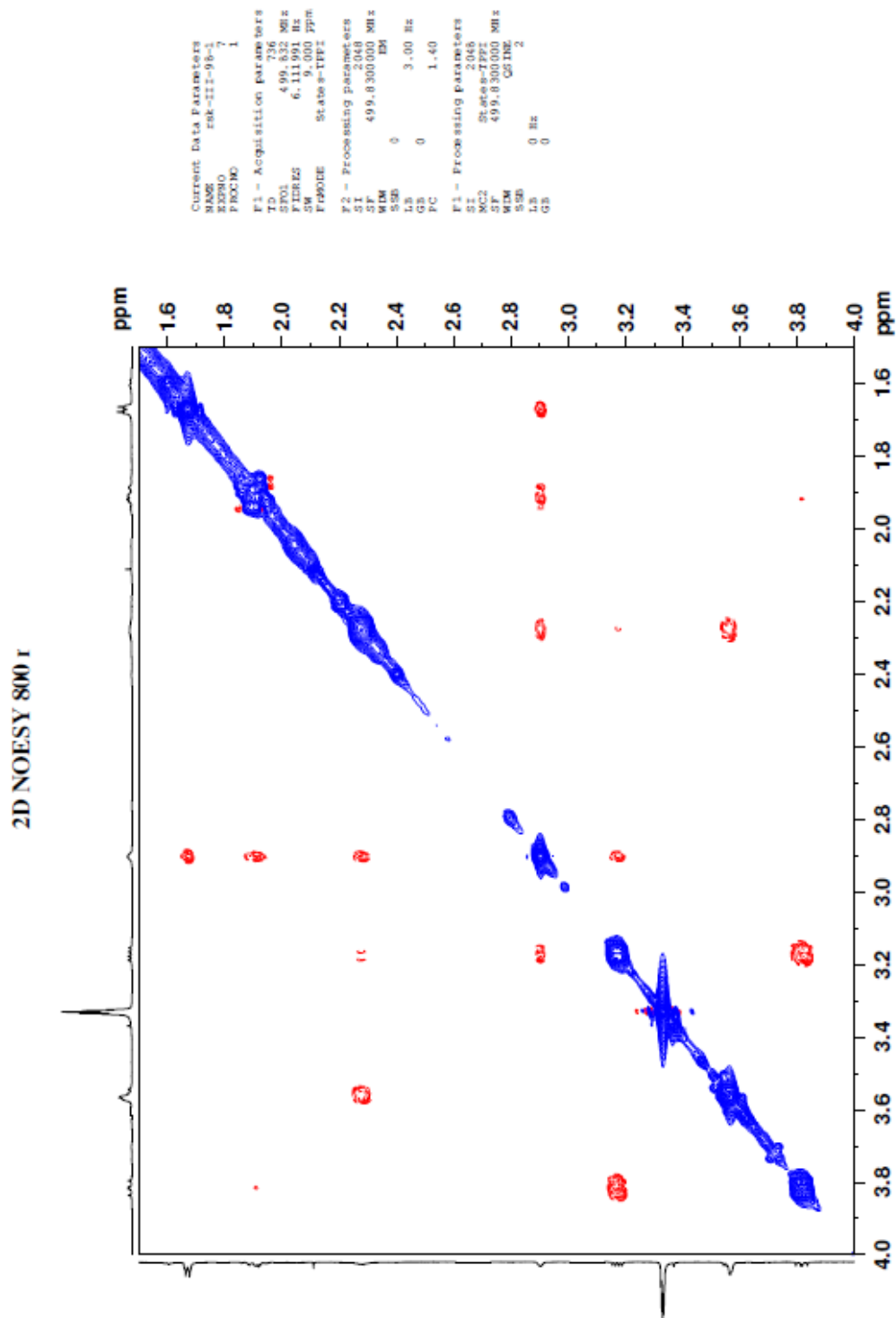


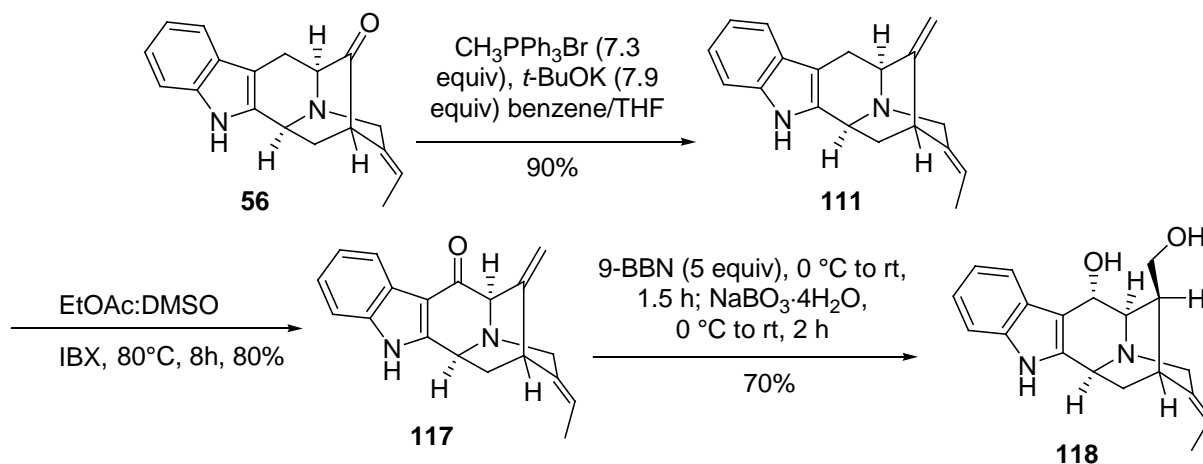
Figure 18. 2D NOESY of ervincidine 89



3.1.5. Completion of the regiospecific, stereospecific total synthesis of the diastereomer (**118**) of Ervincidine

To synthesize the diastereomer with the opposite stereochemistry to that of ervincidine **89** at the C-6 position, diene **111** was treated with IBX to give the ketone **117** at the C-6 position in 80% yield. In order to shorten the synthetic route and also synthesize the other isomer, 9-BBN was chosen which reduces the C-6 keto group to the alcohol and also acts as a hydroborating agent.^{167,168} Since 9-BBN is a bulky group the attack might take place from the top face of the molecule. The boron might coordinate with the C-6 carbonyl oxygen as well as the N_b nitrogen atom thus leading to the formation of the alpha diastereomer **118**. This process was executed as shown in scheme 26 in 70% yield. The optical rotation of **118** [α]_D²⁶ +17.00° (c 0.6, in methanol) was not in agreement with the literature.^{40,137} It is entirely possible that 9-BBN complexed^{127,169} with the N_b-nitrogen function and blocked the attack from the bottom face of the ketone so that the carbonyl reduction occurred from the top face to give **118**.

Scheme 26



4. Conclusion

In conclusion, the first enantiospecific, stereospecific total synthesis of ervincidine **89** has been accomplished from commercially available D-(+)-tryptophan **37** which has served both as the chiral auxiliary and the starting material. Moreover, this is the first synthesis which unequivocally sets the stereochemistry of the hydroxyl group at C-6 in stereospecific fashion, as well as the C-16 hydroxy methyl group. The stereospecific conversion of D-(+)-tryptophan **37** into the key template (-)-*N*_a-H, *N*_b-benzyl tetracyclic ketone **49** via the asymmetric Pictet-Spengler reaction (600 gram scale) and Dieckmann cyclization on multi-hundred gram scale was reduced to only two reaction vessels. The optically active tetracyclic ketone **49** was converted into the core pentacyclic framework **56** using the intramolecular palladium-mediated enolate cross coupling reaction which was developed here in Milwaukee¹³⁰ to afford the core pentacyclic framework **56**. This robust reaction could be scaled up to multigram scale in this series. Important to success here were the sequence of chemical reactions which included a Wittig reaction, a regiospecific hydroboration and protection/deprotection steps in order to provide regiospecific oxidation at C-6. The IBX mediated oxidation and the Luche reduction using CeCl₃ · 7H₂O in the presence of NaBH₄ afforded the first enantiospecific, stereospecific total synthesis of ervincidine **89**. The indole alkaloid ervincidine **89** could be prepared from D-(+)-tryptophan **37** in 13 reaction vessels in 19.2% overall yield. Another important experiment was the epimerization of the C-6 alcohol with 0.2N HCl which indicated the care that must be employed in isolation of these alkaloids which contain a benzylic hydroxyl group. This research process developed here also provides a

general entry into C-6 hydroxy substituted indole alkaloids either alpha or beta stereochemistry.

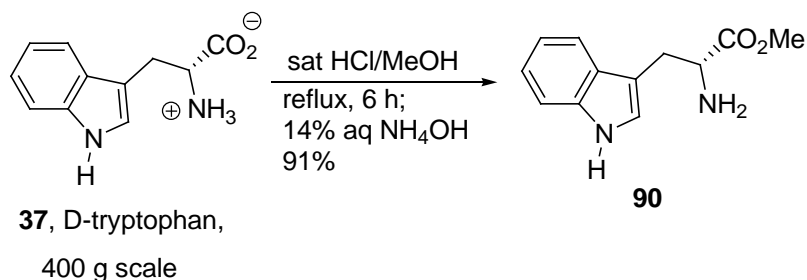
Two other diastereomers were made to rule them out as potential structures. This research corrects the errors in Glasby's book¹³⁷ and Lousnamma's review⁴⁰ and clarifies the work of Yunusov et al as well as providing the correct absolute configuration of the C-6 hydroxyl function in ervincidine **89**.¹³⁶

5. Experimental Details

General Experimental Considerations:

All reactions were carried out under an argon atmosphere with dry solvents using anhydrous conditions unless otherwise stated. Tetrahydrofuran (THF) and diethyl ether were freshly distilled from Na/benzophenone ketyl prior to use. Dichloromethane was distilled from calcium hydride prior to use. Methanol was distilled over magnesium sulfate prior to use. Benzene and toluene were distilled over Na prior to use. Acetonitrile was distilled over CaH₂ prior to use. Reagents were purchased of the highest commercial quality and used without further purification unless otherwise stated. Thin layer chromatography (TLC) was performed using Dynamic Adsorbents Inc. UV active silica gel, 200 μm, plastic backed plates or; Dynamic Adsorbents Inc. UV active alumina N, 200 μm, F-254 plastic backed plates. Flash and gravity chromatography were performed using silica gel P60A, 40-63 μm purchased from Silicycle. Basic alumina (Act I, 50-200 μm) for chromatography was purchased from Dynamic Adsorbents. Neutral alumina (Brockman I, ~150 mesh) for chromatography was purchased from Sigma-Aldrich. TLC

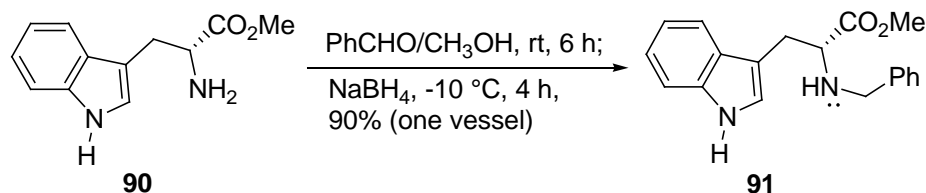
plates were visualized by exposure to short wavelength UV light (254 nm). Indoles were visualized with a saturated solution of ceric ammonium sulfate in 50% sulfuric acid.¹⁷⁰ Elemental analyses were performed on a Carlo Erba model EA-1110 carbon, hydrogen, and nitrogen analyzer. All samples submitted for CHN analyses were first dried under high vacuum for a minimum of six hours using a drying pistol with isopropyl alcohol or benzene as the solvent with potassium hydroxide pellets in the drying bulb. Melting points were taken on a Stuart melting point apparatus SMP3 manufactured by Barloworld Scientific US Ltd. Proton (¹H NMR) and carbon high resolution nuclear magnetic resonance spectra (¹³C NMR) were obtained on a Bruker 300-MHz or a GE 500-MHz NMR spectrometer. ¹H NMR data are reported as follows: chemical shift, multiplicity (s = singlet, d = doublet, t = triplet, q = quartet, dd = doublet of doublets, dt = doublet of triplets, ddd = doublet of doublet of doublet, td = triplet of doublets, qd = quartet of doublets, sex = sextet, m = multiplet), integration, and coupling constants (Hz). ¹³C NMR data are reported in parts per million (ppm) on the δ scale. The low resolution mass spectra (LRMS) were obtained as electron impact (EI, 70eV), which were recorded on a Hewlett-Packard 5985B gas chromatography-mass spectrometer, while high resolution mass spectra (HRMS) were recorded on a VG Autospec (Manchester, England) mass spectrometer. HRMS recorded by electrospray ionization (ESI) methods were performed at the Laboratory for Biological Mass Spectrometry at Texas A&M University on a API QStar Pulsar model, manufactured by MDS Sciex. Optical rotations were measured on a JASCO Model DIP-370 digital polarimeter. Infra-red spectra were recorded on a Thermo Nicolet Nexus 870 FT-IR or a Perkin Elmer 1600 series FT-IR spectrometer.



D-(-)-Tryptophan methyl ester **90**

To a round bottom flask (5000 mL) which contained a freshly saturated solution of anhydrous methanolic hydrogen chloride (2500 mL), D-(+)-tryptophan **37** (400 g, 1.96 mol) was added. The mixture which resulted was heated to reflux for 8 h and then allowed to cool to rt. The crystalline product which formed upon cooling was collected by filtration and washed with cold ether to provide D-(-)-tryptophan methyl ester·HCl. The free base **90** was prepared by treatment of the corresponding HCl salt with cold aq NH₄OH (10%), followed by extraction with CH₂Cl₂ in methanol (4:1, 3 x 1000 mL). The solvent was evaporated under reduced pressure, after which the solid was redissolved in CH₂Cl₂ and dried (K₂CO₃). The DCM layer was removed under reduced pressure to provide D-(-)-tryptophan methyl ester **90** (392 g, 91%). **mp** 92-93 °C (free base); $[\alpha]_D^{27} = -37.2$ (*c* 1.0 in MeOH); **IR** (KBr) 1730 cm⁻¹; **¹H NMR** (250 MHz, CDCl₃, free base) δ 1.62 (2H, s), 3.05 (1H, dd, *J* = 14.5, 7.5 Hz), 3.29 (1H, dd, *J* = 14.6, 5.8 Hz), 3.74 (3H, s), 3.86 (1H, dd, *J* = 7.5, 4.8 Hz), 7.04-7.23 (3H, m), 7.35 (1H, d, *J* = 7.5 Hz), 7.61 (1H, d, *J* = 7.5 Hz), 8.24 (1 H, s); **¹³C NMR** (62.8 MHz, CDCl₃, free base) δ 30.83, 51.86, 55.06, 111.19, 118.73, 119.49, 122.11, 122.87, 127.57, 136.37, 175.71; **EIMS** (*m/e*, relative

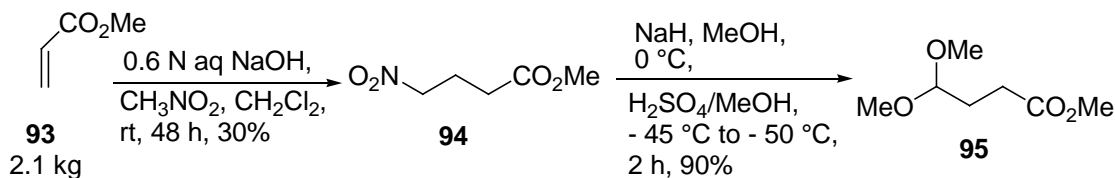
intensity) 218 (M^+ , 78), 159 (57), 130 (100), 117 (33). **Anal. Calcd. for $C_{12}H_{14}O_2N_2$:** C, 66.06; H, 6.42, N, 12.84. Found: C, 66.14; H, 6.33; N, 12.77.



D-(+)- N_1 -Benzyltryptophan methyl ester **91**

To a round bottom flask (3000 mL) which contained a solution of D-(-)-tryptophan methyl ester **90** (408 g, 2.0 mol) in dry CH_3OH (1500 mL), benzaldehyde (260.0 g, 2.3 mol) was added. The solution which resulted was stirred with an overhead stir for 6 h at 22 °C, until examination by TLC (silica gel) indicated the disappearance of **90**. The mixture was then cooled in an ice-salt bath to -5 °C [It was much easier to maintain the inside temperature between -10°C to -5°C by the employment of a dry ice bath (without solvent)]. If the temperature falls below -15°C, a large amount of solid will appear and it is too difficult to stir the reaction mixture. Sodium borohydride (42 g, 1.1 mol) was then added portionwise at -5 °C over a period of 2.5 h [The slow addition and lower temperature of this process are critical to avoid racemization of the chiral center]. The solution was allowed to stir for 3 h and then followed by the addition of ice water (50 mL). The solvent was removed under reduced pressure. The residue was dissolved in CHCl_3 (2000 mL) and washed with brine (2 x 500 mL). The organic layer was dried (K_2CO_3) and the solvent was removed under reduced pressure to give the free base **3** (525 g, 90%) which could be further purified by crystallization from EtOH. **mp** 109-110 °C;

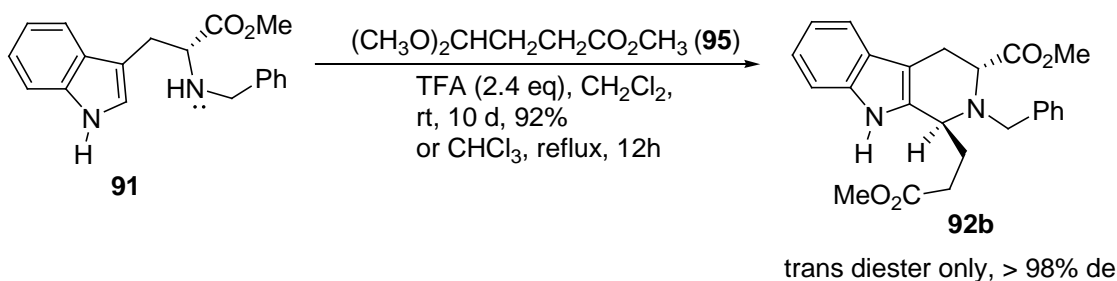
$[\alpha]_D^{22} = +9.07^\circ$ (c 1.0 in CH_3OH), [lit.¹⁵² $[\alpha]_D^{22} = +8.65^\circ$ (c 1.0 in CH_3OH)]; **IR** (film) 1745 cm^{-1} ; **$^1\text{H NMR}$** (250 MHz, CDCl_3) δ 2.10 (1H, s), 3.15 (2H, m), 3.65 (3H, s), 3.75 (3H, s), 3.80 (3H, m), 6.90 (1H, s), 7.10 (1H, t, $J = 8.2$ Hz), 7.25 (5H, m), 7.55 (1H, d, $J = 8.2$ Hz); **$^{13}\text{C NMR}$** (62.8 MHz, CDCl_3) δ 29.35, 51.68, 52.20, 61.38, 111.18, 111.38, 118.84, 119.45, 122.07, 122.88, 127.03, 127.62, 128.19, 128.32, 136.30, 139.79, 175.36; **EIMS** (m/e , relative intensity) 308 (M^+ , 28), 249 (22), 178 (57), 130 (100).
Anal. Calcd. for $\text{C}_{19}\text{H}_{20}\text{O}_2\text{N}_2$: C, 74.03; H, 6.49; N, 9.08. Found: C, 73.99; H, 6.56; N, 8.99.



Preparation of methyl 4,4-dimethoxybutyrate 95¹⁷¹

To a round bottom flask (12 L) equipped with an overhead stir which contained a solution of methyl acrylate **93** (1075 g, 12.5 mol) and nitromethane (762.5 g, 12.5 mol) in CH_2Cl_2 (2500 mL) at 0 °C, was added a solution of NaOH (60 g) in water (2500 mL) at 0 °C. The mixture which resulted was stirred at rt for 48 h. The organic layer was separated and washed with water (2 x 500 mL) and dried (MgSO_4). The solvent was then removed under reduced pressure and the residue was distilled under reduced pressure (95-100 °C/8 mm of Hg) to give the pure methyl γ -nitro butyrate **94** (540 g, 30%). This was dissolved in methanolic sodium methoxide [5400 mL, 0.8 N, freshly prepared from 173 g of NaH (60% dispersion in mineral oil)] and the solution which resulted was added dropwise with

an overhead stirrer at a rate of 1 drop per second to a round bottom flask (12 L) which contained a solution of conc sulfuric acid (1350 mL) in methanol (4050 mL) at -45 to -50 °C. After the addition was completed, the reaction mixture was poured into CH₂Cl₂ (8 L). The organic layer was separated and washed with ice water (2 x 1000 mL), aq 4 N NaOH (2 x 600 mL) and dried (K₂CO₃). The solvent was removed under reduced pressure and the residue was distilled (110-115 °C/8 mm of Hg) to provide methyl 4,4-dimethoxybutyrate **95** (540 g, 90%). ¹H NMR (250 MHz, CDCl₃) δ 1.92 (2H, q, *J* = 7.5 Hz), 2.37 (2H, t, *J* = 7.5 Hz), 3.31 (6H, s), 3.66 (3H, s), 4.38 (1H, t, *J* = 15.8 Hz); ¹³C NMR (62.8 MHz, CDCl₃) δ 27.92, 29.07, 51.45, 53.14, 103.14; CIMS (*m/e*, relative intensity) 375 (M⁺ + 1, 100). The spectral data for **95** were identical to the published values.¹⁷¹

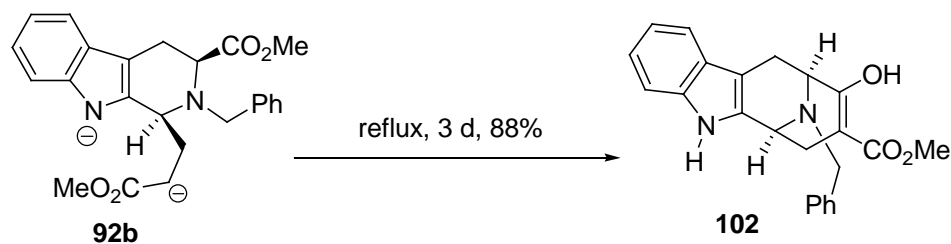


Diastereospecific preparation of the *trans*-(1*S*,3*R*)-(-)-2-benzyl-3-methoxycarbonyl-1-methoxycarbonylethyl-1,2,3,4-tetrahydro-9*H*-pyrido-[3,4-*b*]indole (92b**) via the newly modified Pictet-Spengler reaction.**

To a round bottom flask (5000 mL) which contained a solution of optically active *N*_b-benzyl-D-tryptophan methyl ester **90** (400 g, 1.3 mol) in CH₂Cl₂ (2500 mL) was added methyl 4,4-dimethoxybutyrate acetal **95** (315 g, 1.9 mol) and TFA (180 g, 2.4 eq) at 0 °C

with stirring. The reaction mixture which resulted was allowed to stir at rt for 10 d and then cooled in an ice bath and brought to pH = 8 with a cold aq solution of NaOH (3 N). The aq layer was separated and extracted with CH₂Cl₂ (3 x 1500 mL). The combined organic layers were washed with brine (2 x 600 mL) and dried (K₂CO₃). The volume of the solution was reduced to 300 mL under reduced pressure and EtOAc (100 mL) and hexanes (300 mL) were added to the above solution. The solution was cooled to -20 °C. The *trans* diester **109b** (402 g, 76%) precipitated out as white crystals and the mother liquor was concentrated. The residue which resulted was purified by flash chromatography (silica gel, EtOAc/hexane, 1/4) to provide additional **109b** (83 g, 16%). The combined yield of **92b** (485 g) was 92%. mp 152-153 °C; $[\alpha]_D^{27} = -35.7^\circ$ (*c* 1.4, in CHCl₃), [lit.¹¹⁴ $[\alpha]_D^{27} = -38.0^\circ$ (*c* 1.0 in CHCl₃)]; IR (film) 3310, 1731, 1707 cm⁻¹; ¹H NMR (250 MHz, CDCl₃) δ 1.85-2.15 (2H, m), 2.20-2.50 (2H, m), 3.03 (1H, dd, *J* = 15.8, 5.3 Hz), 3.12 (1H, dd, *J* = 15.8, 8.8 Hz), 3.48 (3H, s), 3.59 (1H, d, *J* = 13.6 Hz), 3.75 (3H, s), 3.84 (1H, d, *J* = 13.6 Hz), 3.87-3.93 (1H, m), 3.98 (1H, dd, *J* = 8.8, 5.3 Hz), 7.07-7.35 (8H, m), 7.43 (1H, d, *J* = 7.2 Hz), 7.98 (1H, s); ¹³C NMR (62.8 MHz, CDCl₃) δ 21.39, 28.94, 29.88, 51.45, 51.85, 53.51, 54.81, 56.79, 107.51, 110.99, 118.16, 119.51, 121.77, 127.08, 127.13, 128.28, 129.13, 134.26, 136.50, 139.41, 173.42, 174.18; EIMS (*m/e*, relative intensity) 406 (M⁺, 60), 347 (45), 319 (100), 169 (50).

Anal. Calcd. for C₂₄H₂₆O₄N₂: C, 70.91; H, 6.45; N, 6.89. Found: C, 70.88; H, 6.47; N, 6.91.

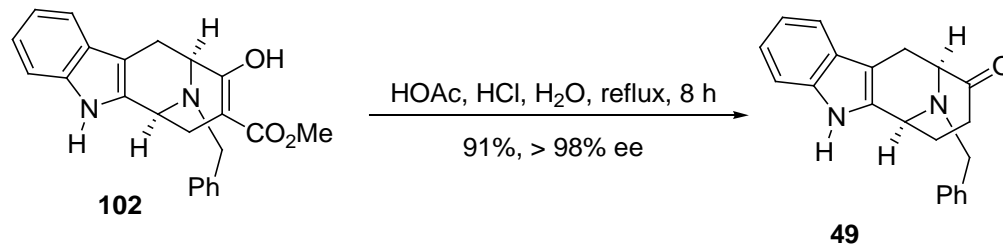


Dieckmann cyclization of the N_a -H diester **92b to provide (6*S*,10*S*)-(-)-methyl-9-oxo-12-benzyl-6,7,8,9,10,11-hexahydro-6,10-imino-5*H*-cyclooct[*b*]indole-8-carboxylate **102****

To a round bottom flask (5000 mL) which contained a solution of N_a -H, *trans* diester **92b** (100 g, 0.25 mol) in toluene (3000 mL), which had been predried by azeotropic removal of H_2O by a DST (refluxed 6 h), was added sodium hydride (88.7 g, 2.2 mol, 60% dispersion in mineral oil) at 0 °C. Anhydrous CH_3OH (174 mL, 4.3 mol) was then added into the above mixture dropwise under Ar at 0 °C. The solution which resulted was held at reflux for 72 h (the flask was covered with aluminum foil on the top to keep the temperature at reflux without carbonizing any compound on the sides of the flask). The reaction was quenched with ice. The aq layer was extracted with CH_2Cl_2 (3 x 1 L). The combined organic extracts were washed with brine and dried (K_2CO_3). The solvent was removed under reduced pressure and the mineral oil was separated by decantation. The residue which resulted was purified by flash chromatography (silica gel, EtOAc/hexane, 1/4) to provide the N_a -H, β -ketoester **102** (82 g, 88%). mp 149-150 °C; $[\alpha]_D^{27} = -177.4^\circ$ (*c*, 1.0 in CHCl_3); IR (KBr) 1670, 1630 cm^{-1} ; $^1\text{H NMR}$ (250M Hz, CDCl_3) δ 2.30 (1H, d, $J = 15.6$ Hz), 2.82 (1H, dd, $J = 15.5, 5.6$ Hz), 2.90 (1H, d, $J = 15.3$ Hz), 3.18 (1H, dd, $J = 15.9, 5.9$ Hz), 3.66 (3H, s), 3.71 (1H, d, $J = 13.4$ Hz), 3.77 (1H, d,

$J = 5.3$ Hz), 3.82 (1H, d, $J = 13.4$ Hz), 3.98 (1H, d, $J = 5.4$ Hz), 7.11 (1H, t, $J = 7.1$ Hz), 7.16 (1H, t, $J = 7.0$ Hz), 7.24-7.39 (6H, m), 7.50 (1H, d, $J = 7.1$ Hz), 7.63 (1H, s), 11.98 (1H, s); ^{13}C NMR (75.5 MHz, CDCl_3) δ 22.2, 28.6, 49.7, 51.3, 55.2, 55.9, 94.3, 106.2, 110.8, 118.1, 119.5, 121.6, 127.0, 127.2, 128.4, 128.7, 133.4, 135.7, 138.3, 171.6, 172.5; CIMS (CH_4) (m/e , relative intensity) 389 ($\text{M}^+ + 1$, 100).

Anal. Calcd. for $\text{C}_{23}\text{H}_{22}\text{N}_2\text{O}_3$: C, 73.78; H, 5.92; N, 7.48. Found: C, 74.19; H, 6.23; N, 7.35.

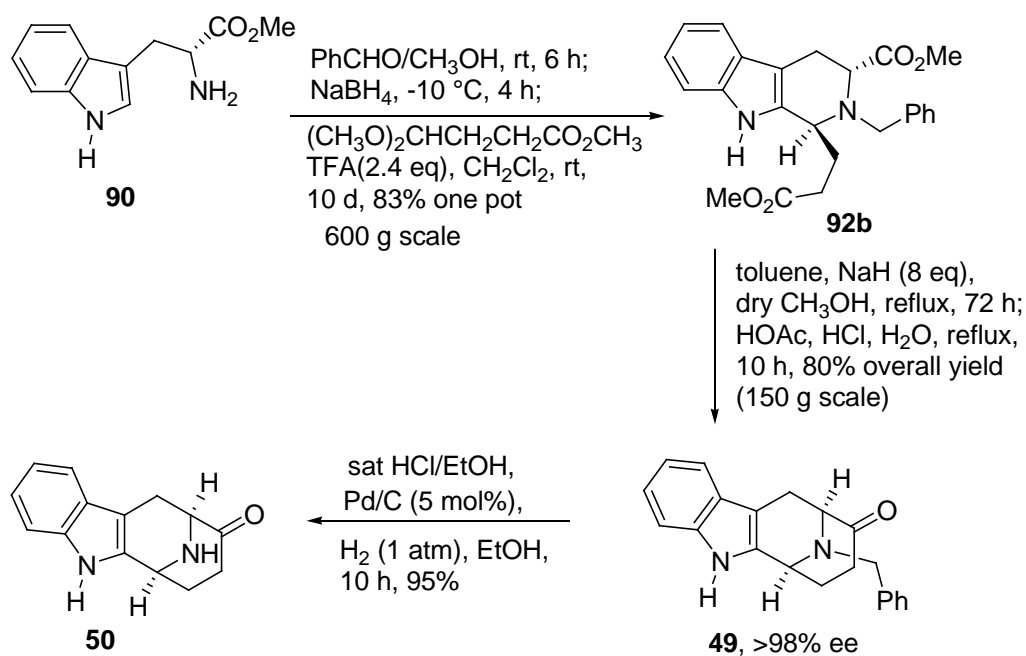


Preparation of (6*S*,10*S*)-(-)-9-oxo-12-benzyl-6,7,8,9,10,11-hexahydro-6,10-imino-5*H*-cyclo-oct[*b*]indole **49 via acid mediated hydrolysis of the N_a -H, β -ketoester **102****

To a round bottom flask (500 mL) which contained the N_a -H, β -ketoester **102** (45.0 g, 0.12 mol) was added glacial acetic acid (167 mL), aq hydrochloric acid (245 mL, conc.) and water (65 mL) with stirring (magnetic stir). The solution which resulted was heated at reflux for 8 h. After removal of the solvent under reduced pressure, the residue was brought to pH = 9 with a cold aq solution of NaOH (3 N). The mixture which resulted was extracted with CH_2Cl_2 (4 x 250 mL) and the combined organic extracts were washed with a saturated aq solution of NH_4Cl (100 mL), brine (2 x 100 mL) and dried (K_2CO_3). Removal of the solvent under reduced pressure afforded an oil. After a short wash column on silica gel, the N_a -H, N_b -benzyltetracyclic ketone **49** (24.5 g, 64%) was

crystallized from EtOAc/ hexane (1:4, 30 mL). The mother liquor was concentrated under reduced pressure and the residue was chromatographed on silica gel with EtOAc/hexane (1:4) to provide additional ketone **49** (10.5 g, 27%). The combined yield of **49** (35.0 g) was 91%. $[\alpha]_D^{27} = -246.7^\circ$ (*c* 1.05 in CHCl_3); **IR** (KBr) 2933, 1715 cm^{-1} ; **$^1\text{H NMR}$** (250 MHz, CDCl_3) δ 2.02(1H, m), 2.15 (1H, m), 2.49 (2H, m), 2.71 (1H, d, $J = 16.9$ Hz), 3.27 (1H, dd, $J = 16.9, 6.8$ Hz), 3.78 (2H, s), 3.80 (1H, s), 4.02 (1H, s), 7.17 (1H, dt, $J = 7.3, 1.0$ Hz), 7.23 (1H, dt, $J = 7.6, 1.0$ Hz), 7.30-7.38 (6H, m), 7.54 (1H, d, $J = 7.6$ Hz), 7.81 (1H, s); **$^{13}\text{C NMR}$** (62.8 MHz, CDCl_3) δ 20.40, 30.37, 34.51, 49.40, 56.13, 65.22, 106.73, 110.94, 118.21, 119.72, 122.01, 126.86, 127.42, 128.43, 128.60, 131.98, 135.85, 138.25, 210.40; **CIMS** (*m/e*, relative intensity) 317 ($\text{M}^+ + 1$).

Anal. Calcd. for $\text{C}_{21}\text{H}_{20}\text{N}_2\text{O}$: C, 79.72; H, 6.37; N, 8.85. Found: C, 79.51; H, 6.37; N, 8.85.



One pot process for converting D-(-)-tryptophan methyl ester **90 into *trans*-(1*S*,3*R*)-(-)-2-benzyl-3-methoxycarbonyl-1-methoxycarbonylethyl-1,2,3,4-tetrahydro-9*H*-pyrido-[3,4-*b*]indole **92b**¹⁰**

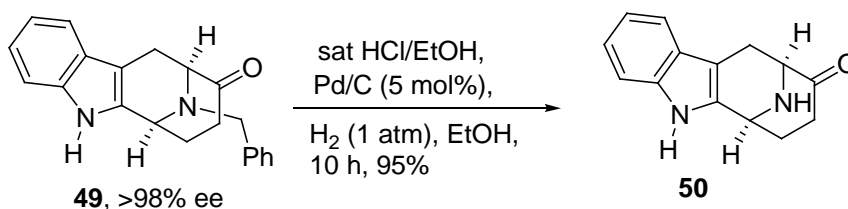
To a round bottom flask (12 L) which contained a solution of D-(-)-tryptophan methyl ester **90** (400 g, 1.83 mol) in CH₃OH (5000 mL) was added benzaldehyde (230 g, 2.2 mol) with stirring (overhead stir). The solution which resulted was stirred for 6 h at rt. The mixture was then cooled to -10 °C and sodium borohydride (55 g, 1.3 mol) was added portionwise over a period of 3 h. The internal pot temperature was kept between -10 °C and -5 °C with a dry ice bath (solid dry ice). After analysis by TLC (silica gel, EtOAc/hexane, 1/1) indicated the disappearance of imine, the mixture was allowed to stir for an additional 0.5 h followed by the slow addition of CF₃COOH (260 mL) at 0 °C. The solvent was removed under reduced pressure and the residue was dissolved in CH₂Cl₂ (3000 mL). After the solution which resulted was cooled to 0 °C, methyl 4,4-dimethoxybutyrate acetal **95** (324 g, 2.0 mol) and TFA (500 g, 2.4 eq) were added to this vessel at 0 °C. The reaction mixture was stirred at rt for 10 d, after which it was cooled in an ice bath and brought to pH = 8 with a cold aq solution of NaOH (3 N). The aq layer was separated and extracted with CH₂Cl₂ (3 x 5000 mL). The combined organic layers were washed with brine (2 x 200 mL) and dried (K₂CO₃). The volume of the solution was reduced to 300 mL under reduced pressure and EtOAc (100 mL) and hexanes (300 mL) were added to the above solution. The solution was cooled to -20 °C. The *trans* diester **92b** (510 g, 69%) precipitated as white crystals and the mother liquor was concentrated and the residue which resulted was purified by flash chromatography (silica gel, EtOAc/hexane, 1/4) to provide additional **92b** (114 g, 14%). The combined yield of **92b**

(624 g) was 83% and the solid was identical to the *trans* diester **92b** obtained from *N*_b-benzyl-D-tryptophan methyl ester **90** in an earlier experiment.

One pot process for converting *trans*-(1*S*,3*R*)-(-)-2-benzyl-3-methoxy carbonyl-1-methoxycarbonylethyl-1,2,3,4-tetrahydro-9*H*-pyrido[3,4-*b*]indole **92b into (6*S*,10*S*) - (-)-9-oxo-12-benzyl-6,7,8,9,10,11-hexahydro-6,10-imino-5*H*-cyclooct[*b*] indole **49****¹⁰

The *trans* diester **92b** (150 g, 246 mmol) was dissolved in dry toluene (3500 mL) in a round bottom flask (5000 mL) equipped with an overhead stirrer, Dean Stark trap (DST) and a reflux condenser. The solution which resulted was heated to reflux for 6 h with stirring. The above predried solution was cooled to 0 °C and sodium hydride (150 g of 60% dispersion NaH in mineral oil) was added to the above vessel under an atmosphere of Ar. Dry CH₃OH (170 mL) was added carefully (a large amount of H₂ was evolved at this point). The mixture was stirred at rt for 0.5 h, and then heated to reflux for an additional 72 h. **Note: The top of the flask was covered with aluminium foil to keep the reflux and prevent carbonization of the lactam intermediate during the Dieckmann process.** After analysis by TLC (silica gel, EtOAc/hexane, 1/4) indicated the disappearance of **92b**, the reaction mixture was cooled to 0 °C and then quenched carefully with glacial acetic acid (300 mL). The solvent was removed under reduced pressure and glacial acetic acid (480 mL), aq hydrochloric acid (750 mL, conc.) and water (200 mL) were added to the above vessel. The mixture which resulted was heated at reflux for 8 h. After removal of the solvent under reduced pressure, the residue was brought to pH = 9 by addition of an aq solution of cold NaOH (3 N). The mixture which resulted was extracted with CH₂Cl₂ (4 x 1000 mL) and the combined organic extracts were washed with brine (2 x 500 mL) and dried (K₂CO₃). Removal of the solvent under

reduced pressure afforded an oil which was chromatographed on silica gel with EtOAc/hexane (3:7) to provide the tetracyclic ketone **50** (90 g, 80%), which was identical to the ketone obtained from ketoester **102** (see above). **Note: A lactam intermediate is formed first in the Dieckmann reaction which must open up to isomerize and undergo the Dieckmann reaction. Do not mistake this first product (lactam) for the β -keto ester intermediate by TLC.**

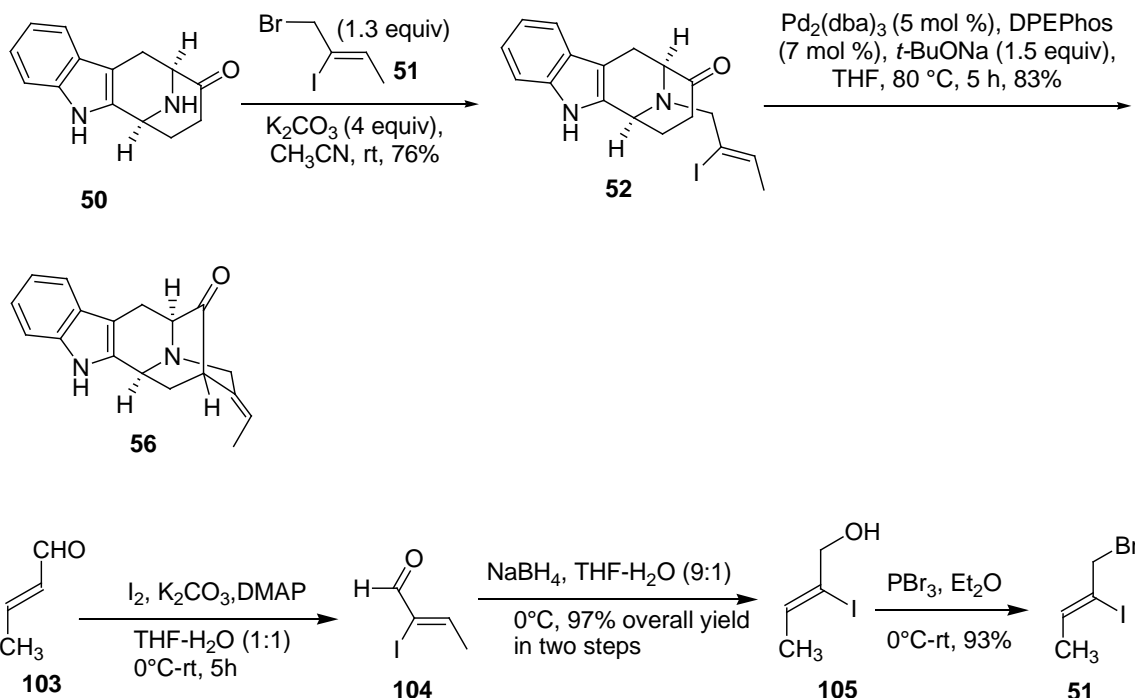


Catalytic debenzoylation of 49 to provide (6*S*,10*S*)-(-)-9-oxo-12-*H*-6,7,8,9,10,11-hexahydro-6,10-imino-5*H*-cyclooct[*b*]indole 50 over Pd/C/H₂

Tetracyclic ketone **49** (40 g, 127 mmol) was dissolved in anhydrous ethanol (1300 mL). A saturated solution of EtOH/HCl (g) was then added dropwise into the above mixture until the solid completely dissolved. The solvent was then removed under reduced pressure to furnish an HCl salt. The residue was then dissolved in dry ethanol (1000 mL) and the solvent was removed under reduced pressure to remove the excess HCl. This process was repeated 3 times to make sure there was no excess HCl. The HCl salt was degassed under reduced pressure at rt and back filled with argon (2 times). Dry Pd/C (10% by wt, 8.1 g, 60 mmol) was added to the above HCl salt, followed by addition (slow addition, initially) of dry ethanol (1300 mL). The mixture was degassed under reduced pressure at rt and back filled with H₂ (3 times). The mixture which resulted was allowed to stir on bench top at rt under an atmosphere of H₂ (balloon) for 10 h. Analysis

by TLC (silica gel plate was exposed to NH_3 vapours) indicated the absence of starting ketone **49**. The catalyst was removed by filtration (Celite) and washed with ethanol (3 x 100 mL). The solvent was removed under reduced pressure. The residue was dissolved in a mixture of CHCl_3 and brought to pH = 8 with 10% aq NH_4OH . The aq layer was extracted with CHCl_3 (3 x 400 mL). The combined organic layers were washed with brine (2 x 200 mL) and dried (K_2CO_3). The solvent was removed under reduced pressure to afford the crude amine which was chromatographed (flash) on silica gel ($\text{CHCl}_3/\text{EtOH}$, 9/1) to provide pure $N_a\text{-H}$, $N_b\text{-H}$ tetracyclic ketone **50** (27.2 g, 95%). **FTIR** (NaCl) 3393, 3382, 1705 cm^{-1} , **^1H NMR** (300 MHz, CDCl_3) δ 2.08-2.15 (2H, m), 2.36-2.50 (3H, m), 2.80 (1H, d, $J = 16.4$ Hz), 3.09 (1H, dd, $J = 16.5, 6.8$ Hz), 3.92 (1H, d, $J = 6.7$ Hz), 4.27 (1H, d, $J = 3.9$ Hz), 7.10 (1H, d, $J = 7.4$ Hz), 7.16 (1H, d, $J = 7.4$ Hz), 7.29 (1H, d, $J = 7.9$ Hz), 7.44 (1H, d, $J = 7.62$ Hz), 8.06 (1H, bs), **^{13}C NMR** (75.5 MHz, CDCl_3) 211.0, 135.7, 134.0, 126.9, 122.1, 119.7, 118.1, 110.9, 107.5, 59.8, 46.1, 35.0, 32, 25.8; **CIMS** (m/e , relative intensity) 227 ($\text{M}^+ + 1$, 100%).

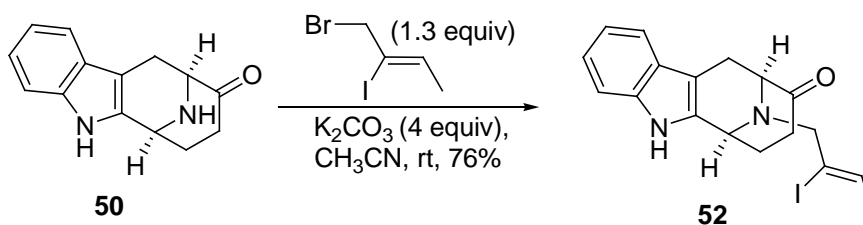
Anal. Calcd. For $\text{C}_{14}\text{H}_{14}\text{N}_2\text{O}$: C, 74.31%; H, 6.24%; N, 12.38%. Found: C, 74.39%; H, 6.35%; N, 12.41%.



(Z)-1-bromo-2-iodobut-2-ene 51¹⁵⁵

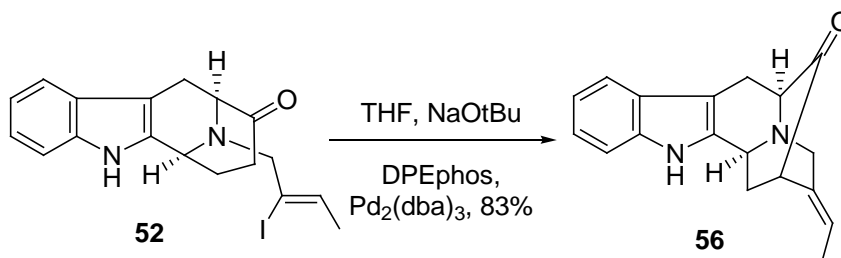
A solution of crotonaldehyde **103** (300mL, 3.63 mol) in THF-H₂O (1:1, 1500mL) was cooled to -15 to -20 °C (dry ice). To the cold solution was added K₂CO₃ (600g, 4.45 mol, 1.2 equiv), I₂ (1383g, 5.45 mol, 1.5 equiv) and DMAP (88.6g, 0.726 mol, 0.2 equiv) successively (the temperature was increased, controlled by the rate of addition of I₂). The reaction was allowed to stir for 12 h until the disappearance of starting material (TLC, silica gel, I₂) during which the temperature was allowed to increase to rt. Then solid Na₂S₂O₃ (600g) and a saturated solution of Na₂S₂O₃ (about 5L) was added until the reaction mixture became colorless. The mixture was extracted with EtOAc (3x8L) and the organic layers were combined. The majority of the solvent was removed under reduced pressure. The residue **104** was dissolved in THF-H₂O (9:1, 8L) and cooled to -5 to -10 °C (dry ice) after which NaBH₄ (70g, 1.8 mol, 0.5 equiv) was added in portions

and the temperature maintained at 0°C. The mixture was extracted with EtOAc (3x8L) and dried (MgSO₄). The solvent was removed under reduced pressure to provide a brown oil. After a simple wash column to remove some baseline material, iodide **105** was obtained as light yellow oil **105** (650g, 90%). ¹H NMR (300 MHz, CDCl₃) δ 6.02 (q, 1H, *J* = 3.9 Hz), 4.30 (s, 2H), 1.85 (t, 3H, *J* = 6.3 Hz). The spectral properties of this iodide were identical to the published values.¹²⁰ (Z)-2-Bromo-2-buten-1-ol **105** (2 g, 10 mmol) was dissolved in anhydrous ethyl ether (20 mL). Phosphorus tribromide (0.380 mL, 4 mmol) was added dropwise to this solution at 0°C. This reaction mixture which resulted was stirred for 18 h at rt. The reaction was quenched with a cold aq solution of K₂CO₃ and extracted with ethyl ether after which it was washed with brine. The organic layer was dried (Na₂SO₄) and concentrated in vacuo to give **51** (2.45 g, 93% yield) which was directly used in the next step.¹⁷² ¹H NMR: 6.08 (q, *J* = 6.4 Hz, 1H); 4.36 (s, 2H); 1.81 (d, *J* = 6.4 Hz, 3H). The spectral properties of this bromide were identical to the published values.¹²¹ This was directly used in the following alkylation.



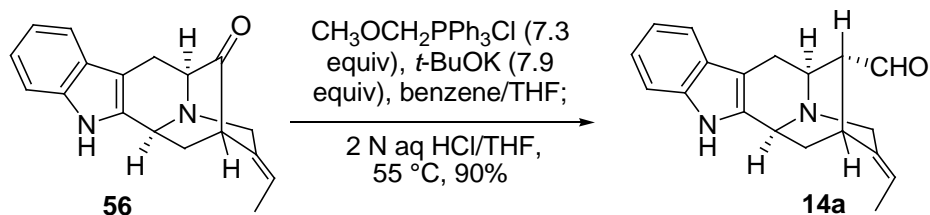
Alkylation of (6S,10S)-(-)-9-oxo-12-H-6,7,8,9,10,11-hexahydro-6,10-imino-5H-cyclooct[b] indole (50) to provide (6S,10S)-(-)-9-oxo-12-(Z-2'-iodo-2'-butenyl)-6,7,8,9,10,11-hexahydro-6,10-imino-5H-cyclooct[b] indole 52

A solution of the N_a-H, N_b-H tetracyclic ketone **50** (1.5g, 6.637mmol) was dissolved in dry CH₃CN (20mL). To this mixture, K₂CO₃ (3.66g, 26.54 mmol) and Z-1-bromo-2-iodo-2-butene **51** (2.6g, 9.95mmol) were added. This reaction mixture was stirred for 14h at rt. Analysis by TLC indicated the absence of tetracyclic ketone. The K₂CO₃ was removed by passing the mixture through a bed of celite with EtOAc. After removal of the solvent under reduced pressure, the crude product was purified by flash chromatography (silica gel, hexane:EtOAc = 9:1) to provide N_b-Z'-2'-iodo-2'-butenyl tetracyclic ketone **52** (2.04g, 76%). FTIR (NaCl) 3393, 1705, 1450cm⁻¹; ¹H NMR (300 MHz, CDCl₃) δ 1.73 (3H, d, J=6.27Hz), 2.19-2.05 (2H, m), 2.37-2.47 (2H,m), 2.65(1H, d, J=16.87Hz), 3.05 (1H, dd, J=16.94, 6.72 Hz), 3.19-3.37 (2H,m), 3.64 (1H, d, J=6.37Hz), 3.96 (1H, bs), 5.76 (1H, q, J=6.17Hz), 6.97-7.16 (2H, m), 7.25 (1H, d, J=7.72Hz), 7.40 (1H, d, J=7.52Hz), 8.05 (1H, bs); ¹³C NMR (75.5 MHz, CDCl₃) δ 20.60, 21.71, 30.35, 34.49, 49.73, 63.36, 64.07, 106.69, 108.47, 110.94, 118.09, 119.62, 121.97, 125.72, 132.11, 132.76, 135.79, 210.40; CIMS (m/e, relative intensity) 407 (M⁺+1, 100%). **Anal. Calcd. For C₁₈H₁₉N₂O**: C, 53.22%; H, 4.71%; N, 6.90%. Found: C, 53.15%; H, 4.80%; N, 6.64%.



Palladium catalyzed cyclization of (6S, 10S)-(-)-9-oxo-12-(Z-2'-iodo-2'-butenyl)-6,7,8,9,10,11-hexahydro-6,10-imino-5H-cyclooct [b] indole (52) to provide pentacyclic ketone (56)

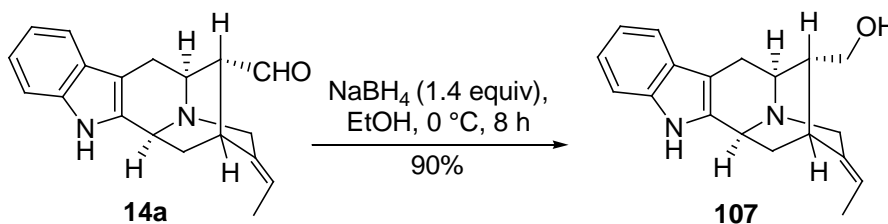
The N_b-Z-2' -iodo-butenyl tetracyclic ketone **52** (1 g, 2.46 mmol) was dissolved in anhydrous THF (20mL). To this mixture NaO^tBu (0.354 g, 3.69 mmol), DPEphos (0.0927 g, 7.0 mol %) and Pd₂ (dba)₃ (0.112g, 5.0 mol %) was added. This reaction mixture was degassed 3-4 times under vacuum and back filled with argon and placed in a preheated oil bath at 80 °C for 5hrs. The reaction was quenched with water and ethyl acetate. The organic layer was separated and dried (Na₂SO₄). The EtOAc was then removed under reduced pressure and the residue was flash chromatographed with CH₂Cl₂/MeOH (4.5:0.5) to provide the coupling product **56** (0.569g, 83% yield). ¹H NMR (300 MHz, CDCl₃) δ 1.63 (3H, *J*=6.86 Hz, d), 2.15-2.20 (1H, m), 2.38 (1H, t, *J*=9.9 Hz), 2.97 (1H, dd, *J*=15.58, 6.20 Hz), 3.27 (1H, d, *J*=14.43 Hz), 3.37 (1H, bs), 3.59 (1H, d, *J*=5.70 Hz), 3.78 (2H, bs), 4.26 (1H, d, *J*=59.11 Hz), 5.49 (1H, q, *J*=6.85 Hz), 7.05-7.15 (2H, m), 7.25 (1H, d, *J*=7.25Hz), 7.47 (1H, d, *J*=4.7Hz), 7.93 (s, 1H); ¹³C NMR (75.5 MHz, CDCl₃) δ 12.68, 22.39, 36.40, 44.55, 50.83, 55.24, 64.17, 105.62, 110.89, 118.54, 119.69, 121.26, 122.00, 126.88, 131.88, 135.87, 136.34, 217.00; CIMS (*m/e*, relative intensity) 291 (M⁺ +1, 100%); EIMS (*m/e*, relative intensity) 278 (M⁺, 10%), 250 (75%), 249 (85%), 182 (6%), 169 (100%), 168 (5%). HRMS C₁₈H₁₈N₂O: calcd. 278.1419; found 278.1437. This material was used directly in the next step.



Conversion of the pentacyclic ketone (56) into (+)-3-ethylidene-1,3,4,7,12,12b-hexahydro-2H, 6H-2,6-methano-indole[2,3,- α]-quinolizine-13-carboxaldehyde[(+)-vellosimine, 14a] via the Wittig reaction followed by acid mediated hydrolysis.

A mixture of anhydrous potassium t-butoxide (12.8g, 0.114 mol) and methoxymethyl triphenylphosphonium chloride (36g, 0.105 mol) in dry benzene (500mL) was allowed to stir at rt for 1h. The pentacyclic ketone **56** (4g, 14.4mmol) in THF (160mL) was then added into the above orange colored solution dropwise at rt. The mixture which resulted was stirred at rt for 24h. The mixture was diluted with EtOAc (3x700mL), washed with H₂O (3x50mL), brine (50mL) and dried (K₂CO₃). The solvent was removed under reduced pressure to afford an oil. The solvent was removed under reduced pressure and the residue was dissolved (without further purification) in a solution of aq HCl (2N) in H₂O-THF (1:1, 400mL). The solution which resulted was refluxed 55 °C (oil bath temperature) under an atmosphere of argon for 6h. The reaction mixture was brought to rt and concentrated under reduced pressure. The reaction mixture was diluted with water and extracted with ether to remove the triphenyl phosphine oxide. The aq layer was brought to pH 8 with an ice cold aq solution of NaOH (1N). The aq layer was extracted with CH₂Cl₂ and the combined organic layers were washed with H₂O (3x100mL), brine (100mL) and dried (K₂CO₃). The solvent was removed under reduced pressure to afford

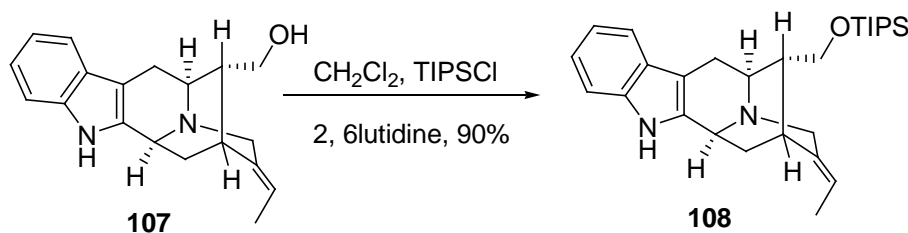
an oil which was crystallized to provide the aldehyde **14a** (3.78g, 90%). The spectral data for (+)-vellosimine **14a** were in good agreement with the published values.^{19,173}



Sodium borohydride mediated reduction of (+)-3-ethylidene-1,3,4,7,12,12b-hexahydro-2H,6H-2,6-methano-indole[2,3- α]-quinolizine-13-carboxaldehyde[(+)-vellosimine, **14a] to provide the (+)-3-ethylidene-1,3,4,7,12,12b-hexahydro-13-hydroxymethyl-2H,6H-2,6-methano-indole [2,3- α]-quinolizine [(+)-normacusine B, **107**].**

The (+)-vellosimine **14a** (100mg, 0.34mmol) was dissolved in EtOH (5mL). The NaBH₄ (12mg, 0.33 mmol) was added to the above solution at 0 °C in one portion. The mixture was then stirred for 8 h. The reaction mixture was diluted with CH₂Cl₂ (50mL) and poured into cold water (10mL). The aq layer was extracted with additional CH₂Cl₂ (3x20mL) and the combined organic layers were washed with brine (10mL) and dried (K₂CO₃). The solvent was removed under reduced pressure to afford the crude product which was chromatographed to provide normacusine B **107** (90mg, 90%). $[\alpha]_{\text{D}}^{28} = +40.5$ ° (c=0.75, C₂H₅OH); lit $[\alpha]_{\text{D}} = +42$ ° (c=1.0, C₂H₅OH)¹⁷⁴; FTIR (NaCl) 3198 cm⁻¹; **¹H NMR** (300 MHz, CDCl₃) δ 1.57 (3H, d, $J=6.76$ Hz), 1.66 (1H, dt, $J=12.54, 3.69$ Hz), 1.78 (1H, q, $J=7.49$ Hz), 1.93 (1H, t, $J=10.00$ Hz), 2.61 (1H, d, $J=15.37$ Hz), 2.72 (1H, s), 2.74 (1H, d, $J=6.51$ Hz), 3.03 (1H, dd, $J=15.39, 5.10$ Hz), 3.43-3.49 (4H, m), 4.07 (1H, d,

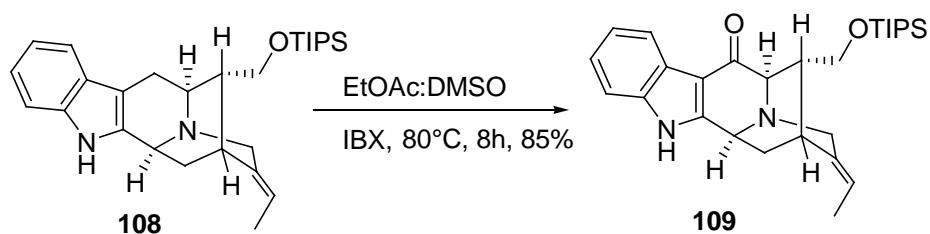
$J=10.29\text{Hz}$), 5.26 (1H, q, $J=6.68\text{Hz}$), 7.03-7.14 (1H, m), 7.28 (1H, d, $J=6.00\text{Hz}$), 7.42 (1H, d, $J=7.00\text{Hz}$), 8.22 (1H, s); $^{13}\text{C NMR}$ (75.5 MHz, CDCl_3) δ 12.75, 26.95, 27.58, 33.37, 44.14, 050/48, 54.47, 55.85, 64.90, 0104.52, 110.99, 116.84, 118.07, 119.35, 121.44, 127.59, 135.33, 136.33, 137.80; **EIMS** (m/e , relative intensity) 294 (M^+ , 84%), 293 (85%), 279 (10%), 263 (30%), 169 (100%), 168 (79%). **HRMS** $\text{C}_{19}\text{H}_{22}\text{N}_2\text{O}$: calcd. 294.1732; found 294.1705. The spectral data were identical to that reported in the literature.¹⁷⁴



Synthesis of 3-ethylidene-13-(triisopropylsilyloxymethyl)-1,3,4,7,12,12b-hexahydro-2H,6H-2,6-methano-indolo [2,3- α] quinolizine 108 from normacusine B 107 with 2,6-lutidine and triisopropylsilyl chloride.

A solution of normacusine B **107** (1.0g, 3.4mmol) was stirred in dry CH_2Cl_2 (30mL) in a 125mL round bottom flask. At 0 °C, 2, 6-lutidine (1.58mL, 13.6mmol), followed by triisopropylsilyl chloride (1.82mL, 6.8mmol) were added. The reaction mixture was allowed to stir for 2h until analysis of the mixture by TLC indicated the absence of starting material. Water (50.0mL) was added to the solution to quench the reaction mixture and it was extracted with CH_2Cl_2 (3x200mL). The organic layer was separated and dried (Na_2SO_4). The organic layer was removed under reduced pressure and the residue was purified by flash chromatography (silica gel, $\text{CH}_2\text{Cl}_2/\text{MeOH}$ (95:5) to

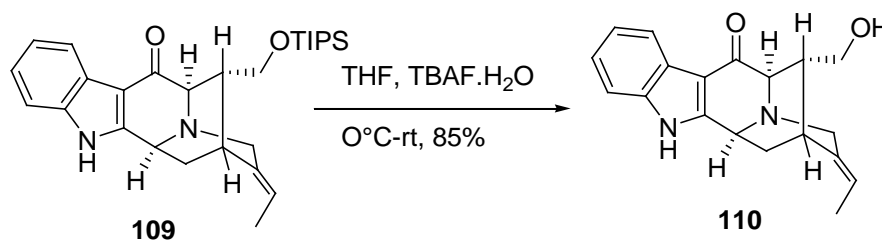
provide **108** (1.38g, 90%). $[\alpha]_D^{25} = +45.14^\circ$ ($c=0.14$ in CH_2Cl_2); $^1\text{H NMR}$ (300 MHz, CDCl_3) δ 1.05 (m, 21H), 1.62 (d, 3H, $J=6.7\text{Hz}$), 1.74 (m, 2H), 2.05 (t, 1H, $J=10.1\text{Hz}$), 2.70 (d, 1H, $J=15.5\text{Hz}$), 2.79 (m, 2H), 3.08 (dd, 1H, $J=15.3$ and 5.3Hz), 3.60 (m, 4H), 4.17 (d, 1H, $J=7.5\text{Hz}$), 5.39 (q, 1H, $J=6.8\text{Hz}$), 7.13 (m, 2H), 7.34 (d, 1H, $J=7.5\text{Hz}$), 7.48 (d, 1H, $J=7.4\text{Hz}$), 8.03(br, 1H); $^{13}\text{C NMR}$ (75.5 MHz, CDCl_3) δ 11.83, 12.73, 17.96, 27.10, 27.29, 33.56, 44.26, 50.55, 54.93, 56.05, 65.56, 104.72, 110.76, 116.44, 118.03, 119.20, 121.23, 127.74, 135.48, 136.18, 137.87; MS (EI) m/e (relative intensity) 450 (M^+ , 16), 263 (45), 182 (31), 169 (89), 168 (100). Anal.Calcd. for $\text{C}_{28}\text{H}_{42}\text{N}_2\text{OSi}$: C, 74.61; H, 9.39; N, 6.22. Found: C, 74.46; H, 9.31, N, 6.06



IBX mediated oxidation to provide (6S,11S,11aR,E)-9-ethylidene-11-((triisopropylsilyl)oxy)methyl)-6,8,9,10,11,11a-hexahydro-6,10-methanoindolo[3,2-b]quinolizin-12(5H)-one (109)¹³⁰

To a solution of triisopropylsilyl ether **108** (100mg, 0.22mmol) in EtOAc/DMSO (10mL/5mL) was added IBX (0.552mg, 0.88mmol) in one portion at rt. The mixture which resulted was stirred at 80°C overnight and the reaction progress was monitored by TLC (silica gel, EtOAc). The reaction mixture was cooled at 0 °C and quenched with a

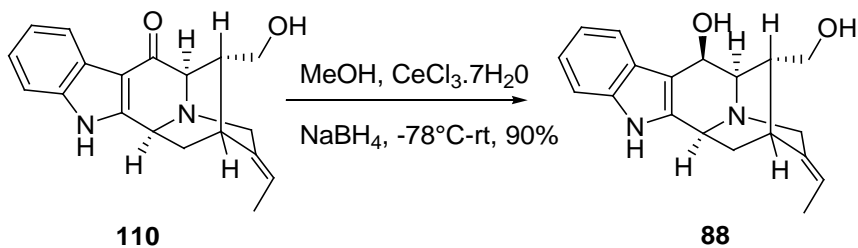
saturated solution of aq NaHCO₃ (4mL), followed by treatment with a saturated solution of aq Na₂S₂O₃ (5mL). After this, the mixture was stirred for an additional 10min at 0°C. The aq layer was extracted with additional amounts of EtOAc (3x10mL) and the combined organic layers was washed with brine (10mL) and dried (K₂CO₃). The solvent was removed under reduced pressure to provide the crude oil which was purified by flash chromatography [silica gel, hexane: EtOAc (1:1)] to provide the benzylic ketone **109** (87mg, 85%). ¹H NMR (300 MHz, CDCl₃) δ 1.05 (m, 21H), 1.66 (d, 3H, *J*=6.3Hz), 1.82 (d, 1H, *J*=6.3Hz), 2.13 (t, 1H, *J*=9.9Hz), 2.86 (d, 1H, *J*=7Hz), 3.17 (s, 1H), 3.5 (m, 3H), 3.8 (dd, 1H, *J*₁=9.6Hz, *J*₂=4.2Hz), 4.3 (d, 1H, *J*=8.4Hz), 5.47 (q, 1H, *J*=7Hz), 7.39 (t, 2H, *J*=7Hz), 7.49 (t, 1H, *J*=7Hz), 7.96 (d, 1H, *J*=7Hz), 8.14 (d, 1H, *J*=7.2Hz), 9.6 (br, 1H); ¹³C NMR (75.5 MHz, CDCl₃) δ 11.91, 12.97, 18.03, 29.72, 32.50, 42.63, 50.48, 54.85, 63.92, 64.60, 106.49, 111.64, 118.52, 121.64, 122.74, 123.61, 124.47, 132.30, 136.14, 154.67, 192.01; HRMS (ESI) calculated for C₂₈H₄₁N₂O₂Si : 465.2937; found : 465.2950.



Synthesis of (6*S*,11*R*,11*aR*,*E*)-9-ethylidene-11-(hydroxymethyl)-6,8,9,10,11,11*a*-hexahydro-6,10-methanoindolo[3,2-*b*]quinolizin-12(5*H*)-one (110)

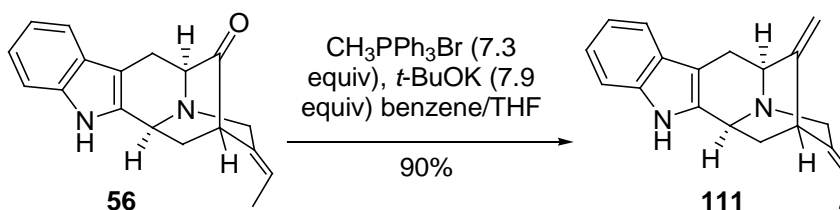
A solution of benzylic ketone **109** (20mg, 0.043mmol) was stirred in THF (1 mL) in a 5mL round bottom flask. At 0°C, excess TBAF hydrate was then added to the mixture and it

was allowed to warm to rt. The reaction mixture was stirred for 2h until analysis of the mixture by TLC indicated the absence of starting material. The reaction was quenched with water (10mL) and extracted with EtOAc (3x10mL), washed with brine and dried (Na_2SO_4). After removal of the solvent under reduced pressure, the residue was purified by flash chromatography [EtOAc : hexane (4:1)] to provide the target monol **110** (0.011g, 85%) . $^1\text{H NMR}$ (300 MHz, CDCl_3) δ 1.68 (d, 3H, $J=6\text{Hz}$), 1.87 (d, 1H, $J=12\text{Hz}$), 2.12 (br, 1H), 2.28 (t, 1H, $J=12\text{Hz}$), 2.84 (d, 1H, $J=6\text{ Hz}$), 3.25 (s, 1H), 3.66 (m, 5H), 4.35 (dd, 1H, $J_1=9\text{Hz}$, $J_2=3\text{Hz}$), 5.55 (q, 1H, $J=7.5\text{Hz}$), 7.25 (m, 2H), 7.43 (d, 1H, $J=7\text{Hz}$), 7.98 (d, 1H, $J=8.4\text{Hz}$); $^{13}\text{C NMR}$ (75.5 MHz, CDCl_3) δ 11.60, 12.52, 19.30, 29.17, 42.58, 50.19, 54.38, 63.17, 64.32, 105.38, 111.63, 117.97, 120.54, 122.24, 123.19, 124.29, 133.29, 136.80, 156.43, 193.70; **HRMS (ESI)** calculated for $\text{C}_{19}\text{H}_{21}\text{N}_2\text{O}_2$: 309.1603; found : 309.1588. This material was used in a later step. The structure of ketone **110** was confirmed by X-ray analysis (see Figure 8).



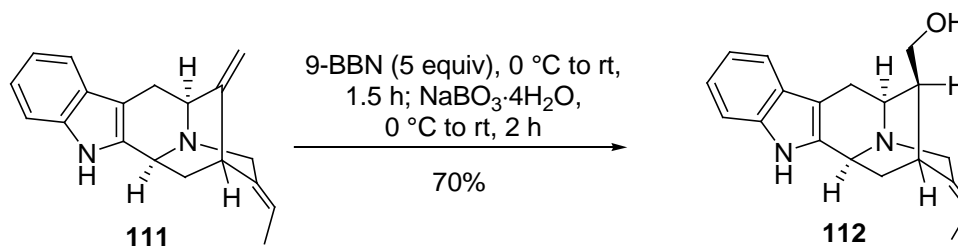
Preparation of (6S,11R,11aR,12R,E)-9-ethylidene-11-(hydroxymethyl)-5,6,8,9,10,11,11a,12-octahydro-6,10-methanoindolo[3,2-b]quinolizin-12-ol (88**)**

A solution of alcohol **110** (15mg, 0.049mmol) was stirred in MeOH (1 mL) in a 5mL flask. At -78°C , $\text{CeCl}_3 \cdot 7\text{H}_2\text{O}$ (19mg, 0.054mmol) and NaBH_4 (2mg, 0.049mmol) was added to the mixture and it was allowed to warm to rt. The reaction mixture was stirred for 3h until analysis of the mixture by TLC indicated the absence of starting material. The reaction was quenched with aq NH_4Cl (5mL) and extracted with CH_2Cl_2 (3x10mL), washed with brine and dried (Na_2SO_4). After removal of the solvent under reduced pressure, the residue was purified by flash chromatography [CH_2Cl_2 : MeOH (90:10)] to provide the target diol **88** (13mg, 90%) ; R_f 0.75 (silica gel, $\text{CH}_2\text{Cl}_2/\text{MeOH}$, 9 : 1); $[\alpha]_D^{25} +79^{\circ}$ (c 0.6 MeOH); $^1\text{H NMR}$ (300 MHz, CDCl_3) δ 1.67 (d, 3H, $J=6.6\text{Hz}$), 1.80 (td, 1H, $J_1=12.6\text{Hz}$, $J_2=6\text{Hz}$), 2.13 (m, 1H), 2.2 (m, 1H), 2.7 (t, 1H, $J=6.6\text{ Hz}$), 3.01 (s, 1H), 3.5 (m, 3H), 3.6 (m, 2H), 4.10 (d, 1H, $J=8\text{Hz}$), 5.23 (d, 1H, $J=6\text{Hz}$), 5.47 (q, 1H, $J=6.6\text{ Hz}$), 7.04 (m, 2H), 7.3 (d, 1H, $J=7.8\text{Hz}$), 7.78 (d, 1H, $J=7.8\text{Hz}$); $^{13}\text{C NMR}$ (75.5 MHz, CDCl_3) δ 11.60, 27.20, 32.46, 39.18, 50.16, 55.58, 59.71, 63.85, 65.98, 102.27, 110.61, 116.86, 118.64, 119.18, 120.78, 126.51, 135.19, 136.91, 138.54; **HRMS (ESI)** calculated for $\text{C}_{19}\text{H}_{23}\text{N}_2\text{O}_2$: 311.1760; found : 311.1758. The structure of diol **88** was confirmed by X-ray analysis (see Figure 9).



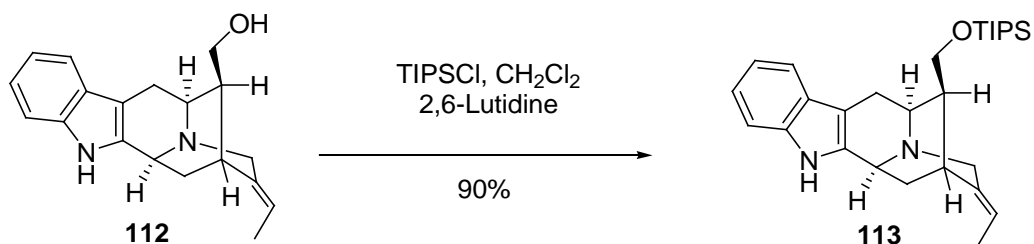
Synthesis of (+)-3-ethylidene-12-methyl-1,3,4,7,12,12b-hexahydro-2H,6H-2,6-methano-13-methylene-indole[2,3-a]quinolizine (111) via the Wittig reaction.

A mixture of anhydrous potassium *tert*-butoxide (3.24g, 2.75mmol) and methyltriphenylphosphonium bromide (8.93 g, 2.5 mmol) in dry benzene (150 mL) was allowed to stir at rt for 1 h. The pentacyclic ketone **56** (1.46 g, 0.50 mmol) in THF (50 mL) was then added into the above orange-colored solution dropwise at rt. The mixture which resulted was stirred at rt for 4 h. The mixture was diluted with EtOAc (500 mL), washed with H₂O (3 x 50 mL), brine (100 mL), and dried (K₂CO₃). The solvent was removed under reduced pressure and the oil which resulted was flash chromatographed (silica gel, CHCl₃/MeOH) 40:1) to provide the olefin **111** (1.30 g, 90%): FTIR (CHCl₃) 3439 cm⁻¹; ¹H NMR (300 MHz, CDCl₃) δ 1.67 (dt, 3H, *J* = 6.8, 1.8 Hz), 1.87 (dt, 1H, *J* = 9.2, 2.8 Hz), 2.25 (ddd, 1 H, *J* = 11.8, 10.0, 1.7 Hz), 3.02 (dd, 1 H, *J* = 15.4, 1.3 Hz), 3.24 (dd, 1 H, *J* = 15.5, 5.2 Hz), 3.35 (m, 1 H), 3.60 (s, 3 H), 3.84 (m, 2 H), 3.93 (m, 1 H), 4.35 (dd, 1 H, *J* = 9.9, 2.3 Hz), 4.86 (t, 2 H, *J* = 2.4 Hz), 5.34 (q, 1 H, *J* = 7.0 Hz), 7.08 (td, 1 H, *J* = 6.9, 1.2 Hz), 7.20 (td, 1 H, *J* = 6.9, 1.1 Hz), 7.27 (d, 1 H, *J* = 7.6 Hz), 7.50 (td, 1 H, *J* = 7.6 Hz); ¹³C NMR (75.5 MHz, CDCl₃) δ 12.4, 26.2, 29.2, 35.3, 36.3, 49.6, 56.1, 56.8, 103.8, 105.4, 108.7, 115.4, 118.1, 118.8, 120.9, 127.0, 136.4, 137.3, 138.2, 151.6; EIMS (*m/z*, relative intensity) 290 (M⁺, 100), 275 (13), 182 (76). **Anal.** **Calcd** for C₂₀H₂₂N₂: C, 82.72; H, 7.04; N, 9.65. Found: C, 82.84; H, 7.29; N, 9.46.



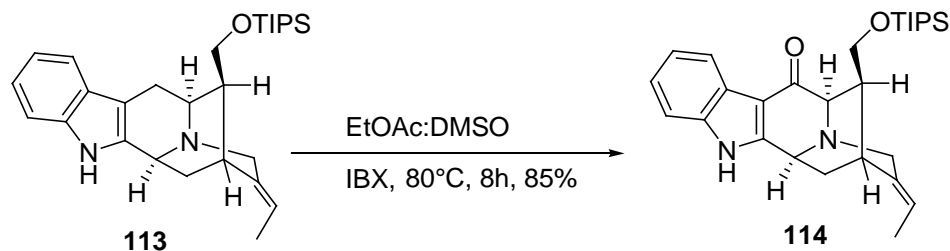
Synthesis of (E) 16-epinormacusine B 112 from (+)-3-ethylidene-12-methyl-1,3,4,7,12,12b-hexahydro-2*H*,6*H*-2,6-methano-13-methylene-indole[2,3-*a*]quinolizine (111)

To a solution of olefin **111** (200 mg, 0.72 mmol) in THF (20 mL) was added 9-BBN (0.5 M in THF, 7.23 mL, 3.6 mmol) dropwise at 0 °C. The solution was allowed to warm to rt and stirred for 1.5 h. The reaction mixture was then cooled to 0 °C and NaBO₃·4H₂O (1.67g, 10.8mmol) was added (Kabalka process) and the reaction temperature allowed to warm to rt. The mixture which resulted was stirred for 2 h at rt, diluted with CH₂Cl₂ (200 mL), washed with H₂O (3 x 50 mL) as well as brine (100 mL), and dried (K₂CO₃). The solvent was removed under reduced pressure and the residue was chromatographed (silica gel, CH₂Cl₂/MeOH; 9:1) to provide alcohol **112** (149 mg, 70%). FTIR (CHCl₃) 3200, 2918 cm⁻¹; [α]_D = +6.92° (c 0.25, MeOH) [lit.1 [α]^D = +3° (c 0.25, MeOH)]; ¹H NMR (300 MHz, CDCl₃) δ 1.64 (dt, 3 H, *J* = 6.8, 1.8 Hz), 1.84 (m, 2 H), 2.24 (m, 1 H), 2.89 (q, 1 H, *J* = 2.8 Hz), 3.01 (m, 2 H), 3.27 (dd, 1 H, *J* = 10.5, 8.5 Hz), 3.48-3.76 (m, 4 H), 4.22 (dd, 1 H, *J* = 9.0, 4.2 Hz), 5.23 (q, 1 H, *J* = 6.8 Hz), 7.08 (td, 1 H, *J* = 7.1, 1.3 Hz), 7.16 (td, 1 H, *J* = 7.1, 1.3 Hz), 7.36 (d, 1 H, *J* = 7.3 Hz), 7.49 (d, 1 H, *J* = 7.3 Hz), 8.60 (s, 1 H); ¹³C NMR (75.5 MHz, CDCl₃) δ 12.7, 22.3, 26.1, 27.0, 41.8, 50.1, 52.8, 55.9, 60.9, 105.6, 111.2, 114.9, 118.1, 119.3, 121.7, 126.0, 135.6, 136.4, 137.4; **Anal. Calcd for C₁₉H₂₂N₂O**: C, 77.52; H, 7.53; N, 9.52. Found: C, 77.80; H, 7.79; N, 9.34



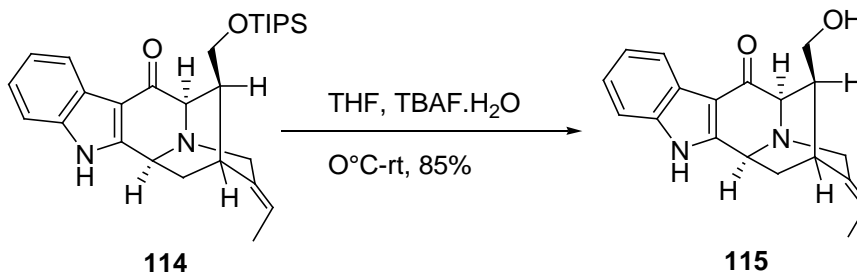
Preparation of (6S,11S,11aS,E)-9-ethylidene-11-(((triisopropylsilyl)oxy)methyl)-5, 6, 8, 9, 10, 11, 11a,12-octahydro-6,10-methanoindolo[3,2-b]quinolizine (113)

The synthesis of 113 (TIPS derivative) from monol 112 was carried out analogous to the preparation of 108 from 107 in 90% yield. ¹H NMR (300 MHz, CDCl₃) δ 1.03 (d, 21H, *J*=3Hz), 1.57 (d, 3H, *J*=6Hz), 2.01 (m, 1H), 2.08 (m, 1H), 2.26 (t, 1H, *J*=12Hz), 2.81 (s, 1H), 2.97 (d, 1H, *J*=15Hz), 3.30 (m, 3H), 3.57 (m, 3H), 4.76 (d, 1H, *J*=9Hz), 5.21 (q, 1H, *J*=9Hz), 7.28 (m, 2H), 7.45 (d, 1H, *J*=9Hz), 9.88 (br, 1H); ¹³C NMR (75.5 MHz, CDCl₃) δ 12.69, 22.80, 26.53, 27.44, 42.99, 50.12, 52.25, 56.65, 61.76, 106.78, 110.55, 112.93, 118.21, 121.23, 126.73, 136.38, 137.26, 141.34; HRMS (ESI) calculated for C₂₈H₄₃N₂OSi : 451.3145; found : 451.3172. This material was employed directly in the next step.



Preparation of (6S,11S,11aR,E)-9-ethylidene-11-((triisopropylsilyl)oxy)methyl)-6,8,9,10,11,11a-hexahydro-6,10-methanoindolo[3,2-b]quinolizin-12(5H)-one (114)

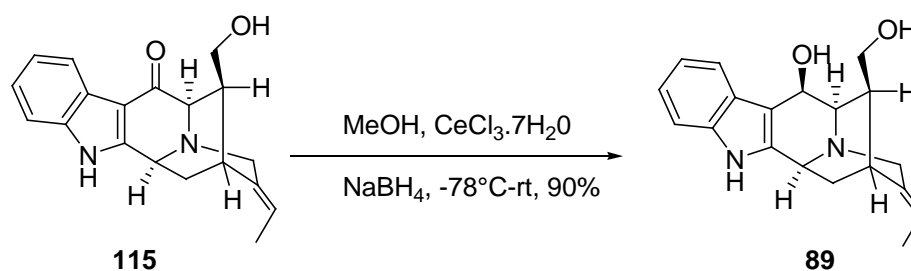
The synthesis of ketone 114 from TIPS derivative 113 was carried out analogous to the preparation of 109 from 108 in 85% yield. $^1\text{H NMR}$ (300 MHz, CDCl_3) δ 0.96 (d, 21H, $J=2.7\text{Hz}$), 1.66 (d, 3H, $J=7\text{Hz}$), 1.81 (t, 1H, $J=11\text{Hz}$), 2.06 (dd, 1H, $J_1=9.9\text{Hz}$, $J_2=3.3\text{Hz}$), 2.25 (m, 1H), 3.35 (d, 1H, $J=2$), 3.47 (t, 1H, $J=11$), 3.74 (d, 2H, $J=2.4\text{Hz}$), 3.78 (s, 1H), 3.84 (dd, 1H, $J_1=10.2\text{Hz}$, $J_2=4.8$), 4.14 (dd, 1H, $J_1=10.5\text{Hz}$, $J_2=4.5$), 5.32 (q, 1H, $J=6.9\text{Hz}$), 7.27 (m, 3H), 8.13 (d, 1H, $J=6.9\text{Hz}$), 8.9 (br, 1H); $^{13}\text{C NMR}$ (75.5 MHz, CDCl_3) δ 11.85, 12.72, 17.94, 25.99, 27.81, 38.52, 50.07, 55.52, 59.87, 63.54, 108.57, 111.27, 114.29, 121.77, 122.82, 123.50, 123.88, 135.75, 139.17, 155.29, 191.47; **HRMS** (ESI) calculated for $\text{C}_{28}\text{H}_{41}\text{N}_2\text{OSi}$: 465.2937; found : 465.2914. This material was employed directly in the next step.



Preparation of (6S,11S,11aR,E)-9-ethylidene-11-(hydroxymethyl)-6,8,9,10,11,11a-hexahydro-6,10-methanoindolo[3,2-b]quinolizin-12(5H)-one (115)

The synthesis of monol 115 from TIPS derivative 114 was carried out analogous to the preparation of 110 from 109 in 85% yield $^{13}\text{H NMR}$ δ 1.68 (td, 3H, $J_1=6.6\text{Hz}$,

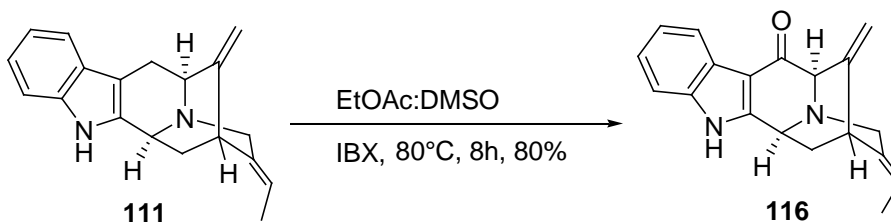
$J_2=3.9\text{Hz}$), 2.06 (m, 2H), 2.26 (m, 1H), 3.3 (m, 1H), 3.67 (dd, 1H, $J_1=11\text{Hz}$, $J_2=5\text{Hz}$), 3.77 (m, 3H), 4.28 (dd, 1H, $J_1=11\text{Hz}$, $J_2=5\text{Hz}$), 5.4 (q, 1H, $J=6\text{Hz}$), 7.27 (m, 2H), 7.47 (m, 1H), 8.01 (m, 1H); ^{13}C NMR (75.5 MHz, CD_3OD) δ 11.47, 24.85, 27.60, 38.07, 49.51, 54.62, 58.32, 63.23, 107.63, 111.63, 114.36, 120.63, 122.40, 123.30, 123.48, 136.70, 138.16, 156.29, 191.83; HRMS (ESI) calculated for $\text{C}_{19}\text{H}_{21}\text{N}_2\text{O}_2$: 309.1603; found: 309.1588. This material was employed directly in the next step.



Preparation of (6S,11S,11aR,12R,E)-9-ethylidene-11-(hydroxymethyl)-5,6,8,9,10,11,11a,12-octahydro-6,10-methanoindolo[3,2-b]quinolizin-12-ol (89)

The synthesis of **89** from **115** was carried out analogous to the preparation of **88** from **110** in 85% yield. R_f 0.71 (silica gel, $\text{CH}_2\text{Cl}_2/\text{MeOH}$, 9 : 1); $[\alpha]_D^{25} +29.0^\circ$ (c 0.6 in MeOH); [lit.¹³⁶ $[\alpha]_D^{22} = +29.5^\circ$ (c 0.6 in CH_3OH)]; ^1H NMR (300 MHz, CD_3OD) δ 1.70 (d, 3H, $J=6.9\text{Hz}$), 1.94 (m, 2H), 2.26 (m, 1H), 2.9 (q, 1H, $J=2.4\text{ Hz}$), 3.14 (dd, 1H, $J_1=11.4\text{Hz}$, $J_2=6\text{Hz}$), 3.61 (dd, 1H, $J_1=10\text{Hz}$, $J_2=5.4\text{Hz}$), 3.6 (s, 3H), 3.8 (m, 1H), 4.2 (dd, 1H, $J_1=8.4\text{Hz}$, $J_2=4\text{Hz}$), 5.4 (m, 2H), 7.0 (t, 1H, $J=7\text{Hz}$), 7.08 (t, 1H, $J=7\text{Hz}$), 7.32 (d, 1H, $J=8.1\text{Hz}$), 7.76 (d, 1H, $J=7.8\text{Hz}$); ^{13}C NMR (300MHz, CD_3OD) δ 11.48, 26.31, 28.15, 42.53, 50.10, 55.66, 58.72, 61.00, 67.33, 110.22, 110.58, 114.22, 118.64, 119.68, 120.85, 125.04, 136.17, 136.99, 138.87; HRMS (ESI) calculated for $\text{C}_{19}\text{H}_{23}\text{N}_2\text{O}_2$:

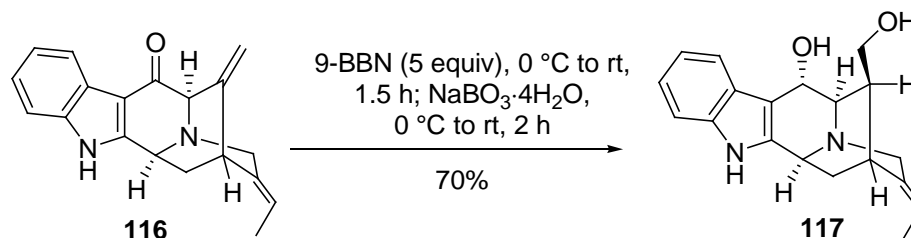
311.1760; found : 311.1773. The optical rotation and mass spectrum were in excellent agreement with the natural product.¹³⁶



Synthesis of (6*S*,11*aR*,*E*)-9-ethylidene-11-methylene-6,8,9,10,11,11*a*-hexahydro-6,10-methanoindolo[3,2-*b*]quinolizin-12(5*H*)-one (116**)**

To a solution of diene **111** (100mg, 0.36mmol) in EtOAc/DMSO (5mL/2.5mL) was added IBX (0.225mg, 1.44mmol) in one portion at rt. The mixture was stirred at 80°C overnight and the reaction progress was monitored by TLC (silica gel, EtOAc). The reaction mixture was cooled at 0 °C and quenched with a saturated solution of aq NaHCO₃ (4mL), followed by treatment with a saturated solution of aq Na₂S₂O₃ (5mL). After this, the mixture was stirred for an additional 10min at 0°C. The aq layer was extracted with additional amounts of EtOAc (3x10mL) and the combined organic layers was washed with brine (10mL) and dried (K₂CO₃). The solvent was removed under reduced pressure to provide the crude oil which was purified by chromatography [silica gel, hexane: EtOAc (3:1)] to provide the benzylic ketone **116** (84mg, 80%). ¹H NMR (300 MHz, CDCl₃) 1.66 (d, 3H, *J*=6Hz), 1.9 (m, 1H), 2.36 (m, 1H), 3.6 (m, 3H), 4.0 (m, 1H), 4.9 (d, 1H, *J*=2Hz), 5.0 (d, 1H, *J*=2Hz), 5.39 (q, 1H, *J*=6.8Hz), 7.27 (m, 2H), 7.4 (m, 1H), 7.6 (m, 2H), 8.0 (m, 1H); ¹³C NMR (75.5 MHz, CDCl₃) δ 11.13, 34.44, 38.50, 50.13, 54.41, 67.44, 105.89, 106.23, 124.30, 128.49, 128.65, 131.60, 131.74, 132.39,

135.75, 136.72, 145.10, 155.95, 190.17; **HRMS** (ESI) calculated for $C_{19}H_{19}N_2O$: 291.1497; found : 291.1513. This material was employed directly in the next step.



Preparation of (6S,11S,11aR,12S,E)-9-ethylidene-11-(hydroxymethyl)-5,6,8,9,10,11,11a,12-octahydro-6,10-methanoindolo[3,2-b]quinolizin-12-ol (117)

To a solution of olefin **116** (100 mg, 0.344 mmol) in THF (10 mL) was added 9-BBN (0.5 M in THF, 1.63 mL, 1.72 mmol) dropwise, at 0 °C. The solution was allowed to warm to rt and stirred for 1.5 h. The reaction mixture was then cooled to 0 °C and $\text{NaBO}_3 \cdot 4\text{H}_2\text{O}$ (0.795g, 5.16mmol) was added and the reaction temperature allowed to warm to rt. The mixture which resulted was stirred for 2 h at rt, diluted with CH_2Cl_2 (50 mL), washed with H_2O (3 x 50 mL) as well as brine (50 mL), and dried (K_2CO_3). The solvent was removed under reduced pressure and the residue was chromatographed (silica gel, $\text{CH}_2\text{Cl}_2/\text{MeOH}$; 9:1) to provide alcohol **117** (74mg, 70% yield). R_f 0.73 (silica gel, $\text{CH}_2\text{Cl}_2/\text{CH}_3\text{OH}$, 9 : 1); $[\alpha]_D^{25} = +17.0^\circ$ (c 0.6 in CH_3OH); [lit. $^{136} [\alpha]_D^{22} = +29.5^\circ$ (c 0.6 in CH_3OH)]]; $^1\text{H NMR}$ (300 MHz, CD_3OD) δ 1.70 (d, 3H, $J=6\text{Hz}$), 1.92 (m, 2H), 2.27 (m, 1H), 2.9 (s, 1H), 3.16 (dd, 1H, $J_1=11.4\text{Hz}$, $J_2=6\text{Hz}$), 3.61 (m, 3H), 3.8 (m, 1H), 4.2 (m, 1H), 5.3 (q, 1H, $J=6.6\text{Hz}$), 5.36 (d, 1H, $J=4.8\text{Hz}$), 7.0 (m, 2H), 7.35 (s, 1H), 7.82 (d, 1H, $J=7.5\text{Hz}$); $^{13}\text{C NMR}$ (300MHz, CD_3OD) δ 11.48, 26.35, 28.22, 42.59, 50.06,

55.69, 58.72, 59.17, 61.07, 67.42, 110.23, 110.57, 114.09, 118.62, 119.67, 120.81,
125.07, 136.35, 136.98, 139.12; **HRMS** (ESI) calculated for $C_{19}H_{22}N_2O_2$: 311.1760;
found : 311.1748

6. References:

- (1) Bentley, K. W. *The Alkaloids, in the Chemistry of Natural Products* New York, 1957.
- (2) Manske, R. H. F. *The Indole Alkaloids*; Academic Press: New York 1968; Vol. 8.
- (3) Pelletier, S. W. *Chemistry of the Alkaloids*; van Nostrand Reinhold Book Corporation: New York, 1970.
- (4) Raffauf, R. F. *Handbook of Alkaloids and Alkaloid Containing Plants*; Wiley Interscience: New York, 1970.
- (5) Glasby, J. S. *Encyclopedia of the Alkaloids*; Plenum Press: New York, 1975.
- (6) Henry, J. A. *The Plant Alkaloids*; 4 ed.; J. and A. Churchill LTD: London, 1949.
- (7) Kawai, R. S., Y.; Channing, M.; Newman, A. H.; Dunn, B.; Rice, K.C.; Biasberg, R. G. *J. Pharm. Exp. Ther.*, **1990**, 255, 826.
- (8) Cook, J. M.; LeQuesne, P. W. *Phytochemistry* **1971**, 10, 437.
- (9) Chatterjee, A.; Banerji, J.; Banerji, A. *Journal of the Indian Chemical Society* **1974**, 51, 156.
- (10) Wang, T. Enantiospecific Total Synthesis of (+)-Velloimine, (+)-Normacusine B and (-)-Norsuaveoline as well as an Improved Enantiospecific Total Synthesis of (+)-Ajmaline and (+)-Alkaloid G. Ph.D. Thesis, University of Wisconsin-Milwaukee, 2001.
- (11) Lounasmaa, M.; Hanhinen, P.; Westersund, M. *The Alkaloids* **1999**, 52.

- (12) Chatterjee, A. *Fortschr. Chem. Org. Naturstoffe* **1953**, *10*, 390.
- (13) Chatterjee, A.; Prakash, S. C.; Werner, G. *Fortschr. Chem. Org. Naturstoffe* **1956**, *13*, 346.
- (14) Cook, J. M.; LeQuesne, P. W. *J. Org. Chem.* **1971**, *36*, 582.
- (15) Kiang, A. K.; Loh, S. K.; Demanczyk, M.; Gemenden, C. W.; Papariello, G. J.; Taylor, W. I. *Tetrahedron* **1966**, *22*, 3293.
- (16) Chatterjee, A. B., *S. Ind. J. Chem.*, **1979**, *18B*, 87.
- (17) Amer, M. M.; Court, W. E. *Planta Med.* **1980**, *8*.
- (18) Lin, M.; Yang, B. Q.; Yu, D. Q. *Acta Pharmaceutica Sinica* **1986**, *21*, 114.
- (19) Banerji, J. D., B.; Chakrabarti, R.; Shoolery, J.N. *Ind. J. Chem.*, **1987**, *26B*, 709.
- (20) Feng, X. Z.; Fu, F. Y. *Acta Pharmaceutica Sinica* **1981**, *16*, 510.
- (21) Ponglux, D.; Wongseripipatana, S.; Subhairasakul, S.; Takayama, H.; Yokota, M.; Ogata, K.; Phisalaphong, C.; Aimi, N.; Sakai, S. *J. Chem. Soc. Perkin Trans.* **1989**, 5075.
- (22) Liu, G.; Liu, Z.; Feng, X. *Planta Med.* **1988**, *54*, 519.
- (23) Talapatra, S. K.; Chaudhury, N. A. *Science and Culture* **1958**, *24*, 243.
- (24) Isidro, N.; Manalo, G. D. *Journal of the Philippine Pharmaceutical Association* **1967**, *53*, 9.
- (25) Wright, C. W.; Allen, D.; Cai, Y.; Phillipson, J. D.; Said, I. M.; Kirby, G. C.; Warhurst, D. C. *Phytotherapy Research*, **1992**, 121.
- (26) Burke, D. E.; DeMarkey, C. A.; LeQuesne, P. W.; Cook, J. M. *J. Chem. Soc., Chem. Comm.* **1972**, 1346.

- (27) Ghedira, K.; Zeches-Hanrot, M.; Richard, B.; Massiot, G.; LeMen-Oliver, L.; Sevenet, T.; Goh, S. H. *Phytochemistry* **1988**, *27*, 3955.
- (28) Burke, D. E.; Cook, J. M.; LeQuesne, P. W. *J. Am Chem. Soc.* **1972**, *95*, 546.
- (29) Garnick, R. L.; LeQuesne, P. W. *J. Am. Chem. Soc.* **1978**, *100*, 4213.
- (30) Keawpradub, N.; Eno-Amooquaye, E.; Burke, P. J.; Houghton, P. J. *Planta Medica* **1999**, *65*, 311.
- (31) Burkill, I. H. *A Dictionary of the Economic Products of the Malay Peninsular*, 1935; Vol. I (A-H).
- (32) Perry, L. M.; Metzger, J. *Medicinal Plants of East and Southeast Asia*; MIT Press: Cambridge, 1980.
- (33) Achenbach, H.; Schaller, E. *Chem. Ber.* **1976**, *109*, 3527.
- (34) Munoz, V.; Moretti, C.; Sauvain, M.; Caron, C.; Porzel, A.; Massiot, G.; Richard, B.; Le Men-Oliver, L. *Planta Med.* **1994**, *60*, 455.
- (35) Elderfield, R. C. *American Scientist* **1960**, *48*, 193.
- (36) Hesse, M.; Hurzeler, H.; Gemenden, C. W.; Joshi, B. S.; Taylor, W. I.; Schmid, H. *Helv. Chim. Acta.* **1965**, *48*, 689.
- (37) Hesse, M.; Bodmer, F.; Gemenden, C. W.; Joshi, B. S.; Taylor, W. I.; Schmid, H. *Helv. Chim. Acta.* **1966**, 1173.
- (38) Esmond, R. W.; LeQuesne, P. W. *J. Am Chem. Soc.* **1980**, *102*, 7116.
- (39) Garnick, R. L. *Studies on the Chemistry of Indole Alkaloids Ph.D. Thesis*, Northeastern University, 1977.

- (40) Lounasmaa, M.; Hanhinen, P.; Westersund, M. In *The Alkaloids*; Cordell, G., Ed.; Academic Press: 1999; Vol. 52, p 103.
- (41) Hava, M. *The Vinca Alkaloids* Marcel Dekker: New York, 1973.
- (42) Svoboda, G. H.; Blake, D. A. *The Catharanthus Alkaloids*; Dekker: New York, 1975.
- (43) Kingston, D. G.; Li, B. T.; Ionescu, F.; Mangino, M. M.; Sami, S. M. J. *J. Pharm. Sci.* **1978**, *67*, 249.
- (44) Harada, M.; Ozaki, Y.; Ohno, H. *Chem. Pharm. Bull.* **1979**, *27*, 1069.
- (45) Harada, M.; Ozaki, Y. *Chem. Pharm. Bull.* **1978**, *26*, 48.
- (46) Harada, M.; Ozaki, Y. *Chem. Pharm. Bull.* **1976**, *24*, 211.
- (47) Keawpradub, N.; Kirby, G. C.; Steele, J. C.; Houghton, P. J. *Planta Medica* **1999**, *65*, 690.
- (48) Verpoote, R.; Bohlin, L.; Dwuma-Badu, D.; Rolfsen, W.; Strombom, J. J. *J. Nat. Prod.* **1983**, *46*, 572.
- (49) Leclercq, J.; de Pauw-Gillet, M. C.; Bassleer, R.; Angenot, L. *J. Ethnopharm.* **1986**, *15*, 305.
- (50) Keawpradub, N.; Houghton, P. J. *Phytochemistry* **1997**, *46*, 757.
- (51) Tan, G. T.; Pezzuto, J. M.; Kinghorn, A. D.; Hughes, L. S. H. *J. Nat. Prod.* **1991**, *54*, 143.
- (52) Tan, G. T.; Miller, J. F.; Kinghorn, A. D.; Hughes, S. H.; Pezzuto, J. M. *Biochem. Biophys. Res. Comm.* **1992**, *185*, 370.
- (53) Lounasmaa, M.; Hanhinen, P. *The Ajmaline Group of Indole Alkaloids*; Academic Press, 2001; Vol. 55.

- (54) Bi, Y.; Hamaker, L. K.; Cook, J. M. In *Bioactive Natural Products. Part A*; Basha, F. Z., Rahman, A., Eds.; Elsevier Science: Amsterdam, **1993**; Vol. 13 p383.
- (55) Hamaker, L. K.; Cook, J. M. In *Alkaloids: Chemical and Biological Perspectives*; Pelletier, S. W., Ed.; Elsevier Science: New York, 1995; Vol. 9, p 23.
- (56) Le Men, J.; Taylor, W. I. *Experientia* **1965**, 21, 508.
- (57) Koskinen, A.; Lounasmaa, M. In *Progress in the Chemistry of Organic Natural Products* Herz, W., Grisebach, H., Kirby, G. W., Eds.; Springer-Verlag: New York, 1983; Vol. 43, p 267.
- (58) Creasey, W. A. In *Heterocyclic Compounds. Indole Series*; Saxton, J. E., Ed.; John Wiley and Sons: New York, **1983**; Vol. 25, p 783.
- (59) Brugada, J.; Brugada, P. *Am. J. of Cardio.* **1996**, 78, 69.
- (60) Woodward, R. B. *Angew. Chem., Int. Ed. Engl.* **1956**, 68, 13.
- (61) Bartlett, M. F.; Lambert, B. F.; Werblood, H. M.; Taylor, W. I. *J. Am. Chem. Soc.* **1963**, 85, 475.
- (62) van Tamelen, E. E.; Haarstad, V. B.; Orvis, R. L. *Tetrahedron* **1968**, 24, 687.
- (63) Koskinen, A.; Lounasmaa, M. *Planta Medica* **1982**, 45, 248.
- (64) Pfitzner, A.; Stöckigt, J. *Tetrahedron Letters* **1983**, 24, 5197.
- (65) Dogru, E.; Warzecha, H.; Seibel, F.; Haebel, S.; Lottspeich, F.; Stöckigt, J. *Eur.J.of Biochem.* **2000**, 267, 1397.
- (66) Ruppert, M.; Ma, X.; Stöckigt, J. *Curr. Org. Chem.* **2005**, 9, 1431.

- (67) Arambewela, L. S. R.; Ranatunge, T. *Phytochemistry* **1991**, *30*, 1740.
- (68) Garnier, J.; Mahuteau, J. *Planta. Med.* **1986**, *66*.
- (69) Pinchorn, T.-M.; Nuzillard, J.-M.; Richard, B.; Massiot, G.; Le Men-
Oliver, L.; Sevenet, T. *Phytochemistry* **1990**, *29*, 3341.
- (70) Pillay, P. P. R., D. S.; Rao, S. B. *J. Sci. Ind. Res.(India)* **1960**, *19B*, 135.
- (71) Martinez, J. A.; Gomez, C.; Santana, T.; Velez, H. *Planta. Med.* **1989**, *55*,
283.
- (72) Itoh, A.; Kumashiro, T.; Yamaguchi, M.; Nagakara, N.; Mizushina, Y.;
Nish, T.; Tanahashi, T. *J. Nat. Prod.* , *68*, 848.
- (73) Aginiwa, J.; Sakai, S.; Kubo, A.; Hamamoto, T. *Yakugaku Zasshi* **1967**,
87, 1484.
- (74) Naranjo, J.; Pinar, M.; Hesse, M.; Schmid, H. *Helv. Chim. Acta.* **1972**, *55*,
752.
- (75) Monnerat, C. S.; Jorgeane de Souza, J.; Mathias, L.; Braz-Filho, R.;
Vieira, I. J. C. *J. Brazil. Chem. Soc* **2005**, *16*, 1331.
- (76) Wan, A. S. C.; Yokota, M.; Ogata, K.; Aimi, N.; Sakai, S. *Heterocycles*
1987, *26*, 1211.
- (77) Cava, M. P.; Talapatra, S. K.; Weisbach, J. A.; Douglas, B.; Raffauf, R.
F.; Ribeiro, O. *Chem. Ind.* **1964**, 1193.
- (78) Kogure, N. N., C.; Kitajima, M.; Takayama, H. *Tetrahedron. Lett.* **2005**,
46, 5857.
- (79) Forgacs, P. J., A.; Provost, J.; Thal, C.; Geilhem, J.; Pascard, C.; Moretti,
C. *Phytochemistry* **1986**, *25*, 969.

- (80) Bert, M. B., G.; Tillequin, F.; Koch, M. . *Heterocycles* **1985**, *23*, 2505.
- (81) Hu, X.-J.; He, H.-P.; Zhou, H.; Di, Y.-T.; Yang, X.-W.; Hao, X.-J.; Kong, L.-Y. *Helv. Chim. Acta.* **2006**, *89*, 1344.
- (82) Bert, M. B., G.; Tillequin, F.; Koch, M.. *Heterocycles* **1986**, *24*, 1567.
- (83) Cook, J. M.; Le Quesne, P. W.; Elderfield, R. C. *J. Chem. Soc., Chem. Commun.* **1969**, 1306.
- (84) Kam, T. S.; Choo, Y. M. *J. Nat. Prod.* **2004**, *67*, 547.
- (85) Kam, T. S.; Choo, Y. M.; Komiyama, K. *Tetrahedron* **2004**, *60*, 3957.
- (86) Rahman, A.; Nighat, F.; Sultana, A.; Desilva, K. T. D. *J. Nat. Prod. Lett.* **1994**, *5*, 201.
- (87) Kam, T. S.; Lek, I. H.; Choo, Y. M. *Phytochemistry* **1999**, *51*, 839.
- (88) Rahman, A.; Nighat, F.; Nelofer, A.; Zaman, K.; Choudhary, M. I.; DeSilva, K. T. D. *Tetrahedron* **1991**, *47*, 3129.
- (89) Kam, T. S.; Choo, Y. M. *Tetrahedron Lett.* **2003**, *44*, 8787.
- (90) Kam, T. S.; Sim, K. M. *Helv. Chim. Acta.* **2002**, *85*, 1027.
- (91) Lin, X.; Zheng, Q.; Zhang, Y. *J. Struct. Chem* **1987**, *6*, 89.
- (92) Mukherjee, R.; Da Silva, B. A.; Das, B. C.; Keifer, P. A.; Shoolery, J. N. *Heterocycles.* **1991**, *32*, 985.
- (93) Rapoport, H.; Moore, R. E. *J. Org. Chem.* **1962**, *27*, 2981.
- (94) Chuah, C.-H.; Malayas *J. Chem.* **2004**, *6*, 001.
- (95) Kishi, T.; Hesse, M.; Vetter, W.; Gemenden, C. W.; Taylor, W. I.; Schmid, H. *Helv. Chim. Acta.* **1966**, *49*, 946.
- (96) Chatterjee, A. G., A. K.; Hagaman, E. W. *J. Org. Chem.* **1982**, *47*, 1732.

- (97) Morfaux, A.; Mouton, P.; Massiot, G.; Le Men Oliver, L. *Phytochemistry* **1992**, *31*, 1079.
- (98) Morfaux, A.; Mouton, P.; Massiot, G.; Le Men-Oliver, L. *Phytochemistry* **1990**, *29*, 3345.
- (99) Kan-Fan, C. M., G.; Das, B. C.; Potier, P. *J. Org. Chem.* **1981**, *46*, 1481.
- (100) Khan, Z. M.; Hesse, M.; Schmid, H. *Helv. Chim. Acta.* **1967**, *50*, 1002.
- (101) Yoneda, N. *Chem. Pharm. Bull.* **1965**, *13*, 1231.
- (102) Mashimo, K.; Sato, Y. *Tetrahedron Lett.* **1969**, *10*, 905.
- (103) Cloudsale, I. S.; Kluge, A. F.; McClure, N. L. *J. Org. Chem.* **1982**, *47*, 919.
- (104) Hobson, J. D.; Raines, J.; Whiteoak, R. J. **1963**, 3495.
- (105) Soerens, D. Part I. Studies of the Pictet-Spengler Reaction in Aprotic Media. Part II. Studies Directed Toward the Total Synthesis of the Indole Alkaloid Suaveoline. Ph.D. Thesis, University of Wisconsin-Milwaukee, 1978.
- (106) Zhang, L. H.; Cook, J. M. *Heterocycles* **1988**, *27*, 2795.
- (107) Michel, P.; Rassat, A.; Daly, J. W.; Spande, T. F. *J. Org. Chem.* **2000**, *65*, 8908.
- (108) Gennet, D.; Michel, P.; Rassat, A. *Synthesis* **2000**, 447.
- (109) Kuethe, J. T.; Wong, A.; Davies, I. W.; Reider, P. J. *Tetrahedron Lett.* **2002**, *43*, 3871.
- (110) Neipp, C. E.; Martin, S. F. *Synthesis of Bridged Azabicyclic Structures via Ring-Closing Olefin Metathesis* **2003**, *68*, 8867.

- (111) Bailey, P. D.; McLay, N. R. *J. Chem. Soc., Perkin Trans.1* **1993**, 441.
- (112) Magnus, P.; Mugrage, B.; Deluca, M. R.; Cain, G. A. *J. Am. Chem. Soc.* **1990**, *112*, 5220.
- (113) Edwankar, C. R.; Edwankar, R. V.; Rallapalli, S. K.; Cook, J. M. *Nat. Prod. Commun.* **2008**, *3*, 1839.
- (114) Kitajima, M.; Takayama, H.; Sakai, S. *J. Chem. Soc., Perkin Trans.1* **1991**, *1*, 1773.
- (115) Martin, S. F.; Chen, K. X.; Eary, C. T. *Org. Lett.* **1999**, *1*, 79.
- (116) Rawal, V. H.; Michoud, C.; Monestel, R. *J. Organomet. Chem.* **1993**, *115*, 3030.
- (117) Bonjoch, J.; Sole, D.; Bosch, J. *J. Am. Chem. Soc.* **1995**, *117*, 11017.
- (118) Wang, T.; Cook, J. M. *Org. Lett.* **2000**, *2*, 2057.
- (119) Yu, J.; Wang, T.; Liu, X.; Deschamps, J.; Flippen-Anderson, J.; Liao, X.; Cook, J. M. *J. Org. Chem.* **2003**, *68*, 7565.
- (120) Ensley, H. E.; Buescher, R. R.; Lee, K. *J. Org. Chem.* **1982**, *47*, 404.
- (121) Kuehne, M. E.; Wang, T.; Seraphin, D. *J. Org. Chem.* **1996**, *61*, 7873.
- (122) Yang, J.; Rallapalli, S. *Tetrahedron. Lett.* **2010**, *51*, 815.
- (123) Birman, V. B.; Rawal, V. H. *Tetrahedron Lett.* **1998**, *39*, 7219.
- (124) Muratake, H.; Natsume, M. *Tetrahedron Lett.* **1997**, *38*, 7581.
- (125) Liu, X.; Wang, T.; Xu, Q.; Ma, C.; Cook, J. M. *Tetrahedron. Lett.* **2000**, *41*, 6299.
- (126) Liu, X.; Cook, J. M. *Org. Lett.* **2002**, *3*, 4023.

- (127) Liu, X. Enantiospecific, Stereospecific Total Synthesis of the Enantiomers of the Indole Alkaloids N_a-Methylvellosimine, Affinisine and Macroline as well as the Total Synthesis of the Indole Alkaloids Trinervine, Alstophylline and the Antimalarial Bisindole Macralstonine. Ph.D. Thesis, University of Wisconsin-Milwaukee, 2002.
- (128) Liao, X.; Zhou, H.; Yu, J.; Cook, J. M. *J.Org.Chem.* **2006**, *71*, 8884.
- (129) Fox, J. M.; Huang, X.; Chieffi, A.; Buchwald, S. L. *J. Am. Chem. Soc.* **2000**, *122*, 1360.
- (130) Liao, X. The First Total Synthesis of the Indole Alkaloids Macralstonidine, 6-Oxoalstophylline, 10-Methoxyvellosimine, Lochnerine, Sarpagine and Improved Total Synthesis of the Indole Alkaloids Macralstonine and Macroline as well as the Formal Total Synthesis of Dispegatine. Ph.D. Thesis, University of Wisconsin-Milwaukee, 2007.
- (131) van Tamelen, E. E.; Yardley, J. P.; Miyano, M.; Hinshaw Jr., W. B. *J. Am. Chem. Soc.* **1969**, *91*, 7349.
- (132) van Tamelen, E. E.; Oliver, L. K. *J. Am. Chem. Soc.* **1970**, *92*, 2136.
- (133) van Tamelen, E. E.; Oliver, L. K. *Bioorg. Chem.* **1976**, *5*, 309.
- (134) Lounasmaa, M.; Hanhinen, P. *Tetrahedron* **1996**, *52*, 15225.
- (135) Deiters, A.; Chen, K.; Eary, C. T.; Martin, S. F. *J. Am. Chem. Soc.* **2003**, *125*, 4541.
- (136) Malikov, V. M.; Sharipov, M. R.; Yunusov, S. Y. *Khim.Prir. Soedin.* **1972**, *8*, 760.

- (137) Glasby, J. S. *Encyclopedia of the Alkaloids*; Plenum Press: New York, 1976; Vol. 3.
- (138) Rakhimov, D. A. S., M. R.; Aripov, Kh. N.; Malikov, V. M.; Shakirov, T. T.; Yunusov, S. Yu. *Khim.Prir. Soedin.* **1970**, *6*, 724.
- (139) Manske, R. F. T. *The Alkaloids Chemistry and Physiology* **1965**, *VII*.
- (140) Sakai, S.; Kubo, A.; T., H.; Wakabayshi, M.; Takahashi, K.; Ohtani, J.; Haginiwa, J. *Tetrahedron Lett.* **1969**, *19*, 1489.
- (141) Cox, E.; Cook, J. M. *Chem. Rev.* **1995**, *95*, 1797.
- (142) Czerwinski, K.; Cook, J. M. *Stereochemical Control of the Pictet-Spengler Reaction in the Synthesis of Natural Products*; JAI Press: Greenwich, 1996; Vol. 3.
- (143) Han, D.; Försterling, F. H.; Deschamps, J. R.; Parrish, D.; Liu, X.; Yin, W.; Huang, S.; Cook, J. M. *J. Nat. Prod.* **2007**, *70*, 75.
- (144) Kumpaty, H. L.; Van Linn, M. L.; Kabir, M. S.; Försterling, F. H.; Deschamps, J. R.; Cook, J. M. *J. Org. Chem.* **2009**, *74*, 2771.
- (145) Lorenz, M.; Van Linn, M. L.; Cook, J. M. *Curr. Org. Synth.* **2010**, *7*, 189.
- (146) Van Linn, M. L.; Cook, J. M. *J. Org. Chem.* **2010**, *75*, 3587.
- (147) Yu, P.; Wang, T.; Yu, F.; Cook, J. M. *Tetrahedron Lett.* **1997**, *38*, 6819.
- (148) Yu, P. Enantiospecific Total Synthesis of the Indole Alkaloids Talpinine, Talcarpine, Alstonerine and Anhydromacrosalpine-methine as well as Studies Directed Toward the Synthesis of the Oxindole Alkaloid Alstonisine. Ph.D. Thesis, University of Wisconsin-Milwaukee, 1999.
- (149) Yu, P.; Wang, T.; Li, J.; Cook, J. M. *J. Org. Chem.* **2000**, *65*, 3173.

- (150) Cao, H.; Yu, J.; Wearing, X. Z.; Zhang, C.; Liu, X.; Deschamps, J. R.; Cook, J. M. *Tetrahedron Lett.* **2003**, *44*, 8013.
- (151) Zhou, H.; Sarma, P. V. V. S.; Han, D.; Cook, J. M. *Tetrahedron Lett.* **2005**, *46*, 4219.
- (152) Shimizu, M.; Ishikawa, M.; Komoda, Y.; Nakajima, T.; Yamaguchi, K.; Sakai, S. *Chem. Pharm. Bull.* **1984**, *32*, 1313.
- (153) Zhang, L. H.; Bi, Y.; Yu, F.; Menzia, G.; Cook, J. M. *Heterocycles* **1992**, *34*, 517.
- (154) Zhao, S.; Liao, X.; Wang, T.; Flippen-Anderson, J.; Cook, J. M. *J. Org. Chem.* **2003**, *68*, 6279.
- (155) Kraft, M. E.; Cran, J. W. *Synlett* **2005**, *8*, 1263.
- (156) Yin, W.; Ma, J.; Rivas, F. M.; Cook, J. M. *Org. Lett.* **2007**, *9*, 295.
- (157) Wang, T.; Cook, J. M. In *220th ACS National Meeting* Washington, DC, United States, 2000.
- (158) Amatore, C.; Carre, E.; Jutand, A.; M'Barki, M. A. *Organometallics* **1995**, *14*, 1818.
- (159) Beletskaya, I. P.; Cheprakov, A. V. *Chem. Rev.* **2000**, *100*, 3009.
- (160) Wang, T.; Cook, J. M. *Org. Lett.* **2000**, *2*, 2057.
- (161) Sole, D.; Peidro, E.; Bonjoch, J. *Org. Lett.* **2000**, *2*, 2225.
- (162) Sole, D.; Urbaneja, X.; Bonjoch, J. *Adv. Synth. Catal.* **2004**, *346*, 1646.
- (163) Dess, D. B.; Martin, J. C. *J. Am Chem. Soc.* **1991**, *113*, 7277.
- (164) Gemal, A. L.; Luche, A. L. *J. Am Chem. Soc.* **1981**, *103*.
- (165) Frigerio, M.; Santagostino, M.; Sputore, S. *J. Org. Chem.* **1999**, *64*, 4537.

- (166) DeMunari, S.; Frigerio, M.; Santagostino, M. *J. Org. Chem.* **1996**, *61*, 9272.
- (167) Corminboeuf, O.; Overman, L. E.; Pennington, L. D. *J. Org. Chem.* **2009**, *74*, 5458.
- (168) Clive, D. L. J.; Wang, J. *J. Org. Chem.* **2004**, *69*, 2773.
- (169) Brown, H. C.; Kanth, J. V. B.; Dalvi, P. V.; Zaidlewicz, M. *J. Org. Chem.* **1999**, *65*, 4655.
- (170) Li, J. J.; Limberakis, C.; Pflum, D. A. *Modern Organic Synthesis in the Laboratory*; Oxford University Press: New York, 2007.
- (171) Iwasaki, T.; Nishitani, T.; Horikawa, H.; Inoue, I. *J. Org. Chem.* **1982**, *47*, 3799.
- (172) Loh, T.-P.; Cao, G.-Q.; Pei, J. *Tetrahedron Lett.* **1998**, *39*, 1453.
- (173) Pfitzner, A.; Stockigt, J. *Planta Med.* **1983**, *48*, 221.
- (174) Jokela, R.; Lounasmaa, M. *Heterocycles* **1996**, *43*, 1015.

**II. THE SYNTHESIS OF ALPHA 5 SUBTYPE SELECTIVE LIGANDS FOR
GABA (A) /BENZODIAZEPINE RECEPTORS**

1. Introduction

The GABA_A /benzodiazepine receptor (BzR) is the major neurotransmitter in the central nervous system which is inhibitory in action.¹ This receptor is involved in many functions of the CNS as well as in many diseases.² Many of these diseases occur due to the improper balance of neurotransmitters which can be restored using therapeutics. The benzodiazepines continue to be the most widely used drug to treat various disorders such as anxiety disorders³ and epilepsy⁴ but they have side effects including muscle relaxant/ataxic, sedative-hypnotic effects, hypersensitive behavior, phobias, along with effects which lead to or complicate drug abuse⁵.

The γ -aminobutyric acid (GABA_A) receptors are heteroligomeric membrane-bound protein complexes that are composed of several subunits and are termed type A, type B and type C. In the case of type A receptors, the inhibitory effects of GABA mediated by these receptors can be modulated by a number of pharmacological agents that selectively bind to allosteric sites on these ion channels.⁶⁻⁹ GABA_A receptors are pentameric assemblies of proteins derived from a family of subunits ($6\alpha3\beta3\gamma1\delta1\pi1\theta1\varepsilon$ and 3ρ) which form the chloride ion channel. The most common form of native GABA_A receptors contains α , β , and γ subunits in a 2:2:1 stoichiometry.¹⁰⁻¹² It has been shown that recombinant receptors which contain these subunits most closely mimic the biological, electrophysiological and pharmacological properties of native GABA_A receptors which contain a benzodiazepine recognition site (GABA_A/Bz receptors).¹³ The benzodiazepine binding site is located at the interface between ^{14,15} α and γ subunits.¹⁶ While it is clear the γ subunit is also required for benzodiazepine binding,^{11,13} the fact that most native GABA_A receptors contain a $\gamma2$ subunit is in agreement with the α

subunit as the key determinant of benzodiazepine binding and efficacy. However, it is clear the gamma subunit is also required for benzodiazepine binding (see Figure 1) was mentioned. Recent advances in molecular biology have identified 21 subunits which comprise a series of GABA_A/BzR subtypes (ion channels).¹⁷⁻²¹ Importantly, it has now been found that certain disease states, as well as tolerance and dependence are related to the up or down regulation of specific subunits.

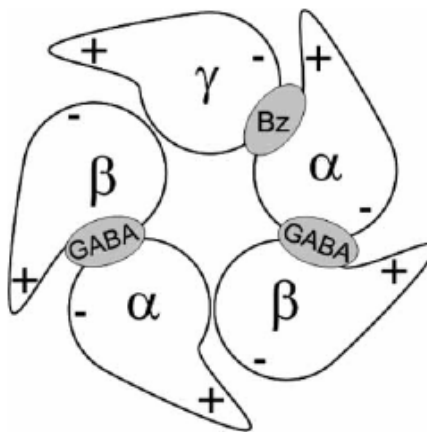
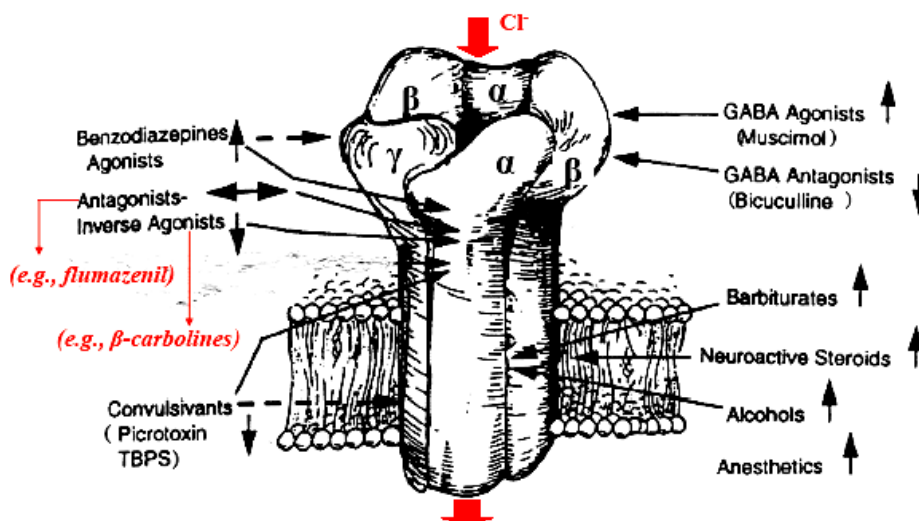


Figure 1. Absolute subunit arrangement of the $\alpha 1\beta 2\gamma 2$ GABA_A receptor when viewed from the synaptic cleft. The GABA binding sites are located at the $\beta^+\alpha^-$ subunit interfaces and the modulatory Bz BS (Bz) is located at the $\alpha^+\gamma^-$ subunit interface.^{22,23}

1.2. Benzodiazepine pharmacology

Ligands that bind to the BZ site can influence the binding of GABA to its receptor and thereby alter the flux of chloride ions through the ion channel.²⁴ Ligands at the BZ site are categorized as agonists, inverse agonists, or antagonists. Agonists enhance the effects of GABA by increasing the frequency of channel opening to provide a net

hyperpolarization of the neuron and a decreased excitability. BZ inverse agonists have the opposite effect and decrease the flow of chloride ions (negative modulators, NAM) which results in a depolarization and an increased neuronal excitability. Between the two efficacy extremes, there is a continuum of partial agonists and partial inverse agonists as well as antagonists, the latter of which do not alter chloride flow and are functionally silent. These different efficacies are reflected in different behavioral effects of BzR site ligands in mammalian species. The schematic diagram of subunits and ligands of the benzodiazepine-GABA receptor-chloride channel complex can be seen in Figure 2.



The five subunits of the GABA_A receptor complex:

- 2 α subunits (comprising of at least six peptides designated $\alpha 1$ - $\alpha 6$)
 - 2 β subunits (comprising of at least 4 peptides designated $\beta 1$ - $\beta 4$)
 - 1 γ gamma subunit (comprising of at least 3 peptides designated $\gamma 1$ - $\gamma 3$)
- Subunits other than α , β , and γ exist.

Figure 2. The schematic diagram of subunits and ligands of the benzodiazepine-GABA receptor-chloride channel complex. Reprinted with permission of the author.

The interaction with benzodiazepines (BZ, Figure 3) has been a major influence in studies on GABA receptors because of the long history of the therapeutic application of BZs as anxiolytics, anticonvulsants, sedative-hypnotics, and muscle relaxants.^{9,25} Although the BZs were first introduced into clinical practice in the early 1960s, it was not until 1975 that these drugs were shown to act by potentiating the inhibitory actions of GABA in the brain.^{1,25} The presence of high-affinity specific binding sites for BZs in the mammalian brain was then demonstrated by Squires, Haefely et al.^{6,26,27} Converging lines of evidence established that these sites were contained in the same macromolecule as the GABA sites and the chloride channel, moreover, that all three elements were coupled allosterically.²⁸⁻³⁰ The term "GABA/BZ receptor" came into use for this complex (and is still encountered). Until recently, progress in this field was driven by the synthesis of a vast range of BZs and BZ-like drugs, which acted at the allosteric BZ sites in the brain. GABA_A receptors exhibited clinical anxiolytic or sedative properties which correlated to their binding potencies in the CNS.³¹ The structures of some ligands which act at the BZ site are shown in Figure 3.

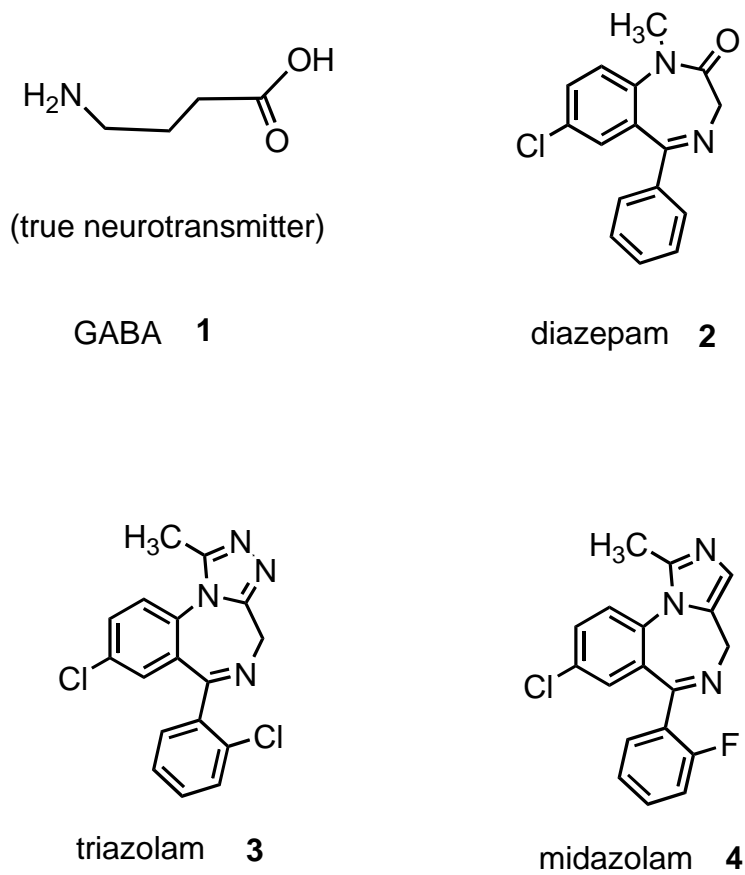


Figure 3. GABA, diazepam, triazolam and midazolam.

BDZs, such as diazepam(2), are the most potent anticonvulsant, muscle relaxant, sedative-hypnotic and anxiolytic compounds in clinical use.³² They do not substitute for GABA, but instead enhance the inhibitory effects of GABA. BDZ's allosterically bind to the receptor at a different location than GABA does and enhance the chloride channels conductance by increasing the frequency of gated channel opening.³³⁻³⁷ BDZ and compounds interacting with the benzodiazepine site of GABA_A receptors can only modulate ongoing GABAergic activity (see Figure 4). These compounds cannot elicit chloride ion flux in the absence of GABA^{33,37} and thus can exhibit an extremely low degree of toxicity. Many different classes of compounds have been shown to interact with the BDZ binding site of GABA_A receptors.³⁸⁻⁴² In each of these classes, compounds

could be identified that enhanced or reduced the action of GABA on GABA_A receptors, as mentioned above.

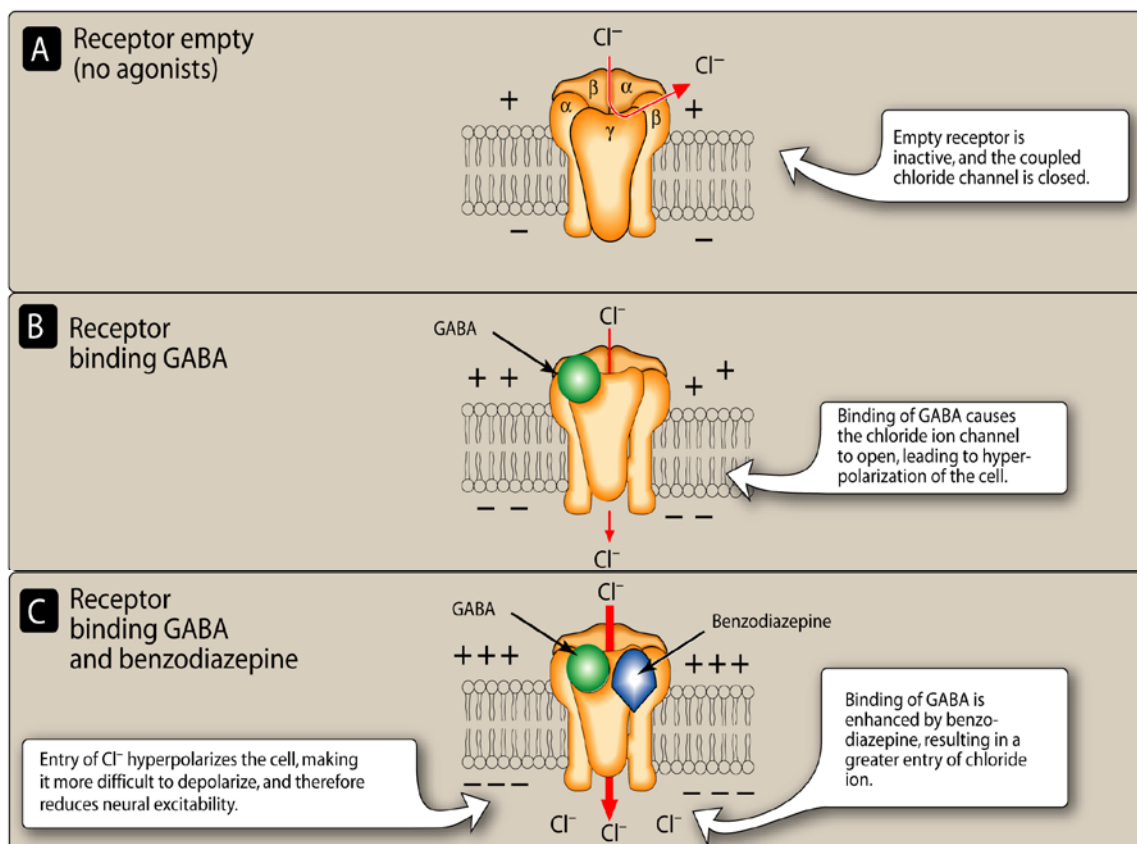


Figure 4: Mode of action of benzodiazepines. Reprinted with permission of the author

1.3. Molecular Modeling

An extensive study of the BzR pharmacophore has been carried out in Milwaukee.⁴²⁻⁴⁷

Based on data from at least 166 ligands at BzR, a unified BzR pharmacophore receptor model of the BDZ receptor has been developed. Outlined in Figure 5 are the proposed descriptors required for high affinity binding to the inclusive pharmacophore.^{43,48} The important points of the model include three anchor points which were termed L₁, H₁, and H₂; region L₁ represents a center of lipophilic interaction with the ligands, while H₁, H₂

and A_2 represent two hydrogen bond donor sites and one hydrogen bond acceptor site on the receptor protein, respectively, in the receptor binding domain.⁴⁹ Three additional lipophilic regions were also proposed, termed L_2 , L_3 and L_{Di} , which are important for binding affinity and selectivity as well as efficacy of ligands. It is noteworthy to mention that lipophilic interactions between a ligand and the receptor include vander Waals interactions, as well as potential π - π and p - π stacking between the aromatic moieties of the ligand and groups on the receptor protein.

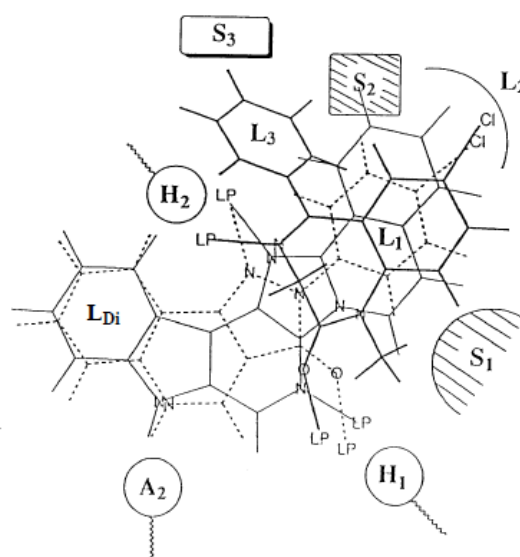


Figure 5. Diazepam in the Pharmacophore/Receptor Model for the BzR Site.

Pyrazolo[3,4-c]quinolin-3-one CGS-9896 (dotted line), a diazadiindole (thin line), and diazepam (thick line) fitted to the inclusive pharmacophore model for the BzR. Sites H1 and H2 represent hydrogen bond donor sites on the receptor protein complex, while A2 represents a hydrogen bond acceptor site necessary for potent inverse activity in vivo. L1, L2, L3 and LDi are four lipophilic regions in the binding pharmacophore. Descriptors S1, S2, and S3 are regions of negative steric repulsion.

Areas of negative steric repulsion with the protein are described as S_1 , S_2 , and S_3 . Examination of the included volumes indicated that the shapes of binding pockets for α_1 , α_2 and α_3 subtypes are very similar to each other. Region L2 for the α_5 containing subtype appeared to be larger in size than the analogous region of the other receptor subtypes. The LDi region in contrast appeared to be larger in the α_1 subtype than in the other subtypes.⁵⁰ The receptor subtype descriptor termed the DI site is related to α_4 and α_6 BzR, which is devoid of or has a very small lipophilic pocket L_3 in comparison to the other four (α_1 , α_2 , α_3 , and α_5) subtypes. The DI region appears to be near the outside of the receptor binding cleft and may be important as well for interactions at the α_1 subtype which results sometimes in increased α_1 subtype selective affinity. With the aid of these models, several series of ligands have been synthesized and evaluated pharmacologically to determine the interaction with the GABA/benzodiazepine receptor subtype selective ligands.

2. Objective of this research

Benzodiazepines and related drugs have been documented to disrupt memory in human and non-human subjects.^{10,13,47,51} Broadly stated, administration of Bz-type drugs can result in a loss of the ability to form new memories. The memory deficits induced by Bz-type drugs are strikingly similar to those associated with lesions of the hippocampus.⁵² Neurons in the hippocampus express structurally diverse $GABA_A$ receptors.^{53,54} The highest density of α_5GABA_A receptors is found in the hippocampus proper (see Figure 6) and these receptors are mostly extra-synaptic.⁵³ The distribution of α_5GABA_A receptors in the hippocampus raises the possibility that this subtype plays a

distinct role in memory deficits induced by Bz-type drugs.⁵⁵ While memory deficits induced by Bz-type drugs represent a clinical burden, understanding the mechanisms underlying these deficits might represent a therapeutic boon.

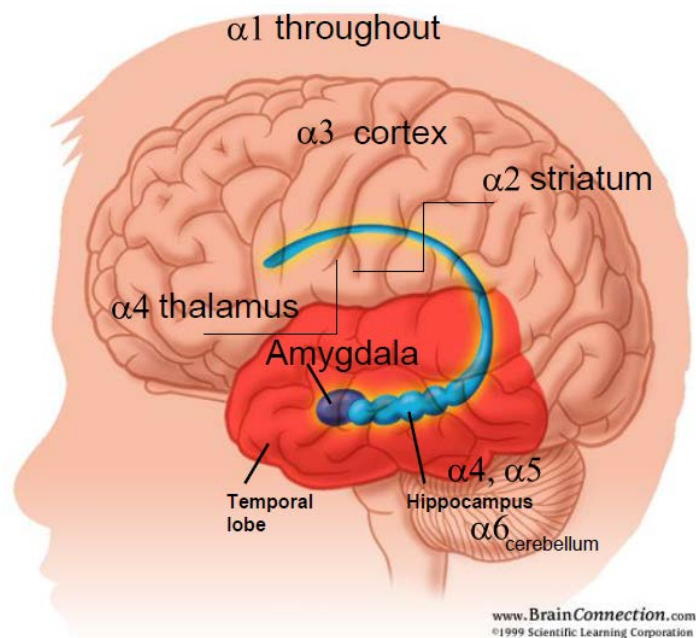


Figure 6: Distribution of $\alpha 5$ receptor in the Hippocampus. Reprinted with permission of author.

In this regard, there is increasing evidence that inverse agonists with selectivity for the $\alpha 5$ GABA_A receptor subtype may enhance cognition.⁵⁶ Since $\alpha 5$ GABA_A subtypes modulate memory processes, the specific aim of this research is to synthesize $\alpha 5$ subtype selective ligands which can be used to treat disorders such as cognitive dysfunction which includes Alzheimer's disease devoid of side effects (sedative, addictive, hypnotic, muscle relaxant and convulsant effects). A key rationale for this

approach is that GABA neurons in the hippocampus and temporal cortical areas are largely preserved in patients^{57,58} with Alzheimer's disease (AD), and these preserved neurons contain $\alpha 5$ GABA_A receptor subtypes that are only moderately reduced in number in AD.⁵⁸

Another critical therapeutic goal of this research is to synthesize ligands which would also reduce anxiety. In fact, BZ-type drugs are commonly given to dementia patients exhibiting "agitation" (usually defined as "inappropriate verbal, vocal, or motor activity not explainable by apparent needs or confusion").⁵⁹ Thus, in addition to enhancing cognition, it would be advantageous to develop analogs which may provide a unique approach to reduce agitation/anxiety in patients with cognitive disorders.

3. Results and Discussion

3.1. Synthesis of $\alpha 5$ selective 1, 4 benzodiazepines

The need for $\alpha 5$ selective ligands to study the hippocampus, as well as results based on previous structure-activity relationships⁶⁰⁻⁶⁴ prompted a study of agonist selectivity by modification of 7-substituted benzodiazepines.⁶⁰⁻⁶³ Earlier in this laboratory,^{49,62-66} a series of acetylene based $\alpha 5$ selective inverse agonists were prepared.⁶⁷ These agents were among the most $\alpha 5$ selective ligands ever reported.⁶⁷ Because the acetylene function (interaction in lipophilic pocket L₂) enhanced selectivity at $\alpha 5$ BzR, it was decided to effect a similar change with orally active benzodiazepines to extend the SAR. In the past two decades computer modeling has evolved into a full-fledged discipline independent from traditional structure-activity-relationships (SAR) and molecular

biology and proven to be a valuable tool in drug discovery.⁶⁸⁻⁷⁶ This technique was important in the development of selective ligands for GABA/BzR subtypes due to the diversity of structural classes of active ligands which bound to these subtypes.^{31,74,76} For this the unified pharmacophore/receptor model (see Figure 5) which was described previously was used.

In order to develop orally active high affinity selective ligands for $\alpha 5$ containing isoforms at the BzR, diazepam was chosen as the starting point. According to classical structure-activity-relationships,⁷⁷ diazepam does not bind to $\alpha 4$ and $\alpha 6$ containing isoforms (these are termed “diazepam insensitive sites”),^{77,78} consequently, interaction at $\alpha 4$ and $\alpha 6$ sites was retarded from the beginning. It was felt diazepam bound to all diazepam sensitive (DS) receptor subtypes at the three anchor points: H₁, H₂ and L₁.^{65,71,79} The imine nitrogen atom was believed to be hydrogen bonded to a hydrogen bond donor site on the receptor protein(H₂), the carbonyl oxygen was felt to be hydrogen bonded to another hydrogen bonding descriptor(H₁), while the benzene A-ring interacted with the receptor protein at a lipophilic site (L₁). In addition, it was felt diazepam also interacted in lipophilic pockets L₂ and L₃, as shown in Figure 7. Lipophilic pocket L₃ was believed to be very small in $\alpha 4$ and $\alpha 6$ containing isoforms which retarded affinity of 1,4-benzodiazepines at these subtypes.^{49,79,80} When the agonist QH-II-066 **11** was aligned in the included volume of pharmacophore/receptor for $\alpha 2\beta 3\gamma 2$ and $\alpha 5\beta 3\gamma 2$ subtypes, the fit was excellent (Figure 9 and Figure 10) respectively.

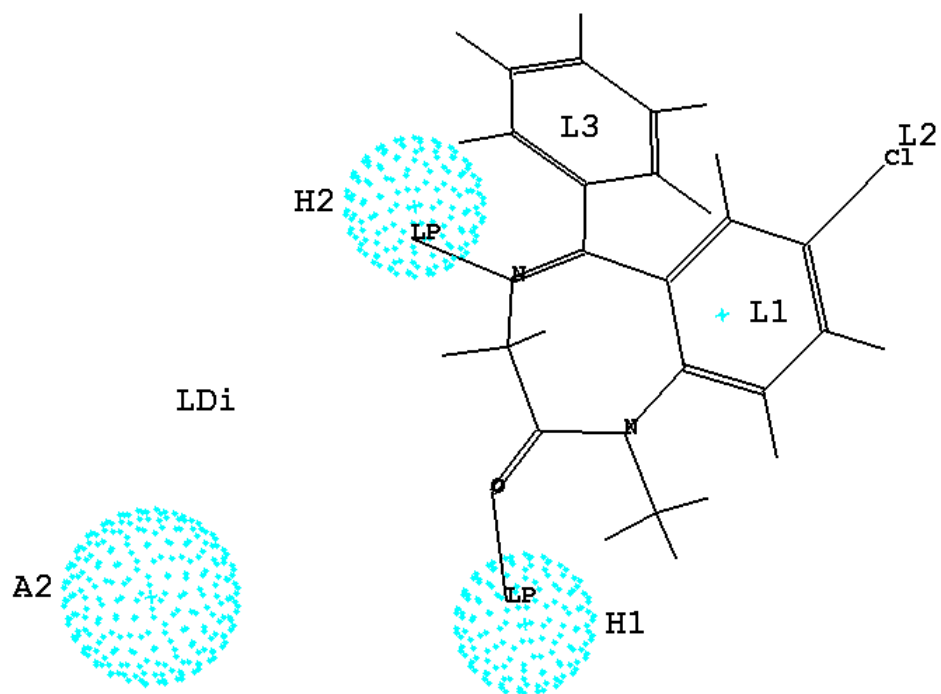


Figure 7. Diazepam (2) aligned in the pharmacophore model.^{75,81}

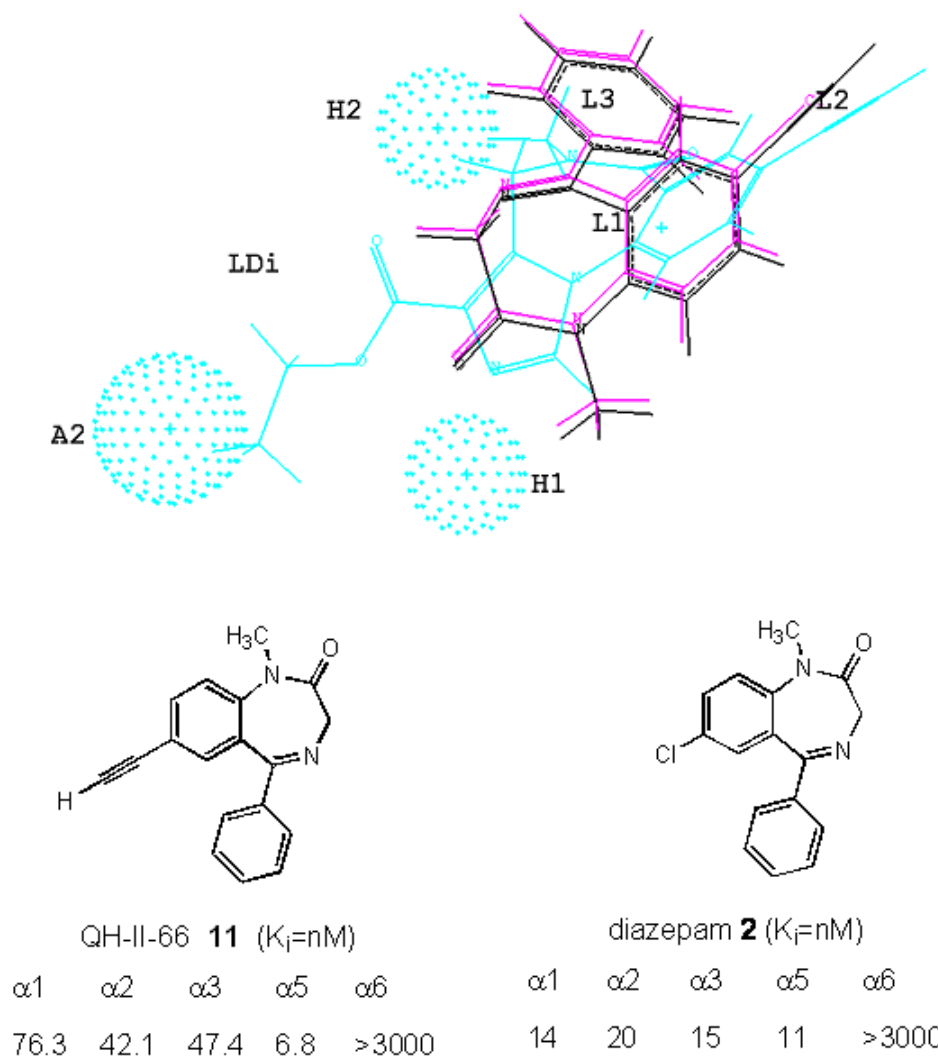


Figure 8: The ligand QH-II-66, (**11**, a 7-acetylenyl-1, 4-benzodiazepine, in black), was designed to offer better occupation of this region and exhibit $\alpha 5$ selectivity. Note that diazepam shown in the Figure was intentionally offset from its original position, which had overlapped completely with QH-II-066, solely for the sake of visualization.^{65, 66}

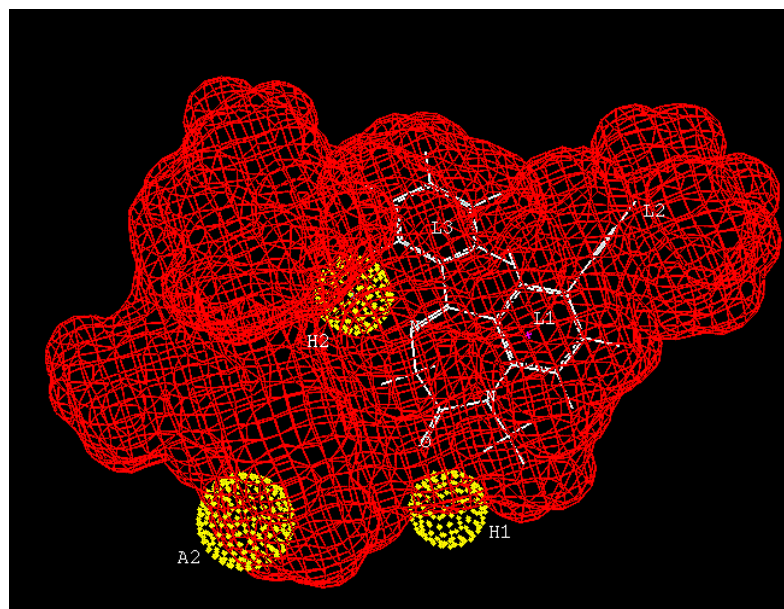


Figure 9. The ligand, QH-II-66 **11**, aligned in the included volume of the pharmacophore/receptor model for the $\alpha_2\beta_3\gamma_2$ subtype.

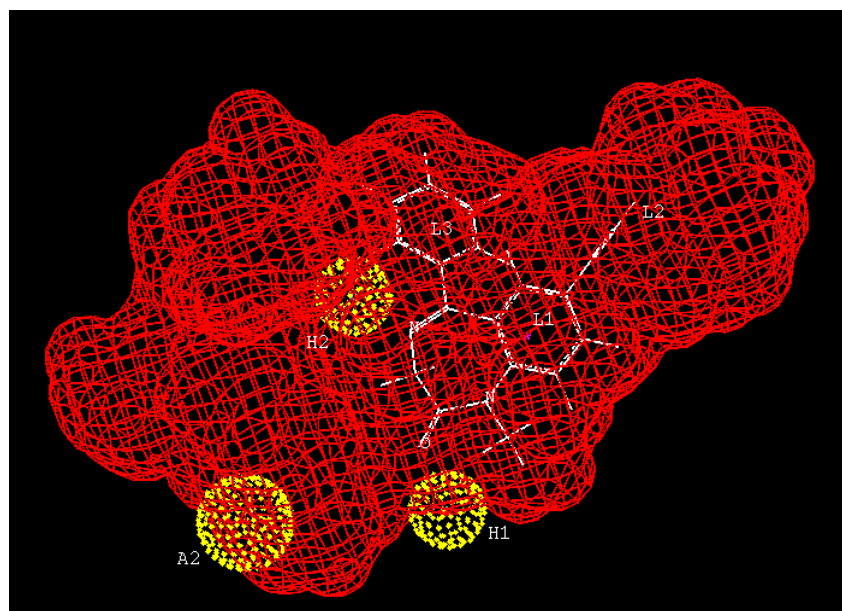


Figure 10. The ligand, QH-II-66 **11**, aligned in the included volume of the pharmacophore/receptor model for the $\alpha_5\beta_3\gamma_2$ subtype.

Based on the findings at $\alpha 5$ containing isoforms^{64,74,76,81} and the results in the imidazobenzodiazepine series described previously,⁶¹⁻⁶³ a diazepam analog with an acetylenic function at position-7(QH-II-066, **11**) was prepared, and better selectivity *in vitro* for $\alpha 5$ containing isoforms was immediately achieved in the agonist series.^{74-76,82} It was felt that lipophilic pocket L₂ was larger in $\alpha 5$ containing subtypes as compared to $\alpha 1$ containing isoforms,^{47,74-76} hence the $\alpha 5$ subtype tolerated a larger lipophilic group in region L₂. To develop ligands more selective for $\alpha 5$ containing BzR subtypes, interactions at H₁, H₂ or L₃ must be modified since not many changes can be done at the L₂ pocket.

3.1.2. Synthesis of gram quantities of the 1, 4 benzodiazepine (QH-II-066)

The large scale synthesis here of this $\alpha 5\beta 3\gamma 2$ selective ligand **11** (Scheme 1), which began from 2-aminobenzophenone **5** and followed the classic work of Fryer, Sternbach et al.^{83,84} as modified by Huang and Liu, was carried out.^{65,85} Benzophenone **5** was acylated on 100 gram scale by bromoacetyl bromide. The bromoacetamide **6** which resulted was then treated with a saturated solution of ammonia (gas) in methanol at reflux to afford benzodiazepine **7** in 99% yield. Regioselective bromination⁸⁴ of this ligand at position-7 was realized after treatment with 2 equivalents of bromine in acetic acid in the presence of 2 equivalents of concentrated sulfuric acid at room temperature. After the reaction was allowed to stir for seven days, ninety percent of the monobrominated benzodiazepine **8** was obtained after alkaline workup. It was necessary to stir the reaction with only 2 equivalents of bromine for several days to prevent

dibromination. Attempts to use additional bromine or to heat the reaction mixture resulted in polybromination. It was difficult to remove the dibrominated side product from the desired 1, 4-benzodiazepine **8**, consequently, the reaction was run over several days. The bromide **8** then was reacted with trimethylsilylacetylene in the presence of a palladium catalyst to provide trimethylsilyl analog **9**.^{62,86,87} This TMS-protected material **9** was then methylated with methyl iodide/sodium hydride to give the N-methyl benzodiazepine **10**. In this manner the acetylenic function was not methylated. This material was subjected to fluoride-mediated desilylation on 20 g scale to furnish gram quantities of **11** (QH-II-066) for studies in rodents and primates.

In agreement with the molecular modeling, QH-II-066 **11** indeed bound more potently to $\alpha 5\beta 3\gamma 2$ subtypes than to $\alpha 1\beta 3\gamma 2$ GABA/BzR receptor sites. This important result indicated that perhaps QH-II-066 might exhibit anxiolytic activity but would exert less sedative-hypnotic, muscle relaxant or ataxic effects when compared to the control (diazepam **2**).

Scheme 1: Synthesis of QH-II-066

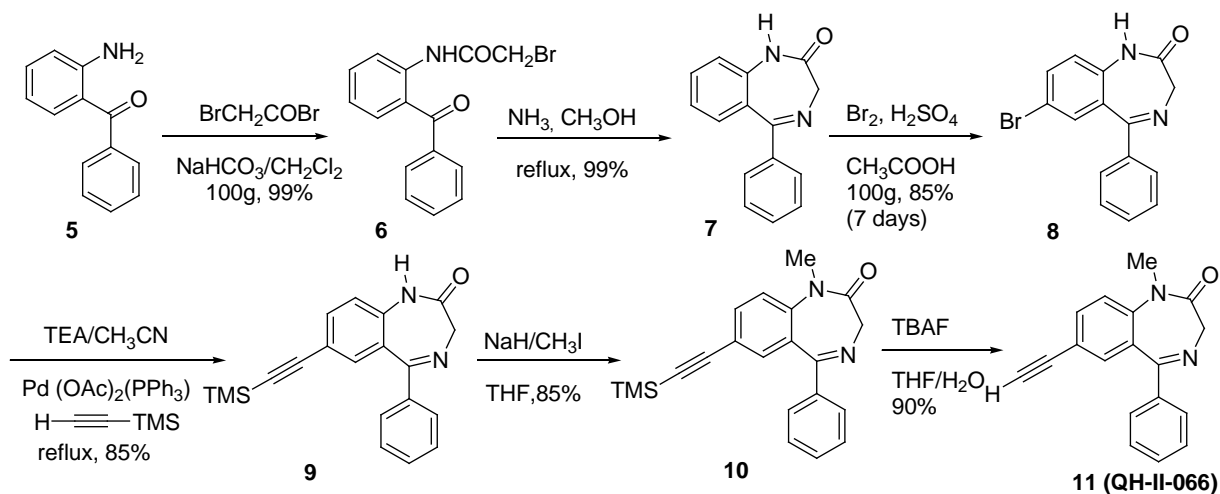


Table 1. *In Vitro* Receptor Binding Data of Diazepam (**2**) and QH-II-066 (**11**). Binding Affinity at $\alpha x\beta 3\gamma 2$ GABA_A/BzR Receptor Subtypes (Values are Reported in nM)

Compound	$\alpha 1$	$\alpha 2$	$\alpha 3$	$\alpha 4$	$\alpha 5$	$\alpha 6$
Diazepam (2)	14	7.8	13.9	ND ^a	13.4	ND ^a
QH-II-066 (11)	76.3	42.1	47.4	ND ^a	6.8	>3000

ND: not determined yet. ^aBinding at $\alpha 4$ and $\alpha 6$ subtypes has not been determined, but since the 6-phenyl group is present, the ligand will not bind to $\alpha 4$ and $\alpha 6$ subtypes.

Studies by Lelas and Cook et al.⁸⁸ reflect that QH-II-066 **11** has functional selectivity *in vivo* with diazepam-like efficacy at $\alpha 5$ and partial efficacy at the $\alpha 1$ subtype. This study showed that QH-II-066 had anxiolytic activity with reduced sedative effects compared to diazepam **2**. This study also indicated that the 7-acetyleno substituted diazepam analog exhibited less potency against ECS induced seizures relative to diazepam than against PTZ-induced seizures. Hence $\alpha 1$ subtype may play an important role in ECS-induced seizures than in PTZ-induced seizures (see Appendix II).

Recent studies by Weiss and Cook et al.⁸⁹ show that activation of GABA (A) receptors induces apoptosis in neuroblastoma. The mechanism by which GABA-A activation inhibited the growth of neuroblastoma cells was assessed. To enhance the signal readout of this pathway, $\alpha 5$ selective GABA-A receptor agonist QH-II-066 was used. Apoptosis was induced in both LAN-5 (high GABA-A expression levels) and Kelly cells (low GABA-A expression levels) (**Figure 11 A and B**), as assessed by annexin V flow cytometry. Immunoblotting revealed that upon addition of GABA and QH-II-066,

cleaved PARP, an indicator of apoptosis, was increased. Notably, immunoblotting revealed a decrease in activity of the PI3K/AKT and MAPK pro-growth and survival pathways, indicated by decreased phosphorylation levels of Akt and Erk, respectively (**Figure 11 C**). Together these data suggest that specific activation of the GABA-A receptor decreases cell viability, induces apoptosis, and suppresses pro-growth and survival signaling pathways in neuroblastoma cell lines (see Appendix III).

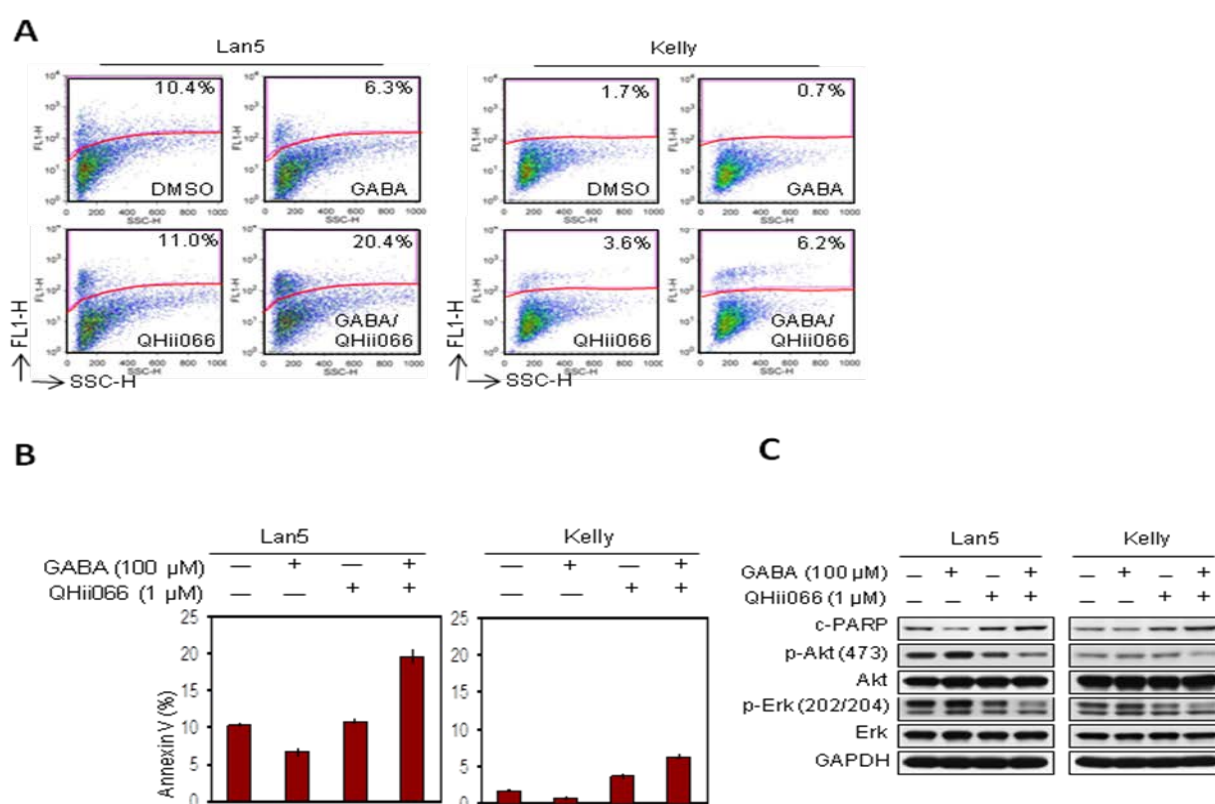


Figure 11. GABA activation decreases viability and induces apoptosis in neuroblastoma cells (A) Lan5 and Kelly cells were treated with GABA 100 μ M or the selective ligand for GABA (QH-II-066, **11**) 1 μ M or both and analyzed by annexin V-FITC flow cytometry for apoptosis after 72h. (B) Percentages of positive cells for apoptotic marker annexin V are mean \pm s.e. for triplicate samples with treatments indicated. (C) Cells analyzed by immunoblot using antisera indicated show decreased phosphorylation of Akt and Erk.

3.1.3. Synthesis of PS-1-37

Since the $\alpha 5$ *in vitro* selectivity and efficacy of QH-II-066 **11** was increased in regard to the potent controls, it was decided to maintain the acetylenic function at C (7) and determine this potential effect at L₂ of other orally active BZ agonists.

PS-I-37 is a stable analog of XHe-II-053 related to an agonist developed by Upjohn, and was prepared for study. A mixture of the bromo benzodiazepine **3** was taken up in pyridine and phosphorous pentasulfide to form the thione **12**. This was further reacted with glycine, Na₂CO₃ in ethanol and a water mixture to form acid **13** as a yellow solid. This was suspended in dry CH₂Cl₂ and DCC was added. The suspension which resulted was stirred at 40°C for 2hrs. The solvent was removed under vacuum to give the ketone **14** as brown oil. The cyclized product was dissolved in benzene, after which dimethylformamide diethyl acetal and triethyl amine were added. The residue was then crystallized from ethyl acetate to give amine **15**. A solution of **15** in dry toluene was treated with 1-methyl piperazine and refluxed for 5hrs and then the solvent was removed under vacuum to give a gum which was crystallized to furnish **16**. To the suspension of compound **16** in acetonitrile and triethyl amine was added bis(triphenylphosphine) palladium(II) acetate to furnish the trimethylsilyl analogue **17**. The trimethyl silyl was removed using TBAF in THF to provide the acetylenic product **18** (PS-I-37) and this material was anxiolytic in monkeys (Dr.Rowlett, Harvard).

Scheme 2: Synthesis of PS-1-37

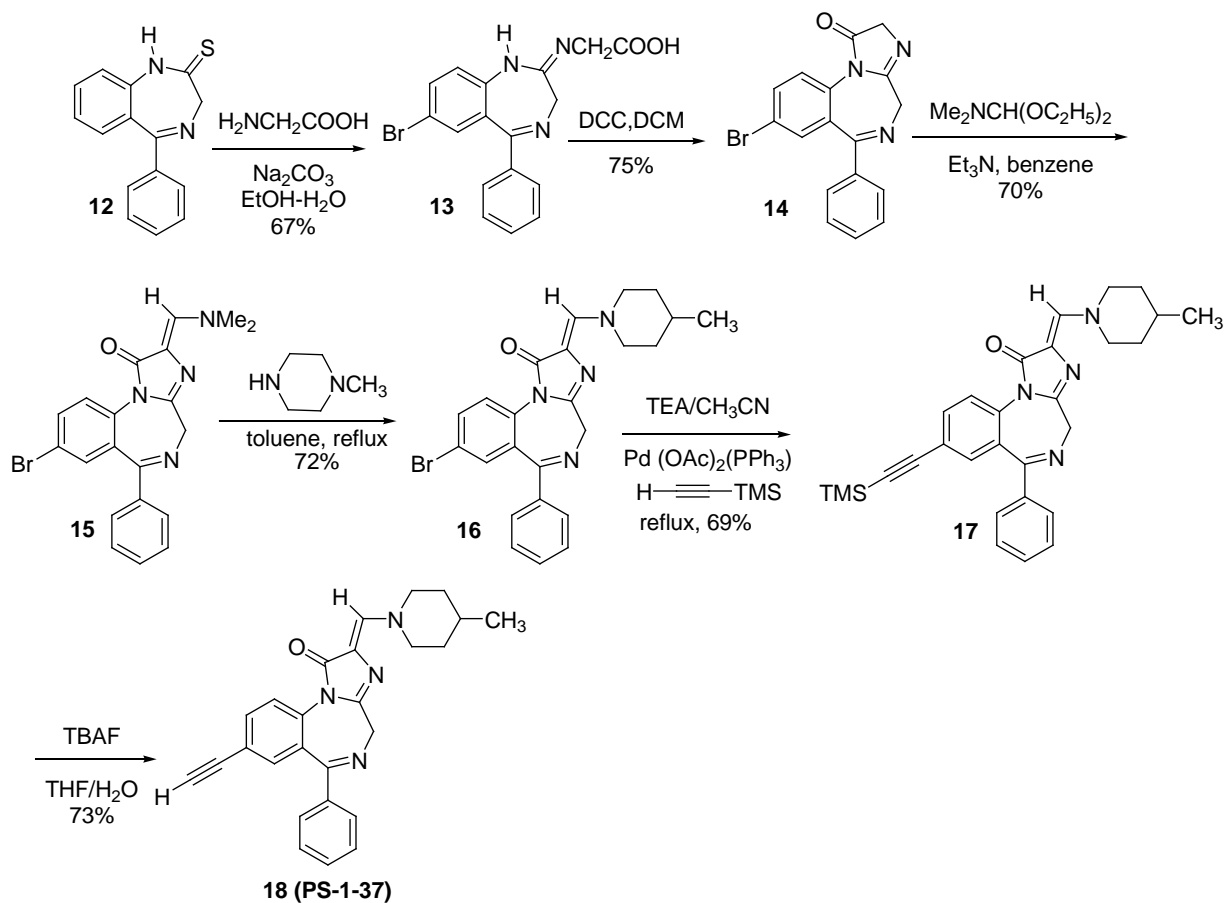


Table 2. *In Vitro* Receptor Binding Data on Diazepam (2) and PS-1-37 (18). Binding Affinity at $\alpha\beta\gamma_2$ GABA_A/BzR Receptor Subtypes (Values are Reported in nM)

Compound	$\alpha 1$	$\alpha 2$	$\alpha 3$	$\alpha 4$	$\alpha 5$	$\alpha 6$
Diazepam (2)	14	7.8	13.9	ND ^a	13.4	ND ^a
PS-1-37 (18)	193	35	435	ND ^a	22	5000

ND: not determined yet. ^aBinding at $\alpha 4$ subtypes has not been determined, but since the 6-phenyl group is present, the ligand will not bind to $\alpha 4$ and $\alpha 6$ subtypes.

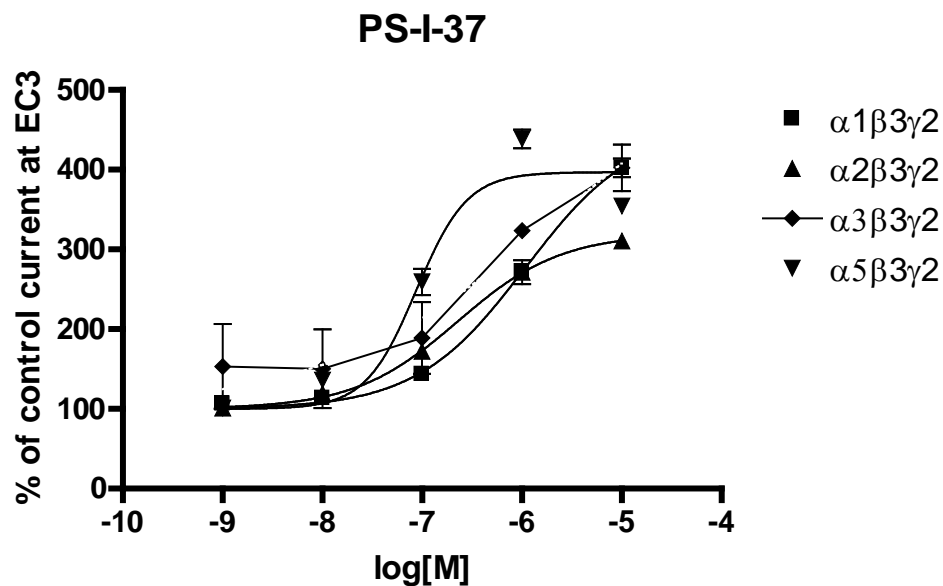


Figure 12. The Oocyte Efficacy Data on **PS-1-37(18)**.

Table 3. EC₅₀ and Hill Slope for Modulation of Control GABA EC₃ by **PS-1-37 (18)** in Xenopus Oocytes Expressing Different GABA_A Receptor Subtypes. Results Represent EC₅₀ (95% Confidence Interval for EC₅₀) and Hill Slope (Nh) ± SD from at Least Four Cells from Two Batches.

		$\alpha 1\beta 3\gamma 2$	$\alpha 2\beta 3\gamma 2$	$\alpha 3\beta 3\gamma 2$	$\alpha 4\beta 3\gamma 2$	$\alpha 5\beta 3\gamma 2$	$\alpha 6\beta 3\gamma 2$
PS-I-37	EC ₅₀	>1,1μM	>228nM	>2,3μM		87nM	
	95% CI					48-158	
	Nh						

Table 4. Modulation of Control GABA EC₃ by Diazepam and **PS-1-37 (18)** on *Xenopus* Oocytes Expressing Different GABA_A Receptor Subtypes. Values are Presented as Mean ± SEM of at Least Four Oocytes from at Least Two Batches

		$\alpha 1\beta 3\gamma 2$	$\alpha 2\beta 3\gamma 2$	$\alpha 3\beta 3\gamma 2$	$\alpha 5\beta 3\gamma 2$
Diazepam(2)	10nM	135±4%	193±5%	167±8%	160±2%
	100nM	246±16%	400±22%	461±34%	322±7%
	1µM	345±27%	508±29%	776±44%	420±12%
	10µM	366±27%	520±14%	749±29%	377±14%
	10nM	114±2%	119%	ns	136±1%
PS-1-37 (18)	100nM	144±1 %	172±3%	ns	259±16%
	1µM	272±3 %	271±15%	324±9%	438±12%
	10µM	402±12%	311±1%	402±29%	345±4%

All the above values were significantly different from the respective control currents ($p < 0.01$, Student's *t*-test) except where indicated (n.s.). NS means not significant.

3.1.4. Synthesis of 8-substituted imidazobenzodiazepines

As mentioned above, the $\alpha 5$ subtypes are primarily found in the hippocampus⁹⁰ which is important for memory and learning⁹¹. Studies done by Mohler et al.⁹² on $\alpha 5$ knockin mice provided strong evidence that hippocampal extrasynaptic $\alpha 5$ GABA_A receptors play a critical role in associative learning.⁹² The 8-substituted imidazobenzodiazepines such as RY-23 and RY-24 exhibited a greater affinity and selectivity at the $\alpha 5$ subtype. Previously, the subtype selective inverse agonist activity^{60-64,85} of a series of $\alpha 5$ subtype selective ligands [(**20**, RY-023), (**21**, RY-024), (**22**, RY-079) and (**23**, RY-080)] was

reported. The design was based on the structure of **19** (Ro 15-4513) and, in addition, McKernan, Atack et al. (see **24**) reported several related ligands as well.^{93,94} These ligands are BzR inverse agonists *in vivo* and have been shown to enhance cognition.¹⁷⁻²¹ One of these ligands was shown by Bailey et al.⁹¹ to be important in the acquisition of fear conditioning and provided further evidence for the involvement of hippocampal GABA_A/benzodiazepine receptors in learning and anxiety. This was supported by the work of DeLorey et al.⁹⁵ in a memory model with a ligand closely related to $\alpha 5$ subtype selective inverse agonists **20** and **21**.

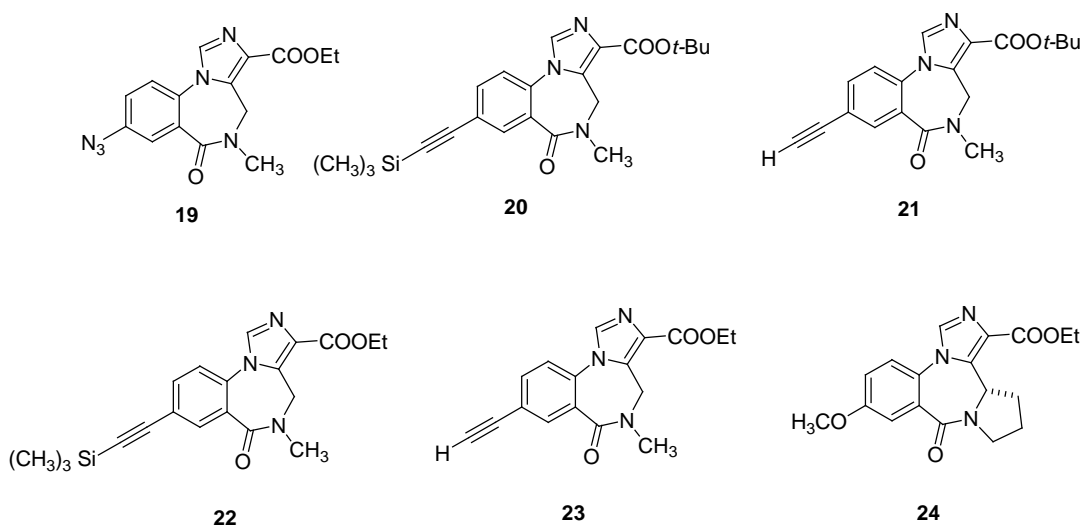


Figure 13. Ro 15-4513 (**19**), RY-023 (**20**), RY-024 (**21**), RY-079 (**22**), RY-80 (**23**) and the Merck compound (**24**).

The ligands **20-23** and **24** depicted in Figure 13 were 40-70 fold more selective for $\alpha 5$ subtypes in comparison to $\alpha 1$ subtypes; however, better selectivity remains a goal of paramount importance. In collaboration with Sieghart *et al.* the efficacy of inverse

agonist RY 24 (**21**) was determined (Figure 46). It was demonstrated that RY 24 (**21**) was a potent inverse agonist at $\alpha 5$ subtypes in oocytes with a much weaker efficacy at the other subtypes.

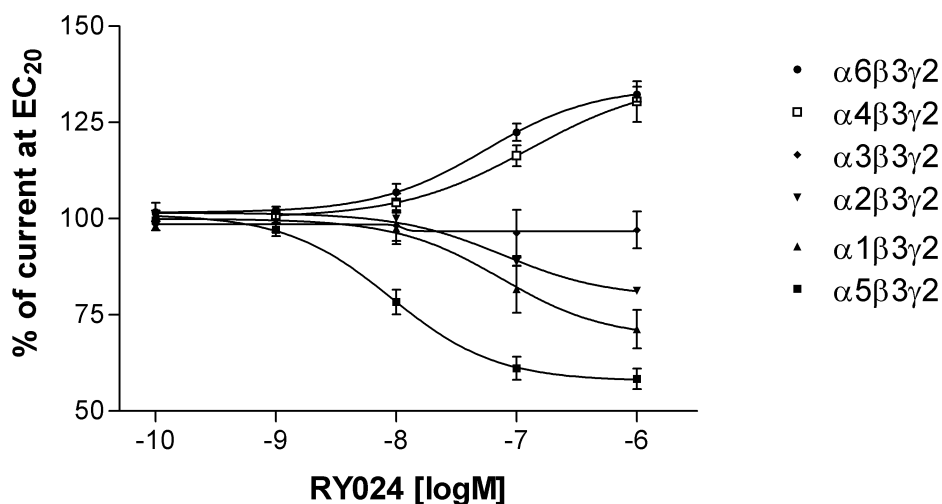
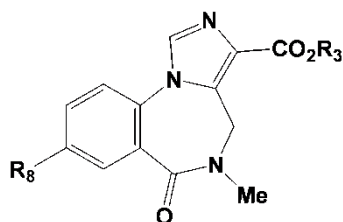


Figure 14. Subtype selective efficacy of **RY-24 (21)**; dose response curves for **RY-24** in oocytes expressing different subunit combinations of GABA_A receptors. Subtype combinations are indicated in legends. cRNA-injected *Xenopus* oocytes were held at –60 mV under two-electrode voltage clamp. Increasing concentrations of **RY-24** were superfused together with a GABA concentration eliciting ~20% of the maximal current amplitude. **RY-24** was pre-applied for 30 sec before the addition of GABA, which was co-applied with the drugs until a peak response was observed. Data were normalized for each curve assuming 100% for the response in the absence of **RY-24**. **RY-24** was made up and diluted as stock solution in DMSO. Final DMSO concentrations perfusing the oocyte were 0.1%. Values are presented as mean \pm SD of at least 4 oocytes from at least 2 batches.

Inspection of the data in Table 4 reveals some observations worth noting. While the lipophilic substituent at R₈ of RY-24 **21** and RY-80 **23** decreased the affinity for α 1, α 2 and α 3 subtypes, it retained affinity for α 5 and actually increased affinity for the α 6 subtype. This data again supports the importance of the occupation of the lipophilic pocket L₂ for potent selectivity at the α 5 subtype.

Table 5. *In Vitro* Receptor Binding Data of α 5 ligands. Binding Affinity at α x β 3 γ 2 GABA_A/BzR Receptor Subtypes (Values are Reported in nM)



Ligand	R ₈	R ₃	K _i (nM) ^a				
			α 1	α 2	α 3	α 5	α 6
RY-24 (21)	—≡—H	<i>t</i> -Bu	26.9	26.3	18.7	0.4	5.1
RY-23 (20)	—≡—TMS	<i>t</i> -Bu	197	143	255	2.61	58.6
RY-80 (23)	—≡—H	Et	28.4	21.4	25.8	0.49	28.8
RY-79 (22)	—≡—TMS	Et	121	142	198	5.0	114

^a "Synthesis and Pharmacological Properties of Novel 8-Substituted Imidazobenzo-diazepines: High Affinity, Selective Probes for α 5 Containing GABA_A Receptors," Liu, R.; Hu, R.; Zhang, P.; Skolnick, P.; Cook, J. M., *J. Med. Chem.*, **39**, 1928-1934 (1996).

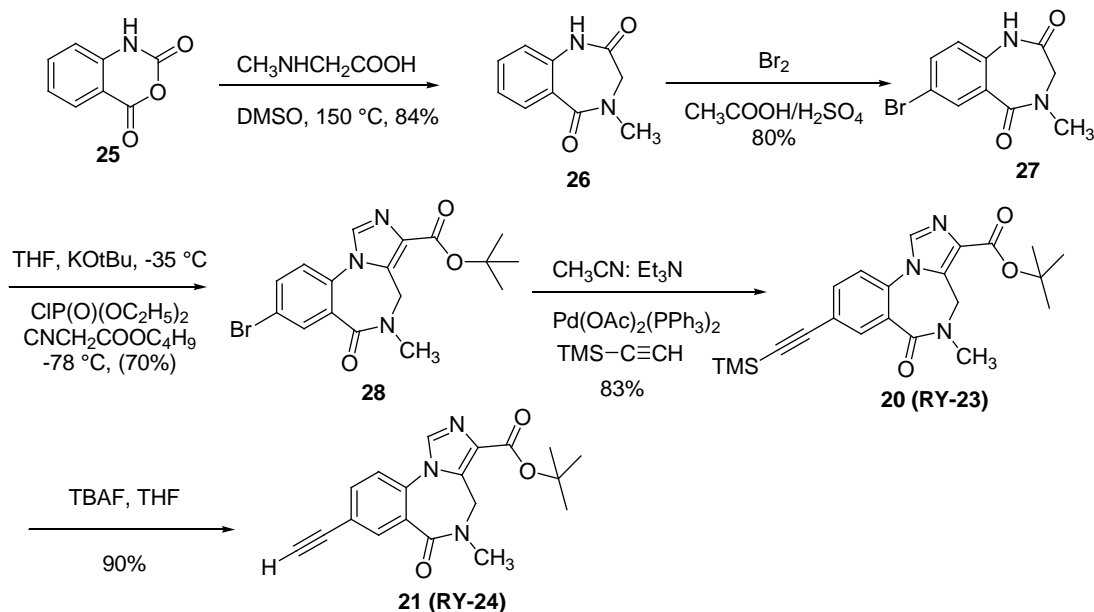
In agreement with previous studies,⁶¹ these $\alpha 5$ selective ligands were highly selective in suppressing ethanol-maintained responding (Figure 25).⁹⁶ As previously stated, the hippocampus contains the greatest concentration of $\alpha 5$ -containing receptors in the CNS,^{90,97} and it is possible that these hippocampal $\alpha 5$ receptors may regulate alcohol-motivated responding following systemic administration of an $\alpha 5$ -selective agent. Furthermore, RY-24 also antagonized the motor-impairing and sedative effects of ethanol in Long-Evans rats. Combined with additional studies within the ventral pallidum (VP), it has been proposed that the GABAergic systems within the VP and hippocampal pathways may represent new extensions of the mesolimbic ethanol reward circuitry. Although these data do not strongly support a direct role for the modulatory influences of intrinsic efficacy in the behaviors examined, the synthesis of $\alpha 5$ subtype selective ligands provides researchers a unique opportunity to explore the role of this subtype in the neurobehavioral effects of alcohol.^{61,98} However, the efficacy (inverse agonist, negative modulation) of RY-23 and RY-24 at $\alpha 1$ and $\alpha 2$ subtypes precludes potential clinical uses of such agents for both agents are proconvulsant and RY-24 is also convulsant.

Additional behavioral studies of RY-24 were performed by Helmstetter *et al.* and provided further support for the role of the hippocampus in anxiety and learning.⁹¹ Moreover, the data suggested that Bz BSs within the hippocampus are important for the acquisition of fear conditioning. Although this subtype selective ligand has been shown to be an inverse agonist at the $\alpha 5$ subtype,^{62,99} this study suggested that RY-24 may act as an agonist at other alpha subtypes because larger doses of RY-24 were not as anxiogenic as the smaller doses and resulted in decreased learning. Consistent with the

studies of Stephens *et al.* using $\alpha 5$ knock-out mice¹⁰⁰ and the efficacy studies of Lüddens, June and Cook *et al.*,¹⁰¹ these findings support the concept that the pharmacology observed depends upon the dose, behavioral paradigm employed and subunit composition activated. Ligands such as RY-24 have proven to be valuable in the study of the biochemical and pharmacological properties of GABA_A receptors and have permitted insight into the role this protein plays in anxiety and learning.

In brief, isatoic anhydride **25** and sarcosine were heated in DMSO to form benzodiazepine **26** in 84% yield. Benzodiazepine **26** was treated with bromine in the presence of CH₃COOH and H₂SO₄ to provide the bromide **27** in 80% yield as illustrated in Scheme 3. Deprotonation of **27** with KO*t*Bu in THF followed by treatment with diethyl chlorophosphate provided the intermediate enol phosphate.¹⁰² The enol phosphate was stirred with a solution of *t*-butyl isocyanoacetate and KO*t*Bu to yield the imidazobenzodiazepine **28** in 70% yield. This bromide was converted into **20** by a Heck-type coupling reaction^{60,62} using bis(acetate) bis(triphenylphosphine) palladium(II) to provide TMS analog **RY 23 (20)** and the silyl group was removed in high yield on treatment with TBAF/H₂O/THF to provide **RY 24 (21)**.⁶⁰

Scheme 3: Synthesis of RY-23 and RY-24



4. Synthesis of $\alpha 5$ selective BzR bivalent ligands

Bivalent ligands have been termed as compounds that contain two pharmacophores joined through a connecting unit. The general structure for bivalent ligands is P-X-P (P: pharmacophore; X: spanner).¹⁰³⁻¹⁰⁵ They may exhibit enhanced selectivity and potency relative to their monovalent analogues (P-X) when a suitable spanner X is employed. The study by Portoghese et al. on bivalent ligands that bind to different opioid receptor subtypes was among one of the most successful reported to date.¹⁰³⁻¹⁰⁵

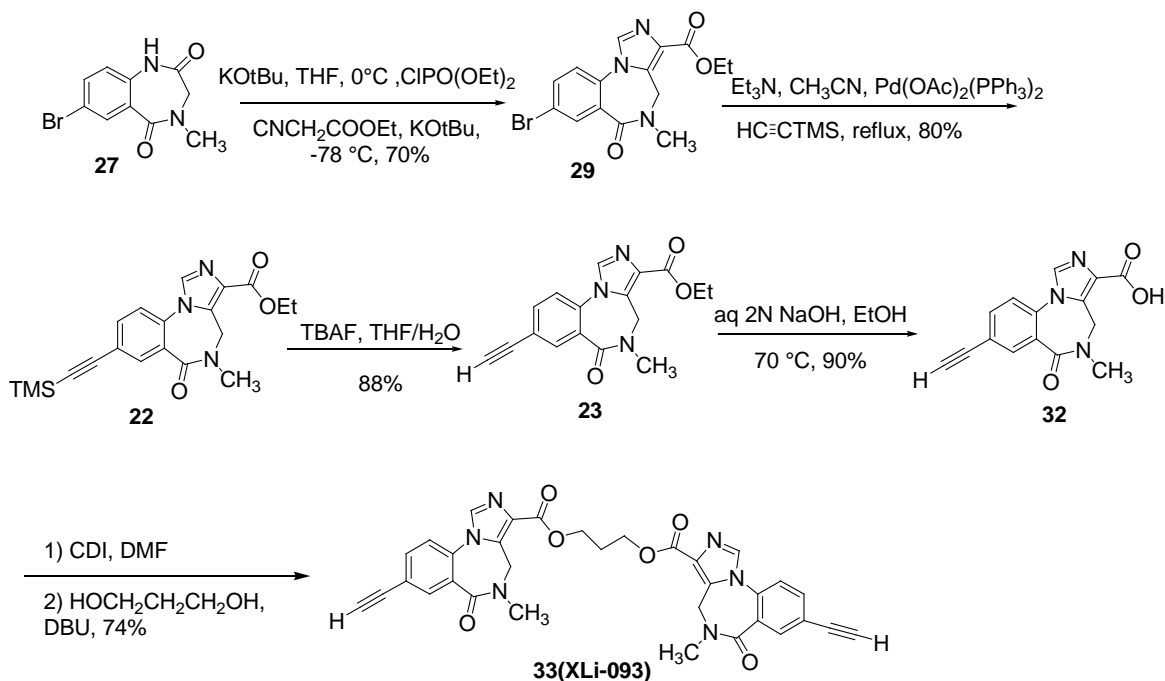
A linker of 3 CH₂- groups is often called the Leonard linker from its founder Nelson J. Leonard.

To enhance subtype selectivity, the bivalent form^{103,104,106} of RY024 (17),^{60,62} that is 1,3-bis(8-acetyleno-5,6-dihydro-5-methyl-6-oxo-4H-imidazo-[1,5a][1,4]-benzodiazepine-3-carboxy) propyl diester, (33, XLi093) was designed and prepared. The

synthesis, $\alpha 5$ subtype selectivity and antagonist properties of this ligand are described below.

Deprotonation of **27** with KO t Bu in THF followed by treatment with diethyl chlorophosphate provided the intermediate enol phosphate. The enol phosphate was stirred with a solution of ethyl isocyanoacetate and KO t Bu to yield the imidazobenzodiazepine **29** in 70% yield.¹⁰² This bromide was converted into **22** by a Heck-type coupling reaction^{60,62} and the silyl group was removed to provide acetylene **23** in high yield on treatment with TBAF/H₂O/THF.⁶⁰ Hydrolysis of the ester function of **23** provided the acid **32** in excellent yield and this material was subjected to a standard CDI-mediated coupling reaction with a three carbon linker to furnish bivalent ligand XLi093 **33** in 73.4% yield on gram scale.

Scheme 4: Synthesis of Bivalent Ligand XLi-093



The binding affinity of XLi093 (**33**) *in vitro* was determined on $\alpha 1$ -6 $\beta 3\gamma 2$ Ltk⁻ cells and is illustrated in Table 6. This ligand XLi093 **33** bound to $\alpha 5\beta 3\gamma 2$ subtypes with a K_i of 15 nM, but exhibited little or no affinity at other BzR/GABA_A subtypes. Although the efficacy at all receptor subtypes was decreased by incorporation of the pharmacophore of **23** into the bivalent structure, the loss of affinity at $\alpha 1$, $\alpha 2$, $\alpha 3$, $\alpha 4$ and $\alpha 6$ subtypes was profound. Presumably, since the second unit of XLi093 **33** lies in the extracellular domain of the BzR, the enriched selectivity is entropic. This has been the most selective $\alpha 5$ subtype selective ligand reported, to date. Depicted in Figure 15 is the ORTEP drawing of the crystal structure of XLi093 (see Appendix VI for coordinates). The J values ($J = 5.38$) calculated from the dihedral angles were in excellent agreement with those from the solution determined NMR spectrum ($J=6.39$), hence support for the conformation as shown (Figure 16) derives from the NMR data. This conformation of XLi093 was then placed in the BzR/GABA_A $\alpha 5$ pharmacophore receptor model previously reported^{42,72,76} from this laboratory; the fit was excellent.

Based on the binding affinity of XLi093 (**33**) and the fit at the $\alpha 5$ subtype, a study of the efficacy of Xli093 was then pursued in oocytes by Sieghart, Furtmueller, Li, Cook et al.¹⁰⁷ The effects of XLi093 (**33**) on chloride currents in GABA_A receptors was determined.¹⁰⁸ The activity of XLi093 on GABA_A receptors was characterized using *Xenopus* oocytes expressing the GABA_A receptor subunits alpha 1 to alpha 6 in combination with beta 3 and gamma 2 subunits. Using the two electrode voltage clamp method, currents in the μ A range were measured for all subunits.

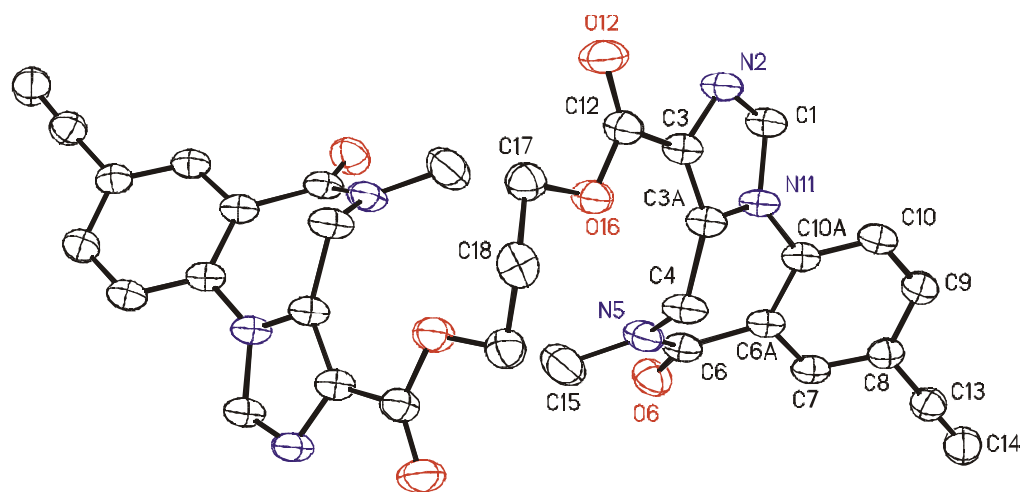


Figure 15. Crystal Structure of Bivalent Ligand XLI093 (**33**).

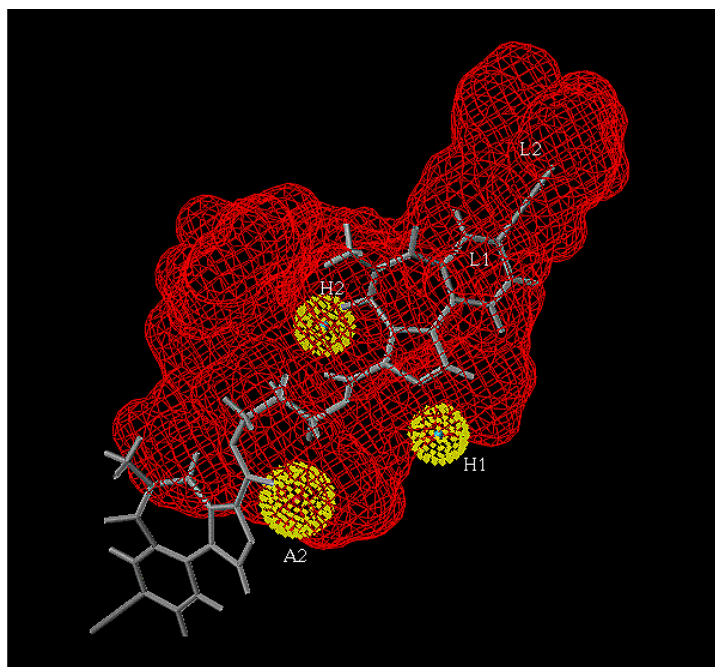


Figure 16. XLI093(**33**) Aligned in the Included Volume of the Pharmacophore/Receptor Model for the $\alpha 5\beta 3\gamma 2$ Subtype.

Table 6. *In Vitro* Binding Affinities at GABA_A/BzR Subtypes. ^aValues Reported are in nM.

Ligand	$\alpha 1$	$\alpha 2$	$\alpha 3$	$\alpha 4$	$\alpha 5$	$\alpha 6$
RY079 (22)	121	142	198	159	5.0	114
RY080 (23)	28.4	21.4	25.8	53	0.49	28.8
XLi093 (33)	>1000	>1000	858	1550	15	>2000

^a K_i values represent the mean of two determinations which differed by less than 10%. Data were generated using Ltk⁻ cell membranes expressing human $\alpha\beta\gamma 2$ receptor combinations in response to application of a saturating concentration of GABA (10 mM). Two electrode voltage clamp experiments were performed to test whether XLi093 triggered chloride currents,^{108,109} modulated GABA-induced currents or antagonized the effects of benzodiazepines in oocytes that express GABA_A receptors.

Bivalent ligand XLi093 **33** at concentrations up to 1 μ M did not trigger chloride currents in any of the tested subtypes of the GABA_A receptor. This dimer, however, at micromolar concentrations modulated GABA-induced currents in an alpha subtype specific manner. To test for agonistic or inverse agonistic effects of XLi093, the compound was coapplied with a concentration of GABA that induced app. 3% of the maximum current amplitude. At concentrations of XLi093 **33** up to 100 nM, this ligand caused no significant modulation of GABA-induced currents in any subtype of GABA_A receptors tested. At a concentration of 1 μ M, XLi093 **33** caused a significant increase in GABA-induced currents in the GABA_A receptor subtypes $\alpha 4\beta 3\gamma 2$ [$+37.6 \pm 2.6$ %

(SEM), $p < 0.0001$ in four oocytes] and $\alpha 6\beta 3\gamma 2$ [$+ 17.0 \pm 2.5$ % (SEM), $p = 0.0014$ in four oocytes]. Furthermore, $1 \mu\text{M}$ XLi093 caused a reduction in GABA induced currents in the subtype $\alpha 5\beta 3\gamma 2$ [-4.0 ± 1.5 % (SEM), $p = 0.0075$ in six oocytes]. However, $1 \mu\text{M}$ of XLi093 caused no significant modulation of GABA-induced currents in the GABA_A receptor subtypes $\alpha 1\beta 3\gamma 2$, $\alpha 2\beta 3\gamma 2$ and $\alpha 3\beta 3\gamma 2$.

Ligand XLi093 (**33**) shifted the dose response curve for diazepam in a subtype specific manner. To test for benzodiazepine antagonistic effects of XLi093, dose response experiments for the stimulation of GABA-induced currents by diazepam in the absence or presence of $1 \mu\text{M}$ XLi093 **33** were performed. Similar conditions for different subtypes were provided by using a concentration of GABA that induced app. 3% of the maximum current amplitude in the respective cell. In oocytes expressing GABA_A receptors of subunit combination $\alpha 5\beta 3\gamma 2$, the presence of $1 \mu\text{M}$ XLi093 (**33**), shifted the dose response curves for the stimulation of GABA induced currents by diazepam to the right (Figure 17). Even high concentrations of diazepam could not fully overcome this inhibition since maximum current stimulations in the presence of XLi093 (**33**) reached only app. 85% of current stimulations that were seen in the absence of XLi093 (**33**).

The dose response curves for diazepam with and without $1 \mu\text{M}$ XLi093 (**33**) in oocytes expressing different subunit combinations of GABA_A receptors are depicted (Figure 17). cRNA–Injected *Xenopus* oocytes were held at -60 mV under two-electrode voltage clamp. Increasing concentrations of diazepam with or without $1 \mu\text{M}$ of XLi093 (**33**) were superfused together with a GABA concentration eliciting app. 3% of the maximal current amplitude. Diazepam and XLi093 were preapplied for 30 sec before the addition

of GABA, which was coapplied with the drugs until a peak response was observed. Data were normalized for each curve assuming 100% for the response in the absence of diazepam and XLI093. Drugs were made up and diluted as stock solutions in DMSO. Final concentrations of DMSO perfusing the oocyte were 0.1%. Values are presented as mean \pm SD of at least four oocytes from at least two batches.

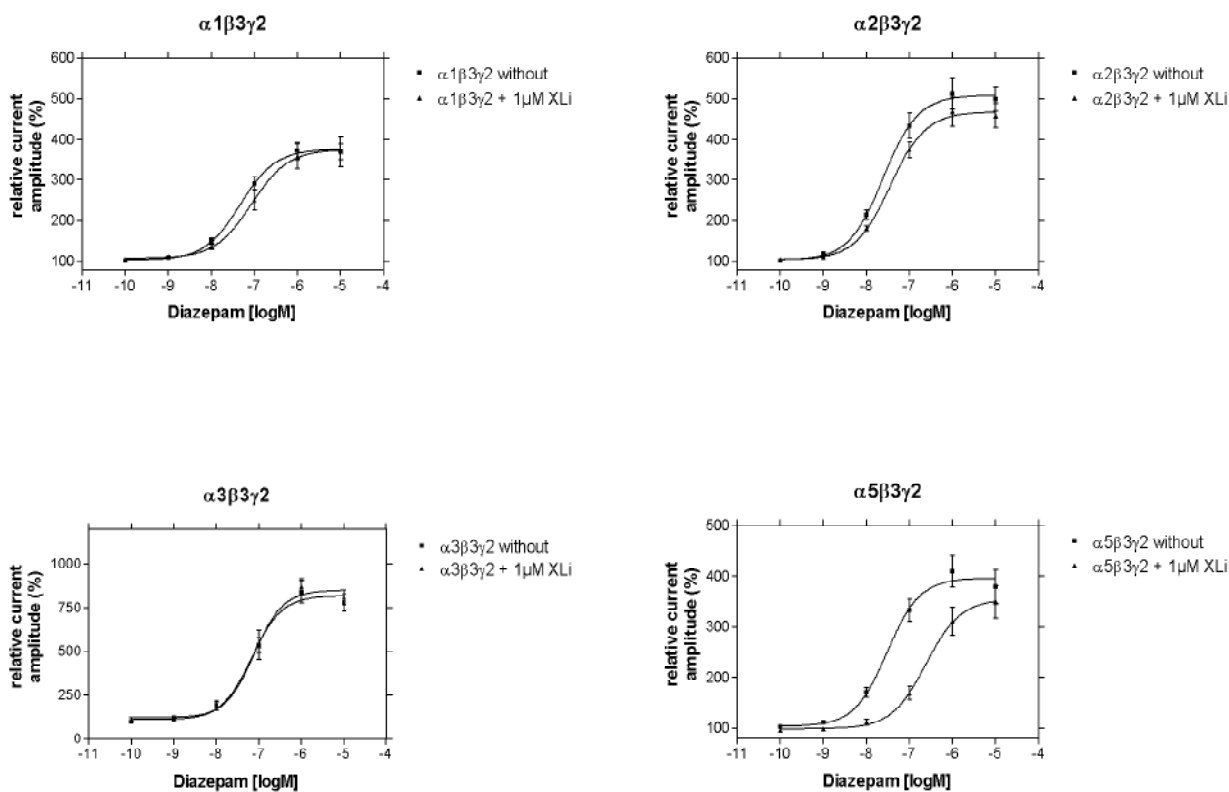


Figure 17. Effects of XLI093 (33) on GABA_A receptors were tested by two-electrode voltage clamp experiments in cRNA injected *Xenopus* oocytes that functionally expressed several subtype combinations of GABA_A receptors. In oocytes expressing GABA_A receptors of the subtypes $\alpha 1\beta 3\gamma 2$, $\alpha 2\beta 3\gamma 2$, or $\alpha 3\beta 3\gamma 2$, 1 μM XLI093 (33)

caused only marginal shifts of dose response curves for the stimulation of GABA-induced currents by diazepam.

Receptor binding studies indicated that the bivalent ligand XLi093 **33** bound almost exclusively to the $\alpha 5$ subtype of GABA_A receptors. In summary, the effect of this compound on various GABA_A receptors expressed in *Xenopus* oocytes was fully investigated by electrophysiological studies. Analysis of the data indicated that bivalent ligand XLi093 up to a concentration of 1 μ M did not trigger chloride currents in any one of the tested GABA_A receptor subtypes. At 1 μ M, XLi093 did not modulate GABA induced chloride flux in $\alpha 1\beta 3\gamma 2$, $\alpha 2\beta 3\gamma 2$, $\alpha 3\beta 3\gamma 2$ but stimulated GABA-induced currents in $\alpha 4\beta 3\gamma 2$ and $\alpha 6\beta 3\gamma 2$ and slightly inhibited currents in $\alpha 5\beta 3\gamma 2$. At 1 μ M, XLi093 only marginally influenced diazepam stimulation of GABA-induced current in $\alpha 1\beta 3\gamma 2$, $\alpha 2\beta 3\gamma 2$ and $\alpha 3\beta 3\gamma 2$, but shifted the diazepam dose response curve to the right in $\alpha 5\beta 3\gamma 2$ receptors. The slight reduction in the maximal diazepam stimulation in the presence of 1 μ M XLi093 might have been due to the previously described reduction in current stimulation at high diazepam concentration¹⁰⁹ or might indicate interaction of XLi093 *via* two different binding sites. Importantly, bivalent ligand XLi093 was able to dose dependently and completely inhibit diazepam stimulated currents in $\alpha 5\beta 3\gamma 2$ receptors. It was a quite selective benzodiazepine receptor site antagonist at $\alpha 5$ receptors. As noted, ligands such as XLi093 have been important in the determination of which physiological function(s) are subserved by this GABA_A $\alpha 5\beta 3\gamma 2$ subtype. There are many scientists who have reversed the amnesic effects of diazepam *in vivo* with XLi-093 in rodents and primates by Savic, Rowlett and Platt et al (see below).

4.1. Binding Studies of XLi-093 (33) *in vivo* by Rowlett and Cook et al.⁵⁵

Recent studies by Rowlett and Cook et al.⁵⁵ have shown that diazepam significantly impaired performance in a hole board memory task, in which mice learned the location of 4 baited holes (out of 16 possible) over the course of 4 trials.

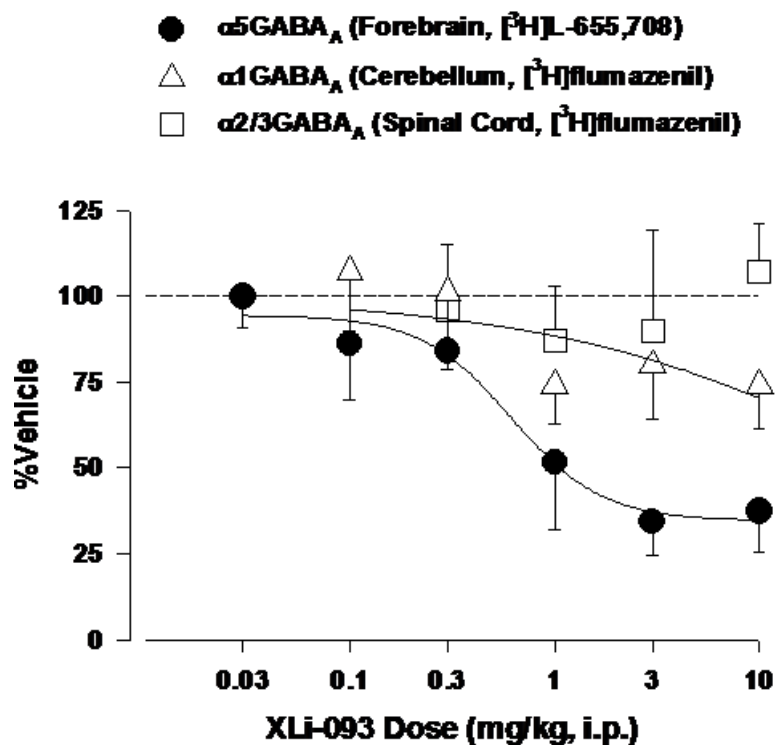


Figure 18: *In vivo* binding of Xli-093. The memory-impairing effects of diazepam were blocked (**Figure 18**) by a dose of (33; 3.0 mg/kg) that occupied ~66% of $\alpha 5$ GABA(A) binding sites but less than 25% (non-significant) of the $\alpha 1$ GABA(A) and $\alpha 2/\alpha 3$ GABA(A) binding sites. Memory impairment measured via the holeboard task occurred at a dose of diazepam that resulted in a relatively high degree of $\alpha 5$ GABA(A) binding site occupancy (64%). Interestingly, even at a saturating dose of diazepam (10 mg/kg), XLi-093 (33) was still able to block the memory impairing effects of diazepam.

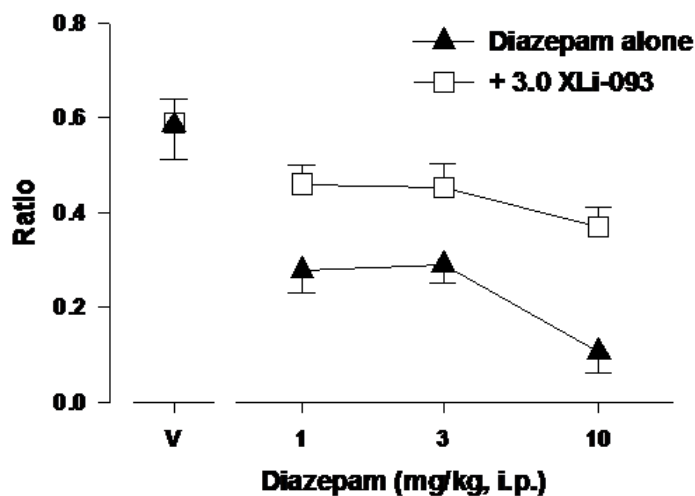


Figure 19: XLi-093 (3.0 mg/kg) blocked the DZ-induced suppression of performance ratio on the holeboard task. Note that XLi-093 showed no effect when administered with vehicle.

This performance impairment suggested that diazepam-induced a working memory deficit. The novel antagonist XLi-093 (**33**) was able to antagonize this deficit and showed appreciable subtype selectivity for the $\alpha 5$ GABA(A) receptor *in vivo* consistent with previous findings. *In vivo* binding studies with XLi-093 showed negligible occupancy of $\alpha 1$ GABA(A) and $\alpha 2/3$ GABA(A) binding sites; however, occupancy of $\alpha 5$ GABA(A) binding sites was significant at 1.0 mg/kg and above (see Figure 18).

The data suggests $\alpha 5$ GABA(A) receptors play an important role in diazepam-induced memory impairments. Identification of compounds with reduced $\alpha 5$ GABA(A) activity may result in sedative-anxiolytics that lack memory-impairing effects of classical benzodiazepines.

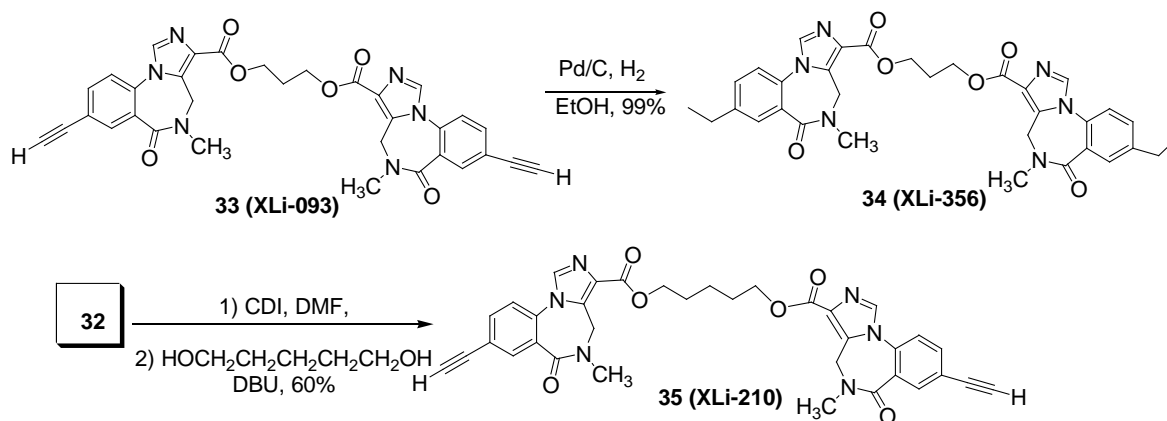
In vivo binding studies (see Table 7) with XLi-093 (**33**) showed negligible occupancy of $\alpha 1$ GABA_A and $\alpha 2/3$ GABA_A binding sites; however, occupancy of $\alpha 5$ GABA(A) binding sites was significant at 1.0 mg/kg and above. The ability of a novel $\alpha 5$ GAB(A) subtype selective antagonist, XLi-093 (**33**; 0.3-10.0mg/kg), to occupy $\alpha 5$ GABA receptors *in vivo* (*in vivo* [3H]L-655,708 binding) had been evaluated. Based on percent binding occupancy, the ability of a range of XLi-093 doses to reverse impairments induced by the minimal effective dose of diazepam (DZ (3.0 mg/kg)) was assessed. Ligand XLi-093 (**33**) reversed DZ-induced impairments at doses of 1.0 and 3.0 mg/kg, which occupied ~50-65% of [3H]L-655,708 binding. In contrast, these doses resulted in only ~20% occupancy of $\alpha 1$ GABA and $\alpha 2/3$ GABA(A) receptors in cerebellum and spinal cord, respectively, (determined by *in vivo* [3H]flumazenil binding). These findings are consistent with a key role for $\alpha 5$ GABA(A) receptors in BZ agonist induced impairments in learning and memory.

Table 7: Percent of $\alpha 5$ GABA (A) binding sites occupied by XLi-093 and DZ at doses used in the behavioral studies.

Ligand (Dose, i.p.)	% $\alpha 5$ GABAA Occupancy
XLi (3.0)	65.8
DZ (1.0)	63.8
DZ(3.0)	83.5
DZ (10.0)	99

It had been demonstrated that bivalent ligand XLi-093 bound tightly to $\alpha 5\beta 3\gamma 2$ receptor subtypes illustrated that bivalent ligands will bind to BzR and since the second unit of this bivalent ligand presumably lies in the extracellular domain of the BzR, this ligand had very poor or no affinity at the other subtypes. It is now obvious that this is the first $\alpha 5$ bivalent ligand which was not only orally active, but also passed through the blood brain barrier. This was an important result for these bivalent ligands in regard to use in science.

Scheme 5: Synthesis of Bivalent Ligands XLi-356 and XLi-210



The bivalent ligand XLi356 (**34**) was obtained from XLi093 (**33**) in 99% yield *via* catalytic hydrogenation (Pd/C , H_2). While XLi093 was found to be an antagonist, ligand XLi356 is an inverse agonist in $\alpha 5\beta 3\gamma 2$ oocytes and a weak agonist at $\alpha 1\beta 3\gamma 2$ sites.

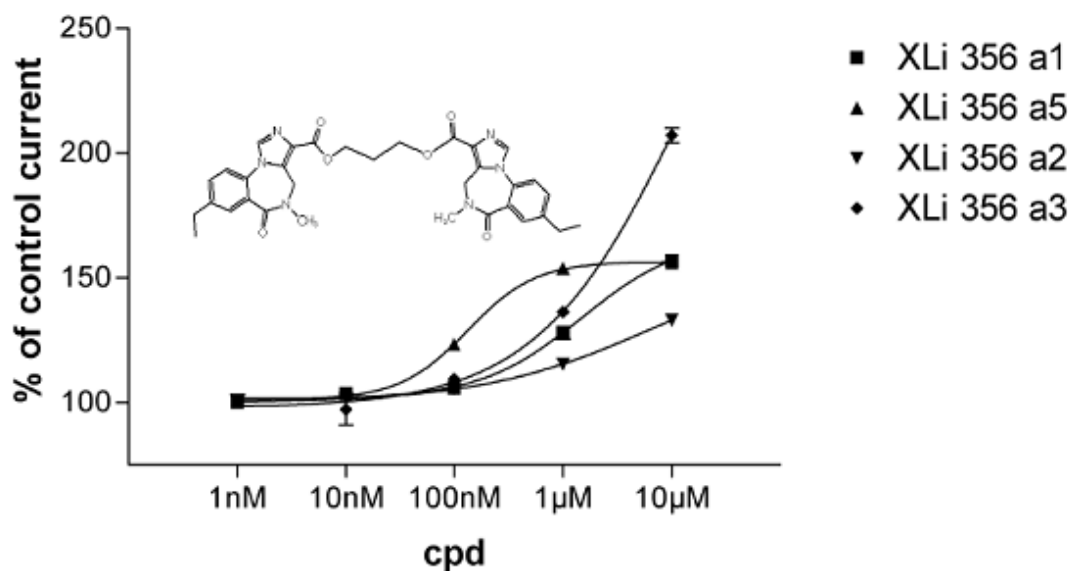


Figure 20: Subtype selective efficacy of XLi356 (34), Dose response curves for XLi356 in oocytes expressing different subunit combinations of GABA_A receptors. Subtype combinations are indicated in legends. cRNA-injected *Xenopus* oocytes were held at –60 mV under two-electrode voltage clamp by Sieghart et al.

Table 8. *In Vitro* Binding affinities of bivalent ligands at GABA_A/BzR subtypes.

^aValues Reported are in nM.

Ligand	α1	α2	α3	α4	α5	α6
XLi356 (34)	1851.5	4202.5	8545	ND	100.5	5000
XLi210 (35)	231	661	2666	ND	5.4	54.22
XLi093 (33)	>1000	>1000	858	1550	15	>2000

^aK_i values represent the mean of two determinations which differed by less than 10%.

Data were generated using Ltk⁻ cell membranes expressing human αxβ3γ2 receptors.

DeLorey has recently shown that XLi-356 (**34**) does potently reverse scopolamine induced memory deficits in rodents. XLi356 was found to reverse scopolamine induced memory deficits in mice. When XLi356 was looked at in audio cued fear conditioning, the results show no activity. This suggests that the effect of XLi356 is selective through $\alpha 5$ receptors which are abundant in the hippocampus which is highly associated with contextual memory. Audio cued memory instead is amygdale-based, and is not affected by an $\alpha 5$ subtype selective compound.¹¹⁰

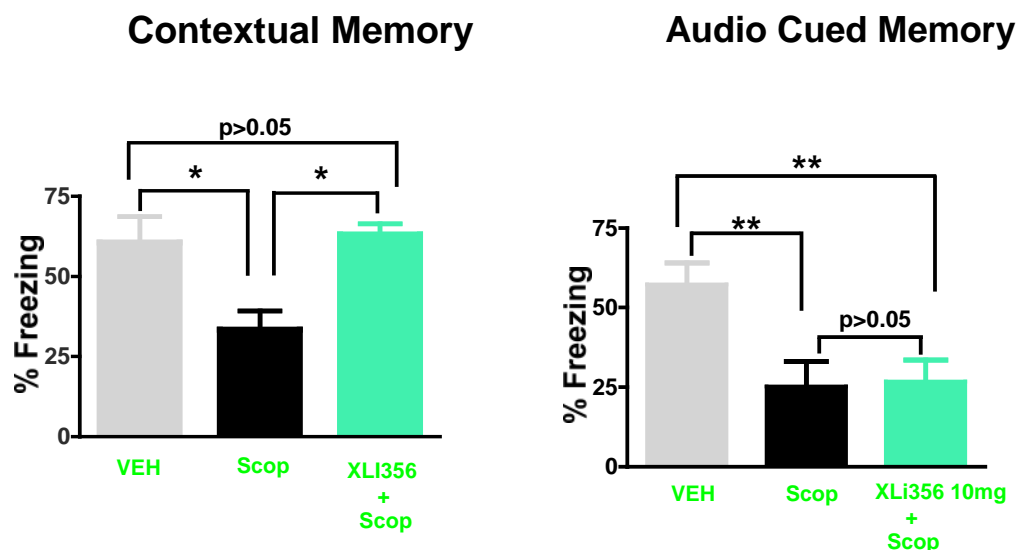


Figure 21: Visual and audio que data for XLI356

As illustrated in Figure 21, scopolamine (1 mg/kg) reduced freezing (ie. impairs memory) typically caused by pairing the context (the cage) with a shock. The drug XLi356 when given at 10mg/kg attenuates the impairment of memory returning the freezing to the level that one typically sees the mouse freeze at (i.e. veh). In the audio cued paradigm, memory was triggered by sound not the context. XLi356 was not able to reverse this type of memory effect which is amygdale driven.

The biology of a bivalent ligand with a 3-carbon linker XLi-093 (**33**) led us to synthesize the analogous bivalent ligand with a 5-carbon linker. The synthesis of XLi-210 (**35**) was done analogous to the conditions employed for XLi-093. The acid **32** was subjected to a standard CDI-mediated coupling reaction using a 5-carbon linker to furnish bivalent ligand XLi210 **35** in 60% yield in dry DMF (Scheme 5).

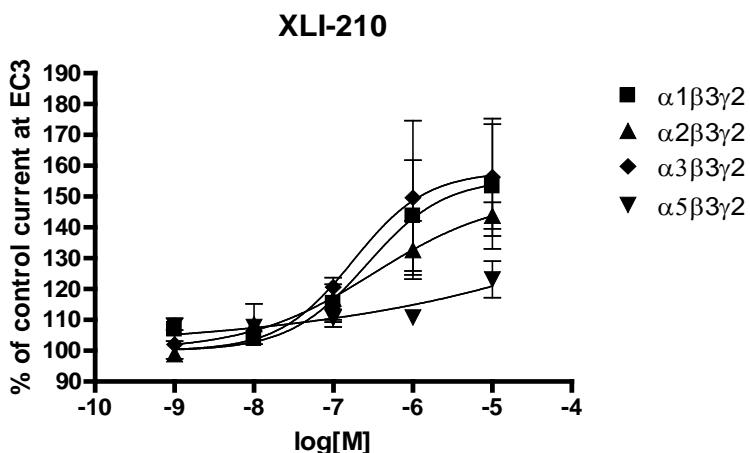


Figure 22: Subtype selective efficacy of XLI210 (**35**): dose response curves for XLI210 in oocytes expressing different subunit combinations of GABA_A receptors. Subtype combinations are indicated in legends. cRNA-injected *Xenopus* oocytes were held at –60 mV under two-electrode voltage clamp.

This bivalent ligand (**35**) showed 50 fold selectivity at $\alpha 5$ over $\alpha 1$ (see Table 8). The efficacy data shows that the ligand is an agonist. This ligand should have properties exactly opposite that of PWZ-029 which is an inverse agonist (NAM). Positive controls and an $\alpha 5$ antagonist render this a very strong approach to hippocampal-mediated drug design in regard to the development of agents to treat cognition deficits in Alzheimer's and age-related memory deficits.

Table 9. EC₅₀ and Hill Slope for Modulation of Control GABA EC₃ by **XLi 210 (35)** in *Xenopus* Oocytes Expressing Different GABA_A Receptor Subtypes. Results Represent EC₅₀ (95% Confidence Interval for EC₅₀) and Hill Slope (Nh) ± SD from at Least Four Cells from Two Batches.

		$\alpha 1\beta 3\gamma 2$	$\alpha 2\beta 3\gamma 2$	$\alpha 3\beta 3\gamma 2$	$\alpha 5\beta 3\gamma 2$
XLi-210	EC ₅₀	262nM	>324nM	175nM	
	95% CI	(15-4543)		(7-4210)	
	Nh	0.89		0.94	

Table 10. Modulation of Control GABA EC₃ by XLi 210 (35) on *Xenopus* Oocytes Expressing Different GABA_A Receptor Subtypes. Values are Presented as Mean ± SEM of at Least Four Oocytes from at Least Two Batches.

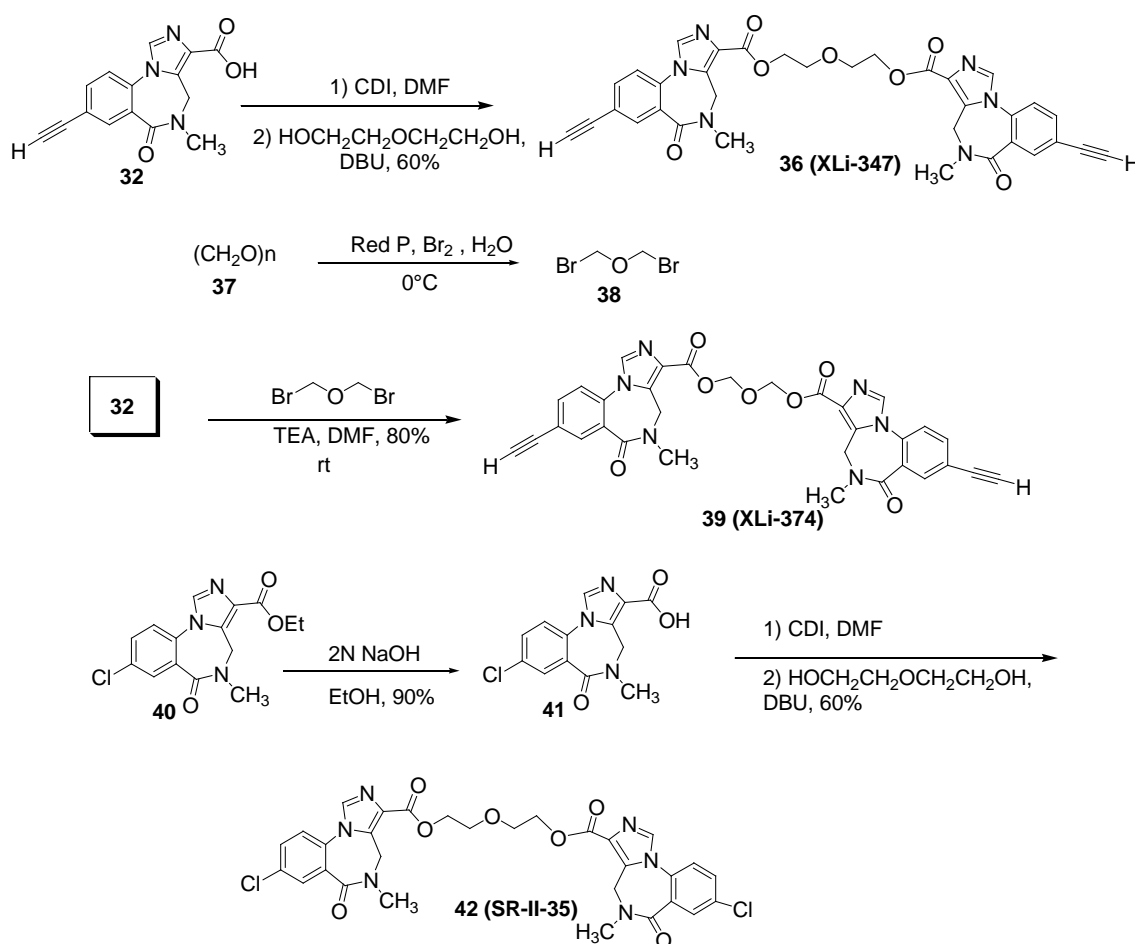
		$\alpha 1\beta 3\gamma 2$	$\alpha 2\beta 3\gamma 2$	$\alpha 3\beta 3\gamma 2$	$\alpha 5\beta 3\gamma 2$
	10nM	ns	ns	ns	ns
XLi210 (35)	100nM	115±6 %	117±7%	121	110±3%
	1μM	143±18 %	133±9%	150±25%	111±2%
	10μM	153±20%	144±4%	156±19%	123±6%

All the above values were significantly different from the respective control currents ($p < 0.01$, Student's-*t*-test) except where indicated (n.s.). n.s. means not significant.

5. Synthesis of Bivalent Ligands with Oxygen Linkers

In order to enhance water solubility and potency, bivalent ligands with an oxygen atom in the linker were synthesized. The insertion of an oxygen atom into the linker might increase the water solubility and hence enhance the molecular hydrophilicity which should play an important role in the pharmacokinetic properties of the ligand.

Scheme 6: Synthesis of Bivalent Ligands with Oxygen Linkers XLi-347, XLi-374 and SR-II-35



The oxygen linked analog XLi 347 (**36**) and SR-II-35 (**42**) were synthesized analogous to the conditions employed for the preparation of XLi-093 (**33**), the synthesis of the 5-carbon atom linked dimer **35** (XLi210) had been carried out. The acid (**32**) available

from Scheme 4, was subjected to a standard CDI-mediated coupling reaction to furnish bivalent ligands XLi 347 (**36**) and SR-II-35 (**39**) in 60% yield in dry DMF (see Scheme 6).

For the synthesis of XLi 374 (**39**), the preparation of the required oxygen-substituted linker (a dibromodimethylether) was based on the method of Tischtschenki and Rabcevitsch-Zubkovski^{111,112}. Bromine was added slowly to water over a four hour period, to which a mixture of paraformaldehyde (**37**) and red phosphorus was also added at a comparable rate. The reaction mixture was ice-water-cooled during this process. The temperature was maintained at 0°C. The final reaction mixture was allowed to stand for 20 hours. The heavy crude dibromo ether layer was then separated, saturated with hydrogen bromide, and dried over P₂O₅ for one day. Distillation at 158°C at 1 atm provided the ether from one fraction as pure dibromodimethyl ether (a colorless liquid). With the dibromodimethyl ether in hand, acid **32** was dissolved in dry dimethylformamide (DMF). To this solution the dibromodimethyl ether (**38**) was added, and this was followed by addition of TEA. After the mixture stirred for 26 hours at ambient temperature, the solvent was removed under reduced pressure and the residue was distributed between CH₂Cl₂ and water. The organic layer was washed multiple times with water and dried over Na₂SO₄, and the solvent was removed under reduced pressure almost to dryness. Subsequent flash chromatography of the crude oil provided the bivalent oxygen (C-O-C) dimer XLi374 (**39**) as a white solid.

The nature of the functional groups in a ligand plays an important role in receptor binding, of course, as well as the conformation in solution. The more the information about the stable conformation(s) of molecules, the better is the understanding of the

structure-activity relationships. It was essential from the beginning of the present study to determine the conformation of these bivalent ligands, which contained 3 to 5 atom linkers, since the steric requirements for affinity to the Bz receptor must be satisfied. In traditional medicinal chemistry, computer assisted molecular modeling programs and X-ray analysis contribute greatly in the search for stable conformations. However, some problems with these methods should not be neglected. Using computer modeling to determine the stable conformation of molecules containing many freely rotating bonds, such as those contained in bivalent ligands is difficult. Although X-ray crystallography is the ultimate arbiter of chemical structure, it has many limitations beyond the obvious need for crystals: it often does not reflect accurately the conformation in solution, nor is it informative regarding conformational equilibria. This information is crucial in drug design. However, NMR spectroscopy is a powerful technique in drug discovery and its role in conformational analysis cannot be surpassed by other spectroscopic methods.^{42,113}

5.1. Low Temperature NMR studies and X-ray Analysis

Herein is described a method utilizing low temperature NMR for the determination of the solution stable conformation of a series of GABA_A-benzodiazepine bivalent ligands with different monomeric units and linkers. The conformations in solution were determined by NMR spectroscopy and compared with those in the crystal structure. The combination of low temperature NMR and X-ray analysis provided accurate structural information required for understanding structure-activity relationships and drug design. The influence of the molecular structure of the linker on the conformation is also discussed.

5.2. Results

Recently it was shown the active dimers XLi093 (**33**) and DMH-D-053 (**31**) existed in a linear conformation in the solid state while dimer dm-III-96 (**43**) with a oxygen containing linker folded back upon itself, as illustrated in Figure 23.¹¹⁴

Since the bioactive conformation in solution may or may not parallel that in the crystal structure, the lowest energy solution structure must be established in order to correlate conformation with biological activity. Thus, NMR experiments at variable temperatures were performed and data were collected in different solvents. In methylene chloride or chloroform at room temperature, only a single set of signals was detected for both bivalent ligands **33** and **42**.

Table 11. *In Vitro* binding affinities of bivalent ligands at GABA_A/BzR subtypes.

^aValues Reported are in nM.

Ligand	$\alpha 1$	$\alpha 2$	$\alpha 3$	$\alpha 4$	$\alpha 5$	$\alpha 6$
RY-080 (23)	28.4	21.4	25.8	5.3	0.49	28.8
XLi-093 (33)	>1000	>1000	858	1550	15	>2000
XLi-374 (39)	3795	2694	1864	ND	76.14	ND
XLi-347 (36)	828.05	690.2	ND	ND	13.87	ND
SR-II-35 (42)	200.7	47.03	94.66	ND	38.38	ND
XHe-II-053 (30)	287	45	96	1504	13.8	1000
dm-III-96 (43)	460	5000	ND	ND	5000	5000
DMH-D-053 (31)	236	7.4	272	>5000	194.2	>5000

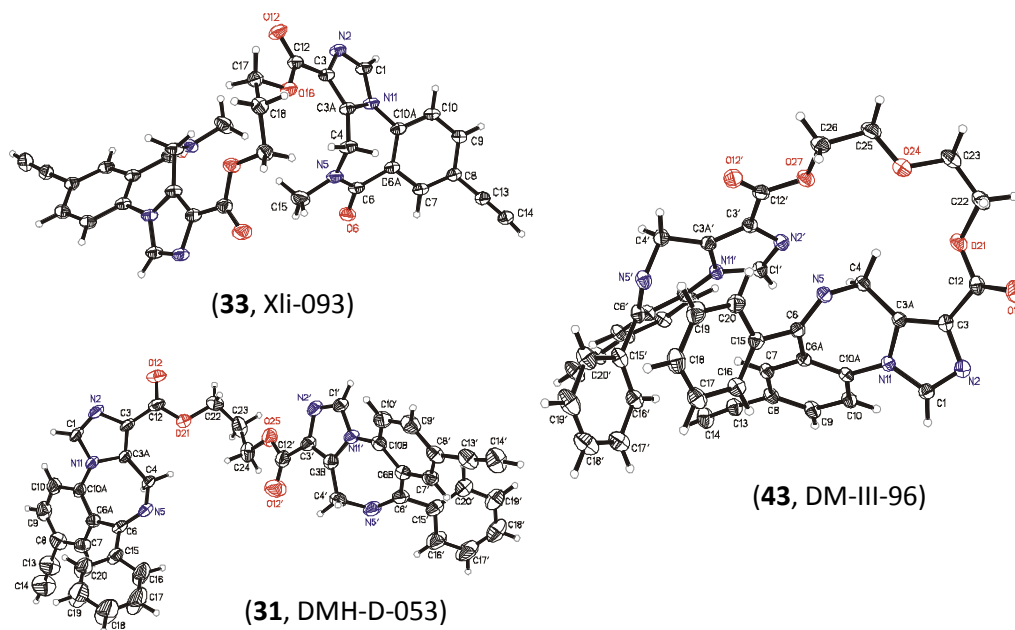
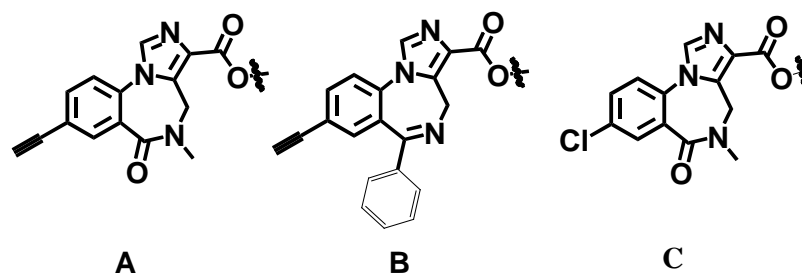


Figure 23. Crystal structures of XLi-093, DMH-D-053, and DM-III-96.

At low temperature, it was found that the linear dimer **33** exhibited only a small splitting of about 3 Hz for some of the aromatic protons in the ^1H NMR spectra(see Figure 24),¹¹⁴ while two clearly separated sets of signals were observed for the folded dimer **43** (Figure 25). For example, as seen in Figure 25 for **43**, the signal of ^1H (7.92 ppm at 298 K) was split into two peaks at δ 7.91 and 7.88 ppm, respectively, at 273° K. The doubling of the signals is consistent with disruption of the symmetry between the two domains of the molecule as expected if **43** adopted a static folded structure similar to the crystalline state.

Table 12. The molecular composition and stable conformation of various Bz BS bivalent ligands. ND = not determined yet.



Ligand	Monounit 1	Monounit 2	Linker	Conformation in solution	Crystal structure
32, RY-080	A	-	-	-	-
33, XLi-093	A	A	(CH ₂) ₃	linear	linear
35, XLi -210	A	A	(CH ₂) ₅	linear	ND
36, XLi -347	A	A	(CH ₂) ₂ O(CH ₂) ₂	folded	ND
39, XLi-374	A	A	CH ₂ OCH ₂	folded	ND
30, XHe-II-053	B	-	-	-	-
31, DMH-D-053	B	B	(CH ₂) ₃	linear	linear
43, dm-III-96	B	B	(CH ₂) ₂ O(CH ₂) ₂	folded	folded
42, SR-II-35	C	C	CH ₂ OCH ₂	folded	ND

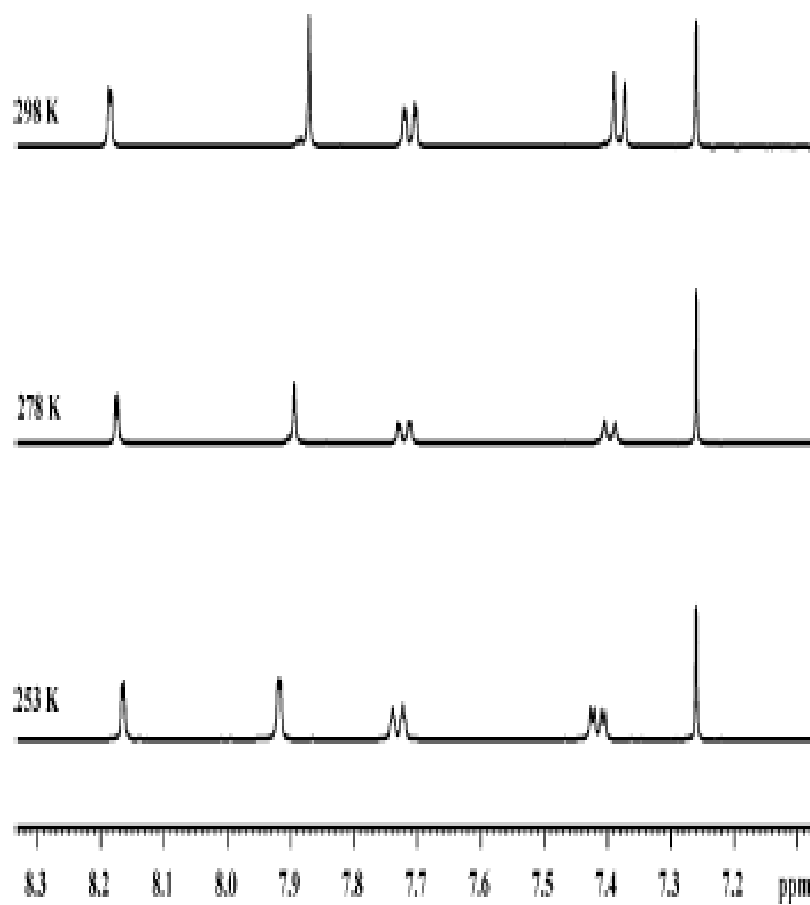


Figure 24. Aromatic region of ^1H NMR spectra of XLi-093 (33) in CD_2Cl_2 at variable temperatures.

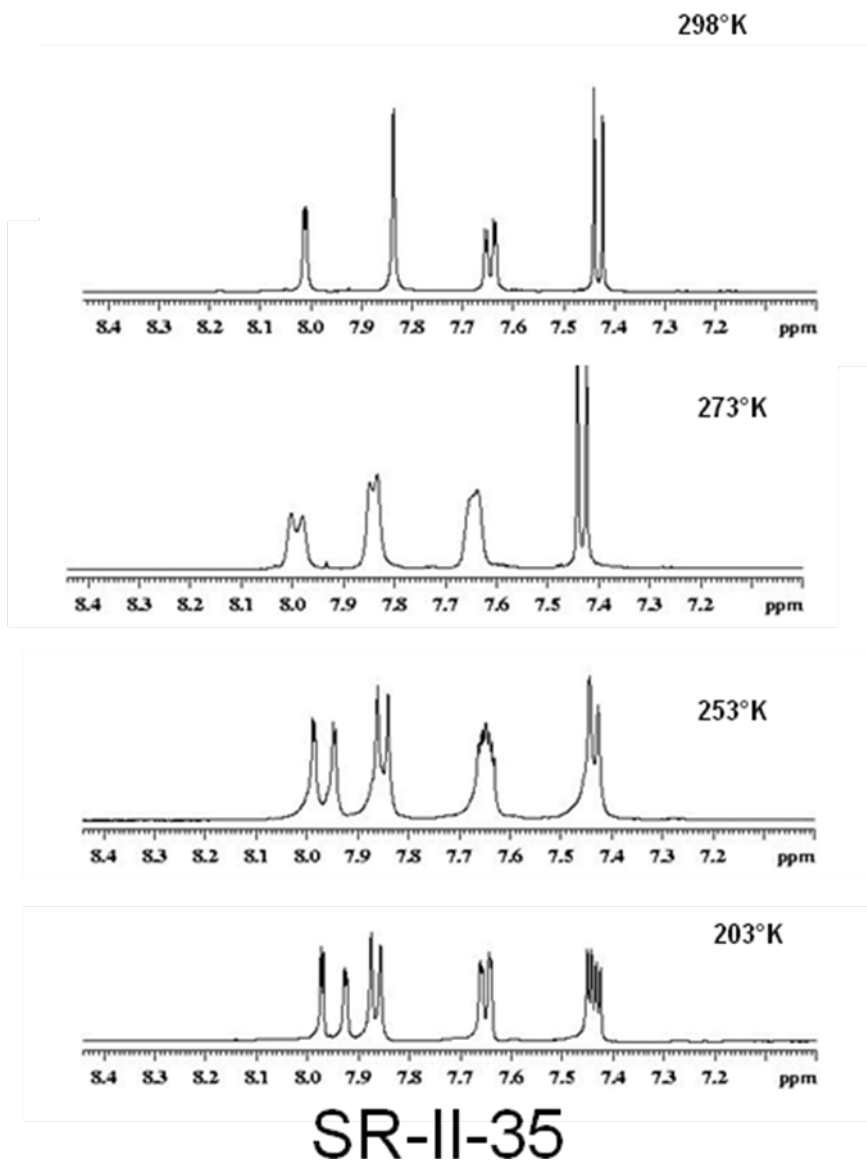


Figure 25. Aromatic region of ^1H NMR spectra of SR-II-35 (42) in CD_2Cl_2 at variable temperatures.

However, the possibility could not be ruled out that the split in the signals was caused by slowing a dynamic process within each domain, such as conformational interconversion of the seven-membered ring.

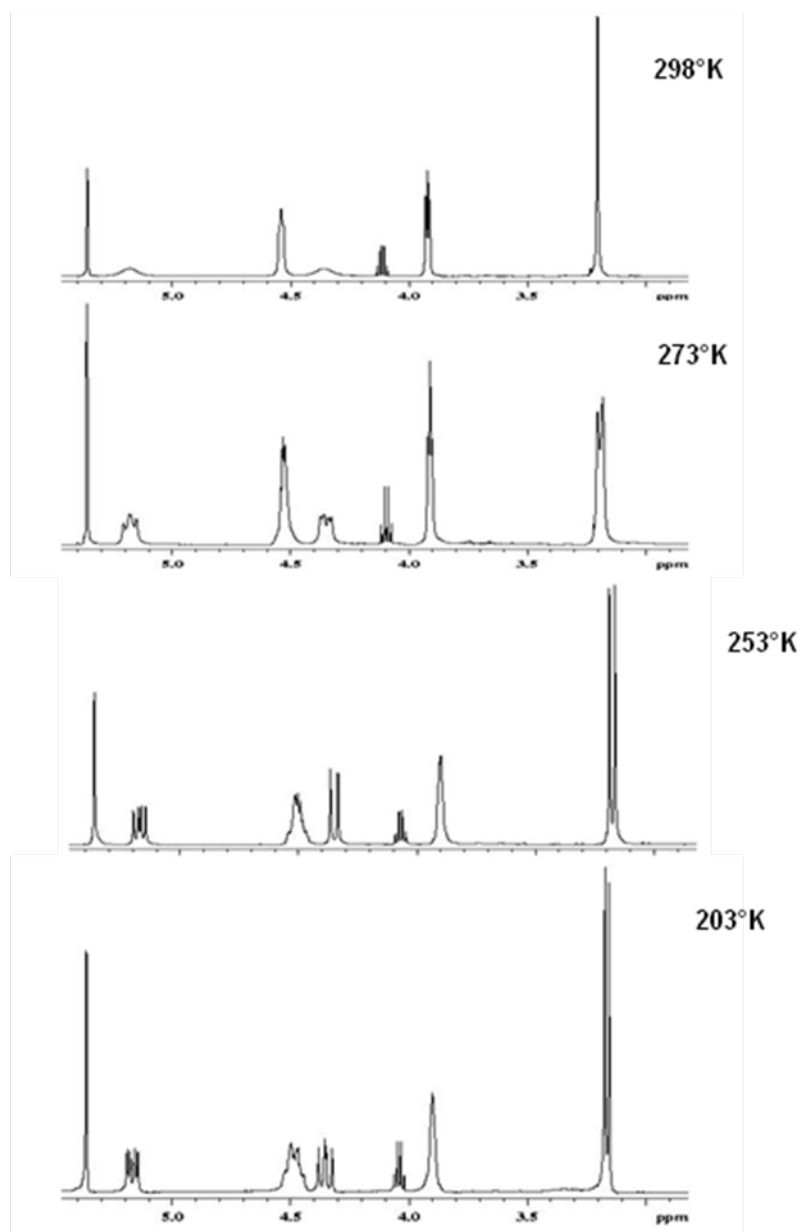


Figure 26. Aliphatic region of ^1H NMR spectra of SR-II-35 (**42**) in CD_2Cl_2 at variable temperatures.

The analysis of these data indicated that the line broadening at the lowest temperature was due to one of the conformational processes mentioned above, whereas the doubling of the peaks in **42** was caused by the presence of two domains. Certainly an interdomain

interaction existed between the two heterocyclic units of **42**. It was therefore concluded the internal mobility of the molecule decreased as expected, when the temperature was lowered which permitted observation of the two sets of signals of **42** on the NMR time scale. It was thus suggested that only when the molecule preferred the folded conformation in solution were two sets of signals observed. The preferred conformations of the molecules in CDCl_3 and CD_2Cl_2 correlated quite well with those observed in the crystal structures (Table 12).

The study was then expanded by varying the nature of the linker and monomer. It was found that **31**, **33**, **34**, and **35** exhibited only one set of NMR signals at low temperature, whereas the NMR signals of ligands **43** and **42** split into two sets at low temperature. Low temperature NMR studies were performed in CD_2Cl_2 . It was concluded that **43** and **42** preferred a folded conformation, while **32**, **33**, **34**, and **35** assumed a linear conformation. These conclusions are supported by a crystal structure obtained for bivalent ligand **33** which indicated **33** was present in a linear conformation in the solid state. These results are illustrated in Table 12.

Attempts to run the NMR experiments in water failed since the ligands were not sufficiently soluble in D_2O . However, the spectra of both the linear and folded dimer **33** and **42** respectively could be carried out in $\text{MeOH-}d_4$. The solvating properties of methanol, of course, more closely resemble those of water and this more closely mimics aqueous physiological conditions as well. The conformations of dimers in $\text{MeOH-}d_4$ were consistent with conformations in hydrophobic solvents.

5.3. Discussion

From the results described above, it is clear that dimers which contain an oxygen atom in the linker tend to adopt a folded conformation. Analysis of these data indicated in the hydrophilic solvent, **43** also had a higher tendency to fold back upon itself than **33**, as it did in the hydrophobic media (Figure 23). In fact, the tendency of **43** to assume a folded structure appeared to be higher in methanol than in CD_2Cl_2 or CDCl_3 , as the free rotation of the molecule was limited (Figure 25). On the other hand, for dimer **33**, which preferred a linear structure in the solid state and in lipophilic solvents, only one set of signals was observed at room temperature in $\text{MeOH-}d_4$ (Figure 27).

It is interesting to note that in the preparation of the samples, dimer **33** was less soluble in $\text{MeOH-}d_4$ than was **42** and **43**. It has been established that ligands are easier to dissolve in a solvent when the ligands surface energy can be minimized. Bivalent ligands **42** and **43** were more polar than dimer **33** and had a higher tendency to fold back. Consequently, **42** was presumably, easier to dissolve in methanol because its surface energy was minimized. On the other hand, when ligand **33** was dissolved in a more polar solvent such as methanol, the surface energy may be forced to be minimized.

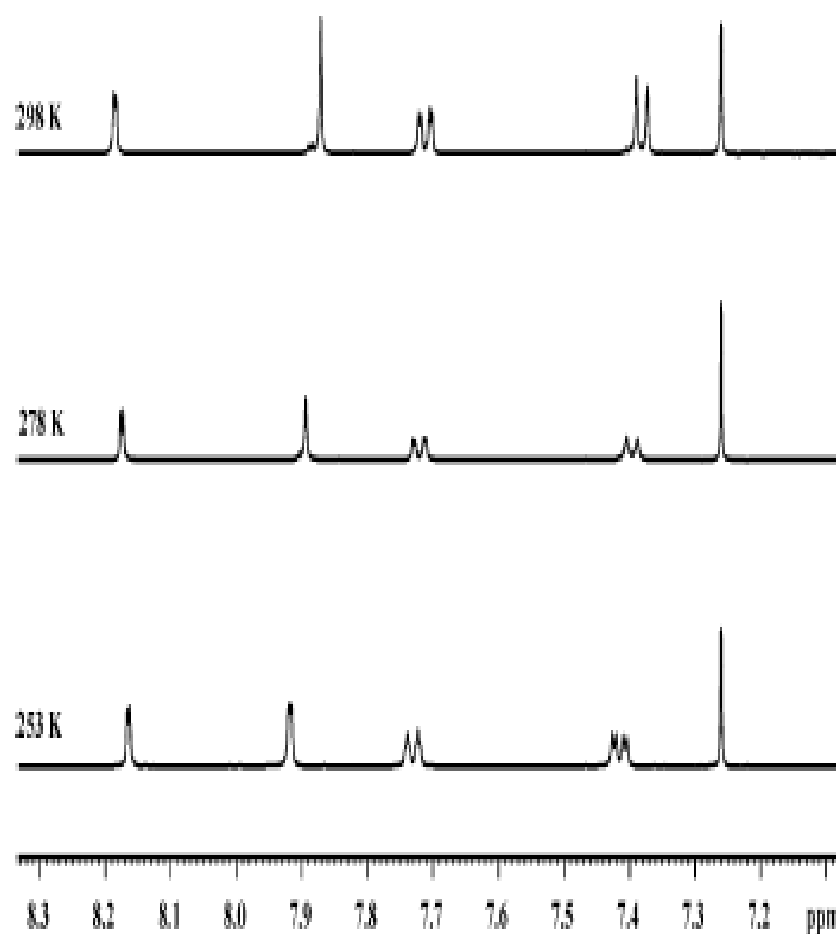


Figure 27. Aromatic region of ¹H NMR spectra of XLi-093 (**33**) in MeOH-*d*₄ at different temperatures.

Since the conformation of molecules XLi-093 (**33**) and SR-II-35 (**42**) in methanol agree with those in CD₂Cl₂ or CDCl₃, the behavior of these ligands in CD₂Cl₂ or CDCl₃ should reflect those in aqueous solution. The stable conformation of the compounds determined in CD₂Cl₂ or CDCl₃ were correlated with the newly generated receptor binding data (Table 11). In the pharmacophore/receptor model, the bivalent ligands in the linear conformation align well (Figure 28).

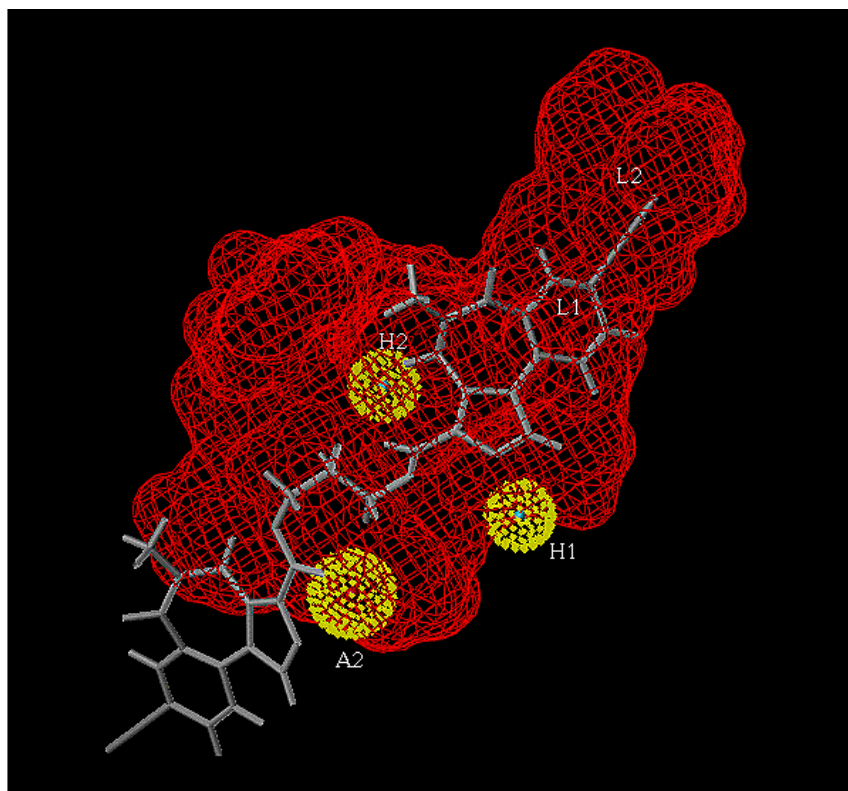


Figure 28. Bivalent ligand XLi093 (**33**) aligned in the included volume of the pharmacophore/receptor model for the $\alpha 5\beta 3\gamma 2$ subtype.

Importantly, bivalent ligands **31**, **33**, **34**, and **35** with carbon only linkers preferred the linear conformation as the stable conformation, independent of the number of linker atoms. In contrast, replacing the middle carbon of either linker $(\text{CH}_2)_3$ or $(\text{CH}_2)_5$ with an oxygen atom altered the stable conformation of the molecules **42** and **43** from linear to folded. The only difference between bivalent pairs **33** and **39** with linear and folded conformations as the stable ones, respectively, was the center atom. In compound **33** (XLi-093) the middle atom was carbon, while in **39** (XLi-374) oxygen was present. Consequently, it was decided to focus attention on the conformational difference between carbon and oxygen containing linkers.

It was well-known^{115,116} that the carbon chain in both small molecules and polymers favored the *anti*-conformation which results in a linear arrangement of atoms. From examination of the linkers (Figure 29), it was easily seen that linkers **C** and **D** can be regarded as oligomers of oxymethylene (OCH₂)₂ and oxyethylene (OCH₂CH₂)₂.

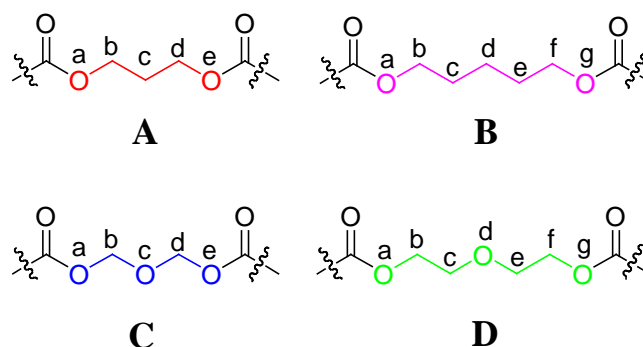


Figure 29. The linkers of the bivalent ligands.

It was well documented that the preference for the *gauche-gauche* conformation¹¹⁷⁻¹¹⁹ of a simple open-chain acetal such as dimethoxymethane (CH₃OCH₂OCH₃) could be predicted on the basis of the anomeric effect and related stereoelectronic effects. In this conformation the polar X–O bonds are favorably oriented such that a lone pair orbital of the oxygen atom was almost antiperiplanar to the X–O bond (Figure 30, lone pair orbital and X–O bond in same color). This permitted maximum overlap of the n orbital of the oxygen atom with the σ^* orbital of the X–O bond. This was not possible in the *anti-anti* or *gauche-trans* conformations and the two rabbit-ear interactions¹¹⁷⁻¹²¹ (Figure 30)

engendered by each pair of adjacent oxygen atoms in the *anti-anti* conformer are avoided.

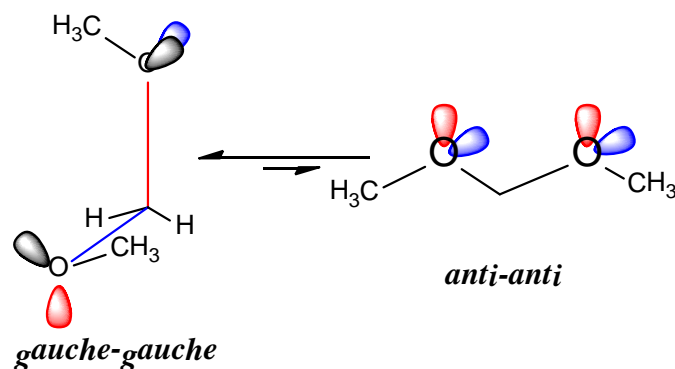


Figure 30. The conformations for dimethoxymethane.

Furthermore, in the related polymer of dimethoxymethane with the two-bond repeating sequence, poly(oxymethylene) (**POM**), the *gauche* conformation was, in fact, markedly preferred over *trans* and the polymer existed in a helical (all *gauche*) conformation^{116,122-124} rather than in the all-*anti* one.

Similarly, much effort has been spent on the investigation of the conformational characteristics of 1,2-dimethoxyethane (glyme, $\text{CH}_3\text{OCH}_2\text{CH}_2\text{OCH}_3$) as a model molecule for understanding the conformations of poly(oxyethylene), **POE**. It had long been established that POE chains have a large fraction of bonds in *gauche* conformation and assumed a helical conformation overall.^{115,116,122-124} It has been proposed that the oxygen gauche effect^{116,125,126} and 1, 5-CHO interaction¹²⁷⁻¹²⁹ within the molecule were responsible for the *gauche*-rich conformations.

Based on this pioneering work, the correlation was made that the conformation of the linkers in the bivalents **33-39** and **42-43** adopt *anti* (**B**), *gauche-gauche* (**C**), *trans*-

gauche-trans (**D**) conformations, respectively, regardless of the monomeric units which comprise them. The arrangement in space (disregarding the direction) of every unit in the linkers is depicted in Figure 31. The end-to-end distance of each unit (**C** and **D**) which adopted the *gauche* conformation was shorter than the one in the *anti*-conformer. The more units in the linker, the shorter the *gauche* linker becomes. Moreover, it was recognized that the X–O bond length (1.43Å) is often appreciably shorter than the C–C bond (1.54 Å).¹³⁰ Therefore, it was believed that the linkers with the oxygen atom in the middle favored the helical conformation and rendered the two monomeric units in each dimer sufficiently close to each other with suitable dihedral angles to facilitate the intramolecular lipophilic-lipophilic (aromatic-aromatic) interaction. This was regarded as one of the most important factors to stabilize the folded structure as the preferred conformation.¹³¹⁻¹³⁵ For these same reasons, bivalent ligands with the linker B adopted the linear conformation.

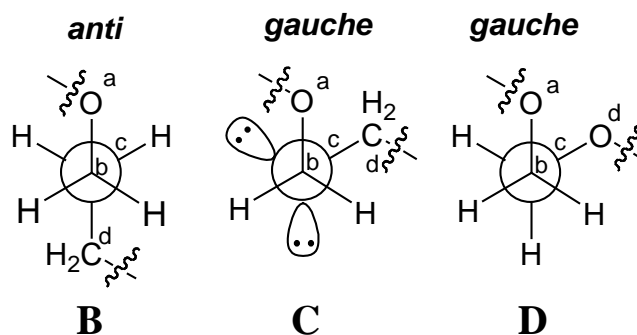


Figure 31. Newman projection for linkers **B**, **C** and **D**.

For the higher analog of **POM** and **POE**, namely, poly(trimethylene oxide) $[(\text{CH}_2)_3\text{O}]_x$ (**POM**₃), *trans-gauche-gauche-trans* was slightly preferred over all-*trans* and *trans-*

trans-gauche-trans conformers in the crystalline state.¹¹⁶ The preference for the *gauche* state in this case was only 0.2 kcal/mol were as in the **POM** and **POE** examples was 1.5 and 0.4 kcal/mol, respectively.¹²² Since the energy difference between *gauche* and *trans* was low, the linker **A** had more flexibility than the other linkers (**C** and **D**) to rotate freely and less tendency to occur as *gauche*. This could lead to improper end-to-end distances or dihedral angles for the interaction between the aromatic monounits. Hence dimers connected with linker **A** could not be stabilized in the folded conformation even though the same aromatic monomeric units were contained in the molecules.

Bivalent ligands were evaluated in competition binding assays for specific GABA_A membrane proteins using [³H] flunitrazepam as the radiolabel. This assay measured the ability of the ligand to displace flunitrazepam. Data is reported as K_i according to the Cheng-Prusoff equation.¹³⁶ Biological data are presented in Table 11 for dimers synthesized using different spanners (or linkers). The linkers in **42** (SR-II-35) and **43** (dm-III-96) contained an oxygen atom. Compounds **31**, **33**, **34**, and **35** contained all carbon linkers. Binding data indicated decreased affinity when bivalents contained an oxygen atom in the linker. Bivalent Ligand **33** (XLi-093) and **35** (XLi-210) showed increased selectivity for the α5 subtype as compared to parent monomer **23**. Bivalent ligand **39** (XLi-374) which was analogous to **33** (XLi-093) with the exception of the oxygen atom present in the linker, bound with less affinity at the α5 subtype. Likewise bivalent ligand **31** (DMH-D-053) showed increased selectivity versus monomer **30** (XHe-II-53). However, the bivalent **43** (dm-III-96) containing an oxygen atom in the linker did not bind. The data suggests that dimers which contain a single oxygen atom

in the linker bind less (decreased affinity) to the Bz/GABA (A) receptor. This is due to their propensity to adopt a folded conformation. One strategy to increase hydrophilicity and avoid a folded conformation is to extend the linker length and insert two opposing oxygen atoms. This approach is currently underway.

Comparison of the results of low temperature NMR studies to crystal structures has provided enough information to demonstrate that low temperature NMR can be used as a quick method to identify dimeric ligands with a tendency to fold back upon themselves, as compared with those preferring a linear conformation. A correlation with binding data shows that the suitability of a ligand in the $\alpha 5$ BzR/Gabaergic subtype is heavily influenced by its conformation in solution. Variable temperature NMR thus can be used as a tool for screening bivalent ligands for their *in vivo* suitability. It was also clear the presence of one oxygen atom in the linker was the principle cause for the dimer to fold back onto itself.

6. Synthesis of $\alpha 5$ subtype selective inverse agonist PWZ-029 on multigram scale

PWZ-029 (**47**) was effective in improving memory and cognition, especially in models with baseline cognitive deficits. The high specificity of PWZ-029 (**47**) for $\alpha 5$ -containing GABA_A receptors has successfully mitigated adverse side effects of seizures and sedation, which are commonly observed with typical benzodiazepines (BZ) and nonselective inverse agonists of the GABA_A complex. The novel ligand PWZ-029, which was synthesized on large scale and characterized electrophysiologically, possesses *in vitro* binding selectivity and moderate inverse agonist functional selectivity

at α_5 -containing GABA_A receptors. This ligand has also been examined in rats in the passive and active avoidance, spontaneous locomotor activity, elevated plus maze and grip strength tests, primarily predictive of the effects on the memory acquisition, basal locomotor activity, anxiety level and muscle tone, respectively. The improvement of task learning was detected at the dose of 5 mg/kg in the passive, but not the active avoidance test. The inverse agonist PWZ-029 had no effect on anxiety nor muscle tone, whereas at higher doses (10 and 20 mg/kg) it decreased locomotor activity in this one paradigm. This effect was antagonized by flumazenil and also by the lower (but not the higher) dose of an agonist (SH-053-2'F-R-CH₃) selective for GABA_A receptors containing the α_5 subunit. The hypolocomotor effect of PWZ-029 was not antagonized by the antagonist β -CCt exhibiting a preferential affinity for α_1 -subunit containing receptors. These data suggest that moderate negative modulation at GABA_A receptors containing the α_5 subunit is a sufficient condition for eliciting enhanced encoding/consolidation of declarative memory, while the influence of higher doses of modulators at these receptors on motor activity shows an intricate pattern whose relevance and mechanism wait to be defined.

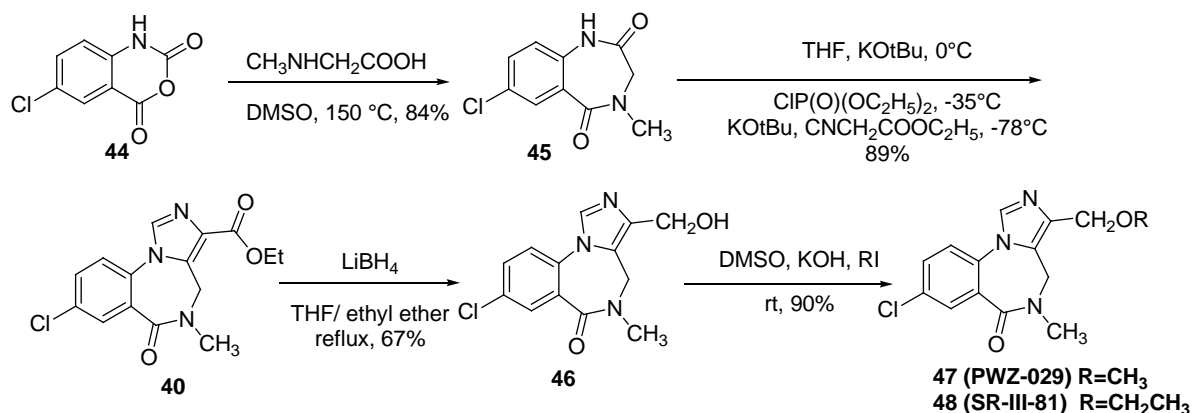
One desirable property in this regard is the pro-amnesic activity of BZ site inverse agonists, repeatedly reported in animal models,^{137,138} as well as in human volunteers.^{139,140} However, this desirable effect is confounded by different concomitant psychomotor effects (increased vigilance, anxiogenic and/or proconvulsant state), some of which have been described in memory studies with non-selective inverse agonists in humans, urging their early termination.¹³⁹ Point mutated mice could not be used to identify the receptor subtypes mediating the promnesic activity of inverse agonists

because an unexplained switch to the agonist mode of action occurs when an inverse agonist at wild type diazepam-sensitive recombinant GABA_A receptors is tested at the respective point-mutated receptors.^{141,142} Thus, inverse agonists exerted agonistic-like sedative and anticonvulsant effects in mice with the point-mutated $\alpha 1$ subunits,¹⁴² while the corresponding experiments in models of learning and memory were not performed.¹⁴² Nevertheless, behavioral examination of genetically modified animals conducted to date has indicated the α_1 and α_5 subunit-containing GABA_A receptors comprise the ‘memory-modulating’ population of these receptors.^{143,144} It is notable that GABA_A receptors containing the α_5 subunit are abundantly expressed in the hippocampus,^{11,145,146} the structure substantially involved in memory formation.¹⁴⁷ Recent evidence from animal studies with affinity-selective¹⁴⁸ or efficacy-selective ligands¹⁴⁹⁻¹⁵¹ has confirmed that the α_5 subunit was significantly involved in cognition enhancement mediated by the negative modulation of GABA_A receptor functions. Moreover, it was shown in humans that pre-treatment with an α_5 efficacy-selective inverse agonist significantly reduces the amnesic effect of alcohol on learning a word list.¹⁵² However, the affinity- or efficacy-selectivity of the ligands, as well as the diversity of the behavioral tasks used in their characterization to date, were of limited extent, which necessitated screening of newer BZ site negative modulatory ligands, to determine the putative therapeutic role of such compounds in various disorders with diminished cognitive capabilities in humans.⁵⁶

In this regard, the BZ site ligand PWZ-029 was synthesized (Scheme 7) and prepared on large scale. A mixture of 5-chloroisatoic anhydride **44** and sarcosine in DMSO was heated to reflux to furnish benzodiazepine **45** in 84% yield. Potassium *t*-butoxide was

added to a solution of **45** in THF at 0 °C and stirred for 20 min. The reaction was cooled to -35°C and diethylchlorophosphate was added slowly. After stirring at 0°C for 30 min, the reaction mixture was cooled to -78°C and ethyl isocyanoacetate was added followed by potassium *t*-butoxide to form **40** in 89% yield. A solution of imidazobenzodiazepine **40** can be reduced with LiBH₄ to furnish alcohol **46** in 67% yield as colorless crystals. To a slurry of KOH in DMSO at room temperature were added alcohol **46** and CH₃I to give PWZ-029 (**47**), as an off-white powder in 95% yield on 1-15 gram scale. The alcohol was dissolved in a solution of KOH in DMSO and treated with CH₃CH₂I at room temperature to give SR-II-81 (**48**).

Scheme 7: Synthesis of PWZ-029



Electrophysiology experiments in *Xenopus* oocytes demonstrated that PWZ-029, at a concentration of 1 μM , significantly reduced GABA initiated control currents, thereby indicating a partial inverse agonist effect of PWZ-029 on GABA_A receptors possessing the $\alpha 5$ isoforms (Figure 32). Illustrated in Figure 32, are the concentration–effects curve

for modulation of GABA_A elicited currents by PWZ-029 on *Xenopus* oocytes expressing GABA_A receptor subtypes $\alpha 1\beta 3\gamma 2$, $\alpha 2\beta 3\gamma 2$, $\alpha 3\beta 3\gamma 2$, and $\alpha 5\beta 3\gamma 2$. Concentrations of GABA_A that elicit 3% of the maximum GABA_A-triggered current of the respective cells were applied alone and with various concentrations of PWZ-029. Control currents represent responses in the absence of PWZ-029. Data points represent means \pm SEM from 4 oocytes from ≥ 2 batches [1 μ M PWZ-029 resulted in 114 \pm 4%, 105 \pm 8%, 118 \pm 5% and 80 \pm 4% of control current (at GABA_A EC₃) in $\alpha 1\beta 3\gamma 2$, $\alpha 2\beta 3\gamma 2$, $\alpha 3\beta 3\gamma 2$, and $\alpha 5\beta 3\gamma 2$ receptors, respectively]. All these values except the one for $\alpha 2\beta 3\gamma 2$ receptors were significantly different from that of the respective control currents (p<0.01, Student's t-test). Note that 100 nM is the pharmacologically relevant concentration.

Table 13. *In Vitro* Binding Affinities of bivalent ligands at GABA_A/BzR subtypes.

Code	MW	$\alpha 1$	$\alpha 2$	$\alpha 3$	$\alpha 4$	$\alpha 5$	$\alpha 6$
Merck	291.73	>300	>300	>300	ND	38.8	>300
Moltech	291.73	920	ND	ND	ND	30	ND
UNC-Roth	291.73	362.4	180.330	328.2	ND	6.185	ND

^aValues Reported are in nM.

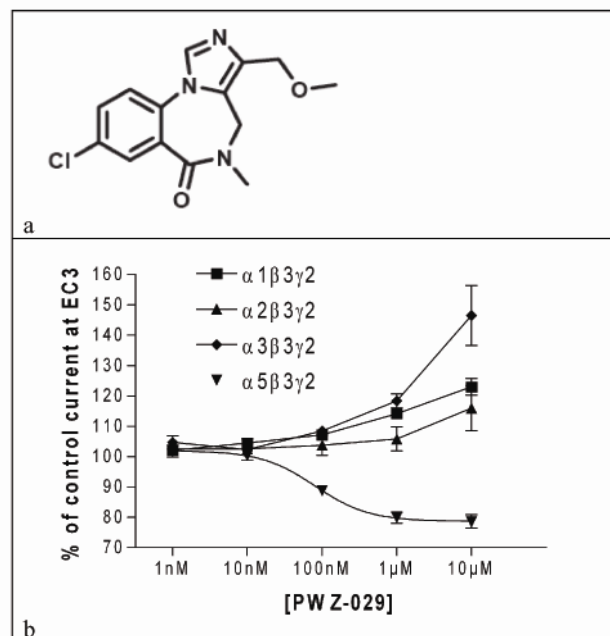


Figure 32. Oocyte data for PWZ-029 by Sieghart et al.¹⁵³

This ligand as mentioned, has also been examined in rats in the passive and active avoidance, spontaneous locomotor activity, elevated plus maze and grip strength tests, primarily predictive of the effects on the memory acquisition, basal locomotor activity, anxiety level and muscle tone, respectively. The improvement of task learning was detected at the dose of 5 mg/kg in the passive avoidance task (Figure 33). The passive avoidance task is a one trial fear-motivated avoidance task in which the mouse learns to refrain from stepping through a door to an apparently safer but previously punished dark compartment. The latency to refrain from crossing into the punished compartment serves as an index of the ability to avoid, and allows memory to be assessed.

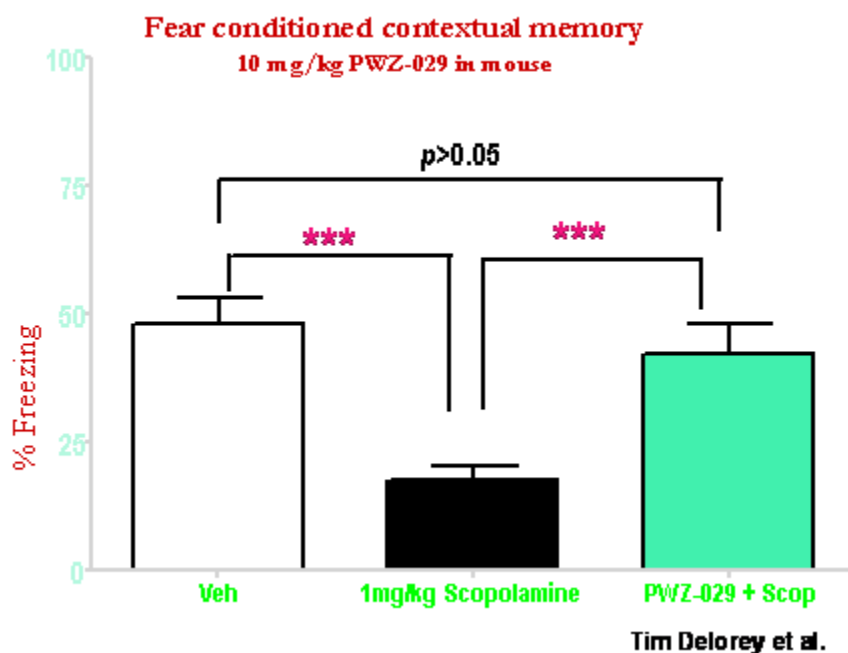


Figure 33. Fear conditioned contextual memory of PWZ-029

The PWZ-029 at 5 mg/kg, administered before the acquisition session, significantly increased retention session latency relative to the control group.¹⁵⁴

The inverse agonist PWZ-029 (**47**) had no effect on anxiety or muscle tone, whereas at higher doses (10 and 20 mg/kg) it decreased locomotor activity. This effect was antagonized by flumazenil and also by the lower (but not the higher) dose of an agonist (SH-053-R-CH3-2'F) selective for GABA_A receptors containing the $\alpha 5$ subunit. The hypolocomotor effect of PWZ-029 (**47**) was not antagonized by the antagonist β CCt, which exhibits a preferential affinity for $\alpha 1$ -subunit-containing receptors. These data suggest that moderate negative modulation at GABA_A receptors containing the $\alpha 5$ subunit is a sufficient condition for eliciting enhanced encoding/consolidation of

declarative memory, while the influence of higher doses of modulators at these receptors on motor activity shows an intricate pattern whose relevance and mechanism await to be defined.¹⁵⁴ In fact, in the conflict paradigm in Rowlett's lab in rhesus monkeys, PWZ-029 was a weak anxiolytic with no sedation observed in either the suppressed or nonsuppressed portion of the test. Recently, Stables et al. at NINDS has shown PWZ-029 to be a weak anticonvulsant. The PWZ-029 (**47**) an $\alpha 5$ inverse agonist cannot be proconvulsant or convulsant (see Appendix IV) and consequently will not exhibit the side effects of other inverse agonists (NAM).

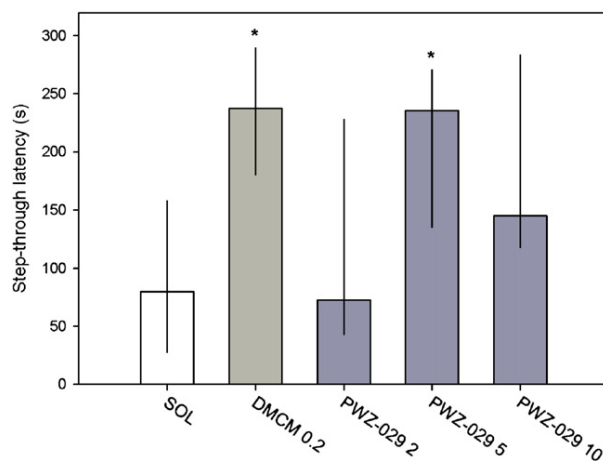


Figure 34. Passive avoidance task¹⁵⁴

The effects of DMCM (0.2 mg/kg) and PWZ-029 (2, 5 and 10 mg/kg) on retention performance in a passive avoidance task (* $p < 0.05$ compared to solvent (SOL) group).

Number of animals per treatment group: 10.

6.1. CANTAB Approach (Rowlett, Rallapalli and Cook et al.)¹⁵⁵

Recent studies by Rowlett, Rallapalli and Cook et al. on PWZ-029 showed that this ligand acted as an inverse agonist at $\alpha 5$ GABA_A receptor subtypes which enhanced memory. Rowlett's used several primate models, including the Cambridge Neuropsychological Test Automated Battery, or CANTAB. A clear strength of the CANTAB approach is that its tasks are based on corresponding procedures developed for human patients, which greatly facilitate the ultimate goal of translating findings from monkeys to humans.

Because PWZ-029 has been shown to be safe and to have cognitive-enhancing effects in rodents¹⁵⁴ experiments were initiated with this compound in rhesus monkeys as mentioned. Initial results, shown in Figure 35, are quite provocative and exciting: PWZ-029 enhanced performance in the DNMS (Delayed non-matching to sample) to task using the 10-min delay with distracters (Figure 35A) and although it had no effect alone, PWZ-029 completely reversed the scopolamine-induced deficit in the ORD (Object Retrieval with Detours) task (Figure 35B). Interestingly, PWZ-029 induced anti-conflict (anxiolytic) effects in monkeys without the concomitant response rate-suppressing effects characteristic of BZ-type drugs (Figure 35C). It is felt that these latter effects are due to PWZ-029's partial agonist effects at $\alpha 2/3$ GABA_A receptor subtypes, whereas the cognition-enhancing effects of this compound are due to inverse agonist (NAM) action at $\alpha 5$ GABA_A receptors.

PWZ-029 (**47**) provides an important lead compound based not only on potential effectiveness against cognitive impairment, but also as a potential treatment for anxiety and agitation in patients with dementias, similar to the anxiolytic effects of classical BZs

(Meehan et al. 2002). Studies will continue with PWZ-029 and expand them to include comparative studies with non-selective agonists and $\alpha 5\text{GABA}_A$ -preferring agonists; as well as with pre-treatments with $\alpha 5\text{GABA}_A$ -preferring antagonists such as XLI-093 (33). In addition, in our initial screens compounds will be sought with similar, and hopefully improved, efficacy profiles. For example, a compound that is an $\alpha 5\text{GABA}_A$ partial inverse agonist, an $\alpha 2/3\text{GABA}_A$ -preferring partial agonist, but ineffective at $\alpha 1\text{GABA}_A$ receptors is both desirable and feasible in our synthesis/screening program.

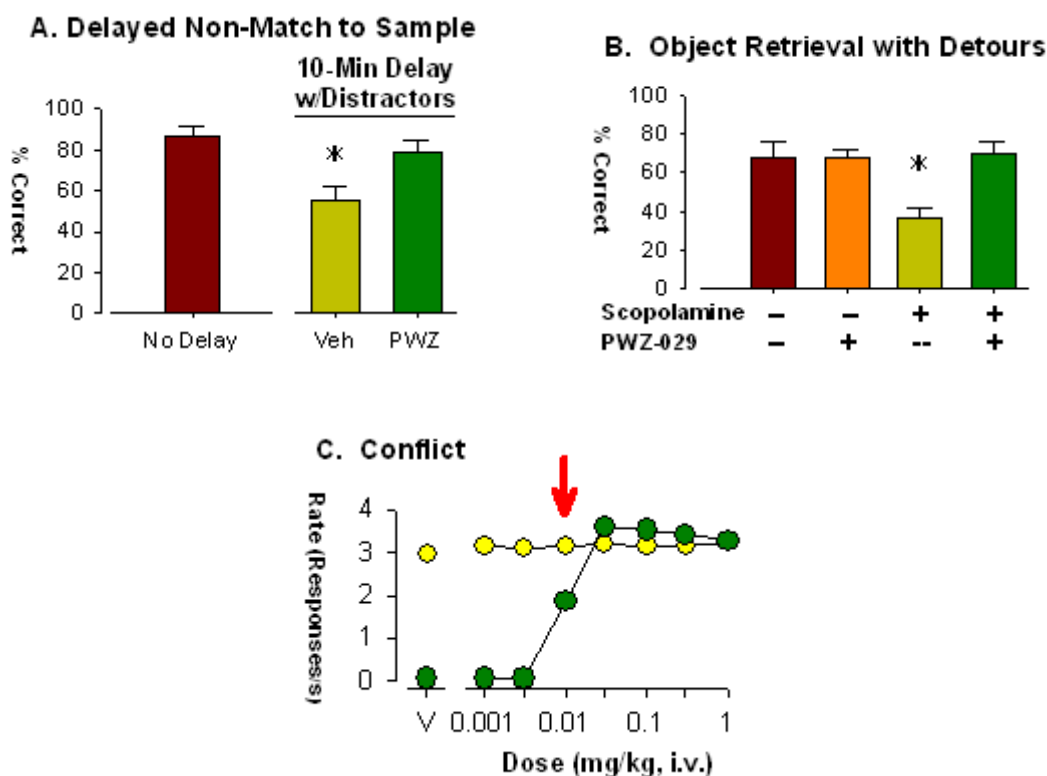


Figure 35: Preliminary profile of cognitive enhancing and anxiolytic like effects of PWZ-029 in monkeys. Data are from n=2 monkeys (A & C) and n=4 monkeys (B). Red arrow indicates the dose (0.01mg/kg, i.v.) of PWZ-029 tested in A & B

Importantly, in the ORD task, PWZ-029 showed only a modest trend for enhancement of performance (Fig. 36A), but when task difficulty was increased by testing with difficult trials only, PWZ-029 robustly increased performance (Fig. 36B). This enhancement was reversed by administration of the $\alpha 5$ GABA_A-preferring antagonist XLi-093, and this antagonism, in turn, was reversed by increasing the dose of PWZ-029 (Fig. 36C). Finally, PWZ-029 completely reversed deficits in performance induced by the memory-impairing anti-cholinergic scopolamine (Fig. 36D).

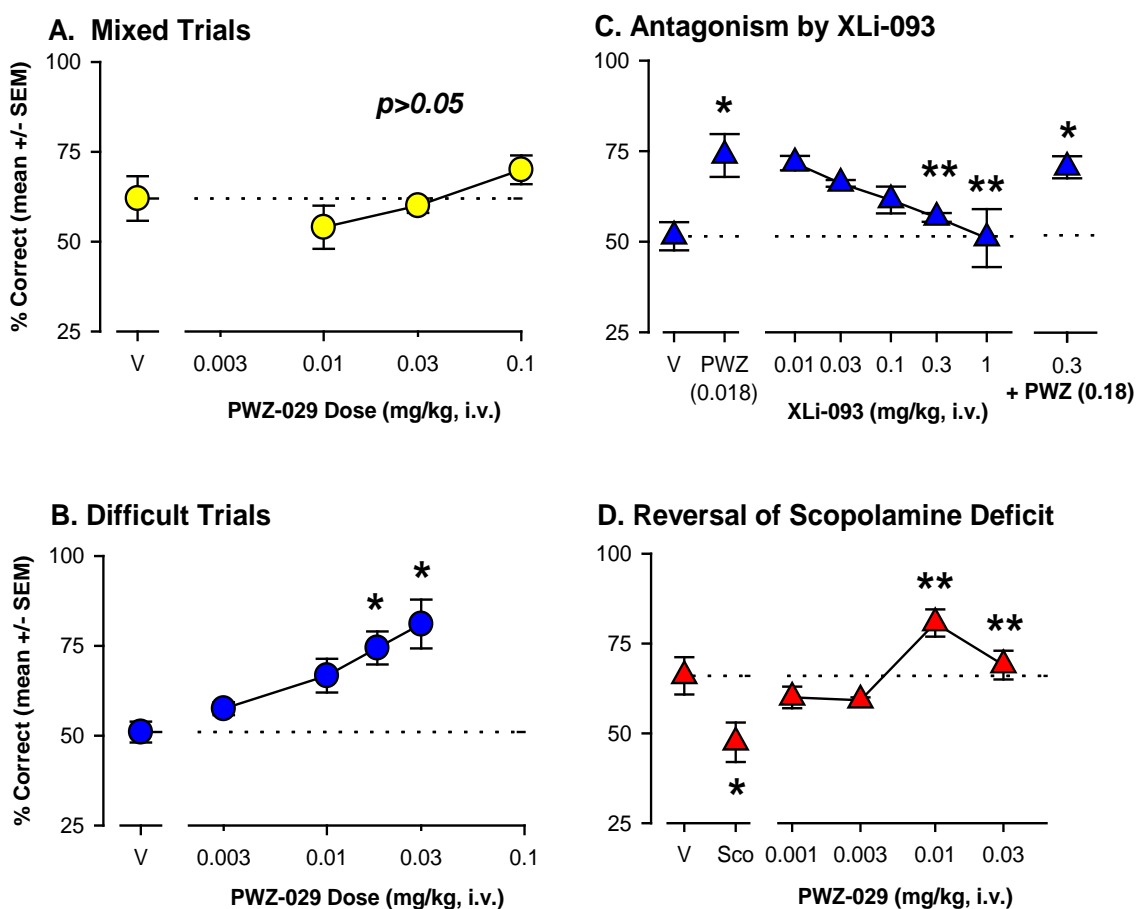


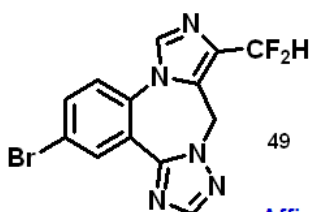
Figure 36. Cognitive-enhancing effects of PWZ-029 in the rhesus monkey Object Retrieval with Detours (ORD) task (N=5 monkeys). **A.** Effects of PWZ-029 on ORD tests consisting of both easy and difficult trials. No effect of the compound was observed

(mean % correct first reaches, $p > 0.05$, repeated measures ANOVA). **B.** PWZ-029 enhanced performance in the ORD task when tested with difficult trials only ($*p < 0.05$ vs. vehicle, V, Bonferroni t-tests). **C.** Enhancement of ORD performance by 0.018 mg/kg of PWZ-029 was attenuated by the $\alpha 5\text{GABA}_A$ -preferring antagonist XLi-093, and this antagonism was surmountable by increasing the PWZ-029 dose ($*p < 0.05$ vs. vehicle, $**p < 0.05$ vs. 0.018 mg/kg PWZ-029, Bonferroni t-tests). **D.** PWZ-029 reversed performance impaired by 0.01 mg/kg of scopolamine. ($*p < 0.05$ vs. vehicle; $**p < 0.05$ vs. scopolamine alone, Bonferroni t-tests).

6.2. Synthesis of PWZ-029 analogs

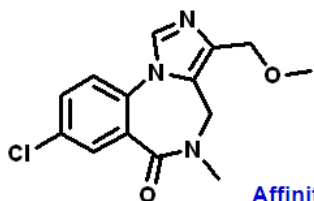
The chemistry used to design fluoro analogs of PWZ-029 (**47**) can be adapted to design ligands of XHE-II-053 (**30**) with less potential for metabolization by esterases. Fluorine atoms in place of the carbonyl group satisfy current included volumes and electronegativity requirements of the Milwaukee-based pharmacophore receptor model. The covalent radius of a hydrogen is 37 pm whereas a fluorine is 71 pm.

This approach is in agreement by a recent compounds patented by Roche.¹⁵⁶ Several new analogs have been proposed and docked in the Milwaukee based pharmacophore by Clayton et al.¹⁵⁷



Affinity for $\alpha\beta\gamma 2$ ($x = 1-6$) benzodiazepine receptor isoforms

	Alpha 1	Alpha 2	Alpha 3	Alpha 4	Alpha 5	Alpha 6
Roche	174.3	185.4	79.6	ND	4.6	ND



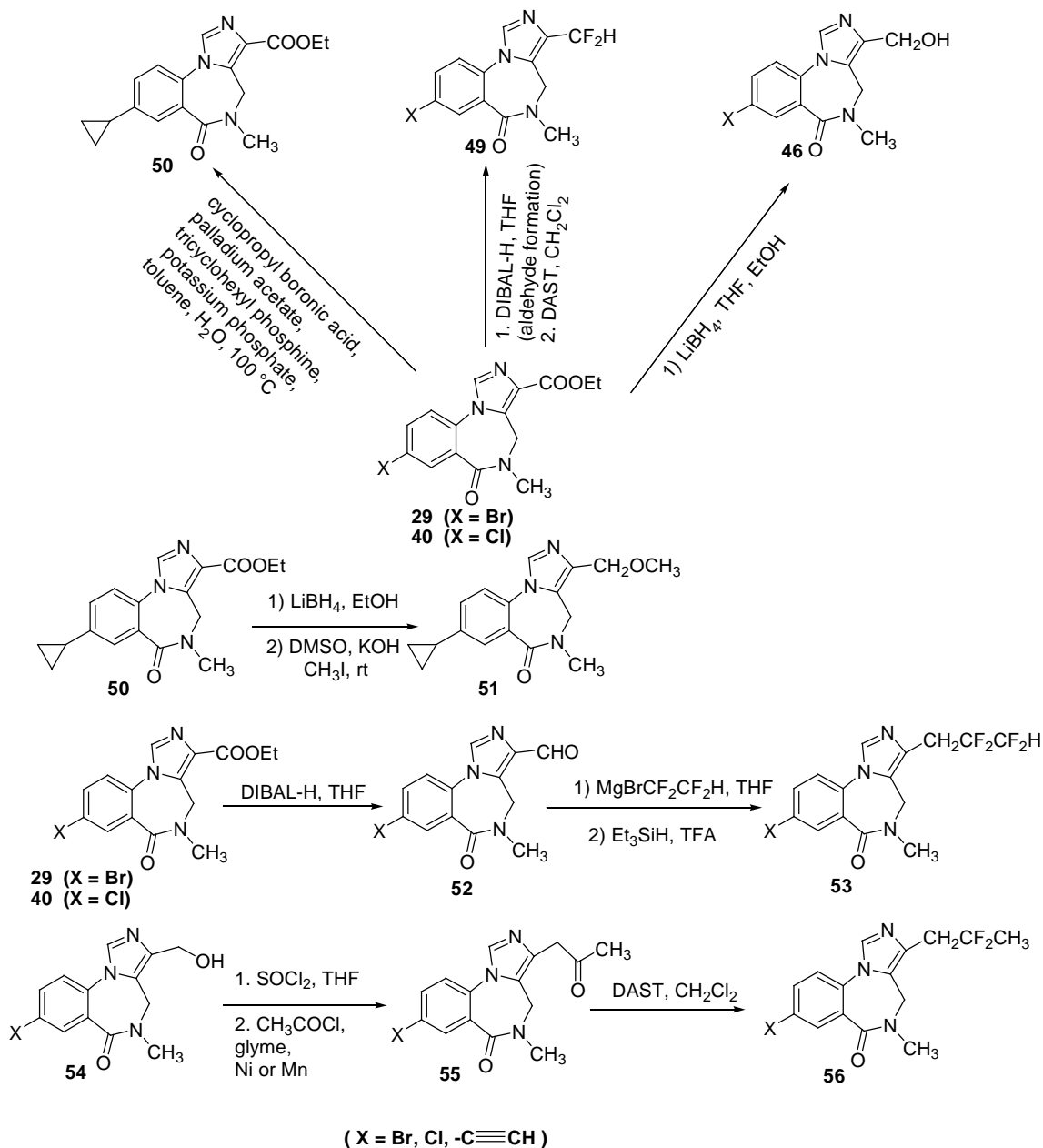
Affinity of PWZ-029 for $\alpha\beta\gamma 2$ ($x = 1-6$) benzodiazepine receptor

	Alpha 1	Alpha 2	Alpha 3	Alpha 4	Alpha 5	Alpha 6
Merck	>300	>300	>300	ND	38.5	>300
Moltech	920	ND	ND	ND	30	ND
UNC-Roth	362.4	180.330	328.2	ND	6.185	ND

Figure 37: Binding affinity data of PWZ-029 (47) and Roche difluoro ligand 49

The new analogs of PWZ-029 are of strong interest due to the recent contextual memory impairment data wherein doses of scopolamine decreased memory while the $\alpha 5$ ligand reversed this (see Scheme 8).

Scheme 8: Synthesis of various analogs of PWZ029



The synthesis of amine analog of PWZ-029 can be seen in Scheme 9. A mixture of imidazobenzodiazepine was refluxed with methyl amine in anhydrous CH_2Cl_2 to give SR-II-097 (**57**) in 78% yield. The efficacy data evaluated by Sieghart et al. (shown in

Figure 38) indicated that the ligand SR-II-097 (**57**) was an inverse agonist at $\alpha 5$ and was an agonist at $\alpha 1$ when compared to PWZ-029 (see Figure 38 and Table 15).

Scheme 9: Synthesis of SR-II-097

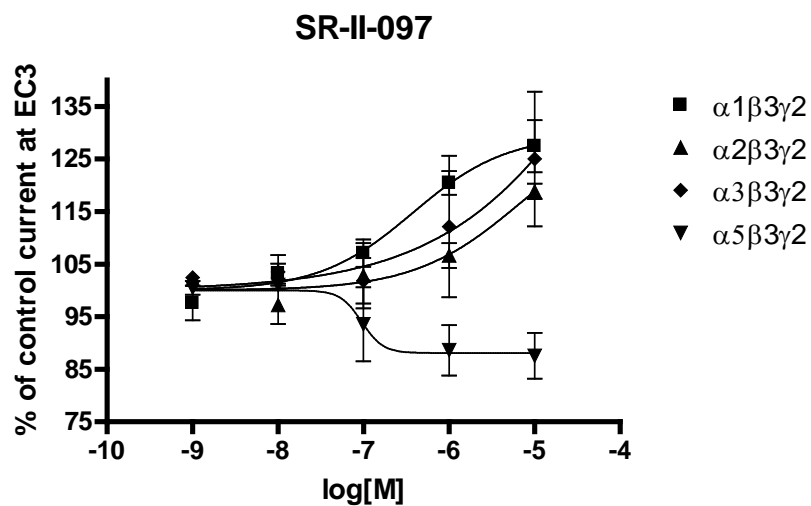
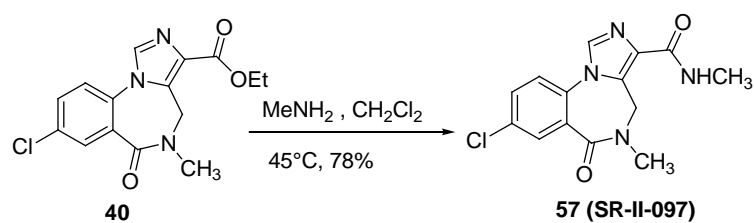


Figure 38: Oocyte data of SR-II-097

Table 14. EC₅₀ and Hill Slope for Modulation of Control GABA EC₃ by **SR-II-097 (57)** in *Xenopus* Oocytes Expressing Different GABA_A Receptor Subtypes. Results represent EC₅₀ (95% confidence interval for EC₅₀) and Hill Slope (Nh) ± SD from at least four cells from two batches.

		$\alpha 1\beta 3\gamma 2$	$\alpha 2\beta 3\gamma 2$	$\alpha 3\beta 3\gamma 2$	$\alpha 5\beta 3\gamma 2$
SR-II-097 (57)	EC ₅₀	378nM	>6μM	>18μM	95nM
	95%CI	(58-2426)			(0.01-6000)
	Nh	0.80			-3.5

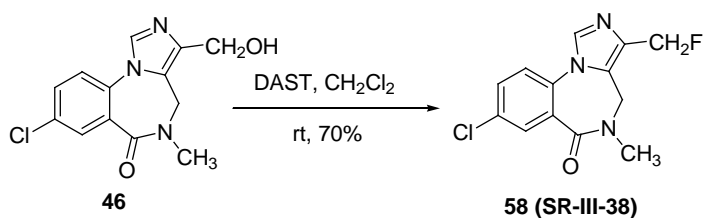
Table 15. Modulation of Control GABA EC₃ by SR-II-097 (57) on *Xenopus* Oocytes Expressing Different GABA_A Receptor Subtypes. Values are presented as mean ± SEM of at least four oocytes from at least two batches.

		$\alpha 1\beta 3\gamma 2$	$\alpha 2\beta 3\gamma 2$	$\alpha 3\beta 3\gamma 2$	$\alpha 5\beta 3\gamma 2$
	10nM	ns	ns	ns	ns
SR-II-097(57)	100nM	ns	ns	ns	ns
	1μM	121±2 %	ns	ns	88±5%
	10μM	123±5%	119±1%	125±13%	88±4%

All the above values were significantly different from the respective control currents ($p < 0.01$, Student's-*t*-test) except where indicated (n.s.). n.s. means not significant.

The fluoro analog SR-III-38 was prepared using DAST (diethylaminosulfur trifluoride) in anhydrous CH_2Cl_2 at room temperature in 70 % yield.

Scheme 10: Synthesis of SR-III-38



Examination of the oocyte data (shown in Figure 39) indicated no significant subtype selective efficacy.

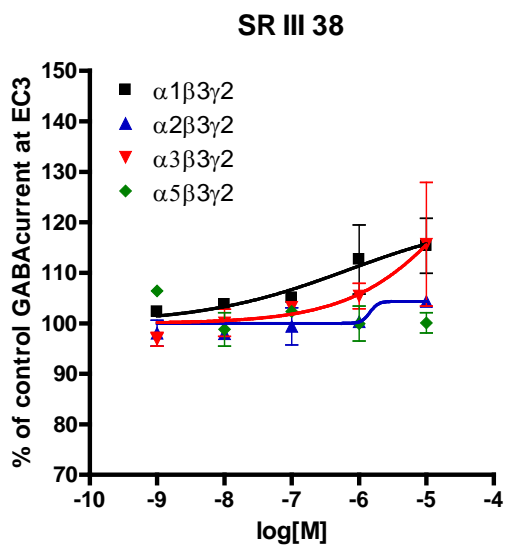


Figure 39: Oocyte data on SR-III-38 by Sieghart et al.

Table 16. EC₅₀ and Hill Slope for Modulation of Control GABA EC₃ by **SR-III-38 (58)** in *Xenopus* Oocytes Expressing Different GABA_A Receptor Subtypes. Results represent EC₅₀ (95% confidence interval for EC₅₀) and Hill Slope (Nh) ± SD from at least four cells from two batches.

		$\alpha 1\beta 3\gamma 2$	$\alpha 2\beta 3\gamma 2$	$\alpha 3\beta 3\gamma 2$	$\alpha 5\beta 3\gamma 2$
SR-III-38 (58)	EC ₅₀	>0.6μM		>43μM	
	95%CI				
	Nh	0.4		1.5	

Table 17. Modulation of Control GABA EC₃ by **SR-III-38 (58)** on *Xenopus* Oocytes Expressing Different GABA_A Receptor Subtypes. Values are presented as mean ± SEM of at least four oocytes from at least two batches.

		$\alpha 1\beta 3\gamma 2$	$\alpha 2\beta 3\gamma 2$	$\alpha 3\beta 3\gamma 2$	$\alpha 5\beta 3\gamma 2$
	10nM	ns	ns	ns	ns
SR-III-38 (58)	100nM	105±1 %	ns	ns	ns
	1μM	112±10 %	ns	105±3%	ns
	10μM	115±7%	ns	115±17%	ns

All the above values were significantly different from the respective control currents ($p < 0.01$, Student's-*t*-test) except where indicated (n.s.). n.s. means not significant.

To improve the selectivity, the difluoro analog SR-III-61 was synthesized from an aldehyde (**59**). The alcohol **46** was treated with Dess Martin periodinane in dry CH_2Cl_2 to afford aldehyde **59** in 96% yield. Treatment of aldehyde in dry CH_2Cl_2 with DAST resulted in the difluoro analog SR-III-61 (**49**) in 65% yield.

Scheme 11: Synthesis of SR-III-61

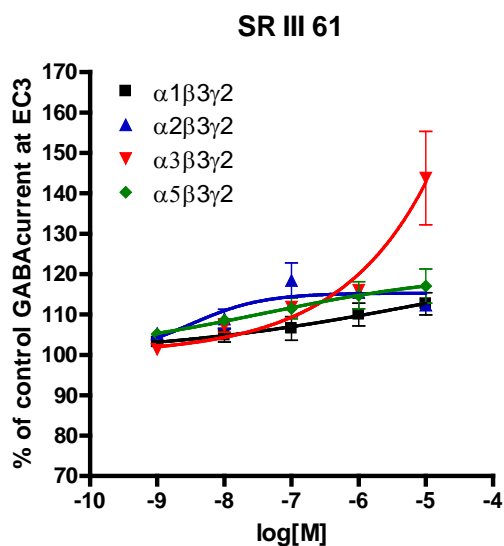
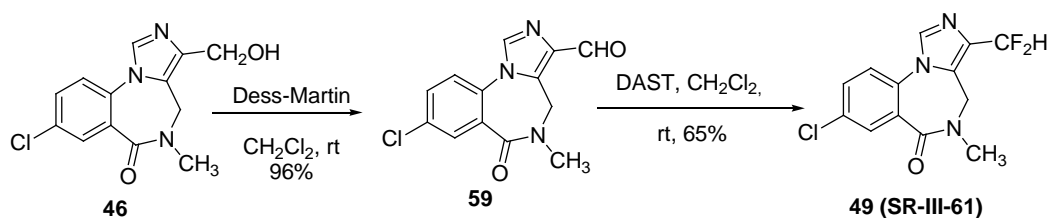


Figure 40: Oocyte data of SR-III-61 by Sieghart et al.

Table 18. EC₅₀ and Hill Slope for Modulation of Control GABA EC₃ by **SR-III-61 (49)** in *Xenopus* Oocytes Expressing Different GABA_A Receptor Subtypes. Results represent EC₅₀ (95% Confidence interval for EC₅₀) and Hill Slope (Nh) ± SD from at least four cells from two batches.

		$\alpha 1\beta 3\gamma 2$	$\alpha 2\beta 3\gamma 2$	$\alpha 3\beta 3\gamma 2$	$\alpha 5\beta 3\gamma 2$
SR-III-61 (49)	EC ₅₀	>10μM	>3nM		>0.03μM
	95%CI		(1-27nM)		
	Nh		0.8		

Table 19. Modulation of Control GABA EC₃ by **SR-III-61 (49)** on *Xenopus* Oocytes Expressing Different GABA_A Receptor Subtypes. Values are presented as mean ± SEM of at least four oocytes from at least two batches.

		$\alpha 1\beta 3\gamma 2$	$\alpha 2\beta 3\gamma 2$	$\alpha 3\beta 3\gamma 2$	$\alpha 5\beta 3\gamma 2$
SR-III-61(49)	10nM	ns	109±4 %	ns	102±7 %
	100nM	ns	119±6%	112±2 %	107±5%
	1μM	110±4 %	116±1%	116±2%	109±8%
	10μM	113±4%	113±1%	144±16%	110±9%

All the above values were significantly different from the respective control currents (p<0.01, Student's-*t*-test) except where indicated (n.s.). n.s. means not significant.

Data of SR-III-61 (**49**) from the electrophysiology indicated (in oocytes) was an agonist at $\alpha 3$ subtypes at high concentrations. However at a pharmacologically relevant concentration (100nM, -7) the ligand demonstrated efficacy at all subtypes. Unfortunately, the efficacy data showed no significant subtype selectivity. The synthesis of the other PWZ analogs is currently underway.

7. Conclusions

In this study, it was clear that QH-II-066 (**11**) which is $\alpha 5$ subtype selective ligand is an agonist. It was shown⁸⁸ that QH-II-066 (**11**) exhibited functional selectivity *in vivo* with potent diazepam-like efficacy at $\alpha 5$ subtypes and partial efficacy at the $\alpha 1$ subtype. Recent studies by Weiss and Cook et al.⁸⁹ have shown that activation of GABA (A) by QH-II-066 (**11**) induces apoptosis in neuroblastoma. This is very important finding. The mechanism by which GABA-A activation inhibited the growth of neuroblastoma cells was assessed by Cho, Cook et al. QH-II-066 (**11**), an $\alpha 5$ agonist passes through the blood brain barrier which opens up the potential to apply in neurology and psychology as chemotherapeutic agent. These results also highlight a possible connection between the role of neurotransmitters in nervous system development and the regulation of neuroblastoma growth as shown by Weiss, Rallapalli and Cook et al. (unpublished, see Appendix III).

Bivalent ligand XLi-093 (**33**) has clearly been shown to be the first subtype selective antagonist at $\alpha 5$ subtypes which is known (Rowlett, Savic et al.) to cross the blood brain barrier. Rowlett showed that the memory impairing effects of diazepam were blocked by

a dose of XLi-093 (3.0mg/kg) that occupied about 66% of the $\alpha 5$ GABA_A binding sites. A series of bivalent ligands with oxygen linker were synthesized based on $\alpha 5$ selectivity of XLi-093 (**33**). Comparison of the results of low temperature NMR studies to crystal structures has provided enough information to demonstrate that low temperature NMR can be used as a quick method to identify dimeric ligands with a tendency to fold back upon themselves, as compared with those preferring a linear conformation. A correlation with binding data shows that the suitability of a ligand in the $\alpha 5$ BzR/Gabaergic subtype is heavily influenced by its conformation in solution. Variable temperature NMR thus can be used as a tool for screening bivalent ligands for their in vivo suitability. It is also clear the presence of one oxygen atom in the linker was the principle cause for the dimer to fold back onto itself, consequently resulted in diminished activity. From the recent work of Rowlett, it was demonstrated that novel $\alpha 5$ selective inverse agonist PWZ-029 (**47**) enhanced cognition in rhesus monkeys in the CANTAB paradigm. This ligand had the ability to reverse cholinergic deficits in performance induced by the antimuscarinic scopolamine under mixed trial conditions. In the ORD task, PWZ-029 showed only a modest trend for enhancement of performance. But when task difficulty was increased by testing with difficult trials only, PWZ-029 robustly increased performance. This enhancement was reversed by administration of the $\alpha 5$ GABA (A) subtype selective antagonist XLi-093 and this antagonism in turn was reversed by increasing the dose of PWZ-029. In addition, PWZ-029 enhanced performance in the DNMS task using the 10 minute delay with distracters. This ligand also exhibited anxiolytic activity in some primates and was a weakly active anticonvulsant in rats (NINDS, Jim Stables et al. see Appendix IV). These findings are

consistent with a role for PWZ-029 (**47**) $\alpha 5$ GABA_A receptors in the treatment of age-associated memory impairment and Alzheimer's disease. It is the subject of an SBIR grant submitted December 5th, 2012 by Physiogenix (see Appendix VII).

8. General Experimental Details

All reactions were carried out under an argon atmosphere with dry solvents using anhydrous conditions unless otherwise stated. Tetrahydrofuran (THF) and diethyl ether were freshly distilled from Na/benzophenone ketyl prior to use. Dichloromethane was distilled from calcium hydride prior to use. Methanol was distilled over magnesium sulfate prior to use. Benzene and toluene were distilled over sodium and acetonitrile was distilled over CaH₂ prior to use. Reagents were purchased of the highest commercial quality and used without further purification unless otherwise stated. Thin layer chromatography (TLC) was performed using Dynamic Adsorbents Inc. UV active silica gel, 200 μ m, plastic backed; Dynamic Adsorbents Inc. UV active alumina N, 200 μ m, F-254 plastic backed plates. Flash and gravity chromatography were performed using silica gel P60A, 40-63 μ m purchased from Silicycle. Elemental analyses were performed on a Carlo Erba model EA-1110 carbon, hydrogen, and nitrogen analyzer. All samples submitted for CHN analyses were first dried under high vacuum for a minimum of six hours using a drying pistol with isopropyl alcohol or benzene as the solvent with potassium hydroxide pellets in the drying bulb. Melting points were taken on a Stuart melting point apparatus SMP3 manufactured by Barloworld Scientific US Ltd. Proton (¹H NMR) and carbon high resolution nuclear magnetic resonance spectra (¹³C NMR) were obtained on a Bruker 300-MHz or a GE 500-MHz NMR spectrometer. ¹H NMR

data are reported as follows: chemical shift, multiplicity (s = singlet, d = doublet, t = triplet, q = quartet, dd = doublet of doublets, dt = doublet of triplets, ddd = doublet of doublet of doublet, td = triplet of doublets, qd = quartet of doublets, sex = sextet, m = multiplet), integration, and coupling constants (Hz). ^{13}C NMR data are reported in parts per million (ppm) on the δ scale. The low resolution mass spectra (LRMS) were obtained as electron impact (EI, 70eV), which were recorded on a Hewlett-Packard 5985B gas chromatography-mass spectrometer, while high resolution mass spectra (HRMS) were recorded on a VG Autospec (Manchester, England) mass spectrometer. HRMS recorded by electrospray ionization (ESI) methods were performed at the Laboratory for Biological Mass Spectrometry at Texas A&M University on an API QStar Pulsar model, manufactured by MDS Sciex.

5-Phenyl -1,4 benzodiazepine-2-one (7) : The 2-amino-benzophenone **5** (100.6g, 0.51mol) and NaHCO_3 (128.6g, 1.5mol) were suspended in dry CH_2Cl_2 (1.3L) at rt. A solution of bromoacetyl bromide (113.2g, 0.56mol, 48.9mL) in dry CH_2Cl_2 (200mL) was added dropwise over 30 min and the mixture was allowed to stir for another 3h. The reaction was allowed to stir until analysis by TLC (silica gel) indicated the absence of starting material, after which the above reaction mixture was concentrated under vacuum to provide amide intermediate **6** which was added directly to a saturated solution of anhydrous ammonia in CH_3OH (1.5L). The mixture was heated to reflux for 6h until analysis by TLC (silica gel) indicated the absence of the 2-bromoacetyl intermediate **6** prepared above. After the solvent was removed under reduced pressure, the solid which remained was washed with hexane/EtOH (1:4) to provide pure benzodiazepine **7** (107g, 95%) as a white powder. **3**: mp: 135-145 °C; **IR** (KBr) 3454, 3185, 3063, 2891, 1681,

1614, 1467 cm^{-1} ; $^1\text{H NMR}$ (CDCl_3 , 300MHz) δ 9.68 (s, 1H), 7.09-7.59 (m, 9H), 4.31 (s, 2H) **MS (EI)** m/e 236 (M^+ , 93), 208 (100), 180 (28), 152 (19); **Anal. Cald for $\text{C}_{15}\text{H}_{12}\text{N}_2\text{O}$** : C, 76.25; H, 5.12; N, 11.86; Found C, 76.21; H, 5.19; N, 11.94. The spectral data were in agreement with the literature.⁶⁵

7-Bromo-5-phenyl-1,4-benzodiazepine-2-one 8: Benzodiazepine **7** (61.4g, 0.274mol) was dissolved in acetic acid (1L) and was treated with H_2SO_4 (15.2mL, 0.55mol, 36N) and bromine (87.1 g, 0.55mol). After stirring at rt for 10d, the reaction mixture was poured into ice water and brought to pH 5-6 with an aq solution of 6N NaOH. The crude bromide **4** precipitated and was collected by vacuum filtration and recrystallized from EtOH to provide the bromide **8** as a white solid in 90% yield. **8**: mp: 188-194 °C; IR (KBr) 3466, 3173, 3075, 2953, 1687, 1602, 1480 cm^{-1} ; $^1\text{H NMR}$ (DMSO-d , 300MHz) δ 10.95(s, 1H), 7.11-7.89 (m, 8H), 4.25 (s, 2H). **MS (CI)** m/e 316 ($\text{M}^+ + 1$, 78), 265 (15), 237 (100), **Anal. Cald for $\text{C}_{15}\text{H}_{12}\text{N}_2\text{O}$** : C, 57.16; H, 3.52; N, 8.89; Found C, 57.56; H, 3.49; N, 8.82. This material was identical to that reported in the literature.⁶⁵

7-Trimethylsilylacetyleno-5-phenyl-1,3-dihydrobenzo[e]-1,4-diazepine-2-one 9: The 6- Bromo-benzodiazepine **8** (5g, 15.86mmol) was dissolved in dry triethyl amine (108mL) and acetonitrile (68mL). This mixture was degassed 3-4 times under vacuum and back filled with argon. To this degassed mixture, bis (triphenylphosphine) palladium (II) acetate (0.713g, 1.1mmol) and trimethylsilylacetylene (4.48mL, 31.72 mmol) was added and the mixture was heated to reflux under argon. After 12 h the reaction mixture was cooled to rt and filtered through a bed of celite with EtOAc. The filtrate was concentrated in vacuo and the residue was purified via flash chromatography [silica gel, EtOAc:hexane (1:1)] to furnish the TMS analog **9** as a yellow powder (4.5g, 85%):

mp: 190.0-191.5 °C; **IR** (KBr) 3011, 2281, 1686, 1610, 1486 cm^{-1} ; **$^1\text{H NMR}$** (CDCl_3 , 300 MHz) δ 10.17 (s, 1H), 7.21-7.61 (br, 7H), 7.09 (d, 1H, $J=8.25\text{Hz}$), 4.31 (s, 2H), 0.21 (s, 9H) ; **MS (CI)** m/e (relative intensity) 333 ($\text{M}^+ +1$, 100). **Anal. Cald for $\text{C}_{20}\text{H}_{20}\text{N}_2\text{OSi}$:** C, 72.25; H, 6.06; N, 8.43; Found C, 72.20; H, 6.11; N, 8.52

1-Methyl-7 - trimethylsilylacetyleno-5- phenyl - 1,3-dihydrobenzo[e]-1,4-diazepine-

2-one 10: The acetyleno amine **9** (1g, 3mmol) was dissolved in dry THF (15mL) at -15°C and NaH (60% mineral oil, 144mg, 3.6mmol) was added to the solution in one portion. The slurry was then stirred for 30 min and then CH_3I (0.28mL, 4.5mmol) was added to the mixture and this mixture was allowed to warm to rt. After the mixture was allowed to stir overnight, the reaction was quenched with water (200mL) and EtOAc (100mL). The mixture was extracted with EtOAc and then washed with brine and dried (Na_2SO_4). After the removal of the solvent under reduced pressure, the residue was purified by flash chromatography [hexane:EtOAc (75:25)] to provide the TMS-analog **10** (0.9g, 85%) as a white solid : **mp:** 177-178 °C; **IR** (KBr) 2954, 2147, 1687, 1612, 1491 cm^{-1} ; **$^1\text{H NMR}$** (CDCl_3 , 300 MHz,) δ 7.20-7.27 (m, 3H), 7.07 (d, 1H, $J=8.58\text{Hz}$), 7.05 (s, 1H), 4.60 (d, 1H, $J=10.8\text{Hz}$), 3.54 (d, 1H, $J=10.8\text{Hz}$), 3.18 (s, 3H); **MS (EI)** m/e 346 (M^+ 90), 318 (100), 303 (19), 165 (22), 151 (20). **Anal. Cald for $\text{C}_{21}\text{H}_{22}\text{N}_2\text{OSi}$:** C, 72.79; H, 6.40; N, 8.08; Found C, 72.50; H, 6.68; N, 8.04

1-Methyl-7-acetyleno-5- phenyl- 1,3-dihydrobenzo[e]-1,4-diazepine-2-one 11: A solution of trimethylsilyl acetyleno benzodiazepine **10** (0.87g, 2.5 mmol) was dissolved in THF (200mL) and the solution was cooled to -30°C . A solution of TBAF (1.0M in THF; 3.01mL, 3mmol) was then added to the mixture and it was allowed to warm to rt. After stirring at rt for 20min the reaction mixture was quenched with water (200mL) and

extracted with EtOAc (200mL), washed with brine and dried (Na₂SO₄). After removal of the solvent under reduced pressure the residue was purified by flash chromatography [EtOAc : hexane (1:1)] to provide the target compound **11 (QH-II-066)** (0.62g, 90%) as light yellow crystals. mp: 163-165 °C; IR (KBr) 2965, 1680, 1605 cm⁻¹; ¹H NMR (CDCl₃, 300 MHz) δ 7.62 (dd, 1H, J=8.5Hz, 2.0Hz), 7.35-7.45 (m, 4H), 7.27-7.42 (d, 1H, J=8.5Hz), 4.80 (d, 1H, J=10.9Hz), 3.85 (d, 1H, J = 10.8Hz), 3.46 (s, 3H), 3.11 (s, 3H); MS (EI) m/e 274 (M⁺, 100), 259(12), 246 (10), 189 (12), 122 (19), 105 (42). **Anal. Cald for C₁₈H₁₄N₂O.2/3H₂O**: C, 75.51; H, 4.89; N, 9.78; Found C, 75.59; H, 5.17; N, 9.62. This material was identical to that reported in the literature.^{47,65}

(Z)-8-Bromo-2-((4-methylpiperidin-1-yl)methylene)-6-phenyl-2,4-dihydro-1H-benzo[f]imidazo[1,2-a][1,4]diazepin-1-one 16: A suspension of 7-bromo-1,3-dihydro-5-phenyl-2H-1,4-benzodiazepin-2-thione **12** (1.6g, 4.83mmol), glycine (1.81g, 24.2mmol) and Na₂CO₃ (1.84g, 17.4mmol) in EtOH (38mL)-H₂O (16mL) was stirred at reflux for 1 h and then poured into water (100mL), after which the mixture was filtered to remove a small amount of 7-bromo-1,3-dihydro-5-phenyl-2H-1,4-benzodiazepin-2-one which remained. The filtrate was extracted with CHCl₃. The CHCl₃ extract was discarded and then the aq layer was adjusted to pH 4 with a solution of aq 2N HCl after which it was extracted with CHCl₃ (3x25mL). Evaporation of the CHCl₃ solution gave pure acid **13** (1.2g, 67%) as a yellow solid. Acid **13** (350mg, 0.941mmol) was suspended in dry CH₂Cl₂ (10mL) and DCC (223mg, 1.08mmol) was added. The suspension which resulted was stirred at 40°C for 2h and then cooled to 0°C. The mixture which resulted was filtered and the solvent was removed under vacuum to give 8-bromo-2,4-dihydro-6-phenyl-1H-imidazo[1,2-a][1,4] benzodiazepine-1-one **14** as a brown oil. The cyclized

amide **14** (250mg) was dissolved in dry benzene (6mL), after which dimethylformamide diethylacetal (130mg, 0.883 mmol) and triethyl amine (89mg, 0.883 mmol) were added. The solution which resulted was stirred at rt for 1 h and the solvent was removed under vacuum. The residue was crystallized from EtOAc-MeOH to give **15** (200mg, 70%). A solution of **15** (180mg, 0.440 mmol) in dry toluene (5mL) was treated with 1-methyl piperazine (1mL) and heated to reflux for 5h. The solvent was removed under vacuum to give a gum which crystallized from CH₂Cl₂-Et₂O to furnish **16** (146mg, 72%) as a yellow solid. **mp** >250 °C; IR (KBr) 3324, 2932, 2787, 1692, 1624, 1475, 1402, 1297, 1137, 933 cm⁻¹; ¹H NMR (CDCl₃, 300MHz) δ 7.95 (d, 1H, *J*=8.8Hz), 7.72 (dd, 1H, *J*₁=8.8Hz, *J*₂=2.3Hz), 7.58-7.55 (m, 2H), 7.49-7.37 (m, 4H), 7.17 (s, 1H), 5.01 (d, 1H, *J*=12Hz), 4.50-4.60 (m, 1H), 4.20-4.30 (m, 1H), 4.16 (d, 1H, *J*=12Hz), 3.50-3.58 (m, 2H), 2.40-2.60 (m, 4H), 2.34 (s, 3H); **MS (m/z)** 465 (100). Anal. Calcd. for C₂₃H₂₂N₅OBr. 1/3H₂O: C, 58.79; H, 4.95; N, 14.89. Found: C, 58.73; H, 4.86; N, 14.83. The spectral data of **16** were identical to the published results.¹⁵⁸

(Z)-2-((4-Methylpiperidin-1-yl)methylene)-6-phenyl-8-((trimethylsilyl)ethynyl)-2,4-dihydro-1H-benzo[f]imidazo[1,2-a][1,4]diazepin-1-one 17: To a suspension of amide **16** (140mg, 0.302mmol) in dry acetonitrile (4mL) and triethylamine (3mL) was added bis (triphenylphosphine)-palladium (II) acetate (22.6mg, 0.03mmol). The solution which resulted was degassed and trimethylsilyl acetylene (0.1mL, 0.7mmol) was added. The mixture was heated to reflux and stirred overnight. After removal of the solvent under vacuum, the residue was dissolved in CH₂Cl₂ and washed with a saturated aq solution of NaHCO₃ and brine. The organic layer was dried (Na₂CO₃), filtered and concentrated under vacuum. The residue was purified by flash column chromatography (EtOAc:

MeOH 9:1) to furnish the trimethylsilyl analog **17** (100mg, 69%) as a pale yellow solid. **mp** >250 °C; **IR** (KBr) 3436, 2936, 2794, 2154, 1682, 1625, 1489, 1136, 847cm⁻¹; **¹H NMR** (CDCl₃, 300MHz) δ 8.80 (d, 1H, J=8.5Hz), 7.68 (dd, 1H, J=1.9Hz, 8.5Hz), 7.55-7.59 (m, 2H), 7.37-7.49 (m, 4H), 7.16 (s, 1H), 4.99 (d, 1H, J=12Hz), 4.50-4.60 (m, 1H), 4.20-4.30(m, 1H), 4.13 (d, 1H, J=12.4Hz), 3.48-3.58(m, 2H), 2.4-2.6 (m, 4H), 2.35 (s, 3H), 0.23 (s, 9H); **MS (m/z)** 482 (100). Anal. Calcd. for C₂₈H₃₁N₅OSi. H₂O: C, 67.60; H, 6.54; N, 13.59. Found: C, 67.30; H, 6.66; N, 14.01.

(Z)-8-Ethynyl-2-((4-methylpiperidin-1-yl)methylene)-6-phenyl-2,4-dihydro-1H-benzo [f]imidazo[1,2-a][1,4]diazepin-1-one 18 (PS-1-37): A solution of the trimethylsilyl analog **17** (65mg, 0.135mmol) in THF (15mL) was stirred with TBAF hydrate (45mg, 0.175mmol) at -5°C for 5min. After this, H₂O (5mL) was added to the solution to quench the reaction and stirring continued at -5°C for one half h. The solution was then extracted with EtOAc (3x40mL) and the organic layer was washed with water. After removal of the solvent under reduced pressure, diethyl ether was added to the residue to precipitate a solid. The solid was filtered and washed with CHCl₃-Et₂O (1:15) to provide the acetyl target **18** (40mg, 73%). **mp** 223-224 °C; **IR** (KBr) 3298, 2935, 2786, 1695, 1628, 1364, 1136, 1002, 778cm⁻¹; **¹H NMR** (CDCl₃, 300MHz) δ 8.04 (d, 1H, J=8.5Hz), 7.71 (dd, 1H, J=1.9Hz, 8.5Hz), 7.55-7.58 (m, 2H), 7.36-7.48 (m, 4H), 7.17 (s, 1H), 5.0 (d, 1H, J=12.1Hz), 4.5-4.6 (m, 1H), 4.2-4.3 (m, 1H), 4.16 (d, 1H, J=12.1Hz), 3.5-3.6 (m, 2H), 3.08 (s, 1H), 2.4-2.6 (m, 4H), 2.35 (s, 3H); **MS (m/z)** (100). The spectral data of **14** were identical to the published results.¹⁵⁹

4-Methyl-3,4-dihydro-1H- benzo[e][1,4]diazepine-2,5-dione(26): A mixture of isatoic anhydride **25** (20g, 101 mmol) and sarcosine (9.02g, 101 mmol) in DMSO (160mL) was heated at 150°C for 5 hr, after which the solution was cooled to rt and poured into ice water (750mL) to furnish a light brown solid. This solid was collected by filtration, washed with water (3x200mL) and dried. The benzodiazepine **26** was obtained as a light brown solid (19g, 84%). This material was used directly in the next experiment.

7-Bromo-4-methyl-3,4-dihydro-1H-benzo[e][1,4]diazepine-2,5-dione(27):

Benzodiazepine **26** (32.4g, 0.17mol) was added to a solution of acetic acid (400mL) in a 3-neck reaction flask. Sodium acetate (27.9g, 0.34mol) was added to this solution. Bromine (13.1mL, 0.255mol) was added using an addition funnel and the solution which resulted was allowed to stir for 18h and then poured into ice water (200mL) to provide a white solid. This solid was collected by filtration and then washed (3x200mL) and dried (Na_2SO_4). The bromobenzodiazepine **27** (36.6g, 80%) was used directly in the next experiment. **mp** 240-242 °C; **^1H NMR** (DMSO- d_6 , 300MHz) δ 10.54 (br s, 1H), 7.81 (d, 1 H, J = 2.2 Hz), 7.67 (dd, 1 H, J = 2.4,8.6 Hz), 7.04 (d,1 H,J = 8.7 Hz),3.87 (s,2 H),3.09 (s,3 H); **MS (CI)** m/z 269 (M + H).

***tert*-Butyl-8-bromo-5,6-dihydro-5-methyl-6-oxo-4H-imidazo[1,5-**

a][1,4]benzodiazepine-3-carboxylate (28): The *t*-BuOK (7.50 g, 66.91 mmol) was added to a solution of benzodiazepine **27** (15 g, 55.76 mmol) in anhydrous THF (1500 mL) at 0 °C and the mixture which resulted was stirred for 20 min. The reaction mixture was cooled to -35 °C and diethyl chlorophosphate (10.47 mL, 72.48 mmol) was added slowly. After stirring at 0°C for 30 min the mixture was cooled to -78°C and *t*-butyl

isocyanoacetate (8.926 mL, 61.33 mmol) was added, and this was followed by the addition of *t*-BuOK (6.88g, 61.33 mmol) at -78°C. After stirring at rt for 4 h the reaction was quenched with a saturated aq NaHCO₃ solution (500 mL) and extracted with EtOAc (3 × 1000 mL). The combined organic layers were dried (Na₂SO₄) and concentrated to give a solid residue. This solid residue was triturated with Et₂O (250 mL) and the ester **28** precipitated as an off-white solid. The mother liquor was further purified by flash chromatography on silica gel (gradient elution 40– 60% EtOAc in hexane) to afford additional ester **28** in a combined yield of (15.3g, 70%). **mp** 180-183 °C; **¹H NMR** (CDCl₃, 300MHz) δ 8.33 (s, 1H), 7.90 (s, 1H), 7.62 (d, 1H, *J* = 10.8 Hz), 7.03 (d, 1H, *J* = 8.6 Hz), 4.71 (br, s, 1H), 4.13 (br, s, 1H), 3.10 (s, 3H), 1.56 (s, 9H); **MS (EI)** *m/e* 394 (M⁺, 100). The spectral data for **28** were identical to the published values.

***tert*-Butyl-8-(trimethylsilyl)-acetylene-5,6-dihydro-5-methyl-6-oxo-4H-imidazo[1,5-a][1,4]benzodiazepine-3-carboxylate (20)**: A mixture of imidazobenzodiazepine **28** (7.5g, 19.12mmol) was dissolved in dry triethyl amine (223mL) and acetonitrile (149mL; 3:2 ratio). This mixture was degassed under argon three times. To this degassed mixture, bis (triphenylphosphine)-palladium (II) acetate (1g, 7 mol %) was added. The mixture was again degassed (with vacuum) three times under argon. Trimethylsilyl acetylene (5.52mL, 38.24mmol) was added and this reaction mixture was heated to reflux for 8h under argon. The reaction mixture was cooled to rt and the solvents were concentrated under reduced pressure. This concentrated mixture was dissolved in ethyl acetate and passed through a bed of celite. After the removal of solvent under reduced pressure the residue was purified by flash chromatography (silica gel, EtOAc) to afford a yellow solid of **RY-23 (20)** (6.5g, 83%). **mp** 199-200 °C. **IR**

(KBr) 2971, 2156, 1723, 1662, 1500 cm^{-1} ; $^1\text{H NMR}$ (CDCl_3 , 300MHz) δ 8.13 (s, 1H), 7.84 (s, 1H), 7.64 (d, 1H, $J = 8.2$ Hz), 7.32 (d, 1H, $J = 8.2$ Hz), 5.11 (br, 1H), 4.31 (br, 1H), 1.63 (s, 9H), 0.25 (s, 9H); **MS (EI)** m/e 409 (M^+ , 4), 354 (19), 353 (82), 335 (45), 307 (100), 279 (23), 251 (16), 143 (13), 160 (21), 107 (14); **Anal. Calcd for $\text{C}_{22}\text{H}_{27}\text{N}_3\text{O}_3\text{Si}$** : C, 64.52; H, 6.64; N, 10.26; Found C, 64.57; H, 6.70; N, 10.46. The spectral data for **20** were in excellent agreement with the literature.⁸⁵

***tert*-Butyl-8-acetylene-5,6-dihydro-5-methyl-6-oxo-4H-imidazo[1,5-**

a][1,4]benzodiazepine-3-carboxylate (21): A solution of **20** (1.2g, 2.93 mmol) in THF (360mL) was treated with a solution of TBAF solution (1.0M in THF; 3.52mL, 3.51mmol) at -30°C . The mixture which resulted was allowed to stir for 30 min at rt, after which the mixture was added to H_2O (50mL) and extracted with EtOAc (3x100mL). The combined organic extracts were washed with brine (50mL) and dried (Na_2SO_4). After removal of the solvent under reduced pressure, the residue was purified by a wash column (silica gel, EtOAc) to give **21 (RY-24)** as a yellow solid (0.89g, 90%): **mp** 213-214 $^\circ\text{C}$. $^1\text{H NMR}$ (CDCl_3 , 300MHz) δ 8.16 (s, 1H), 7.85 (s, 1H), 7.69 (d, 1H, $J = 8.3$ Hz), 7.35 (d, 1H, $J = 8.3$ Hz), 5.15 (br, 1H), 4.32 (br, 1H), 3.23 (s, 3H), 3.20 (s, 1H), 1.63 (s, 9H); **MS (EI)** m/e 337 (M^+ , 2), 282(15), 281 (78), 264 (31), 263(56), 235 (100), 229(22), 207 (36), 138 (16), 101(19); **Anal. Calcd for $\text{C}_{19}\text{H}_{19}\text{N}_3\text{O}_3$** : C, 67.64; H, 5.68; N, 12.45; Found C, 67.50; H, 5.78; N, 12.41. The spectral data for **21** were in excellent agreement with the reported values.

8-Ethynyl-5,6-dihydro-5-methyl-6-oxo-4H-imidazo [1,5-a][1,4] benzodiazepine-3-carboxylic acid 32 : Ethyl-8-ethynyl-5,6-dihydro-5-methyl-6-oxo-4H-imidazo [1,5-a][1,4] benzodiazepine-3-carboxylate **23** (1.5g, 5.3mmol), available from the literature,

was dissolved in EtOH (100mL), after which an aq solution of 2N NaOH (15mL) was added to the solution. The mixture which resulted was heated to 70°C and allowed to stir for 1hr. The mixture was then allowed to cool to rt and the EtOH was removed under reduced pressure. Aq 2N HCl was added to the residue to bring the pH to approximately 3-4. A precipitate formed which was removed by filtration, washed with water (3x50mL) and dried. The 3-carboxylic acid **32** was obtained as a white solid in 90% yield; **mp** 315-316 °C. **¹H NMR** (CD₃OD, 300MHz) δ 8.20 (s, 1H), 7.80 (dd, 1H, *J* =2.5Hz, 10 Hz), 7.69 (s, 1H), 5.22 (br, 1H), 4.50 (br, 1H), 3.74 (s, 1H), 3.28 (s, 3H), ; **MS (EI)** m/e 281 (M⁺, 80), 277(100), 263 (60), 235 (84), 207(55) **Anal. Calcd for C₁₅H₁₁N₃O₃**: C, 64.04; H, 3.94; N, 14.95; Found C, 64.40; H, 4.12; N, 14.76. The spectral data for **20** were in excellent agreement with the published reports.¹⁶⁰

1,3-Bis(8-acetyleno-5,6-dihydro-5-methyl-6-oxo-4H-

imidazo[1,5a][1,4]benzodiazepine-3-carboxy) propyl diester 33 (XLi-093) : To a solution of carbonyl diimidazole (230.3mg, 0.57mmol) in anhydrous DMF (5mL) was added 8-ethyl-5,6-dihydro-5-methyl-6-oxo-4H-imidazo [1,5-a][1,4] benzodiazepine-3-carboxylic acid **24** (200mg, 0.71mmol). The solution which resulted was allowed to stir for 2h at rt. Analysis of the material by TLC (silica gel) indicated the absence of starting material. To this solution, 1, 3 propanediol (27.1mg, 0.36mmol) in dry DMF (0.5mL) and DBU (114.2mg, 0.75mmol) in dry DMF (0.5mL) were added to the solution at rt. The mixture was allowed to stir for 12h until analysis by TLC (silica gel) indicated the absence of starting material. The reaction mixture was then poured into ice water (30mL) and extracted with EtOAc (3x50mL). The combined organic layers were washed with H₂O (5x50mL) and dried (Na₂SO₄). The solvent was removed under reduced

pressure and the residue was purified by flash chromatography (silica gel, EtOAc/MeOH: 4:1) to provide the dimer **33** (**XLi-093** ; 157mg, 74%) as white solid. **mp** >230 °C (dec); **IR** (NaCl) 3247, 1725, 1641, 1359, 1253, 1061 cm⁻¹; **¹H NMR** (CD₃OD, 300MHz) δ 8.20 (d, 2H, *J*=1.76Hz), 7.89 (s, 2H), 7.72 (dd, 2H, *J* =6.43Hz, 1.86 Hz), 7.41 (d, 2H, *J*=8.3Hz), 5.31 (br, 2H), 4.57 (t, 4H, *J*=6.2Hz), 4.40 (s, 2H), 3.26 (s, 6H), 3.24 (s, 2H), 2.37 (m, 2H); **¹³C NMR** (CD₃OD, 300MHz) δ 26.2, 34.4, 40.7, 60.2, 78.7, 79.7, 120.4, 121.6, 127.1, 127.7, 130.1, 133.4, 134.1, 134.9, 161.3, 164.1; **MS (FAB)** m/e 603 (M⁺ +1, 100) **Anal. Calcd for C₃₃H₂₆N₆O₆.2/3 CH₃OH**: C, 64.81; H, 4.63; N, 13.47; Found C, 64.56; H, 4.72; N, 13.76. The spectral data for XLi-093 were identical to the published values.¹⁶⁰

1,3-Bis(8-ethyl-5,6-dihydro-5-methyl-6-oxo-4H-imidazo[1,5a][1,4] benzodiazepine-3-carboxy) propyl diester 34: Bis (8-acetyleno-5,6-dihydro-5-methyl-6-oxo-4H-imidazo[1,5a][1,4]-benzodiazepine-3-carboxy) propyl diester **33** (500mg, 0.83mmol) was dissolved in EtOH (150mL) and degassed 3-4 times with a balloon of hydrogen after which Pd/C (176mg) was added to the solution at rt. The slurry was allowed to stir for 12h under H₂. The catalyst was removed by filtration and washed with EtOH. The EtOH was removed under reduced pressure to furnish a residue. This material was purified by flash chromatography (silica gel, EtOAc:MeOH, 9:1) to provide (**34**)**XLi-356** (504mg, 99%) as white crystals: **mp** 125-133°C; **IR** (NaCl) 3407, 2964, 2358, 1725, 1640, 1499 cm⁻¹; **¹H NMR** (CDCl₃, 300MHz) δ 8.15 (s, 1H), 7.89 (t, 4H, *J*=3.2Hz, 5.3Hz), 7.48 (d, 2H, *J*=1.8Hz), 7.33 (d, 2H, *J*=8.2Hz), 5.16 (br, 2H), 4.56 (t, 4H, *J*=6.1, 12.2 Hz), 4.48 (br, 2H), 3.26 (s, 6H), 2.78 (dd, 4H, *J*=7.5, 15.1Hz), 2.39 (m, 2H), 1.29 (m, 6H) ; **MS (EI)** m/e (relative intensity) 611 (M⁺+1, 100); **Anal Calcd for**

C₃₃H₃₄N₆O₆·2H₂O: C, 61.33; H, 5.92; N, 13.00. Found: C, 61.74; H, 5.91; N, 12.63.

The spectral data of XLi-356 were identical to the published values.¹⁶⁰

1,5-Bis(8-acetyleno-5,6-dihydro-5-methyl-6-oxo-4H-

imidazo[1,5a][1,4]benzodiazepine-3-carboxy) pentyl diester 35: To a solution of carbonyl diimidazole (173mg, 1.06mmol) in anhydrous DMF (5mL) was added 8-ethyl-5,6-dihydro-5-methyl-6-oxo-4H-imidazo [1,5-a][1,4] benzodiazepine-3-carboxylic acid **32** (150mg, 0.534mmol). The solution which resulted was stirred for 2h at rt. Analysis of the mixture by TLC (silica gel) indicated the absence of starting material. To this solution, 1,5 pentanediol (27.8mg, 0.267mmol) in dry DMF (0.5mL) and DBU (114.2mg, 0.75mmol) in dry DMF (0.5mL) were added at rt. The mixture was allowed to stir for 12h until analysis by TLC (silica gel) indicated absence of starting material. The reaction mixture was then poured into ice water (30mL) and extracted with EtOAc (3x50mL). The combined organic layers were washed with H₂O (5x50mL) and dried (Na₂SO₄). The solvent was removed under reduced pressure and the residue was purified by flash chromatography (silica gel, EtOAc/MeOH: 4:1) to provide the dimer **35 XLi-210** (123mg, 89.2%) as a white solid. **mp** 132-138 °C ; **IR** (NaCl) 3422, 3280, 2931, 1714, 1635, 1487, 1249, 1064 cm⁻¹; **¹H NMR** (CD₃OD, 300MHz) δ 8.18 (s, 2H), 7.86 (s, 2H), 7.70 (m, 2H), 7.36 (dd, 2H, *J*=8.1, 16Hz), 5.29 (s, 2H), 4.39 (s, 8H), 3.52 (s, 2H), 3.24 (s, 6H), 1.90 (m, 4H); **MS (FAB)** *m/e* 631 (*M*⁺ +1, 100) Anal. Calcd for C₃₅H₃₀N₆O₆·5/3 H₂O: C, 63.61; H, 4.83; N, 12.72; Found C, 63.16; H, 4.72; N, 13.06.

Bis(8-acetyleno-5,6-dihydro-5-methyl-6-oxo-4H-imidazo[1,5a][1,4]benzodiazepine-3-carboxy) diethylene glycol diester 36 (XLi-347). To a solution of carbonyl

diimidazole (243 mg, 1.50 mmol) in anhydrous DMF (8 mL) was added 8-ethynyl-5, 6-dihydro-5-methyl-6-oxo-4H-imidazo[1,5-a][1,4]-benzodiazepine-3-carboxylic acid **32** (351.4 mg, 1.25 mmol). This solution was stirred for 2 h at rt until analysis by TLC (silica gel) indicated the absence of starting material. To the solution which resulted was then added diethylene glycol (66.3 mg, 0.62 mmol) in dry DMF (0.5 mL) and also DBU (190 mg, 1.25 mmol) in dry DMF (0.10 mL) at rt. The mixture was stirred at rt for 8 h until analysis by TLC (silica gel) indicated the reaction was complete. The reaction mixture was then poured into ice water (30 mL) and extracted with CH₂Cl₂ (3 x 50 mL). The combined organic layer was washed with H₂O (5 x 50 mL), brine and dried (Na₂SO₄). The solvent was removed under reduced pressure and the residue was purified by flash chromatography (silica gel, EtOAc/CH₃OH, 4 : 1) to provide **36** (150 mg) as a white solid in 60% yield. **28**: mp 118-121°C (dec.); IR (NaCl) 3247, 2880, 1725, 1639, 1496, 1253, cm⁻¹; ¹H NMR (500 MHz, CDCl₃) δ 8.19 (d, 2H, *J*=1.76Hz), 7.90(s, 2H), 7.72(dd, 2H, *J*=1.8 Hz and *J*=8.3 Hz), 7.39 (d, 2H, *J*=6.1 Hz), 5.20(br, 2H), 4.37(br, 2H), 3.67 (t, 4H, *J*=5.1Hz), 3.23(s,6H), 3.21(s, 2H); ¹³C NMR (53.4 MHz, CD₂Cl₂) δ 35.4, 42.3, 63.5, 68.9, 79.6, 81.3, 122.2, 122.4, 128.4, 129.4, 131.9, 135.1, 135.7, 135.8, 136.0, 162.5, 165.2; MS (FAB,NBA) *m/e* (relative intensity) 633(M⁺+1, 11). **Anal.** **Calcd** for C₃₄H₂₈N₆O₇ • 1/3 C₂H₅OH: C, 61.38; H, 4.45; N, 12.39. Found: C, 60.99; H, 4.62; N, 12.16.

Dibromodimethyl ether 38¹¹¹. Bromine (120 g) was added slowly via an addition funnel to a capped three-neck flask containing water (22.4 ml) in equal portion intervals over a 2 h period. Paraformaldehyde (120 g) and red phosphorus (27.2 g) were added to the bromine/water solution at a comparable rate in equal portions after each bromine

addition. The reaction vessel and vials containing the starting material were kept capped and only opened briefly to allow sample removal and addition. The reaction mixture was ice water-cooled during the addition period of the process. After completing the addition of all the starting material the final reaction mixture was set aside for 20 h. The heavy crude ether layer, dibromodimethyl ether, was separated, saturated with hydrogen bromide, and dried with phosphorus pentoxide (P₂O₅) for 24 h. Simple distillation at atmospheric pressure afforded the colorless dibromo-dimethyl ether **38** as a fraction with b. p. = 146-159 °C. The data for **38** were identical to the literature values.¹¹²

Bis(8-acetyleno-5,6-dihydro-5-methyl-6-oxo-4H-imidazo[1,5a][1,4]benzodiazepine-3-carboxy) dimethyl glycol diester 39 (XLi374). 8-Ethynyl-5, 6-dihydro-5-methyl-6-oxo-4H-imidazo[1,5-a][1,4]-benzodiazepine-3-carboxylic acid **32** (100 mg, 0.356 mmol) was dissolved in DMF (10 mL) and to this solution dibromodimethyl ether (36.3 mg, 0.178 mmol) was added, followed by TEA(2.0 mL). After 26 h of stirring at ambient temperature the solvent was removed under reduced pressure and the residue was distributed between CHCl₃ and water. The organic phase was washed multiple times with water and dried over Na₂SO₄. The dried crude ether was applied on a column of silica gel to afford dimer **39** (86 mg) in 80% yield. **39**: mp >220 °C (dec.); IR (KBr) 3419, 3237, 2910, 1714, 1635, 1561, 1498 cm⁻¹; ¹H NMR (500 MHz, CD₂Cl₂) δ 8.15 (s, 2H), 7.90 (s, 2H), 7.74(dd, 2H, *J*=1.6Hz, *J*=8.2Hz), 7.40(d, 2H, *J*=8.1 Hz), 5.74 (s, 4H), 5.29(br, 2H), 4.37 (br, 2H), 3.31(s,2H), 3.18(s, 6H); MS(FAB,NBA) *m/e* (relative intensity) 605(M⁺+1, 100). **Anal. Calcd** for C₃₂H₂₄N₆O₇ •3/2 CH₃COOC₂H₅: C, 61.99; H, 4.93; N, 11.41. Found: C, 61.36; H, 4.52; N, 11.96.

8-Chloro-5-methyl-6-Oxo-5,6-dihydro-4H-benzo-[f]-imidazo-[1,5-a]-[1,4]-dizaepine-3-carboxylic acid (41). The ester **40** (2 g, 6 mmol) was dissolved in EtOH (150 mL) to form a solution and then 10% aq sodium hydroxide solution (40 mL) was added to the mixture. The mixture was heated to reflux for 0.5 h and the EtOH was removed under reduced pressure, after which the solution was allowed to cool. The pH was then adjusted to 4 by adding 10% aq HCl dropwise. The solid which precipitated was filtered and the solid acid was washed with water and ether. The solid was dried to provide acid **41**: mp >260°C; IR (neat) 3100, 2424, 1661, 1642, 1562 cm⁻¹; ¹H NMR (300 MHz, DMSO) δ 8.35 (s, 1H), 7.77-7.88 (m, 3H), 5.28 (br s, 1H), 4.55 (br s, 1H), 3.09 (s, 3H); MS (EI) m/e (relative intensity) 291 (M⁺, 44), 273 (61), 245 (100), 230 (47), 217 (62), 75 (37). **Anal. Calcd.** for C₁₃H₁₀ClN₃O₃• 0.3CH₂Cl₂: C, 50.57; H, 3.37; N, 13.32. Found: C, 50.64; H, 3.25; N, 13.12. This material was used directly in a later step.

Bis(8-chloro-5,6-dihydro-5-methyl-6-oxo-4H-imidazo[1,5a][1,4]benzodiazepine-3-carboxy) diethylene glycol diester 42(SR-II-35). To a solution of carbonyl diimidazole (0.197g, 1.22 mmol) in anhydrous DMF (8 mL) was added 8-ethynyl-5,6-dihydro-5-methyl-6-oxo-4H-imidazo[1,5-a][1,4]-benzodiazepine-3-carboxylic acid **41** (0.297g, 1.01 mmol). The solution which resulted was stirred for 2 h at rt until analysis by TLC (silica gel) indicated the absence of starting material. To the solution which resulted was then added diethylene glycol (48 mg, 0.46 mmol) in dry DMF (0.5 mL) and also DBU (186mg, 1.22 mmol) in dry DMF (0.10 mL) at rt. The mixture was stirred at rt for 8 h until analysis by TLC (silica gel) indicated the reaction was complete. The reaction

mixture was then poured into ice water (30 mL) and extracted with CH₂Cl₂ (3 x 50 mL). The combined organic layer was washed with H₂O (5 x 50 mL), brine and dried (Na₂SO₄). The solvent was removed under reduced pressure and the residue was purified by flash chromatography (silica gel, EtOAc/CH₃OH, 4: 1) to provide **41** (177 mg) as a white solid in 60% yield. **41**: ¹H NMR (300 MHz, CDCl₃) δ 8.03 (d, 2H, *J*=2.4Hz), 7.83(s, 2H), 7.72(dd, 2H, *J*=3.3 Hz and *J*=9.3 Hz), 7.40 (s,1H), 7.35(s, 1H), 5.18 (br, 2H), 4.55 (s,4H), 4.36 (br, 2H), 3.93 (t, 4H, *J*=4.8 Hz), 3.26 (s,6H); **MS (EI)** *m/e* 652 (M⁺).

7-Chloro-4-methyl-3,4-dihydro-1H-benzo[e][1,4]diazepine-2,5-dione (45): A mixture of 5-chloroisatoic anhydride **44** (20g, 101 mmol) and sarcosine (9.02g, 101 mmol) in DMSO (160mL) was heated at 150°C for 5 hr, after which it was cooled to rt and poured into ice water (750mL) to furnish a light brown solid. This solid was collected by filtration, washed with water (3x200mL) and dried (Na₂SO₄). The benzodiazepine **45** was obtained as a light brown solid (19g, 84%). This material was used directly in the next experiment.

Ethyl-8-chloro-5, 6-dihydro-5-methyl-6-oxo-4H-imidazo[1,5-][1,4]benzodiazepine-3-carboxylate (40): *t*-BuOK (8.99 g, 80.14 mmol) was added to a solution of amide **45** (15 g, 66.77 mmol) in anhydrous THF (1500 mL) at 0 °C and the solution allowed to stir for 20 min. The reaction mixture which resulted was cooled to -35 °C and diethyl chlorophosphate (12.48 mL, 86.80 mmol) was added slowly. After stirring at 0 °C for 30 min, the mixture was cooled to -78 °C and ethyl isocyanoacetate (8.027 mL, 73.44 mmol) was added and this was followed by the addition of *t*-BuOK (8.24g, 73.44

mmol). After stirring at rt for 4 h, the reaction mixture was quenched with a saturated aq solution of NaHCO₃ (500 mL) and extracted with EtOAc (3 × 1000 mL). The combined organic layers were dried (Na₂SO₄) and concentrated to give a solid residue. This solid residue was treated with Et₂O (250 mL) and the ester **40** was precipitated as an off-white solid. The mother liquor was further purified by flash chromatography on silica gel (gradient elution, 40–60%, EtOAc in hexane) to afford additional ester **40** with an overall yield of (19g, 89%). **mp** 192-193 °C; **¹H NMR** (CDCl₃, 300MHz) δ 8.1 (d, 1H, *J* = 2.4 Hz), 7.90 (s, 1H), 7.62 (dd, 1H, *J* = 8.7, 2.5 Hz), 7.40 (d, 1H, *J* = 8.6 Hz), 5.23 (br, s, 1H), 4.46 (q, 2H, *J*=7.12Hz), 4.13 (br, s, 1H), 3.27 (s, 3H), 1.47 (t, 3H, *J*=7.12Hz); **MS (EI)** *m/e* 319 (M⁺, 100). The data for this material were identical to the published values.¹⁶¹

8-Chloro-5, 6-dihydro-5-methyl-6-oxo-4H-imidazo[1,5- α][1,4]benzodiazepine-3-methyl alcohol (46). A solution of imidazobenzodiazepine **40** (5 g, 15.6 mmol) in a mixture of ethyl ether (50 mL), and THF (50 mL) was stirred with LiBH₄ (2.0 M in THF, 9 mL, 18 mmol). The mixture which resulted was then heated to reflux for 30 min, after which it was cooled to rt and treated with a saturated aq solution of NaHCO₃ (5 mL). The solvent was concentrated and the residue was taken up in EtOAc (100 mL). The organic layer was washed with water (2 × 20 mL), brine (20 mL) and dried (MgSO₄). After removal of the solvent under reduced pressure the residue was purified by flash chromatography (silica gel, EtOAc) to afford alcohol **46** as colorless crystals (2.9 g, 67%): **mp** 252-253 °C; **IR** (KBr) 3500 (br, OH), 3100, 1667, 1612, 823 cm⁻¹; **¹H NMR** (CDCl₃, 300MHz) δ 8.00 (d, 1H, *J* = 2.4 Hz), 7.80 (s, 1H), 7.55 (dd, 1H, *J* = 8.7, 2.4 Hz), 7.30 (d, 1H, *J* = 8.6 Hz), 4.70 (d, 2H, *J* = 4.2 Hz), 4.40 (s, 2H), 3.20 (s, 3H);

MS (EI) m/e 279 (M^+ , 41), 277 (M^+ , 100), 259 (84), 246 (55), 231(41). The data for this material were identical to the published values.¹⁹

Methyl(8-chloro-5,6-dihydro-5-methyl-6-oxo-4H-imidazo[1,5- α][1,4]

benzodiazepin-3-yl)methyl ether (47). To a slurry of KOH (2.41g, 44 mmol) in DMSO (56 mL) at rt were added alcohol **46** (3g, 11 mmol) and excess CH_3I . The mixture which resulted was stirred for 5-10 min and then poured into ice water (100 mL) after which it was extracted with EtOAc (3×100 mL). The combined organic extracts were washed with brine (50mL) and dried ($MgSO_4$). After removal of solvent under reduced pressure, the residue was purified by a wash column on silica gel (EtOAc) to give ether **47 (PWZ-029)** as an off-white powder (2.83g, 90%): **mp** 193-194 °C; **IR** (KBr) 3122, 2973, 1632, 1611, 811 cm^{-1} ; **1H NMR** ($CDCl_3$, 300MHz) δ 8.00 (d, 1H, $J = 2.4$ Hz), 7.80 (s, 1H), 7.55 (dd, 1H, $J = 8.7, 2.5$ Hz), 7.30 (d, 1H, $J = 8.6$ Hz), 4.55 (br, 2H), 4.38 (s, 2H), 3.42 (s, 3H), 3.18 (s, 3H). The data for this material were identical to the published values.

Ethyl (8-chloro-5,6-dihydro-5-methyl-6-oxo-4H-imidazo[1,5- α][1,4] benzodiazepin-3-yl)methyl ether (48). To slurry of KOH (2.41g, 44 mmol) in DMSO (56 mL) at rt were added alcohol **46** (3g, 11 mmol) and excess C_2H_5I . The mixture which resulted was allowed to stir for 5-10 min, poured into ice water (100 mL), and extracted with EtOAc (3×100 mL). The combined organic extracts were washed with brine (50mL) and dried ($MgSO_4$). After removal of the solvent under reduced pressure the residue was purified by a wash column on silica gel (EtOAc) to give ether **48 (SR-III-81)** as an off-white powder (2.98g, 90%): **mp** 137-138 °C; **IR** (KBr) 31282, 2973, 1634, 1601, 810 cm^{-1} ; **1H NMR** ($CDCl_3$, 300MHz) δ 7.92 (d, 1H, $J=2.4$ Hz), 7.86 (s, 1H), 7.50 (dd, 1H, $J=8.5, 2.4$ Hz), 7.30 (d, 1H, $J=8.6$ Hz), 4.55 (s, 2H), 3.60 (q, 2H, $J=7.0$ Hz), 3.12 (s, 3H), 1.22 (t,

3H, $J=7.0\text{Hz}$). **Anal. Calcd. For $\text{C}_{15}\text{H}_{16}\text{ClN}_3\text{O}_2 \cdot 0.0235 \text{H}_2\text{O}$** , C 58.84, H 5.28, N 13.72. Found 58.94, H 5.40, N 13.32

8-Chloro-N,5-dimethyl-6-oxo-5,6-dihydro-4H-benzo[f]imidazo-[1,5-

a][1,4]diazepine-3-carboxamide(57): The ester **40** (100mg, 0.313 mmol) was dissolved in anhydrous CH_2Cl_2 (5mL). To this mixture, a solution of CH_3NH_2 (0.147mL, 1.56 mmol) was added. This reaction mixture (in a sealed tube) was placed in a preheated oil bath at 45°C overnight. The solvent was then removed under reduced pressure and the residue was purified by flash chromatography with $\text{CH}_2\text{Cl}_2/\text{MeOH}$ (4.5:0.5) to provide 3-N-methyl amide **57** (74mg, 78% yield). $^1\text{H NMR}$ (CDCl_3 , 300MHz) δ 8.1 (d, 1H, $J = 2.4\text{Hz}$), 7.90 (s, 1H), 7.62 (dd, 1H, $J = 8.6, 2.5 \text{ Hz}$), 7.40 (d, 1H, $J = 8.6\text{Hz}$), 5.23 (br, 1H), 5.23 (br, 1H), 3.28 (s, 3H), 3.02 (d, 3H, $J=3.9\text{Hz}$) ; **MS (EI) m/e 304 (M^+ , 100)**. **Anal. Calcd. For $\text{C}_{14}\text{H}_{13}\text{ClN}_4\text{O}_2 \cdot 0.28 \text{H}_2\text{O}$** , C 54.25, H 4.41, N 18.07. Found 54.39, H 4.52, N 17.69

8-Chloro-3-(fluoromethyl)-5-methyl-4H-benzo[f]imidazo[1,5-a][1,4]diazepin-6(5H)-

one (58) : The alcohol **46** (100mg, 0.360mmol) was dissolved in anhydrous CH_2Cl_2 (5 mL). At 0°C , DAST (diethylaminosulfur trifluoride, 0.07mL, 0.720mmol) ¹⁶² was added very slowly and the reaction was allowed to stir for 2h. The reaction mixture was then quenched with aq solution of NaHCO_3 and allowed to stir for 1h at 0°C and then extracted with CH_2Cl_2 . The combined organic layers were washed with brine and dried (MgSO_4). After removal of the solvent under reduced pressure the residue was purified by a wash column on silica gel (gradient elution 4:1 EtOAc: hexane) to afford the fluoro analog **58 (SR-III-38; 0.070mg, 70%)**. $^1\text{H NMR}$ (CDCl_3 , 300MHz) δ 8.05 (dd, 1H, $J=2.3\text{Hz}, 1.4\text{Hz}$), 7.89 (d, 1H, $J=1.4\text{Hz}$), 7.62 (m, 1H), 7.37 (dd, 1H, $J = 8.4, 1.2 \text{ Hz}$),

5.57 (s, 1H), 5.41 (s, 1H), 4.40 (br, 2H), 3.25 (d, 3H, $J=1.3\text{Hz}$); $^{19}\text{F NMR}$ (CDCl_3 , 282MHz) δ -205.21 (t, 1F, $J=52\text{Hz}$); **MS (EI)** m/e 279 (M^+ , 100). **Anal. Calcd. For $\text{C}_{13}\text{H}_{11}\text{ClFN}_3\text{O} \cdot 0.13 (\text{C}_2\text{H}_5)_2\text{O}$** , C 56.11, H 4.28, N 14.54. Found 55.86, H 3.97, N 14.17

8-Chloro-3-(difluoromethyl)-5-methyl-4H-benzo[f]imidazo[1,5-a][1,4]diazepin-

6(5H)-one 49: The alcohol **46** (1g, 3.6mmol) was dissolved in dry CH_2Cl_2 (100mL) and Dess-Martin periodinane¹⁶³ (2.29g, 5.41mmol) was added in one portion at 0°C . This solution which resulted was stirred at rt for 2 h. The reaction mixture which resulted was then quenched with a saturated aq solution of $\text{Na}_2\text{S}_2\text{O}_3$, washed with NaHCO_3 and extracted with CH_2Cl_2 . The combined organic layers were washed with brine and dried (MgSO_4). After removal of the solvent under reduced pressure, the residue was purified by a wash column on silica gel (gradient elution 1:9 EtOAc: hexane) to afford the aldehyde **59** (0.953g, 96%). $^1\text{H NMR}$ (CDCl_3 , 300MHz) δ 10.35 (s, 1H), 8.09 (d, 1H, $J=2.43\text{Hz}$), 7.94 (s, 1H), 7.64 (dd, 1H, $J=8.55, 2.41\text{Hz}$), 7.41 (d, 1H, $J=8.6\text{Hz}$), 5.23 (br, s, 1H), 4.6 (br, s, 1H), 3.25 (s, 3H); **HRMS (ESI)** calculated for $\text{C}_{13}\text{H}_{11}\text{ClN}_3\text{O}_2$: 276.0540; found : 276.0536 The aldehyde **59** (100mg, 0.363mmol) was dissolved in anhydrous CH_2Cl_2 (5 mL). At 0°C DAST (diethylaminosulfur trifluoride, 0.07mL, 0.725mmol) was added very slowly and the reaction was allowed to stir for 2h at 0°C . The reaction mixture was then quenched with an aq solution of NaHCO_3 and allowed to stir for 1hr and extracted (CH_2Cl_2). The combined organic layers were washed with brine and dried (MgSO_4). After removal of the solvent under reduced pressure, the residue was purified by a wash column on silica gel (gradient elution 4:1 EtOAc: hexane) to afford the difluoro analog **49** (0.070mg, 65%). $^1\text{H NMR}$ (CDCl_3 , 300MHz) δ 8.05 (dd, 1H, $J=2.4\text{Hz}$), 7.88 (s, 1H), 7.62 (dd, 1H, $J = 8.6 \text{ Hz}, 2.4 \text{ Hz}$), 7.37 (d, 1H, $J =$

8.5Hz), 6.83 (t, 1H, $J=55\text{Hz}$), 4.55 (d, 1H, $J=14\text{Hz}$), 4.45 (d, 1H, $J=14\text{Hz}$), 3.2 (s, 3H); ^{13}C NMR (CDCl_3 , 300MHz) δ 35.41, 42.01, 112.52 (t, $J = 234\text{Hz}$), 123.2, 128.11, 130.38 (d, $J=31.8\text{Hz}$), 132.43, 132.67, 134.50, 134.80, 165.14; ^{19}F NMR (CDCl_3 , 282MHz) δ -111.76 (dd, $J_{(F-F)}=309\text{Hz}$, $J_{(H-F)} =55\text{Hz}$), -109.78 (dd, $J_{(F-F)}=309\text{Hz}$, $J_{(H-F)} =55\text{Hz}$); HRMS (ESI) Calculated for $\text{C}_{13}\text{H}_{11}\text{ClF}_2\text{N}_3\text{O}$: 298.0559; found: 298.0561.

8-Chloro-3-(difluoromethyl)-5-methyl-4H-benzo[f]imidazo[1,5-a][1,4]diazepin-

6(5H)-one 60: The acid **41** (300mg, 1.02 mmol) was dissolved in dry CH_2Cl_2 (5mL) and at 0°C , excess SOCl_2 was added in one portion. The reaction mixture was heated to reflux for 2h until analysis of the mixture by TLC indicated the absence of starting material. The reaction mixture was concentrated under reduced pressure on a rotavapor a few times with CH_2Cl_2 to remove the excess SOCl_2 and dried under vacuum. The solid which resulted was stirred in dry THF at -60°C . In a separate flask, bis[2-(N,N-dimethylamino)ethyl] ether³⁷ (0.239mL, 1.25mmol) was stirred in dry THF (5mL) and at 0°C , EtMgBr (0.419mL, 1.25mmol) was slowly added over 15min. After stirring the reaction mixture for 5min, the mixture which resulted was quenched with an aq solution of NH_4Cl and extracted with EtOAc (3x10mL). The combined organic layers were washed with brine and dried (MgSO_4). After removal of the solvent under reduced pressure the residue was purified by a wash column on silica gel (gradient elution 4:1 EtOAc : hexane) to afford the ketone **60** (0.167g, 53 %). HRMS (ESI) Calculated for $\text{C}_{15}\text{H}_{14}\text{ClN}_3\text{O}_2$: 304.0853; found:304.0861. The ketone **60** (100mg, 0.360mmol) was dissolved in anhydrous CH_2Cl_2 (5 mL). At 0°C , DAST (diethylaminosulfur trifluoride, 0.07mL, 0.720mmol)¹⁶² was added very slowly and the reaction was allowed to stir for 2h. No product formation was observed. Addition of excess DAST (diethylaminosulfur

trifluoride) did not work either. When various fluorinating agents such as Xtal-fluor or Deoxo-fluor were employed they did not yield the product. Excess addition of these fluorinating agents also was futile.

9. Computer Modeling

The core structures of the ligands were taken from available X-ray crystallographic coordinates or generated using the SYBYL fragment library.¹⁶⁴ The structures which resulted were energy minimized using MM2 (molecular mechanics program 2) or MMFF (Merck molecular force field), and the subsequent Monte Carlo conformational searches were carried out on MacroModel 6.0 on a Silicon Graphics Personal Iris 4D/35 workstation or a Silicon Graphics Octane SI 2P 175 R10000 workstation, respectively. The low energy conformations were then fully optimized *via* molecular orbital calculations at the 3-21G basis set with torsional angles fixed. The structures which resulted were further calibrated with 6-31G* single point calculations at an “SCF=TIGHT” convergence criteria *via* Gaussian 92¹⁶⁵ on a Silicon Graphics Indigo R4400 workstation, or Gaussian 94¹⁶⁶ on a Silicon Graphics Octane SI2P175R10000 workstation.⁴³

9.1. Competition Binding Assays (With Dr. Majumder and Dr. Roth)

Competition binding assays were performed in a total volume of 0.5 mL at 4 °C for 1 h using [³H] flunitrazepam as the radiolabel. A total of 6 µg of cloned human GABA_A receptor DNA containing the desired α subtype along with the β2 and γ2 subunits were used for transfecting the HEK 293T cell line using Fugene 6 (Roche Diagnostic) transfecting reagent. Cells were harvested 48 h after transfection, washed with Tris-HCl

buffer (pH 7.0) and Tris Acetate buffer (pH 7.4) and the resulting pellets were stored at -80 °C until assayed. On the day of the assay, pellets containing 20-50 µg of GABA_A receptor protein were resuspended in (50 mM Tris-acetate pH 7.4 at 4 °C) and incubated with the radiolabel as previously described.¹⁶⁷ Nonspecific binding was defined as radioactivity bound in the presence of 100 µM diazepam and represented less than 20% of total binding. Membranes were harvested with a Brandel cell harvester followed by three ice-cold washes onto polyethyleneimine-pretreated (0.3%) Whatman GF/C filters. Filters were dried overnight and then soaked in Ecoscint A liquid scintillation cocktail (National Diagnostics; Atlanta, GA). Bound radioactivity was quantified by liquid scintillation counting. Membrane protein concentrations were determined using an assay kit from Bio-Rad (Hercules, CA) with bovine serum albumin as the standard.

10. Experimental procedures for the electrophysiology using the two-electrode voltage clamp (with Dr. R. Furtmüller and Dr. W. Sieghart)¹⁶⁸⁻¹⁷¹

Ligand effects on GABA_A receptors were tested by two-electrode voltage clamp experiments in cRNA injected *Xenopus* oocytes that functionally expressed several subtype combinations of GABA_A receptors.¹⁶⁸

10.1.1 Preparation of cloned mRNA

Cloning of GABA_A receptor subunits α 1, β 3 and γ 2 into pCDM8 expression vectors (Invitrogen, CA) has been described elsewhere.¹⁷² GABA_A receptor subunit α 4 was cloned in an analogous way. cDNAs for subunits α 2, α 3 and α 5 were gifts from P. Malherbe and were subcloned into a pCI-vector. cDNA for subunit α 6 was a gift from P.

Seeburg and was subcloned into the vector pGEM-3Z (Promega). After linearizing the cDNA vectors with appropriate restriction endonucleases, capped transcripts were produced using the mMessage mMachine T7 transcription kit (Ambion, TX). The capped transcripts were polyadenylated using yeast poly(A) polymerase (USB, OH) and were diluted and stored in diethylpyrocarbonate-treated water at -70°C .

10.1.2 Functional expression of GABA_A receptors

The methods used for isolating, culturing, injecting and defolliculating of the oocytes were identical to those as described previously.^{109,168,173} Briefly, mature female *Xenopus laevis* (Nasco, WI) were anaesthetized in a bath of ice-cold 0.17 % Tricain (Ethyl-m-aminobenzoate, Sigma, MO) before decapitation and removal of the frog ovary. Stage 5 to 6 oocytes with the follicle cell layer around them were singled out of the ovary using a platinum wire loop. Oocytes were stored and incubated at 18°C in modified Barths medium (MB, containing 88 mM NaCl, 10 mM HEPES-NaOH (pH 7.4), 2.4 mM NaHCO₃, 1 mM KCl, 0.82 mM MgSO₄, 0.41 mM CaCl₂, 0.34 mM Ca(NO₃)₂) that was supplemented with 100 U/mL penicillin and 100 µg/mL streptomycin. Oocytes with follicle cell layers still around them were injected with a total of 2.25 ng of cRNA. This solution contained the transcripts for the different α subunits and the β 3 subunit at a concentration of 0.0065 ng/nL as well as the transcript for the γ 2 subunit at 0.032 ng/nL. After injection of the cRNA, oocytes were incubated for at least 36 h before the enveloping follicle cell layers were removed. To this end, oocytes were incubated for 20 min at 37°C in MB that contained 1 mg/mL collagenase type IA and 0.1 mg/mL trypsin inhibitor I-S (both Sigma). This was followed by osmotic shrinkage of the oocytes in doubly concentrated MB medium supplied with 4 mM Na-EGTA. Finally, the oocytes

were transferred to a culture dish containing MB and were gently pushed away from the follicle cell layer which stuck to the surface of the dish. After removal of the follicle cell layer, oocytes were allowed to recover for at least 4 h before being used in electrophysiological experiments.

10.1.3. Electrophysiological experiments^{171,174}

For electrophysiological recordings, oocytes were placed on a nylon-grid in a bath of *Xenopus* Ringer solution (XR, containing 90 mM NaCl, 5 mM HEPES NaOH (pH 7.4), 1 mM MgCl₂, 1 mM KCl and 1 mM CaCl₂). The oocytes were constantly washed by a flow of 6 mL/min XR which could be switched to XR containing GABA and/or drugs. Drugs were diluted into XR from DMSO solutions resulting in a final concentration of 0.1 % DMSO perfusing the oocytes. Drugs were preapplied for 30 sec before the addition of GABA, which was coapplied with the drugs until a peak response was observed. Between the two applications, oocytes were washed in XR for up to 15 min to ensure full recovery from desensitization. For current measurements the oocytes were impaled with two microelectrodes (2–3 mΩ) which were filled with 2 mM KCl. All recordings were performed at rt at a holding potential of –60 mV using a Warner OC-725C two-electrode voltage clamp (Warner Instruments, Hamden, CT). Data were digitized, recorded and measured using a Digidata 1322A data acquisition system (Axon Instruments, Union City, CA). Results of concentration response experiments were fitted using GraphPad Prism 3.00 (GraphPad Software, San Diego, CA). The equation used for fitting the concentration response curves was $Y = \text{Bottom} + (\text{Top} - \text{Bottom}) / (1 + 10^{((\text{LogEC50} - X) * \text{HillSlope}))}$; X represents the logarithm of concentration, Y represents the response; Y starts at Bottom and goes to Top with a sigmoid shape.

10.2. Anticonvulsant screen (with Dr. James Stables)¹⁷⁴

The standard models incorporated into anticonvulsant screening include the maximal electroshock test (MES), the subcutaneous Metrazol test (scMET), and evaluations of toxicity (TOX)-which is sedation in this study. The data for each condition is presented as a ratio of either the number of animals protected or toxicity (loss of locomotor activity) over the number of animals tested at a given time point and dose. Experiments were performed in male rodents (albino Carworth Farms No. 1 mice (intraperitoneal route, ip) and albino Sprague-Dawley rats (oral route and ip). The mice weighed between 18 and 25 g, while rats were between 100 and 150 g. All animals had free access to food and water except during the actual testing period. Housing, handling, and feeding were all in accordance with recommendations contained in the “Guide for the Care and Use of Laboratory Animals”. All of the test ligands were administered in suspensions of 0.5% (w/v) of methyl cellulose in water. The volumes administered were 0.01 mL/g of body weight for mice and 0.04 mL/10 g for rats. Anticonvulsant activity was established using the maximal electroshock seizure (MES) and subcutaneous metrazole seizure threshold (scMET) tests.^{175,176}

10.3. *In Vivo* Experiments (with S. Lelas)⁸⁸

10.3.1. Subjects

All animals were maintained in accordance with the guidelines of the Committee on Animals of the Bristol-Myers Squibb Company and the “Guide for Care and Use of Laboratory Animals” (Institute of Animal Laboratory Resources, 1996). Research

protocols were approved by the Bristol-Myers Squibb Company Institutional Animal Care and Use Committee.

Male CDF rats weighing approximately 350 g at the time of the experiment (conflict), male Sprague-Dawley rats weighing 180-300 g (locomotor activity, rotorod studies, and drug discrimination studies) and male CF1 mice weighing 20-22 g at the time of the experiment (seizure studies) were purchased from Charles River Laboratories (Wilmington, Mass., USA). For the conditioned fear studies, male Sprague-Dawley rats weighing approximately 225 g at the time of the experiment were purchased from Harlan (Indianapolis, Ind., USA). Animals were housed in pairs or fours in clear plastic shoebox cages with Beta Chip bedding in rooms maintained at constant temperature (21-23°C) and humidity (50 ± 10%) with a 12 h light/dark cycle (lights on at 0600 h, except for mice lights were on at 0500 h), except for the drug discrimination study for which animals were housed individually in suspended wire cages.

Animals had *ad libitum* access to food and water throughout the studies, except for the conflict and drug discrimination studies in which animals were restricted to 9 g (conflict) or 12 g (drug discrimination) of laboratory rodent chow (Bio-Serv, Frenchtown, NJ) per day in addition to the food earned in operant box, with unlimited access to water. All training and testing was done between 0600 and 1300 h Monday through Friday of each week.

10.3.2. Procedures

10.3.2.1. GABA_A Binding Assay

HEK293 cells were trypsinized and counted. Cells were transfected using the Amaxa electroporator and 3 million cells per sample. Each transfection was performed in

Amaxa solution “V” using electroporation program Q-01 (Amaxa Inc., Gaithersburg, Md., USA). 1 μg of each GABA subunit (α , β , and γ) was used per transfection. Following electroporation, cells were plated onto poly-lysine coated glass coverslips and used for the experiments.

10.3.2.2. Electrophysiological Studies

Whole-cell patch-clamp experiments were performed using HEK cell lines transiently expressing two different configurations of GABA_A constructs, on the first or second day after the transfection. Cells were plated onto 25 mm Petri dishes and viewed using Nikon TE200 inverted microscope, equipped with the mercury lamp to monitor GFP fluorescence. Cells were continuously perfused with extracellular physiological solution containing (in mM): NaCl 140, KCl 2.5, CaCl₂ 2, MgSO₄ 2, Na₂HPO₄ 1.25, HEPES 10, Glucose 11, pH 7.4 and 340 mOsm (modified from Brown et al., 2002). Patch pipettes were pulled using Narishige vertical puller from fire-polished borosilicate glass capillaries. Pipette resistance was between 3.5 and 6 M Ω . The intracellular solution contained (in mM): CsCl 140, HEPES 10, EGTA 5, MgATP 2, MgCl₂ 3, pH 7.3 and 340 mOsm.

Cells were voltage-clamped at -20 mV via an EPC10 amplifier (HEKA Electronics, Southboro, Mass.). Preliminary experiments have shown that amplitude of the GABA-induced current in these cells was not significantly different at -60, -40 or -20 mV holding potentials. At the same time, -20 mV holding potential facilitated longer experimental time which enabled testing of several concentrations of the test compounds. Drug solutions were applied to the cells via a multi-channel local perfusion

system (AutoMate Scientific, Inc., San Francisco, Calif.) with the estimated solution change time of 20 ms.

GABA was applied to the cell for 20 s with a 60 s washout period between applications, which was found to be a sufficient time period to reverse any desensitization that may occur. In addition, to ensure that there is no desensitization that may affect GABA responses at any given concentration of a GABA modulator, GABA was applied twice during control (no drug) and once at each concentration of the test compound. Test compounds were applied in increasing concentrations (1, 10, 100, or 1000 nM) 60 s prior to GABA (3 μ M) applications.

10.3.3. Geller Conflict with Incremental Shock in Rats

Experiments were conducted in 8 model E10-10 Coulbourn operant chambers (Coulbourn Instruments, Allentown, Penn., USA; 28 x 26 x 31 cm) with an electrified grid floor which were housed in light-proof, sound-attenuated, and fan-ventilated chambers. On one wall of each operant chamber is a house light and a centrally placed food hopper 3 cm from the floor that delivered one 45-mg food pellet (Dustless Precision Pellets, Bio-Serv, Frenchtown, N.J., USA). To the left was mounted a lever response module with cue lights above. Foot-shock was delivered using an H13-16 Universal Shocker. Experiments were controlled with a Compaq DeskPro computer running Graphic State Notation software through Habitest Universal Linc interface equipment (Coulbourn Instruments).

Rats were trained to stability on an alternating multiple Random Interval 30 s/Fixed Ratio 1 Food +Shock paradigm (RI15/FR1 F+S). The paradigm ran through four cycles beginning with the Random Interval (RI) schedule which ran for 12 minutes then

switched to the Fixed Ratio (FR) schedule which was cued and ran for 3 minutes. The RI had a range of 15 to 45 s with the food pellet being delivered with the first lever press after the expiration of the interval. The FR schedule delivered a food pellet after each lever press along with a foot-shock that increased with each lever press beginning at zero on the first lever press then increasing to 0.05 mA on the second lever press and incrementing by 0.05 mA with each subsequent lever press. The shock was reset to zero at the beginning of each RI/FR cycle.

10.3.4. Protection against Pentylentetrazole- and Shock-Induced Seizures in Mice

Pentylentetrazole (PTZ) was administered at 125 mg/kg s.c. The number of animals surviving was recorded at 30 minutes and 60 minutes after administration of PTZ. Electroshock is administered using an Ugo Basile ECT, Unit 7801 seizure apparatus (Ugo Basile, Italy) and corneal electrodes soaked in 0.9% saline. Mice received a shock of 30 mA for 0.3 s. The number of animals that exhibited the hind-limb extensor component of the seizure was recorded.

10.3.5. Conditioned Fear in Rats

Experiments were conducted in standard modular test chambers (ENV-008, Med Associates, St. Albans, Vt., USA, 30.5 x 24.1 x 21 cm) with an electrified grid floor which were housed in light-proof, sound-attenuated, and fan-ventilated chambers. Foot-shock was delivered using a shocker/scrambler module (ENV-414). Experiments were controlled with a desktop computer using Med-PC software through Smart Ctrl™ interface equipment (Med-Associates).

On day 1, rats were placed in the test chambers for a 7-minute conditioning session consisting of 2.5 minutes of habituation, a 2-s foot-shock at 0.7 mA, followed by 2.5

minutes of no foot-shock, another 2-s, 0.7 mA foot-shock, and another 2 minutes with no foot-shock. Twenty-four hours after the conditioning session, rats were placed in the test chamber again for 7 minutes with no foot-shocks and percent time freezing was quantified by video image analysis (Freezeview software using filter 25 and bout length of 0.75 s; Actimetrics and Coulbourn Instruments, Allentown, Penn., USA).

10.3.6. Spontaneous Locomotor Activity in Rats

The testing apparatus consisted of Plexiglas chambers (42 x 42 x 30 cm) equipped with Digiscan activity monitors (Omnitech Electronics, Columbus, Ohio, USA) that detect interruptions of eight photobeams spaced 5 cm apart and 2.5 cm above the floor. Horizontal activity was recorded in 5-minute bins for a total of 60 minutes and expressed as total distance covered (in cm).

10.3.7. Rotorod Performance in Rats

The degree of motor coordination or balance was determined using a standard accelerating rotorod treadmill (Ugo Basile, Comerio-Varese, Italy) that was 6 cm in diameter and 24 cm above the base. The speed was increased gradually from 2 rpm to a maximum speed of 20 rpm. The time each animal remained on the rotating rod was automatically recorded, up to a maximum of 5 minutes. Three acclimation trials were conducted for each animal prior to administration of drugs. The time on rotorod from the third trial was used to counterbalance animals for subsequent drug testing.

10.3.8. Chlordiazepoxide Discrimination in Rats

Twelve model E10-10 Coulbourn operant conditioning chambers (Coulbourn Instruments, Allentown, Penn., USA; 28 x 26 x 31 cm) were housed in light-proof, sound-attenuated, and fan-ventilated chambers. Each operant conditioning chamber was

equipped with two non-retractable levers, requiring a downward force equivalent to 15 g (0.15 N), that were mounted 3 cm from the side wall, 3 cm above the metal grid floor, and 5 cm from a centrally placed food tray that delivered one 45-mg food pellet (Dustless Precision Pellets, Bio-Serv, Frenchtown, N.J.). The experimental chambers were connected to a Micro PDP11/73 computer using a LAB LINC interface. A SKED-11 operating system (State System, Kalamazoo, Mich.) was used to record and control behavior.

After habituation to the operant conditioning chamber, rats were trained to alternate daily between response levers on an FR 1 schedule of food reinforcement. Once lever pressing was well established, the reinforcement contingency was increased incrementally to an FR 10 schedule of food reinforcement, while maintaining the lever alternation. Rats were then trained to discriminate between an intraperitoneal (IP) injection of drug (5.0 mg/kg CDP) and vehicle (0.25% methylcellulose) administered 30 minutes prior to the start of the session. Ten consecutive responses on the injection-appropriate lever resulted in food delivery. Responses on the incorrect lever did not result in pellet delivery. Following an injection of CDP, responding on the right lever was reinforced for half the rats and responding on the left lever was reinforced for the other rats. In each two-week period there were five drug days and five saline days, with the constraint that there not be more than three consecutive drug or vehicle days.

Drug test sessions were conducted once a week (Fridays) with training sessions scheduled on intervening days (Monday – Thursday). The criterion for testing was achieved if no more than three incorrect responses occurred prior to the first reinforcer for at least 9 out of 10 consecutive sessions. During test sessions, the lever on which the

rat first made 10 consecutive responses resulting in delivery of the first food pellet was designated the “selected “ lever and subsequent pellet delivery was made contingent on responding on this selected lever on an FR10 schedule. The selected lever, the number of responses prior to the first food pellet delivery, and the total number of responses in the session were recorded for each rat. The duration of test sessions was ten minutes. Dose-response functions were determined for CDP, diazepam, and QH-ii-066.

11. Experiments of GABA signaling in neuroblastoma (Weiss and Cook et al.)⁸⁹

11.1. Methods Summary:

Backcross mice were generated by crossing *TH-MYCN* transgenic FVB/N mice to wild-type 129/SvJ, and subsequently crossing F1 offspring to wild-type 129/SvJ. Mice were observed for at least one year to be considered tumor-free. DNA was isolated from spleen and genotyped using a combination of microsatellite and SNP markers. RNA from SCG was analyzed using Affymetrix Mouse Exon arrays. Susceptibility linkage was analyzed using R-QTL. Differential gene expression was assessed using Significance Analysis of Microarrays, and eQTL were calculated using custom software as described previously.

11.2. Supplementary Methods:

11.2.1. Mice All mice were obtained from the Jackson Labs (Bar Harbor, ME), and were housed and treated following UCSF IACUC guidelines. Tumor-negative backcross mice were followed until one year of age (the latest tumor was detected at 342 days). Superior cervical ganglia (SCG) were surgically isolated and snap-frozen in liquid nitrogen. SCG were isolated from the parental control groups at 21 days.

11.2.2. Taqman analysis of transgene expression: Taqman expression analysis was performed on 6 mice (3 female, 3 male) from each strain. Proprietary assays for human MYCN and controls L18 and mGUS were obtained from Applied Biosystems (Carlsbad, CA).

11.2.3. Genotyping DNA was isolated from spleen tissue using a proteinase K lysis followed by phenol chloroform extraction. Microsatellite marker genotyping was carried out by the Marshfield Clinic (Marshfield, WI), and CIDR (Baltimore, MD). SNP genotyping was performed using template-directed primer extension with fluorescence polarization detection (FP-TDI, Acycloprime II, Perkin Elmer, Waltham, MA) and SNPStream² 48-plex (Beckman Coulter, Brea, CA). The marker set had an average spacing of 8 MB genome-wide (excluding the high density of markers on chromosome 10).

11.2.4. Linkage analysis Interval mapping was performed using the R-QTL³ package in the R statistical language. Genotypes flagged as probable errors by R-QTL were discarded. The genetic map positions were determined using the physical map positions (NCBI 37/mm9), followed by re-estimation of the map using R-QTL, and likely mis-

mapped markers were discarded. Linkage analysis was performed on a 1-cM grid. Genome-wide significance thresholds were determined by running 1000 permutations for each dataset. Interval analysis was performed using the binary mode of the “EM” model. All results reported as significant were significant at a 5% genome-wide error rate. 95% confidence intervals (CI) were determined using the lodint function in R-QTL. Genes within the confidence intervals were determined by counting all genes in the UCSC genome assembly mapping between markers flanking the 95% CI.

11.2.5. Expression Arrays RNA from superior cervical ganglia was isolated using the RNEasy kit (QIAGEN, Valencia, CA), as we found these buffers were more effective at disrupting the ganglia than Trizol. 1µg of RNA was used as a starting template for the RiboMinus rRNA subtraction (Invitrogen, Carlsbad, CA) followed by the ST labeling protocol (Affymetrix, Santa Clara, CA). Labeled samples were hybridized to Affymetrix Mouse Exon 1.0 arrays. Array quality control was performed using the Affymetrix Expression Console. 2-way comparisons between homogenous groups (e.g. male vs. females or 129/SvJ vs FVB/N males) were performed using the Significance Analysis of Microarrays (SAM) package⁴ using a 5% false discovery rate.

11.2.6. eQTL analysis Arrays were normalized using RMA in the XPS package (<http://www.bioconductor.org/packages/2.6/bioc/html/xps.html>). eQTL were calculated as described in ⁵; briefly, linkage between gene expression and loci was assessed by linear regression with genome-wide significance assessed using a FDR-based method.

11.2.7. Cell Culture Neuroblastoma cell lines were grown in RPMI media with 10% serum and antibiotics with the exception of SK-N-BE(2) (DMEM/F12, 10% serum) and

IMR-32 (DMEM, 10% serum plus non-essential amino acids). Nor-NOHA was obtained from Bachem (Torrance, CA) and dissolved in DMSO. GABA was obtained from Sigma (St. Louis, MO) and dissolved in H₂O. Picrotoxin and bicuculline were obtained from Sigma and dissolved in DMSO.

11.2.8. Western blotting Equal amounts of total protein were loaded for 4%–12% SDS-polyacrylamide gel electrophoresis and transferred to nitrocellulose membranes. After blocking, membranes were blotted with Arg1 (R&D Systems, Minneapolis MN), GABA B R1, Erk (Santa Cruz Biotech, Santa Cruz, CA), GABA A R β 2/3, GABA B R2, β -tubulin (Millipore, Billerica, MA), cleaved-PARP (Asp214), p-Akt (Ser473), Akt, pErk (Thr202/Tyr204) (Cell Signaling Technology, Danvers, MA), and GAPDH (Upstate Biotechnology, Lake Placid NY). Antibodies were detected with HRP-linked anti-mouse, anti-rabbit (Amersham/GE, Piscataway, NJ), or anti-sheep IgG (Calbiochem/EMD, Gibbstown, NJ), followed by enhanced chemiluminescence (Amersham/GE, Piscataway, NJ).

11.2.9. WST-1 assay Cells were grown in 12-well plates and treated for 72 hours prior to the addition of WST-1 reagent (100 μ l per 1ml media). Absorbance was read after 60 minutes. Results were plotted using Graphpad Prism software, and p-values were calculated using a two-tailed Student's t-test.

11.2.10. FACS Cells were plated on 6-well dishes and treated as indicated for 24 hours. They were then harvested, fixed in 70% ethanol for 30 minutes, then stained with a propidium iodide (PI) dye and RNase solution. All samples were analyzed on a FACSCaliber flow cytometer (Becton Dickinson, Franklin Lakes, NJ) and analyzed

using ModFit (Verity Software, Topsham ME). Apoptosis was detected by flow cytometry for annexin V-FITC per manufacturer's protocol (Annexin V-FITC detection kit, BioVision, Milpitas, CA) using FlowJo software (Tree Star, Inc, Ashland, OR).

12. Behavioral experiments (with Savic et al.)¹⁵⁴

Experiments were carried out on male Wistar rats (Military Farm, Belgrade, Serbia), weighing 220-250 g. All procedures in the study conformed to EEC Directive 86/609 and were approved by the Ethical Committee on Animal Experimentation of the Medical Faculty in Belgrade. The rats were housed in transparent plastic cages, six animals per cage, and had free access to pelleted food and tap water. The temperature of the animal room was $22\pm 1^{\circ}\text{C}$, the relative humidity 40-70%, the illumination 120 lux, and the 12/12 h light/dark period (light on at 6:00 h). All handling and testing took place during the light phase of the diurnal cycle. Throughout the study the animals were used only once, with the exception of the grip strength measurement, which was done immediately after the tracking of behavior on the elevated plus maze. Spontaneous locomotor activity and elevated plus maze behavior were analyzed by the ANY-maze Video Tracking System software (Stoelting Co., Wood Dale, IL, USA). All drugs were dissolved/suspended with the aid of sonication in a solvent containing 85% distilled water, 14% propylene glycol, and 1% Tween 80, and were administered intraperitoneally in a volume of 1 ml/kg, 15 min before behavioral testing (for active and passive avoidance test, before the acquisition session). Time of administration, as well as, the doses of DMCM in various tests were chosen based on our previous studies (Savić et al., 2005a; 2005b; 2006). For interaction studies in the locomotor activity assay, the first treatment indicated in

combination was administered into the lower left quadrant of the peritoneum 20 minutes before testing, and the second treatment 5 minutes later into the lower right quadrant of the peritoneum.

12.1. Passive Avoidance (PA) Paradigm

The experiments were performed in an adapted Automatic reflex conditioner (Ugo Basile, Milan, Italy, Model 7051), as described earlier.¹⁷⁷ In short, the apparatus consisted of a shuttle-box, equipped with a grid floor and divided with a sliding door into a lit and a dark compartment, and a programming unit. The animals were submitted to two, 24 hour – separated sessions. The acquisition session started by placing individual subjects in the illuminated compartment. After 30 seconds, the entrance to the dark compartment was opened, and as soon as the rat had entered it with all four paws, the footshock (2 s, 0.3 mA) was delivered. Immediately afterwards, the rat was returned to its home cage. The same procedure was repeated 24 hours later (retention session), without footshock. A cut-off time of 180 seconds was used on the training day, whereas, on the retention trial, a ceiling of 300 seconds was imposed.

13. Two-Way Active Avoidance (AA) Paradigm (with Savic et al.)¹⁵⁴

The AA test was performed in automated two-way shuttle-boxes (Campden Instruments, Sibley, UK), as described earlier.¹⁷⁷ In short, the animals were submitted to two, 24-hour separated sessions. Training and test sessions were procedurally identical. Animals were placed singly into the shuttle box and left to freely explore for 15 minutes, and

habituation crossings were automatically counted. Afterward, they received 30 tone foot shock trials. During the first 5 seconds of each trial, a sound signal was presented (broadband noise of 69 dB), allowing the animal to avoid shocks by moving to the other compartment (avoidance response). If the animal did not respond within this period, a foot shock of 0.5 mA (7-s duration) was applied. Crossing to the adjacent compartment during the shock discontinued its delivery. The animal could move freely in the apparatus between trials (18-s intertrial intervals), and the intertrial crossings were automatically counted.

14. Measurement of Locomotor Activity (with Savic et al)

Activity of single rats in a clear Plexiglas chamber (40 x 25 x 35 cm) under dim red light (20 lux) was recorded for a total of 30 minutes, without any habituation period, using ANY-maze software (as described above). For purposes of improving data analysis, the central 20% of the chamber (200 cm²) was virtually set as a central zone. The minimum percentage of animal that must have been in the zone for an entry to occur was set at 70%, and 50% of the animal must have remained in the zone for an exit not to occur.

15. Behavior on the Elevated Plus Maze (EPM) (with Savic et al)

The apparatus consisted of two open (50 x 10 cm, with a ledge of 0.3 cm) and two enclosed arms (50 x 10 x 40 cm), connected by a junction area (10 x 10 cm). The illumination in the experimental room was 10 lux on the surface of the arms. At the beginning of the experiment, single rats were placed in the center of the maze, facing

one of the enclosed arms, and their behavior was recorded for 5 min. An entry into an open or closed arm was scored when 90% of the animal crossed the virtual line separating the central square of the maze from the arm, whereas an exit occurred when more than 90 % of the animal left the respective arm. After each trial, the maze was cleaned with dry and wet towels.

16. Grip Strength Test (with Savic et al)

Muscle strength was assessed by the grip strength meter (Ugo Basile, Milan, Italy, model 47105). When pulled by the tail, the rat grasps the trapeze connected to a force transducer, and the apparatus measures the peak force of experimenter's pull (in g) necessary to overcome the strength of the animal's forelimbs grip. Each animal was given three consecutive trials, and the median value was used for further statistics.

16.1. Statistical Analysis

All numerical data presented in the figures were given as the mean \pm SEM, except for results from the PA test (median latency with 25th, 75th interquartile range; data were non-parametric because the procedure involved a cut-off). For electrophysiological data Student's t-test was used for statistical analysis. Data from PA test were assessed by a Kruskal-Wallis non-parametric ANOVA, with post-hoc comparison relative to solvent control by a Dunn's test ($\alpha=0.05$). Data from the AA, EPM, grip strength and activity assay were assessed by a one-way ANOVA. If the ANOVA was significant, each treatment condition was compared with control by a Dunnett's test ($\alpha=0.05$). Where appropriate, the assessment of the antagonist influence on the inverse agonist effect was

conducted by a student's t-test. Statistical analyses were performed with ANY-maze Video Tracking System software (Stoelting Co., Wood Dale, IL, USA) and SigmaStat 2.0 (SPSS, Inc., Chicago, IL, USA).

17. *In vivo* studies on XLi-093 in mice (Rowlett and Cook et al)⁵⁵

Subjects

C57BL/6 Male Mice, 6 weeks old, n=8-10 per group

17.1. Drugs

1. Diazepam, Xli-093, flumazenil, bretazenil, and flunitrazepam were injected at doses between 0.3 and 30.0 mg/kg, i.p. and dissolved in a 50% PG and 50% distilled water vehicle
2. [³H]Flumazenil (1.5μCi/30g mouse, i.v), [³H]L655-708 (1.5μCi/30g mouse, i.v.), both were dissolved in a saline vehicle

17.2. HOLEBOARD MEMORY TASK

Apparatus: Holeboard insert containing 16 holes in a sound attenuated locomotor activity chamber (Med Associates, Inc.)

Same 4 holes were baited for 4 consecutive 5-min sessions. Baited holes are changed daily. Mice were trained for 14 days or until they reached criteria. After training, testing

with DZ, XLi-093(XLi), DZ+ flumazenil (FLZ), or DZ+XLi-093 began. Performance was measured as a ratio of the number of novel correct holes (i.e., correct hole visited only once) /Total holes visited. Perfect performance was indicated by a ratio of 1.0.

17.3. *IN VIVO* BINDING ASSAY

1. To determine binding site occupancy at $\alpha 1$ and $\alpha 2/3$ GABAA receptors, mice were injected with [3 H] flumazenil ([3 H]FLZ) (1.5 μ Ci/mouse, i.v.). Pretreatments (30 min): DZ (0.3-10.0 mg/kg, i.p.), XLi-093 (0.03-10.0 mg/kg, i.p.), flunitrazepam (30.0mg/kg, i.p., used to determine non-specific binding). Mice were sacrificed 3 min after i.v. injection of tritiated ligand. Cerebellum and spinal cord were quickly removed, homogenized, and stored in ScintiSafe. All samples were processed with a Packard 1900CA liquid scintillation analyzer.

2. For binding site occupancy at $\alpha 5$ GABA(A)receptors, methods followed those above using [3 H]L655,708 (1.5 μ Ci/mouse, i.v.). Non-specific binding was determined using bretazenil (5.6 mg/kg, i.p.). Mice were sacrificed 1 min after injection with tritiated ligand and the forebrain was quickly removed and prepared as described above.

**18. CANTAB work (Rowlett and Cook et al.)¹⁵⁵:
Preferential inverse agonist action at $\alpha 5$ GABA_A receptors
resulted in enhancement of performance on memory
tasks.**

18.1. Subjects: Experiments were conducted with adult male rhesus monkeys (*Macaca mulatta*), aged 10-15 years (corresponding roughly to “middle aged” monkeys), born and reared at the New England Primate Research Center breeding facility. The monkeys were experimentally naïve at the beginning of the study. Monkeys were prepared with a non-allergic nylon vest (Lomir) and seated in primate chairs (Crisp Instruments) enclosed in ventilated, sound-attenuating chambers (Med Associates); or prepared with the non-allergic nylon vest attached to a flexible, stainless steel tether (Lomir) connected to the top of the monkey's home cage. The restraint chair system was used in CANTAB studies, and the tether system was used in ORD, observational and MAP studies. All monkeys were housed in a temperature- and humidity-controlled housing room and maintained on a 12-hr on/12-hr off light/dark schedule (lights on at 0600 hr). Water was available continuously in the home cage.

18.2. Food availability: The protocol for food restriction developed by Taffe (2004) was used. Briefly, the monkeys in all studies were weighed weekly, and these weights were used to calculate food (LabDiet 5038) allotments based on metabolic energy requirements for rhesus monkeys. The calculation was based on the equation:

$y=15.504x^{-0.8219}$, in which y =food biscuits/kg/day and x =body weight in kg (Taffe 2004). Monkeys were maintained at 100% of this allotment for at least 3 weeks or until weights are stable (no upward or downward trend over three weight determinations). Once stable, the monkeys' food allotments were gradually reduced to 70 to 85% (note that this was not a reduction in *weight*, rather a reduction in *food allotment*), an amount shown to result in stable and accurate performance in CANTAB tasks. Weekly weighing occurred throughout the studies to adjust feeding (within the 70-85% range) based on a combination of weight, performance, and overall health (as determined by routine physical exams conducted by the Clinical Veterinary Staff).

18.3. Surgery and drug delivery: All compounds were administered via the intravenous (i.v.) route. We used this route in order to minimize pharmacokinetic variables and to allow direct comparisons with other procedures at Harvard Medical School (NERPC) designed to study BZ effects in rhesus monkeys (e.g., i.v. self-administration models of abuse potential). Monkeys were implanted with venous catheters using the surgical procedures described by Platt et al. (2005). Surgery was conducted under aseptic conditions using isoflurane/oxygen anesthesia. Catheters were passed by way of a jugular, femoral or brachial vein to the level of the right atrium. The distal end of the catheter was passed subcutaneously to a mid-scapular exit point. Catheters were flushed routinely with saline containing Heparin (100-150 U/ml), and physical exams were conducted that occasionally included contrast-dye infusion into the catheter, followed by X-ray to verify catheter patency and proper placement. Using these procedures, catheters can remain patent for up to 3 years.

18.4. General design and data analyses: Separate groups of 6-8 monkeys were used in the CANTAB vs. the ORD/MAP/observation studies, with each monkey in a group receiving all treatments whenever possible.

Dependent measures for the studies depended on the individual tasks, as described below. The studies employed within-subjects design, in which each subject serves as its own control. This design permits scientifically meaningful results to be obtained with fewer animals than would be required using most other approaches. For individual subject analysis, data during test sessions were compared to data from control sessions and significance of effects were determined on the basis of 95% confidence intervals established under baseline conditions. For comparison of doses within individual tasks, repeated-measures ANOVAs were used to evaluate statistical reliability when warranted. For all studies, multiple comparisons were assessed for statistical reliability using *a priori* Bonferroni t-tests, when applicable. Comparisons of drug potencies were conducted by computing ED₅₀ values (dose engendering 50% of the maximum effect). The ED₅₀s were computed using non-linear regression analysis techniques.

18.5. CANTAB Tasks in Monkeys.

18.5.1 Apparatus: As described above, monkeys were trained to sit in primate chairs that will be placed in a sound-attenuating chamber. Inside this chamber were a computer-controlled touch-screen monitor (Campden or Lafayette Instruments, Inc.), equipped with a dispenser to deliver 190-mg flavored food pellets (BioServe, Inc.).

Experimental events were controlled by the CANTAB software system on a computer in an adjacent room.

18.5.2. Delayed non-matching to sample (DNMS). The DNMS task was a short-term recognition memory task involving sets of visual discriminations. A sample stimulus is presented in the center of the screen, and the animal must touch this stimulus within 30 sec. After a touch, the screen was blanked and following a variable retention interval, two stimuli were presented on the lower left and right of the screen. The retention interval consisted of 0, 1, 3, or 10 min; if performance was highly variable, the delays were adjusted for individual monkeys based on performance such that short, medium, and long delays were tested. Of the two “matching” stimuli, one stimulus was identical to the sample stimulus (“matching” stimulus) and the other was novel (“non-matching” stimulus). A touch directed to the non-matching stimulus was followed by reinforcer delivery. In addition to the four retention interval conditions, a simultaneous condition was included in which the sample stimulus remained present while the matching and non-matching stimuli were present. A session consisted of 10 trials of each retention interval, presented in a randomly intermixed fashion (total trials=50). The CANTAB software used 469 shapes and 7 colors to ensure that discriminations were unique for approximately 120,000 trials. The primary dependent measures for the DNMS task are the percent correct responses at each delay and the latency to respond at each delay. The number of trials completed also was recorded as a measure of motivation and/or ability to perform the task.

18.5.3. Paired associated learning (PAL). Large colored abstract stimuli were displayed in one of 4 positions (top center, bottom center, left middle, right middle).

The subject was required to touch the sample stimulus, which then disappeared. After a 1-sec delay, the same pattern reappears (choice phase) in two or more locations on the screen (the original location plus one or more novel locations). The subject was required to touch the stimulus that was presented in the same location as the sample item to obtain a food pellet. Task difficulty was increased by increasing the number of stimulus-location associations required on each trial. Training was initiated with sessions that present 25 1-stimulus trials and 25 2-stimulus trials until performance averaged >50% correct trials on the 2-stimulus trials. Next, monkeys received sessions of 25 2-stimulus trials and 25 3-stimulus trials until performance averaged >25% correct trials on the 3-stimulus trials. This part of the PAL task measured memory for stimulus-location associations.

Next, a learning component is introduced in which a trial repeats if a mistake was made in attempting to complete this trial (i.e. the monkey gets 0-2 of 3 stimulus-locations correct in a 3-stimulus trial). Up to 6 attempts at a given trial were allowed. Finally, 4-stimulus trials were added when performance of 3-stimulus trials exceeded 50% correct (thus, the PAL task measured both memory and learning of stimulus-location associations). The dependent measures were the percent correct at each difficulty level and the latencies to respond.

18.5.4. Intradimensional/extradimensional set shifting (ID/ED). The ID/ED shift task evaluated the ability of a subject to attend to specific attributes of a stimulus, as well as the ability to shift attention to other attributes when required. This task consisted of a series of eight discrimination learning stages wherein touching only one of two stimuli presented on the screen resulted in food pellet delivery. Within any

given stage of the task, a pair of stimuli was presented and the same stimulus was associated with reinforcement (S+ stimulus) until the performance criteria were met (18 of 20 consecutive trials correct). Correct choices must be made within 30 sec, and following a correct choice the screen was blanked for 5 sec while an incorrect choice (S- stimulus) resulted in a 0.2 sec tone and a 9-sec period of blank screen.

The task consisted of 4 levels of stimulus sets, each progressively more difficult. In the first stimulus set (Level 1), two distinctly shaped stimuli were presented, with touches on one shape resulting in food pellet delivery. This level (and all subsequent levels) included a stimulus reversal, in which the same two shapes are retained but pressing the S+ stimulus now does not result in reinforcement, whereas touching the former S- stimulus did result in food pellet delivery. In Level 2, a compound discrimination was presented. For this discrimination, the two shapes from Level 1 are present, but additional stimuli, consisted of lines, were superimposed onto the existing shapes. Because the shape discrimination from the previous stage did not change, the lines are irrelevant to this discrimination. Level 3 consisted of the intra-dimensional (ID) shift stage. For this discrimination, two new shapes with new lines were presented. This was considered an ID shift due to the fact that despite new shapes and lines being introduced, the shape remained the relevant dimension for the discrimination. In the final level, the extra-dimensional (ED) shift will be introduced. Thus, in Level 4, new shapes and lines were presented; however, the lines—not the shape—were the relevant discriminative stimulus. Performance was determined as the number of errors at each stage, and the data were subjected to a square root transformation to achieve normal distributions.

18.5.5. Progressive-Ratio (PR). PR procedures consisted of response requirements that progressively increased across a session until responding ceases. The last response requirement completed, termed “break point”, provided a quantitative measure of the reinforcing effectiveness of a stimulus. For these studies, a session was initiated by a colored box appearing in the middle of the screen. Touching the box once resulted in food pellet delivery, and the response requirement were progressively increased following each reinforcer by an incremental value beginning at 1 and doubling after 8 response requirements were completed successfully. Thus, the response requirement sequences consisted of: Increment= 1, response requirements= 1, 2, 3, 4, 5, 6, 7, 8; Increment = 2, response requirements = 10, 12, 14, 16, 18, 20, 22, 24; Increment = 4, response requirements = 28, 32, 36, 40, 44, 48, 52, 56; and so on. Sessions were a maximum of 30 min, and were terminated if 3 min elapses without a response. Performance was measured as the break point and number of food pellets delivered per session. This procedure provided a measure of the ability of the animal to respond, as well as an assessment of “motivation” to perform.

18.5.6. Training. Initial training began with shaping the basic response of touching the screen. A large colored square was displayed that occupied most of the screen. Touching the screen inside the box was a “correct” response and results in food reinforcement. With each correct response, the size of the square decreased until the monkey readily pressed a 1-in box in any location on the screen. This initial training typically required up to 5 sessions.

Currently 4 monkeys were trained at various stages of the DNMS and ID/ED task. These monkeys initiated training on PAL (a task that requires a lengthy training period,

Taffe et al. 2004) with “reminder” trials for DNMS and ID/ED scheduled one day per week. We anticipated approximately 5-6 more months of training for PAL performance to reach acceptable performance.

For new monkeys, CANTAB training was initiated by gradually introducing different tasks, and also incorporate training on the ORD task. In the first phase of training, the PAL task was introduced 5 days/week. After approximately 6 months, the DNMS task was introduced on days 1-4 of the week, with PAL training continuing on day 5. In our experience, DNMS training typically took up to 3 months, once criterion performance was met, DNMS training was initiated on days 1-3, with PAL training scheduled for days 4 and 5, respectively. PAL training may take up to and over 12 months, therefore, after 9 months the ID/ED task was introduced into the sequence once or twice per week on randomly chosen days (this task did not require special training, Weed et al., 1999). In the final phase of training, two tasks per day were introduced and the PR schedule introduced according to the schedule: day 1: PR/PAL; day 2: DNMS/PR; day 3: PAL; day 4: DNMS/PR; day 5: ID/ED/PR.

Table 20: Schedule of CANTAB tests for a single dose of compound plus vehicle

	<u>Day 1</u>	<u>Day 2</u>	<u>Day 3</u>	<u>Day 4</u>	<u>Day 5</u>	<u>Day 6</u>	<u>Day 7</u>	<u>Day 8</u>
<u>Cycle 1:</u>	PAL Dose A	ID/ED vehicle	ORD Dose A	DNMS/PR vehicle	DNMS/PR Dose A	ORD vehicle	ID/ED Dose A	PAL vehicle
<u>Cycle 2:</u>	DNMS/PR Dose A	ORD vehicle	ID/ED Dose A	PAL vehicle	PAL Dose A	ID/ED vehicle	ORD Dose A	DNMS/PR vehicle

18.5.7. Testing. Once training criteria were reached on all tasks, the 8-day cycles shown in **Table 20** were initiated. The two cycles shown in the Table allowed a dose of test compound and vehicle to be determined twice in all tasks. For each compound, vehicle plus at least 4 doses were evaluated. All doses of a compound (or dose of compound plus antagonist) were tested in irregular order, with a compound finished prior to moving to the next compound. A test session consisted of i.v. injections of compound(s) at an appropriate pretreatment time prior to the session. Based on the scheduling shown in Table 20, for CANTAB a dose-response function was required approximately 10 weeks to complete.

19. Object Retrieval with Detours (ORD) Task. To augment CANTAB-based testing, parallel assessments were conducted using the ORD Task, which was a manual test sensitive to frontostriatal deficits (Taylor et al. 1990; Jentsch et al. 1999) and has been validated in pharmacological studies at NERPC. The task required the monkey to retrieve a small piece of palatable food from a transparent box that was open on one side only. The box was attached to a tray that can be positioned within easy reach of the monkey. Different levels of task complexity were achieved by varying the orientation of the open side of the box, the position of the box on the tray, and the position of the food relative to the opening. The level of cognitive complexity and motor difficulty of each task was rated *a priori* using the criteria of Taylor et al. (1990). The 12 task configurations varied from those characterized by high cognitive complexity/low motor difficulty to low cognitive complexity/high motor difficulty.

Training on the ORD task typically required 14-21 sessions, and tests were scheduled as described above in Table 20. The primary dependent measure for the ORD task was “percent success”, which was the total number of reaches minus “incorrect” (i.e., a reach in which the food item was not obtained) and “barrier” reaches (i.e., a reach in which the monkey contacted a closed side of the box), divided by total reaches and then multiplied by 100. Barrier reaches were also analyzed separately as a measure of perseverative behavior, and reach latencies (i.e., time to obtain food or maximum trial length of 20 seconds) were recorded as a measure of motor impairment.

20. Assessment of Motor Coordination and Behavioral Effects in Monkeys.

20.1. MAP apparatus and procedure. To evaluate fine motor coordination, monkeys were trained using the movement assessment panel (MAP) system developed by Gash and colleagues (Gash et al. 1999). The MAP (Quanteon, Inc.) consists of a Lexan® box attached to a clear Lexan® panel that was mounted on to home cage (**Figure 41**). Portals in the front panel and on the sides of the food receptacle allowed monkeys to retrieve small food objects (e.g., miniature marshmallows or raisins). Arrays of photocells are attached to the portals on the front panel (Portal A) and food receptacle (Portal B). The amount of time that the photobeams for Portal A were broken was considered a measure of gross motor coordination, whereas the amount of time that the photobeams for Portal B were broken was considered a measure of fine motor

coordination (Gash et al. 1999). MAP studies occurred in the home cage of monkeys prepared with the tether system. The MAP apparatus fit the cage door, and monkeys received initial training by placing food treats in different parts of the apparatus until they consistently retrieved treats from the food receptacle.

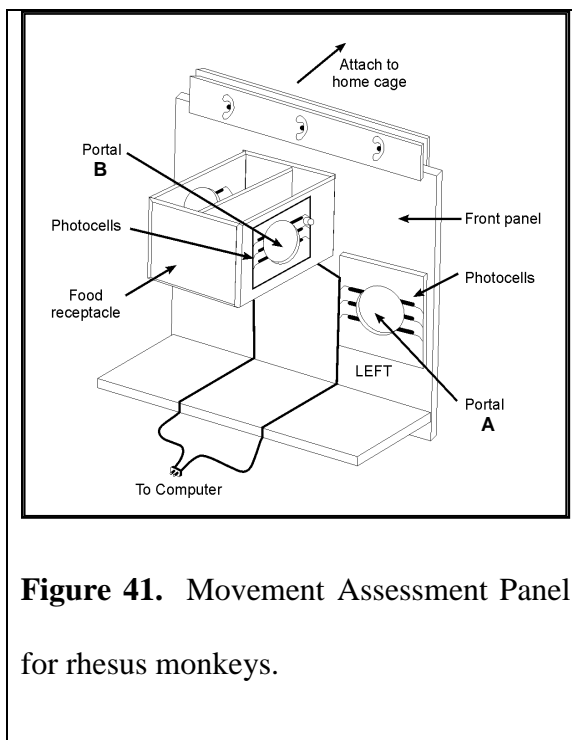


Figure 41. Movement Assessment Panel for rhesus monkeys.

Training occurred 5 days per week until latencies retrieved the treat are stable (no upward or downward trends over 3 consecutive sessions) and testing occurred on day 2 and day 5 of this 5-day cycle.

20.1.1. Observation studies. Observers were trained in the use of the behavioral scoring instrument developed in previous studies at NERPC. Each observer will undergo at least 20 hrs of observational training until they reached a > 90% reliability criterion based on percent agreement scores. The scoring system included 19 categories

encompassing a wide range of species-typical and drug-induced behaviors including locomotion, environmental manipulation, foraging, self-grooming, scratching, stereotypic behavior such as self-grasping, back flipping, and hair pulling, ataxia, sleep posture, moderate and deep sedation. These behavioral categories have proven to be useful for characterization of the sedative and motoric effects of BZ-type compounds in previous research at NERPC.

Observation studies occurred in the same monkeys that were trained on the MAP task. Observation studies were conducted in these monkeys in alternate weeks, on the 2nd and 3rd day of the 5-day cycle (i.e., MAP testing occurred one week, observation tests occurred the following week, and so on). Video cameras were used to record the monkeys' behavior during observation sessions. This provided an archival record of experimental sessions, permitted subsequent scoring of videotapes by independent observers, and eliminated the possibility that an observer's presence disturbed the monkeys' behavior. All behaviors were scored during 5-min sampling periods as described above. Each 5-min period was subdivided into twenty 15-s intervals, and frequency scores were calculated as the proportion of 15-s intervals in which a particular behavior occurred. Data was analyzed separately in individual subjects and for the group when appropriate used the statistical approach described earlier at NERPC.

21. References

- (1) Haefely, W.; Facklam, M.; Schoch, P.; Martin, J. R.; Bonetti, E. P.; Moreau, J. L.; Jenck, F.; Richards, J. G. *Adv. Biochem. Psychoph* **1992**, *47 (GABAergic Synaptic Transm.)*, 379.
- (2) Haefely, W. *J. Psychoactive. Drugs* **1983**, *15*, 19.
- (3) Griebel, G.; Perrault, G.; Simiand, J.; Cohen, C.; Granger, P.; Depoortere, H.; Francon, D.; Avenet, P.; Schoemaker, H.; Evanno, Y.; Sevrin, M.; George, P.; Scatton, B. *CNS Drug Rev.* **2003**, *9*, 3.
- (4) Zingales, I. A. *J. Chromatog.* **1973**, *75*, 55.
- (5) Otto, M. W.; Bruce, S. E.; Deckersbach, T. *J. Clin. Psychiatry* **2005**, *66*, 34.
- (6) Sieghart, W. *Pharmacological Review* **1995**, *47*, 181.
- (7) Squires, R. F.; Braestrup, C. *Nature* **1977**, *266*, 732.
- (8) Möhler, H.; Fritschy, J. M.; Rudolph, U. *J. Pharmacol. Exp. Ther.* **2002**, *300*, 2.
- (9) Barnard, E. A.; Skolnick, P.; Olsen, R. W.; Möhler, H.; Sieghart, W.; Biggio, G.; Braestrup, C.; Bateson, A. N.; Langer, S. Z. *Pharmacol. Rev.* **1998**, *50*, 291.
- (10) Stevenson, I. H.; Browning, M.; Crooks, J.; O'Malley, K. *Br. Med. J.* **1972**, *4*, 322.
- (11) Sieghart, W.; Sperk, G. *Curr. Top. Med. Chem.* **2002**, *2*, 795.

- (12) Garattini, S.; Mussini, E.; Marcucci, F.; Guaitani, A. *Metabolic studies on benzodiazepines in various animal species in the benzodiazepines*, Raven Press, 1973.
- (13) Nayeem, N.; Green, T. P.; Martin, I. L.; Barnard, E. A. *J. Neurochem* **1994**, *62*, 815.
- (14) McKernan, R.; Farrar, S.; Collins, I.; Emms, F.; Asuni, A.; Quirk, K.; Broughton, H. B. *Mol. Pharmacol.* **1998**, *54*, 33.
- (15) McKernan, R. M.; Rosahl, T. W.; Reynolds, D. S.; Sur, C.; Wafford, K. A.; Atack, J. R.; Farrar, S.; Myers, J.; Cook, G.; Ferris, P.; Garrett, L.; Bristow, L.; Marshall, G.; Macaulay, A.; Brown, N.; Howell, O.; Moore, K. W.; Carling, R. W.; Street, L. J.; Castro, J. L.; Ragan, C. I.; Dawson, G. R.; Whiting, P. J. *Nat. Neurosci.* **2000**, *3*, 587.
- (16) Ernst, M.; Brauchart, D.; Boesch, S.; Sieghart, W. *Neuroscience* **2003**, *119*, 933.
- (17) Davies, P. A.; Hanna, M. C.; Hales, T. G.; Kirkness, E. F. *Nature* **1997**, *385*, 820.
- (18) Bonnert, T. P.; McKernan, R. M.; Farrar, S.; le Bourdelles, B.; Heavens, R. P.; Smith, D. W.; Hewson, L.; Rigby, M. R.; Sirinathsinghji, D. J. S.; Brown, N.; Wafford, K. A.; Whiting, P. J. *Proc. Natl. Acad. Sci. U.S.A.* **1999**, *96*, 9891.
- (19) McKernan, R. M. Q., K.; Prince, R.; Cox, P. A.; Gillard, N. P.; Ragan, C. I.; Whiting, P. *Neuron.* **1991**, *7*, 667.

- (20) Baude, A.; Sequier, J. M.; McKernan, R. M.; Olivier, K. R.; Somogyi, P. *Neuroscience* **1992**, *51*, 739.
- (21) McKernan, R. M.; Wafford, K.; Quirk, K.; Hadingham, K. L.; Harley, E. A.; Ragan, C. I.; Whiting, P. J. *J. Recept. Signal Transduct Res.* **1995**, *15*, 173.
- (22) Neish, C. S.; Martin, I. L.; Davies, M.; Henderson, R. M.; Edwardson, J. M. *Nanotechnol.* **2003**, *14*, 864.
- (23) Pritchett, D. B.; Sontheimer, H.; Shivers, B.; Ymer, S.; Kettenmann, H.; Schofield, P. C.; Seeburg, P. *Nature* **1988**, 338.
- (24) Sternfeld, F.; Carling, R. W.; Jelley, R. A.; Ladduwahetty, T.; Merchant, K. J.; Moore, K. W.; Reeve, A. J.; Street, L. J.; O'Connor, D.; Sohal, B.; Atack, J. R.; Cook, S.; Seabrook, G.; Wafford, K.; Tattersall, F. D.; Collinson, N.; Dawson, G. R.; Castro, J. L.; MacLeod, A. M. *J. Med. Chem.* **2004**, *47*, 2176.
- (25) Costa, E.; Guidotti, A.; Mao, C. *Adv. Biochem. Psychopharmacol* **1975**, *14*, 113.
- (26) Sigel, E. B., A. *Trends Pharmacol. Sci.* **1997**, *18*, 425.
- (27) Smith, G. B.; Olsen, R. W. *Trends. Pharmacol. Sci.* **1995**, *16*, 162.
- (28) Sieghart, W. In *GABA*; Enna, S. J., Ed.; Elsevier: San Diego, 2006; Vol. 54, p pp 231.
- (29) Grasshoff, C. D., B.; Rudolph, U.; Antkowiak, B. *Curr. Pharm. Design.* **2006**, *12*, 3665.

- (30) Frolund, B.; Ebert, B.; Kristiansen, U.; Liljefors, T.; Krogsgaard-Larsen, P. *Curr. Top. Med. Chem* **2002**, *2*, 817.
- (31) Haefely, W., Kyburz, E., Gerecke, M., and Mohler, H. *Recent Advances in the Molecular Pharmacology of Benzodiazepine Receptors and in the Structure-Activity Relationships of their Agonists and Antagonists*; Academic Press: New York, 1985; Vol. 99.
- (32) Woods, J. H.; Katz, J. L.; Winger, G. *Pharmacol. Rev.* **1992**, *44*, 151.
- (33) MacDonald, R. L.; Olsen, R. W. *Annu. Rev. Neurosci.* **1994**, *17*, 569.
- (34) McKernan, R. M.; Whiting, P. J. *Trends. Neurosci.* **1996**, *19*, 139.
- (35) Atack, J. R.; Pike, A.; Clarke, A.; Cook, S. M.; Sohal, B.; McKernan, R. M.; Dawson, G. R. *Drug. Metab. Dispos.* **2006**, *34*, 887.
- (36) Campo-Soria, C.; Chang, Y.; Weiss, D. S. *Br. J. Pharmacol.* **2006**, *148*, 984.
- (37) Study, R. E.; Barker, J. L. *Proc. Natl. Acad. Sci. USA* **1981**, *78*, 7180.
- (38) Atack, J. R. *Expert Opin. Investig. Drugs.* **2005**, *14*, 601.
- (39) Korpi, E. R.; Grunder, G.; Luddens, H. *Prog. Neurobiol.* **2002**, *67*, 113.
- (40) Adkins, C. E.; Pillai, G. V.; Kerby, J.; Bonnert, T. P.; Haldon, C.; McKernan, R. M.; Gonzalez, J. E.; Oades, K.; Whiting, P. J.; Simpson, P. *B. J. Boil. Chem.* **2001**, *276*, 38934.
- (41) Teuber, L.; Watjen, F.; Jensen, L. H. *Curr. Pharm. Des.* **1999**, *5*, 317.
- (42) Huang, Q.; He, X.; Ma, C.; Liu, R.; Yu, S.; Dayer, C. A.; Wenger, G. R.; McKernan, R.; Cook, J. M. *J. Med. Chem.* **2000**, *43*, 71.

- (43) He, X.; Huang, Q.; Ma, C.; Yu, S.; McKernan, R.; Cook, J. M. *Drug Des. Discov.* **2000**, *17*, 131.
- (44) Allen, M. S. H., T. J.; Trudell, M. L.; Coddington, P. W.; Skolnick, P.; Cook, J. M. *J. Med. Chem.* **1988**, *31*, 1854.
- (45) Yu, S.; He, X.; Ma, C.; McKernan, R.; Cook, J. M. *Med. Chem. Res.* **1999**, *9*, 186.
- (46) He, X. H., Q.; Yu, S.; Ma, C.; McKernan, R.; Cook, J. M. *Drug Des. Disc.* **1999**, *16*, 77.
- (47) Huang, Q.; Cox, E.; Gan, T.; Ma, C. R.; Bennett, D. A.; McKernan, R.; Cook, J. *Drug Des. Discov.* **1999**, *16*, 55.
- (48) Zhang, W.; Koehler, K. F.; Zhang, P.; Cook, J. M. *Drug Des. Discov.* **1995**, *12*, 193.
- (49) Huang, Q.; Zhang, W. J.; Liu, R. Y.; McKernan, R. M.; Cook, J. M. *Med. Chem. Res.* **1996**, *6*, 384.
- (50) He, X. B.; Huang, Q.; Ma, C. R.; Yu, S.; McKernan, R.; Cook, J. *Drug Des. Discov.* **2000**, *17*, 131.
- (51) Ebert, B.; Wafford, K. A.; Whiting, P. J.; Krogsgaard-Larsen, P.; Kemp, J. A. *Mol. Pharmacol.* **1994**, *46*, 957.
- (52) Hillestad, L.; Hansen, T.; Melsom, H. *Clin. Pharmacol. Ther* **1974**, *16*, 485.
- (53) Sperk, G.; Schwarzer, C.; Tsunashima, K.; Fuchs, K.; Sieghart, W. *Neuroscience* **1997**, *80*, 987.
- (54) McKernan, R. M.; Whiting, P. J. *Trends in Neurosciences* **1996**, *19*, 139.

- (55) Shinday, N.; Rallapalli, S.; Cook, J. M.; Rowlett, J. K. In *Society for Neuroscience* Washington D.C., 2008.
- (56) Maubach, K. *Drug Targets-CNS & Neuro. Disorders* **2003**, 2, 233.
- (57) Howell, O.; Atack, J. R.; Dewar, D.; McKernan, R. M.; Sur, C. *Neuroscience* **2000**, 98, 669.
- (58) Rissman, R. A.; De Blas, A. L.; Armstrong, D. M. *J. Neurosci.* **2007**, 103, 1285.
- (59) Cohen-Mansfield, J. *J. Am. Geriatr. Soc.* **1986**, 34, 722.
- (60) Skolnick, P.; Hu, R. J.; Cook, C. M.; Hurt, S. D.; Trometer, J. D.; Liu, R.; Huang, Q.; Cook, J. M. *J. Pharmacol. Exp. Ther.* **1997**, 283, 488.
- (61) Liu, R.; Zhang, P.; McKernan, R. M.; Wafford, K.; Cook, J. M. *Med. Chem. Res.* **1995**, 5, 700.
- (62) Liu, R.; Hu, R. J.; Zhang, P.; Skolnick, P.; Cook, J. M. *J. Med. Chem.* **1996**, 39, 1928.
- (63) Liu, R.; Zhang, P.; Gan, T.; McKernan, R. M.; Cook, J. M. *Med. Chem. Res.* **1997**, 7, 25.
- (64) Huang, Q.; Zhang, W.; Liu, R.; McKernan, R. M.; Cook, J. M. *Med. Chem. Res.* **1996**, 6, 384.
- (65) Huang, Q. Part I: A Chemical And Computer Assisted Approach To Pharmacophore/Receptor Models for GABA_A/Bz Receptor Subtypes Part II: Predictive Models for GABA(A)/Bzr Subtypes *Via* Comparative Molecular Field Analysis. PhD Thesis, University of Wisconsin-Milwaukee, 1998.

- (66) He, X. Studies of Molecular Pharmacophore Receptor Models for GABA (A)/BzR Subtypes. Chemical and Computer Assisted Approach in Search of Selective Ligands for GABA (A)/ BzR Subtypes. Ph.D Thesis, University of Wisconsin-Milwaukee,WI, 2000.
- (67) Cook, J. M.; Huang, Q.; He, X.; Li, X.; Yu, J.; Han, D.; Lelas, S.; McElroy, J. US Pat. 60/368,408, Applied for March 28, 2002 (pending), 2002.
- (68) Rein, R.; Golombek, A. E. in *Computer-assisted Modeling of Receptor-Ligand Interactions*; Alan R. Liss, Inc.: New York, 1989.
- (69) Damewood, J. R. in *Reviews in Computational Chemistry*; Lipkowitz, K.B., Boyd, D.B. Ed., VHC., 1996; Vol. 9.
- (70) Zhang, W. Part I: Chemical and Computer Assisted Development of an Inclusive Pharmacophore for the Benzodiazepine Receptor. Studies Directed Toward the Synthesis of Anxiolytic Anxiolytics. Part II: Molecular Yardsticks: Probes to study the Actual Dimensions of Benzodiazepine Receptors. Ph. D Thesis, University of Wisconsin-Milwaukee, 1994.
- (71) Zhang, W.; Diaz-Araujo, H.; Allen, M. S.; Koehler, K. F.; Cook, J. M. In *Studies in Medicinal Chemistry*; Choudhary, M. I., Ed.; Harwood Academic Publishers: 1996; Vol. 2, p 303.
- (72) Zhang, W.; Koehler, K. F.; Zhang, P.; Cook, J. M. *Drug Des. Discov.* **1995**, *12*, 193.

- (73) Huang, Q.; Liu, R.; Zhang, W.; Zhang, P.; Cox, E. D.; Gan, T.; Cook, J. *M. J. Med. Chem.* **1998**.
- (74) Huang, Q.; He, X.; Ma, C.; Liu, R.; Yu, S.; Dayer, C. A.; Wenger, G. R.; McKernan, R.; Cook, J. M. *J. Med. Chem.* **2000**, *43*, 71.
- (75) He, X.; Huang, Q.; Yu, S.; Ma, C.; McKernan, R.; Cook, J. M. *Drug Des. Discov.* **1999**, *16*, 77.
- (76) He, X.; Huang, Q.; Ma, C.; Yu, S.; McKernan, R.; Cook, J. M. *Drug Des. Discov.* **2000**, *17*, 131.
- (77) Sieghart, W.; Eichinger, A.; Richards, J. G.; Möhler, H. *J. Neurochem.* **1987**, *48*, 46.
- (78) Wisden, W.; Herb, A.; Wieland, H.; Keinänen, K.; Luddens, H.; Seeburg, P. H. *FEBS Lett.* **1991**, *289*, 227.
- (79) Zhang, P.; Zhang, W.; Liu, R.; Harris, B.; Skolnick, P.; Cook, J. M. *J. Med. Chem.* **1995**, *38*, 1679.
- (80) Hadingham, K. L.; Wingrove, P. B.; Wafford, K. A.; Bain, C.; Kemp, J. A.; Palmer, K. J.; Wilson, A. W.; Wilcox, A. S.; Sikela, J. M.; Ragan, C. I.; Whiting, P. J. *Molecular Pharmacology* **1993**, *44*, 1211.
- (81) Yu, S.; Ma, C.; He, X.; McKernan, R.; Cook, J. M. *Med. Chem. Res.* **1999**, *9*, 71.
- (82) Huang, Q.; Cox, E. D.; Gan, T.; Ma, C.; Bennett, D. W.; McKernan, R. M.; Cook, J. M. *Drug Des. Discov.* **1999**, *16*, 55.
- (83) Fryer, R. I.; Schmidt, R. A.; Sternbach, L. H. *J. Pharm. Sci.* **1964**, *53*, 264.

- (84) Sternbach, L. H.; Fryer, R. I.; Metlesics, W.; Sach, G.; Stempel *J. Org. Chem.* **1962**, *27*, 3788.
- (85) Liu, R., Part I : An Enantiospecific Synthesis of 5-Methoxy (D) Tryptophan and Related Indole Amino Acids Which Serve as Building Blocks Required for the Synthesis Of Alkaloids and Cyclic Peptides Part II: Synthesis and Pharmacological Properties of Novel Imidazobenzodiazepines: High Affinity, Selective Probes For Alpha 5 Containing GABA(A) Receptors. PhD Thesis, University of Wisconsin-Milwaukee, 1996.
- (86) Austin, W. B.; Bilow, N.; Kelleghan, W. J.; Lau, K. S. Y. *J. Org. Chem.* **1981**, *46*, 2280.
- (87) Sternbach, L. H.; Reeder, E.; Archer, G. A. *J. Org. Chem.* **1963**, *28*, 2456.
- (88) Lelas, S.; Rohrbach, K.; Glick, S. D.; Zeller, K.; Bourin, C.; Sieracki, K.; Bertekap, R.; Chen, J.; Cook, C. M.; Helmstetter, F. J.; Li, X. H.; Westphal, R.; Lindner, M.; Tertysnikova, S.; Rallapalli, S.; Cook, J. M.; McElroy, J. F. *manuscript in preparation*.
- (89) Hackett, C. S.; Quigley, A.; Fan, Q.; Cheng, C.; Song, Y. K.; Pawlikowska, L.; Chen, J.; Bao, Y.; Goldenberg, D. D.; Nguyen, K.; Cho, Y. J.; Rallapalli, S.; Cook, J. M.; Kozlov, S.; Ma, J.; Van Dyke, T.; Kowk, P.; Khan, J.; Balmain, A.; Weiss, W. A. *Manuscript in preparation*.

- (90) Wisden, W.; Laurie, D. J.; Monyer, H.; Seeburg, P. H. *J. Neurosci.* **1992**, *12*, 1040.
- (91) Bailey, D. J.; Tetzlaff, J. E.; Cook, J. M.; He, X. H.; Helmstetter, F. J. *Neurobiol. Learn. Mem.* **2002**, *78*, 1.
- (92) Crestani, F.; Keist, R.; Fritschy, J.-M.; Benke, D.; Vogt, K.; Prut, L.; Bluthmann, H.; Mohler, H.; Rudolph, U. *Neurobiology* **2002**, *99*, 8980.
- (93) Chambers, M. S.; Atack, J. R.; Bromidge, F. A.; Broughton, H. B.; Cook, S.; Dawson, G. R.; Hobbs, S. C.; Maubach, K. A.; Reeve, A. J.; Seabrook, G. R.; Wafford, K.; MacLeod, A. M. *J. Med. Chem.* **2002**, *45*, 1176.
- (94) Sur, C.; Quirk, K.; Dewar, D.; Atack, J. R.; McKernan, R. *Mol Pharmacol* **1998**, *54*, 928.
- (95) DeLorey, T.; Lin, R.; McBrad, B.; He, X.; Cook, J. M.; Lamah, J.; Loew, G. *Eur J Pharmacol* **2001**, *426*, 45.
- (96) Kelly, M. D.; Smith, A.; Banks, G.; Wingrove, P.; Whiting, P. W.; Atack, J.; Seabrook, G. R.; Maubach, K. A. *Br. J. Pharmacol.* **2002**, *135*, 248.
- (97) Turner, D.; Sapp, D.; Olsen, R. W. *J. Pharmacol. Exp. Ther.* **1991**, *257*, 1236.
- (98) McKay, P. F.; Foster, K. L.; Mason, D.; Cummings, R.; Garcia, M.; Williams, L. S.; Grey, C.; McCane, S.; He, X. H.; Cook, J. M.; June, H. L. *Psychopharmacology* **2004**, *172*, 455.
- (99) June, H. L.; Harvey, S. C.; Foster, K. L.; McKay, P. F.; Cummings, R.; Garcia, M.; Mason, D.; Grey, C.; McCane, S.; Williams, L. S.; Johnson, T. B.; He, X. H.; Rock, S.; Cook, J. M. *J. Neurosci.* **2001**, *21*, 2166.

- (100) Stephens, D. N.; Pistovcakova, J.; Worthing, L.; Atack, J. R.; Dawson, G. *R. Eur. J. Pharmacol.* **2005**, *526*, 240.
- (101) Lüddens, H.; June, H. L.; Cook, J. (**In preparation**).
- (102) Yang, J.; Teng, Y.; Ara, S.; Rallapalli, S.; Cook, J. M. *Synthesis* **2009**, 1036.
- (103) Portoghese, P. *Trends in pharmacological Sciences* **1989**, *10*, 230.
- (104) Portoghese, P.; Lin, C.; Farouz-Grant, F.; Takemori, A. E. *J Med Chem* **1994**, 37.
- (105) Erez, M.; Takemori, A. E.; Portoghese, P. *J. Med. Chem* **1982**, *25*, 847.
- (106) Halazy, S. In *Exp. Opin. Ther. Pat.* 9 1999, p 431.
- (107) Li, X.; Cao, H.; Zhang, C.; Furtmueller, R.; Fuchs, K.; Huck, S.; Sieghart, W.; Deschamps, J.; Cook, J. M. *J Med Chem* **2003**, *46*, 5567.
- (108) Furtmuller, R.; Schlag, M. G.; Berger, M.; Hopf, R.; Huck, S.; Sieghart, W.; Redl, H. *J. Pharmacol. Exp. Ther.* **2002**, *301(1)*, 168.
- (109) Sigel, E.; Baur, R.; Trube, G.; Möhler, H.; Malherbe, P. *Neuron* **1990**, *5*, 703.
- (110) Delorey, T. M.; Cook, J. M. unpublished results
- (111) Beeby, M. H.; Mann, F. G. *J. Chem. Soc* **1949**, 9.
- (112) Tischchenki, R.-Z. *J. Russ. Phys. Chem. Soc* **1914**, *46*, 705.
- (113) *Burger's Medicinal Chemistry & Drug Discovery*; 6 ed.; John Wiley & Sons Inc., 2003; Vol. 1.
- (114) Han, D. M.; Forsterling, F. H.; Li, X. Y.; Deschamps, J. R.; Cao, H.; Cook, J. M. *Bioorg. Med. Chem. Lett.* **2004**, *14*, 1465.

- (115) Eliel, E. L.; Wilen, S. H. *Stereochemistry of Organic Compounds*; Wiley-Interscience: New York, 1994.
- (116) Flory, P. J. *Statistical Mechanics of Chain Molecules*; Interscience Publishers: New York, 1968.
- (117) Lemieux, R. U. *Molecular Rearrangement*; Interscience Publishers: New York, 1964.
- (118) Eliel, E. L. *J. Acc. Chem. Res.* **1970**, *3*, 1.
- (119) Graczyk, P. P.; Mikolajczyk, M. *Topics in Stereochemistry*; John Wiley & Sons: New York, 1994; Vol. 21.
- (120) Hutchins, R. O.; Kopp, L. D.; Eliel, E. L. *J. Am. Chem. Soc.* **1968**, *90*, 7174.
- (121) Eliel, E. L.; Giza, C. A. *J. Org. Chem.* **1968**, *33*, 3754.
- (122) Uchida, T.; Kurita, Y.; Kubo, M. *J. Polym. Sci.* **1956**, *19*, 365.
- (123) Abe, A.; Mark, J. E. *J. Am. Chem. Soc.* **1976**, *98*, 6468.
- (124) Ohsaku, M. *Macromolecules* **1978**, *11*, 970.
- (125) Wolfe, S. *Acc. Chem. Res.* **1972**, *5*, 102.
- (126) Jaffe, R. J.; Smith, G. D.; Yoon, D. Y. *Phys. Chem.* **1993**, *97*, 12745.
- (127) Bultinck, P.; Van Alsenoy, C.; Goeminne, A. *J. Phys. Chem.* **2001**, *105*, 9203.
- (128) Bultinck, P.; Goeminne, A.; Van de Vondel, D. *J. Mol. Struct.* **1999**, *467*, 211.
- (129) Glendening, E. D.; Feller, D.; Thompson, M. A. *J. Am. Chem. Soc.* **1994**, *116*, 10657.

- (130) Glasstone, S.; Laidler, K. J.; Eyring, H. *The Theory of Rate Processes*; McGraw-Hill: New York, 1941.
- (131) Azumaya, I.; Uchida, I.; Kato, T.; Yokoyama, A.; Tanatani, A.; Takayanagi, H.; Yokozawa, T. *Agnew. Chem. Int. Ed.* **2004**, *43*, 1360.
- (132) Rashkin, M. J.; Waters, M. L. *J. Am. Chem. Soc.* **2002**, *124*, 1860.
- (133) Tsuzuki, S.; Honda, K.; Uchimarui, T.; Mikami, M.; Tanabe, K. *J. Am. Chem. Soc.* **2002**, *124*, 104.
- (134) Hobza, P.; Selzle, H. L.; Schlag, E. W. *J. Am. Chem. Soc.* **1994**, *116*, 3500.
- (135) Burley, S. K.; Petsko, G. A. *Sci.* **1985**, *229*, 23.
- (136) Cheng, Y., Prusoff, W.H. *Biochem. Pharmacol.* **1973**, *22*, 3099.
- (137) Venault, P.; Chapouthier, G.; de Carvalho, L. P.; Simiand, J.; Morre, M.; Dodd, R. H.; Rossier, J. *Nature* **1986**, *321*, 864.
- (138) Jensen, L. H.; Stephens, D. N.; Sarter, M.; Petersen, E. *Brain Res. Bull.* **1987**, *9*, 359.
- (139) Dorow, R.; Horowitz, B.; Paschelke, G.; Amin, M. *Lancet* **1983**, *2*, 98.
- (140) Duka, T.; Ott, H.; Rohloff, A.; Voet, B. *Psychopharmacology* **1996**, *123*, 361.
- (141) Benson, J. A.; Low, K.; Keist, R.; Mohler, H.; Rudolph, U. *FEBS Lett.* **1998**, *431*, 400.
- (142) Crestani, F.; Assandri, R.; Tauber, M.; Martin, J.; Rudolph, U. *Neuropharmacology* **2002**, *43*, 679.

- (143) Rudolph, U.; Crestani, F.; Benke, D.; Brunig, I.; Benson, J. A.; Fritschy, J. M.; Martin, J. R.; Bluethmann, H.; Mohler, H. *Nature* **1999**, *401*, 796.
- (144) Collinson, N.; Kuenzi, F. M.; Jarolimek, W.; Maubach, K. A.; Cothliff, R.; Sur, C.; Smith, A.; Otu, F. M.; Howell, O.; Atack, J. R.; McKernan, R. M.; Seabrook, G. R.; Dawson, G. R.; Whiting, P. J.; Rosahl, T. W. *J. Neurosci.* **2002**, *22*, 5572.
- (145) Pirker, S.; Schwarzer, C.; Wieselthaler, A.; Sieghart, W.; Sperk, G. *Neuroscience* **2000**, *101*, 815.
- (146) Crestani, F.; Low, K.; Keist, R.; Mandelli, M. J.; Mohler, H.; Rudolph, U. *Mol. Pharmacol.* **2001**, *59*, 442.
- (147) Izquierdo, I.; Medina, J. H.; Vianna, M. R.; Izquierdo, L. A.; Barros, D. M. *Behav. Brain Res* **1999**, *103*, 1.
- (148) Atack, J.; Bayley, P. J.; Seabrook, G.; Wafford, K. A.; McKernan, R.; Dawson, G. R. *Neuropharmacology* **2006**, *51*, 1023.
- (149) Collinson, N.; Atack, J.; Laughton, P.; Dawson, G. R.; Stephens, D. N. *Psychopharmacology* **2006**, *188*, 619.
- (150) Chambers, M. S.; Atack, J. R.; Broughton, H. B.; Collinson, N.; Cook, S.; Dawson, G. R.; Hobbs, S. C.; Marshall, G.; Maubach, K. A.; Pillai, G. V.; Reeve, A. J.; MacLeod, A. M. *J. Med. Chem.* **2003**, *46*, 2227.
- (151) Dawson, G. R.; Maubach, K. A.; Collinson, N.; Cobain, M.; Everitt, B. J.; MacLeod, A. M.; Choudhury, H. I.; McDonald, L. M.; Pillai, G.; Rycroft, W.; Smith, A. J.; Sternfeld, F.; Tattersall, F. D.; Wafford, K. A.;

- Reynolds, D. S.; Seabrook, G. R.; Atack, J. R. *J. Pharmacol. Exp. Ther.* **2006**, *316*, 1335.
- (152) Nutt, D.; Besson, M.; Wilson, S. J.; Dawson, G. R.; Lingford-Hughes, A. *Neuropharmacology* **2007**, *53*, 810.
- (153) Sieghart, W. *Unpublished* **2009**.
- (154) Savic, M. M.; Clayton, T.; Furtmueller, R.; Gavrilovic, I.; Samardzic, J.; Savic, S.; Huck, S.; Sieghart, W.; Cook, J. M. *Brain Res.* **2008**, *1208*, 150.
- (155) Moran, C. A.; Rowlett, J. K.; Clayton, T.; Rallapalli, S.; Majumder, S.; Roth, B. L.; Cook, J. M. In *Society of Neuroscience* Chicago, IL, October 17-21 2009.
- (156) Knust, H.; USPTO, Ed.; Hoffman-La Roche Inc.: USA, 2009; Vol. US 7,514,426 B2, p 1.
- (157) Clayton, T. Part I. Unified Pharmacophoric Protein Models of the Benzodiazepine Receptor Subtypes Part II. Subtype Selective Ligands For 5 GABA_A/Bz Receptors. PhD Thesis, University of Wisconsin-Milwaukee, 2011.
- (158) Zimprich, F.; Zezula, J.; Sieghart, W.; Lassmann, H. *Neurosci. Lett.* **1991**, *127*, 125.
- (159) McKernan, R. M.; Cox, P.; Gillard, N. P.; Whiting, P. *FEBS. Lett.* **1991**, *286*, 44.
- (160) Li, X., Synthesis of Selective Ligands for GABA_A/Benzodiazepine Receptors, PhD Thesis, University of Wisconsin-Milwaukee, 2004.

- (161) Cook, J. M. Zhou, H.; Huang, S.; Sarma, P.V.V.S.; Zhang, C USA, 2009; Vol. US 7,618,958B2.
- (162) Beaulieu, F.; Beauregard, L. P.; Courchesne, G.; Couturier, M.; LaFlamme, F.; L'Heureux, A. *Org. Lett* **2009**, *11*, 5050.
- (163) Kalesse, M.; Lorenz, M. Synthesis of the C10-C32 Core Structure of Spirangien A. PhD Thesis, Zentrum für Biomolekulare Wirkstoffe (BMWZ).
- (164) Mohamadi, F.; Richards, N. G. J.; Guida, W. C.; Liskamp, R.; Caufield, C.; Chang, G.; Hendrickson, T.; Still, W. C. *J. Comput. Chem.* **1990**, *11*, 440.
- (165) Inc, G.; Gaussian 92 ed. ed.; Carnegie office park, bldg. 6, Pittsburgh, PA-15106.
- (166) Chambers, M. S.; Atack, J. R.; Carling, R. W.; Collinson, N.; Cook, S. M.; Dawson, G. R.; Ferris, P.; Hobbs, S. C.; O'Connor, D.; Marshall, G.; Rycroft, W.; MacLeod, A. M. *J. Med. Chem.* **2004**, *47*, 5829.
- (167) Choudhary, M. S.; Craigo, S.; Roth, B. L. *Mol. Pharmacol.* **1992**, *42*, 627.
- (168) Li, X. C., H.; Zhang, C.; Furtmüller, R.; Fuchs, K.; Huck, S.; Sieghart, W.; Deschamps, J.; Cook, J. M. *J. Med. Chem.* **2003**, *46*, 5567.
- (169) El Hadri, A.; Abouabdellah, A.; Thomet, U.; Baur, R.; Furtmüller, R.; Sigel, E.; Sieghart, W.; Dodd Robert, H. *J. Med. Chem.* **2002**, *45*, 2824.
- (170) Sieghart, W. *J. Psychiatr. Neurosci.* **1994**, *19*, 24.

- (171) Schreibmayer, W.; Lester, H. A.; Dascal, N. *Pflugers Arch.: Eur. J. Physiol* **1994**, *426*, 453.
- (172) Fuchs, K.; Zezula, J.; Slany, A.; Sieghart, W. *Eur. J. Pharmacol.* **1995**, *289*, 87.
- (173) Sigel, E. *J. Physiol.* **1987**, *386*, 73.
- (174) Rivas, F. M.; Stables, J. P.; Murphree, L.; Edwankar, R. V.; Edwankar, C. R.; Huang, S.; Jain, H. D.; Zhou, H.; Majumder, S.; Sankar, S.; Roth, B. L.; Ramerstorfer, J.; Furtmüller, R.; Sieghart, W.; Cook, J. M. *J. Med. Chem.* **2009**, 1795.
- (175) Krall, R. L.; Penry, J. K.; White, B. G.; Kupferberg, H. J.; Swinyard, E. A. *Epilepsia.* **1978**, *19*, 409.
- (176) Stables, J. P.; Kupferberg, H. J. In *Molecular and Cellular Targets for Anti-Epileptic Drugs*; 1 ed.; Avanzini, G., Regesta, G., Tanganelli, P., Avoli, M., Ed.; John Libbey: London, 1997, p pp 191.
- (177) Savic, M. M.; Obradovic, D. I.; Ugresic, N. D.; Cook, J. M.; Sarma, P.; Bokonjic, D. R. *Psychopharmacology* **2005**, *180*, 455.

III. Appendix I: Crystal Data for **110** and **111**

X-ray Crystal Structure Determination for **110** and **111**

Single-crystal X-ray diffraction data on **110** and **111** were collected at 296 and 100 °K respectively. All data were collected using MoK α radiation ($\lambda = 0.71073 \text{ \AA}$) and a Bruker APEX 2 CCD area detector. Samples were prepared for data collection by coating with high viscosity microscope oil (Paratone-N, Hampton Research). The oil-coated crystal was mounted on a MicroMesh mount (MiTeGen, Inc.) and transferred immediately to the diffractometer. Corrections were applied for Lorentz, polarization, and absorption effects. All structures were solved by direct methods and refined by full-matrix least squares on F^2 values using the programs found in the SHELXTL suite (Bruker, SHELXTL v6.10, 2000, Bruker AXS Inc., Madison, WI). Parameters refined included atomic coordinates and anisotropic thermal parameters for all non-hydrogen atoms.

Full information on data collection, refinement, and results of the x-ray studies are given in Tables 1 to 14

Table 1. Crystal data and structure refinement for **110**.

Empirical formula	$C_{19}H_{20}N_2O_2$	
Formula weight	308.37	
Temperature	296(2) K	
Wavelength	0.71073 Å	
Crystal system	Orthorhombic	
Space group	$P 2_12_12_1$	
Unit cell dimensions	$a = 9.6247(4)$ Å	$\alpha = 90^\circ$
	$b = 11.6485(5)$ Å	$\beta = 90^\circ$
	$c = 13.7072(5)$ Å	$\gamma = 90^\circ$
Volume	$1536.76(11)$ Å ³	
Z	4	
Density (calculated)	1.333 Mg/m ³	
Absorption coefficient	0.087 mm ⁻¹	
F(000)	656	
Crystal size	0.549 x 0.141 x 0.104 mm ³	
Theta range for data collection	2.29 to 29.23°	
Index ranges	$-12 \leq h \leq 13$, $-15 \leq k \leq 15$, $-18 \leq l \leq 18$	
Reflections collected	17885	
Independent reflections	4117 [R(int) = 0.0313]	
Completeness to theta = 29.23°	99.4 %	
Absorption correction	Semi-empirical from equivalents	
Max. and min. transmission	0.9910 and 0.9537	
Refinement method	Full-matrix least-squares on F ²	
Data / restraints / parameters	4117 / 0 / 208	
Goodness-of-fit on F ²	1.051	
Final R indices [I > 2sigma(I)]	R1 = 0.0441, wR2 = 0.1120	
R indices (all data)	R1 = 0.0560, wR2 = 0.1197	
Absolute structure parameter	0.9(14)	
Largest diff. peak and hole	0.275 and -0.226 e.Å ⁻³	

Table 2. Atomic coordinates ($\times 10^4$) and equivalent isotropic displacement parameters ($\text{\AA}^2 \times 10^3$) for **110**. $U(\text{eq})$ is defined as one third of the trace of the orthogonalized U^{ij} tensor.

	x	y	z	$U(\text{eq})$
N(1)	1218(2)	4427(1)	8185(1)	37(1)
C(2)	2099(2)	5027(2)	8752(1)	33(1)
C(3)	3328(2)	5685(2)	8403(1)	34(1)
N(4)	3535(1)	6617(1)	9129(1)	34(1)
C(5)	3857(2)	6092(1)	10089(1)	34(1)
C(6)	2664(2)	5348(2)	10454(1)	35(1)
O(6)	2569(2)	5140(1)	11332(1)	47(1)
C(7)	1757(2)	4884(2)	9725(1)	33(1)
C(8)	551(2)	4152(2)	9753(1)	33(1)
C(9)	-305(2)	3714(2)	10488(1)	42(1)
C(10)	-1425(2)	3030(2)	10227(2)	47(1)
C(11)	-1703(2)	2774(2)	9258(2)	49(1)
C(12)	-880(2)	3187(2)	8508(2)	43(1)
C(13)	242(2)	3876(2)	8775(1)	35(1)
C(14)	4643(2)	4903(2)	8333(1)	39(1)
C(15)	5780(2)	5425(2)	8987(1)	37(1)
C(16)	5253(2)	5408(2)	10054(1)	37(1)
C(17)	6311(2)	5866(2)	10792(2)	53(1)
O(17)	6185(2)	7054(1)	10952(1)	60(1)
C(18)	8403(2)	6398(2)	7934(2)	60(1)
C(19)	7098(2)	7033(2)	8158(1)	44(1)
C(20)	6001(2)	6639(2)	8636(1)	37(1)
C(21)	4712(2)	7351(2)	8821(2)	41(1)

Table 3. Bond lengths [Å] and angles [°] for **110**.

N(1)-C(2)	1.345(2)	N(1)-C(13)	1.395(2)
N(1)-H(1A)	0.8600	C(2)-C(7)	1.384(2)
C(2)-C(3)	1.489(2)	C(3)-N(4)	1.485(2)
C(3)-C(14)	1.562(3)	C(3)-H(3A)	0.9800
N(4)-C(21)	1.480(2)	N(4)-C(5)	1.484(2)
C(5)-C(6)	1.523(2)	C(5)-C(16)	1.563(2)
C(5)-H(5A)	0.9800	C(6)-O(6)	1.231(2)
C(6)-C(7)	1.432(2)	C(7)-C(8)	1.441(2)
C(8)-C(9)	1.398(2)	C(8)-C(13)	1.411(2)
C(9)-C(10)	1.387(3)	C(9)-H(9A)	0.9300
C(10)-C(11)	1.387(3)	C(10)-H(10A)	0.9300
C(11)-C(12)	1.384(3)	C(11)-H(11A)	0.9300
C(12)-C(13)	1.395(3)	C(12)-H(12A)	0.9300
C(14)-C(15)	1.541(3)	C(14)-H(14A)	0.9700
C(14)-H(14B)	0.9700	C(15)-C(20)	1.509(3)
C(15)-C(16)	1.548(2)	C(15)-H(15A)	0.9800
C(16)-C(17)	1.531(3)	C(16)-H(16A)	0.9800
C(17)-O(17)	1.406(3)	C(17)-H(17A)	0.9700
C(17)-H(17B)	0.9700	O(17)-H(17C)	0.8200
C(18)-C(19)	1.490(3)	C(18)-H(18A)	0.9600
C(18)-H(18B)	0.9600	C(18)-H(18C)	0.9600
C(19)-C(20)	1.325(3)	C(19)-H(19A)	0.9300
C(20)-C(21)	1.514(3)	C(21)-H(21A)	0.9700
C(21)-H(21B)	0.9700		
C(2)-N(1)-C(13)	109.18(14)	C(2)-N(1)-H(1A)	125.4
C(13)-N(1)-H(1A)	125.4	N(1)-C(2)-C(7)	110.16(15)
N(1)-C(2)-C(3)	125.62(14)	C(7)-C(2)-C(3)	124.10(15)
N(4)-C(3)-C(2)	105.51(13)	N(4)-C(3)-C(14)	111.05(14)
C(2)-C(3)-C(14)	111.26(14)	N(4)-C(3)-H(3A)	109.6
C(2)-C(3)-H(3A)	109.6	C(14)-C(3)-H(3A)	109.6
C(21)-N(4)-C(3)	109.31(14)	C(21)-N(4)-C(5)	109.49(14)
C(5)-N(4)-C(3)	108.68(13)	N(4)-C(5)-C(6)	111.59(14)
N(4)-C(5)-C(16)	111.26(13)	C(6)-C(5)-C(16)	111.64(13)
N(4)-C(5)-H(5A)	107.4	C(6)-C(5)-H(5A)	107.4
C(16)-C(5)-H(5A)	107.4	O(6)-C(6)-C(7)	124.21(16)
O(6)-C(6)-C(5)	119.25(16)	C(7)-C(6)-C(5)	116.46(14)
C(2)-C(7)-C(6)	118.78(15)	C(2)-C(7)-C(8)	106.74(14)
C(6)-C(7)-C(8)	134.12(15)	C(9)-C(8)-C(13)	118.55(16)
C(9)-C(8)-C(7)	135.20(16)	C(13)-C(8)-C(7)	106.24(14)
C(10)-C(9)-C(8)	118.74(18)	C(10)-C(9)-H(9A)	120.6
C(8)-C(9)-H(9A)	120.6	C(11)-C(10)-C(9)	121.41(18)
C(11)-C(10)-H(10A)	119.3	C(9)-C(10)-H(10A)	119.3
C(12)-C(11)-C(10)	121.72(18)	C(12)-C(11)-H(11A)	119.1
C(10)-C(11)-H(11A)	119.1	C(11)-C(12)-C(13)	116.67(18)
C(11)-C(12)-H(12A)	121.7	C(13)-C(12)-H(12A)	121.7
C(12)-C(13)-N(1)	129.41(16)	C(12)-C(13)-C(8)	122.91(16)
N(1)-C(13)-C(8)	107.67(15)	C(15)-C(14)-C(3)	108.01(14)
C(15)-C(14)-H(14A)	110.1	C(3)-C(14)-H(14A)	110.1
C(15)-C(14)-H(14B)	110.1	C(3)-C(14)-H(14B)	110.1
H(14A)-C(14)-H(14B)	108.4	C(20)-C(15)-C(14)	106.53(15)
C(20)-C(15)-C(16)	111.10(15)	C(14)-C(15)-C(16)	108.14(14)
C(20)-C(15)-H(15A)	110.3	C(14)-C(15)-H(15A)	110.3

Table 3. (continued)

C(16)-C(15)-H(15A)	110.3	C(17)-C(16)-C(15)	113.68(15)
C(17)-C(16)-C(5)	111.96(15)	C(15)-C(16)-C(5)	107.71(13)
C(17)-C(16)-H(16A)	107.8	C(15)-C(16)-H(16A)	107.8
C(5)-C(16)-H(16A)	107.8	O(17)-C(17)-C(16)	112.84(17)
O(17)-C(17)-H(17A)	109.0	C(16)-C(17)-H(17A)	109.0
O(17)-C(17)-H(17B)	109.0	C(16)-C(17)-H(17B)	109.0
H(17A)-C(17)-H(17B)	107.8	C(17)-O(17)-H(17C)	109.5
C(19)-C(18)-H(18A)	109.5	C(19)-C(18)-H(18B)	109.5
H(18A)-C(18)-H(18B)	109.5	C(19)-C(18)-H(18C)	109.5
H(18A)-C(18)-H(18C)	109.5	H(18B)-C(18)-H(18C)	109.5
C(20)-C(19)-C(18)	127.06(19)	C(20)-C(19)-H(19A)	116.5
C(18)-C(19)-H(19A)	116.5	C(19)-C(20)-C(15)	126.46(17)
C(19)-C(20)-C(21)	123.16(16)	C(15)-C(20)-C(21)	110.16(14)
N(4)-C(21)-C(20)	111.02(14)	N(4)-C(21)-H(21A)	109.4
C(20)-C(21)-H(21A)	109.4	N(4)-C(21)-H(21B)	109.4
C(20)-C(21)-H(21B)	109.4	H(21A)-C(21)-H(21B)	108.0

Table 4. Anisotropic displacement parameters ($\text{\AA}^2 \times 10^3$) for **110**. The anisotropic displacement factor exponent takes the form: $-2\pi^2 [h^2 a^{*2} U^{11} + \dots + 2 h k a^* b^* U^{12}]$

	U^{11}	U^{22}	U^{33}	U^{23}	U^{13}	U^{12}
N(1)	39(1)	46(1)	27(1)	0(1)	1(1)	-5(1)
C(2)	33(1)	36(1)	30(1)	1(1)	2(1)	1(1)
C(3)	34(1)	38(1)	30(1)	2(1)	2(1)	-4(1)
N(4)	33(1)	33(1)	38(1)	2(1)	2(1)	1(1)
C(5)	36(1)	34(1)	32(1)	-3(1)	0(1)	-4(1)
C(6)	37(1)	36(1)	30(1)	-2(1)	3(1)	-1(1)
O(6)	54(1)	58(1)	27(1)	-1(1)	2(1)	-13(1)
C(7)	33(1)	37(1)	30(1)	1(1)	3(1)	-3(1)
C(8)	33(1)	35(1)	31(1)	2(1)	1(1)	2(1)
C(9)	42(1)	48(1)	36(1)	4(1)	5(1)	-1(1)
C(10)	41(1)	47(1)	53(1)	8(1)	13(1)	-8(1)
C(11)	40(1)	47(1)	59(1)	3(1)	0(1)	-11(1)
C(12)	41(1)	43(1)	45(1)	-2(1)	-4(1)	-6(1)
C(13)	34(1)	37(1)	34(1)	0(1)	1(1)	1(1)
C(14)	42(1)	36(1)	39(1)	-4(1)	10(1)	-2(1)
C(15)	32(1)	32(1)	47(1)	2(1)	5(1)	3(1)
C(16)	37(1)	33(1)	41(1)	5(1)	-1(1)	-2(1)
C(17)	50(1)	54(1)	54(1)	7(1)	-13(1)	-5(1)
O(17)	42(1)	63(1)	76(1)	-22(1)	1(1)	-12(1)
C(18)	48(1)	61(1)	72(2)	-5(1)	20(1)	-5(1)
C(19)	44(1)	42(1)	47(1)	1(1)	9(1)	-6(1)
C(20)	35(1)	35(1)	42(1)	2(1)	0(1)	-3(1)
C(21)	39(1)	33(1)	50(1)	8(1)	5(1)	-2(1)

Table 5. Hydrogen coordinates ($\times 10^4$) and isotropic displacement parameters ($\text{\AA}^2 \times 10^3$) for **110**.

	x	y	z	U(eq)
H(1A)	1251	4390	7559	44
H(3A)	3128	6019	7762	41
H(5A)	3978	6719	10557	40
H(9A)	-127	3878	11140	50
H(10A)	-2001	2738	10711	56
H(11A)	-2462	2312	9109	58
H(12A)	-1066	3013	7859	52
H(14A)	4421	4131	8550	47
H(14B)	4963	4863	7663	47
H(15A)	6643	4984	8929	44
H(16A)	5050	4609	10225	44
H(17A)	6188	5466	11407	63
H(17B)	7241	5701	10558	63
H(17C)	6767	7260	11352	91
H(18A)	9023	6889	7577	90
H(18B)	8190	5733	7548	90
H(18C)	8838	6162	8531	90
H(19A)	7048	7787	7939	53
H(21A)	4904	7913	9325	49
H(21B)	4462	7761	8231	49

Table 6. Torsion angles [°] for **cook106**.

C(13)-N(1)-C(2)-C(7)	0.8(2)	C(13)-N(1)-C(2)-C(3)	176.81(16)
N(1)-C(2)-C(3)-N(4)	152.43(16)	C(7)-C(2)-C(3)-N(4)	-32.1(2)
N(1)-C(2)-C(3)-C(14)	-87.0(2)	C(7)-C(2)-C(3)-C(14)	88.4(2)
C(2)-C(3)-N(4)-C(21)	-177.83(13)	C(14)-C(3)-N(4)-C(21)	61.50(17)
C(2)-C(3)-N(4)-C(5)	62.83(16)	C(14)-C(3)-N(4)-C(5)	-57.84(17)
C(21)-N(4)-C(5)-C(6)	178.61(14)	C(3)-N(4)-C(5)-C(6)	-61.93(16)
C(21)-N(4)-C(5)-C(16)	-55.97(17)	C(3)-N(4)-C(5)-C(16)	63.48(16)
N(4)-C(5)-C(6)-O(6)	-158.11(16)	C(16)-C(5)-C(6)-O(6)	76.7(2)
N(4)-C(5)-C(6)-C(7)	25.1(2)	C(16)-C(5)-C(6)-C(7)	-100.12(18)
N(1)-C(2)-C(7)-C(6)	173.05(16)	C(3)-C(2)-C(7)-C(6)	-3.0(3)
N(1)-C(2)-C(7)-C(8)	-1.0(2)	C(3)-C(2)-C(7)-C(8)	-177.07(16)
O(6)-C(6)-C(7)-C(2)	-169.54(18)	C(5)-C(6)-C(7)-C(2)	7.1(2)
O(6)-C(6)-C(7)-C(8)	2.5(3)	C(5)-C(6)-C(7)-C(8)	179.14(18)
C(2)-C(7)-C(8)-C(9)	-178.1(2)	C(6)-C(7)-C(8)-C(9)	9.1(4)
C(2)-C(7)-C(8)-C(13)	0.80(19)	C(6)-C(7)-C(8)-C(13)	-171.94(19)
C(13)-C(8)-C(9)-C(10)	-0.2(3)	C(7)-C(8)-C(9)-C(10)	178.7(2)
C(8)-C(9)-C(10)-C(11)	0.2(3)	C(9)-C(10)-C(11)-C(12)	-0.1(3)
C(10)-C(11)-C(12)-C(13)	-0.1(3)	C(11)-C(12)-C(13)-N(1)	-178.39(19)
C(11)-C(12)-C(13)-C(8)	0.2(3)	C(2)-N(1)-C(13)-C(12)	178.43(18)
C(2)-N(1)-C(13)-C(8)	-0.3(2)	C(9)-C(8)-C(13)-C(12)	0.0(3)
C(7)-C(8)-C(13)-C(12)	-179.15(17)	C(9)-C(8)-C(13)-N(1)	178.81(16)
C(7)-C(8)-C(13)-N(1)	-0.32(19)	N(4)-C(3)-C(14)-C(15)	-4.76(18)
C(2)-C(3)-C(14)-C(15)	-121.97(15)	C(3)-C(14)-C(15)-C(20)	-56.62(17)
C(3)-C(14)-C(15)-C(16)	62.88(17)	C(20)-C(15)-C(16)-C(17)	-65.57(19)
C(14)-C(15)-C(16)-C(17)	177.85(16)	C(20)-C(15)-C(16)-C(5)	59.09(18)
C(14)-C(15)-C(16)-C(5)	-57.49(17)	N(4)-C(5)-C(16)-C(17)	121.05(16)
C(6)-C(5)-C(16)-C(17)	-113.56(17)	N(4)-C(5)-C(16)-C(15)	-4.63(18)
C(6)-C(5)-C(16)-C(15)	120.75(15)	C(15)-C(16)-C(17)-O(17)	90.4(2)
C(5)-C(16)-C(17)-O(17)	-31.9(2)	C(18)-C(19)-C(20)-C(15)	-5.5(4)
C(18)-C(19)-C(20)-C(21)	-179.5(2)	C(14)-C(15)-C(20)-C(19)	-108.6(2)
C(16)-C(15)-C(20)-C(19)	133.8(2)	C(14)-C(15)-C(20)-C(21)	65.96(18)
C(16)-C(15)-C(20)-C(21)	-51.6(2)	C(5)-N(4)-C(21)-C(20)	65.37(19)
C(3)-N(4)-C(21)-C(20)	-53.6(2)	C(19)-C(20)-C(21)-N(4)	164.91(18)
C(15)-C(20)-C(21)-N(4)	-9.9(2)		

Table 7. Hydrogen bonds for **110** [Å and °].

D-H...A	d(D-H)	d(H...A)	d(D...A)	<(DHA)
N(1)-H(1A)...O(6)#1	0.86	2.10	2.8409(19)	143.7
O(17)-H(17C)...N(4)#2	0.82	2.25	2.743(2)	119.5

Symmetry transformations used to generate equivalent atoms:

#1 $-x+1/2, -y+1, z-1/2$ #2 $x+1/2, -y+3/2, -z+2$

Table 8. Crystal data and structure refinement for **111**.

Empirical formula	$C_{21}H_{30}N_2O_4$	
Formula weight	374.47	
Temperature	100(2) K	
Wavelength	0.71073 Å	
Crystal system	Orthorhombic	
Space group	P 21 21 21	
Unit cell dimensions	a = 8.3186(7) Å	$\alpha = 90^\circ$
	b = 12.4731(10) Å	$\beta = 90^\circ$
	c = 19.1532(16) Å	$\gamma = 90^\circ$
Volume	1987.3(3) Å ³	
Z	4	
Density (calculated)	1.252 Mg/m ³	
Absorption coefficient	0.086 mm ⁻¹	
F(000)	808	
Crystal size	0.463 x 0.429 x 0.091 mm ³	
Theta range for data collection	1.95 to 29.14°	
Index ranges	-11<=h<=11, -17<=k<=16, -24<=l<=26	
Reflections collected	22977	
Independent reflections	5326 [R(int) = 0.0221]	
Completeness to theta = 29.14°	99.6 %	
Absorption correction	Semi-empirical from equivalents	
Max. and min. transmission	0.9931 and 0.9658	
Refinement method	Full-matrix least-squares on F ²	
Data / restraints / parameters	5326 / 2 / 252	
Goodness-of-fit on F ²	1.103	
Final R indices [I>2sigma(I)]	R1 = 0.0356, wR2 = 0.1041	
R indices (all data)	R1 = 0.0367, wR2 = 0.1055	
Absolute structure parameter	0.3(7)	
Largest diff. peak and hole	0.329 and -0.273 e.Å ⁻³	

Table 9. Atomic coordinates ($\times 10^4$) and equivalent isotropic displacement parameters ($\text{\AA}^2 \times 10^3$) for **111**. $U(\text{eq})$ is defined as one third of the trace of the orthogonalized U^{ij} tensor.

	x	y	z	$U(\text{eq})$
N(1)	8034(1)	7267(1)	1454(1)	19(1)
C(2)	9226(1)	6894(1)	1016(1)	16(1)
C(3)	9215(1)	5825(1)	663(1)	16(1)
N(4)	10222(1)	5969(1)	23(1)	14(1)
C(5)	11870(1)	6313(1)	231(1)	14(1)
C(6)	11787(1)	7506(1)	449(1)	14(1)
O(6)	13218(1)	7827(1)	813(1)	18(1)
C(7)	10356(1)	7674(1)	908(1)	15(1)
C(8)	9838(1)	8606(1)	1287(1)	17(1)
C(9)	10416(1)	9662(1)	1352(1)	21(1)
C(10)	9558(2)	10381(1)	1759(1)	25(1)
C(11)	8144(2)	10067(1)	2108(1)	26(1)
C(12)	7541(2)	9036(1)	2053(1)	23(1)
C(13)	8393(1)	8315(1)	1633(1)	19(1)
C(14)	9850(1)	4886(1)	1124(1)	19(1)
C(15)	11491(1)	4539(1)	832(1)	18(1)
C(16)	12574(1)	5545(1)	793(1)	17(1)
C(17)	14318(1)	5261(1)	620(1)	22(1)
O(18)	15055(1)	4601(1)	1132(1)	29(1)
C(19)	12250(2)	2212(1)	268(1)	40(1)
C(20)	11531(2)	3126(1)	-134(1)	27(1)
C(21)	11204(1)	4106(1)	107(1)	19(1)
C(22)	10360(1)	4933(1)	-348(1)	18(1)
O(1S)	5487(1)	6196(1)	2188(1)	26(1)
C(1S)	6066(2)	6072(2)	2882(1)	39(1)
O(2S)	13630(1)	7920(1)	2198(1)	34(1)
C(2S)	12416(2)	8163(1)	2687(1)	34(1)

Table 10. Bond lengths [Å] and angles [°] for **110**.

N(1)-C(2)	1.3796(14)	N(1)-C(13)	1.3849(16)
N(1)-H(1A)	0.8800	C(2)-C(7)	1.3681(15)
C(2)-C(3)	1.4956(15)	C(3)-N(4)	1.4957(14)
C(3)-C(14)	1.5580(15)	C(3)-H(3A)	1.0000
N(4)-C(22)	1.4790(13)	N(4)-C(5)	1.4898(14)
C(5)-C(6)	1.5469(14)	C(5)-C(16)	1.5569(15)
C(5)-H(5A)	1.0000	C(6)-O(6)	1.4362(13)
C(6)-C(7)	1.4942(14)	C(6)-H(6A)	1.0000
O(6)-H(6B)	0.8400	C(7)-C(8)	1.4366(15)
C(8)-C(9)	1.4073(16)	C(8)-C(13)	1.4191(16)
C(9)-C(10)	1.3856(17)	C(9)-H(9A)	0.9500
C(10)-C(11)	1.4089(19)	C(10)-H(10A)	0.9500
C(11)-C(12)	1.384(2)	C(11)-H(11A)	0.9500
C(12)-C(13)	1.3988(16)	C(12)-H(12A)	0.9500
C(14)-C(15)	1.5377(16)	C(14)-H(14A)	0.9900
C(14)-H(14B)	0.9900	C(15)-C(21)	1.5081(17)
C(15)-C(16)	1.5462(16)	C(15)-H(15A)	1.0000
C(16)-C(17)	1.5302(16)	C(16)-H(16A)	1.0000
C(17)-O(18)	1.4209(15)	C(17)-H(17A)	0.9900
C(17)-H(17B)	0.9900	O(18)-H(18A)	0.8400
C(19)-C(20)	1.4994(19)	C(19)-H(19A)	0.9800
C(19)-H(19B)	0.9800	C(19)-H(19C)	0.9800
C(20)-C(21)	1.3352(17)	C(20)-H(20A)	0.9500
C(21)-C(22)	1.5219(16)	C(22)-H(22D)	0.9900
C(22)-H(22E)	0.9900	O(1S)-C(1S)	1.4221(17)
O(1S)-H(1S)	0.8400	C(1S)-H(1SC)	0.9800
C(1S)-H(1SB)	0.9800	C(1S)-H(1SA)	0.9800
O(2S)-C(2S)	1.4099(17)	O(2S)-H(2S)	0.8402(10)
C(2S)-H(2SA)	0.9800	C(2S)-H(2SB)	0.9800
C(2S)-H(2SC)	0.9800		
C(2)-N(1)-C(13)	108.26(10)	C(2)-N(1)-H(1A)	125.9
C(13)-N(1)-H(1A)	125.9	C(7)-C(2)-N(1)	110.26(10)
C(7)-C(2)-C(3)	124.79(10)	N(1)-C(2)-C(3)	124.78(10)
C(2)-C(3)-N(4)	105.01(8)	C(2)-C(3)-C(14)	114.34(9)
N(4)-C(3)-C(14)	111.40(9)	C(2)-C(3)-H(3A)	108.6
N(4)-C(3)-H(3A)	108.6	C(14)-C(3)-H(3A)	108.6
C(22)-N(4)-C(3)	107.98(8)	C(22)-N(4)-C(3)	109.36(8)
C(5)-N(4)-C(3)	109.37(8)	N(4)-C(5)-C(6)	107.96(8)
N(4)-C(5)-C(16)	110.68(8)	C(6)-C(5)-C(16)	114.89(9)
N(4)-C(5)-H(5A)	107.7	C(6)-C(5)-H(5A)	107.7
C(16)-C(5)-H(5A)	107.7	O(6)-C(6)-C(7)	109.63(8)
O(6)-C(6)-C(5)	111.23(8)	C(7)-C(6)-C(5)	109.26(9)
O(6)-C(6)-H(6A)	108.9	C(7)-C(6)-H(6A)	108.9
C(5)-C(6)-H(6A)	108.9	C(6)-O(6)-H(6B)	109.5
C(2)-C(7)-C(8)	107.02(10)	C(2)-C(7)-C(6)	122.41(10)
C(8)-C(7)-C(6)	130.54(10)	C(9)-C(8)-C(13)	119.14(10)
C(9)-C(8)-C(7)	134.35(11)	C(13)-C(8)-C(7)	106.46(10)
C(10)-C(9)-C(8)	118.66(11)	C(10)-C(9)-H(9A)	120.7
C(8)-C(9)-H(9A)	120.7	C(9)-C(10)-C(11)	121.11(12)
C(9)-C(10)-H(10A)	119.4	C(11)-C(10)-H(10A)	119.4
C(12)-C(11)-C(10)	121.62(11)	C(12)-C(11)-H(11A)	119.2
C(10)-C(11)-H(11A)	119.2	C(11)-C(12)-C(13)	117.21(12)

Table 10. (continued)

C(11)-C(12)-H(12A)	121.4	C(13)-C(12)-H(12A)	121.4
N(1)-C(13)-C(12)	129.79(11)	N(1)-C(13)-C(8)	107.97(10)
C(12)-C(13)-C(8)	122.22(11)	C(15)-C(14)-C(3)	107.85(9)
C(15)-C(14)-H(14A)	110.1	C(3)-C(14)-H(14A)	110.1
C(15)-C(14)-H(14B)	110.1	C(3)-C(14)-H(14B)	110.1
H(14A)-C(14)-H(14B)	108.5	C(21)-C(15)-C(14)	107.15(9)
C(21)-C(15)-C(16)	109.83(9)	C(14)-C(15)-C(16)	107.80(9)
C(21)-C(15)-H(15A)	110.7	C(14)-C(15)-H(15A)	110.7
C(16)-C(15)-H(15A)	110.7	C(17)-C(16)-C(15)	111.98(9)
C(17)-C(16)-C(5)	110.40(9)	C(15)-C(16)-C(5)	108.26(9)
C(17)-C(16)-H(16A)	108.7	C(15)-C(16)-H(16A)	108.7
C(5)-C(16)-H(16A)	108.7	O(18)-C(17)-C(16)	113.16(10)
O(18)-C(17)-H(17A)	108.9	C(16)-C(17)-H(17A)	108.9
O(18)-C(17)-H(17B)	108.9	C(16)-C(17)-H(17B)	108.9
H(17A)-C(17)-H(17B)	107.8	C(17)-O(18)-H(18A)	109.5
C(20)-C(19)-H(19A)	109.5	C(20)-C(19)-H(19B)	109.5
H(19A)-C(19)-H(19B)	109.5	C(20)-C(19)-H(19C)	109.5
H(19A)-C(19)-H(19C)	109.5	H(19B)-C(19)-H(19C)	109.5
C(21)-C(20)-C(19)	126.91(14)	C(21)-C(20)-H(20A)	116.5
C(19)-C(20)-H(20A)	116.5	C(20)-C(21)-C(15)	127.85(11)
C(20)-C(21)-C(22)	121.13(11)	C(15)-C(21)-C(22)	110.94(9)
N(4)-C(22)-C(21)	110.67(9)	N(4)-C(22)-H(22D)	109.5
C(21)-C(22)-H(22D)	109.5	N(4)-C(22)-H(22E)	109.5
C(21)-C(22)-H(22E)	109.5	H(22D)-C(22)-H(22E)	108.1
C(1S)-O(1S)-H(1S)	109.5	O(1S)-C(1S)-H(1SC)	109.5
O(1S)-C(1S)-H(1SB)	109.5	H(1SC)-C(1S)-H(1SB)	109.5
O(1S)-C(1S)-H(1SA)	109.5	H(1SC)-C(1S)-H(1SA)	109.5
H(1SB)-C(1S)-H(1SA)	109.5	C(2S)-O(2S)-H(2S)	110.8(3)
O(2S)-C(2S)-H(2SA)	109.5	O(2S)-C(2S)-H(2SB)	109.5
H(2SA)-C(2S)-H(2SB)	109.5	O(2S)-C(2S)-H(2SC)	109.5
H(2SA)-C(2S)-H(2SC)	109.5	H(2SB)-C(2S)-H(2SC)	109.5

Table 11. Anisotropic displacement parameters ($\text{\AA}^2 \times 10^3$) for **110**. The anisotropic displacement factor exponent takes the form: $-2\pi^2 [h^2 a^{*2} U^{11} + \dots + 2 h k a^* b^* U^{12}]$

	U^{11}	U^{22}	U^{33}	U^{23}	U^{13}	U^{12}
N(1)	13(1)	25(1)	18(1)	-1(1)	4(1)	-1(1)
C(2)	13(1)	21(1)	13(1)	1(1)	1(1)	1(1)
C(3)	12(1)	19(1)	15(1)	3(1)	1(1)	-2(1)
N(4)	13(1)	16(1)	14(1)	0(1)	0(1)	-1(1)
C(5)	12(1)	17(1)	13(1)	1(1)	0(1)	0(1)
C(6)	11(1)	19(1)	12(1)	0(1)	1(1)	-1(1)
O(6)	14(1)	26(1)	14(1)	0(1)	0(1)	-5(1)
C(7)	13(1)	19(1)	14(1)	0(1)	1(1)	1(1)
C(8)	14(1)	22(1)	14(1)	-2(1)	-1(1)	2(1)
C(9)	19(1)	24(1)	21(1)	-3(1)	-1(1)	-1(1)
C(10)	24(1)	25(1)	28(1)	-8(1)	-3(1)	2(1)
C(11)	23(1)	33(1)	23(1)	-10(1)	-1(1)	8(1)
C(12)	18(1)	34(1)	18(1)	-5(1)	2(1)	4(1)
C(13)	14(1)	26(1)	15(1)	-2(1)	0(1)	3(1)
C(14)	18(1)	21(1)	18(1)	6(1)	2(1)	-1(1)
C(15)	17(1)	19(1)	20(1)	5(1)	0(1)	1(1)
C(16)	13(1)	20(1)	16(1)	5(1)	-2(1)	2(1)
C(17)	14(1)	27(1)	25(1)	5(1)	-1(1)	3(1)
O(18)	24(1)	32(1)	32(1)	5(1)	-8(1)	9(1)
C(19)	41(1)	25(1)	54(1)	3(1)	-6(1)	13(1)
C(20)	27(1)	24(1)	32(1)	-1(1)	-3(1)	6(1)
C(21)	17(1)	18(1)	23(1)	3(1)	0(1)	0(1)
C(22)	20(1)	16(1)	17(1)	-1(1)	-2(1)	-1(1)
O(1S)	19(1)	37(1)	21(1)	6(1)	0(1)	-1(1)
C(1S)	33(1)	57(1)	25(1)	9(1)	-5(1)	0(1)
O(2S)	29(1)	56(1)	18(1)	-3(1)	-2(1)	11(1)
C(2S)	38(1)	41(1)	23(1)	5(1)	7(1)	13(1)

Table 12. Hydrogen coordinates ($\times 10^4$) and isotropic displacement parameters ($\text{\AA}^2 \times 10^3$) for **110**.

	x	y	z	U(eq)
H(1A)	7191	6900	1596	22
H(3A)	8089	5657	516	19
H(5A)	12571	6265	-192	16
H(6A)	11666	7957	21	17
H(6B)	13840	8142	535	26
H(9A)	11375	9876	1123	25
H(10A)	9928	11098	1802	30
H(11A)	7592	10575	2390	31
H(12A)	6589	8826	2290	28
H(14A)	9965	5125	1614	23
H(14B)	9087	4278	1111	23
H(15A)	11990	3979	1136	22
H(16A)	12547	5916	1256	20
H(17A)	14347	4886	164	26
H(17B)	14946	5931	572	26
H(18A)	15198	4957	1500	44
H(19A)	12363	1588	-40	60
H(19B)	11547	2028	661	60
H(19C)	13309	2421	445	60
H(20A)	11281	2993	-610	33
H(22D)	10974	5035	-785	21
H(22E)	9274	4670	-472	21
H(1S)	4845	6716	2172	39
H(1SC)	6968	6564	2959	58
H(1SB)	6429	5333	2951	58
H(1SA)	5202	6236	3213	58
H(2S)	13284(9)	7984(18)	1788(1)	51
H(2SA)	12095	8915	2635	51
H(2SB)	12826	8045	3161	51
H(2SC)	11485	7699	2606	51

Table 13. Torsion angles [°] for **110**.

C(13)-N(1)-C(2)-C(7)	0.34(13)	C(13)-N(1)-C(2)-C(3)	-175.08(10)
C(7)-C(2)-C(3)-N(4)	-20.77(14)	N(1)-C(2)-C(3)-N(4)	153.99(10)
C(7)-C(2)-C(3)-C(14)	101.63(12)	N(1)-C(2)-C(3)-C(14)	-83.61(13)
C(2)-C(3)-N(4)-C(22)	177.07(9)	C(14)-C(3)-N(4)-C(22)	52.78(11)
C(2)-C(3)-N(4)-C(5)	59.02(10)	C(14)-C(3)-N(4)-C(5)	-65.27(11)
C(22)-N(4)-C(5)-C(6)	166.16(8)	C(3)-N(4)-C(5)-C(6)	-74.93(10)
C(22)-N(4)-C(5)-C(16)	-67.31(10)	C(3)-N(4)-C(5)-C(16)	51.60(11)
N(4)-C(5)-C(6)-O(6)	165.99(8)	C(16)-C(5)-C(6)-O(6)	41.96(12)
N(4)-C(5)-C(6)-C(7)	44.82(10)	C(16)-C(5)-C(6)-C(7)	-79.21(11)
N(1)-C(2)-C(7)-C(8)	-1.32(13)	C(3)-C(2)-C(7)-C(8)	174.09(10)
N(1)-C(2)-C(7)-C(6)	-179.39(10)	C(3)-C(2)-C(7)-C(6)	-3.98(17)
O(6)-C(6)-C(7)-C(2)	-130.32(11)	C(5)-C(6)-C(7)-C(2)	-8.19(14)
O(6)-C(6)-C(7)-C(8)	52.11(15)	C(5)-C(6)-C(7)-C(8)	174.24(11)
C(2)-C(7)-C(8)-C(9)	-175.80(13)	C(6)-C(7)-C(8)-C(9)	2.1(2)
C(2)-C(7)-C(8)-C(13)	1.77(12)	C(6)-C(7)-C(8)-C(13)	179.63(11)
C(13)-C(8)-C(9)-C(10)	0.58(17)	C(7)-C(8)-C(9)-C(10)	177.92(12)
C(8)-C(9)-C(10)-C(11)	0.79(19)	C(9)-C(10)-C(11)-C(12)	-1.1(2)
C(10)-C(11)-C(12)-C(13)	-0.09(19)	C(2)-N(1)-C(13)-C(12)	178.83(12)
C(2)-N(1)-C(13)-C(8)	0.81(12)	C(11)-C(12)-C(13)-N(1)	-176.27(12)
C(11)-C(12)-C(13)-C(8)	1.51(18)	C(9)-C(8)-C(13)-N(1)	176.43(10)
C(7)-C(8)-C(13)-N(1)	-1.59(12)	C(9)-C(8)-C(13)-C(12)	-1.78(17)
C(7)-C(8)-C(13)-C(12)	-179.79(11)	C(2)-C(3)-C(14)-C(15)	-109.10(11)
N(4)-C(3)-C(14)-C(15)	9.75(12)	C(3)-C(14)-C(15)-C(21)	-64.15(11)
C(3)-C(14)-C(15)-C(16)	54.00(11)	C(21)-C(15)-C(16)-C(17)	-72.68(12)
C(14)-C(15)-C(16)-C(17)	170.90(9)	C(21)-C(15)-C(16)-C(5)	49.27(12)
C(14)-C(15)-C(16)-C(5)	-67.15(11)	N(4)-C(5)-C(16)-C(17)	135.38(9)
C(6)-C(5)-C(16)-C(17)	-102.04(11)	N(4)-C(5)-C(16)-C(15)	12.47(12)
C(6)-C(5)-C(16)-C(15)	135.05(10)	C(15)-C(16)-C(17)-O(18)	-62.10(13)
C(5)-C(16)-C(17)-O(18)	177.19(10)	C(19)-C(20)-C(21)-C(15)	0.8(2)
C(19)-C(20)-C(21)-C(22)	-175.55(14)	C(14)-C(15)-C(21)-C(20)	-120.57(14)
C(16)-C(15)-C(21)-C(20)	122.61(13)	C(14)-C(15)-C(21)-C(22)	56.12(12)
C(16)-C(15)-C(21)-C(22)	-60.71(12)	C(5)-N(4)-C(22)-C(21)	56.56(11)
C(3)-N(4)-C(22)-C(21)	-62.36(11)	C(20)-C(21)-C(22)-N(4)	-176.72(11)
C(15)-C(21)-C(22)-N(4)	6.34(13)		

Table 14. Hydrogen bonds for **110** [Å and °].

D-H...A	d(D-H)	d(H...A)	d(D...A)	<(DHA)
N(1)-H(1A)...O(1S)	0.88	2.02	2.8717(13)	163.7
O(6)-H(6B)...N(4)#1	0.84	1.92	2.7569(12)	172.2
O(18)-H(18A)...O(1S)#2	0.84	2.05	2.8593(15)	162.8
O(1S)-H(1S)...O(2S)#3	0.84	1.81	2.6472(15)	173.4
O(2S)-H(2S)...O(6)	0.8402(10)	1.880(3)	2.6783(13)	158.3(7)

Symmetry transformations used to generate equivalent atoms:

#1 $x+1/2, -y+3/2, -z$ #2 $x+1, y, z$ #3 $x-1, y, z$

IV. Appendix II: Data on QH-II-066

In vivo and *in vitro* profiles of the GABA_A/α5-preferring agonist QH-ii-066 and the non-selective agonist diazepam

Snjezana Lelas¹, Kenneth W. Rohrbach¹, Susan Glick¹, Kim L. Zeller¹, Clotilde Bourin¹, Kristine K. Sieracki¹, Robert L. Bertekap¹, Qi Huang², Catherine Cook³, Fred Helmstetter³, Xiaoyan Li², Sundari K. Rallapalli², Ryan Westphal¹, Mark D. Lindner¹, Svetlana M. Tertyshnikova¹, James M. Cook², and John F. McElroy¹

¹Discovery Neuroscience, Bristol-Myers Squibb Company, Wallingford, CT, ² Department of Chemistry and ³ Department of Psychology, University of Wisconsin, Milwaukee, WI

Correspondence to: Snjezana Lelas, D.Phil., Bristol-Myers Squibb Company, PO Box 5100, 5 Research Parkway 3CD/355D, Wallingford, CT 06492, phone (203) 677-7441, fax (203) 677-7569, e-mail: snjezana.lelas@bms.com

ABSTRACT

In order to investigate the possible role of GABA_A/α5 receptors in behavioral effects of benzodiazepines (BZ), the effects of QH-ii-066, the GABA_A/α5-preferring agonist, were compared with diazepam in binding and electrophysiology assays and behavioral models of anxiety, epilepsy, and side effects (activity, motor coordination, and subjective effects). QH-ii-066, while having similar affinity for BZ-sensitive GABA_A receptor subtypes, showed functional selectivity for GABA_A/α5 receptors over GABA_A/α1 receptors. QH-ii-066 increased punished responding in the Geller conflict test in rats and protected against pentylenetetrazole (PTZ)-induced seizures in mice at doses similar to those of diazepam, but was less potent than diazepam in protecting against electroconvulsive shock (ECS)-induced seizures, suggesting that GABA_A/α1 receptors may play a bigger role in ECS- than PTZ-induced seizures. QH-ii-066 showed a larger separation between doses effective in the conflict model and those effective in the conditioned fear, locomotor activity, rotorod, and chlordiazepoxide drug discrimination. In the case of locomotor activity and chlordiazepoxide drug discrimination, the decreased potency of QH-ii-066 compared with diazepam indicate that GABA_A/α1 receptors play a more prominent role in sedative and chlordiazepoxide-like subjective effects of BZs. These data suggest that compounds like QH-ii-066 with reduced efficacy at GABA_A/α1 receptors may be effective anxiolytics with a reduced potential for side effects.

Although benzodiazepines (BZ) are the most frequently prescribed anxiolytics, their use is accompanied by significant side effects, most notably, sedation, ataxia, memory impairment, potentiation of their effects by ethanol, development of tolerance and dependence, and abuse liability. Efforts to discover anxiolytics with reduced side effect profiles have centered on two types of compounds, those acting by a different mechanism (e.g., 5-HT_{1A} receptor agonists and CRF₁ receptor antagonists) and BZ-like compounds showing functional selectivity, i.e., acting with high efficacy at some GABA_A receptors and with low or no efficacy on other GABA_A receptors. The latter approach assumes that the therapeutic and adverse effects of classical BZs are mediated by different GABA_A receptors and that reducing binding affinity and/or efficacy at receptors mediating adverse effects will result in a superior anxiolytic compared with classical BZs.

Zolpidem and zaleplon, two compounds with selectivity for GABA_A/α1 receptors, decrease sleep latency and increase sleep duration (e.g., Fry et al., 2000) and are marketed for treatment of insomnia. In addition, recent studies with transgenic mice and GABA_A receptor-selective compounds have indicated that GABA_A/α1 receptors mediate sedative/ataxic effects of classical BZs (Rudolph et al., 1999; McKernan et al., 2000; Kralic et al., 2002).

The role of other BZ-sensitive GABA_A receptors, containing α2, α3, or α5 subunits, in the behavioral effects of classical BZs is less clear. Mice with a point mutation rendering GABA_A/α2 receptors insensitive to diazepam (GABA_A/α2 receptor knock-in mice) do not exhibit anxiolytic or myorelaxant effects when treated with diazepam, whereas GABA_A/α3 receptor knock-in mice showed a normal anxiolytic response to diazepam, with reduced myorelaxant effects (Lów et al., 2000; Crestani et al., 2001). However, selective GABA_A/α3 receptor inverse agonists appear to be anxiogenic (Collins et al., 2002), indicating that GABA_A/α3 receptors may be involved in anxiolytic effects of BZs. In addition, compounds with higher intrinsic efficacy at GABA_A/α2 and GABA_A/α3 receptors, and lower or no efficacy at GABA_A/α1 and GABA_A/α5 receptors,

show anxiolytic and anticonvulsant effects in rodents (Griebel et al., 2001). These studies suggest that both GABA_A/α2 and GABA_A/α3 receptors may play a role in the anxiolytic effects of classical BZs. Thus, an ideal compound, an anxiolytic with reduced motoric side effect profile, would have no affinity or, at least, no efficacy at the GABA_A/α1 receptors and high affinity and high efficacy at GABA_A/α2 and GABA_A/α3 receptors.

The role of GABA_A/α5 receptors remains to be elucidated. Thus far, only one study used GABA_A/α5 receptor knock-in mice to investigate the role of GABA_A/α5 receptors. Collinson et al. (2002) showed that these mice show no overt phenotype: their baseline anxiety-related response, as measured by elevated plus maze, did not differ from those of wild-type mice, they showed no spontaneous seizures, no impairment in rotorod performance, and normal anxiolytic-like responses to chlordiazepoxide (CDP). These animals did show faster learning of a Morris water maze task, suggesting that GABA_A/α5 receptors may play a role in the memory-impairing effects of classical BZs. This result is consistent with the finding that most GABA_A/α5 receptors are located in the hippocampus, a brain region shown to be involved in learning and memory. Furthermore, inverse agonists at this site show memory-enhancing effects in animals (Chambers et al., 2003), and some of these compounds also show anxiogenic and proconvulsant effects (Navarro et al., 2002).

As is the case with GABA_A/α2- and GABA_A/α3 receptor-selective compounds, studies with agonists selective for GABA_A/α5 receptors are scarce. QH-ii-066 (7-acetyleno-1,3-dihydro-1-methyl-5-phenyl-2H-1,4-benzodiazepin-2-one), a compound with 6-fold selectivity for GABA_A/α5 receptors compared with GABA_A/α2 and GABA_A/α3 receptors and 11-fold selectivity compared with GABA_A/α1 receptors (Huang et al., 2000), differs from classical BZs in that it did not share subjective effects with triazolam in squirrel monkeys (Lelas et al., 2002). Like classical BZs, QH-ii-066 protected against seizures induced by BZ inverse agonists DMCM and RY-24 (Skolnick et al., 1997).

The present studies were designed to compare the effects of QH-ii-066 and diazepam in an array of *in vitro* and *in vivo* assays. QH-ii-066 is a 7-acetyleno congener of diazepam (Figure 1) and thus, diazepam was chosen as the classical BZ for comparison. The two compounds were characterized in binding and electrophysiology functional assays (HEK whole-cell patch clamp) and in models of anxiety (conflict), pentylenetetrazole (PTZ)- and electroconvulsive shock (ECS)- induced seizures, learning and memory (conditioned fear), sedation (locomotor activity), ataxia (rotorod performance), and BZ-like subjective effects (CDP drug discrimination) in rodents. Differences observed between QH-ii-066 and diazepam in these assays would provide an indication of the potential contribution of GABA_A/α5 receptors to these effects of classical BZs.

METHODS

Subjects

All animals were maintained in accordance with the guidelines of the Committee on Animals of the Bristol-Myers Squibb Company and the “Guide for Care and Use of Laboratory Animals” (Institute of Animal Laboratory Resources, 1996). Research protocols were approved by the Bristol-Myers Squibb Company Institutional Animal Care and Use Committee.

Male CDF rats weighing approximately 350 g at the time of the experiment (conflict), male Sprague-Dawley rats weighing 180-300 g (locomotor activity, rotorod studies, and drug discrimination studies) and male CF1 mice weighing 20-22 g at the time of the experiment (seizure studies) were purchased from Charles River Laboratories (Wilmington, Mass., USA). For the conditioned fear studies, male Sprague-Dawley rats weighing approximately 225 g at the time of the experiment were purchased from Harlan (Indianapolis, Ind., USA). Animals were housed in pairs or fours in clear plastic shoebox cages with Beta Chip bedding in rooms maintained at constant temperature (21-23°C) and humidity (50 ± 10%) with a 12 h light/dark cycle (lights on at 0600 h, except for mice lights were on at 0500 h), except for the drug discrimination study for which animals were housed individually in suspended wire cages.

Animals had *ad libitum* access to food and water throughout the studies, except for the conflict and drug discrimination studies in which animals were restricted to 9 g (conflict) or 12 g (drug discrimination) of laboratory rodent chow (Bio-Serv, Frenchtown, NJ) per day in addition to the food earned in operant box, with unlimited access to water. All training and testing was done between 0600 and 1300 h Monday through Friday of each week.

Procedures

GABA_A Binding Assay

HEK293 cells were trypsinized and counted. Cells were transfected using the Amaxa electroporator and 3 million cells per sample. Each transfection was performed in Amaxa solution “V” using electroporation program Q-01 (Amaxa Inc., Gaithersburg, Md., USA). 1 μ g of each GABA subunit (α , β , and γ) was used per transfection. Following electroporation, cells were plated onto poly-lysine coated glass coverslips and used for the experiments.

Electrophysiological Studies

Whole-cell patch-clamp experiments were performed using HEK cell lines transiently expressing two different configurations of GABA_A constructs, on the first or second day after the transfection. Cells were plated onto 25 mm Petri dishes and viewed using Nikon TE200 inverted microscope, equipped with the mercury lamp to monitor GFP fluorescence. Cells were continuously perfused with extracellular physiological solution containing (in mM): NaCl 140, KCl 2.5, CaCl₂ 2, MgSO₄ 2, Na₂HPO₄ 1.25, HEPES 10, Glucose 11, pH 7.4 and 340 mOsm (modified from Brown et al., 2002). Patch pipettes were pulled using Narishige vertical puller from fire-polished borosilicate glass capillaries. Pipette resistance was between 3.5 and 6 M Ω . The intracellular solution contained (in mM): CsCl 140, HEPES 10, EGTA 5, MgATP 2, MgCl₂ 3, pH 7.3 and 340 mOsm.

Cells were voltage-clamped at -20 mV via an EPC10 amplifier (HEKA Electronics, Southboro, Mass.). Preliminary experiments have shown that amplitude of the GABA-induced current in these cells was not significantly different at -60, -40 or -20 mV holding potentials. At the same time, -20 mV holding potential facilitated longer experimental time which enabled testing of several concentrations of the test compounds. Drug solutions were applied to the cells via a multi-channel local perfusion system

(AutoMate Scientific, Inc., San Francisco, Calif.) with the estimated solution change time of 20 ms.

GABA was applied to the cell for 20 s with a 60 s washout period between applications, which was found to be a sufficient time period to reverse any desensitization that may occur. In addition, to ensure that there is no desensitization that may affect GABA responses at any given concentration of a GABA modulator, GABA was applied twice during control (no drug) and once at each concentration of the test compound. Test compounds were applied in increasing concentrations (1, 10, 100, or 1000 nM) 60 s prior to GABA (3 μ M) applications.

Geller Conflict with Incremental Shock in Rats

Experiments were conducted in 8 model E10-10 Coulbourn operant chambers (Coulbourn Instruments, Allentown, Penn., USA; 28 x 26 x 31 cm) with an electrified grid floor which were housed in light-proof, sound-attenuated, and fan-ventilated chambers. On one wall of each operant chamber was a houselight and a centrally placed food hopper 3 cm from the floor that delivered one 45-mg food pellet (Dustless Precision Pellets, Bio-Serv, Frenchtown, N.J., USA). To the left was mounted a lever response module with cue lights above. Foot-shock was delivered using an H13-16 Universal Shocker. Experiments were controlled with a Compaq DeskPro computer running Graphic State Notation software through Habitest Universal Linc interface equipment (Coulbourn Instruments).

Rats were trained to stability on an alternating multiple Random Interval 30 s/Fixed Ratio 1 Food +Shock paradigm (RI15/FR1 F+S). The paradigm ran through four cycles beginning with the Random Interval (RI) schedule which ran for 12 minutes then switched to the Fixed Ratio (FR) schedule which was cued and ran for 3 minutes. The RI had a range of 15 to 45 s with the food pellet being delivered with the first lever press after the expiration of the interval. The FR schedule delivered a food pellet after each lever press along with a foot-shock that increased with each lever press beginning at zero on the first lever press then increasing to 0.05 mA on the second lever press and incrementing by

0.05 mA with each subsequent lever press. The shock was reset to zero at the beginning of each RI/FR cycle.

Protection against Pentylenetetrazole- and Shock-Induced Seizures in Mice

Pentylenetetrazole (PTZ) was administered at 125 mg/kg s.c. The number of animals surviving was recorded at 30 minutes and 60 minutes after administration of PTZ. Electroshock is administered using a Ugo Basile ECT, Unit 7801 seizure apparatus (Ugo Basile, Italy) and corneal electrodes soaked in 0.9% saline. Mice received a shock of 30 mA for 0.3 s. The number of animals that exhibited the hind-limb extensor component of the seizure was recorded.

Conditioned Fear in Rats

Experiments were conducted in standard modular test chambers (ENV-008, Med Associates, St. Albans, Vt., USA, 30.5 x 24.1 x 21 cm) with an electrified grid floor which were housed in light-proof, sound-attenuated, and fan-ventilated chambers. Foot-shock was delivered using a shocker/scrambler module (ENV-414). Experiments were controlled with a desktop computer using Med-PC software through Smart Ctrl™ interface equipment (Med-Associates).

On day 1, rats were placed in the test chambers for a 7-minute conditioning session consisting of 2.5 minutes of habituation, a 2-s foot-shock at 0.7 mA, followed by 2.5 minutes of no foot-shock, another 2-s, 0.7 mA foot-shock, and another 2 minutes with no foot-shock. Twenty-four hours after the conditioning session, rats were placed in the test chamber again for 7 minutes with no foot-shocks and percent time freezing was quantified by video image analysis (Freezeview software using filter 25 and bout length of 0.75 s; Actimetrics and Coulbourn Instruments, Allentown, Penn., USA).

Spontaneous Locomotor Activity in Rats

The testing apparatus consisted of Plexiglas chambers (42 x 42 x 30 cm) equipped with Digiscan activity monitors (Omnitech Electronics, Columbus, Ohio, USA) that detect interruptions of eight photobeams spaced 5 cm apart and 2.5 cm above the floor.

Horizontal activity was recorded in 5-minute bins for a total of 60 minutes and expressed as total distance covered (in cm).

Rotorod Performance in Rats

The degree of motor coordination or balance was determined using a standard accelerating rotorod treadmill (Ugo Basile, Comerio-Varese, Italy) that was 6 cm in diameter and 24 cm above the base. The speed was increased gradually from 2 rpm to a maximum speed of 20 rpm. The time each animal remained on the rotating rod was automatically recorded, up to a maximum of 5 minutes. Three acclimation trials were conducted for each animal prior to administration of drugs. The time on rotorod from the third trial was used to counterbalance animals for subsequent drug testing.

Chlordiazepoxide Discrimination in Rats

Twelve model E10-10 Coulbourn operant conditioning chambers (Coulbourn Instruments, Allentown, Penn., USA; 28 x 26 x 31 cm) were housed in light-proof, sound-attenuated, and fan-ventilated chambers. Each operant conditioning chamber was equipped with two non-retractable levers, requiring a downward force equivalent to 15 g (0.15 N), that were mounted 3 cm from the side wall, 3 cm above the metal grid floor, and 5 cm from a centrally placed food tray that delivered one 45-mg food pellet (Dustless Precision Pellets, Bio-Serv, Frenchtown, N.J.). The experimental chambers were connected to a Micro PDP11/73 computer using a LAB LINC interface. A SKED-11 operating system (State System, Kalamazoo, Mich.) was used to record and control behavior.

After habituation to the operant conditioning chamber, rats were trained to alternate daily between response levers on an FR 1 schedule of food reinforcement. Once lever pressing was well established, the reinforcement contingency was increased incrementally to an FR 10 schedule of food reinforcement, while maintaining the lever alternation. Rats were then trained to discriminate between an intraperitoneal (IP) injection of drug (5.0 mg/kg CDP) and vehicle (0.25% methylcellulose) administered 30

minutes prior to the start of the session. Ten consecutive responses on the injection-appropriate lever resulted in food delivery. Responses on the incorrect lever did not result in pellet delivery. Following an injection of CDP, responding on the right lever was reinforced for half the rats and responding on the left lever was reinforced for the other rats. In each two-week period there were five drug days and five saline days, with the constraint that there not be more than three consecutive drug or vehicle days.

Drug test sessions were conducted once a week (Fridays) with training sessions scheduled on intervening days (Monday – Thursday). The criterion for testing was achieved if no more than three incorrect responses occurred prior to the first reinforcer for at least 9 out of 10 consecutive sessions. During test sessions, the lever on which the rat first made 10 consecutive responses resulting in delivery of the first food pellet was designated the “selected “ lever and subsequent pellet delivery was made contingent on responding on this selected lever on an FR10 schedule. The selected lever, the number of responses prior to the first food pellet delivery, and the total number of responses in the session were recorded for each rat. The duration of test sessions was ten minutes. Dose-response functions were determined for CDP, diazepam, and QH-ii-066.

Drugs

GABA, diazepam, PTZ, and CDP HCl were purchased from Sigma (St. Louis, Mo., USA). QH-ii-066 was synthesized by Xiaoyan Li, Wenyuan Yin, and Dongmei Han at the University of Wisconsin. Compounds were prepared as suspensions in an aqueous vehicle of 0.25% methylcellulose (Type A15c, Dow Chemicals), except for diazepam in the conditioned fear study which was prepared in 40% propylene glycol / 10% ethanol / 50% benzoic acid solution. Stock suspensions were bead-milled overnight using three layers of 4-mm glass beads. Dilutions were made using the 0.25% methylcellulose vehicle. Compounds were administered orally by gavage (PO) 60 minutes before

behavioral testing in a volume of 2 ml/kg body weight. Doses of all drugs were calculated and are expressed in terms of the free base weight.

Data Analysis

In the electrophysiology experiments, the amplitude of the I_{GABA} in each cell was normalized to I_{GABA} produced by 3 μ M GABA in the absence of drug in the same cell. Data (% increase of I_{GABA}) from 3-6 cells for each concentration were averaged and concentration-response curves for each test compound were constructed using ExcelFit. All data are presented as mean \pm 1 SEM.

Results for conflict, locomotor activity, and rotorod performance are expressed as the mean \pm 1 SEM. Results for the PTZ- and ECS-induced seizures are presented as the percent of animals protected from death and percent of animals protected from the hind-limb extensor component of the seizure, respectively. Results for the drug discrimination study are expressed as the percent of animals selecting the CDP-appropriate lever. A drug was considered to substitute fully for CDP if 75% of the animals selected the CDP-appropriate lever. Response rates were expressed as percentage of control rate (average of the vehicle training session immediately before and the vehicle session immediately after the test) for individual animals, averaged across animals, and plotted as a function of dose (mean \pm 1 SEM). All data were subjected to analysis of variance (ANOVA) followed by individual mean comparisons using Fisher's Least Significant Difference Test (Kirk, 1968) where appropriate. The significance level was set at $P < 0.05$. ED_{50} values were calculated by linear regression.

RESULTS

GABA_A Binding Assay

Binding affinities of QH-ii-066 and diazepam at different rat GABA_A receptor subtypes are shown in Table 1. QH-ii-066 showed similar affinity for the six rat GABA_A receptors examined (range of $K_i = 40\text{-}72$ nM). Similarly, diazepam showed comparable binding affinity at all GABA_A receptor subtypes studied (range of K_i values was 20-28 nM). QH-ii-066 had a 2- to 3-fold lower affinity than diazepam at the six receptors studied.

Electrophysiological Studies

Application of GABA resulted in a dose-dependent increase in Cl⁻ currents in GABA_A/α1β2γ2 and GABA_A/α5β2γ2 receptors transiently expressed in HEK cells (data not shown). The EC₅₀ value for GABA was 7.55±0.58. Diazepam and QH-ii-066 both potentiated GABA-induced Cl⁻ currents at both GABA_A/α1β2γ2 and GABA_A/α5β2γ2 receptors in a concentration-dependent manner (Figure 2). At the GABA_A/α1β2γ2 receptors, maximum potentiation of I_{GABA} by diazepam occurred at 1 μM and reached 389% of control, whereas maximum potentiation of I_{GABA} by QH-ii-066 occurred at 100 nM and reached only 200% (at 1 μM, the potentiation of I_{GABA} by QH-ii-066 reached 180% of control). In contrast, at the GABA_A/α5β2γ2 receptors, maximum potentiation of I_{GABA} by diazepam and QH-ii-066 occurred at the same concentration (1 μM) and reached similar levels (282% and 289% of control, respectively).

Geller Conflict with Incremental Shock in Rats

Diazepam and QH-ii-066 increased punished responding without altering the rate of responding in the unpunished component (Figure 3). Diazepam significantly increased responding in the punished component to 178% of control at the dose of 3.0 mg/kg PO [F(3,21)=3.38, $P=0.04$]. QH-ii-066 significantly increased punished responding to 149% of control at the dose of 10 mg/kg PO [F(3,15)=3.7, $P=0.04$]. Thus, QH-ii-066 is 3-fold less potent than diazepam in increasing punished responding in rats. The doses of

diazepam and QH-ii-066 that produced a significant increase in punished responding did not alter rates of responding in the punished component [$F(3,21)=1.72$, $P=0.19$ for diazepam; $F(3,15)=3.14$, $P=0.06$ for QH-ii-066].

Protection from Pentylentetrazole- and Shock-Induced Seizures in Mice

Diazepam and QH-ii-066 both fully protected against both PTZ- (at 1.0 and 10 mg/kg PO, respectively) and ECS- (10 and 100 mg/kg PO, respectively) induced seizures in mice (Figure 4). The ED_{50} values for the protective effects of diazepam and QH-ii-066 are 0.27 mg/kg and <3 mg/kg against PTZ-induced seizures, respectively. The ED_{50} values for the protective effects of diazepam and QH-ii-066 are 0.88 mg/kg and 18.57 mg/kg against ECS-induced seizures, respectively. Thus, QH-ii-066 is approximately 11-fold and 21-fold less potent in protecting against PTZ- and ECS-induced seizures, respectively, than diazepam. Both compounds are more potent in protecting against PTZ- than ECS-induced seizures, 3-fold more potent in the case of diazepam and more than 6-fold more potent in the case of QH-ii-066.

Conditioned Fear in Rats

For both diazepam and QH-ii-066 experiments, vehicle-treated rats showed an increase in freezing observed on test day (day 2) compared with animals who did not receive shock (diazepam study: $F(1,95)=19.88$, $P<0.0001$; QH-ii-066 study: $F(1,95)=13.27$, $P<0.0004$). Diazepam significantly decreased freezing on test day relative to the vehicle-treated group (Figure 5, left panel). A dose of diazepam comparable to that which was effective in the conflict model (2.5 mg/kg) decreased percent freezing by 44% ($F(1,95)=6.46$, $P=0.01$) and a higher dose (5.0 mg/kg) also significantly decreased percent freezing by 39% ($F(1,95)=5.11$, $P=0.03$). Unlike diazepam, QH-ii-066 did not alter freezing on test day relative to the vehicle-treated group at doses up to and including 10 mg/kg (Figure 5, right panel; $F(1,95)=0.5$, $P=0.48$), the lowest effective dose in the conflict model.

Spontaneous Locomotor Activity in Rats

Diazepam and QH-ii-066 dose-dependently decreased spontaneous locomotor activity recorded 60-120 minutes after oral administration (corresponding to the 60-min pretreatment time and 60-min test duration in the conflict test) [diazepam $F(5,42)=16.66$, $P<0.0001$, Figure 6, left panel; QH-ii-066 $F(6,49)=4.17$, $P=0.002$, Figure 6, right panel]. The lowest effective dose of diazepam in the conflict model (3.0 mg/kg) did not alter locomotor activity; however, a 3-fold higher dose (10 mg/kg) resulted in a significant reduction of locomotor activity (by 34%, $P=0.001$), as did the doses of 30 and 100 mg/kg (38%, $P=0.0004$ and 75%, $P<0.0001$, respectively). In comparison, the lowest effective dose of QH-ii-066 in the conflict model (10 mg/kg) also did not alter locomotor activity; however, a 10-fold higher dose (100 mg/kg) resulted in a significant decrease in locomotor activity (by 49%; $P=0.04$).

Rotorod Performance in Rats

Diazepam dose-dependently decreased motor coordination in rats as measured by time on rotorod [$F(3,28)=5.43$, $P<0.005$, Figure 7, left panel]. The dose of 100 mg/kg of diazepam resulted in a significant decrease in time on rotorod to 72% of control ($P=0.001$). The dose of 3.0 mg/kg of diazepam, the lowest effective dose of diazepam in the conflict model, did not alter the time on rotorod ($P=0.84$); thus, the difference between the lowest effective dose of diazepam in the conflict model compared with rotorod performance is 33-fold.

Unlike diazepam, QH-ii-066 did not alter time on rotorod in rats up to 100 mg/kg [$F(3,27)=1.0$, $P=0.41$, Figure 7, right panel]. The lowest effective dose of QH-ii-066 in the conflict model (10 mg/kg) did not alter rotorod performance ($P=0.96$) and neither did the highest dose of QH-ii-066 tested (100 mg/kg, $P=0.44$). Thus, the difference between the lowest effective dose of QH-ii-066 in the conflict model compared with rotorod performance is greater than 10-fold.

Chlordiazepoxide Discrimination in Rats

All rats acquired stimulus control with the training dose of CDP of 5.0 mg/kg (IP, administered 30 minutes before session). These data were reported by Lelas et al. (2003). Briefly, the mean response rates (responses/min \pm SEM) for vehicle and CDP were 67.1 ± 8.5 and 91.7 ± 9.8 , respectively. The ED₅₀ value for CDP was 1.7 mg/kg. All three doses of CDP significantly increased response rates relative to vehicle control rates.

Both diazepam and QH-ii-066 dose-dependently increased the percent of rats selecting the CDP lever (Figure 8). At the lowest effective dose of diazepam in the conflict model (3.0 mg/kg) 86% of animals selected the CDP lever, and at 10 mg/kg 100% of animals selected the CDP lever. The ED₅₀ value for diazepam is 2.82 mg/kg. In comparison, the lowest effective dose of QH-ii-066 in the conflict model (10 mg/kg) resulted in 63% of animals selecting the CDP lever, and at 30 mg/kg 100% of animals selected the CDP lever. The ED₅₀ value for QH-ii-066 is 8.56 mg/kg. Thus, in the case of diazepam, there is no separation between the doses effective in the conflict model and those resulting in CDP-lever selection, whereas for QH-ii-066 this separation is 3-fold.

Diazepam increased mean response rates, expressed as percent of control, at 5.0 mg/kg to 158% of control [$t(6)=2.69$, $P=0.04$], but did not alter rates of responding at the lower (1.0 mg/kg) or the higher (10 mg/kg) dose tested. The highest dose of QH-ii-066 tested (30 mg/kg) decreased response rates to 77% of control [$t(8)=2.38$, $P=0.04$].

DISCUSSION

The purpose of the present studies was to compare the *in vitro* and *in vivo* profiles of diazepam, a non-selective classical BZ agonist, and QH-ii-066, a 7-acetyleno congener of diazepam. In contrast to the previously published data (Huang et al., 2000), the present study showed that QH-ii-066 did not bind selectively to any GABA_A receptor subtype. Affinity of QH-ii-066 at GABA_A/α1, GABA_A/α2, GABA_A/α3, and GABA_A/α5 receptors was similar, ranging between 40 and 72 nM. Binding affinity of QH-ii-066 and diazepam at the GABA_A/α1 and GABA_A/α5 receptors was similar in the presence of either β2 or β3 subunits. In the previous publication (Huang et al., 2000), QH-ii-066 showed a 6-fold selectivity for GABA_A/α5 over GABA_A/α2 and GABA_A/α3 receptors and 11-fold selectivity over GABA_A/α1 receptors. Thus, the difference in binding affinity for the GABA_A/α5 receptors between the two studies is 6-fold. It is possible that this discrepancy is due to the fact that the Huang et al. (2000) study used cells expressing human GABA receptors, whereas the present study used rat GABA receptors. When compared with diazepam, binding data from the present study show that the 7-acetyleno congener of diazepam exhibits approximately 2-fold lower affinity for all BZ-sensitive GABA_A receptor subtypes.

In contrast to the binding data, electrophysiology studies showed a functional selectivity of QH-ii-066 compared with diazepam. The intrinsic efficacy of QH-ii-066 at the GABA_A/α5 receptor was similar to the efficacy of diazepam, as measured by potentiation of GABA-induced Cl⁻ currents in HEK cells transiently expressing GABA_A/α5 receptors. However, QH-ii-066 was approximately half as efficacious as diazepam in HEK cells transiently expressing GABA_A/α1 receptors. Thus, while QH-ii-066 did not show binding selectivity, it did exhibit functional selectivity, with diazepam-like efficacy at GABA_A/α5 receptors and partial efficacy at GABA_A/α1 receptors.

In vivo, the effects of QH-ii-066 and diazepam were compared directly in behavioral models of anxiety, epilepsy, and side effects (sedation, motor incoordination,

and subjective effects). QH-ii-066 and diazepam administered orally significantly increased punished responding in the Geller conflict test with incremental shock, an index of anxiolytic-like activity in rats. QH-ii-066 was 3-fold less potent in this model compared with diazepam. This loss of potency could be accounted for by lower affinity of QH-ii-066 at all BZ-sensitive GABA_A receptors. The present data suggest that QH-ii-066 retained anxiolytic-like activity despite loss of efficacy at the GABA_A/α1 receptors. These data support the conclusion from studies using the GABA_A/α1 receptor knock-out or knock-in mice showing normal anxiolytic-like response to diazepam in these animals (Kralic et al., 2002; Rudolph et al., 1999; McKernan et al., 2000), suggesting that GABA_A/α1 receptors do not play an important role in the anxiolytic effects of BZs. While efficacy of QH-ii-066 at the GABA_A/α2 or GABA_A/α3 receptors was not investigated in the present study, the similar effects of QH-ii-066 and diazepam in the conflict model suggest that QH-ii-066 retained diazepam-like intrinsic efficacy at these receptors.

In addition to the anxiolytic-like effects, QH-ii-066 and diazepam also showed protective effects against PTZ- and ECS-induced seizures. Diazepam was 3-fold less potent in protecting against ECS-induced seizures compared with PTZ-induced seizures; this difference was increased to 6-fold in the case of QH-ii-066. When the two compounds are compared in potency in protecting against each type of seizures, diazepam was 11-fold more potent than QH-ii-066 in protecting against PTZ-induced seizures and 21-fold more potent against ECS-induced seizures. Thus, it appears that the 7-acetyleno substituted diazepam analog QH-ii-066 showed a greater loss of potency in protecting against ECS-induced seizures relative to diazepam than against PTZ-induced seizures. These data may suggest that GABA_A/α1 receptors play a more prominent role in the ECS-induced seizures than in PTZ-induced seizures. SL651498, a compound with lower efficacy at GABA_A/α1 receptors (Griebel et al., 2001), and bretazenil, a low-efficacy agonist at many GABA_A subtypes including GABA_A/α1 receptors (Martin et al., 1988), were also more potent in reversing PTZ- than ECS-induced seizures. In addition, Griebel

et al. (1999) showed that β -CCT, an GABA_A/ α 1 receptor-preferring antagonist, did not alter protective effects of diazepam and zolpidem against PTZ-induced seizures, whereas it blocked the effects of the agonists against isoniazid-induced seizures. Taken together, these data suggest that PTZ-induced seizures are less dependent on the activity at the GABA_A/ α 1 receptors than ECS-induced seizures.

The conditioned fear model has been used to study “cognitive-affective” processes in anxiety disorders (e.g., Uys et al., 2003). In this model, animals are exposed to pairings of a neutral stimulus (conditioned stimulus (CS); e.g., tone or context) with an aversive stimulus (unconditioned stimulus (UCS); e.g., shock). Following acquisition, behaviors typically seen after the presentation of UCS (e.g., startle, freezing, or suppression of water-drinking) are now seen when the CS is presented alone. BZs reduced expression of UCS-appropriate behaviors in the presence of the CS (e.g., Davis, 1979; Sanger and Joly, 1985). The same effects are obtained following administration of scopolamine (e.g., Rudy, 1996; Lindner et al., 2003), a memory-impairing agent without any anxiolytic-like activity, suggesting that the conditioned fear assay is more sensitive to memory-impairing rather than anxiolytic-like effects of BZs. In the present study, diazepam at the doses of 2.5 and 5.0 mg/kg PO resulted in a decrease in freezing, whereas QH-ii-066 did not affect freezing at the doses up to and including 10 mg/kg, PO. Thus, QH-ii-066 appears to be 2-fold less potent in producing memory deficits in the conditioned fear test. It has been suggested that GABA_A/ α 5 receptors mediate memory-impairing effects of BZs (e.g., Collinson et al., 2002). Our electrophysiology studies showed comparable efficacy of QH-ii-066 and diazepam in potentiating the GABA currents through the GABA_A/ α 5 receptors. The observed difference in potency in the conditioned fear assay could be due to lower affinity of QH-ii-066 at all GABA_A receptors studied. Therefore, higher doses of QH-ii-066 would need to be tested to determine if lower efficacy of QH-ii-066 at GABA_A/ α 1 receptors compared with diazepam would result in lower potential to produce memory deficits in animals. However, the present study indicates that QH-ii-066 may have a better

therapeutic index than diazepam with respect to memory impairment since the doses of diazepam effective in the conflict and conditioned fear models effects were, whereas QH-ii-066 showed at least a 3-fold separation between doses effective in these tests.

Effects of QH-ii-066 and diazepam on motoric behaviors were assessed using the locomotor activity assay as an index of sedative effects and the rotorod performance as an index of motor incoordination. QH-ii-066 was 10-fold less potent than diazepam in reducing locomotor activity and at least 3-fold less potent in reducing time on rotorod. These differences in potency to produce sedation and motor incoordination lead to a better therapeutic index for QH-ii-066 compared with diazepam, despite a 3-fold loss of potency in producing anxiolytic-like effects (Table 2). Thus, QH-ii-066 shows a 10-fold or greater separation between its effects on motoric behavior and its anxiolytic-like effects in rats. By comparison, diazepam showed only a 3-fold separation in dose between the sedative and anxiolytic-like effects and a better (33-fold) separation in dose between the ataxic and anxiolytic-like effects.

Since QH-ii-066 has only 2-fold lower affinity for the six GABA_A receptors compared with diazepam, the 10-fold loss of potency of QH-ii-066 in reducing locomotor activity suggests that diminished intrinsic efficacy of QH-ii-066 at the GABA_A/α1 receptors also contributed to its reduced potency in producing sedative effects. These data support studies with transgenic mice and GABA_A/α1-selective agonists in indicating that GABA_A/α1 receptors mediate sedative/ataxic effects of classical BZs (e.g., Rudolph et al., 1999; McKernan et al., 2000; Kralic et al., 2002; Fry et al., 2000).

Finally, effects of QH-ii-066 and diazepam were compared in animals trained to discriminate CDP. Drug discrimination may be used as an index of abuse liability when compounds of the same pharmacological class are compared. In the present studies, animals were trained to discriminate CDP, a classical BZ with no apparent receptor selectivity. Diazepam at 3.0 mg/kg and QH-ii-066 at 30 mg/kg fully substituted for CDP, suggesting that at some dose, both compounds produce CDP-like subjective effects. As

was the case for locomotor activity, lower affinity of QH-ii-066 at GABA_A receptors alone does not account entirely for the lower potency of QH-ii-066 compared with diazepam in substituting for CDP, suggesting that GABA_A/α1 receptors may be an important part of the CDP stimulus in rat drug discrimination. In addition, these data also suggest that compounds like QH-ii-066 with lower efficacy at GABA_A/α1 receptors may have reduced abuse liability compared with classical BZs.

In summary, QH-ii-066, the 7-acetyleno congener of diazepam, showed a 2-fold loss of affinity at all GABA_A receptors studied relative to diazepam. However, QH-ii-066 also showed a loss of efficacy at the GABA_A/α1 receptors compared with diazepam, while retaining diazepam-like efficacy at the GABA_A/α5 receptors. *In vivo*, QH-ii-066 showed anxiolytic-like and protective effects against PTZ-induced seizures in rodents at doses similar to those of diazepam. QH-ii-066 was less potent than diazepam in protecting against ECS-induced seizures, indicating that ECS-induced seizures are mediated by GABA_A/α1 receptors to a greater extent than PTZ-induced seizures. QH-ii-066 was also less potent than diazepam in reducing activity and in producing CDP-like subjective effects, suggesting that QH-ii-066 and other compounds with lower intrinsic efficacy at the GABA_A/α1 receptors may be effective anxiolytics in humans with a reduced potential for side effects.

Table 1.
Binding affinity of QH-ii-066 and diazepam for rat GABA_A receptors.

Compound	GABA _A Receptor K _i (nM)					
	α1β2γ2	α1β3γ2	α2β3γ2	α3β3γ2	α5β2γ2	α5β3γ2
QH-ii-066	52±3*	56±1***	51±2**	72±8**	44±1**	40±8***
Diazepam	18	20	20	28	22	20
Ratio ^a	2.9	2.8	2.6	2.6	2.0	2.0

* n=5 determinations

** n=3 determinations

*** n=2 determinations

^a Ratio of binding affinity, QH-ii-066:diazepam

Table 2.

Lowest effective doses (mg/kg) and therapeutic indices for QH-ii-066 and diazepam in behavioral models.

Assay	QH-ii-066	Diazepam	Ratio
Conflict	10	3.0	3-fold
Conditioned Fear	>10	2.5	>4-fold
Locomotor Activity (LMA)	100	10	10-fold
Rotorod	>100	100	≥3-fold
Chlordiazepoxide Drug Discrimination (DD)	30	3.0	10-fold
Conflict:LMA Ratio	10-fold	3-fold	
Conflict:Rotorod Ratio	>10	33-fold	
Conflict:DD Ratio	3-fold	0	

REFERENCES

Brown et al. (2002)

Chambers MS, Atack JR, Broughton HB, Collinson N, Cook S, Dawson GR, Hobbs SC, Marshall G, Maubach KA, Pillai GV, Reeve AJ, MacLeod AM (2003) Identification of a novel, selective GABA_A α 5 receptor inverse agonist which enhances cognition. *J Med Chem* 46:2227-2240.

Collins I, Moyes C, Davey WB, Rowley M, Bromidge FA, Quirk K, Atack JR, McKernan RM, Thompson SA, Wafford K, Dawson GR, Pike A, Sohal B, Tsou NN, Ball RG, Castro JL (2002) 3-Heteroaryl-2-pyridones: benzodiazepine site ligands with functional selectivity for alpha 2/alpha 3-subtypes of human GABA(A) receptor-ion channels. *J Med Chem* 45:1887-1900.

Collinson N, Kuenzi FM, Jarolimek W, Maubach KA, Cothliff R, Sur C, Smith A, Out FM, Howell O, Atack JR, McKernan RM, Seabrook GR, Dawson GR, Whiting PJ, Rosahl TW (2002) Enhanced learning and memory and altered GABAergic synaptic transmission in mice lacking the α 5 subunit of the GABA_A receptor. *J Neurosci* 22:5572-5580.

Crestani F, Löw K, Keist R, Mandelli M, Möhler H, Rudolph U (2001) Molecular targets for the myorelaxant action of diazepam. *Mol Pharmacol* 59:442-445.

Davis M (1979) Diazepam and flurazepam: effects on conditioned fear as measured with the potentiated startle paradigm. *Psychopharmacology* 62:1-7.

Fry J, Scharf M, Mangano R, Fujimori M (2000) Zaleplon improves sleep without producing rebound effects in outpatients with insomnia. Zaleplon Clinical Study Group. *Int Clin Psychopharmacol* 15:141-152.

Griebel G, Perrault G, Letang V, Granger P, Avenet P, Shoemaker H, Sanger DJ (1999) New evidence that the pharmacological effects of benzodiazepine receptor ligands can be associated with activities at different BZ (ω) receptor subtypes. *Psychopharmacology* 146:205-213.

Griebel G, Perrault G, Simiand J, Cohen C, Granger P, Decobert M, Francon D, Avenet P, Depoortere H, Tan S, Oblin A, Shoemaker H, Evanno Y, Sevrin M, George P, Scatton B (2001) SL651498: An anxiolytic compound with functional selectivity for α_2 - and α_3 -containing γ -aminobutyric acid_A (GABA_A) receptors. *J Pharmacol Exp Ther* 298:753-768.

Huang Q, He X, Ma C, Liu R, Yu S, Dayer CA, Wenger GR, McKernan R, Cook JM (2000) Pharmacophore/Receptor models for GABA_A/BzR subtypes ($\alpha_1\beta_3\gamma_2$, $\alpha_5\beta_3\gamma_2$, and $\alpha_6\beta_3\gamma_2$) via a comprehensive ligand-mapping approach. *J Med Chem* 43:71-95.

Institute of Laboratory Animal Resources, Commission on Life Sciences, National Research Council (1996) Guide for the Care and Use of Laboratory Animals, 7th edn. National Academy Press, Washington, DC

Kirk RE (1968) Experimental Design: Procedures for the Behavioral Sciences. Brooks/Cole, Belmont, Calif.

Kralic JE, O'Buckley TK, Khisti RT, Hodge CW, Homanics GE, Morrow AL (2002) GABA_A receptor alpha-1 subunit deletion alters receptor subtype assembly, pharmacological and behavioral responses to benzodiazepines and zolpidem. *Neuropharmacology* 43:685-694.

Lelas S, Rowlett JK, Spealman RD, Cook JM, Ma C, Li X, Yin W (2002) Role of GABA_A/benzodiazepine receptors containing $\alpha 1$ and $\alpha 5$ subunits in the discriminative stimulus effects of triazolam in squirrel monkeys. *Psychopharmacology* 161:180-188.

Lelas S, Zeller KL, Ward KA, McElroy JF (2003) The anxiolytic CRF₁ antagonist DMP696 fails to function as a discriminative stimulus and does not substitute for chlordiazepoxide in rats. *Psychopharmacology* 166:408-415.

Lindner MD, Hodges DB Jr, Hogan JB, Orié AF, Corsa JA, Barten DM, Polson C, Robertson BJ, Guss VL, Fillman KW, Starrett JE Jr, Gribkoff VK (2003) An assessment

of the effects of serotonin 6 (5-HT₆) receptor antagonists in rodent models of learning. *J Pharmacol Exp Ther* 307:682-691.

Löw K, Crestani F, Keist R, Benke D, Brünig I, Benson JA, Fritschy J-M, Rüllicke T, Bluethmann H, Möhler H, Rudolph U (2000) Molecular and neuronal substrate for the selective attenuation of anxiety. *Science* 290:131-134.

Martin JR, Pieri L, Bonetti EP, Schaffner R, Burkard WP, Cumin R, Haefely WE (1988) Ro 16-6028: a novel anxiolytic acting as a partial agonist at the benzodiazepine receptor. *Pharmacopsychiatry* 21:360-362.

McKernan RM, Rosahl TW, Reynolds DS, Sur C, Wafford KA, Atack JR, Farrar S, Myers J, Cook G, Ferris P, Garrett L, Bristow L, Marshall G, Macaulay A, Brown N, Howell O, Moore KW, Carling RW, Street LJ, Castro JL, Ragan CI, Dawson GR, Whiting PJ (2000) Sedative but not anxiolytic properties of benzodiazepines are mediated by the GABA_A receptor α 1 subtype. *Nature Neurosci* 3:587-530.

Navarro JF, Buron E, Martin-Lopez M (2002) Anxiogenic-like activity of L-655,708, a selective ligand for the benzodiazepine site of GABA_A receptors which contain the α 5 subunit, in the elevated plus maze. *Prog Neuropsychopharmacol Biol Psychiatry* 26:1389-1392.

Rudolph U, Crestani F, Benke D, Brünig I, Benson JA, Fritschy J-M, Martin JR, Bluethmann H, Möhler H (1999) Benzodiazepine actions mediated by specific γ -aminobutyric acid_A receptor subtypes. *Nature* 401:796-800.

Rudy JW (1996) Scopolamine administered before and after training impairs both contextual and auditory-cue fear conditioning. *Neurobiol Learn Mem* 65:73-81.

Sanger DJ, Joly D (1985) Anxiolytic drugs and the acquisition of conditioned fear in mice. *Psychopharmacology* 85:284-288.

Skolnick P, Hu RJ, Cook CM, Hurt SD, Trometer JD, Liu R, Huang Q, Cook JM (1997) [³H]RY-80: a high affinity, selective ligand for GABA_A receptors containing α 5 subunits. *J Pharmacol Exp Ther* 283:488-495.

Uys JD, Stein DJ, Daniels WM, Harvey BH (2003) Animal models of anxiety disorders. *Curr Psychiatry Rep* 5:274-281.

LEGENDS FOR FIGURES

Figure 1. Chemical structures of QH-ii-066 and diazepam.

Figure 2. Effects of diazepam and QH-ii-066 on GABA-induced Cl^- currents in two GABA_A constructs ($\alpha 1\beta 2\gamma 2$ and $\alpha 5\beta 2\gamma 2$). Abscissae: concentration (log, nM). Ordinates: Percent control (3 μM GABA without drug) I_{GABA} for $n=3-6$ cells per concentration.

Figure 3. Anxiolytic-like effects of diazepam and QH-ii-066 in the Geller conflict with incremental shock test in rats. Abscissae: dose (mg/kg). Ordinates: mean ($\pm\text{SEM}$) response rates expressed as percent of control rates (vehicle training days) for $n=6-8$ animals per dose. Diazepam and QH-ii-066 were administered in 0.25% methylcellulose PO, 60 minutes prior to testing. * $P<0.05$.

Figure 4. Effect of diazepam and QH-ii-066 on pentylenetetrazole- and electroconvulsive shock-induced seizures in mice. Abscissae: dose (mg/kg). Ordinates: percent animals protected for $n=12$ animals per dose. Diazepam and QH-ii-066 were administered in 0.25% methylcellulose PO, 60 minutes prior to testing.

Figure 5. Effect of diazepam and QH-ii-066 in conditioned fear test in rats. Abscissae: dose (mg/kg). Ordinates: mean ($\pm\text{SEM}$) percent time spent freezing for $n=16-24$ animals per dose. Diazepam and QH-ii-066 were administered in 0.25% methylcellulose PO, 60 minutes prior to behavioral testing. * $P<0.05$.

Figure 6. Effect of diazepam and QH-ii-066 on spontaneous locomotor activity in rats. Abscissae: dose (mg/kg). Ordinates: mean (\pm SEM) distance traveled (in cm) for $n=8$ animals per dose. Diazepam and QH-ii-066 were administered in 0.25% methylcellulose PO, 60 minutes prior to behavioral testing. * $P<0.05$.

Figure 7. Effect of diazepam and QH-ii-066 on motor coordination in the rotorod test in rats. Abscissae: dose (mg/kg). Ordinates: mean (\pm SEM) time on rotorod (in seconds) for $n=7-8$ animals per dose. Diazepam and QH-ii-066 were administered in 0.25% methylcellulose PO, 60 minutes prior to behavioral testing. * $P<0.05$.

Figure 8. Discriminative stimulus and rate-decreasing effects of chlordiazepoxide, diazepam, and QH-ii-066 in rats ($n=7-12$) discriminating between chlordiazepoxide and vehicle. Abscissae: dose (mg/kg). Ordinates: percent of rats selecting the chlordiazepoxide lever (upper panel) and mean response rates (\pm SEM) expressed as percent control rates (vehicle training days) (lower panel). Chlordiazepoxide was administered in 0.25% methylcellulose IP, 30 minutes before testing. Diazepam and QH-ii-066 were administered in 0.25% methylcellulose PO, 60 minutes prior to behavioral testing. * $P<0.05$. The dashed line in the upper panel refers to 75% of animals selecting the drug lever (criterion for substitution).

Figure 1

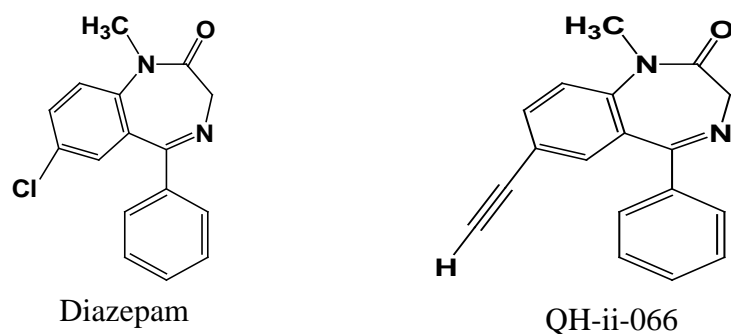


Figure 2 EP

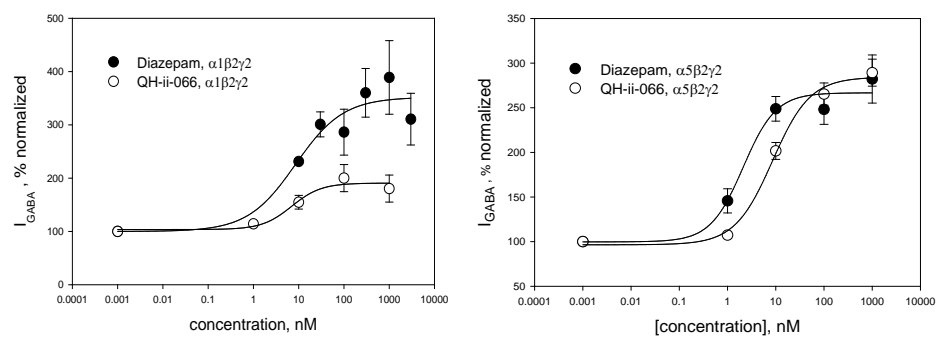


Figure 3 Conflict model with incremental shock (anxiety)

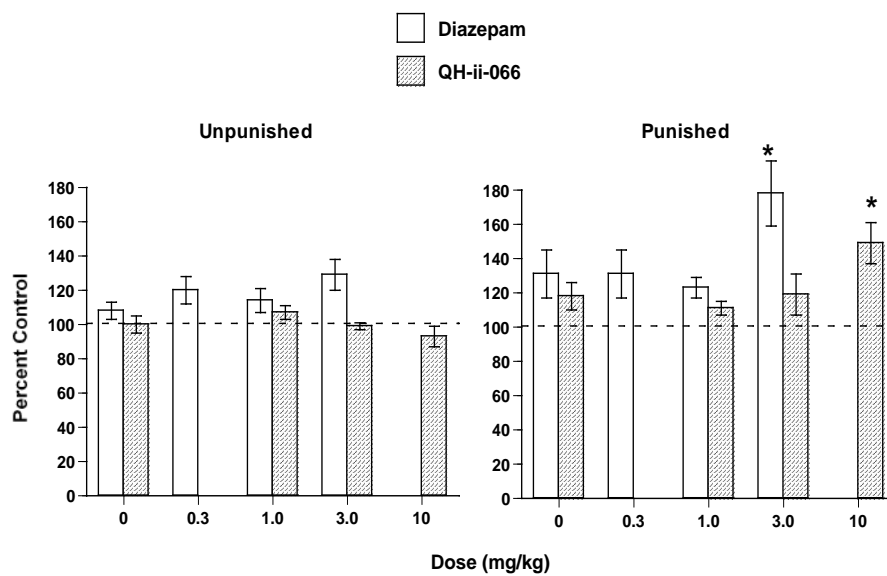


Figure 4 PTZ- and ECS-induced seizures

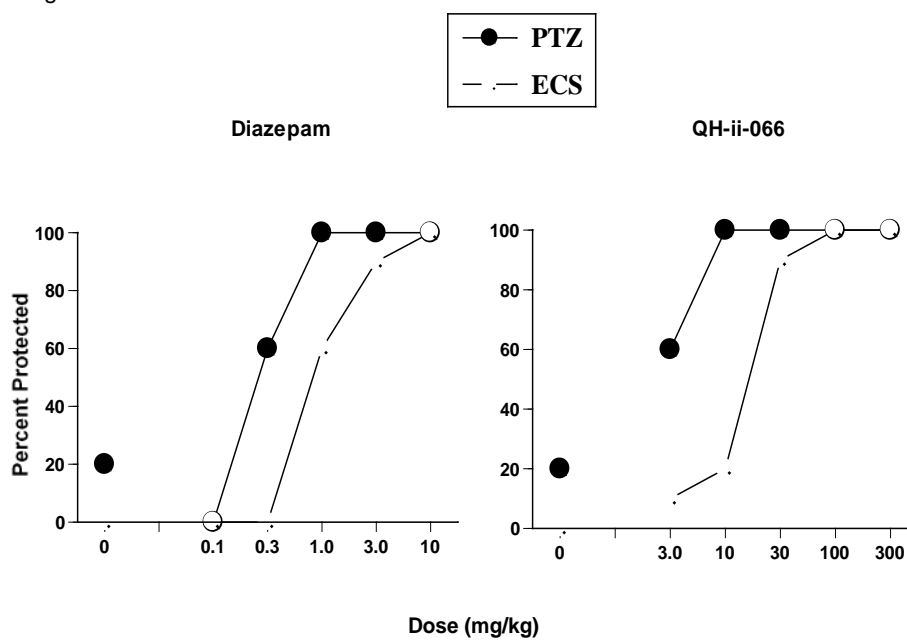


Figure 5 Conditioned fear model

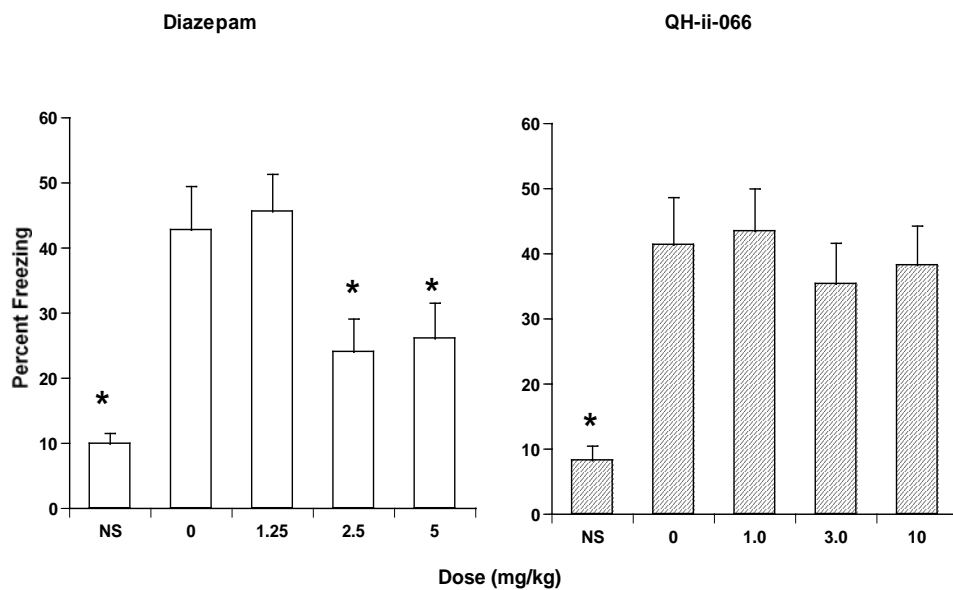


Figure 6 Locomotor activity (sedation)

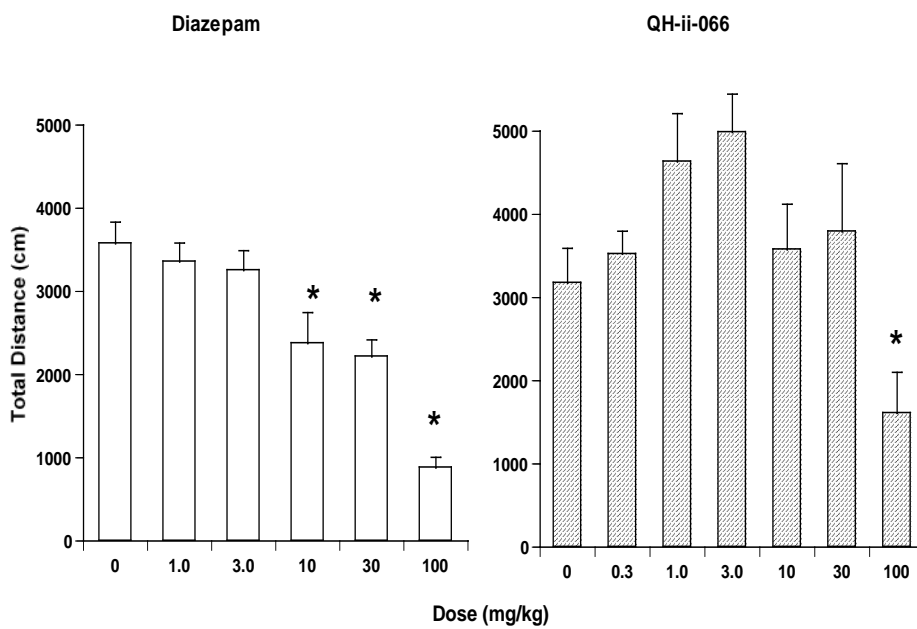


Figure 7 Rotorod performance (ataxia)

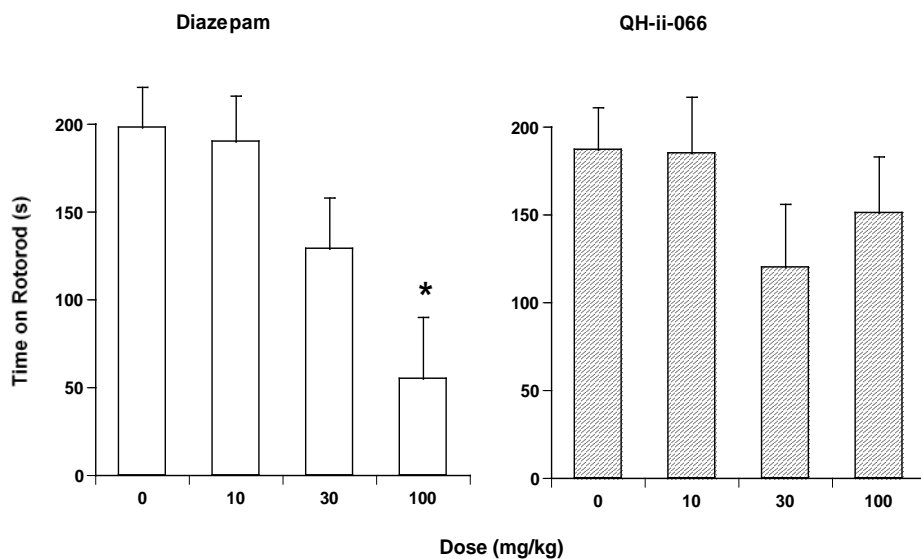
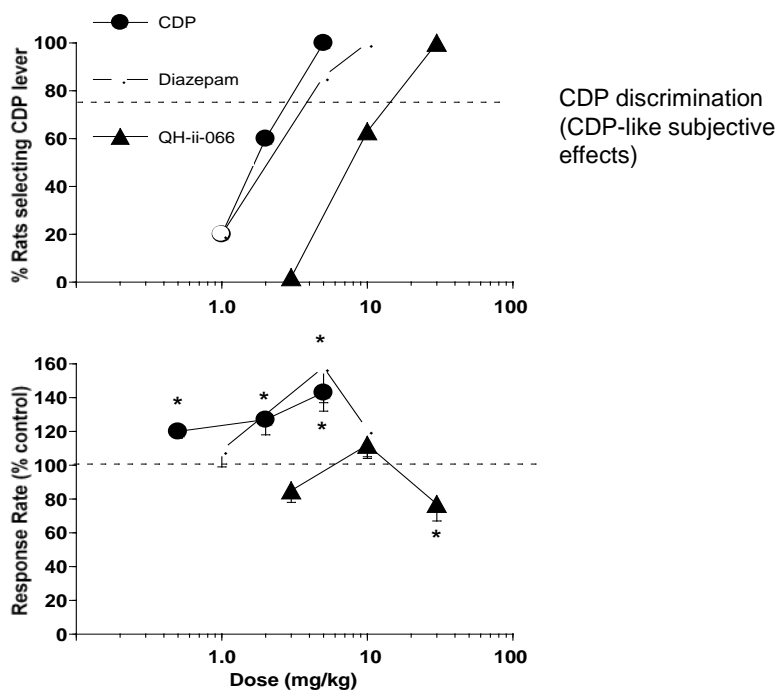


Figure 8



V. Appendix III: Data on QH-II-066

eQTL and receptor pharmacology implicate GABA signaling in neuroblastoma

Christopher S. Hackett^{1,2}, David A. Quigley³, QiWen Fan², Christine Cheng², Young K. Song⁴, Ludmila Pawlikowska^{5,6}, Justin Chen^{1,2}, Yun Bao², David D. Goldenberg², Kim Nguyen², Yoon Jae Cho¹³, Sundari K. Rallapalli¹⁴, James M. Cook¹⁴, Serguei Kozlov⁷, Jian-Hua Mao⁸, Terry Van Dyke⁷, Pui-Yan Kwok^{6,9,10}, Javed Khan⁴, Allan Balmain³, and William A. Weiss^{2,11,12,†}

¹Biomedical Sciences Graduate Program, Departments of ²Neurology, ³Helen Diller Family Comprehensive Cancer Center, ⁵Anesthesia, ⁶Institute for Human Genetics, ⁸Epidemiology and Biostatistics, ⁹Dermatology, ¹⁰Cardiovascular Research Institute, ¹¹Pediatrics, and ¹²Neurological Surgery, University of California, San Francisco, CA USA.

⁴Oncogenomics Section, Pediatric Oncology Branch, National Cancer Institute, Gaithersburg, MD USA.

⁷Mouse Cancer Genetics Program, Center for Advanced Preclinical Research, National Cancer Institute, Frederick, Maryland, USA.

¹³Department of Neurology, Stanford University School of Medicine, Stanford, CA, USA.

¹⁴Chemistry Department, University of Wisconsin, Milwaukee, WI, USA.

†To whom correspondence should be addressed: email waweiss@gmail.com

Summary

The signaling pathways driving neuroblastoma, a tumor derived from neural progenitors, remain largely unidentified. In an engineered mouse model for neuroblastoma, susceptibility to tumors is strain-specific and genetically complex. To identify genes involved in tumor susceptibility, we analyzed genetic control of gene expression (eQTL) in the peripheral sympathetic nervous system. Here we show that genes controlling GABA neurotransmitter signaling, including arginase (*Arg1*), co-localized with susceptibility loci. Activation of GABA-A receptors in human neuroblastoma cells induced apoptosis, while inhibition of arginase slowed proliferation. These results demonstrate the ability of a neurotransmitter to regulate cell growth, and present novel neuroblastoma therapeutic targets.

Introduction

Neuroblastoma, a pediatric tumor of the peripheral nervous system, arises from sympathetic neural progenitors that normally differentiate into post-mitotic neurons shortly after birth. Mutations that drive myeloid, epithelial, and glial tumors are largely not present in neuroblastoma, suggesting this tumor arises from disruption of growth pathways specific to the neural lineage. In a transgenic model driven by the MYCN proto-oncogene, amplification of which is a hallmark of high-risk neuroblastoma^{1,2}, mice develop tumors with histological and genomic characteristics of human neuroblastoma^{3,4}. In this model, tumor incidence varies among mouse strains, and we exploited this genetic variance to identify novel molecular pathways driving neuroblastoma development.

In this study, genetic linkage analysis revealed a locus on chromosome 10 that interacted with numerous secondary loci to influence tumor susceptibility. To identify candidate genes at these loci, we superimposed expression quantitative trait loci (eQTL) in sympathetic superior cervical ganglia (SCG) from backcross mice. Liver arginase (*Arg1*), a component of both the urea cycle and the gamma-amino butyric acid (GABA) biosynthetic pathway, was the strongest eQTL at the primary chromosome 10 locus. Multiple genes and eQTL involved in GABA neurotransmitter signaling were located at the secondary susceptibility loci, providing an intriguing genetic link between this pathway and neuroblastoma biology. We tested this link using compounds targeting the *Arg1*-GABA pathway in human neuroblastoma cell lines. Both nor-NOHA, an *Arg1* inhibitor, and, more strikingly, nanomolar concentrations of the neurotransmitter GABA, inhibited cell growth and viability in vitro. The GABA response was dependent on GABA-A receptor expression and was rescued with GABA-A-specific antagonists.

Activation of GABA-A signaling induced apoptosis and was associated with decreased activity of PI3K/AKT and MAPK signaling, two central pathways in cell growth and survival. The implication of arginine metabolism and GABA signaling in the pathogenesis of neuroblastoma presents a combination of therapeutic targets. Additionally, the demonstration that the neurotransmitter GABA inhibits growth of tumor cells derived from a neural lineage highlights an emerging role for neurotransmitters in regulating development of the peripheral nervous system.

Results

Neuroblastoma penetrance in TH-MYCN mice is strain-dependent

Transgenic mice were generated on a Balb/c x C57B6/J background and showed ~10% incidence of tumors. As mice were crossed into strain FVB/NJ, incidence decreased to zero by 2 generations (**Supplementary Figure 1A**). Conversely, penetrance of tumors steadily increased with each successive backcross into strain 129/SvJ, leveling out at ~60%⁵. Levels of transgene expression were similar between genetic backgrounds (**Supplementary Figure 1B**).

We next crossed resistant transgenic FVB/NJ mice to susceptible wild-type 129/SvJ. The resulting F1 mice showed 4% incidence of tumors, suggesting that resistance was genetically dominant. To generate a genetically diverse population for linkage mapping, we backcrossed transgenic F1 animals to wild-type 129/SvJ mice. Incidence of tumors in the resulting N1 backcross generation was 38% (N=203), with an average survival (109 days) identical to that of mice carrying the transgene in a pure 129/SvJ background⁵

Linkage analysis identifies a tumor susceptibility modifier on chromosome 10

To identify genomic loci associated with tumor susceptibility, we genotyped 203 mice using a combination of microsatellite and SNP markers (see **Supplementary Methods**). Interval mapping for linkage to tumor susceptibility produced a maximum LOD (log of odds) score on chromosome 10 at marker RS36323433 (LOD=4.1, **Figure**

1A, B, significant at a 5% genome-wide error rate, see **Supplementary Methods**). However, at this locus, heterozygous mice were tumor prone (55%), while mice homozygous for the 129/SvJ allele were resistant (25% incidence) (**Figure 1C**). Additionally, tumor susceptibility was strongly influenced by gender. Performing the analysis using sex as an interacting covariate increased the LOD score to 4.9. When mice were segregated by sex and analyzed independently, this locus was not significant in female mice but was in males (LOD=4.3, N=82). It may be relevant in this regard that neuroblastoma is slightly more prevalent in boys (1.3:1) than in girls⁶.

Since the segregation of genotypes with tumor susceptibility at the chromosome 10 locus did not match the patterns of tumor susceptibility in the parent strains, we next considered a more complex genetic model to explain susceptibility. A 2-QTL test identified several loci that interacted with the chromosome 10 locus, with similar LOD scores (**Figure 1D, Supplementary Table 1**). Interestingly, while all of these loci interacted with the chromosome 10 locus, they did not interact with each other.

Expression QTL analysis identifies *Arg1* as a candidate modifier

The 95% confidence interval of the peak on chromosome 10 spanned 47Mb and contained over 281 genes (see **Supplementary Methods**), complicating identification of candidates. Hypothesizing that susceptibility to tumors may be governed by differential expression of genes within this locus, we narrowed our field of candidates by comparing mRNA expression levels in neural crest-derived sympathetic superior cervical ganglia (SCG) from transgenic male and female 129/SvJ and FVB/NJ mice using Affymetrix

Mouse Exon arrays. Surprisingly, only 8 genes were differentially expressed between sexes, and with the exception of a RIKEN clone on chromosome 2, all mapped to either the X or Y chromosomes (**Supplementary Figure 1C, Supplementary Table 3**), excluding gender-specific gene expression as a mechanism for the gender effect at the chromosome 10 locus. When males of the two strains were compared, however, 9,820 genes were differentially expressed genome-wide (**Supplementary Figure 1D, Supplementary Table 3**), including 137 within the 95% confidence interval for the chromosome 10 susceptibility locus (representing almost half of all genes within the locus).

Gene expression levels can be influenced by complex interactions among cis- and trans- acting factors. One method for distinguishing these factors involves generating a genetically heterogeneous population (such as our backcross population), measuring gene expression levels, and treating the expression level of each gene as a quantitative trait (expression QTL or eQTL^{7,8}). Using this method, the cis- and trans- acting alleles influencing gene expression are decoupled from each other, and genes whose differential expression is due to cis-acting factors at a locus can be distinguished from genes under the control of trans-acting factors at other loci. Genes with eQTL overlapping with QTL for physiological phenotypes have been shown to control these phenotypes^{8,9}. We thus utilized this technique to identify eQTL within our chromosome 10 locus, as well as at the numerous other secondary loci identified in the 2-QTL tumor susceptibility analysis.

We measured mRNA expression levels in 116 SCG from the backcross population and tested for linkage between gene-level expression calls for each gene and germline variation, to identify 342 eQTL acting both locally and on another

chromosomes (**Supplementary Table 4**). Four eQTL mapped to the susceptibility locus on chromosome 10, with *Arg1* (liver arginase) showing the strongest eQTL. When this measurement was refined by interval mapping, *Arg1* expression was linked to a QTL at chromosome 10 with a LOD score of 18.2 (**Figure 2A**). *Arg1* overlapped directly with our tumor susceptibility locus, making *Arg1* our top candidate gene (**Figure 2C, Table 1**). Mice heterozygous at that locus had almost 2-fold higher expression of *Arg1* compared to mice homozygous for the 129/SvJ allele (**Figure 2B**). Notably, among 137 genes differentially expressed at the chromosome 10 locus in parental strains, only four showed significant eQTL mapping to the locus, with *Arg1* showing the strongest eQTL in backcross animals. These data suggest that differential expression of the other genes in the parents was due in part to *trans*-acting factors, illustrating the power of eQTL analysis in dissecting control of gene expression at a genetic locus and filtering candidate genes.

eQTL for GABA-related genes map to secondary susceptibility loci

We next looked for eQTL that mapped to the secondary tumor susceptibility loci that interacted with the chromosome 10 locus, and noted eQTL for genes related to GABA neurotransmitter signaling at two of the loci (**Table 1**). Notably, a *trans*-eQTL on chromosome 2 controlled expression of the *Gabra3* receptor subunit on the X chromosome (**Figure 3A-C**). This eQTL overlapped directly with the secondary susceptibility locus on chromosome 2 (**Figure 3G, Supplementary Figure 2A, Table 1**). Mice harboring alleles resulting in high *Arg1* expression and low *Gabra3* expression

showed the strongest susceptibility to tumors (**Figure 3C**). Similarly, an eQTL for the GABA transporter *Slc6a1* (**Figure 3D-F**) mapped to a secondary susceptibility locus on chromosome 4 (**Figure 3G, Supplementary Figure 2B, Table 1**), though the gene was on chromosome 6. Importantly, the chromosome 2 and 4 secondary susceptibility loci showed the highest LOD scores in male mice (**Supplementary Table 2**).

We next investigated secondary susceptibility loci that lacked GABA-related eQTL candidates and found several GABA-related genes mapping within 10Mb of susceptibility peaks. The locus on chromosome 1 (LOD 7.8) flanked by markers RS5056599 (116Mb) and D1MIT1001 (131Mb), LOD 7.8) is in close proximity to *Dbi* (diazepam binding inhibitor, 122Mb), a gene that modulates GABA receptor activity¹⁰. Similarly, the locus on chromosome 9 centered near 117Mb (D9MIT201, LOD 7.9) is 4 Mb from the *Trak1* gene, which encodes a trafficking factor that modulates GABA receptor homeostasis¹¹. The locus on chromosome 7 centered at 144Mb (RS13479509, LOD 6.4) is 4 MB from ornithine aminotransferase (*Oat*), which converts ornithine to glutamate (the substrate for GABA synthesis). Finally, the locus on chromosome 17 centered near 35Mb (D17MIT231, LOD 6.7) is 2 Mb from the GABA-B receptor 1. Together, at least 6 secondary susceptibility loci co-localized with genes in the GABA pathway, and/or eQTL controlling these genes (**Table 1**).

Inhibition of *Arg1* decreases viability of human neuroblastoma cells

The higher-expressing Arginase allele conferring tumor susceptibility is nested within an overall resistant genetic background in purebred mice (either FVB/NJ or

FVB/NJ x 129/SvJ F1). The allelic variation in the secondary loci (harboring components of the GABA pathway) only showed an effect in combination with alleles at other loci. This genetic complexity precluded validation *in vivo*. The association of a gene with susceptibility to tumors does not necessarily imply an ongoing role in tumor maintenance. Nevertheless, since our ultimate goal was to identify clinically-relevant biochemical pathways, we next analyzed *Arg1* and GABA in human neuroblastoma cell lines. As there is little precedent for these pathways in regulation of cell growth and thus little basis for the specific downstream pathways involved, we assessed the effect of compounds targeting this pathway on overall growth and viability.

We detected *Arg1* by western blot across a panel of human neuroblastoma cell lines (**Figure 4A**). We treated this panel with the reversible arginase inhibitor nor-NOHA (N-Omega-hydroxy-nor-arginine)¹² to test whether inhibition of arginase could impair tumor growth. Viability was decreased in CHP-126, SY5Y, and Kelly cells at 100 μ M (**Supplementary Figure 3A**). Both Kelly and SY5Y cultures accumulated in G1 phase with decreased numbers of cells in S phase, without a significant apoptotic fraction assessed by flow cytometry (**Supplementary Figure 3B**). In SY5Y cells this effect was nearly equivalent to the potent PI3K/mTOR inhibitor PI-103. We conclude that *Arg1* expression modulates viability and proliferation in human neuroblastoma cells.

GABA-A activation induces apoptosis in neuroblastoma

We next investigated the role of GABA signaling in the control of viability. While all neuroblastoma cell lines tested expressed the two human GABA-B receptors,

expression of the GABA-A receptor subunits was variable (**Figure 4A**). In response to GABA, viability was unchanged in cell lines CHP-126, Kelly and SY5Y, all of which expressed low levels of the GABA-A receptor (**Supplementary Figure 3C**). In contrast, the cell line LAN-5, which expressed high levels of the GABA-A receptor, was particularly sensitive to GABA, showing a 40% decrease in viability at doses as low as 100nM. To demonstrate that this effect was specific to the GABA-A receptor, we co-treated cells with GABA and either picrotoxin or bicuculline. Picrotoxin, a non-competitive GABA-A channel blocker, was able to fully rescue the effects of both 100nM and 1mM GABA. In contrast, the competitive inhibitor bicuculline was able to reverse the effects of GABA in a dose-dependent manner; 10 μ M bicuculline reversed the effects of 100nM but not 1mM GABA treatment (**Figure 4B**). The dose-dependent and independent effects of bicuculline and picrotoxin, respectively, are consistent with the pharmacological mechanisms of each molecule on the GABA-A receptor, and demonstrate the specificity of the GABA-A receptor's role in cell viability.

We next assessed the mechanism by which GABA-A activation inhibited the growth of neuroblastoma cells. To enhance the signal readout of this pathway, we utilized the potent, selective GABA-A receptor agonist QHii066, a benzodiazepine derivative^{13,14}. Apoptosis was induced in both LAN-5 (high GABA-A expression levels) and Kelly cells (low GABA-A expression levels) (**Figure 4 C and D**), as assessed by annexin V flow cytometry. Immunoblotting revealed that upon addition of GABA and QHii066, cleaved PARP, an indicator of apoptosis, was increased. Notably, immunoblotting revealed a decrease in activity of the PI3K/AKT and MAPK pro-growth and survival pathways, indicated by decreased phosphorylation levels of Akt and Erk,

respectively (**Figure 4E**). Together these data suggest that specific activation of the GABA-A receptor decreases cell viability, induces apoptosis, and suppresses pro-growth and survival signaling pathways in neuroblastoma cell lines.

Discussion

The pathways regulating development of the peripheral nervous system are distinct from those controlling epithelial and other cell types. Perhaps as a consequence, common genomic aberrations driving tumorigenesis in epithelial and glial tumors rarely show abnormalities in neuroblastoma, a tumor of the sympathetic peripheral nervous system.

Mouse model systems have provided a tremendous resource for the identification and validation of genes involved in cancer. Though the influence of strain background on tumor penetrance is frequently observed in mouse models of cancer, only a handful of genes underlying this susceptibility have been identified¹⁵⁻²⁰, mostly due to the limited resolution of quantitative trait linkage mapping. To decipher biological mechanisms underlying genetic linkage to tumor susceptibility in our mouse neuroblastoma model, we investigated patterns of gene expression in peripheral sympathetic nervous tissue. Analysis of gene expression as a function of genotype (in other words, treating gene expression levels as heritable traits and performing linkage analysis) has facilitated identification of candidate genes for quantitative trait loci underlying physiological differences⁷⁻⁹. Genetic control of gene expression is more direct than genetic influence over complex physiological phenotypes. Thus, analysis of expression quantitative trait loci or eQTL provides a relatively strong signal in linkage analysis, enabling the direct identification of specific candidate genes among hundreds of genes at an overlapping QTL for a physiological phenotype. eQTL analysis has identified several genes modifying tumor susceptibility in mouse models for cancer²¹⁻²³. In the current study, eQTL suggested candidate genes from a common biological pathway at multiple loci

simultaneously, including genes located on chromosomes that were controlled in *trans* by unidentified elements at the QTL loci, a phenomenon that would have been missed by conventional analysis of candidate genes at the susceptibility loci.

eQTL analysis identified *Arg1* as a candidate neuroblastoma modifier gene at chromosome 10. One of the strongest secondary susceptibility loci, a locus on chromosome 2, overlapped with a particularly prominent eQTL governing expression of a GABA-A neurotransmitter receptor subunit. Numerous other susceptibility loci overlapped with other GABA-related genes, suggesting a mechanism for the pattern of genetic linkage to tumor susceptibility and implicating an interaction between up-regulation of arginase activity and down-regulation of GABA receptors as cooperating mechanisms promoting susceptibility to tumors.

While *Arg1* is associated with the urea cycle in liver, it is also expressed in a number of tissues that do not carry out the urea cycle, including sympathetic nerve ganglia²⁴, suggesting a role in other biochemical pathways. In neurons, *Arg1* is part of the GABA synthesis pathway, producing ornithine, a precursor of glutamate and of GABA. The biochemical link between *Arg1* and the GABA pathway potentially explains our unique genetic pattern of several secondary loci interacting with a single gene/locus. Only one cytoplasmic arginase gene exists (*Arg1*). However, the GABA signaling pathway may be perturbed at several genomic loci, including several components of the GABA-A receptor, genes for which are dispersed throughout the genome. Thus, in a genetic model involving perturbation of arginase and GABA signaling, many GABA-related genes could interact with the single *Arg1* gene on chromosome 10 with similar

effects (disrupting two connected pathways), while GABA genes may not interact with each other (as multiple disruptions would have redundant effects on the same pathway).

While emerging evidence supports the role for GABA signaling in the control of neural cell growth (see below), a role for *Arg1* is less obvious. Several downstream outputs could account for increased expression of *Arg1* predisposing mice to tumors. Arginase may act as an immunosuppressant^{25,26}, a competitor for the substrate arginine with the growth-inhibitory nitric oxide synthases (NOSs)²⁷⁻³⁰, or a producer of ornithine, the substrate for polyamine synthesis linked to tumorigenesis³¹ and neural proliferation³². The rate-limiting polyamine synthetic enzyme, ornithine decarboxylase (ODC), is a well-established target for c-myc and MYCN³³. ODC inhibitors inhibit neuroblastoma development *in vitro* and in TH-MYCN mice^{34,35}, and are currently in clinical trials for neuroblastoma (<http://www.nmtrc.org/phase-i-dfmo/>). Ornithine is also a substrate for synthesis of glutamate and GABA. Notably, ornithine aminotransferase (*Oat*), which converts ornithine to glutamate, maps to a susceptibility locus. GABA inhibits neuronal growth and promotes differentiation³⁶. Thus, at least one ultimate output of *Arg1* activity (GABA) could inhibit both induction and further growth of tumors, driving selection for secondary genetic lesions that disable this pathway.

While *Arg1* activity has not been studied extensively in cancer, inhibition of arginase has been shown to disrupt growth of breast cancer cells³⁷. Arginase expression has also been linked to neuronal viability. Clinically, *Arg1* mutations cause arginemia, characterized by neurodegeneration (OMIM 207800). While hepatic production of neurotoxic metabolites are speculated to cause this neurodegeneration^{38,39}, our data, coupled with detection of *Arg1* expression in neural tissues^{24,40,41}, suggest that *Arg1* may

be involved in growth and survival signaling in neuroblasts, and inhibition of Arg1 may have an intrinsic cytotoxic effect in neurons and neuroblastoma cells.

The observation that mice with lower expression of GABA-A receptor subunits are tumor prone is consistent with GABA's known role in neuronal cell growth and differentiation^{36,42}, and suggest that the association of down-regulation of GABA-A receptors with more aggressive human neuroblastomas has biological significance⁴³. However, since the receptor is formed as a pentameric combination of 19 possible subunits, with changing expression patterns and biological roles⁴², testing this hypothesis is not straightforward. GABA signaling has been shown to negatively regulate growth of neural crest stem cells³⁶. In our hands, neuroblastoma cells expressing the GABA-A receptor showed decreased viability, increased apoptosis, and diminished activity of mitogenic signaling pathways in response to GABA-A activation, supporting a role of GABA signaling in tumor cell growth and survival. These results parallel the neurotrophin model, based on the observation that dysregulation of TRK neurotrophin receptors correlates with clinical outcome in neuroblastoma⁴⁴. Our results are consistent with this paradigm, suggesting that decreased signaling through the GABA pathway (rather than TRKs) may promote neuroblastoma development.

Neuroblastoma is a common pediatric tumor with a unique biology, making the development of novel targeted therapeutics problematic. As a result, improvements in clinical outcomes have been modest over the last several decades. Arginase inhibitors are under investigation for highly prevalent diseases such as hypertension²⁷. Additionally, the implication of GABA and other neurotransmitters in regulating growth of neuroblastoma opens up the potential to apply numerous clinically-approved drugs used

in neurology and psychology as chemotherapeutic agents. These results also highlight a possible connection between the role of neurotransmitters in nervous system development and the regulation of neuroblastoma growth.

Acknowledgements:

The authors are grateful to the Marshfield Clinic and CIDR for genotyping, and to Fernando Pardo Manuel de Villena, Gary Churchill, Saunak Sen, Clay Gustafson, and Roger Nicoll for experimental advice and comments on the manuscript. This work was supported by the March of Dimes, the Concern Foundation, the UCSF Academic Senate, NIH R01CA102321, R01NS055750 and ARRA supplement for NIH R01NS055750.

Author Contributions:

CSH performed the majority of the experiments and data analysis in the manuscript. DQ performed the eQTL and statistical analysis and helped prepare the manuscript. QF, CC and YB performed biochemical assays. DDG and KN assisted with mouse work. LP, JC, JM, and PK provided technical support for genotyping data generation and analysis. YKS, JC, SK, TVD, and JK provided technical support for expression array data generation and analysis. AB, JK, YJC, JMC and TVD helped design experiments and prepare the manuscript. WAW supervised the project. CSH and WAW designed experiments and wrote the paper.

Methods Summary:

Backcross mice were generated by crossing *TH-MYCN* transgenic FVB/N mice to wild-type 129/SvJ, and subsequently crossing F1 offspring to wild-type 129/SvJ. Mice were observed for at least one year to be considered tumor-free. DNA was isolated from spleen and genotyped using a combination of microsatellite and SNP markers. RNA

from SCG was analyzed using Affymetrix Mouse Exon arrays. Susceptibility linkage was analyzed using R-QTL. Differential gene expression was assessed using Significance Analysis of Microarrays, and eQTL were calculated using custom software as described previously²¹. Cell viability and cell-cycle status were assessed using a WST-1 assay and flow cytometry. For details see **Supplementary Methods**.

Table 1: Candidate genes at susceptibility loci

A. Candidate eQTL at susceptibility loci

chromosome	susceptibility locus (Mb)	LOD	eQTL gene	eQTL locus (Mb)	eQTL p-val	perm. p-val
10	28	5.0	<i>Arg1</i>	25	2.92E-20	<0.001
2	166	7.0	<i>Gabra3</i>	178	5.57E-34	<0.001
4	115	7.4	<i>Slc6a1</i>	129	2.81E-05	0.001

B. GABA genes at susceptibility loci

chromosome	susceptibility locus (Mb)	LOD	gene	gene location (Mb)
1	131	7.8	<i>Dbi</i>	122
9	117	7.8	<i>Trak1</i>	121
17	35	6.9	<i>Gabbr1</i>	37
7	144	6.3	<i>Oat</i>	140

C. Gene descriptions

gene	location (chromosome)	description
<i>Arg1</i>	10	liver arginase
<i>Gabra3</i>	X*	GABA-A receptor, subunit alpha 3
<i>Slc6a1</i>	6*	GABA transporter, removes GABA from synaptic cleft
<i>Dbi</i>	1	diazepam binding inhibitor; modulates the action of the GABA receptor
<i>Trak1</i>	9	trafficking protein, kinesin binding 1, regulates GABA receptor
<i>Gabbr1</i>	17	GABA-B receptor, 1
<i>Oat</i>	7	ornithine aminotransferase (produces glutamate, a GABA precursor)

*controlled by trans eQTL

Figure 1. A locus on chromosome 10 and multiple secondary loci are linked to tumor susceptibility. (A) LOD plot for tumor susceptibility shows a single significant locus on chromosome 10. Dotted line indicates 5% genome-wide significance threshold (LOD=2.81, 1000 permutations). (B) LOD plot of chromosome 10 only. Hash marks on the horizontal axis indicate marker positions. Dotted line indicates 5% genome-wide significance threshold (LOD=2.81, 1000 permutations). (C) Effect plot for the marker closest to the maximum LOD score (RS36323433) showing incidence of tumors as a function of genotype. (D) Two-QTL analysis using sex as an interacting covariate reveals that multiple secondary loci interact with the chromosome 10 locus. The top left half shows the results of the additive model (no epistatic interactions), and the bottom right half shows results of the “full” model, which accounts for epistatic interactions. The bar on the right displays the correspondence between color on the chart and LOD scores (the left side of the bar corresponds to the additive analysis on the top left half of the plot, while the right side of the bar, with a different scale, corresponds to the full model analysis on the bottom right). Locations of the maximum LOD scores are shown in **Supplementary Table 1**.

Figure 2. An eQTL for *Arg1* co-localizes with the tumor susceptibility locus on chromosome 10. (A) Interval mapping for *Arg1* expression, the most significant eQTL in the chromosome 10 region, showing a LOD score of 18.2 on chromosome 10, centered at the physical location of the *Arg1* gene. Line indicates 5% genome-wide significance threshold. (B) Log₂ *Arg1* expression level as a function of genotype. (C) A plot of LOD

scores on chromosome 10 for susceptibility (black line) and the *Arg1* eQTL (blue line) showing co-localization of the peaks.

Figure 3. Secondary susceptibility loci co-localize with eQTL for GABA-related genes.

(A) A trans-eQTL on chromosome 2 controls expression of the GABA-A receptor subunit 3 (*Gabra3*) on the X chromosome (arrow) (LOD=30.9). (B) *Gabra3* expression as a function of D2MIT148 genotype. (C) Plot of tumor incidence as a function of genotypes at the chromosome 2 and 10 loci. (D) Expression QTL for the *Slc6a1* GABA transporter on chromosome 4 (LOD=4.1). Arrow indicates the physical location of *Slc6a1* on chromosome 6. (E) *Slc6a1* expression as a function of D4MIT203 genotype. (F) Tumor incidence as a function of genotypes at loci on chromosomes 4 and 10. (G) Genome-wide plot of LOD scores for the *Gabra3* (black), *Slc6a1* (green), *Arg1* (blue) eQTL and tumor susceptibility for a single-locus model (purple) and the combined effect of the peak of the chromosome 10 locus plus points across the rest of the genome (red), showing correspondence between eQTL peaks and primary and secondary susceptibility loci. Two-dimensional plots for *Gabra3* and *Slc6a1* are shown in **Supplementary Figure 2**.

Figure 4. GABA activation decreases viability and induces apoptosis in neuroblastoma cells (A) Western blot for *Arg1*, GABA-A, and GABA-B receptors in neuroblastoma cell lines. (B) GABA treatment of LAN-5, a GABA-A expressing cell line, results in decreased viability that is rescued by the GABA competitive inhibitor bicuculline (bic) at 10 μ M, in a GABA dose-dependent manner; and by the non-competitive channel blocker picrotoxin (picro) at 100 μ M in a GABA dose-independent manner. (C) Lan5 and Kelly cells were treated with GABA 100 μ M or the selective ligand for GABA QHii066 1 μ M or both and analyzed by annexin V-FITC flow cytometry for apoptosis after 72h. (D) Percentages of positive cells for apoptotic marker annexin V are mean \pm s.e. for triplicate samples with treatments indicated. (E) Cells analyzed by immunoblot using antisera indicated show decreased phosphorylation of Akt and Erk.

Figure 1

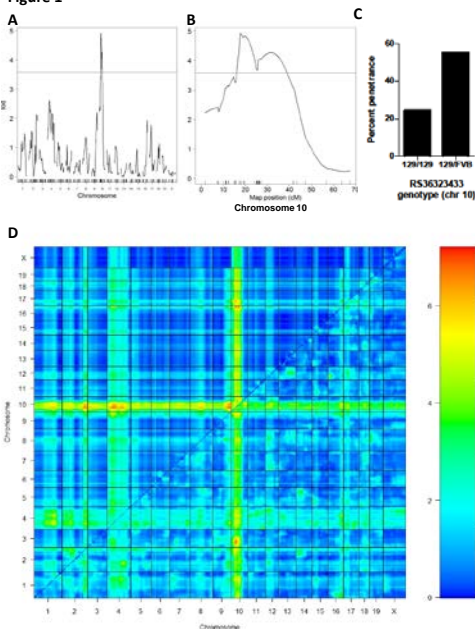


Figure 2

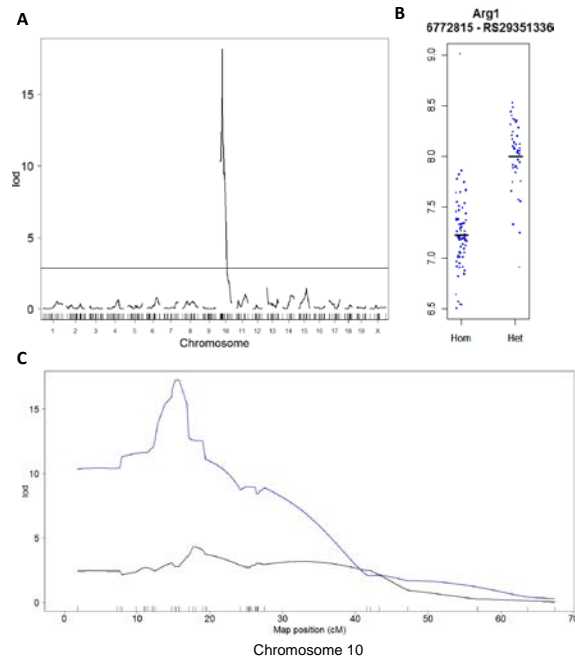
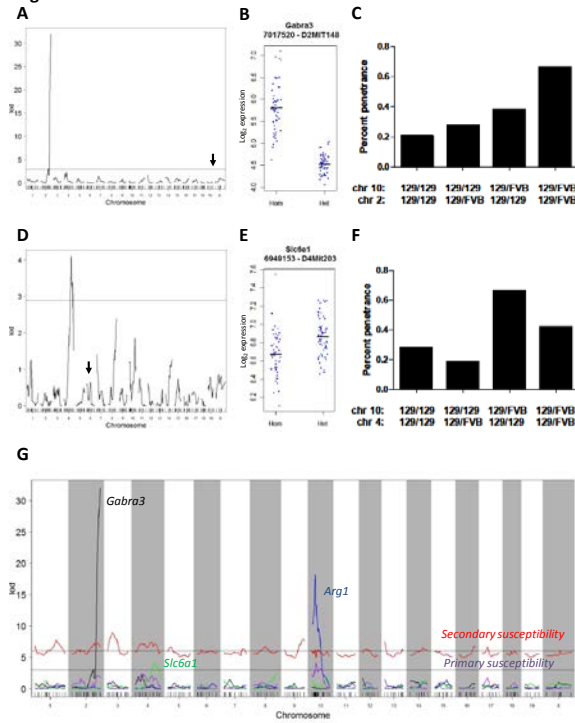
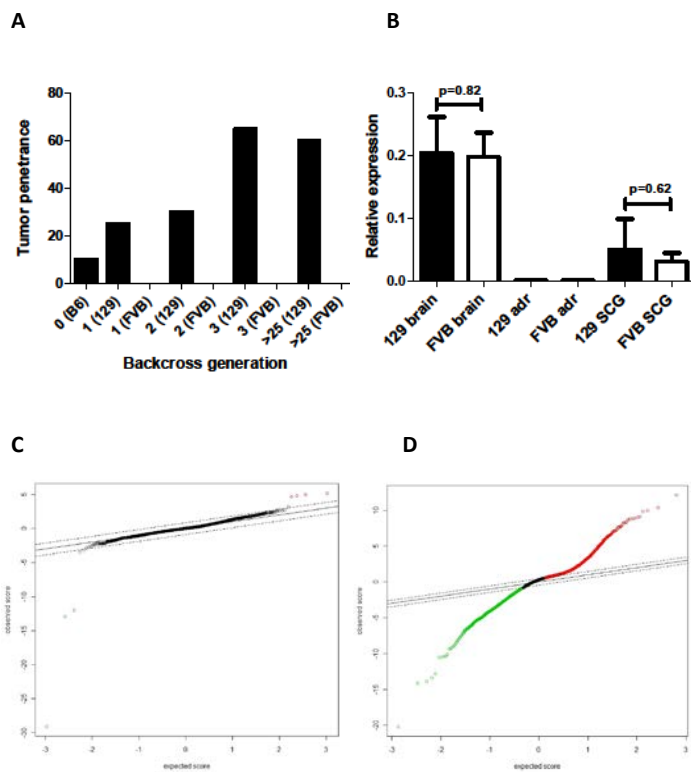


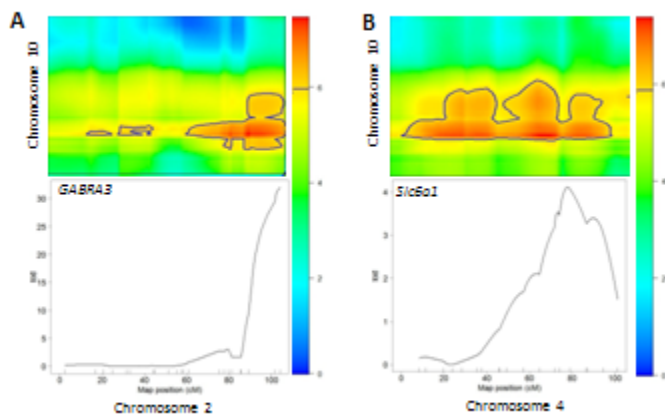
Figure 3



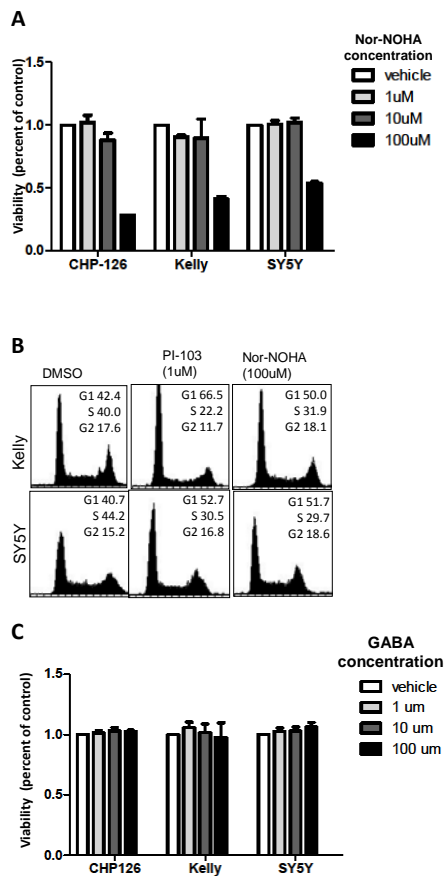
Supplementary Figure 1



Supplementary Figure 2



Supplementary Figure 3



References

1. Brodeur, G.M., Seeger, R.C., Schwab, M., Varmus, H.E. & Bishop, J.M. Amplification of N-myc in untreated human neuroblastomas correlates with advanced disease stage. *Science* **224**, 1121-4 (1984).
2. Schwab, M. et al. Chromosome localization in normal human cells and neuroblastomas of a gene related to c-myc. *Nature* **308**, 288-91 (1984).
3. Weiss, W.A., Aldape, K., Mohapatra, G., Feuerstein, B.G. & Bishop, J.M. Targeted expression of MYCN causes neuroblastoma in transgenic mice. *EMBO J* **16**, 2985-95 (1997).
4. Hackett, C.S. et al. Genome-wide array CGH analysis of murine neuroblastoma reveals distinct genomic aberrations which parallel those in human tumors. *Cancer Res* **63**, 5266-73 (2003).
5. Chesler, L. et al. Malignant progression and blockade of angiogenesis in a murine transgenic model of neuroblastoma. *Cancer Res* **67**, 9435-42 (2007).
6. Hale, G., Gula, M.J. & Blatt, J. Impact of gender on the natural history of neuroblastoma. *Pediatr Hematol Oncol* **11**, 91-7 (1994).
7. Brem, R.B., Yvert, G., Clinton, R. & Kruglyak, L. Genetic dissection of transcriptional regulation in budding yeast. *Science* **296**, 752-5 (2002).
8. Schadt, E.E. et al. Genetics of gene expression surveyed in maize, mouse and man. *Nature* **422**, 297-302 (2003).
9. Yang, X. et al. Validation of candidate causal genes for obesity that affect shared metabolic pathways and networks. *Nat Genet* **41**, 415-23 (2009).

10. Gray, P.W., Glaister, D., Seeburg, P.H., Guidotti, A. & Costa, E. Cloning and expression of cDNA for human diazepam binding inhibitor, a natural ligand of an allosteric regulatory site of the gamma-aminobutyric acid type A receptor. *Proc Natl Acad Sci U S A* **83**, 7547-51 (1986).
11. Gilbert, S.L. et al. Trak1 mutation disrupts GABA(A) receptor homeostasis in hypertonic mice. *Nat Genet* **38**, 245-50 (2006).
12. Tenu, J.P. et al. Effects of the new arginase inhibitor N(omega)-hydroxy-nor-L-arginine on NO synthase activity in murine macrophages. *Nitric Oxide* **3**, 427-38 (1999).
13. He, X. et al. Pharmacophore/receptor models for GABA(A)/BzR alpha2beta3gamma2, alpha3beta3gamma2 and alpha4beta3gamma2 recombinant subtypes. Included volume analysis and comparison to alpha1beta3gamma2, alpha5beta3gamma2, and alpha6beta3gamma2 subtypes. *Drug Des Discov* **17**, 131-71 (2000).
14. Huang, Q. et al. Pharmacophore/receptor models for GABA(A)/BzR subtypes (alpha1beta3gamma2, alpha5beta3gamma2, and alpha6beta3gamma2) via a comprehensive ligand-mapping approach. *J Med Chem* **43**, 71-95 (2000).
15. MacPhee, M. et al. The secretory phospholipase A2 gene is a candidate for the Mom1 locus, a major modifier of ApcMin-induced intestinal neoplasia. *Cell* **81**, 957-66 (1995).
16. Ewart-Toland, A. et al. Identification of Stk6/STK15 as a candidate low-penetrance tumor-susceptibility gene in mouse and human. *Nat Genet* **34**, 403-12 (2003).
17. Mao, J.H. et al. Genetic variants of Tgfb1 act as context-dependent modifiers of mouse skin tumor susceptibility. *Proc Natl Acad Sci U S A* **103**, 8125-30 (2006).
18. Park, Y.G. et al. Sipa1 is a candidate for underlying the metastasis efficiency modifier locus Mtes1. *Nat Genet* **37**, 1055-62 (2005).

19. Wakabayashi, Y., Mao, J.H., Brown, K., Girardi, M. & Balmain, A. Promotion of Hras-induced squamous carcinomas by a polymorphic variant of the Patched gene in FVB mice. *Nature* **445**, 761-5 (2007).
20. Crawford, N.P. et al. Bromodomain 4 activation predicts breast cancer survival. *Proc Natl Acad Sci U S A* **105**, 6380-5 (2008).
21. Quigley, D.A. et al. Genetic architecture of mouse skin inflammation and tumour susceptibility. *Nature* **458**, 505-8 (2009).
22. La Merrill, M., Gordon, R.R., Hunter, K.W., Threadgill, D.W. & Pomp, D. Dietary fat alters pulmonary metastasis of mammary cancers through cancer autonomous and non-autonomous changes in gene expression. *Clin Exp Metastasis* **27**, 107-16.
23. Crawford, N.P. et al. The Diasporin Pathway: a tumor progression-related transcriptional network that predicts breast cancer survival. *Clin Exp Metastasis* **25**, 357-69 (2008).
24. Yu, H. et al. Widespread expression of arginase I in mouse tissues. Biochemical and physiological implications. *J Histochem Cytochem* **51**, 1151-60 (2003).
25. Yachimovich-Cohen, N., Even-Ram, S., Shufaro, Y., Rachmilewitz, J. & Reubinoff, B. Human embryonic stem cells suppress T cell responses via arginase I-dependent mechanism. *J Immunol* **184**, 1300-8.
26. Bak, S.P., Alonso, A., Turk, M.J. & Berwin, B. Murine ovarian cancer vascular leukocytes require arginase-1 activity for T cell suppression. *Mol Immunol* **46**, 258-68 (2008).
27. Durante, W., Johnson, F.K. & Johnson, R.A. Arginase: a critical regulator of nitric oxide synthesis and vascular function. *Clin Exp Pharmacol Physiol* **34**, 906-11 (2007).
28. Jenkins, D.C. et al. Roles of nitric oxide in tumor growth. *Proc Natl Acad Sci U S A* **92**, 4392-6 (1995).

29. Ortiz-Ortiz, M.A. et al. Nitric oxide-mediated toxicity in paraquat-exposed SH-SY5Y cells: a protective role of 7-nitroindazole. *Neurotox Res* **16**, 160-73 (2009).
30. Ciani, E., Severi, S., Contestabile, A. & Bartesaghi, R. Nitric oxide negatively regulates proliferation and promotes neuronal differentiation through N-Myc downregulation. *J Cell Sci* **117**, 4727-37 (2004).
31. Gerner, E.W. & Meyskens, F.L., Jr. Polyamines and cancer: old molecules, new understanding. *Nat Rev Cancer* **4**, 781-92 (2004).
32. Huang, Y., Higginson, D.S., Hester, L., Park, M.H. & Snyder, S.H. Neuronal growth and survival mediated by eIF5A, a polyamine-modified translation initiation factor. *Proc Natl Acad Sci U S A* **104**, 4194-9 (2007).
33. Bello-Fernandez, C., Packham, G. & Cleveland, J.L. The ornithine decarboxylase gene is a transcriptional target of c-Myc. *Proc Natl Acad Sci U S A* **90**, 7804-8 (1993).
34. Koomoa, D.L., Yco, L.P., Borsics, T., Wallick, C.J. & Bachmann, A.S. Ornithine decarboxylase inhibition by alpha-difluoromethylornithine activates opposing signaling pathways via phosphorylation of both Akt/protein kinase B and p27Kip1 in neuroblastoma. *Cancer Res* **68**, 9825-31 (2008).
35. Hogarty, M.D. et al. ODC1 is a critical determinant of MYCN oncogenesis and a therapeutic target in neuroblastoma. *Cancer Res* **68**, 9735-45 (2008).
36. Andang, M. et al. Histone H2AX-dependent GABA(A) receptor regulation of stem cell proliferation. *Nature* **451**, 460-4 (2008).
37. Singh, R., Pervin, S., Karimi, A., Cederbaum, S. & Chaudhuri, G. Arginase activity in human breast cancer cell lines: N(omega)-hydroxy-L-arginine selectively inhibits cell proliferation and induces apoptosis in MDA-MB-468 cells. *Cancer Res* **60**, 3305-12 (2000).

38. De Deyn, P.P., Marescau, B. & Macdonald, R.L. Guanidino compounds that are increased in hyperargininemia inhibit GABA and glycine responses on mouse neurons in cell culture. *Epilepsy Res* **8**, 134-41 (1991).
39. Deignan, J.L. et al. Increased plasma and tissue guanidino compounds in a mouse model of hyperargininemia. *Mol Genet Metab* **93**, 172-8 (2008).
40. Yu, H. et al. Arginase expression in mouse embryonic development. *Mech Dev* **115**, 151-5 (2002).
41. Yu, H. et al. Expression of arginase isozymes in mouse brain. *J Neurosci Res* **66**, 406-22 (2001).
42. Le-Corronc, H., Rigo, J.M., Branchereau, P. & Legendre, P. GABA(A) Receptor and Glycine Receptor Activation by Paracrine/Autocrine Release of Endogenous Agonists: More Than a Simple Communication Pathway. *Mol Neurobiol*.
43. Roberts, S.S. et al. GABAergic system gene expression predicts clinical outcome in patients with neuroblastoma. *J Clin Oncol* **22**, 4127-34 (2004).
44. Brodeur, G.M. et al. Trk receptor expression and inhibition in neuroblastomas. *Clin Cancer Res* **15**, 3244-50 (2009).

Supplementary Methods:

Mice: All mice were obtained from the Jackson Labs (Bar Harbor, ME), and were housed and treated following UCSF IACUC guidelines. Tumor-negative backcross mice were followed until one year of age (the latest tumor was detected at 342 days). Superior cervical ganglia (SCG) were surgically isolated and snap-frozen in liquid nitrogen. SCG were isolated from the parental control groups at 21 days.

Taqman analysis of transgene expression: Taqman expression analysis was performed on 6 mice (3 female, 3 male) from each strain. Proprietary assays for human MYCN and controls L18 and mGUS were obtained from Applied Biosystems (Carlsbad, CA). MYCN relative to mGUS is shown in **Supplementary Figure 1B**.

Genotyping: DNA was isolated from spleen tissue using a proteinase K lysis followed by phenol chloroform extraction. Microsatellite marker genotyping was carried out by the Marshfield Clinic (Marshfield, WI), and CIDR (Baltimore, MD). SNP genotyping was performed using template-directed primer extension with fluorescence polarization detection (FP-TDI¹, Acycloprime II, Perkin Elmer, Waltham, MA) and SNPStream² 48-plex (Beckman Coulter, Brea, CA). Markers and map positions are shown in **Supplementary Table 5**. The marker set had an average spacing of 8 MB genome-wide (excluding the high density of markers on chromosome 10).

Linkage analysis: Interval mapping was performed using the R-QTL³ package in the R statistical language. Genotypes flagged as probable errors by R-QTL were discarded. The genetic map positions were determined using the physical map positions (NCBI

37/mm9), followed by re-estimation of the map using R-QTL, and likely mis-mapped markers were discarded. Linkage analysis was performed on a 1-cM grid. Genome-wide significance thresholds were determined by running 1000 permutations for each dataset. Interval analysis was performed using the binary mode of the “EM” model. All results reported as significant were significant at a 5% genome-wide error rate. 95% confidence intervals (CI) were determined using the lodint function in R-QTL. Genes within the confidence intervals were determined by counting all genes in the UCSC genome assembly mapping between markers flanking the 95% CI.

Expression Arrays: RNA from superior cervical ganglia was isolated using the RNEasy kit (QIAGEN, Valencia, CA), as we found these buffers were more effective at disrupting the ganglia than Trizol. 1µg of RNA was used as a starting template for the RiboMinus rRNA subtraction (Invitrogen, Carlsbad, CA) followed by the ST labeling protocol (Affymetrix, Santa Clara, CA). Labeled samples were hybridized to Affymetrix Mouse Exon 1.0 arrays. Array quality control was performed using the Affymetrix Expression Console. 2-way comparisons between homogenous groups (e.g. male vs. females or 129/SvJ vs FVB/N males) were performed using the Significance Analysis of Microarrays (SAM) package⁴ using a 5% false discovery rate. Results are presented in **Supplementary Table 3** and plotted in **Supplementary Figures 1C** and **1D**.

eQTL analysis: Arrays were normalized using RMA in the XPS package (<http://www.bioconductor.org/packages/2.6/bioc/html/xps.html>). eQTL were calculated as described in ⁵; briefly, linkage between gene expression and loci was assessed by linear regression with genome-wide significance assessed using a FDR-based method.

Cell Culture: Neuroblastoma cell lines were grown in RPMI media with 10% serum and antibiotics with the exception of SK-N-BE(2) (DMEM/F12, 10% serum) and IMR-32 (DMEM, 10% serum plus non-essential amino acids). Nor-NOHA was obtained from Bachem (Torrance, CA) and dissolved in DMSO. GABA was obtained from Sigma (St. Louis, MO) and dissolved in H₂O. Picrotoxin and bicuculline were obtained from Sigma and dissolved in DMSO.

Western blotting: Equal amounts of total protein were loaded for 4%–12% SDS-polyacrylamide gel electrophoresis and transferred to nitrocellulose membranes. After blocking, membranes were blotted with Arg1 (R&D Systems, Minneapolis MN), GABA B R1, Erk (Santa Cruz Biotech, Santa Cruz, CA), GABA A R β 2/3, GABA B R2, β -tubulin (Millipore, Billerica, MA), cleaved-PARP (Asp214), p-Akt (Ser473), Akt, pErk (Thr202/Tyr204) (Cell Signaling Technology, Danvers, MA), and GAPDH (Upstate Biotechnology, Lake Placid NY). Antibodies were detected with HRP-linked anti-mouse, anti-rabbit (Amersham/GE, Piscataway, NJ), or anti-sheep IgG (Calbiochem/EMD, Gibbstown, NJ), followed by enhanced chemiluminescence (Amersham/GE, Piscataway, NJ).

WST-1 assay: Cells were grown in 12-well plates and treated for 72 hours prior to the addition of WST-1 reagent (100 μ l per 1ml media). Absorbance was read after 60 minutes. Results were plotted using Graphpad Prism software, and p-values were calculated using a two-tailed Student's t-test.

FACS: Cells were plated on 6-well dishes and treated as indicated for 24 hours. They were then harvested, fixed in 70% ethanol for 30 minutes, then stained with a propidium

iodide (PI) dye and RNase solution. All samples were analyzed on a FACSCaliber flow cytometer (Becton Dickenson, Franklin Lakes, NJ) and analyzed using ModFit (Verity Software, Topsham ME). Apoptosis was detected by flow cytometry for annexin V-FITC per manufacturer's protocol (Annexin V-FITC detection kit, BioVision, Milpitas, CA) using FlowJo software (Tree Star, Inc, Ashland, OR).

Supplementary Figure Legends

Supplementary Figure 1. Incidence of neuroblastoma and SCG gene expression, but not MYCN transgene expression, are dependent on strain. (A) Incidence of tumors in FVB/NJ and 129/SvJ as a function of backcross number. (B) Taqman expression showing equivalent levels of *TH-MYCN* transgene expression in all tissues tested. Analysis of brain, adrenal gland, and superior cervical ganglia from each strain showed equivalent levels of expression (C) SAM analysis showing 3 genes differentially regulated between male and female FVB/NJ mice (N=5 in each group) (D) SAM analysis showing 9,820 genes differentially expressed between strains in male ganglia

Supplementary Figure 2. Correspondence between *Gabra3* and *Slc6a1* eQTL and secondary susceptibility loci. (A) 2-qtL lod scores are plotted for the intersection of chromosomes 10 (vertical) and 2 (horizontal) in the top panel, with the scale at right indicating LOD scores for the full (additive plus interaction) model. The contour line indicates a 1.5 LOD drop from the maximal value for the chromosome (See Table 1). The bottom panel shows the eQTL LOD plot for *Gabra3* expression, indicating that the peak LOD score falls within a 1.5-LOD (95%) confidence interval for the susceptibility locus. (B) plot similar to A, showing chromosome 4 on the horizontal axis and the eQTL lod score for *Slc6a1* in the bottom panel.

Supplementary Figure 3. Treatment of neuroblastoma cell lines with arginase inhibitors inhibits proliferation, while the effect of GABA on viability is GABRA-A expression dependent. (A) WST-1 assay showing a dose-dependent decrease in viability following 72h treatment of neuroblastoma cells with varying doses of the Arg1

inhibitor nor-NOHA. (C) FACS plot showing increased G1 phase in Kelly and SY5Y cells treated with nor-NOHA for 24 hours. The dual PI3K/mTOR inhibitor PI103 is shown for comparison. (C) Three neuroblastoma cell lines with low GABA-A expression show no change in viability in response to GABA. Viability was assessed by WST-1 assay at 72h.

Supplementary Tables:

Supplementary Table 1: Tumor susceptibility interaction LOD scores, all mice, sex as an interacting covariate.

Supplementary Table 2: Tumor susceptibility interaction LOD scores, male mice only.

Supplementary Table 3: Genes differentially expressed between 129/SvJ and FVB/N

Supplementary Table 4: eQTL significant at a 5% genome-wide error rate

Supplementary Table 5: Markers and map positions

Supplementary References:

1. Hsu, T.M., Chen, X., Duan, S., Miller, R.D. & Kwok, P.Y. Universal SNP genotyping assay with fluorescence polarization detection. *Biotechniques* **31**, 560, 562, 564-8, passim (2001).

2. Bell, P.A. et al. SNPstream UHT: ultra-high throughput SNP genotyping for pharmacogenomics and drug discovery. *Biotechniques Suppl*, 70-2, 74, 76-7 (2002).
3. Broman, K.W., Wu, H., Sen, S. & Churchill, G.A. R/qtl: QTL mapping in experimental crosses. *Bioinformatics* **19**, 889-90 (2003).
4. Tusher, V.G., Tibshirani, R. & Chu, G. Significance analysis of microarrays applied to the ionizing radiation response. *Proc Natl Acad Sci U S A* **98**, 5116-21 (2001).
5. Quigley, D.A. et al. Genetic architecture of mouse skin inflammation and tumour susceptibility. *Nature* **458**, 505-8 (2009).

VI. Appendix IV: Anticonvulsant Screening Data

Anticonvulsant Screening Program Test 8 Results - Anticonvulsant Identification (Rats I.P.)

Add ID: 412007 D Screen ID: 1

Solvent Code: MC Solvent Prep: M&P,SB
 Animal Weight: 105.0 - 140.0 g
 Date Started: 20-Nov-2012 Date Completed: 20-Nov-2012

Reference: 480: 216

Response

Time (Hours)		0.25	0.5	1.0	2.0	4.0	6.0	8.0	24	3.0
Test	Dose	Dths	N / F C	N / F C	N / F C	N / F C	N / F C	N / F C	N / F C	N / F C
MES	30.0		1 / 4	0 / 4	0 / 4	0 / 4	0 / 4	/	/	/
TOX	30.0		0 / 4	0 / 4	0 / 4	0 / 4	0 / 4	/	/	/

Note: N/F = number of animals active or toxic over the number tested.

C= Comment code

Comments to Supplier:

Anticonvulsant Screening Program
Test 8 Results - Anticonvulsant Identification (Rats I.P.)

Add ID: 412007 D Screen ID: 1

Solvent Code: MC Solvent Prep: M&P,SB

Animal Weight: 105.0 - 140.0 g

Date Started: 20-Nov-2012 Date Completed: 20-Nov-2012

Reference: 480: 216

Response

Time (Hours)				0.25		0.5		1.0		2.0		4.0		6.0		8.0		24		3.0	
Test	Dose		Dths	N / F	C	N / F	C	N / F	C	N / F	C	N / F	C	N / F	C	N / F	C	N / F	C	N / F	C
MES	30.0			1 / 4		0 / 4		0 / 4		0 / 4		/		/		/		/		/	
TOX	30.0			0 / 4		0 / 4		0 / 4		0 / 4		/		/		/		/		/	

Note: N/F = number of animals active or toxic over the number tested.

C= Comment code

Comments to Supplier:

VII. Appendix V: Data on QH-II-066

Modulation of $\alpha 5$ subunit-containing GABA_A receptors alters alcohol drinking by rhesus monkeys

Daniela Rüedi-Bettschen, PhD¹, James K. Rowlett, PhD, Sundari Rallapalli, PhD, Terry Clayton, PhD, James M. Cook, PhD, and Donna M. Platt, PhD

Harvard Medical School, New England Primate Research Center, Southborough, MA, USA (DR-B, JKR, DMP)

Department of Chemistry, University of Wisconsin-Milwaukee, Milwaukee, WI, USA (SR, TC, JMC)

¹Current address: Department of Pharmacology and Toxicology, College of Medicine, University of Arkansas for Medical Sciences, 4301 W. Markham, #611, Little Rock, AR, 72205, USA

Correspondence: Donna M. Platt, Ph.D., Harvard Medical School, New England Primate Research Center, One Pine Hill Drive, PO Box 9102, Southborough, MA 01772-9102, USA; phone: 508-624-8090; fax: 508-624-8197; e-mail: donna_platt@hms.harvard.edu

Supported by: AA16179 (DMP), RR00168 (DMP), DA11792 (JKR), MH46851 (JMC), The Lynde and Harry Bradley Foundation (JMC)

Abstract

Background: Alcohol's ability to potentiate the activity of γ -aminobutyric acid (GABA) at GABA_A receptors has been implicated as a key mechanism underlying the behavioral effects of alcohol. The complex molecular biology of these receptors raises the possibility that particular receptor subtypes may play unique roles in alcohol's abuse-related effects and that subtype-selective ligands with therapeutic specificity against alcohol might be developed. This study evaluated the capacity of α 5GABA_A receptor ligands to alter selectively the reinforcing effects of alcohol. *Methods:* Two groups of rhesus monkeys were trained to orally self-administer alcohol or sucrose under fixed-ratio schedules and limited daily access conditions. Additionally, following daily self-administration sessions, the behavior of each monkey was scored for both species-typical and drug-induced behaviors. *Results:* Concentrations of 1-6% alcohol maintained self-administration above water levels, engendered pharmacologically-relevant blood alcohol levels ranging from 90-160 mg/dl, and produced changes in behavior typical of alcohol intoxication. Concentrations of 0.3-3% sucrose also reliably maintained self-administration. The α 5GABA_A receptor agonist QH-ii-066 enhanced and the α 5GABA_A receptor inverse agonist L-655,708 inhibited alcohol but not sucrose drinking. The changes in alcohol drinking could be reversed with the α 5GABA_A receptor antagonist XLi-093. However, L-655,708 increased yawning in both alcohol- and sucrose-drinkers, possibly indicative of an anxiogenic effect. *Conclusions:* These findings suggest a prominent and specific role for α 5GABA_A receptor mechanisms in the reinforcing effects of alcohol. Moreover, these results suggest that α 5GABA_A receptors may represent a novel pharmacological target for the development of medications to reduce drinking. Of ligands modulating this receptor, α 5GABA_A receptor inverse agonists may hold the most promise as alcohol pharmacotherapies.

Keywords: GABA_A receptors, alcohol self-administration, monkey, pharmacotherapy, QH-ii-066, L-655,708, XLi-093, naltrexone

Introduction

Alcohol's ability to potentiate the activity of γ -aminobutyric acid (GABA) at GABA_A receptors has been implicated as a key mechanism underlying the abuse-related effects of alcohol in both human and non-human subjects (e.g., Hyytiä and Koob, 1995; June et al., 1995; 1998; Korpi, 1994; Söderpalm and Hansen, 1998). Molecular biological studies have shown that the mammalian GABA_A receptor is a pentamer consisting of subunits from at least five different families, including the α , β , and γ subunits (McKernan and Whiting, 1996; Pritchett et al., 1989; Rudolph et al., 2001). In addition, most of these subunits have a number of different isoforms (e.g., α 1- α 6, β 1- β 3, γ 1- γ 3; Olsen and Sieghart, 2008). The complex molecular biology of GABA_A receptors raises the possibility that subtype-selective agents with therapeutic specificity against alcohol might be developed.

GABA_A receptors expressing the α 5 subunit (α 5GABA_A receptors) comprise only a small proportion of native GABA_A receptors and are found primarily in the hippocampus (Sur et al., 1999; Uusi-Oukari and Korpi, 2010). Projections from the CA1 and CA3 hippocampal fields have been shown to innervate brain regions implicated in the reinforcing effects of alcohol (e.g., Sesack and Grace, 2010). Several lines of evidence support a potential role for α 5GABA_A receptor mechanisms in the abuse-related effects of alcohol. In this regard, using data from the Collaborative Study on the Genetics of Alcoholism, Song and colleagues (2003) reported a significant association between *GABRA5* (the gene encoding the α 5 subunit of the GABA_A receptor) and alcohol dependence. In alcohol discrimination studies in squirrel monkeys, we have shown that the α 5GABA_A receptor-selective agonists QH-ii-066 and panadiplon mimicked the discriminative stimulus effects of alcohol (Platt et al., 2005). Moreover, the discriminative stimulus effects of alcohol and the alcohol-like discriminative stimulus

effects of QH-ii-066 were dose-dependently blocked by L-655,708, an $\alpha 5$ GABA_A receptor-selective inverse agonist (Platt et al., 2005). With respect to the reinforcing effects of alcohol, intrahippocampal or i.p. administration of other $\alpha 5$ GABA_A receptor-selective inverse agonists decreased alcohol self-administration in rats at doses that did not disrupt self-administration of saccharin or water (June et al., 2001; McKay et al., 2004). Finally, mice lacking the $\alpha 5$ subunit of the GABA_A receptor show both reduced preference for and reduced consumption of alcohol (Boehm et al., 2004).

The purpose of the present study was to evaluate the contribution of $\alpha 5$ GABA_A receptor mechanisms to the reinforcing effects of alcohol in rhesus monkeys. We determined the ability of $\alpha 5$ GABA_A receptor-selective ligands to augment and/or attenuate alcohol self-administration. The selective ligands included the agonist QH-ii-066, the antagonist XLi-093 and the inverse agonist L-655,708. Results with the $\alpha 5$ GABA_A receptor ligands were compared with results obtained with naltrexone, an FDA approved pharmacotherapy to treat alcohol dependence. Drugs that reduce alcohol self-administration may have potential as candidate anti-alcohol medications. An important consideration in the development of an alcohol pharmacotherapy is the pharmacological specificity of the candidate medication's effects. One technique used to evaluate the specificity of a medication's effect is to compare the doses of a drug to reduce behaviour maintained by alcohol relative to behaviour maintained by a non-drug reinforce. To that end, we investigated the extent to which L-655,708 modulated the reinforcing effects of alcohol at doses that did not alter sucrose self-administration. Finally, compliance with any medication regimen is tied closely with the extent to which the medication produces untoward side effects. We evaluated the observable behavioral effects of $\alpha 5$ GABA_A receptor ligands in both alcohol- and sucrose-drinking

monkeys to assess the degree to which the drugs elicited behavioral effects that might limit their clinical utility (e.g., sedation, anxiety, convulsions).

Materials and Methods

Subjects. Nine adult male rhesus monkeys (*Macaca mulatta*), weighing 9.5 to 12.1 kg, were studied in daily experimental sessions. Three of the monkeys (two assigned to the alcohol group; one assigned to the sucrose group) had prior experience in operant i.v. self-administration (either cocaine or midazolam) procedures. The remaining monkeys were experimentally naive. Monkeys were housed in a colony room with a 12-h light/dark cycle. Monkeys had unrestricted access to water via the standard cage-associated automatic sipper line and were fed a diet of monkey chow (Harlan Teklad Monkey Diet, Harlan Teklad, Madison, WI), supplemented with fresh fruit. All animals were maintained in accordance with the guidelines of the Committee on Animals of the Harvard Medical School and the "Guide for Care and Use of Laboratory Animals" of the Institute of Laboratory Animal Resources, National Research Council, Department of Health, Education and Welfare Publication No. (NIH) 85-23, revised 1996. Research protocols were approved by the Harvard Medical School Institutional Animal Care and Use Committee.

Apparatus. Monkeys were housed individually in stainless steel primate cages that also served as the experimental chambers. One side of the cage was customized to form an operant drinking panel. The panel consisted of two retractable sippers (model #: ENV-652AM; Med Associates, Inc., Georgia, VT) equipped with solenoids to minimize dripping. Each sipper was connected with Tygon tubing to a stainless steel liquid reservoir mounted on the outside of the drinking panel. A response lever (Med Associates, Inc., Georgia, VT) was positioned below each sipper. Each press of a lever

produced an audible click and was recorded as a response. Colored lights mounted above the sippers could be illuminated to serve as visual stimuli. In these experiments, only one side of the drinking panel was active.

Alcohol self-administration. Five monkeys were trained to respond under a fixed-ratio (FR) schedule of oral alcohol reinforcement. In the presence of a white light, completion of every 10th response (FR 10) resulted in a change in illumination from white to red light and extension of the drinking spout. Displacement of the drinking spout up, down, left or right during extension resulted in alcohol delivery. Fluid flow continued for as long as the monkey displaced the spout or for 30-s, whichever was shorter. Within the 30-s sipper extension time, the monkey could stop drinking (i.e., release the spout) and resume drinking (i.e., displace the spout) as many times as it wanted. The actual duration and volume of intake, within the constraints of the schedule, were under the control of the subject. Between extensions of the drinking spout, all lights were off briefly, and responses had no scheduled consequences. Daily self-administration sessions lasted 3-h. The reinforcing effects of a range of concentrations of alcohol (0.5 – 16% w/v), as well as water, were evaluated initially in each monkey. Each alcohol concentration (or water) was made available for a minimum of five consecutive self-administration sessions and until stable intake was observed (i.e., no upward or downward trend in mls and/or g/kg consumed over a period of at least three consecutive days).

The effects of pretreatment with varying doses of the $\alpha 5\text{GABA}_A$ agonist QH-ii-066 (0.1 – 5.6 mg/kg), the $\alpha 5\text{GABA}_A$ antagonist XLi-093 (0.03 – 0.3 mg/kg) or the $\alpha 5\text{GABA}_A$ inverse agonist L-655,708 (0.1 – 1.8 mg/kg) and their vehicles were determined on self-administration of a 2% alcohol solution. This alcohol concentration

was chosen because it maintained intakes significantly higher than that of water. In addition, it was on the ascending limb of the alcohol concentration-response function, allowing for detection of both increases and decreases in intake as a consequence of drug pretreatment. Each dose of QH-ii-066, XLi-093 and L-655,708 was studied for a minimum of five consecutive sessions and until intake was stable. Between evaluation of different doses of the $\alpha 5\text{GABA}_A$ ligands, monkeys were returned to baseline self-administration (i.e., a minimum of five days of self-administration of a 2% alcohol solution in the absence of any pretreatment). This step allowed assessment of baseline levels of intake over the course of the study. The $\alpha 5\text{GABA}_A$ ligands were studied in random order in individual animals, and all doses of a given ligand were studied before moving on to another drug. For comparison, the effects of the opioid antagonist naltrexone (0.01 – 0.3 mg/kg) also were determined.

Subsequently, maximally effective doses of QH-ii-066 (0.3 mg/kg) and L-655,708 (1.8 mg/kg) and their vehicles were given as pretreatments before sessions in which a wider range of alcohol concentrations were made available for self-administration. These studies determined the degree to which the ligands altered the shape and/or position of the alcohol concentration-response function. Finally, the capacity of XLi-093 to reverse the effects of QH-ii-066 and L-655,708 was determined. In all instances, the effects of the $\alpha 5\text{GABA}_A$ ligands at each alcohol concentration were studied for a minimum of five consecutive sessions and until intake was stable.

Sucrose self-administration. A separate group of four monkeys was trained to respond under a FR 10 schedule of oral sucrose reinforcement. This schedule and solution delivery was identical to that for alcohol self-administration, except that a sucrose solution instead of alcohol was available for self-administration. The reinforcing

effects of a range of concentrations of sucrose (0.1 – 3% w/v), as well as water, were evaluated initially in each monkey. Each sucrose concentration (or water) was made available for a minimum of five consecutive self-administration sessions and until stable intake was observed.

The effects of pretreatment with varying doses of the QH-ii-066 or L-655,708 and their vehicles were determined on self-administration of a 0.3% sucrose solution. This sucrose concentration was chosen because it maintained intakes that were significantly higher than that of water and roughly equivalent to intakes maintained by 2% alcohol in the alcohol self-administration group. Each dose of QH-ii-066 and L-655,708 was studied for a minimum of five consecutive sessions and until intake was stable. Between evaluation of different doses of the $\alpha 5\text{GABA}_A$ ligands, monkeys were returned to baseline self-administration. The $\alpha 5\text{GABA}_A$ ligands were studied in irregular order in individual animals, and all doses of a given ligand were studied before moving on to another test drug.

Observable behavior. Following daily self-administration sessions, the behavior of each monkey (regardless of whether the animal self-administered alcohol or sucrose) was scored during a five-min sampling period using a focal animal approach as described in Platt et al. (2000; 2002) and as modified for the rhesus monkey. That is, after the self-administration session, an observer who was not informed about the drugs under investigation watched a specific animal for five min. During this sampling period, the observer recorded each instance a particular behavior (Table 1) occurred in 15-s intervals during the period. Scores were calculated from these data as the number of 15-s intervals in which a particular behavior occurred (maximum possible score for each behavior was 20). A randomization schedule was employed so that order effects

between animals were minimized. Eight observers performed the scoring across the duration of the study. Typically, two observers were used daily – one observing the alcohol drinkers, one observing the sucrose drinkers. To ensure reliability across observers, each individual underwent at least 20 h of training until they reached an inter-observer reliability criterion of $\geq 90\%$ based on percent agreement scores calculated between all possible pairs.

Blood alcohol levels (BAL). At select time points across the study (e.g., once stable intake was obtained at a particular alcohol concentration or after a particular drug treatment), monkeys self-administering alcohol were anesthetized with ketamine immediately following the session and three – five mls of blood were collected from the femoral vein. Samples were immediately centrifuged at 3200 rpm for 8-12 minutes. The plasma was drawn off, transferred to polypropylene tubes, and then frozen until analysis. Triple determinations of BALs were conducted using a rapid high performance plasma alcohol analysis using alcohol oxidase with an AM1 series analyzer and Analox Kit GMRD-113 (Analox Instruments USA, Lunenburg, MA). This process detects BAL ranges from 0 to 350 mg/dl using an internal standard of 100 mg/dl.

Data analysis. After each alcohol self-administration session, intake for individual subjects was determined in two ways: volume (mls) and alcohol dose (g/kg) consumed. Dose was calculated as: [volume consumed (mls) X alcohol concentration (g/ml)]/weight (kg). After each sucrose self-administration session, intake for individual subjects was the volume consumed (mls). Data are expressed as mean intake over the last three sessions of water or alcohol/sucrose availability. Because the intake measurements for alcohol self-administration are correlated, with the exception of Fig. 1, we present only the data representing alcohol dose. A one-way repeated measures

ANOVA was used to evaluate the effect of alcohol/sucrose concentration on total volume consumed.

To compare the effects of the $\alpha 5\text{GABA}_A$ ligands and naltrexone on alcohol self-administration, intakes following pretreatment with QH-ii-066, XLi-093; L-655,708 or naltrexone were converted to % of baseline intake. Baseline intake was considered to be the mean dose of alcohol consumed across the three days of no pretreatment immediately prior to tests with a given dose of a compound. Separate one-way repeated measures ANOVAs followed by Bonferroni t-tests compared the effects of the pretreatment drugs to the effect of vehicle on intake. In curve-shifting experiments, separate two-way repeated measures ANOVAs compared the effects of either QH-ii-066 or L-655,708, alone or combined with XLi-093, to the effect of vehicle on intake.

To compare the effects of the $\alpha 5\text{GABA}_A$ ligands on sucrose self-administration, intakes following pretreatment with QH-ii-066 or L-655,708 were converted to % of baseline intake. Baseline intake was considered to be the mean mls of sucrose consumed across the three days of no pretreatment immediately prior to tests with a given dose of a compound. Separate one-way repeated measures ANOVAs compared the effects of the pretreatment drugs to the effect of vehicle on intake.

Observational data were treated in two ways. To evaluate the effect of increasing intake of alcohol on observable behavior, frequency scores for each behavior were averaged across the alcohol self-administration subjects to obtain group means. Mean scores (\pm SEM) for each behavior then were plotted as a function of intake. For these analyses, intake (g/kg) was converted to "number of drinks". We use an operational definition of a "drink" as 0.25 g/kg alcohol or 17 g alcohol in a 70 kg human, representing the upper range of worldwide definitions of a drink (cf. Grant and Bennett, 2003; Kalant and Poikolainen, 1999). To determine statistical reliability of treatment

effects on each behavior, the effect of drink number was determined by separate one-way ANOVAs. Only the behavioral data generated during determination of the alcohol-concentration response function were included in these analyses. To evaluate the effect of $\alpha 5\text{GABA}_A$ ligands on observable behavior, frequency scores for each behavior were averaged separately across the alcohol self-administration subjects and the sucrose self-administration subjects to obtain means. For each group, mean scores (\pm SEM) for each behavior were plotted as a function of dose. For normally distributed data (as assessed using the Shapiro-Wilk test), separate two-way mixed factor ANOVAs determined the effects of the between-group factor (alcohol vs. sucrose) and within-group factor (dose) and their interaction on each behavior. In all cases, significant main effects were examined post-hoc with Bonferroni t-tests. The alpha level for all tests was $P \leq 0.05$.

Drugs. Ethanol (95%; Pharmco Products, Brookfield, CT) and diluted to the appropriate concentrations with tap water. QH-ii-066 and XLi-093 were synthesized as described in Huang et al. (2000) and Li et al. (2003), respectively. These compounds were dissolved in 50-80% propylene glycol/20-50% 0.9% saline solution. L-655,708 (Tocris Bioscience, Ellsville, MO) was dissolved in 50% propylene glycol/50% 0.9% saline solution. Naltrexone HCl (Sigma/RBI, St. Louis, MO) was dissolved in 0.9% saline solution. Intramuscular injection volumes were 0.02 – 0.05 ml/kg body weight. Pretreatment times were 10 min for the $\alpha 5\text{GABA}_A$ ligands and 30 min for naltrexone.

Results

Alcohol self-administration. Oral presentation of alcohol maintained self-administration in all monkeys under the FR schedule of alcohol delivery and limited

access conditions (Fig. 1). As the concentration of alcohol was increased, intake first increased and then decreased, resulting in an inverted u-shaped concentration-response function. For the group, alcohol concentrations between 1 and 6% (w/v) maintained intakes significantly higher than that during water availability (Fig. 1A; $F(7,28)=17.6$, $P<0.001$, Bonferroni t-tests, $P<0.05$). At these concentrations, monkeys drank approximately 0.8 – 1.9 g/kg of alcohol (Fig. 1B). Analysis of blood samples verified that the volumes consumed when concentrations $\geq 2\%$ (w/v) were available produced BALs in excess of 80 mg/dl in all monkeys (Fig. 1C).

In addition to producing orderly effects on drinking behavior, alcohol altered several observable behaviors (Fig. 2). All five self-administration monkeys had self-administration episodes resulting in intake of 1 – 8 drinks; while three of the five monkeys had self-administration episodes resulting in intake of nine or more drinks. These higher intakes were observed after 13% of the self-administration sessions. While intakes below the equivalent of 7 drinks failed to alter any observable behavior, intakes of at least 7 drinks produced reliable changes in measures of passive visual, locomotion, tactile/oral exploration, stereotypy, scratching, and ataxia compared to levels of these behaviors observed during water availability. Locomotion, across a range of 7 – 9 drinks, was significantly increased compared to levels observed during water availability ($F(10,716)=6.2$, $P<0.001$, Bonferroni t-tests, $P<0.05$). At the highest intake (≥ 10 drinks), though, locomotion returned to water levels, likely coinciding with a significant increase in passive visual behavior ($F(10,716)=2.0$, $P<0.05$, Bonferroni t-tests, $P<0.05$). During water availability, ataxia was not observed. However, a significant drink-dependent increase in ataxia occurred at intakes of ≥ 8 drinks ($F(10,716)=4.0$, $P<0.001$, Bonferroni t-tests, $P<0.05$). Significant drink-dependent decreases in behaviors also were observed. At intakes ≥ 7 drinks, scratching was significantly reduced compared to water levels ($F(10,716)=8.0$, $P<0.001$, Bonferroni t-tests, $P<0.05$). Alcohol also

produced an overall drink-dependent decrease in levels of tactile/oral exploratory behavior ($F(10,716)=2.2$, $P<0.05$, Bonferroni t-tests, n.s.) and stereotypic behavior ($F(10,716)=2.4$, $P<0.01$, Bonferroni t-tests, n.s.). Alcohol had no other significant effects on observable behavior over the range of intakes observed during determination of the alcohol concentration-response function.

$\alpha 5GABA_A$ ligands and alcohol self-administration. Daily pretreatment with the $\alpha 5GABA_A$ ligands or naltrexone produced qualitatively different effects on alcohol (2% w/v) intake depending on the compound (Fig. 3). For example, the two lowest doses (0.1 and 0.3 mg/kg) of QH-ii-066 induced small but significant increases in alcohol consumption (125 – 135% of the baseline intake of 1.4 ± 0.2 g/kg) compared to vehicle ($F(5,20)=18.2$, $P<0.001$, Bonferroni t-tests, $P<0.05$). At higher doses of QH-ii-066, intake returned to baseline levels and did not differ from that following vehicle administration. Problems with solubility prohibited testing higher doses of QH-ii-066. In the case of XLi-093, none of the doses evaluated altered self-administration of alcohol compared to vehicle, and intake was maintained at baseline levels (1.8 ± 0.02 g/kg). In contrast, daily pretreatment with L-655,708 resulted in dose-dependent reductions in alcohol self-administration compared to vehicle ($F(4,16)=37.6$, $P<0.001$), with the two highest doses (1 and 1.8 mg/kg) producing significant decreases in intake (Bonferroni t-tests, $P<0.05$). At the highest dose of L-655,708, intake was suppressed maximally to approximately 40% of the baseline intake of 1.6 ± 0.2 g/kg. The suppression of alcohol self-administration by L-655,708 was similar to that induced by naltrexone. As expected, naltrexone engendered dose-dependent decreases in alcohol self-administration that reliably differed from vehicle at doses of 0.1 and 0.3 mg/kg ($F(4,16)=7.7$, $P<0.01$, Bonferroni t-tests, $P<0.05$). The highest dose of naltrexone maximally suppressed

alcohol self-administration to 38% of the baseline intake of 1.7 ± 0.2 g/kg. In general, for all drugs, the effect observed on the first day of a given pretreatment was similar to that observed on the final day of administration (5 – 7 days), providing no evidence of the development of tolerance to the effects of QH-ii-066, L-655,708 or naltrexone (data not shown).

Based on the results of the study described above, doses of the $\alpha 5\text{GABA}_A$ ligands that maximally altered alcohol self-administration were studied in combination with a wider range of alcohol concentrations (Fig. 4). In general, pretreatment with QH-ii-066 (0.3 mg/kg) enhanced self-administration of 0.5 – 4% (w/v) alcohol solutions and resulted in a leftward shift in the ascending limb of the alcohol concentration-response function (Fig. 4, left). By and large, this leftward shift could be reversed if the animals also received a pretreatment of the highest dose of XLi-093 (0.3 mg/kg). These findings are confirmed by a significant alcohol concentration X treatment interaction ($F(6,24)=5.2$, $P<0.01$, Bonferroni t-tests, $P<0.05$). In contrast, pretreatment with L-655,708 (1.8 mg/kg) attenuated self-administration of 1 – 6% (w/v) alcohol solutions and resulted in an overall rightward shift in the ascending limb of the alcohol concentration-response function (Fig. 4, right). As with QH-ii-066, pretreatment with the highest dose of XLi-093 completely reversed the L-655,708-induced rightward shift in the alcohol concentration-response function. These findings are confirmed by a significant alcohol concentration X treatment interaction ($F(6,24)=3.9$, $P<0.01$, Bonferroni t-tests, $P<0.05$).

$\alpha 5\text{GABA}_A$ ligands and sucrose self-administration. Oral presentation of sucrose maintained self-administration in all monkeys under the FR schedule of sucrose delivery and limited access conditions (Fig. 5A). As the concentration of sucrose was increased, intake also increased. Patterns of responding were comparable to those

observed during alcohol self-administration (data not shown). For the group, sucrose concentrations between 0.3 and 3% (w/v) maintained intakes significantly higher than that during water availability ($F(4,12)=9.5$, $P<0.01$, Bonferroni t-tests, $P<0.05$). At 0.3% (w/v), individual subjects displayed intakes ranging from ~ 450 to 1100 mls. The average intake (\pm SEM) for the group at this concentration was 839 ± 157 mls and did not differ significantly from the intake of the alcohol self-administration group at 2% (w/v) (906 ± 92 mls; $t(7)=0.4$, $P=n.s.$). Daily pretreatment with either QH-ii-066 or L-655,708 did not markedly alter sucrose self-administration at any dose compared to their respective vehicles (Fig. 5B).

$\alpha 5GABA_A$ ligands and observable behavior. In the absence of drug pretreatment and under water availability, the alcohol- and sucrose-drinking monkeys did not differ from each other for the majority of behaviors (Supplemental Figure 1). However, the sucrose drinkers did exhibit significantly higher levels of tactile/oral exploration ($t(7)=-4.3$, $P<0.005$) and locomotion ($t(7)=-2.4$, $P<0.05$) and tended to present more ($t(7)=-2.5$, $P<0.05$). Neither QH-ii-066 nor L-655,708, at any dose evaluated, markedly altered the majority of observable behaviors. Likewise, naltrexone failed to alter any of the behaviors. There were, however, two exceptions (Fig. 6A and 6B). QH-ii-066 dose-dependently decreased tactile/oral exploration in both the alcohol-drinking and sucrose-drinking monkeys, with a dose of 3 mg/kg significantly reducing this behavior compared to vehicle levels. This effect was confirmed by a significant main effect of QH-ii-066 dose on this behavior (Shapiro-Wilk Normality test – passed; $F(4,28)=4.6$, $P<0.01$, Bonferroni t-tests, $P<0.05$). On the other hand, L-655,708 dose-dependently increased yawning in both self-administration groups, with the highest dose (1.8 mg/kg) engendering significantly more yawning compared to vehicle (Shapiro-Wilk Normality test – passed; $F(4,28)=2.8$, $P<0.05$, Bonferroni t-tests, $P<0.05$).

Discussion

In the present study, alcohol served as a reinforcer in all monkeys, maintaining intake levels above those of water. At concentrations of $\geq 2\%$ (w/v), monkeys self-administered pharmacologically relevant doses of alcohol and produced BALs ranging from 90 – 160 mg/dl. The overall intakes (i.e., g/kg) observed in this study are generally typical of intakes observed for macaques self-administering alcohol under limited access conditions (Grant and Johanson, 1988; Henningfield and Meisch, 1978; 1979; 1981; Katner et al., 2004; Vivian et al., 1999). Differences in intake between the present study and those cited could be due to a number of methodological differences including length of self-administration session, addition of flavorants, induction techniques, concentrations of alcohol made available for self-administration, and the self-administration apparatus itself. In fact, the latter difference could be especially important in the cases where the intakes observed in the present study are higher than those of the cited studies. In our procedure, the monkey must press a lever to gain access to a drinking spout connected to an alcohol reservoir. Depression of the drinking spout during extension results in alcohol delivery and fluid flow continues for as long as the monkey displaces the spout or for 30-s, whichever is shorter. The actual duration and volume of intake, within the constraints of the schedule, is under the control of the subject. Depending upon the available alcohol concentration, we observed average volumes of 12.5 mls of alcohol delivered per spout extension (range: ~3.5 mls/extension at 16% w/v; ~21 mls/extension at 2% w/v; data not shown). This average volume/delivery is much larger than the volumes/delivery in the cited studies in which the drinking spouts are designed to deliver a set amount of alcohol (typically 0.5 – 1 ml) each delivery. Evidence from rats would suggest that alcohol intake should increase as the volume per reinforcement increases (Henningfield and Meisch, 1975).

When given the opportunity to consume a wide range of alcohol concentrations, monkeys drank sufficient quantities of alcohol to alter observable behavior. In many instances, these behavioral changes mirrored the effects of alcohol in intoxicated humans or those exposed to an acute alcohol challenge. For example, it is well-established that alcohol has a biphasic effect on activity (e.g., Martin et al., 1993; Morean and Corbin, 2010) such that, in human subjects, alcohol-induced stimulant effects (e.g., feelings of energized, stimulated, vigorous) are generally observed at lower BALs on the ascending limb of the blood alcohol curve, and alcohol-induced sedative effects (e.g., feelings of heavy head, inactive, sluggish) are reported at higher BALs on the descending limb of the blood alcohol curve. In monkeys, we observed a reliable increase in locomotor activity across a lower range of drinks (and presumably lower BALs) compared to the range where we observed increases in passive visual behavior and decreases in tactile/oral exploration, possible indices of sedative-like effects. Alcohol also is known to reduce the response to stressors and can produce anxiolytic-like effects in humans (e.g., Eckardt et al., 1998; Thomas et al., 2003). Similarly, alcohol produced a drink-dependent decrease in stereotypy and scratching, two behaviors that have been associated with anxiety in nonhuman primates and which are amenable to reduction by typical anxiolytics (e.g., Birkett et al., 2005; Castles et al., 1999; Schino et al., 1996; Tiefenbacher et al., 2005a; 2005b; Troisi, 2002). Finally, alcohol has been shown to dose-dependently increase the amount of body sway or static ataxia in humans (e.g., Schuckit, 1985); likewise, in monkeys, observable ataxia increased in a drink-dependent manner. Together, these findings illustrate and reinforce the translational nature of our non-human primate drinking model.

Using this model and GABA_A receptor subtype-selective ligands, we assessed the contribution of α 5GABA_A receptor mechanisms to the reinforcing effects of alcohol. We found that the agonist QH-ii-066 modestly increased, and the inverse agonist L-

655,708 decreased, intake of alcohol (2% w/v). Subsequently, the maximally effective dose of QH-ii-066 was found to enhance intake of a wider range of alcohol concentrations; whereas, the maximally effective dose of L-655,708 was found to inhibit intake of a wider range of alcohol concentrations. Both leftward (QH-ii-066) and rightward (L-655,708) shifts in the alcohol concentration-response function were abolished by XLi-093, despite it not altering drinking on its own. These observations are in agreement with results from rodent studies showing that other $\alpha 5$ GABA_A receptor inverse agonists can reduce drinking (June et al., 2001; McKay et al., 2004). In conjunction with observations that $\alpha 5$ GABA_A receptor-subunit knockout mice exhibit reduced preference for and consumption of alcohol (Boehm et al., 2004), these findings suggest a prominent role for $\alpha 5$ GABA_A receptor mechanisms in the reinforcing effects of alcohol. Moreover, the lack of effect on drinking behavior with XLi-093 alone raises the possibility that neutral efficacy (i.e., antagonism) at this specific GABA_A receptor subtype is not sufficient to inhibit drinking, rather inverse efficacy is required.

In our hands, L-655,708 was as effective as the prototypical alcohol pharmacotherapy naltrexone in reducing drinking in the monkeys. Coupled with the observation that L-655,708 also can attenuate the subjective/interoceptive effects of alcohol (Platt et al., 2005), a growing body of research suggests that $\alpha 5$ GABA_A receptor inverse agonists may have potential as candidate anti-alcohol medications. An important consideration in the development of an alcohol pharmacotherapy is the pharmacological specificity of the candidate medication's effect. One technique used to evaluate the specificity of a medication's effect is to compare the doses of a drug needed to reduce behavior maintained by alcohol relative to behavior maintained by a non-drug reinforcer. For example, if a drug reduces alcohol-maintained behavior to a greater extent than it reduces behavior maintained by the non-drug reinforcer, then the

drug may have selective effects on alcohol self-administration (c.f. Mello and Negus, 1996). In the present study, L-655,708, across the same dose range studied in the alcohol drinkers, did not alter drinking in the sucrose drinkers. This result suggests that the inhibitory effects of L-655,708 are selective for alcohol. Moreover, that sucrose drinking also was not modified by QH-ii-066 provides additional support for a key role for $\alpha 5\text{GABA}_A$ receptor mechanisms in modulating the abuse-related effects of alcohol in particular, rather than drinking behavior in general.

Because adverse side effects can limit the utility of a pharmacotherapy, and because non-selective inverse agonists at the GABA_A /benzodiazepine site often can have convulsant/proconvulsant effects (e.g., Braestrup et al., 1983), it was of interest to determine the behavioral profile of L-655,708. In both alcohol- and sucrose-drinkers, L-655,708 was relatively benign and there was no indication of any interaction between L-655,708 and alcohol. Notably, even with repeated administration, L-655,708 was devoid of convulsant activity. This agrees with studies in rats showing that L-655,708 does not induce seizures on its own, nor does it alter the dose of pentylenetetrazole required to induce seizures (Atack et al., 2006). The sole observable effect of L-655,708 was to increase yawning in both groups of monkeys. In nonhuman primates, increases in yawning often have been interpreted as indicating increased stress and anxiety (Castles et al., 1999; Lutz et al., 2004), and yawning can be induced in monkeys with administration of an anxiogenic drug (Major et al., 2009). Likewise, L-655,708 exhibited anxiogenic-like activity in mice in an elevated plus-maze procedure (Navarro et al., 2002). While the effects of L-655,708 have not been determined in alcoholics, there is evidence for transient anxiogenic effects of flumazenil, a benzodiazepine receptor antagonist, in alcoholics in early withdrawal (Nutt et al., 1993). Taken together, these findings certainly would suggest that an $\alpha 5\text{GABA}_A$ receptor inverse agonist is likely to

have anxiogenic effects in humans. While a relatively mild side effect, anxiogenesis would likely limit how an L-655,708-type drug might be used effectively in a treatment setting. For example, given that stress-induced negative affective states and withdrawal-induced anxiety are important facilitators of relapse to excessive alcohol use (e.g., Breese et al., 2005; Heilig et al., 2010), a drug that induces anxiety would not be a practical anti-relapse medication. Rather, our results would suggest that an $\alpha 5\text{GABA}_A$ receptor inverse agonist may be most useful as a pharmacotherapy to assist individuals with achieving abstinence.

In summary, our findings suggest a prominent and selective role for $\alpha 5\text{GABA}_A$ receptor mechanisms in the reinforcing effects of alcohol. The results implicate $\alpha 5\text{GABA}_A$ receptors as potential pharmacological targets for medications to reduce drinking and assist individuals in achieving abstinence. In particular, $\alpha 5\text{GABA}_A$ receptor inverse agonists may hold the most promise as alcohol pharmacotherapies.

Acknowledgments

We thank A. Duggan, S. Harper-Castle, K. Bano, S. Curran, A. Duke, S. Langer, N. Shinday, J. Perrault, C. Moran, B. Fischer and the Division of Veterinary Resources for assistance with data collection.

References

- Atack JR, Bayley PJ, Seabrook GR, Wafford KA, McKernan RM, Dawson GR (2006) L-655,708 enhances cognition in rats but is not proconvulsant at a dose selective for $\alpha 5$ -containing GABA_A receptors. *Neuropharmacology* 51:1023-1029.
- Birkett MA, Platt DM, Tiefenbacher S, Rowlett JK (2005) A "pharmacological stressor" model of anxiolysis in monkeys: Alprazolam attenuation of the behavioral and physiological effects of yohimbine. *Neuropsychopharmacology* 30:S235.
- Boehm SL, Ponomarev I, Jennings AW, Whiting PJ, Rosahl TW, Garrett EM, Blednov YA, Harris RA (2004) γ -aminobutyric acid A receptor subunit mutant mice: New perspectives on alcohol actions. *Biochem Pharmacol* 68:1581-1602.
- Braestrup C, Nielsen M, Honore T, Jensen LH, Petersen EN (1983) Benzodiazepine receptor ligands with positive and negative efficacy. *Neuropharmacology* 22:1451-1457.
- Breese GR, Overstreet DH, Knapp DJ (2005) Conceptual framework for the etiology of alcoholism: A "kindling"/stress hypothesis. *Psychopharmacology* 178:367-380.
- Castles DL, Whiten A, Aureli F (1999) Social anxiety, relationships and self-directed behaviour among wild female olive baboons. *Anim Behav* 58:1207-1215.
- Eckardt MJ, File SE, Gessa GL, Grant KA, Guerri C, Hoffman PL, Kalant H, Koob GF, Li T-K, Tabakoff B (1998) Effects of moderate alcohol consumption on the central nervous system. *Alcohol Clin Exp Res* 22:998-1040.
- Grant KA, Johanson CE (1988) Oral ethanol self-administration behavior in free-feeding rhesus monkeys. *Alcohol Clin Exp Res* 12:780-784..
- Grant KA, Bennett AJ (2003) Advances in nonhuman primate alcohol abuse and alcoholism research. *Pharmacol Ther* 100:235-255.

- Heilig M, Egli M, Crabbe JC, Becker HC (2010) Acute withdrawal, protracted abstinence and negative affect in alcoholism: Are they linked? *Addict Biol* 15:169-184.
- Henningfield JE, Meisch RA (1975) Ethanol-reinforced responding and intake as a function of volume per reinforcement. *Pharmacol Biochem Behav* 3:437-441.
- Henningfield JE, Meisch RA (1978) Ethanol drinking by rhesus monkeys as a function of concentration. *Psychopharmacology* 57:133-136.
- Henningfield JE, Meisch RA (1979) Ethanol drinking by rhesus monkeys with concurrent access to water. *Pharmacol Biochem Behav* 10:777-782.
- Henningfield JE, Meisch RA (1981) Ethanol and water drinking by rhesus monkeys. *J Stud Alcohol* 42:192-201.
- Huang Q, He X, Ma C, Liu R, Yu S, Dayer CA, Wenger GR, McKernan R, Cook JM (2000) Pharmacophore/receptor models for GABA_A/BzR subtypes ($\alpha 1\beta 3\gamma 2$, $\alpha 5\beta 3\gamma 2$, and $\alpha 6\beta 3\gamma 2$) via a comprehensive ligand mapping approach. *J Med Chem* 43:71-95.
- Hyytiä P, Koob GF (1995) GABA_A receptor antagonism in the extended amygdala decreases ethanol self-administration in rats. *Eur J Pharmacol* 283:151-159.
- June HL, Lin M, Greene TL, Lewis MJ, Murphy JM (1995) Effects of negative modulators of GABAergic efficacy on ethanol intake: Correlation of biochemical changes with pharmacological effect using a behavioral paradigm. *J Exp Clin Psychopharmacol* 3:252-260.
- June HL, Torres L, Cason CR, Hwang BH, Braun MR, Murphy JM (1998) The novel benzodiazepine inverse agonist RO19-4603 antagonizes ethanol motivated behaviors: Neuropharmacological studies. *Brain Res* 784:256-275.
- June HL, Harvey SC, Foster KL, McKay PF, Cummings R, Garcia M, Mason D, Grey C, McCane S, Williams L, Johnson TB, He X, Rock S, Cook JM (2001) GABA_A

receptors containing $\alpha 5$ subunits in the CA1 and CA3 hippocampal fields regulate ethanol-motivated behaviors: An extended ethanol reward circuitry. *J Neurosci* 21:2166-2177.

- Kalant H, Poikolainen K (1999) Moderate drinking: Concepts, definitions and public health significance, in *Health Issues Related to Alcohol Consumption* (MacDonald I, ed), pp 1-26. Blackwell, Oxford.
- Katner SN, Flynn CT, Von Huben SN, Kirsten AJ, Davis SA, Lay CC, Cole M, Roberts AJ, Fox HS, Taffe MA (2004) Controlled and behaviorally relevant levels of oral ethanol intake in rhesus macaques using a flavorant-fade procedure. *Alcohol Clin Exp res* 28:873-883.
- Korpi ER (1994) Role of GABA_A receptors in the actions of alcohol and in alcoholism: Recent advances. *Alcohol Alcohol* 29:115-129.
- Li X, Cao H, Zhang C, Furtmuller R, Fuchs K, Huck S, Sieghart W, Deschamps J, Cook JM (2003) Synthesis, in vitro affinity, and efficacy of a bis 8-ethynyl-4*H*-imidazo[1,5*a*]-[1,4]benzodiazepine analogue, the first bivalent $\alpha 5$ subtype selective BzR/GABA_A antagonist. *J Med Chem* 46:5567-5570.
- Lutz C, Tiefenbacher S, Meyer J, Novak M (2004) Extinction deficits in male rhesus macaques with a history of self-injurious behavior. *Am J Primatol* 63:41-48.
- Major CA, Kelly BJ, Novak MA, Davenport MD, Stonemetz KM, Meyer JS (2009) The anxiogenic drug FG7142 increases self-injurious behavior in male rhesus monkeys (*Macaca mulatta*). *Life Sci* 85:753-758.
- Martin CS, Earleywine M, Musty RE, Perrine MW, Swift RM (1993) Development and validation of the biphasic alcohol effects scale. *Alcohol Clin Exp Res* 17:140-146.
- McKay PF, Foster KL, Mason D, Cummings R, Garcia M, Williams L, Grey C, McCane S, He X, Cook JM, June HL (2004) A high affinity ligand for GABA_A-receptor

- containing $\alpha 5$ subunit antagonizes ethanol's neurobehavioral effects in Long-Evans rats. *Psychopharmacology* 172:455-462.
- McKernan RM, Whiting PJ (1996) Which GABA_A-receptor subtypes really occur in the brain? *Trends Pharmacol Sci* 19:139-143.
- Mello NK, Negus SS (1996) Preclinical evaluation of pharmacotherapies for treatment of cocaine and opioid abuse using drug self-administration procedures. *Neuropsychopharmacology* 14:375-424.
- Morean ME, Corbin WR (2010) Subjective response to alcohol: A critical review of the literature. *Alcohol Clin Exp Res* 34:385-395.
- Navarro JF, Buron E, Martin-Lopez M (2002) Anxiogenic-like activity of L-655,708, a selective ligand for the benzodiazepine site of GABA_A receptors which contain the alpha-5 subunit, in the elevated plus-maze test. *Prog Neuropsychopharmacol Biol Psychiatry* 26:1389-1392.
- Novak MA, O'Neill P, Suomi SJ (1992) Adjustments and adaptations to indoor and outdoor environments: Continuity and change in young adult rhesus monkeys. *Am J Primatol* 28:124-138.
- Nutt D, Glue P, Wilson S, Groves S, Coupland N, Bailey J (1993) Flumazenil in alcohol withdrawal. *Alcohol Alcohol Suppl* 2:337-341.
- Olsen RW, Sieghart W (2008) International Union of Pharmacology. LXX. Subtypes of γ -aminobutyric acid_A receptors: Classification on the basis of subunit composition, pharmacology, and function. Update. *Pharmacol Rev* 60:243-260.
- Platt DM, Rowlett JK, Spealman RD (2000) Dissociation of cocaine-antagonist properties and motoric effects of the D1 receptor partial agonists SKF 83959 and SKF 77434. *J Pharmacol Exp Ther* 293:1017-1026.

- Platt DM, Rowlett JK, Spealman RD, Cook J, Ma C (2002) Selective antagonism of the ataxic effects of zolpidem and triazolam by the GABA_A/α₁-preferring antagonist β-CCt in squirrel monkeys. *Psychopharmacology* 164:151-159.
- Platt DM, Duggan A, Spealman RD, Cook JM, Li X, Yin W, Rowlett JK (2005) Contribution of α₁GABA_A and α₅GABA_A receptor subtypes to the discriminative stimulus effects of ethanol in squirrel monkeys. *J Pharmacol Exp Ther* 313:658-667.
- Pritchett DB, Lüddens H, Seeburg PH (1989) Type I and type II GABA_A-benzodiazepine receptors produced in transfected cells. *Science* 245:1389-1392.
- Rudolph U, Crestani F, Möhler H (2001) GABA_A receptor subtypes: Dissecting their pharmacological functions. *Trends Pharmacol Sci* 22:188-194.
- Schino G, Perretta G, Taglioni AM, Monaco V, Troisi A (1996) Primate displacement activities as an ethopharmacological model of anxiety. *Anxiety* 2:186-191.
- Schuckit MA (1985) Ethanol-induced changes in body sway in men at high alcoholism risk. *Arch Gen Psychiatry* 42:375-379.
- Sesack SR, Grace AA (2010) Cortico-basal ganglia reward network: Microcircuitry. *Neuropsychopharmacology* 35:27-47.
- Söderpalm AHV, Hansen S (1998) Benzodiazepines enhance the consumption and palatability of alcohol in the rat. *Psychopharmacology* 137:215-222.
- Song J, Koller DL, Foroud T, Carr K, Zhao J, Rice J, Nurnberger Jr JI, Begleiter H, Porjesz B, Smith TL, Schuckit MA, Edenberg HJ (2003) Association of GABA_A receptors and alcohol dependence and the effects of genetic imprinting. *Am J Med Gen* 117B:39-45.

- Sur C, Farrar SJ, Kerby J, Whiting PJ, Atack JR, McKernan RM (1999) Preferential coassembly of alpha4 and delta subunits of the gamma-aminobutyric acid_A receptor in rat thalamus. *Mol Pharmacol* 56:110-115.
- Thomas SE, Randall CL, Carrigan MH (2003) Drinking to cope in socially anxious individuals: A controlled study. *Alcohol Clin Exp Res* 27:1937-1943.
- Tiefenbacher S, Fahey MA, Rowlett JK, Meyer JS, Pouliot AL, Jones BM, Novak MA (2005a) The efficacy of diazepam treatment for the management of acute wounding episodes in captive rhesus macaques. *Comp Med* 55:387-392.
- Tiefenbacher S, Novak MA, Lutz CK, Meyer JS (2005b) The physiology and neurochemistry of self-injurious behavior: A nonhuman primate model. *Front Biosci* 10:1-11.
- Troisi A (2002) Displacement activities as a behavioral measure of stress in nonhuman primates and human subjects. *Stress* 5:47-54.
- Uusi-Oukari M, Korpi ER (2010) Regulation of GABA_A receptor subunit expression by pharmacological agents. *Pharmacol Rev* 62:97-135.
- Vivian JA, Higley JD, Linnoila M, Woods JH (1999) Oral ethanol self-administration in rhesus monkeys: Behavioral and neurochemical correlates. *Alcohol Clin Exp Res* 23:1352-1361.
- Weerts EM, Ator NA, Grech DM, Griffiths RR (1998) Zolpidem physical dependence assessed across increasing doses under a once-daily dosing regimen in baboons. *J Pharmacol Exp Ther* 285:41-53.

Table 1. Behavioral categories, abbreviations, and definitions^a.

SPECIES-TYPICAL:		
Passive visual	(VIS)	Animal is standing or sitting motionless with eyes open
Rest/Sleep posture	(RSP)	Idiosyncratic posture adopted by monkeys during rest or sleep; eyes closed, easily roused by external stimulation (e.g., tapping on cage)
Locomotion	(LOC)	At least two directed steps in the horizontal and/or vertical plane
Tactile/oral exploration	(TAC)	Any tactile or oral manipulation of the cage or environment
Forage	(FOR)	Sweeping and/or picking through wood chip substrate
Self-groom	(GRM)	Picking, scraping, spreading or licking of an animal's own hair
Scratch	(SCR)	Vigorous strokes of the hair with the finger or toenails
Vocalization	(VOC)	Species-typical sounds emitted by monkey (not differentiated into different types)
Yawn	(YWN)	To open mouth wide and expose teeth
Present	(PRE)	Posture involving presentation of rump, belly, flank, and/or neck) to observer or other monkey
Threat/aggress	(THR)	Multifaceted display involving one or more of the following: open mouth stare with teeth partially exposed, eyebrows lifted, ears flattened or flapping, rigid body posture, piloerection, attack (e.g., biting, slapping) of inanimate object or other monkey
Fear grimace	(FGR)	Grin-like facial expression involving the retraction of the lips exposing clenched teeth; may be accompanied by flattened ears, stiff, huddled body posture, screech/chattering vocalizations
Body spasm	(BSP)	An involuntary twitch or shudder of the entire body; also "wet dog" shake
Lip smack	(LIP)	Pursing the lips and moving them together to produce a smacking sound; often accompanied by moaning
Cage shake	(CSH)	Any vigorous shaking of the cage that may or may not make noise
Stereotypy	(STY)	Any repetitive, ritualized pattern of behavior that serves no obvious function
Other	(OTH)	Any notable behavior not indicated above (e.g., masturbation, nose rub, lip droop, vomit/retch)
PROCEDURE-RELATED:		
Lever press	(LVR)	Depression of lever manipulanda on the drinking panel
Drink	(DRI)	Mouth contact to fluid delivery sippers
DRUG-INDUCED:		
Ataxia	(ATX)	Any slip, trip, fall or loss of balance
Procumbent posture	(PRO)	Loose-limbed posture (sitting or lying on cage bottom) accompanied by eye closure; not easily aroused by external stimulation (e.g., tapping on cage)

^a Adapted from Novak et al., 1992; Weerts et al., 1998; Platt et al., 2000, 2002.

Figure Legends

- Figure 1 Oral self-administration of varying alcohol concentrations and water under a fixed-ratio schedule and limited access conditions in monkeys. For each monkey, mean intakes for the last three sessions at each concentration were calculated. Data points represent the mean intake \pm SEM (A. mls; B. g/kg) for the group (N = 5). * $P < 0.05$ vs. water (gray bar = SEM for water availability). C. Mean \pm SEM blood alcohol levels (mg/dl) determined once stable intake was obtained at a particular alcohol concentration for the group (N = 5).
- Figure 2 Effects of increasing number of drinks on observable behavior (one drink = 0.25 g/kg alcohol). Data points represent the mean \pm SEM at each drink (N = 34 – 115). * $P < 0.05$ vs. water (gray bar = SEM for water availability).
- Figure 3 Effects of daily pretreatment with QH-ii-066, XLi-093, L-655,708 or naltrexone on intake maintained by a 2% (w/v) alcohol solution. For each monkey, mean intakes for the last three sessions at each dose were calculated. Data points represent the mean intake \pm SEM presented as a % of baseline g/kg for the group (N = 5). * $P < 0.05$ vs. vehicle. Baseline intake for QH-ii-066 = 1.4 ± 0.2 g/kg; XLi-093 = 1.8 ± 0.02 g/kg; L-655,708 = 1.6 ± 0.2 g/kg; naltrexone = 1.7 ± 0.2 g/kg (one-way ANOVA; $F(3,16) = 0.97$, n.s.).
- Figure 4 Modulation by QH-ii-066 and L-655,708, administered alone or in conjunction with XLi-093, of alcohol self-administration in monkeys. Points are group means \pm SEM based on the last three sessions at each alcohol concentration in five monkeys. * $P < 0.05$ vs. vehicle.
- Figure 5 A. Oral self-administration of varying sucrose concentrations and water under a fixed-ratio schedule and limited access conditions in monkeys. For each monkey, mean intakes for the last three sessions at each concentration were calculated. Data points represent the mean intake \pm SEM (mls) for the group (N

= 4). * $P < 0.05$ vs. water (gray bar = SEM for water availability). B. Effects of daily pretreatment with QH-ii-066 or L-655,708 on intake maintained by a 0.3% (w/v) sucrose solution. For each monkey, mean intakes for the last three sessions at each dose were calculated. Data points represent the mean intake \pm SEM presented as a % of baseline mls for the group (N = 4). Baseline intake for QH-ii-066 = 739 ± 178 mls; L-655,708 = 953 ± 142 mls (t-test; $t(6) = -0.94$, n.s.).

Figure 6 Observable effects of QH-ii-066 on tactile/oral exploration (A) and L-655,708 on yawning (B). Bars/points are group means \pm SEM in the sucrose self-administration group (N = 4) and the alcohol self-administration group (N = 5). * $P < 0.05$ vs. vehicle.

Supplemental Figure 1 Behavioral profile of alcohol and sucrose self-administration monkeys under water availability (see Table 1 for abbreviations). * $P < 0.05$

Figure 1:

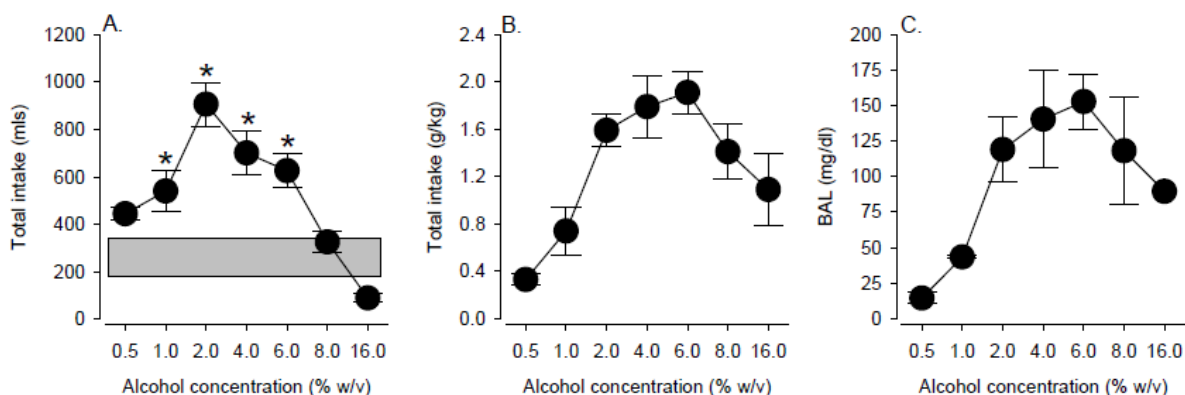


Figure 2:

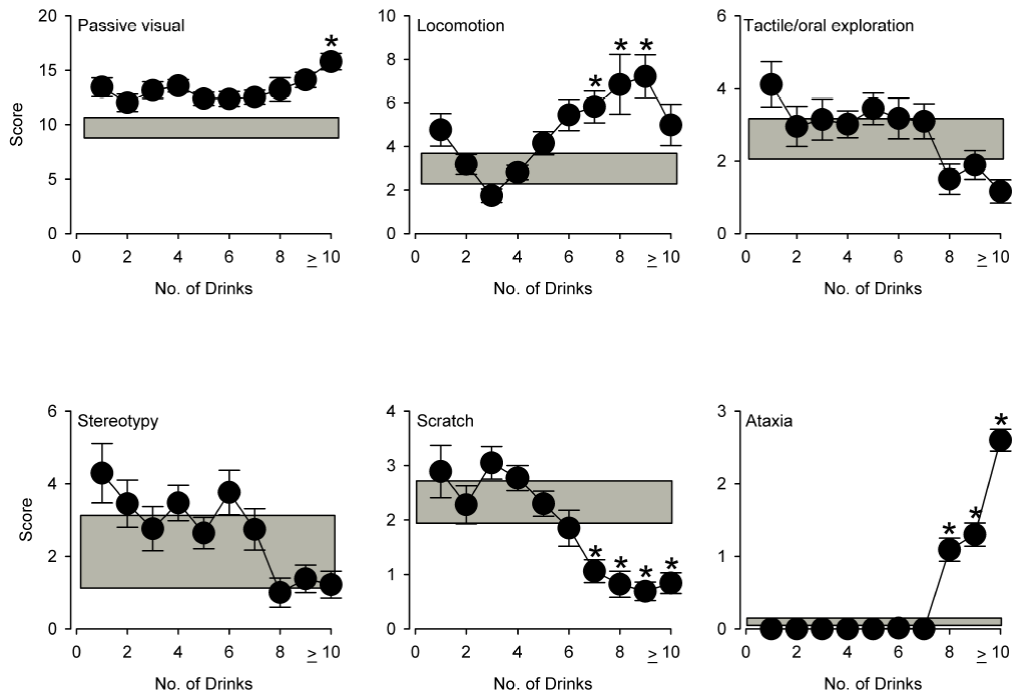


Figure 3:

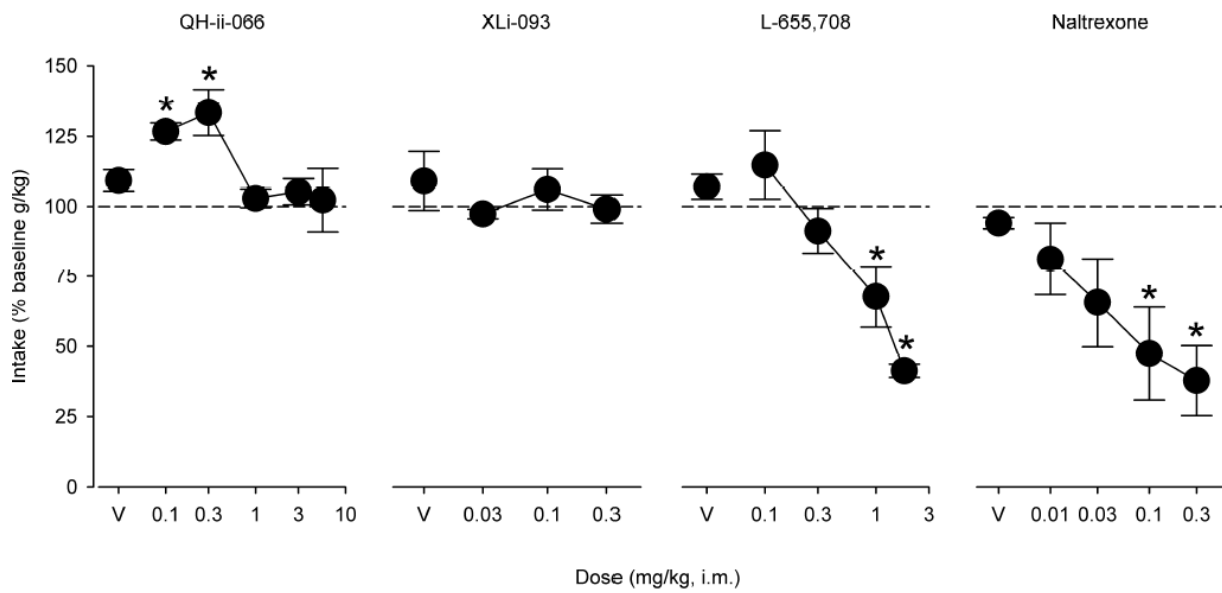


Figure 4:

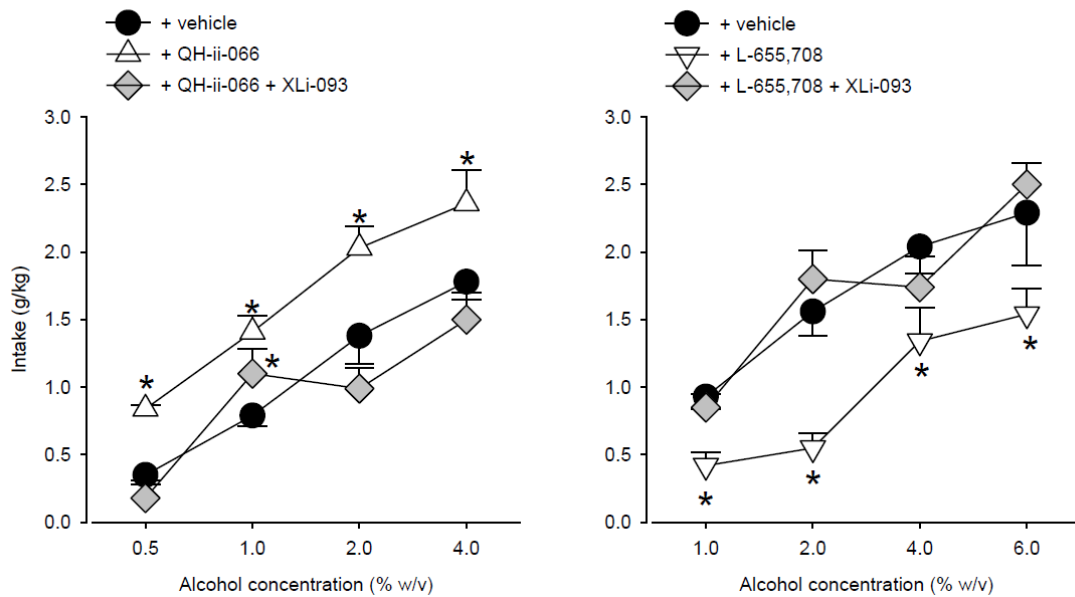


Figure 5:

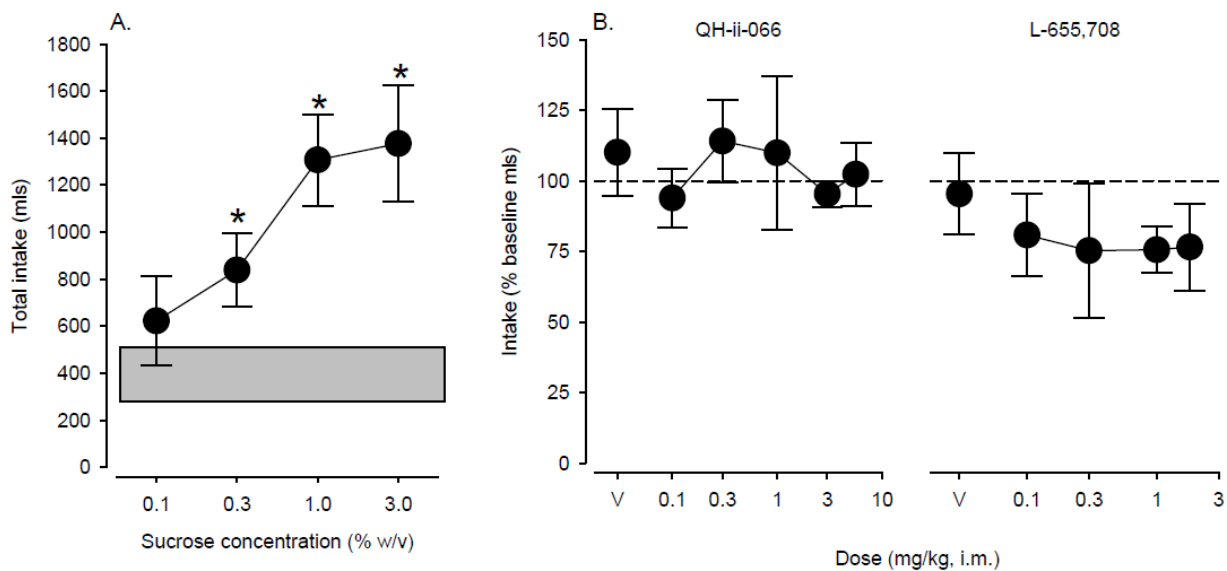
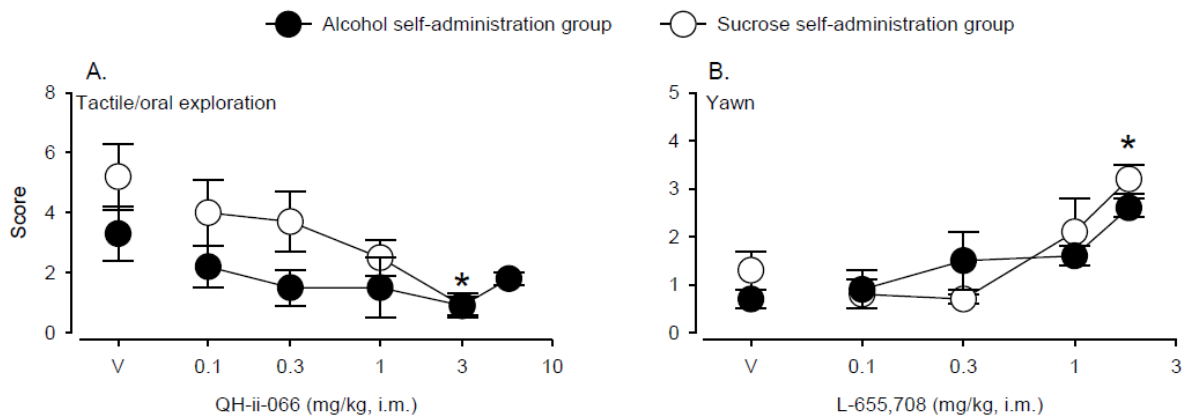


Figure 6:



VIII. Appendix VI (a). Crystal data and structure refinement for XLi093 (**33**).

Identification code	(33)	
Empirical formula	C ₃₃ H ₂₆ N ₆ O ₆	
Formula weight	602.60	
Temperature	295(2) K	
Wavelength	1.54178 Å	
Crystal system	Monoclinic	
Space group	P2/n	
Unit cell dimensions	a = 6.9314(1) Å	α = 90°.
	b = 9.2889(1) Å	β = 95.316(1)°.
	c = 22.5403(4) Å	γ = 90°.
Volume	1445.02(4) Å ³	
Z	2	
Density (calculated)	1.385 Mg/m ³	
Absorption coefficient	0.809 mm ⁻¹	
F(000)	628	
Crystal size	0.24 x 0.10 x 0.02 mm ³	
Theta range for data collection	3.94 to 66.97°.	
Index ranges	-7 ≤ h ≤ 7, -10 ≤ k ≤ 10, -22 ≤ l ≤ 26	
Reflections collected	7178	
Independent reflections	2450 [R(int) = 0.0286]	
Completeness to theta = 66.97°	95.3 %	
Absorption correction	Semi-empirical from equivalents	
Max. and min. transmission	0.984 and 0.823	
Refinement method	Full-matrix least-squares on F ²	
Data / restraints / parameters	2450 / 0 / 211	
Goodness-of-fit on F ²	1.045	
Final R indices [I > 2σ(I)]	R1 = 0.0451, wR2 = 0.1276	
R indices (all data)	R1 = 0.0574, wR2 = 0.1378	
Extinction coefficient	0.0020(6)	
Largest diff. peak and hole	0.369 and -0.181 e.Å ⁻³	

Appendix III(b). Atomic coordinates ($\times 10^4$) and equivalent isotropic displacement parameters ($\text{\AA}^2 \times 10^3$) for XLi093(33).

U(eq) is defined as one third of the trace of the orthogonalized U^{ij} tensor.

	x	y	z	U(eq)
C(1)	583(3)	4957(2)	3838(1)	60(1)
N(2)	-713(2)	5543(2)	4205(1)	66(1)
C(3)	302(3)	6423(2)	4553(1)	63(1)
N(4)	2206(2)	6468(2)	4437(1)	58(1)
C(5)	3729(3)	7252(2)	4757(1)	56(1)
C(6)	3678(3)	7399(2)	5366(1)	62(1)
C(7)	5123(3)	8119(2)	5706(1)	64(1)
C(8)	6661(3)	8721(2)	5433(1)	60(1)
C(9)	6658(3)	8620(2)	4822(1)	60(1)
C(10)	5230(3)	7871(2)	4466(1)	57(1)
C(11)	5409(3)	7917(2)	3806(1)	63(1)
O(11)	6076(2)	9000(2)	3588(1)	79(1)
N(12)	4863(2)	6755(2)	3477(1)	68(1)
C(13)	4333(3)	5396(2)	3747(1)	67(1)
C(14)	2394(3)	5524(2)	3978(1)	57(1)
C(15)	-123(3)	3891(2)	3389(1)	62(1)
O(15)	-1791(2)	3537(2)	3294(1)	88(1)
O(16)	1313(2)	3338(2)	3099(1)	66(1)
C(17)	735(3)	2297(3)	2632(1)	68(1)
C(18)	2500	1438(4)	2500	70(1)
C(19)	5152(4)	6746(4)	2849(1)	103(1)
C(20)	8236(3)	9416(2)	5781(1)	70(1)
C(21)	9564(4)	9941(3)	6065(1)	92(1)

Appendix III(c). Bond lengths [\AA] and angles [$^\circ$] for XLi093(33).

C(1)-C(14)	1.371(3)
C(1)-N(2)	1.386(3)
C(1)-C(15)	1.468(3)
N(2)-C(3)	1.295(3)
C(3)-N(4)	1.369(2)
N(4)-C(14)	1.370(3)
N(4)-C(5)	1.423(2)
C(5)-C(6)	1.384(3)
C(5)-C(10)	1.403(3)
C(6)-C(7)	1.377(3)
C(7)-C(8)	1.397(3)
C(8)-C(9)	1.379(3)
C(8)-C(20)	1.437(3)
C(9)-C(10)	1.401(3)
C(10)-C(11)	1.504(3)
C(11)-O(11)	1.229(2)
C(11)-N(12)	1.344(3)
N(12)-C(19)	1.448(3)
N(12)-C(13)	1.464(3)
C(13)-C(14)	1.491(3)
C(15)-O(15)	1.203(2)
C(15)-O(16)	1.342(2)
O(16)-C(17)	1.457(3)
C(17)-C(18)	1.513(3)
C(18)-C(17)#1	1.513(3)
C(20)-C(21)	1.177(3)
C(14)-C(1)-N(2)	109.99(18)
C(14)-C(1)-C(15)	131.11(18)
N(2)-C(1)-C(15)	118.90(17)
C(3)-N(2)-C(1)	105.25(16)
N(2)-C(3)-N(4)	112.49(18)
C(3)-N(4)-C(14)	106.56(16)
C(3)-N(4)-C(5)	126.97(17)

C(14)-N(4)-C(5)	126.31(15)
C(6)-C(5)-C(10)	120.76(18)
C(6)-C(5)-N(4)	117.91(17)
C(10)-C(5)-N(4)	121.33(18)
C(7)-C(6)-C(5)	121.08(18)
C(6)-C(7)-C(8)	119.6(2)
C(9)-C(8)-C(7)	118.85(19)
C(9)-C(8)-C(20)	120.46(18)
C(7)-C(8)-C(20)	120.7(2)
C(8)-C(9)-C(10)	122.81(18)
C(9)-C(10)-C(5)	116.79(19)
C(9)-C(10)-C(11)	115.74(17)
C(5)-C(10)-C(11)	127.30(17)
O(11)-C(11)-N(12)	122.2(2)
O(11)-C(11)-C(10)	119.17(19)
N(12)-C(11)-C(10)	118.64(18)
C(11)-N(12)-C(19)	119.2(2)
C(11)-N(12)-C(13)	122.06(19)
C(19)-N(12)-C(13)	117.7(2)
N(12)-C(13)-C(14)	110.26(17)
N(4)-C(14)-C(1)	105.71(16)
N(4)-C(14)-C(13)	117.83(16)
C(1)-C(14)-C(13)	136.41(19)
O(15)-C(15)-O(16)	123.6(2)
O(15)-C(15)-C(1)	124.09(19)
O(16)-C(15)-C(1)	112.30(17)
C(15)-O(16)-C(17)	115.99(16)
O(16)-C(17)-C(18)	108.60(16)
C(17)#1-C(18)-C(17)	116.3(3)
C(21)-C(20)-C(8)	177.6(3)

Symmetry transformations used to generate equivalent atoms:

#1 $-x+1/2, y, -z+1/2$

Appendix III(d). Anisotropic displacement parameters ($\text{\AA}^2 \times 10^3$) for XLi093 (33).

The anisotropic displacement factor exponent takes the form: $-2\pi^2 [h^2 a^{*2} U^{11} + \dots + 2 h k a^* b^* U^{12}]$

	U ¹¹	U ²²	U ³³	U ²³	U ¹³	U ¹²
C(1)	45(1)	62(1)	74(1)	0(1)	14(1)	-3(1)
N(2)	42(1)	77(1)	81(1)	-6(1)	17(1)	-4(1)
C(3)	43(1)	66(1)	82(1)	-6(1)	18(1)	-2(1)
N(4)	40(1)	56(1)	79(1)	-6(1)	16(1)	-4(1)
C(5)	43(1)	49(1)	77(1)	-1(1)	13(1)	0(1)
C(6)	51(1)	60(1)	78(1)	1(1)	19(1)	-6(1)
C(7)	59(1)	65(1)	70(1)	2(1)	13(1)	-6(1)
C(8)	50(1)	57(1)	74(1)	1(1)	8(1)	-3(1)
C(9)	45(1)	54(1)	81(1)	3(1)	14(1)	-4(1)
C(10)	43(1)	52(1)	77(1)	0(1)	13(1)	-1(1)
C(11)	45(1)	68(1)	79(1)	-2(1)	17(1)	-8(1)
O(11)	76(1)	81(1)	81(1)	3(1)	21(1)	-24(1)
N(12)	52(1)	80(1)	77(1)	-13(1)	23(1)	-12(1)
C(13)	48(1)	62(1)	94(2)	-16(1)	23(1)	-5(1)
C(14)	45(1)	53(1)	75(1)	-4(1)	15(1)	-1(1)
C(15)	50(1)	70(1)	68(1)	3(1)	13(1)	-5(1)
O(15)	49(1)	116(1)	100(1)	-28(1)	14(1)	-17(1)
O(16)	53(1)	72(1)	73(1)	-10(1)	15(1)	-8(1)
C(17)	63(1)	77(1)	65(1)	-4(1)	9(1)	-9(1)
C(18)	78(2)	69(2)	66(2)	0	10(1)	0
C(19)	94(2)	135(2)	87(2)	-28(2)	37(2)	-31(2)
C(20)	61(1)	73(1)	77(1)	8(1)	10(1)	-12(1)
C(21)	77(2)	114(2)	82(2)	12(2)	1(1)	-40(2)

Appendix III (e). Hydrogen coordinates ($\times 10^4$) and isotropic displacement parameters ($\text{\AA}^2 \times 10^3$) for XLi093 (**33**).

	x	y	z	U(eq)
H(3)	-205	6965	4848	75
H(6)	2650	7006	5549	75
H(7)	5076	8205	6116	77
H(9)	7646	9068	4639	72
H(13B)	5296	5148	4070	80
H(13A)	4303	4633	3452	80
H(17B)	199	2793	2276	82
H(17A)	-250	1659	2763	82
H(18)	3010(40)	810(30)	2867(10)	84
H(19A)	5480	7698	2726	155
H(19B)	3983	6437	2623	155
H(19C)	6186	6096	2780	155
H(21)	10530(50)	10430(40)	6280(14)	119

Appendix III (f). Torsion angles [°] for XLi093(33).

C(14)-C(1)-N(2)-C(3)	-0.3(2)
C(15)-C(1)-N(2)-C(3)	179.53(19)
C(1)-N(2)-C(3)-N(4)	0.5(2)
N(2)-C(3)-N(4)-C(14)	-0.4(2)
N(2)-C(3)-N(4)-C(5)	-176.01(19)
C(3)-N(4)-C(5)-C(6)	34.5(3)
C(14)-N(4)-C(5)-C(6)	-140.2(2)
C(3)-N(4)-C(5)-C(10)	-144.9(2)
C(14)-N(4)-C(5)-C(10)	40.4(3)
C(10)-C(5)-C(6)-C(7)	-1.9(3)
N(4)-C(5)-C(6)-C(7)	178.69(18)
C(5)-C(6)-C(7)-C(8)	0.5(3)
C(6)-C(7)-C(8)-C(9)	2.2(3)
C(6)-C(7)-C(8)-C(20)	-176.9(2)
C(7)-C(8)-C(9)-C(10)	-3.5(3)
C(20)-C(8)-C(9)-C(10)	175.54(19)
C(8)-C(9)-C(10)-C(5)	2.1(3)
C(8)-C(9)-C(10)-C(11)	177.80(18)
C(6)-C(5)-C(10)-C(9)	0.6(3)
N(4)-C(5)-C(10)-C(9)	-179.99(16)
C(6)-C(5)-C(10)-C(11)	-174.48(19)
N(4)-C(5)-C(10)-C(11)	4.9(3)
C(9)-C(10)-C(11)-O(11)	-32.8(3)
C(5)-C(10)-C(11)-O(11)	142.3(2)
C(9)-C(10)-C(11)-N(12)	145.98(19)
C(5)-C(10)-C(11)-N(12)	-38.9(3)
O(11)-C(11)-N(12)-C(19)	3.0(3)
C(10)-C(11)-N(12)-C(19)	-175.8(2)
O(11)-C(11)-N(12)-C(13)	171.04(19)
C(10)-C(11)-N(12)-C(13)	-7.7(3)
C(11)-N(12)-C(13)-C(14)	73.5(3)
C(19)-N(12)-C(13)-C(14)	-118.2(2)
C(3)-N(4)-C(14)-C(1)	0.2(2)
C(5)-N(4)-C(14)-C(1)	175.81(18)

C(3)-N(4)-C(14)-C(13)	178.00(19)
C(5)-N(4)-C(14)-C(13)	-6.4(3)
N(2)-C(1)-C(14)-N(4)	0.1(2)
C(15)-C(1)-C(14)-N(4)	-179.8(2)
N(2)-C(1)-C(14)-C(13)	-177.1(2)
C(15)-C(1)-C(14)-C(13)	3.0(4)
N(12)-C(13)-C(14)-N(4)	-64.7(3)
N(12)-C(13)-C(14)-C(1)	112.3(3)
C(14)-C(1)-C(15)-O(15)	-176.2(2)
N(2)-C(1)-C(15)-O(15)	3.9(3)
C(14)-C(1)-C(15)-O(16)	4.6(3)
N(2)-C(1)-C(15)-O(16)	-175.23(18)
O(15)-C(15)-O(16)-C(17)	2.4(3)
C(1)-C(15)-O(16)-C(17)	-178.41(17)
C(15)-O(16)-C(17)-C(18)	-161.41(18)
O(16)-C(17)-C(18)-C(17)#1	-52.04(12)
C(9)-C(8)-C(20)-C(21)	-78(6)
C(7)-C(8)-C(20)-C(21)	101(6)

Symmetry transformations used to generate equivalent atoms:

#1 $-x+1/2, y, -z+1/2$

IX. Appendix VII: SBIR grant by Physiogenix

Research Strategy

A. Significance

Alzheimer's disease (AD) is a complex and progressive neurodegenerative pathology that currently affects 5.4 million Americans at an estimated total cost of \$200 billion [Alzheimer's Association, 2012]. Although the monetary costs greatly impact our economy, the emotional and social burdens the disease imparts on individuals and their families are immeasurable. The complexity of the disease is due in part to the multiple stages of AD, ranging from pre-symptomatic to severe dementia. As the disease progresses into the symptomatic phase of pathogenesis, individuals begin losing basic cognitive and learning abilities, which eventually can lead to the complete loss of memory, cognition, and executive functions [1, 2]; a point at which many AD sufferers lose the freedom of independent living. Along with the complexity of defining the exact causes of AD, there is a multitude of controversies and gaps in our understanding of the disease progression, which has made the treatment and prevention of AD especially difficult. Furthermore, current treatments for AD have variable successes [2-5] and demonstrate efficacy in approximately half of the treated individuals [National Institute of Aging, Alzheimer's Association, 2012], thus substantiating the need for new approaches to AD therapeutics [1, 2]. Here, we propose our ligand PWZ-029, an inverse agonist with functional selectivity at gamma-aminobutyric acid class A (GABA_A) receptors containing $\alpha 5$ subunits, for the mitigation of cognitive deficits associated with AD and age-related dementias.

Current treatments of Alzheimer's disease are largely ineffective and recent approaches to treating and preventing the disease have lost momentum in clinical trials. Currently, there are five drug therapies that are FDA-approved for the treatment of

cognitive symptoms associated with AD. Cholinesterase inhibition is the mechanism of action utilized by four of the five AD therapies (e.g., donepezil) while N-methyl-D-aspartate (NMDA) antagonism constitutes the action of memantine, which is prescribed to treat moderate to severe AD [2]. Unfortunately, the efficacy of these drugs is variable, with positive results reported in only half of the users [3-5]. Thus, the necessity to further characterize the mechanism of disease progression, which will theoretically identify novel targets for drug therapies, is increasingly evident. Since the mid-1990s, the bulk of AD drug development efforts have surrounded the amyloid cascade hypothesis, which postulates that the neurotoxicity associated with AD pathogenesis is largely the result of alterations in the processing of amyloid precursor proteins in the brain. The result of these alterations can lead to the production and eventual aggregations of plaque-forming amyloid-beta ($A\beta$) peptides [2, 6-9]. Although the presence of extracellular $A\beta$ plaques and intracellular neurofibrillary tangles are generally recognized as hallmarks of AD, recent attempts to commercialize compounds that reduce the accumulation of or increase the clearance of $A\beta$ have been met by failure during clinical trials [2]. Thus, new approaches to treating or preventing AD are of immediate need. Recent approaches to characterizing the neuronal processes and alterations that result in or from hallmark anatomical changes of AD pathology are gaining momentum [10-12], thereby leading to novel targets for treating and preventing AD, such as the $GABA_A$ receptor complex [2, 7, 8, 13-15]. To this end, we aim to develop PWZ-029, a selective inverse agonist of $\alpha 5GABA_A$ receptors, to mitigate cognitive deficits associated with early (i.e., mild and moderate) stages of AD, as well as age-associated dementias.

The $GABA_A$ receptor complex is the primary modulator of neuronal inhibition and possesses diverse functionalities. The pathogenesis of AD targets neuronal networks that are especially vulnerable to the toxic effects of disease progression. Cholinergic neurons of the forebrain and the glutamatergic receptors and neurons in the

hippocampus are prime examples of networks affected by AD pathology. These excitatory networks of the brain are predominantly modulated by gamma-aminobutyric (GABA) neurotransmissions. GABA is the chief inhibitory neurotransmitter of the mammalian central nervous system (CNS) [7, 8, 14, 16, 17] and is regulated by three classes of GABA receptors, GABA_A, GABA_B, and GABA_C, with the GABA_A receptor complex being the primary regulator of GABA-induced CNS depression [7, 8, 16] and the primary target for benzodiazepine (BZ) pharmaceuticals [7, 8, 14, 17].

The GABA_A receptor complex is a pentameric, chloride-ion-gated channel through which GABA regulates fast synaptic inhibitory neurotransmissions [7, 16]. The heterogeneity of this ionotropic receptor is due to the diversity of subunit compositions. Characterizations of the GABA_A receptor complex define 8 subunits with a total of 20 different subtypes: α 1-6, β 1-4, γ 1-3, ρ 1-3, δ , ϵ , π , and θ [13, 16-24]. Although the exact characterization of subtype and subunit composition in relation to GABA_A receptor functionality is yet unclear, research supports that the majority of these complexes are composed of at least two α and β subunits [14, 16, 25-27] and one γ subunit [8, 14, 16, 27]. These findings suggest that GABA_A receptors have immense structural and functional diversity, and the implications for this diverse functioning potential have profound implications for the specificity and resulting pharmacological effects of ligands targeting the GABA_A complex [14]. For instance, many established BZ drugs (e.g., diazepam) have non-specific binding behaviors, which have been shown to elicit side effects like sedation, hypnotic behavior, and affected motor coordination [14]; side effects that are not attractive for AD therapeutics aiming to improve memory and cognition. The α 1 subtype, for example, is ubiquitously distributed in mammalian CNS [13, 14, 16] and has been shown to play a paramount role in the sedative side effects associated with ligands of the GABA_A receptor [13, 14, 28]. Conversely, α 5 subtypes, which are targeted by PWZ-

029, are predominantly concentrated in the hippocampus, specifically in the Ammon's horn of the dorsal CA1 region of rodent brains [13, 14, 16], and are characterized as modulators of memory and cognition [13, 14, 16, 24, 29-31]. These findings support the hypothesis that highly specific ligands that selectively bind $\alpha 5$ subtypes are promising targets for potent mitigators of AD-associated cognitive decline [15]. Our preliminary data for PWZ-029 substantiates this hypothesis and shows practical evidence that our compound significantly improves cognition without the sedative side effects common to other BZ ligands.

Down-regulating compensatory mechanisms related to AD pathology may reduce the cognitive impairments associated with mild and moderate stages of the disease. Neuronal death that is commonly observed in the brains of AD patients has been shown to be caused partly by overstimulation of NMDA and 2-amino-3-(3-hydroxy-5-methyl-isoxazol-4-yl) propanoic acid (AMPA) receptors via toxic amounts of the excitatory neurotransmitter, glutamate [32, 33]. Researchers speculate that these overstimulated pathways lead to compensatory mechanisms that aim to maintain the excitatory/inhibitory (E/I) balance of the brain's regulatory processes. In other words, a pathologically overactive excitatory pathway can lead to the compensatory up-regulation of inhibitory processes, specifically GABA-mediated CNS inhibition [7, 8]. These findings, in combination with research showing the relative conservation of the GABAergic hippocampal networks in AD pathology [7, 29, 34-37], suggest that inverse agonist ligands that selectively act on GABA_A receptors to inhibit the action of GABA in the brain are excellent candidates for memory and cognition therapeutics [15], such as PWZ-029.

B. Innovation

Preliminary preclinical data strongly suggests that PWZ-029 is effective in improving memory and cognition, especially in models with baseline cognitive deficits. The high specificity of PWZ-029 for $\alpha 5$ -containing GABA_A receptors has successfully mitigated adverse side effects of seizures and sedation, which are commonly observed with benzodiazepines (BZ). Furthermore, the unique functional selectivity of PWZ-029 has successfully overcome functional interference and side effects that have stopped previous attempts to commercialize nonselective inverse agonists of the GABA_A complex. Furthermore, because the core chemical structure of PWZ-029 classifies it as a benzodiazepine (Figure 1A) we are confident that the safety and toxicology experiments proposed here would be consistent with the vast body of research demonstrating the established safety and toxicological profiles of the BZ class of compounds.

Our collaborator, Dr. James Cook, synthesized PWZ-029 as part of an effort to explore the difference between the pharmacophores for the diazepam-sensitive versus the diazepam-insensitive GABA_A receptors [38]. One of the products of his laboratory's research was PWZ-029, which was designed to be a partial inverse agonist with functional selectivity for the $\alpha 5$ subunit-containing GABA_A receptor [39]. Our approach to mitigating the cognitive impairments of AD is innovative because PWZ-029 acts with a novel GABA-reducing mechanism rather than targeting cholinergic, glutamatergic, or A β pathways. Success in the proposed experiments will drive our team towards commercializing a benzodiazepine drug that improves memory and cognition in AD patients without eliciting unwanted sedative and convulsive side effects. These strides in our research will not only lead to a marketable product with strong intellectual property, but we will also publish our sensitive findings so that scientific understanding for treatment and mitigation of AD will advance.

C. Approach

C1. PHASE I FINAL REPORT/PRELIMINARY STUDIES

Our successful Phase I milestone data combined with significant findings from our company-sponsored preliminary studies encouraged us to pursue a Phase II SBIR grant for our cognition-enhancing compound, PWZ-029. In summary, our significant findings demonstrate: 1) a selective binding affinity of PWZ-029 to $\alpha 5$ subunits on GABA_A receptors, which was substantiated by an auspicious in-vitro efficacy profile, 2) minimal behavioral side effects of PWZ-029 compared to benzodiazepines and other inverse agonists with non-specific binding affinities, and 3) the ability of PWZ-029 to improve cognition and overcome impaired baseline performance in a myriad of memory tests that were carried out in multiple species.

In-vitro characterization of binding affinity and efficacy. Extensive in vitro binding and efficacy experiments that showed a selective affinity of PWZ-029 to $\alpha 5$ GABA_A receptors (Figure 1.); in vitro data that were exemplified by enhanced performance in behavioral assays [39], specifically the contextual fear conditioning paradigm [30] (Figure 3). These data, in addition to binding and electrophysiological assays carried out by our collaborator, Dr. James Cook (University of Wisconsin-Milwaukee), demonstrate that PWZ-029 binds selectively (i.e., ≈ 20 - to 30-fold greater selectivity) to $\alpha 5$ subunit-containing receptors compared to the other isoforms of the GABA_A receptor complex, specifically the $\alpha 1$ subunit-containing receptors, which are associated with sedative side effects of non-selective BZ ligands (Figure 1B and 1C). Electrophysiology experiments in *Xenopus* oocytes demonstrated that PWZ-029, at a concentration of 1 μ M, significantly reduced GABA initiated control currents, thereby indicating a partial inverse agonist effect of PWZ-029 on GABA_A receptors possessing the $\alpha 5$ isoforms (Figure 1B). Additional experiments carried out by the NIMH Psychoactive Drug Screening Program

(PDSP) at the University of North Carolina Chapel Hill Medical School showed that PWZ-029 is a highly selective ligand of the BZ-binding site, confidently indicating that the observed cognitive enhancing effects elicited by this ligand are likely the result of binding at the GABA_A receptor complex and not other receptor classes, such as cannabinoids, histamines, prostaglandins, glutamate, Ca⁺ channel, transporters, adrenergic, acetylcholine, dopamine, serotonin, and opiates (data not shown).

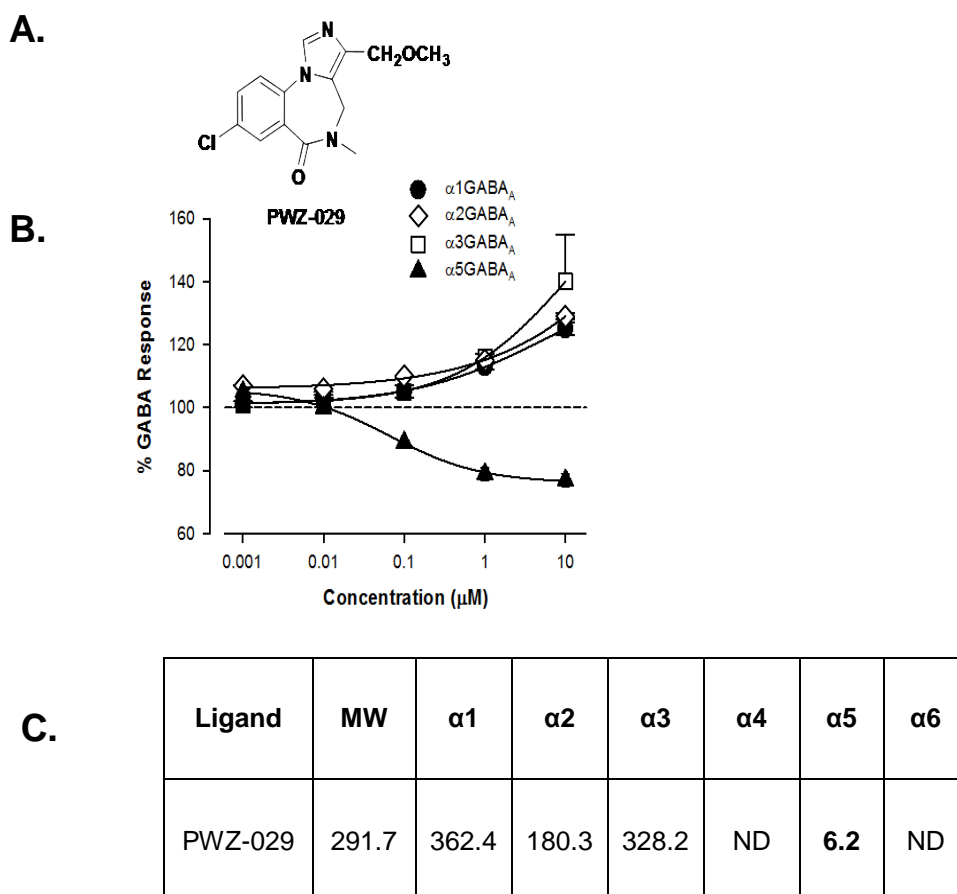


Figure 1. Structural, electrophysiological, and binding characterizations of PWZ-029 show the ligand is a partial inverse agonist with functional selectivity and in vitro efficacy at α5 subunit-containing GABA_A receptors. *Panel A.* Chemical structure of PWZ-029 classifies the compound as a benzodiazepine, a class of compounds with a well-characterized safety profile. *Panel B.* Oocyte electrophysiology data demonstrating the selectivity of GABA attenuation by inverse activity with α5 isoforms. *Panel C.* Binding affinity (K_i, nM) and selectivity of PWZ-029 against the various α-containing GABA_A receptors.

Preliminary profiling of PWZ-029 pharmacokinetics, maximum tolerated dose, and oral bioavailability (data not shown).

In our Phase I rat experiments, we showed that peak plasma concentrations were detected by LC/MS at 0.25 hours (h) post-dose when PWZ-029 was administered by intravenous (1 mg/kg, i.v.) and oral gavage (5 mg/kg, p.o.) routes. These preliminary data indicate a rapid absorption into the blood compartment via the oral route. The concentration-time curves for both i.v. and p.o. administrations indicated at least two separate phases of redistribution with significant amounts of compound in the plasma compartment at 4 h and remaining detectable for 24 h post-dose. The bioavailability of PWZ-029 was found to be roughly 11% when calculated by the area under the curve method and when accounting for the larger concentration used for the p.o. dose. In addition, brain samples were taken from rats 2 h after dosing to determine the potential of PWZ-029 to traverse the blood brain barrier. PWZ-029 was detected in brain tissue at 2 h after oral dosing and represented 2.1% of peak plasma concentration. A brain/blood ratio of 0.7 was determined for PWZ-029, with a brain/blood ratio of greater than 0.3-0.5 serving as our reference for sufficient access to the target organ. This was the first report showing both the oral bioavailability and target organ accessibility of PWZ-029.

Additionally, a dose escalation experiment investigated oral doses of PWZ-029 at 30, 100, 300, and 1000 mg/kg. Doses were given in single administrations, animals were observed for toxicological effects for 48 h post-dose, and then the next escalating dose was administered with the same experimental design followed for all phases of the escalation paradigm. All experimental animals survived each arm of dosing, and body weight loss was not observed for the duration of the experiment. Although mild tremors and facial twitches were noted, specifically at 300 and 1000 mg/kg, there were no overt signs of toxicity observed.

Minimal side effects observed with PWZ-029 administrations in mice, rats, and non-human primates.

Single-dose proconvulsant studies utilizing male Swiss mice (Crl:CFW(SW)) treated with pentylenetetrazole (PTZ) were conducted at NINDS and at PsychoGenics (Tarrytown, NY). Results demonstrated that PWZ-029 is not proconvulsant at any dose (10, 20, or 40 mg/kg) in the PTZ mouse model (data not shown). Furthermore, Harris et al. [30] found that systemic dose administrations in mice of PWZ-029 at a dose of 30 mg/kg did not result in convulsions.

Our Phase I experiments utilized a standard battery of behavioral and motor coordination tests to elucidate side effects that are common to the BZ class of compounds. The rotarod test was used to assess motor coordination effects of single oral doses of PWZ-029 at 5, 10, and 20 mg/kg versus saline- and diazepam-treated rats in the Dahl/SS rat strain. No signs of impaired motor coordination or sedation were observed at any of the three PWZ-029 doses (data not shown). The Dahl/SS rat strain was also utilized for the elevated plus maze and the open field test. Oral doses of PWZ-029 at 5, 10, and 20 mg/kg were tested against saline-treated and DMCM-treated rats in both assays. The combined results of these experiments suggest that PWZ-029 activity does not elicit anxiogenic side effects relative to the DMCM- or diazepam-treated control rats (data not shown). We suspect that the overall data suggest a mild sedative effect of PWZ-029; however, a sedative effect was not observed in the rotarod studies.

Targeted studies in monkeys were conducted in order to assess possible anxiolytic-like effects, abuse potential, and sedative-motor effects. In a rhesus monkey conflict model of the anxiolytic effects of drugs [40], PWZ-029 was ineffective over a 1000-fold dose range (up to 1.0 mg/kg, i.v.), suggesting that although this compound is a weak agonist at α_1 , α_2 , and α_3 subunit-containing receptors, the efficacy at these subtypes is insufficient to induce anxiolysis-like behavior or alter operant responding. Similarly,

PWZ-029 lacked reinforcing effects over a 300-fold dose range in monkeys self-administering the BZ, midazolam (i.v.), under a progressive-ratio procedure, suggesting that this compound has no abuse potential (data not shown).

Figure 2 represents the results of sedation studies in rhesus monkeys treated with 3.0 mg/kg PWZ-029 (i.v., panel A) or alprazolam (i.v., panel B) and then monitored for 120 minutes (min) post-dose. PWZ-029 did not induce significant signs of sedation at doses 200-300 times higher than the lowest dose shown to enhance performance in cognitive tasks (see below). Conversely, the non-selective BZ, alprazolam, induced significant rest/sleep posture and deep sedation, thus providing a positive comparator.

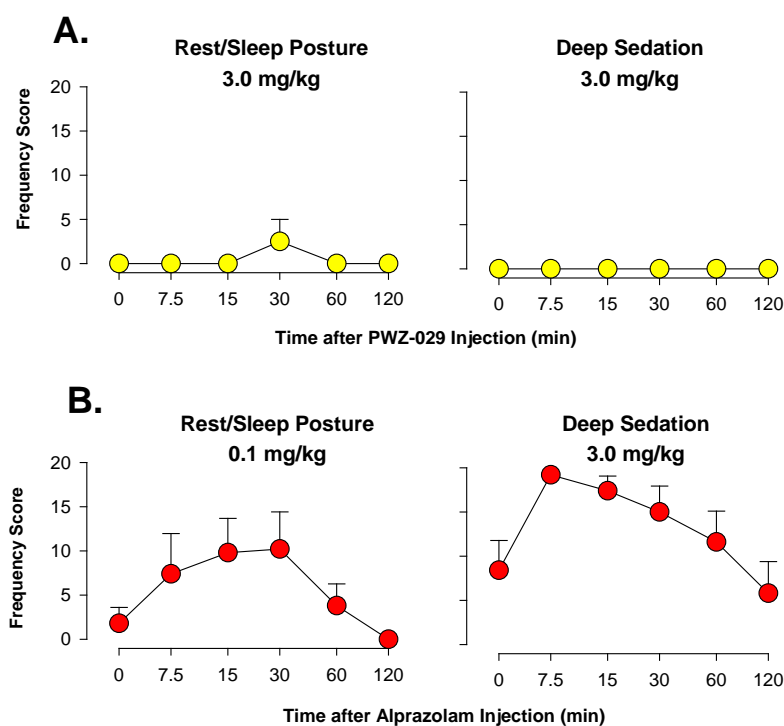


Figure 2. Sedation studies carried out with PWZ-029- (A) and alprazolam- (B) treated rhesus monkeys (n=5). Data were obtained as modified frequency scores by trained observers unaware of the treatments or purpose of the studies (inter-rater reliability scores > 90%). “Rest/sleep posture” was defined as the monkey assuming a posture associated with rest or assumed sleep, with eyes closed for at least 3 sec, but responsive to an auditory cue. “Deep sedation” was recorded if the monkey assumed an atypical posture, with eyes closed for at least 3 sec, and non-responsive to an auditory cue. These measures are adapted from the American Association for Anesthesiology standards for levels of sedation. All data presented as mean \pm SEM.

PWZ-029 demonstrates efficacy in the attenuation of cognitive deficits in mice,

rats, and NHP. Assessments of the contextual fear response (i.e., % freezing) to stimulus (Figure 3) in scopolamine-treated, male C57BL/6 mice demonstrated that PWZ-029 attenuated the scopolamine-induced impairment of contextual memory (Harris, et al., 2008).

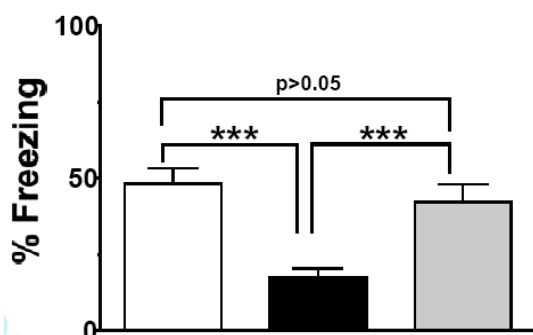


Figure 3. Pavlovian fear conditioned contextual memory test in scopolamine-treated C57BL/6 mice. Each mouse was injected via intraperitoneal injection with vehicle (white bar), 1.5 mg/kg scopolamine (black bar), or 1.5 mg/kg scopolamine plus 10 mg/kg PWZ-029 (gray bar). N=12 mice/group. *P<0.05 versus scopolamine-treated mice (Harris et al., 2008)

In a company-sponsored Morris Water Maze (MWM) experiment, we examined the effects of PWZ-029 in a novel rat model of Alzheimer's disease (AD) - the FAB-Samaritan rat (Taconic Farms, Inc., Hudson, NY). FAB-Samaritan rats were carried through the MWM task (1 day of visible acquisition followed by 2 days of hidden platform tests) in subsequent weeks following brain infusions of an AD-inducing solution [41]. Infusion pumps were installed in the animals, and rats received brain infusions of saline (positive model control) or a proprietary FAB solution (negative control and test groups). Animals (n=8/group) were dosed for ≈28 days via p.o. gavage with vehicle (positive model and negative controls), donepezil (positive drug control, 3 mg/kg), or PWZ-029

(10 mg/kg) at \approx 30 minutes prior to entering the maze. In the second arm of testing for the animals, PWZ-029-treated rats performed significantly better on Day 2 of the hidden phase in both latency to platform and distance travelled when compared to the FAB-Samaritan negative control animals ($P < 0.05$ versus negative control, data not shown).

As an additional part of our SBIR Phase I project, we conducted preliminary experiments to evaluate the extent to which PWZ-029 could alter memory processes in a translationally-relevant primate species. Figure 3 shows very promising results with PWZ-029 in the Object Retrieval with Detours (ORD) task in rhesus monkeys. The ORD task in monkeys is often described as providing a measure of executive functioning [42, 43]. Impairments in executive functioning (i.e., decision making, planning, response inhibition, cognitive flexibility) often emerge after mild cognitive impairment in the progression to AD [44]. Importantly, Ballard et al. reported that an inverse agonist with selectivity for $\alpha 5$ -containing receptors enhanced performance in the ORD task, providing initial proof-of-concept support for our studies [42].

The ORD task consists of a food-retrieval procedure in which a small food treat (e.g., banana slice) is placed in a transparent box with one open side, and the animal's ability to retrieve the treat is measured (see Figure 4). Performance in the ORD task was not enhanced (mean percentage of successfully-completed trials in a daily session) by i.v. injections of PWZ-029 when the task included easy trials (i.e., open side directly in front of monkey, Figure 4A); however, performance was robustly enhanced when trials were difficult (i.e., open side on right or left, treat deep within the box, Figure 4B). When performance on the ORD task was attenuated by the cholinergic agent, scopolamine, PWZ-029 treatment effectively reversed this deficit (Figure 4C). Finally, the enhancement of ORD performance induced by PWZ-029 could be blocked by an antagonist selective for $\alpha 5$ -containing GABA_A receptors (Figure 4D). Together, these

findings provide strong support for PWZ-029 as a cognitive enhancer of executive functioning in a primate species with close genetic similarity to humans.

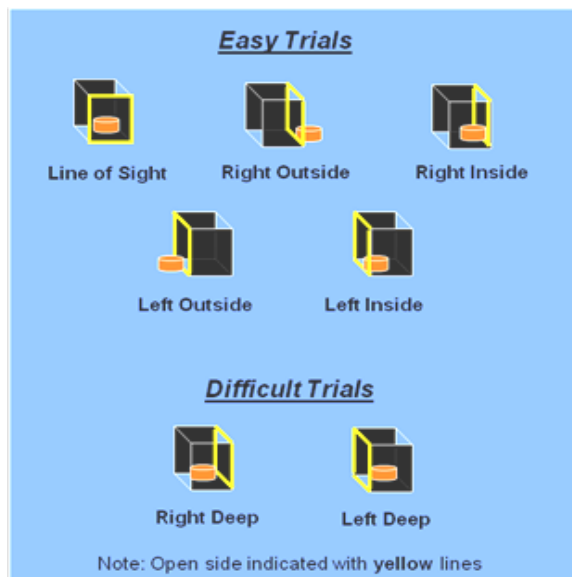
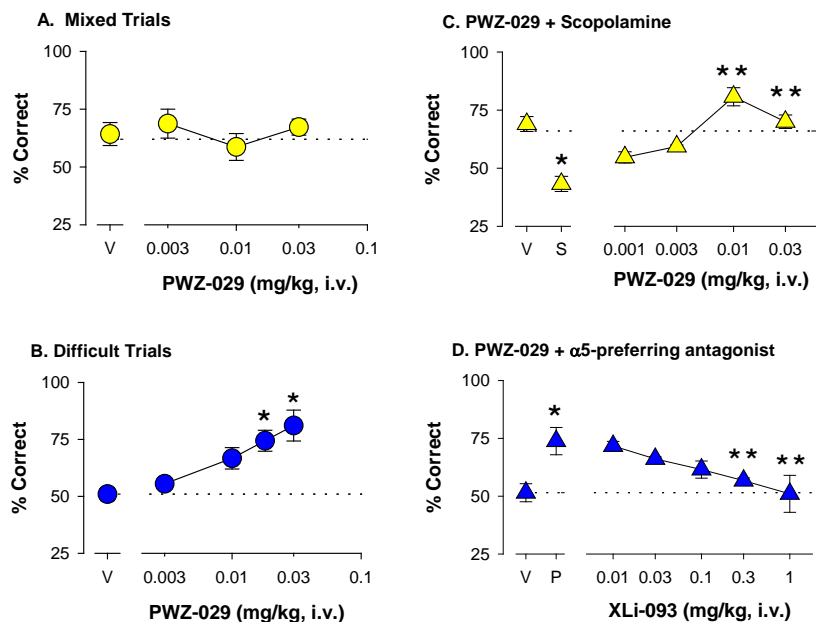


Figure 4. Effects of PWZ-029 in the Object Retrieval with Detour (ORD) task. Monkeys were trained to retrieve food from an opaque box with one open end (above right). *Panel A.* PWZ-029 was ineffective when tested with a combination of Easy and Difficult Trials. *Panel B.* PWZ-029 enhanced performance when only Difficult Trials were tested (* $p < 0.05$ vs. vehicle, V). *Panel C.* Scopolamine (S, 0.01 mg/kg) inhibited ORD performance, which was reversed by PWZ-029 (** $p < 0.05$ vs. S). *Panel D.* Enhanced performance with PWZ-029 in Difficult Trials was blocked by the antagonist XLi-093 (* $p < 0.05$ vs. V; ** $p < 0.05$ vs. PWZ-029 alone, P).

C2. EXPERIMENTAL APPROACH

Aim 1. Define the exposure/safety relationship of PWZ-029 in rats to determine whether this compound exhibits a sufficient level of safety to support Phase I clinical trials. The safety and potential target-organ toxicity of a drug must be established to demonstrate a sufficient efficacy/safety margin prior to entering a compound into clinical trials [45]. Here, escalating-dose and 7-day repeat dosing studies will be carried out in rats with the goal of establishing the no observable adverse effects level (NOAEL), dose-limiting toxicities (DLT), maximum tolerated dose (MTD), and the safety/exposure relationship of PWZ-029. We will use these data to support the definitive, IND-enabling GLP safety studies needed prior to initiating a Phase I clinical trial.

Rationale: Determining the toxicology and safety of a compound prior to testing in humans is crucial to the process of drug development [45]. As multiple benzodiazepines are currently on the market, their general safety profile is well documented. To establish the specific safety profile of PWZ-029, a series of safety/toxicological experiments will be carried out to assess the MTD and NOAEL in acute and multiple dosing paradigms. The toxicology assessments will be carried out in Sprague Dawley (SD) rats. We will determine the general safety profile of PWZ-029 and incorporate pharmacokinetic measurements to establish its safety/exposure relationship. Potential differences in toxicological responses between genders will also be evaluated. In parallel to the in vivo safety studies, standard in vitro assays for selectivity, mutagenicity, and clastogenicity/aneugenicity will be conducted to assess the potential for 'off-target' toxicity.

Experimental Design: Information gained from the escalating-dose MTD studies will drive the doses of PWZ-029 to be used in subsequent 7-day toxicological studies, and the outcomes of these studies will then determine the ultimate design of the GLP-safety

studies. A preliminary dose-ranging study in rats (using doses up to 1000 mg/kg) has already been conducted as part of an initial safety evaluation of PWZ-029. Although no overt findings of toxicological significance were observed, increased facial movements (twitching) were noted, especially at 300 and 1000 mg/kg. Therefore, a second MTD study will be conducted in rats using doses up to 2000 mg/kg, paying particular attention to potential abnormal muscular activity (i.e., twitching/tremors).

In addition to the Phase I single dose pharmacokinetic (PK) analysis that has already been conducted with PWZ-029 in rats, PK analysis will be carried out after a single dose and after 4 daily doses to assess the potential for drug accumulation or the potential for induction of liver metabolism that may affect drug exposure upon chronic dosing. Results from these rat safety studies will be used to seek funding from other sources for further study and to design PK, single-dose MTD, and sub-chronic safety studies in beagle dogs. Additionally, in vitro safety assessment will be conducted by an established contract research organization (Cerep Inc., Redmond, WA). The desired outcome of these studies is to further define the safety and selectivity profile of PWZ-029.

PK analysis to establish safety/exposure ratio in rats. Three male SD rats (8-weeks old, 250 g) will be dosed p.o. with 10 mg/kg of PWZ-029. Blood will be sampled after 0.08, 0.25, 0.5, 1, 2, 4, 8, 18 and 24 h to assess PWZ-029 exposure and to determine single dose PK parameters. Subsequently, rats will be dosed at 24 h intervals, and after the fourth daily dose, blood will be sampled following the schedule utilized on Day 1 to determine whether multiple-day dosing affects any of the PK parameters.

Escalating-dose MTD studies. Male SD rats (8-weeks old, 250 g) will be dosed via p.o. gavage with either vehicle (n = 5) or with escalating doses of PWZ-029 (100, 500 and 2000 mg/kg; n = 5/group). On day 1 of the study, rats will be dosed with vehicle or the lowest dose of PWZ-029 (100 mg/kg) and then observed for behavioral effects. For the first 120 minutes, animals will be intensely monitored for signs of acute toxicity (i.e.

morbidity and mortality) with special attention being paid toward unusual muscular activity (i.e., twitching, tremors and/or convulsions). Animals will be subsequently monitored for an additional 46 h for overt signs of toxicity such as ataxia, greater than 10% decrement in body weight, tremors, loss of righting response, morbidity, and mortality. Following the initial dose, rats will be dosed at 48 h intervals with either vehicle or the escalating doses of PWZ-029 and monitored as described for the 100-mg/kg dose. Forty-eight hours after the final vehicle or 2000 mg/kg dose of PWZ-029, animals will be terminated and gross pathological observations documented. Blood will be collected to assess clinical chemistries, and the adrenals, brain, heart, kidneys, liver, spleen, thyroid with parathyroid, skeletal muscle and thymus will be weighed, collected, and stored in formalin for histological analysis.

In vivo safety assessment in rats (7-day repeat dose study). A low, mid, and high dose of PWZ-029 will be established based upon the findings from the dose-ranging experiments. A total of 32 SD rats will be distributed among 8 experimental groups.

- 16 female SD rats will be distributed into 4 experimental groups (n=4/group): Control group, low dose group, mid dose group and high dose group.
- 16 male SD rats will be distributed among 4 dose groups as with the females.

All experimental animals will be dosed via p.o. gavage once a day for 7 consecutive days. Detailed clinical observations including unusual muscular activity (i.e., twitching, tremors and/or convulsions), body weights, and food consumption will be recorded daily. On day 7, blood will be collected 1 h after administering the final dose for drug exposure and clinical chemistries. Animals will be terminated, and the adrenals, brain, heart, kidneys, liver, spleen, thyroid with parathyroid, skeletal muscle, and thymus will be collected, weighed, and stored in formalin for histology. The 1 h post-dose timing was chosen based on the PK data obtained from Phase I experiments.

In vitro selectivity and gene safety assessment. The potential for off-target pharmacology/toxicology will be assessed using a broad panel of ~150 human receptors and enzymes. The potential for genetic toxicity will be assessed using the Ames fluctuation assay and the in vitro micronucleus assays run in the presence and absence of S9 liver fractions (Cerep Inc., Redmond, WA).

Benchmark for Success. Results from the PK study will refine the PK parameters estimated in the preliminary studies that indicated rapid oral absorption of PWZ-029 into the blood compartment with a bioavailability of about 11% and biphasic elimination kinetics. Success will be determined from the escalating-dose MTD studies if we observe of a sufficiently high MTD to proceed to a multiple-dose safety assessment in rats. Successful outcomes of the 7-day repeat dosing study will establish a relationship between chronic dosing and DLT, define a therapeutic index (TI) sufficient for continued development of PWZ-029, and demonstrate that PWZ-029 does not induce its own metabolism nor show drug accumulation upon multiple-day dosing. Successful outcomes will Finally, in vitro analyses will be successful will demonstrate that PWZ-029 does not induce its own metabolism nor show drug accumulation upon multiple-day dosing. Finally, successful in vitro analyses will be defined as demonstration of an in vitro selectivity profile ≥ 50 -fold and a lack of gene toxicity.

Anticipated Problems and Solutions. The increased facial movements (i.e., twitching) that were observed in the preliminary dose-ranging study may be confirmed or another unanticipated DLT may be discovered. If increased facial twitching is confirmed, we will determine whether it decreases or stops in a multiple-day dosing study (i.e., toleration). Assessment of any toxicological observations will require their assessment in multiple-day dosing studies and protocols will be designed to incorporate the necessary measurements. Identification of off-target activity in the selectivity panel would first require confirmation in secondary enzyme and/or cell-based assays. Confirmed off-

target activity would require the evaluation of potential side effects and further toxicology studies would need to incorporate assessment of these in study designs. Positive results in the genetic toxicity assays would require the identification of a back-up compound devoid of this activity.

Aim 2. Examine the potential of PWZ-029, an inverse agonist of $\alpha 5$ GABA_A receptors, to mitigate cognitive deficits in a transgenic mouse model of AD.

Despite an ever-growing population of aged individuals, there are few, effective therapeutic options for individuals suffering from cognitive deficits associated with AD. To expand on our preliminary evidence that suggests inverse agonist action at $\alpha 5$ -subunit containing GABA_A receptors can mitigate AD-associated cognitive decline, we will test the efficacy of PWZ-029 to improve performance in the contextual-fear conditioning assay with the APP^{swe} Tg2576 mouse model of AD. All behavioral experiments will be controlled with age-matched, non-transgenic littermates, as well as positive and negative drug controls (n=10 mice/group). From these experiments, we expect to gain proof-of-concept data that supports inverse agonist action at $\alpha 5$ GABA_A receptors as a novel therapeutic option for improving cognition in those suffering from AD.

Rationale: Research carried out to characterize the distribution of the various GABA_A receptor subtypes in rodent brains shows that $\alpha 5$ GABA_A subunits are highly concentrated in the Ammon's horn of the hippocampus, specifically in the CA1 dorsal region [13, 14, 16]; a region of the hippocampus that is specifically targeted in context-dependent fear conditioning assays [46-50]. Furthermore, studies have shown that the $\alpha 5$ GABA_A subunits are spared in the hippocampus, even with the pathophysiological brain shrinkage and neuronal death that is commonly associated with AD [7, 29, 34-37]. To this end, we hypothesize that PWZ-029, an inverse agonist that has repeatedly demonstrated high selectivity for $\alpha 5$ GABA_A receptors, will improve performance in

context-dependent fear conditioning experiments, thereby establishing proof-of-concept for a novel therapeutic mechanism to mitigate AD-associated cognitive decline.

Experimental Design: The following experiments will have oversight by Dr. Catherine Kaczorowski, a leading AD expert from the Medical College of Wisconsin. The evidence gained from these experiments will guide the direction in which impactful and successful commercialization of PWZ-029 is most likely.

Formulation. *Formulation of PWZ-029 will be carried out identically for all Aims.* All compounds will be administered via p.o. gavage 30-60 minutes prior to entering the fear conditioning experiments. PWZ-029 will be synthesized by Cambridge Major Laboratories (Germantown, WI). PWZ-029 will be administered to the animals only on the day of training (see conditioning protocol below) at 10 mg/kg, a dose shown to improve performance on memory tasks in adult mice (Figure 3) and rats (refer to MWM data in the preliminary data section of this proposal), suggesting that a 10 mg/kg dose of PWZ-029 will enhance cognition in the APP^{swe} model [30, 39]. Premeasured amounts of PWZ-029 will be dissolved in a widely used solvent that contains 85% distilled water, 14% propylene glycol, and 1% Tween 80 [30, 38, 39]. Donepezil (catalog # D6821), which will serve as the positive drug control, will be purchased from Sigma-Aldrich (St. Louis, MO), formulated in vehicle, and administered daily at 0.3 mg/kg for 6 weeks prior to the fear-conditioning assay, including the training day of the behavioral assay [51, 52]. Triazolam, a non-selective BZ agonist that has been shown to inhibit performance in fear conditioning assays [53] will serve as the negative drug control, and will also be purchased from Sigma Aldrich (catalog # T9772), formulated in vehicle, and administered at 0.03 mg/kg prior to the training phase of the fear conditioning protocol. To acclimate all mice to the same handling/dosing exposure and to maintain blinded treatments, PWZ-029 and triazolam groups will be dosed with vehicle for the 6-week period that donepezil will be dosed prior to the conditioning assay. There will be no

doses administered on the testing day when freezing behaviors are scored.

Research Model. Taconic Farms, Inc. (Hudson, NY) will provide male APP^{swe} Tg2576 mice (001349-T-RD1) along with the age-matched, non-transgenic, wild type littermates (001349-W-RD1). Prior to being shipped to the PhysioGenix Animal Facility, the mice will be screened for the RD1 mutation, which causes blindness. Any animal carrying the mutation will be excluded and replaced. Animals will be shipped from Taconic at ≈6 months of age and housed at PhysioGenix until the animals are aged to 9-12 months, which is the age where A β deposition notably affects performance in memory tasks [54]. Body weights will be collected weekly for the entire duration that the animals are housed at PhysioGenix as a means of monitoring animal health and to calculate dosing volumes for each study animal.

Contextual fear conditioning assay to assess associative learning and memory.

Behavioral assays will be carried out in an isolated laboratory where traffic and sound inference is negligible. Experiments will be carried out during the light phase of a 12/12hr light/dark cycle, and all technicians will be blinded to the treatments of the animals. Fear chambers will be procured from Med Associates (St. Albans, VT). Study animals will be acclimated to the experimental room for 60-90 minutes before entering into the fear-conditioning assay. After the period of acclimation, an animal will be placed into the fear chamber, which will serve as the novel context, i.e., conditioned stimulus. The animal will be allowed to explore the novel context for 148 s, at the end of which a foot shock (duration of 2 s at 0.4 mA) will be introduced [55, 56]. The animal will remain in the chamber for 30 s following the foot shock before returning to the home cage. Twenty-four hours later, the animal will be returned to the experimental room, allowed to acclimate in the room, and placed back into the chamber. Freezing, which will be defined

as the complete absence of movement, except for respiratory actions, will be scored every 10 s for 4 min.

Benchmark for Success. Success will be defined as a significant increase ($P < 0.05$) in percent freezing at the 24-hour time point for APP^{swe} transgenic and/or non-transgenic mice treated with PWZ-029 relative to the negative controls (vehicle and triazolam).

Anticipated Problems and Solutions. If differences are not observed between the treatment groups, we will consult Dr. Kaczorowski for procedural amendments that may enhance the differentiating potential of the fear conditioning assay (e.g., condition mice to the context prior to administering unconditioned stimulus training). We may still find that PWZ-029 does not enhance performance in this mouse model and in this assay. If these results are encountered, in our next round of funding, we will test the ability of PWZ-029 to mitigate cognitive deficits in mouse models of 'normal' aging.

Aim 3. Examine the potential of PWZ-029 to enhance executive function and memory in rhesus monkeys. Our research during the SBIR Phase I project showed that PWZ-029 enhanced performance on the ORD task of executive function in a manner consistent with a role for $\alpha 5$ -containing GABA_A receptors. We first will expand these findings to assess specific aspects of executive function, including set-shifting and response inhibition. In addition, we will introduce studies on working memory—a cognitive domain regulated by and influencing executive function [57]. Notably, deficits of this domain are considered a hallmark of AD [2, 44]. Finally, we will evaluate fundamental processes that may influence results from executive function and memory tasks, specifically attention and motivation.

Rationale: In order to evaluate the extent to which PWZ-029 enhances executive function and memory, our proposal will utilize the Cambridge Neuropsychological Test Automated Battery (CANTAB). A clear strength of the CANTAB approach is that its tasks

are based on corresponding procedures developed for human patients, which will greatly facilitate our ultimate goal of translating findings from monkeys to humans. For executive function, we will use two tasks, including the intradimensional/extradimensional (ID/ED) set-shifting task, which evaluates the ability of a subject to acquire discriminations, attend to specific stimulus attributes, and shift attention to other attributes, thus providing an assessment of cognitive flexibility. To evaluate “impulsivity,” a behavior shown to be impaired in AD [58], we will use the delayed reinforcement choice (DRC) task, in which monkeys must choose between a delayed, large reward or an immediate, small reward. To assess memory, we will use the self-ordered spatial search (SOSS) task, which is a short-term spatial working memory task similar to the radial-arm maze procedure used in rodents [59]. Attention will be assessed with the serial-reaction time (SRT) task [60], and motivational processes will be assessed with a progressive-ratio (PR) procedure. Altogether, these tasks will provide a comprehensive evaluation of the ability of PWZ-029 to enhance executive function and memory, as well as to assess the relative roles of attentional and motivational variables that potentially contribute to PWZ-029’s ability to enhance cognition.

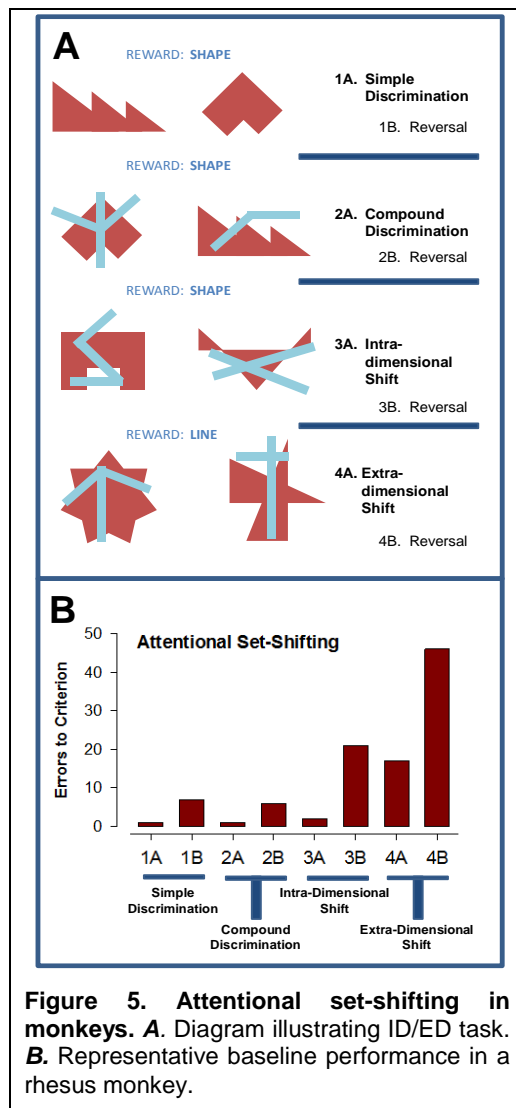
Experimental Design: Our overall approach will be similar to that described for our ORD results in the preliminary data section of this proposal (see Figure 4): (1) examine a range of doses of PWZ-029 (0.001-1.0 mg/kg) compared to a positive control (donepezil, 0.01 or 0.03 mg/kg [61]); (2) assess the ability of PWZ-029 to reverse the performance-attenuating effects of scopolamine (0.01 mg/kg, which will serve as a negative control; and (3) assess the ability of the preferential α 5-containing receptor antagonist, XLi-093 (0.1-1.0 mg/kg), to block enhanced performance, if present, of a maximally effective dose of PWZ-029.

Route of Administration. In order to compare our results with the results from the Phase I studies, we will initially administer all drugs via the i.v. route using indwelling chronic venous catheters (implanted using the methods described in detail by Platt et al., 2011) [62]. The use of the i.v. route will also help to minimize limitations of interpretation due to differences in pharmacokinetic variables. Oral dosing is a key consideration, however, and in the event that a positive effect of PWZ-029 emerges for a cognitive task, we will evaluate targeted doses using the intragastric (i.g.) route via a nasogastric tube in awake monkeys. Our co-PI, Dr. Rowlett, has extensive experience with this methodology [63-69]. We will choose the maximally effective dose, assuming a decrease in potency when switching from i.v. to i.g. administration, and increase (or decrease) the dose by $\frac{1}{2}$ log unit in order to adjust for potency differences across the two routes.

Subjects. Experiments will be conducted with adult male and female rhesus monkeys (*Macaca mulatta*), born and reared at the New England Primate Research Center breeding facility and/or obtained from outside sources. Based on our research during the Phase I grant, as well as power analyses derived from the literature, we are proposing a sample size of at least N=6 monkeys. For cognitive testing, monkeys will be prepared with a non-allergenic nylon vest (Lomir Biomedical, Inc., Malone, NY) and seated in primate chairs (Crist Instruments, Hagerstown, MD) enclosed in ventilated, sound-attenuating chambers (Med Associates). All animals will be monitored for food intake, and will undergo relatively mild food restriction, based on limiting caloric intake (for detailed methods, see Taffe, 2004 [70]). The monkeys will be weighed and assessed for body condition once per week. Weekly weighing of the conflict monkeys will occur throughout the studies to adjust feeding based on a combination of weight, performance, and overall health (assessed in consultation with the clinical veterinary staff).

CANTAB tasks for assessing executive function, memory, attention, and motivation. All

monkeys to be used in this application will receive training to sit in the chair, with different stages of training for the individual tasks (most monkeys will be trained and ready by the project start date). During a given experimental session, the monkey will be placed into the chair and brought to a sound-attenuated chamber (Med Associates) with ventilation, white noise, and a CANTAB touch screen unit. Sessions typically last no more than 2 hours, and 1 or 2 tasks are conducted per session (usually a single session/day). During tests with PWZ-029 (administered 5-10 min before the session), only a single task will be scheduled.



Intradimensional/Extradimensional Set Shifting (ID/ED). This task consists of a series of four discrimination learning stages, plus reversals, wherein touching only one of two stimuli presented on the screen results in food pellet delivery (for summary, see Figure 5). Within any given stage of the task, a pair of stimuli is presented and the same stimulus is associated with reinforcement (S+ stimulus) until the performance criteria are met (18 of 20 consecutive trials correct). Correct choices must be made within 30 s, and following a correct choice, the screen is blanked for 5 sec while an incorrect choice (S- stimulus) results in a 0.2 s tone and a 9-s period of blank screen. Four distinct stimulus sets will be used in 4 stages. In the first stimulus set (stage 1A), two distinctly shaped stimuli will be presented, with touches on one shape resulting in food pellet delivery. Stage 1B will consist of a stimulus reversal, in which the same two shapes are retained, but pressing the S+ stimulus now does not result in reinforcement, whereas touching the former S- stimulus will result in food pellet delivery. In Stage 2A, a compound discrimination is presented. For this discrimination, the two shapes from Stage 1B are present, but additional stimuli, consisting of lines, will be superimposed onto the existing shapes. Because the shape discrimination from the previous stage does not change, the lines are irrelevant to this discrimination. Stage 2B will consist of a shape reversal, similar to Stage 1B.

Stage 3A will consist of the ID shift stage. For this discrimination, two new shapes with new lines will be presented. This is considered an ID shift due to the fact that despite new shapes and lines being introduced, the shape remains the relevant dimension for the discrimination. Stage 3B will consist of a reversal of the shape S+ and S- from Stage 3A. In the final two stages, the ED shift will be introduced. Thus, in Stage 4A, new shapes and lines will be presented; however, the lines—not the shape—will be the relevant discriminative stimulus. Stage 4B will consist of a reversal of the line S+ and S-

contingencies. Performance is determined as the number of errors at each stage, and the data will be subjected to a square root transformation to achieve normal distributions [59]. Data will be analyzed with repeated measures ANOVA and Bonferroni t-tests for multiple comparisons.

Delayed Reinforcement Choice (DRC). Our preliminary data with the ORD task suggested the possibility that PWZ-029 enhances the ability of the monkey to withhold or inhibit prepotent responding. The ID/ED task will allow recording of persistent incorrect responding, similar to barrier reaches in the ORD task. A prominent interpretation of this type of behavior is dysfunctional inhibitory control, or “impulsivity.” A more complex form of inhibitory control involves choice behavior, which can be investigated using the DRC task, also commonly referred to as “delayed discounting” task.

The CANTAB “Impulsive Choice” task offers subjects a choice between two reinforcers, which can differ in magnitude, probability, and delay. We are focusing on delay of reinforcement in the DRC task, based on pharmacological studies [71, 72]. In this task, a

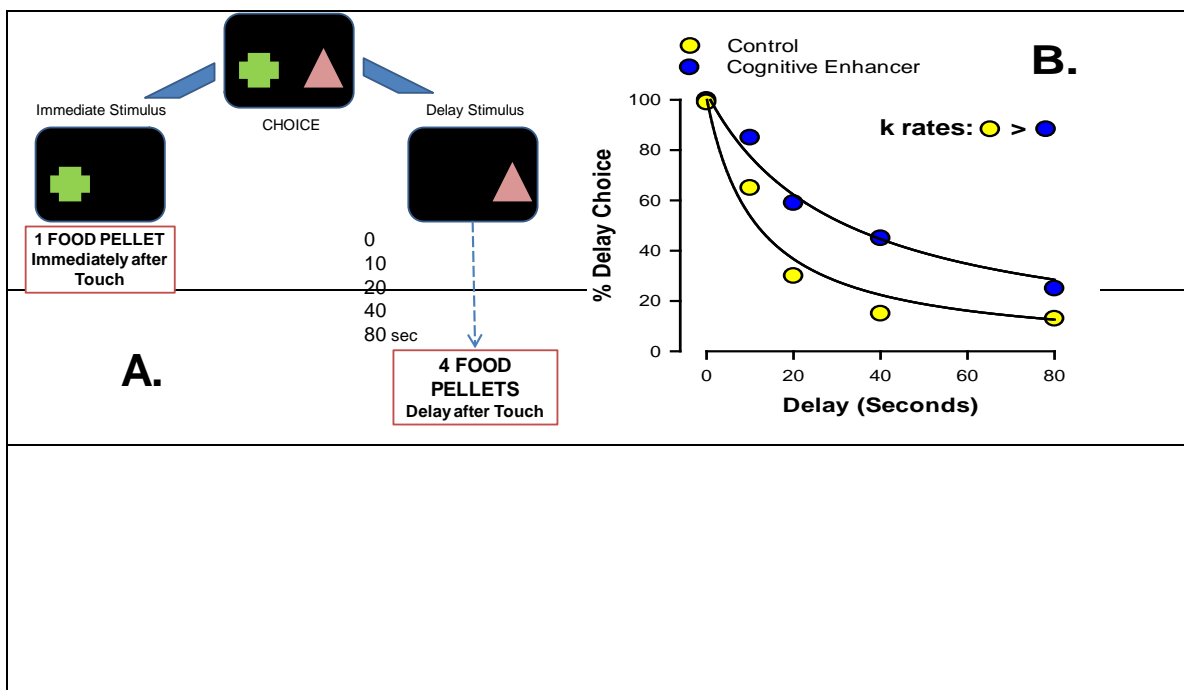


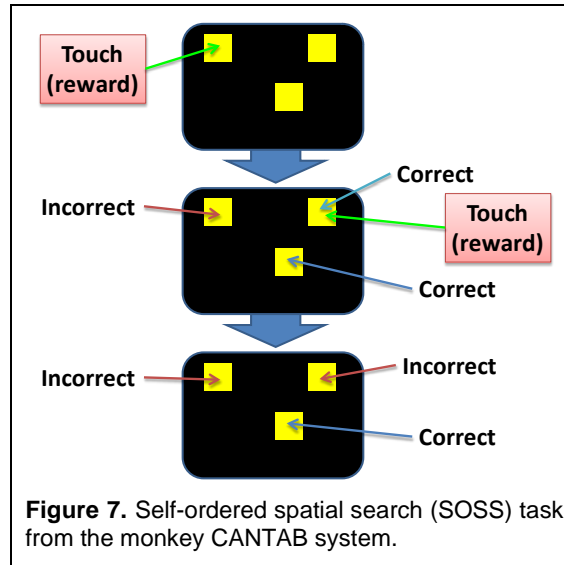
Figure 6. Delayed reinforcement choice task from the monkey CANTAB system.

A. Schematic of the task.

B. Prediction of the effects of a cognitive enhancer on data analyzed by discount functions. The k rate is the slope of discounting for the hyperbolic function—in this example, k is reduced by the cognitive enhancer, indicating a higher degree of choice for the larger, but delayed, reward.

choice is offered between a relatively large reward (4 or more food pellets) and a small reward (1 food pellet). A trial will initiate by a touch of a single stimulus, which is replaced by two stimuli, referred to as the “delay” and “immediate” stimulus. Touching the delay stimulus results in a blank screen for a specified duration (e.g., 0-80 s), followed by a signaled delivery of the large reward. Touching the immediate stimulus will result in signaled delivery of the small reward with no delay. After reward, the screen will be blank for 10 s. Data will be analyzed initially by comparing the percentage of delay stimulus responding as a function of delay (typical delay sequence= 0, 10, 20, 40, 80 s, randomly presented). As the delay is increased, animals characteristically choose the large reward less [71] (for summary, see Figure 6A). An improvement in performance by PWZ-029 would be manifested as a significant increase in percentage of choices for the delayed, yet larger reward, relative to control conditions. Data also may be analyzed using a hyperbolic discounting function [73], which provides a rate (k) of discounting value (Figure 6B). Enhancement of performance by PWZ-029 would be reflected as a significant decrease in the k value.

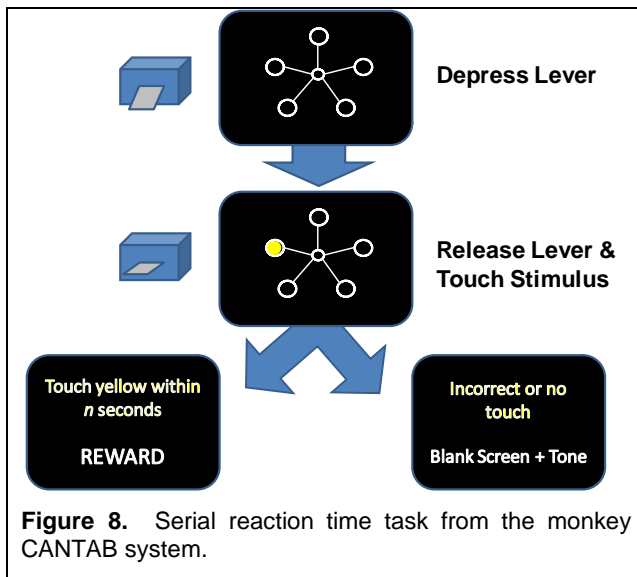
Self-Ordered Spatial Search (SOSS). The SOSS task is a short-term spatial working memory task similar to the radial-arm maze procedure used in rodents (see Figure 7, [59]).



In each trial, two, three or four small, colored, rectangular boxes are displayed on the screen in positions randomly allocated from 16 possible locations. The monkey must touch a box within 30 s of stimulus onset. After each successful touch, the color of the touched box is briefly (100 ms) changed and the screen is then blanked and a reinforcer delivered. After a 2-s delay, the boxes are re-displayed and the monkey must touch a box that was not previously touched in the trial in order to receive a food pellet. The trial is completed when the animal has either touched all boxes without a repetition (correct), touched a box that had previously been selected in that trial (error), or failed to touch a box within 30 s of stimulus presentation (omission). A tone and a 4-s screen blank will follow errors and omissions. After 5 s, another trial is presented with stimuli in new (randomly allocated) positions. A session will consist of 40 trials grouped into 6 blocks that differ according to the number of boxes presented. The different blocks, with

number of trials in parentheses, will be: 2 boxes (5), 3 boxes (7), 4 boxes (7), 3 boxes (8), 4 boxes (8), and 2 boxes (5). Accuracy scores will be calculated for each trial type by dividing the number of correctly completed trials by the number of trials in which there was at least one response (omissions will be excluded from the calculation). Accuracy scores will be analyzed by repeated measures ANOVA and Bonferroni t-tests, with trial type and PWZ-029 dose as factors.

Serial Reaction Time (SRT). This task is based on methods described in detail by Weed and Gold [60]. Briefly, the task consists of a discrete-trials procedure in which each trial begins with the presentation of a grid with 5 open circles (3 cm diameter) on the touch screen. The monkeys will be trained to press and hold a lever for a variable duration (between 0.75 to 2.5 s, randomly determined) and then to release the lever at the onset of a 2 cm yellow stimulus presented in one of the 5 circles. If the monkey touches this circle within 2 s, the screen will go blank and 2 food pellets will be delivered, and a 3 s inter-trial interval will begin. The yellow stimulus duration will consist of brief flashes of 0.02, 0.1, and 1.0 s durations. If the monkey fails to press the lever or fails to respond to the screen within the allotted time, or touches an incorrect circle, then a tone will sound and the screen will go blank for 4 s until the next trial, with no food reward given (for summary, see Figure 8).

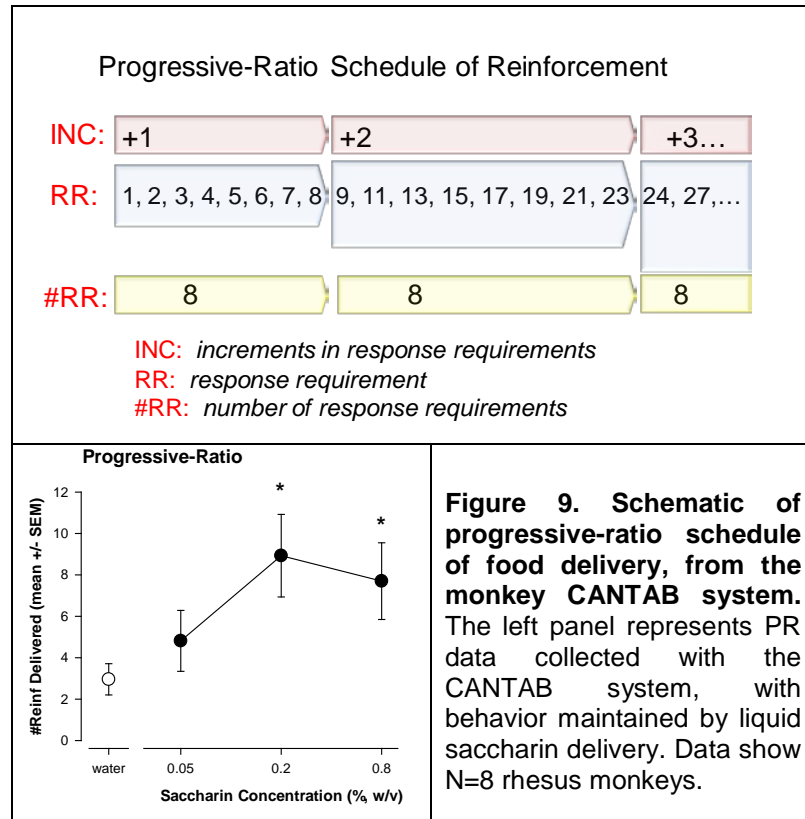


Each session will consist of 45 trials with the 3 flash durations presented randomly 3 times in each of the 5 choice circles.

Data that will be analyzed include latency to release the lever following stimulus onset and the time taken to move the hand from the lever to the screen. Failure to touch the screen after pressing the lever will be considered an omission error, which will be analyzed as the average number of errors per trial. All data will be analyzed with repeated measures ANOVA with dose and stimulus duration as factors, as well as with Bonferroni t-tests for multiple comparisons.

Progressive-Ratio (PR) schedule of reinforcement. PR procedures consist of response requirements that progressively increase across a session until responding ceases (Figure 9). The last response requirement completed, termed “break point,” provides a quantitative measure of the reinforcing effectiveness of a stimulus. For these studies, a colored box appearing in the middle of the screen will initiate a session. Touching the box once will result in food pellet delivery, and the response requirement will progressively increase following each reinforcer by an incremental value beginning at 1 and doubling after 8 response requirements are completed successfully. Thus, the

response requirement sequences will consist of: Increment=1, response requirements=1, 2, 3, 4, 5, 6, 7, 8; Increment=2, response requirements=10, 12, 14, 16, 18, 20, 22, 24; Increment=4, response requirements=28, 32, 36, 40, 44, 48, 52, 56; and so on.



Sessions will be a maximum of 20 min and will be terminated if 3 min elapses without a response. Performance will be measured as the break point and number of food pellets delivered per session. This procedure provides a measure of the ability of the animal to respond, as well as an assessment of “motivation” to perform. We do not anticipate that PWZ-029 will significantly alter the mean break points or number of food pellets delivered, which would rule out changes in motivational levels as an interpretation for changes in cognitive performance.

Benchmark for Success. Success will be defined as $\alpha 5$ -containing receptor mediated enhancements in ID/ED, DRC, and SOSS performance, in the absence of robust changes in SRT and PR.

Anticipated Problems and Solutions. SRT enhancements might suggest that broader cognitive processes are augmented simply due to an enhancement in attention, which in and of itself might be therapeutically useful. Change in PR performance, however, is a more significant issue, given that increases in motivation might explain increases in task performance by a non-cognitive mechanism (e.g., enhanced food palatability). We are unaware of any precedent in the literature for this type of effect.

Recent evidence has suggested an age-dependency for cognitive-enhancing effects of inverse agonists at $\alpha 5$ subunit-containing GABA_A receptors [15]. For our ORD studies, the monkeys generally were in the “middle-aged” category (≈ 15 -20 years old), a time period documented to show mostly moderate cognitive impairments [57, 74] and a similar group of monkeys will be available for the present project. If warranted, future plans will involve targeted cognitive tests with PWZ-029 in aged monkeys (20+ years old) depending on availability of monkeys in this age range.

References Cited

1. Pimplikar, S.W., et al., *Amyloid-independent mechanisms in Alzheimer's disease pathogenesis*. J Neurosci, 2010. **30**(45): p. 14946-54.
2. Selkoe, D.J., *Resolving controversies on the path to Alzheimer's therapeutics*. Nat Med, 2011. **17**(9): p. 1060-5.
3. Birks, J. and L. Flicker, *Donepezil for mild cognitive impairment*. Cochrane Database Syst Rev, 2006(3): p. CD006104.
4. Birks, J. and R.J. Harvey, *Donepezil for dementia due to Alzheimer's disease*. Cochrane Database Syst Rev, 2006(1): p. CD001190.
5. McShane, R., A. Areosa Sastre, and N. Minakaran, *Memantine for dementia*. Cochrane Database Syst Rev, 2006(2): p. CD003154.
6. Bishop, G.M. and S.R. Robinson, *The amyloid hypothesis: let sleeping dogmas lie?* Neurobiol Aging, 2002. **23**(6): p. 1101-5.
7. Rissman, R.A., A.L. De Blas, and D.M. Armstrong, *GABA(A) receptors in aging and Alzheimer's disease*. J Neurochem, 2007. **103**(4): p. 1285-92.
8. Rissman, R.A. and W.C. Mobley, *Implications for treatment: GABAA receptors in aging, Down syndrome and Alzheimer's disease*. J Neurochem, 2011. **117**(4): p. 613-22.
9. Robinson, S.R. and G.M. Bishop, *Abeta as a bioflocculant: implications for the amyloid hypothesis of Alzheimer's disease*. Neurobiol Aging, 2002. **23**(6): p. 1051-72.
10. Kaczorowski, C.C., et al., *Mechanisms underlying basal and learning-related intrinsic excitability in a mouse model of Alzheimer's disease*. Neurobiol Aging, 2011. **32**(8): p. 1452-65.

11. Kaczorowski, C.C. and J. Disterhoft, *Memory deficits are associated with impaired ability to modulate neuronal excitability in middle-aged mice*. Learn Mem, 2009. **16**: p. 362-366.
12. Oakley, H., et al., *Intraneuronal beta-amyloid aggregates, neurodegeneration, and neuron loss in transgenic mice with five familial Alzheimer's disease mutations: potential factors in amyloid plaque formation*. J Neurosci, 2006. **26**(40): p. 10129-40.
13. Pirker, S., et al., *GABA(A) receptors: immunocytochemical distribution of 13 subunits in the adult rat brain*. Neuroscience, 2000. **101**(4): p. 815-50.
14. Sieghart, W. and G. Sperk, *Subunit composition, distribution and function of GABA(A) receptor subtypes*. Curr Top Med Chem, 2002. **2**(8): p. 795-816.
15. Koh, M.T., S. Rosenzweig-Lipson, and M. Gallagher, *Selective GABA(A) alpha5 positive allosteric modulators improve cognitive function in aged rats with memory impairment*. Neuropharmacology, 2013. **64**: p. 145-52.
16. Sperk, G., et al., *GABA(A) receptor subunits in the rat hippocampus I: immunocytochemical distribution of 13 subunits*. Neuroscience, 1997. **80**(4): p. 987-1000.
17. Sigel, E. and A. Buhr, *The benzodiazepine binding site of GABAA receptors*. Trends Pharmacol Sci, 1997. **18**(11): p. 425-9.
18. Olsen, R.W. and A.J. Tobin, *Molecular biology of GABAA receptors*. FASEB J, 1990. **4**(5): p. 1469-80.
19. Macdonald, R.L. and R.W. Olsen, *GABAA receptor channels*. Annu Rev Neurosci, 1994. **17**: p. 569-602.
20. Rabow, L.E., S.J. Russek, and D.H. Farb, *From ion currents to genomic analysis: recent advances in GABAA receptor research*. Synapse, 1995. **21**(3): p. 189-274.

21. Mohler, H., et al., *The GABAA receptors. From subunits to diverse functions*. Ion Channels, 1996. **4**: p. 89-113.
22. Barnard, E.A., et al., *International Union of Pharmacology. XV. Subtypes of gamma-aminobutyric acidA receptors: classification on the basis of subunit structure and receptor function*. Pharmacol Rev, 1998. **50**(2): p. 291-313.
23. Bonnert, T.P., et al., *theta, a novel gamma-aminobutyric acid type A receptor subunit*. Proc Natl Acad Sci U S A, 1999. **96**(17): p. 9891-6.
24. Whiting, P.J., et al., *Molecular and functional diversity of the expanding GABA-A receptor gene family*. Ann N Y Acad Sci, 1999. **868**: p. 645-53.
25. Li, M. and A.L. De Blas, *Coexistence of two beta subunit isoforms in the same gamma-aminobutyric acid type A receptor*. J Biol Chem, 1997. **272**(26): p. 16564-9.
26. Jechlinger, M., et al., *Subunit composition and quantitative importance of heterooligomeric receptors: GABAA receptors containing alpha6 subunits*. J Neurosci, 1998. **18**(7): p. 2449-57.
27. Farrar, S.J., et al., *Stoichiometry of a ligand-gated ion channel determined by fluorescence energy transfer*. J Biol Chem, 1999. **274**(15): p. 10100-4.
28. McKernan, R.M., et al., *Sedative but not anxiolytic properties of benzodiazepines are mediated by the GABA(A) receptor alpha1 subtype*. Nat Neurosci, 2000. **3**(6): p. 587-92.
29. Howell, O., et al., *Density and pharmacology of alpha5 subunit-containing GABA(A) receptors are preserved in hippocampus of Alzheimer's disease patients*. Neuroscience, 2000. **98**(4): p. 669-75.
30. Harris, D., et al., *Selective influence on contextual memory: physiochemical properties associated with selectivity of benzodiazepine ligands at GABAA receptors containing the alpha5 subunit*. J Med Chem, 2008. **51**(13): p. 3788-803.

31. Sur, C., et al., *Rat and human hippocampal alpha5 subunit-containing gamma-aminobutyric AcidA receptors have alpha5 beta3 gamma2 pharmacological characteristics*. Mol Pharmacol, 1998. **54**(5): p. 928-33.
32. Pellegrini-Giampietro, D.E., et al., *The GluR2 (GluR-B) hypothesis: Ca(2+)-permeable AMPA receptors in neurological disorders*. Trends Neurosci, 1997. **20**(10): p. 464-70.
33. Arundine, M. and M. Tymianski, *Molecular mechanisms of glutamate-dependent neurodegeneration in ischemia and traumatic brain injury*. Cell Mol Life Sci, 2004. **61**(6): p. 657-68.
34. Rossor, M.N., et al., *A post-mortem study of the cholinergic and GABA systems in senile dementia*. Brain, 1982. **105**(Pt 2): p. 313-30.
35. Mountjoy, C.Q., et al., *Correlation of cortical cholinergic and GABA deficits with quantitative neuropathological findings in senile dementia*. Brain, 1984. **107** (Pt 2): p. 507-18.
36. Reinikainen, K.J., et al., *A post-mortem study of noradrenergic, serotonergic and GABAergic neurons in Alzheimer's disease*. J Neurol Sci, 1988. **84**(1): p. 101-16.
37. Lowe, S.L., et al., *Gamma-aminobutyric acid concentration in brain tissue at two stages of Alzheimer's disease*. Brain, 1988. **111** (Pt 4): p. 785-99.
38. Zhang, P., et al., *Synthesis of novel imidazobenzodiazepines as probes of the pharmacophore for "diazepam-insensitive" GABAA receptors*. J Med Chem, 1995. **38**(10): p. 1679-88.
39. Savic, M.M., et al., *PWZ-029, a compound with moderate inverse agonist functional selectivity at GABA(A) receptors containing alpha5 subunits, improves passive, but not active, avoidance learning in rats*. Brain Res, 2008. **1208**: p. 150-9.

40. Rowlett, J.K., et al., *Anti-conflict effects of benzodiazepines in rhesus monkeys: relationship with therapeutic doses in humans and role of GABAA receptors*. *Psychopharmacology (Berl)*, 2006. **184**(2): p. 201-11.
41. Lecanu, L., J. Greeson, and V. Papadopoulos, *Beta-amyloid and oxidative stress jointly induce neuronal death, amyloid deposits, gliosis, and memory impairment in the rat brain*. *Pharmacology*, 2006. **76**(1): p. 19-33.
42. Ballard, T.M., et al., *RO4938581, a novel cognitive enhancer acting at GABAA alpha5 subunit-containing receptors*. *Psychopharmacology (Berl)*, 2009. **202**(1-3): p. 207-23.
43. Jentsch, J.D., et al., *Altered frontal cortical dopaminergic transmission in monkeys after subchronic phencyclidine exposure: involvement in frontostriatal cognitive deficits*. *Neuroscience*, 1999. **90**(3): p. 823-32.
44. Baudic, S., et al., *Executive function deficits in early Alzheimer's disease and their relations with episodic memory*. *Arch Clin Neuropsychol*, 2006. **21**(1): p. 15-21.
45. Ng, R. and John Wiley & Sons., *Drugs from discovery to approval*, 2004, Wiley-Liss, Hoboken, NJ.
46. Kim, J.J. and M.S. Fanselow, *Modality-specific retrograde amnesia of fear*. *Science*, 1992. **256**(5057): p. 675-7.
47. Phillips, R.G. and J.E. LeDoux, *Differential contribution of amygdala and hippocampus to cued and contextual fear conditioning*. *Behav Neurosci*, 1992. **106**(2): p. 274-85.
48. Misane, I., et al., *GABA(A) receptor activation in the CA1 area of the dorsal hippocampus impairs consolidation of conditioned contextual fear in C57BL/6J mice*. *Behav Brain Res*, 2012. **238C**: p. 160-169.

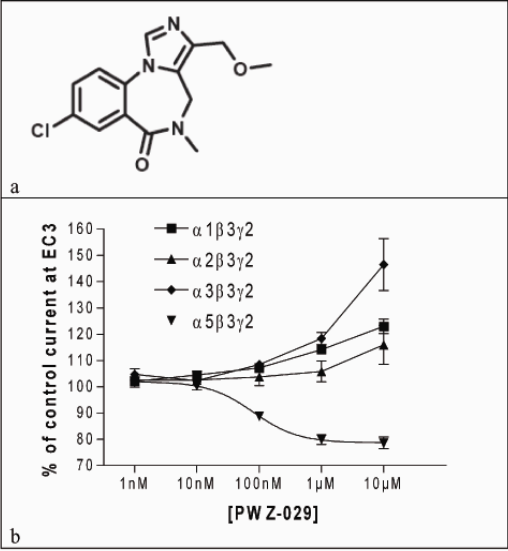
49. Selden, N.R., et al., *Complementary roles for the amygdala and hippocampus in aversive conditioning to explicit and contextual cues*. *Neuroscience*, 1991. **42**(2): p. 335-50.
50. Stiedl, O., et al., *Impairment of conditioned contextual fear of C57BL/6J mice by intracerebral injections of the NMDA receptor antagonist APV*. *Behav Brain Res*, 2000. **116**(2): p. 157-68.
51. Dong, H., et al., *Acetylcholinesterase inhibitors ameliorate behavioral deficits in the Tg2576 mouse model of Alzheimer's disease*. *Psychopharmacology (Berl)*, 2005. **181**(1): p. 145-52.
52. Dong, H., et al., *Effects of donepezil on amyloid-beta and synapse density in the Tg2576 mouse model of Alzheimer's disease*. *Brain Res*, 2009. **1303**: p. 169-78.
53. Sanger, D.J., D. Joly, and B. Zivkovic, *Effects of zolpidem, a new imidazopyridine hypnotic, on the acquisition of conditioned fear in mice. Comparison with triazolam and CL 218,872*. *Psychopharmacology (Berl)*, 1986. **90**(2): p. 207-10.
54. Hsiao, K., et al., *Correlative memory deficits, Abeta elevation, and amyloid plaques in transgenic mice*. *Science*, 1996. **274**(5284): p. 99-102.
55. Fukushima, H., et al., *Upregulation of calcium/calmodulin-dependent protein kinase IV improves memory formation and rescues memory loss with aging*. *J Neurosci*, 2008. **28**(40): p. 9910-9.
56. Suzuki, A., et al., *Activation of LVGCCs and CB1 receptors required for destabilization of reactivated contextual fear memories*. *Learn Mem*, 2008. **15**(6): p. 426-33.
57. Zeamer, A., et al., *Attention, executive functioning and memory in normal aged rhesus monkeys*. *Behav Brain Res*, 2011. **219**(1): p. 23-30.
58. Rochat, L., et al., *A multidimensional approach to impulsivity changes in mild Alzheimer's disease and control participants: Cognitive correlates*. *Cortex*, 2011.

59. Weed, M.R., et al., *Performance norms for a rhesus monkey neuropsychological testing battery: acquisition and long-term performance*. Brain Res Cogn Brain Res, 1999. **8**(3): p. 185-201.
60. Weed, M.R. and L.H. Gold, *The effects of dopaminergic agents on reaction time in rhesus monkeys*. Psychopharmacology (Berl), 1998. **137**(1): p. 33-42.
61. Buccafusco, J.J., et al., *Sex dimorphisms in the cognitive-enhancing action of the Alzheimer's drug donepezil in aged Rhesus monkeys*. Neuropharmacology, 2003. **44**(3): p. 381-9.
62. Platt, D.M., G. Carey, and R.D. Spealman, *Intravenous self-administration techniques in monkeys*. Curr Protoc Neurosci, 2005. **Chapter 9**: p. Unit 9 21.
63. Acteo, M.D., et al., *Zipeprol: preclinical assessment of abuse potential*. Drug Alcohol Depend, 1996. **42**(2): p. 93-104.
64. France, C.P., et al., *Progress report from the testing program for stimulant and depressant drugs (1996)*. NIDA Res Monogr, 1998. **178**: p. 429-39.
65. Rowlett, J.K. and W.L. Woolverton, *Discriminative stimulus effects of zolpidem in pentobarbital-trained subjects: I. Comparison with triazolam in rhesus monkeys and rats*. J Pharmacol Exp Ther, 1997. **280**(1): p. 162-73.
66. Rowlett, J.K. and W.L. Woolverton, *Discriminative stimulus effects of benzodiazepine agonists and partial agonists in pentobarbital-trained rhesus monkeys*. Behav Pharmacol, 1998. **9**(2): p. 81-92.
67. Rowlett, J.K., et al., *Reinforcing and discriminative stimulus effects of the neuroactive steroids pregnanolone and Co 8-7071 in rhesus monkeys*. Psychopharmacology (Berl), 1999. **145**(2): p. 205-12.
68. Rowlett, J.K. and W.L. Woolverton, *Discriminative stimulus effects of panadiplon (U-78875), a partial agonist at the benzodiazepine site, in pentobarbital-trained rhesus monkeys*. Drug Alcohol Depend, 2001. **61**(3): p. 229-36.

69. Woolverton, W.L., et al., *Evaluation of the reinforcing and discriminative stimulus effects of gamma-hydroxybutyrate in rhesus monkeys*. Drug Alcohol Depend, 1999. **54**(2): p. 137-43.
70. Taffe, M.A., *Effects of parametric feeding manipulations on behavioral performance in macaques*. Physiol Behav, 2004. **81**(1): p. 59-70.
71. Evenden, J.L. and C.N. Ryan, *The pharmacology of impulsive behaviour in rats: the effects of drugs on response choice with varying delays of reinforcement*. Psychopharmacology (Berl), 1996. **128**(2): p. 161-70.
72. Cardinal, R.N., T.W. Robbins, and B.J. Everitt, *The effects of d-amphetamine, chlordiazepoxide, alpha-flupenthixol and behavioural manipulations on choice of signalled and unsignalled delayed reinforcement in rats*. Psychopharmacology (Berl), 2000. **152**(4): p. 362-75.
73. Freeman, K.B., et al., *Delay discounting in rhesus monkeys: equivalent discounting of more and less preferred sucrose concentrations*. Learn Behav, 2012. **40**(1): p. 54-60.
74. Peters, A., et al., *Neurobiological bases of age-related cognitive decline in the rhesus monkey*. J Neuropathol Exp Neurol, 1996. **55**(8): p. 861-74.

PWZ-029 Preliminary Data Compilation

BINDING AFFINITY

Experiment	Type of Test	Model	Figure	Summary of Results																																
Functional and subtype selectivity of PWZ-029	Used to determine the subtype selectivity of PWZ-029 to the GABA _A receptors, especially the $\alpha 5$ subtype.	Xenopus oocytes electrophysiology	 <p>The figure consists of two parts. Part (a) shows the chemical structure of PWZ-029, which is a benzodiazepine derivative with a 7-chlorophenyl ring, a 5-methoxy-1H-imidazol-2-ylmethyl group, and a 1-methyl-2-oxoethyl group. Part (b) is a line graph showing the percentage of control current at EC3 for four GABA_A receptor subtypes: $\alpha 1\beta 3\gamma 2$ (squares), $\alpha 2\beta 3\gamma 2$ (triangles), $\alpha 3\beta 3\gamma 2$ (diamonds), and $\alpha 5\beta 3\gamma 2$ (inverted triangles). The x-axis represents the concentration of PWZ-029 from 1 nM to 10 μM. The y-axis represents the percentage of control current from 70 to 160. The $\alpha 5\beta 3\gamma 2$ subtype shows a significant decrease in current (agonistic effect) at 1 μM and 10 μM, while the other subtypes show an increase in current (partial inverse agonist effect).</p>	PWZ-029 concentrations of up to 1 μ M demonstrated a significant 20% reduction of control GABA elicited current indicating a partial inverse agonist effect at GABA _A receptors possessing the $\alpha 5$ subtype. PWZ-029 also exhibited agonistic selectivity for the $\alpha 1$ and $\alpha 3$ bearing GABA _A receptors. P<0.01, Student's t-test.																																
Binding Affinity of PWZ-029	Used to determine the affinity of PWZ-029 to the GABA _A receptor subtype, $\alpha 5$.	Mouse fibroblast L(tk ⁻) cells expressing recombinant human GABA _A receptor subunits	<p style="text-align: center;">Affinity of PWZ-029 for $\alpha x\beta 3\gamma 2$ (x = 1-6) benzodiazepine receptor isoforms</p> <table border="1" style="width: 100%; border-collapse: collapse; text-align: center;"> <thead> <tr> <th>Code</th> <th>MW</th> <th>$\alpha 1$</th> <th>$\alpha 2$</th> <th>$\alpha 3$</th> <th>$\alpha 4$</th> <th>$\alpha 5$</th> <th>$\alpha 6$</th> </tr> </thead> <tbody> <tr> <td>Merck</td> <td>291.73</td> <td>>300</td> <td>>300</td> <td>>300</td> <td>ND</td> <td style="color: red;">38.8</td> <td>>300</td> </tr> <tr> <td>Moltech</td> <td>291.73</td> <td>920</td> <td>ND</td> <td>ND</td> <td>ND</td> <td style="color: red;">30</td> <td>ND</td> </tr> <tr> <td>UNC-Roth</td> <td>291.73</td> <td>362.4</td> <td>180.330</td> <td>328.2</td> <td>ND</td> <td style="color: red;">6.185</td> <td>ND</td> </tr> </tbody> </table>	Code	MW	$\alpha 1$	$\alpha 2$	$\alpha 3$	$\alpha 4$	$\alpha 5$	$\alpha 6$	Merck	291.73	>300	>300	>300	ND	38.8	>300	Moltech	291.73	920	ND	ND	ND	30	ND	UNC-Roth	291.73	362.4	180.330	328.2	ND	6.185	ND	PWZ-029 binding affinity for $\alpha 5$ sutypes are near 60 fold times that of $\alpha 1$ subunits.
Code	MW	$\alpha 1$	$\alpha 2$	$\alpha 3$	$\alpha 4$	$\alpha 5$	$\alpha 6$																													
Merck	291.73	>300	>300	>300	ND	38.8	>300																													
Moltech	291.73	920	ND	ND	ND	30	ND																													
UNC-Roth	291.73	362.4	180.330	328.2	ND	6.185	ND																													

PWZ-029 Preliminary Data Compilation

SIDE-EFFECTS

Experiment	Type of Test	Model	Figure	Summary of Results																								
Convulsant/ Proconvulsant Effects	Used to determine the convulsant/proconvulsant drug side-effects.	Male Swiss mice (CrI:CFW(SW)) treated with pentylenetetrazole (PTZ)	N/A	PWZ-029 did not cause convulsions at any concentration (10, 20, or 40 mg/kg) in the PTZ mouse model.																								
Rotarod	Rotarod tests are used to assess motor coordination. The longer an animal stays on the rotating rod, the more coordination their motor skills. The test further assesses drug side-effects, such as dizziness and muscle relaxation. If these effects are present the subject is expected to spend less time on the rotating rod.	Dahl Salt-Sensitive (SS) rats (n=12/group) were treated per os with either vehicle, diazepam, or one of three concentrations of PWZ-029. After a training period, the animals were subjected to the rotating rod test for a maximum of 300 seconds.	<p>A. Rotarod Test: Motor Coordination in Dahl/SS Rats</p> <table border="1"> <caption>Latency to Fall (s)</caption> <thead> <tr> <th>Treatment Group</th> <th>Latency to Fall (s)</th> </tr> </thead> <tbody> <tr> <td>Group 1: Vehicle - Saline</td> <td>~160</td> </tr> <tr> <td>Group 2: Diazepam (3 mg/kg)</td> <td>~160</td> </tr> <tr> <td>Group 3: PWZ-029 (5 mg/kg)</td> <td>~180</td> </tr> <tr> <td>Group 4: PWZ-029 (10 mg/kg)</td> <td>~170</td> </tr> <tr> <td>Group 5: PWZ-029 (20 mg/kg)</td> <td>~170</td> </tr> </tbody> </table> <p>B. Rotarod Test: Percent Success in Dahl/SS Rats</p> <table border="1"> <caption>Success Rate (%)</caption> <thead> <tr> <th>Treatment Group</th> <th>Success Rate (%)</th> </tr> </thead> <tbody> <tr> <td>Group 1: Vehicle - Saline</td> <td>~65</td> </tr> <tr> <td>Group 2: Diazepam (3 mg/kg)</td> <td>~65</td> </tr> <tr> <td>Group 3: PWZ-029 (5 mg/kg)</td> <td>~90</td> </tr> <tr> <td>Group 4: PWZ-029 (10 mg/kg)</td> <td>~85</td> </tr> <tr> <td>Group 5: PWZ-029 (20 mg/kg)</td> <td>~75</td> </tr> </tbody> </table>	Treatment Group	Latency to Fall (s)	Group 1: Vehicle - Saline	~160	Group 2: Diazepam (3 mg/kg)	~160	Group 3: PWZ-029 (5 mg/kg)	~180	Group 4: PWZ-029 (10 mg/kg)	~170	Group 5: PWZ-029 (20 mg/kg)	~170	Treatment Group	Success Rate (%)	Group 1: Vehicle - Saline	~65	Group 2: Diazepam (3 mg/kg)	~65	Group 3: PWZ-029 (5 mg/kg)	~90	Group 4: PWZ-029 (10 mg/kg)	~85	Group 5: PWZ-029 (20 mg/kg)	~75	No significant decrease in motor coordination was observed at any of the three PWZ-029 concentrations. However, the success rate of rats increased with PWZ-029 treatment.
Treatment Group	Latency to Fall (s)																											
Group 1: Vehicle - Saline	~160																											
Group 2: Diazepam (3 mg/kg)	~160																											
Group 3: PWZ-029 (5 mg/kg)	~180																											
Group 4: PWZ-029 (10 mg/kg)	~170																											
Group 5: PWZ-029 (20 mg/kg)	~170																											
Treatment Group	Success Rate (%)																											
Group 1: Vehicle - Saline	~65																											
Group 2: Diazepam (3 mg/kg)	~65																											
Group 3: PWZ-029 (5 mg/kg)	~90																											
Group 4: PWZ-029 (10 mg/kg)	~85																											
Group 5: PWZ-029 (20 mg/kg)	~75																											

PWZ-029 Preliminary Data Compilation

SIDE-EFFECTS Continued

Experiment	Type of Test	Model	Figure	Summary of Results																								
Operant Responding	Very basically assesses the individual's response that is required to carry out cognitive tasks. This experiment is highly sensitive to sedative-motor effects of conventional benzodiazepines (e.g. alprazolam).	Rhesus monkeys treated with vehicle and then increasing concentrations of alprazolam or PWZ-029. This Operant Responding task required the animal to press the lever 20 times to receive a food pellet.	<p>C. Operant Responding</p> <table border="1"> <caption>Data for Figure C: Operant Responding Rate (Responses/s)</caption> <thead> <tr> <th>Dose (mg/kg, i.v.)</th> <th>PWZ-029 (Responses/s)</th> <th>alprazolam (Responses/s)</th> </tr> </thead> <tbody> <tr> <td>V</td> <td>~3.0</td> <td>~2.8</td> </tr> <tr> <td>0.001</td> <td>~3.2</td> <td>~3.0</td> </tr> <tr> <td>0.01</td> <td>~3.1</td> <td>~2.8</td> </tr> <tr> <td>0.01</td> <td>~3.2</td> <td>~3.2</td> </tr> <tr> <td>0.1</td> <td>~3.2</td> <td>~2.4</td> </tr> <tr> <td>0.1</td> <td>~3.2</td> <td>~1.1</td> </tr> <tr> <td>1</td> <td>~3.2</td> <td>~0.0</td> </tr> </tbody> </table>	Dose (mg/kg, i.v.)	PWZ-029 (Responses/s)	alprazolam (Responses/s)	V	~3.0	~2.8	0.001	~3.2	~3.0	0.01	~3.1	~2.8	0.01	~3.2	~3.2	0.1	~3.2	~2.4	0.1	~3.2	~1.1	1	~3.2	~0.0	PWZ-029 showed no evidence of inhibition in the baseline levels of operant responding maintained by food.
Dose (mg/kg, i.v.)	PWZ-029 (Responses/s)	alprazolam (Responses/s)																										
V	~3.0	~2.8																										
0.001	~3.2	~3.0																										
0.01	~3.1	~2.8																										
0.01	~3.2	~3.2																										
0.1	~3.2	~2.4																										
0.1	~3.2	~1.1																										
1	~3.2	~0.0																										
Observational Studies	Based on defined behaviors observed in animals under baseline conditions, post-dose observations are indicative of drug side-effects.	Rhesus monkeys were treated with vehicle, alprazolam, zolpidem, or PWZ-029. Post-dose observations were documented as no change, increase, decrease or increase and decrease in respective behavior.	<p>Table 2. Analysis of all behavioral categories following multiple doses of the three test compounds. Significant effects were identified as at least one dose significantly different from vehicle (N=4-5 monkeys). See Table 1 for definitions of abbreviations.</p> <table border="1"> <thead> <tr> <th>Compounds</th> <th>No Change</th> <th>Increase</th> <th>Decrease</th> <th>Increase & Decrease</th> </tr> </thead> <tbody> <tr> <td>Alprazolam</td> <td>Loc, Grm, Scr, Ste, For, Voc, Thr, Yaw, BSm, Pre, Dri, NRu, LSm, CSh, LDr</td> <td>RSP, MSe, DSe, Atx</td> <td>Pas, Tac</td> <td></td> </tr> <tr> <td>Zolpidem</td> <td>Loc*, Grm, Scr, Ste, For, Voc, Thr, Yaw, BSm, Pre, Dri, NRu, LSm, RSP, MSe, CSh, LDr</td> <td>DSe, Atx</td> <td>Pas</td> <td>Tac</td> </tr> <tr> <td>PWZ-029</td> <td>Pas, Loc, Grm, Tac, Scr, Ste, For, Voc, Thr, Yaw, BSm, Pre, Dri, NRu, Atx, LSm, RSP, CSh, MSe, DSe, LDr</td> <td></td> <td></td> <td></td> </tr> </tbody> </table> <p>*Loc was associated with a significant overall main effect of dose (ANOVA) but none of the doses were significantly different from vehicle (Bonferroni t-tests, P>0.05).</p>	Compounds	No Change	Increase	Decrease	Increase & Decrease	Alprazolam	Loc, Grm, Scr, Ste, For, Voc, Thr, Yaw, BSm, Pre, Dri, NRu, LSm, CSh, LDr	RSP, MSe, DSe, Atx	Pas, Tac		Zolpidem	Loc*, Grm, Scr, Ste, For, Voc, Thr, Yaw, BSm, Pre, Dri, NRu, LSm, RSP, MSe, CSh, LDr	DSe, Atx	Pas	Tac	PWZ-029	Pas, Loc, Grm, Tac, Scr, Ste, For, Voc, Thr, Yaw, BSm, Pre, Dri, NRu, Atx, LSm, RSP, CSh, MSe, DSe, LDr				No increase or decrease in behavior were observed for PWZ-029.				
Compounds	No Change	Increase	Decrease	Increase & Decrease																								
Alprazolam	Loc, Grm, Scr, Ste, For, Voc, Thr, Yaw, BSm, Pre, Dri, NRu, LSm, CSh, LDr	RSP, MSe, DSe, Atx	Pas, Tac																									
Zolpidem	Loc*, Grm, Scr, Ste, For, Voc, Thr, Yaw, BSm, Pre, Dri, NRu, LSm, RSP, MSe, CSh, LDr	DSe, Atx	Pas	Tac																								
PWZ-029	Pas, Loc, Grm, Tac, Scr, Ste, For, Voc, Thr, Yaw, BSm, Pre, Dri, NRu, Atx, LSm, RSP, CSh, MSe, DSe, LDr																											

PWZ-029 Preliminary Data Compilation

SIDE-EFFECTS Continued

Experiment	Type of Test	Model	Figure	Summary of Results																																																	
Sedation Measures	Based on defined sedative postures for primates, sedative side-effects can be measured with these experiments.	Rhesus monkeys were treated with 3.0 mg/kg PWZ-029 (i.v.) or one of two concentrations of alprazolam and then monitored for 120-minutes post-dose.	<p>The figure consists of six line graphs arranged in a 2x3 grid. The top row shows results for PWZ-029 at 3.0 mg/kg, and the bottom row shows results for Alprazolam at 0.1 mg/kg and 1 mg/kg. Each graph plots a sedation measure (0-20) against time (0, 7.5, 15, 30, 60, 120 minutes). Error bars are included for each data point.</p> <table border="1"> <caption>Approximate data from the sedation measure graphs</caption> <thead> <tr> <th>Time (min)</th> <th>PWZ-029 3.0 mg/kg (Sleep Posture)</th> <th>PWZ-029 3.0 mg/kg (Moderate Sedation)</th> <th>PWZ-029 3.0 mg/kg (Deep Sedation)</th> <th>Alprazolam 0.1 mg/kg (Sleep Posture)</th> <th>Alprazolam 1 mg/kg (Moderate Sedation)</th> <th>Alprazolam 1 mg/kg (Deep Sedation)</th> </tr> </thead> <tbody> <tr> <td>0</td> <td>0</td> <td>0</td> <td>0</td> <td>2</td> <td>2</td> <td>8</td> </tr> <tr> <td>7.5</td> <td>0</td> <td>0</td> <td>0</td> <td>8</td> <td>1</td> <td>18</td> </tr> <tr> <td>15</td> <td>0</td> <td>0</td> <td>0</td> <td>10</td> <td>2</td> <td>17</td> </tr> <tr> <td>30</td> <td>3</td> <td>0</td> <td>0</td> <td>10</td> <td>4</td> <td>15</td> </tr> <tr> <td>60</td> <td>0</td> <td>0</td> <td>0</td> <td>4</td> <td>3</td> <td>11</td> </tr> <tr> <td>120</td> <td>0</td> <td>0</td> <td>0</td> <td>0</td> <td>3</td> <td>5</td> </tr> </tbody> </table>	Time (min)	PWZ-029 3.0 mg/kg (Sleep Posture)	PWZ-029 3.0 mg/kg (Moderate Sedation)	PWZ-029 3.0 mg/kg (Deep Sedation)	Alprazolam 0.1 mg/kg (Sleep Posture)	Alprazolam 1 mg/kg (Moderate Sedation)	Alprazolam 1 mg/kg (Deep Sedation)	0	0	0	0	2	2	8	7.5	0	0	0	8	1	18	15	0	0	0	10	2	17	30	3	0	0	10	4	15	60	0	0	0	4	3	11	120	0	0	0	0	3	5	<p>PWZ-029 did not alter either species-specific behavior or induce significant signs of sedation at doses 200-300 times higher than the lowest dose that enhanced ORD performance.</p> <p>Conversely, the non-selective benzodiazepine alprazolam suppressed some aspects of normal, species-typical behavior and engendered rest/sleep posture, moderate and deep sedation; thus providing a positive control for the PWZ-029 data.</p>
Time (min)	PWZ-029 3.0 mg/kg (Sleep Posture)	PWZ-029 3.0 mg/kg (Moderate Sedation)	PWZ-029 3.0 mg/kg (Deep Sedation)	Alprazolam 0.1 mg/kg (Sleep Posture)	Alprazolam 1 mg/kg (Moderate Sedation)	Alprazolam 1 mg/kg (Deep Sedation)																																															
0	0	0	0	2	2	8																																															
7.5	0	0	0	8	1	18																																															
15	0	0	0	10	2	17																																															
30	3	0	0	10	4	15																																															
60	0	0	0	4	3	11																																															
120	0	0	0	0	3	5																																															

PWZ-029 Preliminary Data Compilation

IMPAIRED BASELINE RECOVERY AND COMPLEX MEMORY

Experiment	Type of Test	Model	Figure	Summary of Results								
<p>Pavlovian Fear Conditioned Contextual Memory</p>	<p>Assesses the contextual fear response (i.e. freezing) to stimulus.</p>	<p>Scopolamine-treated C57BL/6 mice (n=12/group) - Each mouse received i.p. injections with either vehicle (0.9% saline containing 2.5% encapsin), 1.5 mg/kg scopolamine, or 1.5 mg/kg scopolamine plus 10 mg/kg PWZ-029.</p>	<table border="1"> <caption>Data from Figure: % Freezing</caption> <thead> <tr> <th>Group</th> <th>% Freezing (approx.)</th> </tr> </thead> <tbody> <tr> <td>Vehicle</td> <td>50</td> </tr> <tr> <td>Scopolamine</td> <td>20</td> </tr> <tr> <td>PWZ-029 + Scop</td> <td>45</td> </tr> </tbody> </table>	Group	% Freezing (approx.)	Vehicle	50	Scopolamine	20	PWZ-029 + Scop	45	<p>PWZ-029 attenuated the scopolamine-induced impairment of contextual memory [3]. ***$p < 0.05$.</p>
Group	% Freezing (approx.)											
Vehicle	50											
Scopolamine	20											
PWZ-029 + Scop	45											

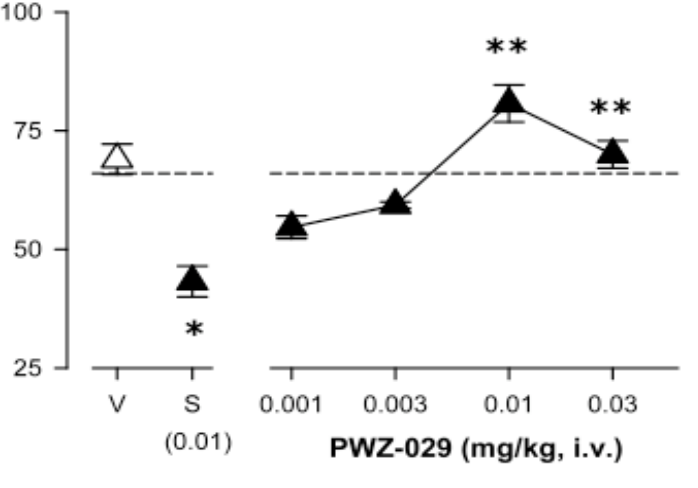
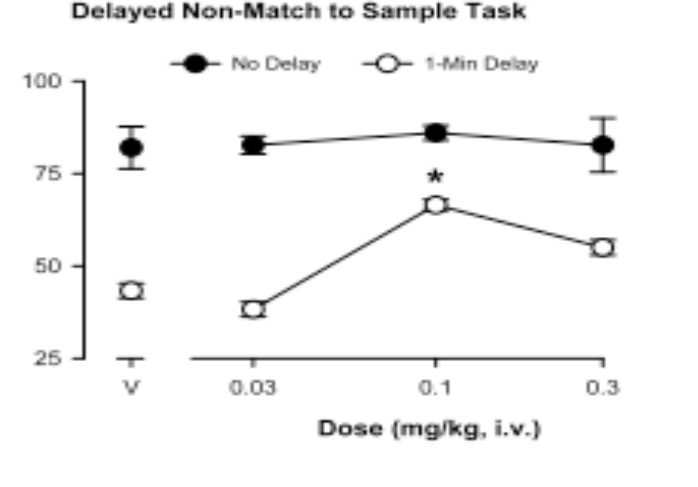
PWZ-029 Preliminary Data Compilation

IMPAIRED BASELINE RECOVERY AND COMPLEX MEMORY Continued

Experiment	Type of Test	Model	Figure	Summary of Results																				
Object Retrieval with Detours (ORD)	ORD is a manual test sensitive to frontostriatal deficits that investigates executive function.	Rhesus monkeys were treated with vehicle or 1 of 3 concentrations of PWZ-029 and then subjected to 15 mixed or difficult task configurations over 14-21 experimental sessions. The percent success rate of object retrieval was measured.	<p>A. Mixed Trials</p> <table border="1"> <thead> <tr> <th>PWZ-029 Dose (mg/kg, i.v.)</th> <th>Success Rate (%)</th> </tr> </thead> <tbody> <tr> <td>V</td> <td>~65</td> </tr> <tr> <td>0.003</td> <td>~68</td> </tr> <tr> <td>0.01</td> <td>~58</td> </tr> <tr> <td>0.03</td> <td>~68</td> </tr> </tbody> </table> <p>B. Difficult Trials</p> <table border="1"> <thead> <tr> <th>PWZ-029 Dose (mg/kg, i.v.)</th> <th>Success Rate (%)</th> </tr> </thead> <tbody> <tr> <td>V</td> <td>50</td> </tr> <tr> <td>0.003</td> <td>~55</td> </tr> <tr> <td>0.01</td> <td>~65</td> </tr> <tr> <td>0.03</td> <td>~80*</td> </tr> </tbody> </table>	PWZ-029 Dose (mg/kg, i.v.)	Success Rate (%)	V	~65	0.003	~68	0.01	~58	0.03	~68	PWZ-029 Dose (mg/kg, i.v.)	Success Rate (%)	V	50	0.003	~55	0.01	~65	0.03	~80*	PWZ-029 enhanced cognition under conditions in which baseline performance was impaired (i.e. difficult trials). *P<0.05 vs. vehicle (V)
PWZ-029 Dose (mg/kg, i.v.)	Success Rate (%)																							
V	~65																							
0.003	~68																							
0.01	~58																							
0.03	~68																							
PWZ-029 Dose (mg/kg, i.v.)	Success Rate (%)																							
V	50																							
0.003	~55																							
0.01	~65																							
0.03	~80*																							

PWZ-029 Preliminary Data Compilation

IMPAIRED BASELINE RECOVERY AND COMPLEX MEMORY Continued

Experiment	Type of Test	Model	Figure	Summary of Results																					
Object Retrieval with Detours (ORD)	ORD is a manual test sensitive to frontostriatal deficits that investigates executive function.	Rhesus monkeys were treated with vehicle, scopolamine, or 1 of 3 concentrations of PWZ-029 and then subjected to 15 mixed or difficult task configurations over 14-21 experimental sessions. The percent success rate of object retrieval was measured.	 <p>Detailed description: This line graph plots the percent success rate of object retrieval in the ORD task against different treatments. The y-axis ranges from 25 to 100. The x-axis shows treatments: Vehicle (V), Scopolamine (S), and three doses of PWZ-029 (0.001, 0.003, 0.01, 0.03 mg/kg, i.v.). A dashed horizontal line at approximately 68% represents the baseline performance. The S treatment significantly reduces performance to about 42% (*). PWZ-029 treatments show a dose-dependent recovery, with the 0.01 mg/kg dose showing the highest performance at approximately 82% (**).</p> <table border="1"> <caption>ORD Performance Data</caption> <thead> <tr> <th>Treatment</th> <th>Percent Success Rate</th> <th>Significance</th> </tr> </thead> <tbody> <tr> <td>V</td> <td>~68</td> <td></td> </tr> <tr> <td>S</td> <td>~42</td> <td>*</td> </tr> <tr> <td>0.001</td> <td>~55</td> <td></td> </tr> <tr> <td>0.003</td> <td>~60</td> <td></td> </tr> <tr> <td>0.01</td> <td>~82</td> <td>**</td> </tr> <tr> <td>0.03</td> <td>~70</td> <td>**</td> </tr> </tbody> </table>	Treatment	Percent Success Rate	Significance	V	~68		S	~42	*	0.001	~55		0.003	~60		0.01	~82	**	0.03	~70	**	Scopolamine-induced deficits in ORD performance were reduced with PWZ-029. *P<0.05 vs. Vehicle (V); **P<0.05 vs. scopolamine (S)
Treatment	Percent Success Rate	Significance																							
V	~68																								
S	~42	*																							
0.001	~55																								
0.003	~60																								
0.01	~82	**																							
0.03	~70	**																							
Delayed Non-Match to Sample Task (DNMS)	Short-term recognition memory task	Rhesus monkeys treated with vehicle or increasing concentrations of PWZ-029 (n=2-3), and subjected to DNMS tasks with and without delay.	 <p>Detailed description: This line graph shows performance on a DNMS task with and without a 1-minute delay. The y-axis is percent success rate (25-100). The x-axis shows doses: Vehicle (V), 0.03, 0.1, and 0.3 mg/kg, i.v. The 'No Delay' series (filled circles) remains consistently high, around 80-85%. The '1-Min Delay' series (open circles) shows significantly lower performance, which is improved by PWZ-029 treatment, reaching approximately 65% at the 0.1 mg/kg dose (*).</p> <table border="1"> <caption>DNMS Performance Data</caption> <thead> <tr> <th>Dose (mg/kg, i.v.)</th> <th>No Delay (%)</th> <th>1-Min Delay (%)</th> <th>Significance (1-Min)</th> </tr> </thead> <tbody> <tr> <td>V</td> <td>~80</td> <td>~42</td> <td></td> </tr> <tr> <td>0.03</td> <td>~82</td> <td>~38</td> <td></td> </tr> <tr> <td>0.1</td> <td>~85</td> <td>~65</td> <td>*</td> </tr> <tr> <td>0.3</td> <td>~82</td> <td>~55</td> <td></td> </tr> </tbody> </table>	Dose (mg/kg, i.v.)	No Delay (%)	1-Min Delay (%)	Significance (1-Min)	V	~80	~42		0.03	~82	~38		0.1	~85	~65	*	0.3	~82	~55		Performance was not affected by PWZ-029 without delay. A 0.1 mg/kg dose of PWZ-029 significantly enhanced performance when a 1-minute delay was introduced. *P<0.05	
Dose (mg/kg, i.v.)	No Delay (%)	1-Min Delay (%)	Significance (1-Min)																						
V	~80	~42																							
0.03	~82	~38																							
0.1	~85	~65	*																						
0.3	~82	~55																							

PWZ-029 Preliminary Data Compilation

IMPAIRED BASELINE RECOVERY AND COMPLEX MEMORY Continued

Experiment	Type of Test	Model	Figure	Summary of Results															
DNMS	Short-term recognition memory task	Rhesus monkeys treated with vehicle or 0.01 mg/kg of PWZ-029 (n=4), and subjected to DNMS tasks without delay, as well as with a 10-minute delay and distractors.	<p>A. Delayed Non-Match to Sample</p> <p>10-Min Delay w/Distractors</p> <table border="1"> <caption>Data for Figure A: Delayed Non-Match to Sample</caption> <thead> <tr> <th>Condition</th> <th>% Correct</th> </tr> </thead> <tbody> <tr> <td>No Delay</td> <td>~88</td> </tr> <tr> <td>Veh</td> <td>~55*</td> </tr> <tr> <td>PWZ</td> <td>~80</td> </tr> </tbody> </table>	Condition	% Correct	No Delay	~88	Veh	~55*	PWZ	~80	At 0.01 mg/kg, PWZ-029 significantly enhances recognition memory in the DNMS task when a 10-minute delay and distractors are introduced. *P<0.05							
Condition	% Correct																		
No Delay	~88																		
Veh	~55*																		
PWZ	~80																		
Object Retrieval with Detours	Theorized to assess Executive Function	Rhesus Monkeys treated with and without scopolamine and/or PWZ-029 (n=4).	<p>B. Object Retrieval with Detours</p> <table border="1"> <caption>Data for Figure B: Object Retrieval with Detours</caption> <thead> <tr> <th>Scopolamine</th> <th>PWZ-029</th> <th>% Correct</th> </tr> </thead> <tbody> <tr> <td>--</td> <td>--</td> <td>~68</td> </tr> <tr> <td>--</td> <td>+</td> <td>~68</td> </tr> <tr> <td>+</td> <td>--</td> <td>~38*</td> </tr> <tr> <td>+</td> <td>+</td> <td>~70</td> </tr> </tbody> </table>	Scopolamine	PWZ-029	% Correct	--	--	~68	--	+	~68	+	--	~38*	+	+	~70	PWZ-029 appeared to recover the scopolamine-induced deficit of retrieving the objects. *P<0.05 vs. no treatment (first bar)
Scopolamine	PWZ-029	% Correct																	
--	--	~68																	
--	+	~68																	
+	--	~38*																	
+	+	~70																	

PWZ-029 Preliminary Data Compilation

IMPAIRED BASELINE RECOVERY AND COMPLEX MEMORY Continued

Experiment	Type of Test	Model	Figure	Summary of Results
Acquisition Phase of MWM	Assess spatial learning and working memory	Male, Dahl SS, n=10, red bars = 10 mg/kg PWZ-029	<p>Distance (m)</p> <p>Day</p> <p>P<.05 vs. Vehicle</p>	PWZ-029 significantly improves the ability of SS rats to acquire the location of the hidden platform after four days of acquisition training.
MWM	Assess spatial learning and working memory	Male, FAB-Samaritan rats; blue bars = positive control, red bars = negative control, green bars = donepezil, 3 mg/kg; turquoise bars = PWZ-029, 10 mg/kg	<p>Distance (m)</p> <p>Platform Phase</p>	On the second week of the MWM protocol, PWZ-029 significantly improved performance in the experiment compared to the Group 2 (negative control).
MWM	Assess spatial learning and working memory	Male, FAB-Samaritan rats; blue bars = positive control, red bars = negative control, green bars = donepezil, 3 mg/kg; turquoise bars = PWZ-029, 10 mg/kg	<p>Latency (sec)</p> <p>Platform Phase</p>	On the second week of the MWM protocol, PWZ-029 significantly improved performance in the experiment compared to the Group 2 (negative control).

CURRICULUM VITAE

Full Name: Sundari K. Rallapalli

Place of birth: Secunderabad, India, March 26

Education:

University of Wisconsin-Milwaukee	08/2006-12/2012	Ph. D.
Tennessee Tech. Univ., Cookeville, TN	08/1999-08/2001	M.S.
Osmania University, Hyderabad, India	06/1996-06/1998	M.Sc.

Dissertation Title:

- I. The First Enantiospecific, Stereospecific Total Synthesis of the Indole Alkaloid Ervincidine
- II. Synthesis of Alpha 5 Subtype Selective Ligands for GABA(A)/Benzodiazepine Receptors

Affiliation:

Member of the American Chemical Society

Publications

1. "A Study of the Structure-activity Relationship of GABA_A-benzodiazepine Receptor Bivalent Ligands by Conformational Analysis with low Temperature NMR and X-ray Analysis", Han, D., Forsterling, H.F., Li, X., Deschamps, J.R., Parrish, D., Cao, H., **Rallapalli, S.**, Clayton, T. , Teng, Y., Majumder, S., Sankar,

- S., Roth, B.L., Sieghart, W., Furtmuller, R., J.K. , Weed, M.R., Cook, J.M. *Bioorg. and Med. Chem.*, **16**, 8853-8862 (2008).
2. “General Approach to the Total Synthesis of Macroline Related Sarpagine and Ajmaline Alkaloids”, Edwankar, C., Edwankar, R. V., **Rallapalli, S.**, Cook, J. *Natural Product Communications*, **11**, 1839-1870 (2008).
 3. “Effects of a Novel Inverse Agonist Selective for Alpha5 GABA(A) Receptors on Spatial Memory: Comparison with the Standard Non-Selective Inverse Agonist DMCM”, Samardzic, J.,Savic, M., Clayton, T., **Rallapalli, S.**, Obradovic, D., Joksimovic, S.M. Seighart, W. Cook, J. Congress of the European-College-of-Neuropsychopharmacology, Aug 30-Sept 03, 2008, Barcelona, Spain, *European Neuropsychopharmacology*, S285-S-285 Supplement, Suppl.4 (18 pages), published August 2008.
 4. “An Improved Process for the Synthesis of 4H-Imidazo [1,5-a][1,4]benzodiazepines”, Yang, J., Teng, Y., Ara, S., **Rallapalli, S.**, Cook, J. *Synthesis*, **6**, 1036-1040 (2009).
 5. “The Differential Role of $\alpha 1$ and $\alpha 5$ Containing GABA_A Receptors in Mediating Diazepam Effects on Spontaneous Locomotor Activity and Water Maze Learning and Memory in Rats”, Savic, M.M.; Milinkovic, M.M.; Clayton, T., **Rallapalli, S.**, Joksimovic, Van linn, M., Cook, J.M. *International Journal of Neuropsychopharmacology*, **12**, 1179-1193 (2009).
 6. “Recent Progress in the Total Synthesis of Indole Alkaloids”, Edwankar, C. R., Edwankar, R, V., Namjoshi, O. A., **Rallapalli, S. K.**, Yang, J., Cook, J. M. *Curr. Opin. Drug Discovery Dev.* **12 (6)**, 752-771 (2009).
 7. “The First Enantiospecific Total Synthesis of the 3-Oxygenated Sarpagine Indole Alkaloids Affinine and 16-Epiaffinine as well as Vobasinediol and 16-

- Epivobasinediol”, Yang, J., **Rallapalli, S. K.**, Cook, J. M. *Tetrahedron Lett.*, **51**, 815-817 (2010).
8. “Enantiospecific Total Synthesis of the Important Biogenetic Intermediates along the Ajmaline Pathway, (+)-Polyneuridine and (+)-Polyneuridine Aldehyde, as well as 16-Epivellosimine and Macusine A”, Yin, W., Kabir, M. S., Wang, Z., **Rallapalli, S. K.**, Ma, J., Cook, J. M. *J. Org. Chem.* **75**, 3339-3349 (2010).
 9. “ α 4-Containing GABA (A) Receptors are Required for Antagonism of Ethanol-Induced Motor Incoordination and Hypnosis by the Imidazobenzodiazepine Ro15-4513,” Iyer, S. V.; Benavides, R. A.; Chandra, D.; **Rallapalli, S.**; Cook, J.; June, H. L.; Homanics, G. E., *Frontiers in Pharmacology*, **2**, 18, 1-7 (2011).
 10. “Lifelong CRF Overproduction is Associated with Altered Gene Expression and Sensitivity of Discrete GABA_A and mGlu Receptor Subtypes,” Vinkers, C.; Hendriksen, H.; Oorshot, R.; Cook, J.; **Rallapalli, S.**; Huang, S.; Millian, M.; Oliver, B.; Groenink, L., *Psychopharmacology*, **219** (3), 897-908 (2012).
 11. “The Role of α 1 and α 5 Subunit-Containing GABA_A Receptors in Motor Impairment Induced by Benzodiazepines in Rats”, Milic, M.; Divljakovic, J.; **Rallapalli, S.**; Van Linn, M.L.; Timic, T.; Cook, J. M.; Savic, M. M., *Behav. Pharmacol.*, **23** (2), 191-197(2012).
 12. “Modulation of α 5 Subunit-Containing GABA_A Receptors Alters Alcohol Drinking by Rhesus Monkeys”, Ru“edi-Bettschen, D.; Rowlett, J. K.; **Rallapalli, S.**; Clayton, T.; Cook, J. M.; Platt, D. M., *Alcoholism Clin. and Exp. Res.*, DOI: 10.1111/acer.12018 (2012).

13. "Search for $\alpha 3 \beta 2/3 \gamma 2$ Subtype Selective Ligands That are Stable on Human Liver Microsomes", Namjoshi, O.; Wang, Z.; **Rallapalli, S.**; Johnson, E. M.; Johnson, Yun-Teng; Ng, H.; Ramerstorger, J.; Sieghart, W.; Roth, B.; Rowlett, J.K.; Cook, J. M., *Bioorg. and Med. Chem.*, accepted (2012).
14. "Cognition Impairing Effects of Benzodiazepine Type Drugs: Evaluation of the Role of GABA_A Receptor Subtypes in Spatial Recognition Memory and Executive Function Tasks", Makaron, L.; Moran, C.; Namjoshi, O.; **Rallapalli, S.**; Cook, J.; Rowlett, J., *Eur. J. Neuropsychopharmacology*, **00**, 0000-0000 (2013).
15. "Subtype Selectivity of $\alpha + \beta -$ Site Ligands of GABA_A Receptors-Identification of the First Highly Specific Positive Modulators at $\alpha 6 \beta (2/3) \gamma 2$ Receptors", Varagic, Z.; Ramerstorfer, J.; Huang, S.; **Rallapalli, S.**; Sarto-Jackson, I.; Cook, J.; Sieghart, W.; Margot, E., *J. British Pharmacol.*, **00**, 0000-0000 (2013).
16. "Allosteric Modulation of GABA (A) Receptors Compared to Non-GABAergic Compounds: Effects on Visuo Spatial Memory in Rhesus Monkeys", P. Soto, N. Ator, S. Rallapalli, P. Biawat, T. Clayton, C. Brayton, J. Cook, M. Weed., *Psychopharmacology*, **00**, 0000-0000 (2013).
17. "The First Enantiospecific, Stereospecific Total Synthesis of Indole Alkaloid Ervincidine", **Rallapalli, S. K.**; Cook, J.M., *Org. Lett., Manuscript in preparation.*
18. "eQTL and receptor pharmacology implicate GABA signaling in neuroblastoma", Hackett, C. S.; Quigley, D. A.; Fan, Q.; Cheng, C.; Song, Y. K.; Pawlikowska L.;

Chen, J.; Bao, Y.; Goldenberg, D.D.; Nguyen, K.; Cho, Y.C.; Rallapalli, S.K.; Cook, J. M.; Kozlov, S.; Mao, J.; Van Dyke, T.; Kwok, P. Y.; Khan, J.; Balmain, A.; Weiss, W. A., *Nature*, **00**, 0000-0000 (2013).

Patents

1. “GABAergic Agents to Treat Memory Deficits”, Cook, J. M. Clayton, T., Teng, Y., **Rallapalli, S. K.**, Han, D., U. S. Patent publication no 2010/0130479 A1, Published May 27, 2010.
2. “Gabaergic Receptor Subtype Selective Ligands and their Uses”, Cook, J. M., **Rallapalli, S.**; Clayton, T.; Jain, H.; Yang, J.; Teng, Y.; Poe, M.M., Namjoshi, O.; Wang, Z., U.S. Patent publication no 2012/0295892 A1, Published November 22, 2012.

Major: Organic Chemistry

Minor: Physical Chemistry